Contents

Notation and Abbreviations

Ai(z)	:	The Airy function
BA	:	Baker–Akhiezer
$\boldsymbol{B(x,\delta)}$	:	ball centered at x with radius δ
$\boldsymbol{B_{\theta,\phi}(x,\delta)}$	:	See Figure 3.1.1
$\boldsymbol{\mathcal{B}^+(\Gamma)}$	:	The weighted Bergman space $\mathcal{B}^+(\Gamma) = \{f \text{ holomorphic in } \Gamma^+ : \|f\|_{B^+(\Gamma)} < \infty\}$,
$\boldsymbol{C}$	:	A generic positive constant
$\mathbb{C}^{\pm}$	:	The upper $(+)$ and lower $(-)$ half planes: $\{z \in \mathbb{C} : \pm \operatorname{Im} z > 0\}$
$\boldsymbol{\mathcal{C}_\Gamma}$	:	$\mathcal{C}_\Gamma f(z) = \int_\Gamma \frac{f(s)}{s-z} \bar{d}s$
$\boldsymbol{\mathcal{C}_\Gamma^{\pm}}$	:	The boundary values of $\mathcal{C}_\Gamma$
$\boldsymbol{\mathcal{C}[G;\Gamma]}$	:	The operator $u \mapsto u - \mathcal{C}_\Gamma^- u \cdot (G - I)$
$\boldsymbol{\mathcal{C}'[G;\Gamma]}$	:	The operator $u \mapsto u - \mathcal{C}_\Gamma^- [u(G - I)]$
$\boldsymbol{\mathcal{C}[X_+, X_-;\Gamma]}$	:	The operator $u \mapsto \mathcal{C}_\Gamma^+ u \cdot X_+^{-1} - \mathcal{C}_\Gamma^- u \cdot X_-^{-1}$
$\boldsymbol{\mathcal{C}'[X_+, X_-;\Gamma]}$	:	The operator $u \mapsto \mathcal{C}_\Gamma^+ [uX_+] - \mathcal{C}_\Gamma^- [uX_-]$
$\boldsymbol{\mathcal{C}_n[G;\Gamma]}$	:	A finite-dimensional approximation of $\mathcal{C}[G;\Gamma]$
$\boldsymbol{C^{0,\alpha}(\Gamma)}$	:	The Banach space of uniformly α-Hölder continuous functions on Γ
$\boldsymbol{C^k(\Gamma)}$	:	The Banach space of k-times differentiable functions
$\boldsymbol{C_c^\infty(\Gamma)}$	:	C^∞ functions with compact support inside of Γ
$\boldsymbol{\chi_A}$	:	The indicator (or characteristic) function of a set A
$\boldsymbol{\operatorname{codim} X}$	:	The dimension of the vector space $Y \diagup X$, $X \subset Y$, Y is implied
$\boldsymbol{D \Subset \Omega}$	:	D is a connected component of Ω
$\boldsymbol{Df}$	:	Weak differentiation of f on a self-intersecting contour

$\boldsymbol{\dim X}$	:	The dimension of a vector space X
$\boldsymbol{\bar{d}s}$	:	$\bar{d}s = 1/(2\pi i)ds$
$\boldsymbol{D_\nu(z)}$	:	Parabolic Cylinder function
$\boldsymbol{\mathcal{E}^p(D)}$	:	The L^p-based Hardy space on a general domain D
$\boldsymbol{\mathcal{E}^p(D_-)}$	:	The L^p-based Hardy space on the domain $D^c \setminus \partial D$
$\boldsymbol{\mathcal{E}^\pm(\Gamma)}$	:	L^2-based Hardy spaces of functions holomorphic off a self-intersecting contour
Γ^+	:	The domain lying above a Lipschitz graph Γ
$\boldsymbol{H^k(\Gamma)}$	:	$W^{k,2}(\Gamma)$
$\boldsymbol{\mathcal{H}^p}$	:	The L^p-based Hardy space on $\mathbb{U}$
$\boldsymbol{H^k_\pm(\Gamma)}$	:	The Sobolev spaces of Zhou: $H^k_\pm(\Gamma) = \{f \in L^2(\Gamma) : f \in H^k_z(\partial D) \text{ for every } D \Subset \Omega_\pm\}$
$\boldsymbol{\tilde{H}^k_\pm(\Gamma)}$	:	$H^k_\pm(\Gamma) \oplus \mathbb{C}^{n\times n}$
$\boldsymbol{I}$	:	The identity matrix, dimensionality is implied
$\mathbb{I}$	:	The interval $[-1,1]$ with left-to-right orientation
$\boldsymbol{\operatorname{ind} T}$	:	Fredholm index of an operator T: $\dim\ker T - \operatorname{codim}\operatorname{ran} T$
$\operatorname{ind}_\Gamma f$	:	The index of f with respect to Γ: $\operatorname{ind}_\Gamma f = \frac{1}{2\pi i}[\log f]_\Gamma$
KdV	:	Korteweg-de Vries
$\boldsymbol{\ker T}$	:	The kernel of an operator T
$\boldsymbol{\mathcal{K}(X,Y)}$	:	The space of compact operators from X to Y
$\boldsymbol{L^p(\Gamma)}$	:	The Lebesgue space (with respect to arclength) on the oriented contour Γ with norm $\|\cdot\|_p = \|\cdot\|_{L^p(\Gamma)}$
$\boldsymbol{\mathcal{L}(X,Y)}$	:	The space of operators from X to Y
$\boldsymbol{\mathcal{L}(X)}$	:	$\mathcal{L}(X,X)$
$\boldsymbol{[\cdot,\cdot]}$	:	Matrix commutator: $[M,N] = MN - NM$
NLS	:	Nonlinear Schrödinger
$\boldsymbol{\|\cdot\|_X}$	:	The norm on a linear space X
$\boldsymbol{\|\cdot\|_u}$	:	The uniform norm: For $f : \Gamma \to \mathbb{C}$, $\|f\|_u = \sup_{z\in\Gamma} \|f(z)\|$
ODE	:	ordinary differential equation
operator	:	bounded linear operator

PDE	:	partial differential equation
$\boldsymbol{\Phi_\pm}$ or $\boldsymbol{\Phi^\pm}$	:	The boundary values of an analytic function Φ
$\mathbf{ran}\, \boldsymbol{T}$	:	The range of an operator T
RHP	:	Riemann–Hilbert problem
$[\boldsymbol{G};\boldsymbol{\Gamma}]$	:	An L^2 Riemann–Hilbert problem $$\Phi^+(s) = \Phi^-(s)G(s), \quad s \in \Gamma, \quad \Phi(\infty) = I$$
$\boldsymbol{R_\pm(\Gamma)}$	:	Functions whose restrictions to appropriate contours are rational
$\boldsymbol{\mathcal{S}(\mathbb{R})}$	:	Schwarz class of rapidly decaying functions
$\boldsymbol{\mathcal{S}_\delta(\mathbb{R})}$	:	For $\delta > 0$ $$\{f \in \mathcal{S}(\mathbb{R}) : \sup_{x\in\mathbb{R}} e^{\delta\|x\|}\|f^{(j)}(x)\| < \infty, \quad j = 0, 1, \ldots\}$$
$\boldsymbol{\Phi^\dagger}$	:	Schwarz conjugate: $\Phi^\dagger(z) = (\overline{\Phi(\bar{z})})^T$
$\boldsymbol{\Sigma_\infty}$	:	Contours that tend to straight lines at infinity
$\boldsymbol{\mathcal{T}[G;\Gamma]}$	:	The operator $u \mapsto \mathcal{C}_\Gamma^- u \cdot (G - I)$
$\boldsymbol{T_k(x)}$	:	Chebyshev polynomial of the first kind
$\mathbb{U}$	:	The unit sphere
$\boldsymbol{U_k(x)}$	:	Chebyshev polynomial of the second kind
$\boldsymbol{W^{k,p}(\Gamma)}$	:	The kth-order L^p-based Sobolev space on a self-intersecting contour
$\boldsymbol{W_z^{k,p}(\Gamma)}$	:	Functions in $W^{k,p}(\Gamma)$ satisfying the $(k-1)$th-order zero-sum condition

Chapter 1

Introduction

1.1 What are special functions?

A special function is shorthand for a mathematical function which arises in many physical, biological and computational applications or in mathematical settings. In addition, a special function should be sufficiently basic so as to allow the mathematical community to identify, prove and make use of many of its properties. A simple example is the cosine function $x \mapsto \cos(x)$. The cosine function, to a calculus student does not seem so 'special'. Indeed, nearly all of the elementary properties are found and hopefully understood during a year-long calculus course. This is the exact purpose, ironically, of special functions. We identify and catalog important properties to allow easy assimilation of knowledge and thus, making the function, to the experienced user, seem mundane; certainly, not special.

For centuries, mathematicians have been studying special functions. The relative importance of the subject is determined by applications throughout engineering and the physical sciences. The catenary, discovered by Leibniz, Huygens and Bernoulli in the 1600s, describes the shape of a freely-hanging rope in terms of the hyperbolic cousin of the cosine function, $x \mapsto \cosh(x)$. An illustration of the importance of this work in early construction can be found in King's College Chapel, Cambridge, UK where it was used to guide the curvature of the ceiling.

An important feature that separates cos and cosh from lines and parabolas is that they necessarily take a *transcendental*[1] form. Thus, they have infinite series representations

$$\cos(x) = \sum_{n=0}^{\infty} \frac{(-1)^n}{(2n)!} x^{2n}, \tag{1.1.1}$$

$$\cosh(x) = \sum_{n=0}^{\infty} \frac{1}{(2n)!} x^{2n}. \tag{1.1.2}$$

The study of transcendental functions continued with the discovery of the Airy and Bessel functions which share similar but more complicated series representations. These series representations are oft derived using a differential equation that is satisfied by the given special function. Such a derivation succeeds in many cases when the differential equation

[1] In this context transcendental means that the function cannot be expressed as a finite number of algebraic steps, including rational powers, applied to a variable or variables [62].

is linear.

The 19th century was a golden age for special function theory. Techniques from the field of complex analysis were invoked to study the so-called elliptic functions. These functions are of a fundamentally nonlinear nature: elliptic functions are solutions of nonlinear differential equations. The use of complex analysis greatly aids in the theory of elliptic functions.

The early twentieth century marked the work of Paul Painlevé and his collaborators in identifying the so-called Painlevé transcendents. The Painlevé transcendents are solutions of nonlinear differential equations that possess important properties in the complex plane. Independent of their mathematical properties, which are described at length in [51], the Painlevé transcendents have found use in the asymptotic study of water wave models [5, 39, 34] and in statistical mechanics [113]. We discuss these applications further in Section 1.3.

1.2 How are special functions studied?

As we will see, an expression for a special function is not enough. As an example, consider the formula (1.1.1) for $\cos(x)$. The important fact that $\cos(0) = \cos(2\pi)$ is not evident from this formula. Indeed, there exists an infinite product expansion that makes this fact much clearer. Furthermore, (1.1.1) does not make it clear that the cosine function grows exponentially in the complex plane while being bounded on the real line.

Another question one may ask is how to compute $\cos(x)$. The series in (1.1.1) may be approximated by truncating it at some finite number of terms. With this methodology $\cos(0)$ is obtained exactly, and

$$\left|\cos(.1) - \sum_{n=0}^{3} \frac{(-1)^n}{(2n)!}(.1)^{2n}\right| < 10^{-12},$$

a very good approximation using just the first four terms in the series. When $x = 2\pi$ it takes 17 terms to achieve the same degree of accuracy. It requires more than a naive summing of the series (*i.e.* use periodicity) to compute $\cos(x)$ for large values of x.

We have identified three of the many ways to study special functions:

1. the derivation of alternate representations,
2. behavior for large values of x (*i.e.* asymptotic expansions), and
3. numerical computations.

In this manuscript we discuss all three methodologies but concentrate on numerical computations. We also demonstrate their interdependencies.

1.3 Modern applications of nonlinear special functions

We study *nonlinear special functions*. Nonlinear special functions are the subclass of special functions that are uniquely defined by a nonlinear relationship. The solutions of certain nonlinear ordinary differential equations are nonlinear special functions, see Chapter 8.

So are the solutions of nonlinear partial differential equations (PDEs), see Chapters 6, 9, and 7. Additionally, orthogonal polynomials with respect to a given measure depend nonlinearly on the measure, see Chapter 10.

1.3.1 Reduction to the Korteweg-de Vries equation

We consider the reduction of the classical Euler equations that describe 1-D invicid fluid flow, driven by gravity. We use subscripts to denote partial derivatives.

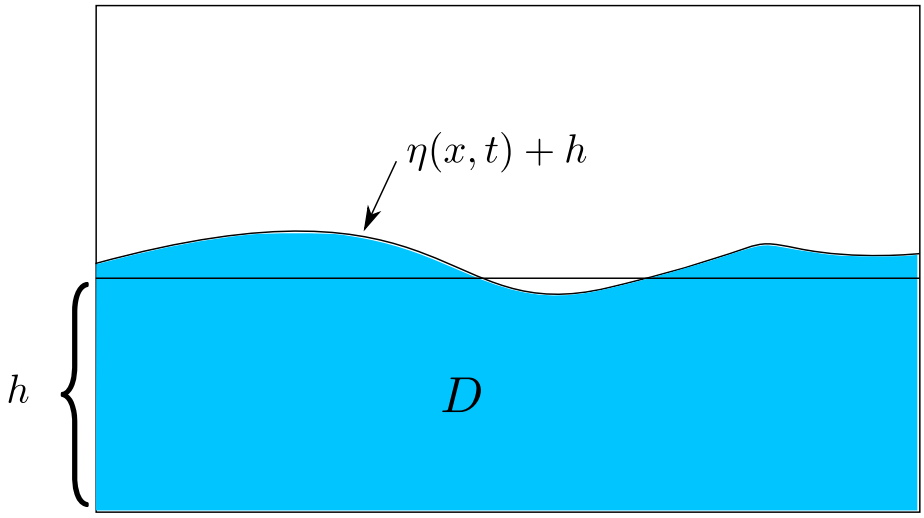

Figure 1.3.1: A schematic for (1.3.1).

$$\begin{aligned} \phi_{xx}+\phi_{zz} &= 0, \quad (x,z)\in D, \\ \phi_z &= 0, \quad z=0, \\ \eta_t+\eta_x\phi_x &= \phi_z, \quad z=h+\eta, \\ \phi_t+\frac{1}{2}\left(\phi_x^2+\phi_z^2\right)+g(\eta+h) &= 0, \quad z=h+\eta, \end{aligned} \tag{1.3.1}$$

Here the fluid domain is $D=\{(x,z):-\infty<x<\infty, 0<z<h+\eta(x,t)\}$. The function ϕ is the velocity potential, $\eta(x,t)$ is the surface elevation above the at-rest depth h, see Figure 1.3.1. Define the parameter l to be the typical wavelength and a to be the typical amplitude. In a particular long-wave ($h^2/l^2\to 0$), shallow-water ($a/h\to 0$) limit, a multiple scales analysis produces the Korteweg-de Vries (KdV) equation [69, 111]:

$$\eta_t+\eta_x+\frac{3}{2}\frac{a}{h}\eta\eta_x+\frac{1}{6}\frac{h^2}{l^2}\eta_{xxx}+\mathcal{O}\left(\left(\frac{h^2}{l^2}\right)^2+\left(\frac{a}{h}\right)^2\right)=0.$$

Using non-dimensional variables, in a moving frame, to first order we obtain

$$q_t+6qq_x+q_{xxx}=0. \tag{1.3.2}$$

We see in Chapters 6 and 9 that the solutions of the KdV equation possesses the requisite structure and universality to be considered special functions in $(1+1)$-dimensions.

With a sufficiently smooth and decaying initial condition, the KdV equation can be reduced further in different regions of the (x,t)-plane. Consider the region $|x| \leq Ct^{1/3}$ for some constant $C > 0$. The solution q of (1.3.2) satisfies [5]

$$q(x,t) - U(x,t) = \mathcal{O}(t^{-1}),$$

where

$$U(x,t) = \frac{1}{(3t)^{2/3}} \left(v^2 \left(\frac{x}{(3t)^{1/3}} \right) + v' \left(\frac{x}{(3t)^{1/3}} \right) \right),$$

and v is a specific solution of the equation

$$v_{xx} = xv + 2v^3. \tag{1.3.3}$$

This is the famous homogeneous Painlevé II equation which will be discussed in Chapter 8. With the exception of elliptic functions, the Painlevé transcendents (transcendental solutions of (1.3.3)) are the most well-known and widely-used nonlinear special functions.

1.3.2 The 2-D Ising model

The 2-D Ising model is a mathematical idealization originating in ferromagnetism, see [72] for a sketch of the model. Unlike the water wave models above, the Ising model is discrete. Each variable $\sigma_{j,k}$ arranged in a 2-dimensional lattice, can take the values (spins) ± 1 and may only interact with its nearest neighbors. An interaction energy exists between neighbors of $-E$ if spins differ and $+E$ if spins agree. Thus, in its simplest form, the total interaction energy is given by

$$\mathcal{E} = -\sum_{j=1}^{L_v} \sum_{k=1}^{L_h} (E\sigma_{j,k}\sigma_{j,k+1} + E\sigma_{j,k}\sigma_{j+1,k}).$$

The free energy and specific heat of the Ising model was explicitly calculated by Onsager [92] in the limit as $L_v, L_h \to \infty$. Kaufman and Onsager computed the two-spin correlation function

$$\langle \sigma_{0,0}\sigma_{M,N} \rangle = \lim_{L_v, L_h \to \infty} Z^{-1} \sum_{\text{states}} \sigma_{0,0}\sigma_{M,N} e^{\mathcal{E}/k_B T},$$

where k_B is Boltzmann's constant, T is the associated temperature and Z is the partition function. Onsager established the existence of a critical temperature T_c where the specific heat becomes infinite. The important results of Wu, McCoy, Tracy and Barouch showed that near T_c, the correlation function can be expressed in terms of a Painlevé III transcendent [113]. Furthermore, the work of Jimbo and Miwa expressed the diagonal correlation function $\langle \sigma_{0,0}\sigma_{N,N} \rangle$ in terms of a Painlevé VI transcendent [67]. Theoretical physics and statistical mechanics has great dependence on nonlinear special functions.

It is worth noting that due to the strong connections between statistical mechanics and

random matrix theory, it is not surprising to see Painlevé transcendents arising in random matrix theory. See Chapter 10 for further discussion of this.

1.4 Overview

As mentioned above, the approach presented here is mainly computational. We develop methods for the computation of both linear and nonlinear special functions. We consider solutions of linear, constant-coefficient evolution PDEs as linear special functions in $(1+1)$ dimensions. Additionally, solutions of integrable nonlinear PDEs are nonlinear special functions, also in $(1+1)$ dimensions. Much of the code that is used below can be found in `ISTPackage` [105], a `Mathematica` package that is built off [85].

This dissertation is laid out as follows. In the remainder of this section we fix notation and discuss some essential background material that is necessary for much of the analysis that follows. In Chapter 2, we discuss a unification of Fourier transform PDE solution techniques for linear and nonlinear problems. This unification extends to the numerical analysis required to solve the respective problems. The unification of these numerical analysis techniques has not been discussed previously in the literature. Furthermore, the method presented for the solution of linear constant-coefficient PDEs appears to not be present in the existing literature.

The techniques that unify linear and nonlinear problems rely on the theory of Riemann–Hilbert problems (RHPs). In short, a RHP consists of finding a piecewise-analytic function in the complex plane where the behavior of its discontinuities is specified. More precisely, a RHP consists of finding a function $\phi(z)$ that satisfies the following jump condition

$$\lim_{\substack{z\to s \\ z \text{ left of } \Gamma}} \phi(z) = \left(\lim_{\substack{z\to s \\ z \text{ right of } \Gamma}} \phi(z) \right) g(s) + f(s), \quad s \in \Gamma, \tag{1.4.1}$$

for some definite functions f, g defined on an oriented contour Γ. In Chapter 3 we discuss a comprehensive theory for RHPs. In particular, we present results that often, in practice, allow one to establish both the existence and the uniqueness of a solution of a given RHP. This theory includes properties of singular integrals and singular integral equations along with developments related to Hardy spaces and rational approximation in Hardy spaces (Appendix A). The new contributions made here to singular integral equations are summarized by Definition 3.7.7 and Theorems 3.7.9, 3.8.10, 3.8.21 and 3.9.1. While the results presented in Appendix A on rational approximation are not new, we expose the full proof of the sketches that can be found in [116] and [8].

In Chapter 4 we review the inverse scattering transform (IST) as applied to the defocusing nonlinear Schrödinger equation. As is discussed in Chapter 2 the IST is a generalization of the Fourier transform solution technique to nonlinear, integrable PDEs. We immediately obtain a transform method that recovers the initial condition at $t = 0$. The so-called dressing method is introduced to demonstrate that we obtain a solution for $t > 0$. This method depends fundamentally on the theory of RHPs. We proceed to complete the asymptotic analysis for the RHP derived with the IST via the Deift and Zhou method of nonlinear steepest descent [33]. This entire process includes an elegant application of the theory in Chapter 3.

Chapter 5 discusses the numerical solution of RHPs, and in particular, the numerical solution of singular integral equations. Not surprisingly, Chapter 5 has heavy dependence on Chapter 3. In this chapter, a general framework is developed (introduced by the author in [90]) that allows one to prove that after certain preconditioning steps (deformations) a numerical method applied to a parameter-dependent RHP can maintain accuracy for arbitrarily large values of said parameter. In this numerical setting, we refer to this type of behavior as *asymptotic stability*. This establishes links between the numerical ideas used in the rest of the manuscript with the method of nonlinear steepest descent [33].

Chapter 6 presents the application of the theory of Chapters 2-5 to the Korteweg-de Vries (KdV) and modified KdV equations. This presents the first known numerical implementation of the celebrated inverse scattering transform that can be evaluated for all (x,t) and for all allowable initial conditions. Here asymptotic stability is realized and verified through numerical tests and comparison with asymptotic formulae. In specific regions of the (x,t)-plane the asymptotic stability of the numerical method is proved in a straightforward way with a new application of the theory of Chapter 5.

This chapter is followed by more new results: the same techniques applied to the KdV equation are applied to the focusing and defocusing nonlinear Schrödinger equations. Similar results are demonstrated: provable asymptotic stability of the numerical method. Darboux transformations are used to solve problems with homogeneous Robin boundary conditions. Finally, solutions with vertical asymptotes are computed. Traditional numerical methods cannot capture these solutions.

The computation of asymptotic formulae in Chapter 6 requires the computation of a Painlevé II transcendent. In Chapter 8 we examine the computation of solutions of Painlevé II equation on the real line. We present the computation of solutions that often arise in applications. This represents the first time the deformed RHP for the Painlevé II transcendent has been solved in the literature and we include a proof of asymptotic stability for some parameter ranges.

In Chapter 9 we present a new method for computing all finite-genus solutions of the KdV equation. The finite-genus solutions are special periodic and quasi-periodic multi-phase solutions of the KdV equations. These solutions arise in the analysis of the periodic Cauchy problem for the KdV equation. The finite-genus solutions are computed from the asymptotics of an associated Baker–Akhiezer function which is holomorphic on a finite-genus Riemann surface except at infinity. The method we present first phrases a RHP that is solved by the Baker–Akhiezer function. This RHP is solved via the techniques in Chapter 5 and a uniformly accurate approximation to solutions of the KdV equation is produced.

We conclude this manuscript with a discussion of a different kind of nonlinear special function: orthogonal polynomials. Polynomials that are orthogonal with respect to a measure depend nonlinearly on that measure. We present the first-known method to solve the Fokas–Its–Kitaev [66] RHP numerically. This requires the construction of the so-called equilibrium measure, see [88]. This method has important applications to random matrix theory. In many cases, the measure

$$\mu_n(B) = \int_B \mathcal{K}_n(x,x)dx,$$

that represents the expected fraction of eigenvalues of a random $n \times n$ Hermitian matrix that lie in the set B can be computed using orthogonal polynomials. We compute this measure and demonstrate its convergence to the so-called equilibrium measure. In addition, we use the numerical method to compute other eigenvalue statistics of some random matrix ensembles.

1.5 Background material

1.5.1 Notation

On a given metric space we use $B(x, \delta)$ to denote the ball centered at x with radius δ. We reserve C to denote a generic positive constant. We use χ_A to denote the indicator function of the set A. The notation $D \Subset \Omega$ is used when D is a connected component of Ω. We reserve k, z and λ to be complex parameters.

1.5.2 Lebesgue spaces

Unless otherwise stated, we assume that $\Gamma \subset \mathbb{C}$ is a piecewise smooth oriented contour with at most a finite number of transverse self-intersections. Additionally we assume that any unbounded component of Γ tends to a straight line at infinity. The theory can be developed under more general assumptions but this suffices for our purposes. We represent $\Gamma = \Gamma_1 \cup \cdots \cup \Gamma_n$ where each Γ_i is non-self-intersecting.

Definition 1.5.1.

$$L^p(\Gamma) = \left\{ f : \Gamma \to \mathbb{C} : f|_{\Gamma_i} \text{ measurable}, \int_{\Gamma_i} |f(k)|^p |dk| < \infty, \forall i \right\}.$$

We make $L^p(\Gamma)$ into a Banach space by equipping it with the norm

$$\|f\|_{L^p(\Gamma)} = \left(\sum_{i=1}^{n} \int_{\Gamma_i} |f(k)|^p dk \right)^{1/p}.$$

The notation $\|f\|_p = \|f\|_{L^p(\Gamma)}$ is used when Γ is clear from context.

1.5.3 Fredholm theory

Let X and Y be Banach spaces. Denote the set of operators from X to Y by $\mathcal{L}(X, Y)$ and we equip the space with its standard induced operator norm which makes the space into a Banach algebra if $X = Y$. We use the term *operator* for an element of $\mathcal{L}(X, Y)$.

Definition 1.5.2. *$K \in \mathcal{L}(X, Y)$ is said to be compact if the image of a bounded set in X is precompact in Y. Or, equivalently, the image of the unit ball in X is precompact in Y. Let $\mathcal{K}(X, Y)$ denote the closed subspace of compact operators in $\mathcal{L}(X, Y)$.*

This allows us to define a (semi-)Fredholm operator.

Definition 1.5.3. *$T \in \mathcal{L}(X, Y)$ is called left(right) semi-Fredholm if there exists $S \in \mathcal{L}(X, Y)$, called a* regulator*, such that $ST = I + K$ ($TS = I + K$) where $K \in \mathcal{K}(X, Y)$. An operator is Fredholm if it is both left and right semi-Fredholm.*

Theorem 1.5.4. *[41] If X is a Banach space, then an operator T on X is a Fredholm operator if and only if* $\dim\ker T$ *and* $\operatorname{codim}\operatorname{ran} T$ *is finite.*

Definition 1.5.5. *The* Fredholm index *denoted* $\operatorname{ind} T$ *is defined by*

$$\operatorname{ind}(T) = \dim\ker T - \operatorname{codim}\operatorname{ran} T.$$

Theorem 1.5.6. *Let T be a Fredholm operator with index κ. There exists $\epsilon > 0$ such that if $\|S - T\| < \epsilon$ then S is Fredholm with index κ.*

1.5.4 Additional results

We include two theorems that are of great use in what follows.

Theorem 1.5.7. *Let X and Y be two normed linear spaces with at least one being a Banach space. Let $L \in \mathcal{L}(X,Y)$ and $L^{-1} \in \mathcal{L}(Y,X)$. Let $M \in \mathcal{L}(X,Y)$ satisfy*

$$\|M - L\| < \frac{1}{\|L^{-1}\|}.$$

Then M is invertible, $M^{-1} \in \mathcal{L}(Y,X)$ and

$$\|M^{-1}\| \leq \frac{\|L^{-1}\|}{1 - \|L^{-1}\|\|M - L\|},$$
$$\|M^{-1} - L^{-1}\| \leq \frac{\|L^{-1}\|^2\|M - L\|}{1 - \|L^{-1}\|\|M - L\|}.$$

Theorem 1.5.8. *Let V be a Banach space, $L \in \mathcal{L}(V)$. Assume for some integer $m \geq 1$ that $\|L\| < 1$. Then $I - L$ is a bijection on V and its inverse satisfies*

$$\|(I - L)^{-1}\| \leq \frac{1}{1 - \|L^m\|} \sum_{i=0}^{m-1} \|L^i\|.$$

Throughout we are interested in matrix-valued functions so we need to define function spaces that contain them. For $M \in \mathbb{C}^{n\times x}$ we define the appropriate L^p-based matrix norms:

$$|M|_p = \left(\sum_{j=1}^{n} \sum_{i=1}^{n} |M_{ij}|^p \right)^{1/p}.$$

Note that when $p = 2$

$$|M|_2 = \sqrt{\operatorname{tr} M^* M},$$

where * denotes conjugate transpose.

This allows us to define the space, abusing notation,

$$L^p(\Gamma) = \{f : \Gamma \to M(n,\mathbb{C}), \quad \text{measurable} : \||f(k)|_p\|_p < \infty\}$$

equipped with the obvious norm. For $p = 2$ we set $W^{k,p}(\Gamma) = H^k(\Gamma)$ and this retains the Hilbert space structure with the inner product

$$\langle f, g\rangle = \sum_{j=1}^{k} \int_\Gamma f^{(j)}(g^{(j)})^* |dk|.$$

Remark 1.5.9. *Another important property of $H^k(\Gamma)$ for $k \geq 1$ is that there exists a constant $c > 0$ such that*

$$\|fg\|_{H^k(\Gamma)} \leq c\|f\|_{H^k(\Gamma)}\|g\|_{H^k(\Gamma)}.$$

This makes the space into an algebra and with a redefinition of the norm, the space is a Banach algebra ($c = 1$).

Chapter 2

Linear and Nonlinear Partial Differential Equations

In this chapter we discuss the solution, analytical and numerical, of a simple linear evolution PDE. At their essence the ideas presented here extend to the nonlinear case. The nonlinearization of the solution technique we present is the celebrated inverse scattering transform. The nonlinearization of the method for calculating long-time asymptotics is the method of nonlinear steepest descent. Finally, the nonlinearization of the numerical method presented in this section is the numerical method discussed in the remainder of this manuscript.

2.1 Solution of a prototypical linear PDE

Consider the solution of the initial-value problem

$$\begin{aligned} iq_t + q_{xx} &= 0, \\ q(x,0) &= q_0(x) \in \mathcal{S}(\mathbb{R}), \end{aligned} \tag{2.1.1}$$

where $\mathcal{S}(\mathbb{R})$ is the Schwarz class of rapidly decaying functions. For simplicity, we assume more. Define for $\delta > 0$,

$$\mathcal{S}_\delta(\mathbb{R}) = \{f \in \mathcal{S}(\mathbb{R}) : \sup_{x\in\mathbb{R}} e^{\delta|x|}|f^{(j)}(x)| < \infty, \quad j = 0, 1, \ldots\}.$$

For the remainder of this chapter we assume $q_0(x) \in \mathcal{S}_\delta(\mathbb{R})$. Consider the system of ordinary differential equations

$$\mu_x - ik\mu = q, \quad k \in \mathbb{R}, \tag{2.1.2}$$

$$\mu_t + ik^2\mu = iq_x - kq. \tag{2.1.3}$$

It is straightforward to check that $\mu_{xt} = \mu_{tx}$ if and only if $iq_t + q_{xx} = 0$. This fact, for linear PDEs, was first noticed by Gel'fand and Fokas in [50]. The system (2.1.2) and (2.1.3) is a

Lax pair for (2.1.1). Assuming decay in q, we solve (2.1.2)

$$\mu(x,t) = C_1(t)e^{ikx} + \int_{-\infty}^{x} e^{ik(x-s)}q(s,t)ds.$$

By choosing $C_1(t) = 0$ and $C_1(t) = \int_{-\infty}^{\infty} e^{-iks}q(s,t)ds$ we obtain two solutions

$$\mu_+(x,t;k) = \int_{-\infty}^{x} e^{ik(x-s)}q(s,t)ds, \quad \mu_-(x,t) = -\int_{x}^{\infty} e^{-ik(s-x)}q(s,t)ds.$$

Note that $\mu_\pm$ is analytic in k for $k \in \mathbb{C}^\pm = \{z \in \mathbb{C} : \pm \operatorname{Im} z > 0\}$. Furthermore, integration by parts shows that $\mu_\pm = \mathcal{O}(k^{-1})$ as $|k| \to \infty$ in the respective domains of analyticity. Additional integration by parts shows that $(\mu_\pm)_x = \mathcal{O}(k^{-1})$ as $|k| \to \infty$. Thus (2.1.2) implies

$$q(x,t) = i \lim_{|k|\to\infty} k\mu(x,t;k). \tag{2.1.4}$$

Remark 2.1.1. *To apply this technique with weaker assumptions on $q_0(x)$ we need to invoke the theory of Hardy spaces. See Example 3.5.15 for an example of this technique.*

Consider the difference

$$\nu(x,t;k) = \mu_+(x,t;k) - \mu_-(x,t;k) = \int_{-\infty}^{\infty} e^{ik(x-s)}q(s,t)ds. \tag{2.1.5}$$

It follows that ν satisfies

$$\begin{aligned} \nu_x - ik\nu &= 0, \\ \nu_t + ik^2\nu &= 0. \end{aligned}$$

The first equation implies $\nu(x,t;k) = A(t;k)e^{ikx}$ and the second, $\nu(x,t;k) = B(x;k)e^{-ik^2t}$. Evaluating at $t = 0$, $A(0;k)e^{ikx} = B(x;k)$ and therefore $\nu(x,t;k) = A(0;k)e^{ikx-ik^2t}$. Evaluating this at $x = t = 0$, we find

$$A(0;k) = \hat{q}_0(k) = \int_{-\infty}^{\infty} e^{-iks}q_0(s)ds.$$

We arrive at the relation (see Figure 2.1.1)

$$\begin{aligned} &\mu_+(x,t;k) - \mu_-(x,t;k) = e^{ikx-ik^2t}\hat{q}_0(k), \\ &\mu_\pm(x,t;k) = \mathcal{O}(k^{-1}), \text{ as } k \to \infty. \end{aligned}$$

This is a scalar RHP (see (1.4.1) or Chapter 3) for a piecewise analytic function

$$\mu(x,t;k) = \begin{cases} \mu_+(x,t;k), & \text{if } k \in \mathbb{C}^+, \\ \mu_-(x,t;k), & \text{if } k \in \mathbb{C}^-. \end{cases}$$

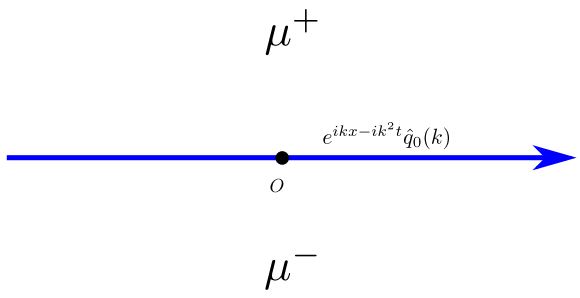

Figure 2.1.1: The piecewise definition of μ. The contour in the figure represents $\mathbb{R}$.

The solution techniques in Chapter 3 apply (see (3.2.1)) and we find the solution

$$\mu(x,t;k) = \frac{1}{2\pi i}\int_{-\infty}^{\infty} \frac{e^{isx-is^2t}\hat{q}_0(s)}{s-k}ds, \quad k \notin \mathbb{R}.$$

We use the reconstruction formula, (2.1.4), along with Lemma 3.6.9 to obtain

$$q(x,t) = \frac{1}{2\pi}\int_{-\infty}^{\infty} e^{ikx-ik^2t}\hat{q}_0(k)dk. \tag{2.1.6}$$

Remark 2.1.2. *The Lax pair* (2.1.2) *and* (2.1.3) *can be written in an equivalent way using differential forms [49]. It follows that*

$$d\left(e^{-ikx+ik^2t}\mu\right) = e^{-ikx+ik^2t}(qdx+\tilde{q}dt), \quad \tilde{q} = iq_x - kq,$$

is equivalent to (2.1.2) *and* (2.1.3)*. Therefore μ_+ is obtained by integrating this differential form in the (x,t)-plane from $(-\infty,t)$ to (x,t) and μ_- is obtained by integration from (∞,t) to (x,t). This approach generalizes to the nonlinear case. This also provides an alternative approach to the linear periodic problem [106].*

2.2 An asymptotic formula

Because $q_0 \in \mathcal{S}_\delta(\mathbb{R})$ it follows that $\hat{q}_0$ is analytic in the strip $T_\delta = \{k \in \mathbb{C} : |\operatorname{Im} k| < \delta\}$. Additionally, for each $n > 0$, $|\hat{q}_0(k)| \leq A_n/(1+|k|)^n$ for $k \in \overline{T}_{\delta'}$ for $\delta' < \delta$. A similar bound follows for every derivative of $\hat{q}_0(k)$ in the same strip. This follows from the fact that $e^{\pm\delta' x}q_0(x) \in \mathcal{S}(\mathbb{R})$. We use this decay to deform the integral over the real axis. To guide the deformation, we use the method of steepest descent for integrals. Define $\Theta(k) = ikx - ik^2t$. We look for the stationary point, k_0 such that $\Theta'(k_0) = 0$, or $k_0 = x/(2t)$. Expand Θ around the stationary point, $\Theta(k) = ix^2/(4t) - it(k-k_0)^2$. To find the path of steepest descent we set $k - k_0 = re^{i\theta}$ thus $\Theta(k) = ix^2/(4t) - itr^2e^{2i\theta}$. If $\theta = -\pi/4$ then $\Theta(k) = ix^2/(4t) - tr^2$: the imaginary part is constant while the real part is negative and decreasing away from the stationary point.

The estimate $|\hat{q}_0(k)| \leq A_n/(1+|k|)^n$ allows the deformation of the integral to a contour

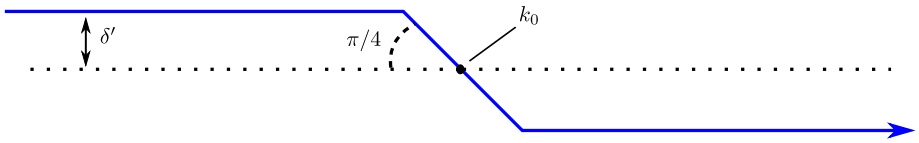

Figure 2.2.1: The contour $C_{\delta'} + k_0$.

that passes along the local path of steepest descent. Define (see Figure 2.2.1)

$$C_{\delta'} = (-\infty + i\delta', -\delta' + i\delta'] \cup \{re^{-i\pi/4} : -\sqrt{2}\delta' < r < \sqrt{2}\delta'\} \cup [\delta' - i\delta', \infty + i\delta).$$

Consider the integral, for $s < k_0$

$$\begin{aligned} I_s &= \left| \int_s^{s+i\delta'} e^{ikx - ik^2 t} \hat{q}_0(k) dk \right| \\ &\leq \left| \int_0^{\delta'} e^{i(s+ir)x - i(s+ir)^2 t} \hat{q}_0(s+ir) i dr \right| \leq \int_0^{\delta'} e^{-rx+2srt} \frac{A_n}{(1+|s+ir|)^n} dr \\ &\leq \frac{A_n}{(1+|s|)^n} e^{-rx+2k_0 rt} \delta'. \end{aligned} \tag{2.2.1}$$

Thus $I_s \to 0$ as $s \to -\infty$. Note that this follows when $n = 0$— $\hat{q}$ need only be bounded for this deformation to proceed for $t > 0$. The same argument applied to a similar contour from $s > k_0$ to $s - i\delta'$ justifies the equality

$$q(x,t) = \frac{1}{2\pi} \int_{-\infty}^{\infty} e^{ikx - ik^2 t} \hat{q}_0(k) dk = \frac{1}{2\pi} \int_{C_{\delta'} + k_0} e^{ikx - ik^2 t} \hat{q}_0(k) dk \tag{2.2.2}$$

A change of variables shows

$$q(x,t) = \frac{1}{2\pi} e^{ix^2/(4t) - i\pi/4} \int_{-\sqrt{2}\delta'}^{\sqrt{2}\delta'} e^{-tr^2} \hat{q}_0(k_0 + re^{-i\pi/4}) dr + \mathcal{O}(t^{-n}) \text{ for all } n > 0,$$

as $t \to 0$. A full asymptotic expansion of q can be found via a modification of Watson's Lemma [79, pg. 58]. In particular,

$$q(x,t) = \frac{\hat{q}_0(x/(2t))}{2\sqrt{\pi}} e^{ix^2/(4t) - i\pi/4} \frac{1}{\sqrt{t}} + \mathcal{O}(t^{-1}) \text{ as } t \to \infty. \tag{2.2.3}$$

2.3 A steepest descent-based numerical technique

We develop a numerical technique based on applying quadrature routines to (2.2.2). We first concentrate on the computation of the inverse Fourier transform, assuming that $\hat{q}_0$ can be computed accurately. Our approach is related to that of Asheim and Huybrechs [6]. To do so, we must truncate the infinite integral. With this goal, define

$$C_{\delta',L} = C_{\delta'} \cap \{k \in \mathbb{C} : |\operatorname{Re} k| \leq L\}.$$

The same estimates used in (2.2.1) show that for any $\epsilon > 0$, there exists an M, depending only on $\hat{q}_0$ and δ', so that

$$\left| \frac{1}{2\pi} \int_{C_{\delta'}+k_0} e^{ikx-ik^2t} \hat{q}_0(k)dk - \frac{1}{2\pi} \int_{C_{\delta',M}+k_0} e^{ikx-ik^2t} \hat{q}_0(k)dk \right| < \epsilon, \text{ for } L > M.$$

In practice, we choose L so that the integrand is less than machine precision on $C_{\delta'} \setminus C_{\delta',L}$. In what follows, we always assume such an L is chosen.

There is a subtle complication. If δ' is fixed, the derivative of the integrand on the contour $\{re^{-i\pi/4} : -\sqrt{2}\delta' < r < \sqrt{2}\delta'\} + k_0$ will increase with t. We scale the contour. Define for $t \geq 1$, $S_{\delta',L,k_0} = t^{-1/2}C_{\delta',L} + k_0$. We have $|q(x,t) - q_L(x,t)| < \epsilon$ where

$$q_L(x,t) = \frac{1}{2\pi} \int_{S_{\delta',L,k_0}} e^{ikx-ik^2t} \hat{q}_0(k)dk.$$

Use $k = t^{-1/2}z + k_0 \in S_{\delta',L,k_0}$ for $z \in C_{\delta',L}$ as a change of variables in the integral along with $ikx + ik^2t = ix^2/(4t) - it(k-k_0)^2$ to find

$$q_L(x,t) = \frac{1}{2\pi} t^{-1/2} e^{ix^2/(4t)} \int_{C_{\delta',L}} e^{-z^2} \hat{q}_0(t^{-1/2}z + k_0)dz.$$

From the uniform boundedness of every derivative of $\hat{q}_0(k)$ in $\overline{T}_{\delta'}$ we find that a quadrature routine applied to

$$\int_{C_{\delta',L}} e^{-z^2} \hat{q}_0(t^{-1/2}z + k_0)dk,$$

will converge uniformly in the half plane $\{(x,t) : x \in \mathbb{R}, t \geq c > 0\}$. This implies that the computational cost to compute a solution at any given (x,t) value is bounded. This method for computing $q_L(x,t)$ will have its relative error tend to zero. Furthermore, if a spectral method, such as Clenshaw–Curtis quadrature is used, the convergence is spectral.

This is all, of course, assuming that we may compute $\hat{q}_0$ accurately in the complex plane. To do this we use a spectral collocation method, see Appendix B to solve (2.1.2) for an approximation of $\tilde{\mu}_\pm(x,k)$ of $\mu_\pm(x,0;k)$. We solve the truncated, approximate boundary-value problems

$$(\tilde{\mu}_\pm)_x - ik\tilde{\mu}_\pm = q_0, \quad \mu_\pm(\pm l) = 0, \quad l \text{ sufficiently large.} \tag{2.3.1}$$

Then

$$\tilde{\mu}^+(0,k) - \tilde{\mu}^-(0,k) \approx \mu^+(0,0;k) - \mu^-(0,0;k) = \int_{-\infty}^{\infty} e^{-ikx} q_0(x)dx.$$

This is an approximation of the Fourier transform. Furthermore, if k is complex there is no barrier to solving (2.3.1) numerically, provided q_0 has sufficient decay and smoothness.

What we have described here is a Levin-type collocation method [64] for oscillatory integrals. One could compute the Fourier transform directly using quadrature but the

high oscillation destroys accuracy for k outside a small neighborhood of the origin. The accuracy of the Levin-type method is seen to increase as $|k| \to \infty$ for $k \in T_{\delta'}$. Additionally, since $q_0 \in \mathcal{S}_\delta(\mathbb{R})$, the spectral method in Appendix B converges spectrally.

2.4 Numerical results

To demonstrate the numerical method we use $q_0(x) = (1+x)e^{-x^2}$ so that

$$\hat{q}_0(k) = \frac{\sqrt{\pi}}{2} e^{-\frac{k^2}{4}} (2 - ik).$$

We demonstrate the spectral convergence of the method described above for computing $\hat{q}_0(k)$. We numerically solve (2.3.1) with 15, 30 and 60 collocation points. The error in the resulting approximations are shown in Figure 2.4.1.

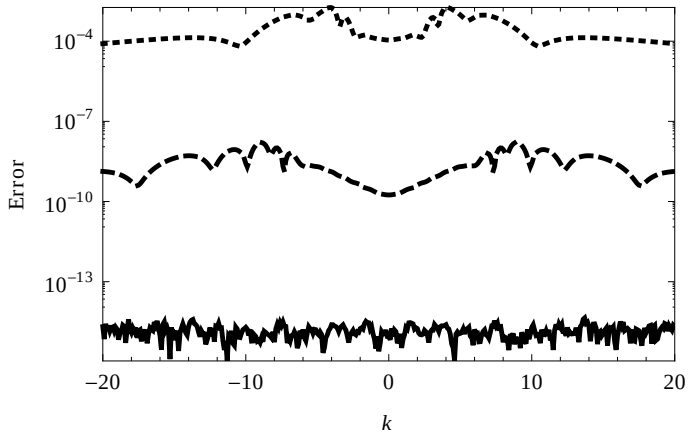

Figure 2.4.1: An approximation of $\hat{q}_0(k)$ when $q_0(x) = (1+x)e^{-x^2}$ by solving (2.3.1) with $l = 10$. The error is shown using the analytical formula for $\hat{q}_0$ for 15 (dotted), 30 (dashed) and 60 (solid) collocation points. Notice that doubling the number of collocation points gives about 5 digits of accuracy. This demonstrates spectral convergence.

The corresponding solution of (2.1.1) can be computed over large spatial ranges. In Figure 2.4.2 we show the initial condition along with the solution when $t = 5$. Notice the high oscillation due to dispersion.

We also examine the validity of (2.2.3). Define the an estimate of the relative error to be

$$E_{\text{rel}}(x,t) = \sqrt{t} \left| \frac{1}{2\sqrt{\pi}} e^{ix^2/(4t) - i\pi/4} \frac{1}{\sqrt{t}} - q(x,t) \right|.$$

We use the numerical approximation $q(x,t)$ in this formula and plot $E_{\text{rel}}(-2t,t)$ as t increases. See Figure 2.4.3 for a validation of both the numerical method and the asymptotic formula.

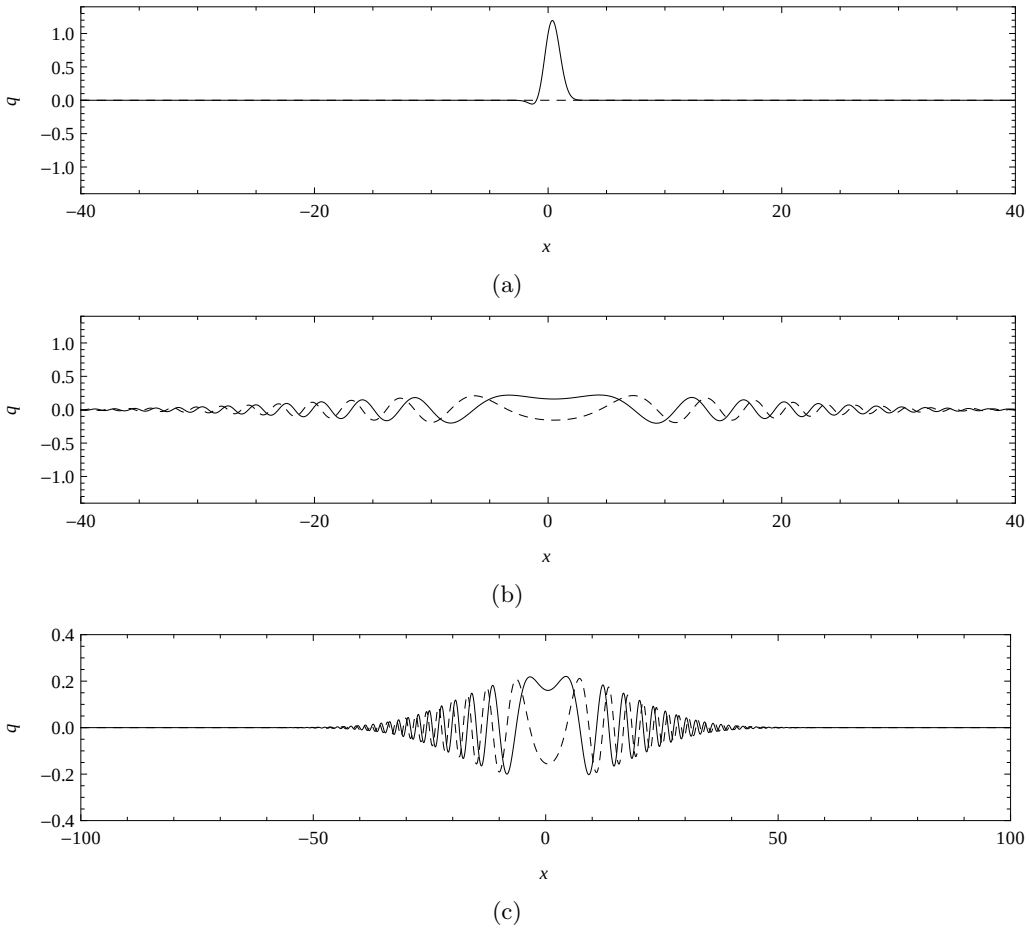

Figure 2.4.2: The numerically computed solution of (2.4.2). We plot both real (solid) and imaginary (dashed) parts of the solution. (a) The initial condition $q_0(x)$. (b) The solution at $t = 5$. (c) A scaled plot of the solution at $t = 5$. Notice the high oscillation due to dispersion.

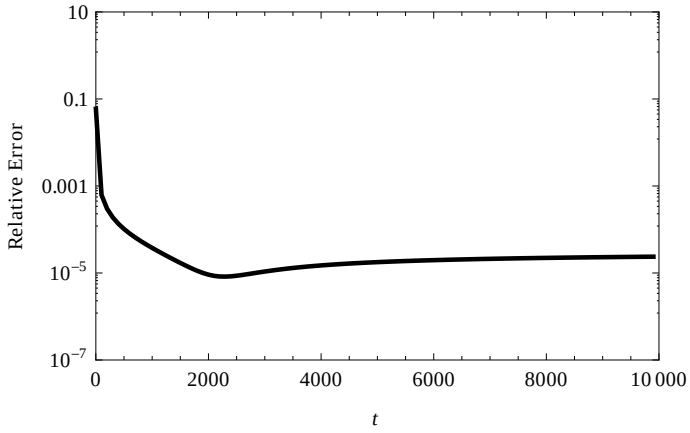

Figure 2.4.3: A plot of $E(-2t, t)$ using the numerical method outlined here. This validates both the numerical accuracy and the asymptotic formula. Since we expect uniform, relative convergence we assume that our numerical approximation to $q(x, t)$ is much more accurate than the asymptotic formula.

2.5 An extension to nonlinear problems

Consider the solution of the initial-value problem for the nonlinear Schrödinger (NLS) equation

$$\begin{aligned} iq_t + q_{xx} + 2\lambda|q|^2 q = 0, \quad \lambda = \pm 1, \\ q(x, 0) = q_0(x) \in \mathcal{S}(\mathbb{R}). \end{aligned} \tag{2.5.1}$$

We discuss the solution of this problem with the inverse scattering in loose terms. A rigorous discussion is found in Chapter 4.

This system has the following Lax pair [49]

$$\mu_x + ik[\sigma_3, \mu] = Q\mu, \tag{2.5.2}$$

$$\mu_t + 2ik^2[\sigma_3, \mu] = \tilde{Q}\mu, \tag{2.5.3}$$

where

$$Q(x,t) = \begin{bmatrix} 0 & q(x,t) \\ -\lambda\bar{q}(x,t) & 0 \end{bmatrix}, \quad \tilde{Q}(x,t) = 2kQ - iQ_x\sigma_3 + i\lambda|q|^2\sigma_3, \quad \sigma_3 = \begin{bmatrix} 1 & 0 \\ 0 & -1 \end{bmatrix}$$

and $[\cdot, \cdot]$ is the standard matrix commutator. Following similar ideas that are present in Remark 2.1.2, this Lax pair is equivalent to the differential form

$$d\left(e^{i(kx-2k^2t)\hat{\sigma}_3}\mu(x,t,k)\right) = e^{i(kx+2k^2t)\hat{\sigma}_3}(Q\mu dx + \tilde{Q}\mu dt), \quad e^{\alpha\hat{\sigma}_3}A = e^{\alpha\sigma_3}Ae^{-\alpha\sigma_3}. \tag{2.5.4}$$

Integrating this differential form over various contours in the (x, t)-plane yields different integral equations, and different solutions μ. For any solution μ, it follows that $M =$

$\mu e^{-i(kx+2k^2t)\sigma_3}$ solves

$$M_x + ik\sigma_3 M = QM,$$
$$M_t + 2ik^2\sigma_3 M = \tilde{Q}M.$$

For any two solutions M_1, M_2 of this system $M_1(x,t,k) = M_2(x,t,k)S(k)$ for some matrix S. Thus for any two solutions μ_1, μ_2 of (2.5.4),

$$\mu_1(x,t,k) = \mu_2(x,t,k)e^{-i(kx+2k^2t)\hat{\sigma}_3}S(k), \tag{2.5.5}$$

for some matrix $S(k)$. We follow [49] and define μ_1, μ_2 to be the solutions of

$$\begin{aligned}\mu_1(x,t,k) &= I + \int_{(-\infty,t)}^{(x,t)} e^{-ik(x-\xi)\hat{\sigma}_3}[Q(\xi,t)\mu(\xi,\tau,k)]d\xi,\\ \mu_2(x,t,k) &= I + \int_{(\infty,t)}^{(x,t)} e^{-ik(x-\xi)\hat{\sigma}_3}[Q(\xi,t)\mu(\xi,\tau,k)]d\xi.\end{aligned} \tag{2.5.6}$$

Combining, standard results on Volterra integral equations (see Chapter 4) with the boundedness properties of the exponential, we find that the first column μ_1^+ of μ_1 is analytic in the upper-half plane and the second column μ_1^- is analytic in the lower-half plane. The reverse is true for μ_2: the first column μ_2^- is analytic in the lower-half plane and the second column μ_2^+ is analytic in the upper-half plane. This is, of course, dependent on some mild conditions on Q: $q \in \mathcal{S}_\delta(\mathbb{R})$ is certainly sufficient.

It follows from Chapter 4 that $S(k)$ in (2.5.5) may be written in the form (see also [49])

$$S(k) = \begin{bmatrix} \overline{a(\bar{k})} & b(k) \\ -\lambda\overline{b(\bar{k})} & a(k) \end{bmatrix}.$$

for some functions a, b. Generally, $a(k)$ is analytic in the upper-half plane, and for $q \in \mathcal{S}_\delta(\mathbb{R})$ both $a(k)$ and $b(k)$ are analytic in a strip that contains the real line. For simplicity we assume that $a(k)$ never vanishes. This is true when $\lambda = -1$ for the defocusing NLS equation. A discussion of how to proceed when this is not the case is found in Chapter 7.

The reflection coefficient is defined by the ratio $\rho(k) = b(k)/a(k)$. Define a sectionally analytic function

$$\Phi = \begin{cases} \Phi^+, & \text{in } \mathbb{C}^+, \\ \Phi^-, & \text{in } \mathbb{C}^-, \end{cases}$$
$$\Phi^+ = \begin{bmatrix} \dfrac{\mu_1^+}{a(k)}, \mu_2^+ \end{bmatrix}, \quad \Phi^- = \begin{bmatrix} \mu_2^+, \dfrac{\mu_1^-}{\overline{a(\bar{k})}} \end{bmatrix}.$$

It follows [49] that $\Phi(x,t,k)$ solves the following *matrix Riemann–Hilbert problem*

$$\Phi^+(x,t,s) = \Phi^-(x,t,s)J(x,t,s), \quad s \in \mathbb{R}, \quad \Phi(x,t,\infty) = I, \tag{2.5.7}$$
$$J(x,t,k) = \begin{bmatrix} 1 + \lambda\overline{\rho(\bar{k})}\rho(k) & \lambda\overline{\rho(\bar{k})}e^{-2ikx-4ik^2t} \\ \rho(k)e^{2ikx+4ik^2t} & 1 \end{bmatrix}.$$

Once this is solved for Φ the solution q may be found via

$$q(x,t) = \lim_{|k|\to\infty} 2ik(\Phi - I)_{12}, \tag{2.5.8}$$

where the subscript denotes the $(1,2)$ entry of the matrix. Unfortunately, this Riemann–Hilbert problem can only be solved in closed form for extremely simple initial conditions. A numerical treatment is necessary.

Remark 2.5.1. *In the method of inverse scattering the linear dispersion relation always appears in the jump matrix. On first glance it may seem that this is not the case as the exponential in* (2.5.7) *differs from that in* (2.1.6)*, even if we allow scalings of the spectral k variable. This can be rectified by noting that $\bar{q}(x,t)$ can be recovered from the $(2,1)$-entry of Φ and the complex conjugate of* (2.5.1) *has the dispersion relation that appears in* (2.5.7)*.*

2.6 An asymptotic formula for the nonlinear problem

The long-time asymptotics of (2.5.1) are computed by Deift and Zhou [36] when $\lambda = -1$ (defocusing NLS). A full derivation of the results of this section is found in Chapter 4. The long-time behavior is seen to differ from the linear problem in a fundamental way. This comparison is important from a physical and mathematical perspective. Deift and Zhou use the method of nonlinear steepest descent for Riemann–Hilbert problems [33] to analyze the long-time behavior of solutions of (2.5.7). From this, the long-time behavior of $q(x,t)$, the solution of (2.5.1), can be rigorously established. The result from [36] is for $|x/(4t)| \leq C$,

$$q(x,t) = \frac{\alpha(-x/(4t))}{\sqrt{t}} e^{ix^2/(4t) - i\nu(-x/(4t))\log 8t} + \mathcal{O}(t^{-1}\log t), \tag{2.6.1}$$

where

$$\begin{aligned} \nu(k) &= -\frac{1}{2\pi}\log(1-|\rho(k)|^2), \quad |\alpha(k)|^2 = \nu(k)/2, \\ \arg\alpha(k) &= \frac{1}{\pi}\int_{-\infty}^{k} \log(k-\xi)d(\log(1-|\rho(\xi)|^2)) + \pi/4, \\ &\quad + \arg\Gamma(i\nu(k)) - \arg\rho(k), \end{aligned}$$

and Γ is the classical Gamma function [84]. This formula shows that the behavior of $\exp(-x^2/(4t) + i\pi/4)$, present in the case of the linear problem, appears in the formula for the nonlinear problems. From the presence of the $\log 8t$ term in (2.6.1) it follows that the solution $q(x,t)$ to the nonlinear problem never 'becomes linear'. There is a fundamental difference between the solutions, always. For numerical results for the focusing and defocusing NLS equations, see Chapter 7.

2.7 Quantifying nonlinearity

In this section we use numerical methods to quantify and demonstrate the fundamental differences between solutions of (2.1.1) and (2.5.1) with $\lambda = -1$ (defocusing). This provides

an important motivation for studying nonlinear problems: even in solvable[1] nonlinear problems, the behavior differs consistently from the corresponding linear case. With the extensive numerical techniques we develop below, we can examine the effect of nonlinearity precisely. This shows to all scientists that linearization of nonlinear problems must always be considered carefully.

Furthermore, our results demonstrate the transition of the corresponding solutions into their asymptotic regimes. We use $q_0(x) = \alpha(x+1)e^{-x^2}$ as the initial condition for both equations, for varying constants α. The notation $q_N(x,t)$ is used to denote the corresponding solution to the defocusing NLS equation and $q_L(x,t)$ will be used to denote the solution of (2.1.1). We ignore any error due to the numerical algorithms and treat the numerical results as the true solution.

2.7.1 Small time

With $\alpha = 1$ we look at the small-time evolution of the function $d(x,t) = q_N(x,t) - q_L(x,t)$. The numerical results indicate that $d(x,t) = \mathcal{O}(e^{at})$ as $t \to 0^+$, $a > 0$, see Figure 2.7.1 for a demonstration of this.

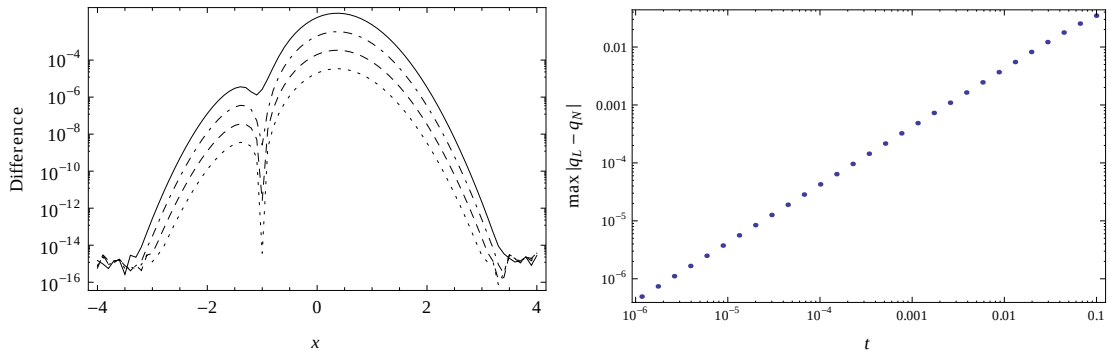

(a) (b)

Figure 2.7.1: (a) The difference $|q_N(x,t) - q_L(x,t)|$ plotted as a function of x for fixed times: $t = 0.00001$ (dotted), $t = 0.0001$ (dashed), $t = 0.001$ (dot-dashed), and $t = 0.01$ (solid). (b) A demonstration of the error: this plot indicates $\max_{x\in[-30,30]} |q_N(x,t) - q_L(x,t)| = \mathcal{O}(e^{at})$ as $t \to 0^+$, $a > 0$.

[1]Though general solution formulas for the NLS equations cannot be written down, the IST provides a constructive existence and uniqueness proof for the PDE with access to asymptotics. In this sense the problem is solved.

2.7.2 Long time

The analysis is more interesting in the large-time regime. We use (2.2.3) as a guide and consider solutions along the trajectory $x = -4\beta t$ for $\beta > 0$. We find

$$\begin{aligned} q_L(-2\beta t, t) &= \frac{\hat{q}_0(-2\beta)}{2\sqrt{\pi}} e^{-i\beta x - i\pi/4} \frac{1}{\sqrt{t}} + \mathcal{O}(t^{-1}) \text{ as } t \to \infty, \\ Q_L(t) &= q_L(-2\beta t, t)\sqrt{t}. \end{aligned}$$

Define $x_j = j2\pi/n$ and $\mathbb{S}_n = (x_0, x_1, \ldots, x_{n-1})$. Consider the vector of values

$$V_L(t^*) = Q_L(t^* + M/\beta \mathbb{S}_n).$$

For $M \geq 1$ and n sufficiently large the discrete Fourier transform of this vector will limit to a fixed vector with only one entry non-zero as $t^* \to \infty$.

In the nonlinear case we have

$$\begin{aligned} q_N(-2\beta t, t) &= \frac{\alpha(\beta)}{\sqrt{t}} e^{-i\beta x - i\nu(\beta)\log 8t} + \mathcal{O}(t^{-1}\log t), \\ Q_N(t) &= q_N(-2\beta t, t)\sqrt{t}. \end{aligned}$$

Consider the vector $Q_N(t^* + M/\beta \mathbb{S}_n)$. For fixed M, a simple calculation shows that

$$e^{-i\beta x - i\nu(\beta)\log 8t} = e^{-i\beta x - i\nu(\beta)\log 8t^*} + \mathcal{O}(1/t^*),$$

$x \in -4\beta[t^*, t^* + 2\pi M/\beta]$ and $t \in [t^*, t^* + 2\pi M/\beta]$. Therefore the discrete Fourier transform of $V_N(t^*) = Q_N(t^* + M/\beta \mathbb{S}_n)$ will limit to a vector with only one non-zero component as $t^* \to \infty$ but this will not be a fixed vector. The logarithm will change the phase of the non-zero component.

We also consider the discrete Fourier transform of the first term in the asymptotic expansions. Define

$$\begin{aligned} q_L^{\text{asym}}(x,t) &= \frac{\hat{q}_0(x/(2t))}{2\sqrt{\pi}} e^{ix^2/(4t) - i\pi/4} \frac{1}{\sqrt{t}}, \\ q_N^{\text{asym}}(x,t) &= \frac{\alpha(-x/(4t))}{\sqrt{t}} e^{ix^2/(4t) - i\nu(-x/(4t))\log 8t}, \\ Q_L^{\text{asym}}(t) &= q_L^{\text{asym}}(-2\beta t, t)\sqrt{t}, \\ Q_N^{\text{asym}}(t) &= q_N^{\text{asym}}(-2\beta t, t)\sqrt{t}, \\ V_L^{\text{asym}}(t^*) &= Q_L^{\text{asym}}(t^* + M/\beta \mathbb{S}_n), \\ V_N^{\text{asym}}(t^*) &= Q_N^{\text{asym}}(t^* + M/\beta \mathbb{S}_n). \end{aligned}$$

We use a variety tests to examine solutions. First, we compute the discrete Fourier transform of $V_L(t^*), V_N(t^*), V_L^{\text{asym}}(t^*)$ and $V_N^{\text{asym}}(t^*)$ with $n \approx M/2$. Call these vectors $FV_L(t^*), FV_N(t^*), FV_L^{\text{asym}}(t^*)$ and $FV_N^{\text{asym}}(t^*)$.

In the first test, we normalize the transformed vectors so that their maximum entry has absolute value one. This entry is then removed and the norm of the resulting vector is compared and we call this the *residual power*. A small norm indicates that the vector

has extremely localized support showing that the solution is close to the linear asymptotic formula. See Figure 2.7.2 for a plot of the residual power as t^* varies from 2π to 10000. This figure shows the dramatic affect that amplitude has on the solution of the nonlinear problem. The residual power decays much slower, initially, in the larger amplitude case.

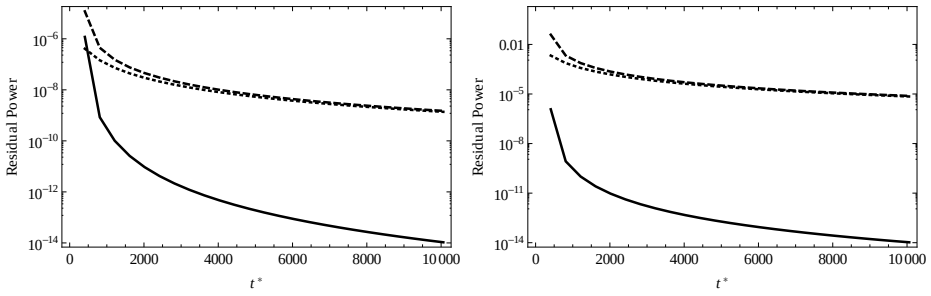

(a) (b)

Figure 2.7.2: All plots show the residual power for $FV_N(t^*)$ (dotted), $FV_N^{\text{asym}}(t^*)$ (dashed) and $FV_L(t^*)$ (solid). (a) A small amplitude initial condition ($\alpha = 0.1$), and (b) A medium amplitude initial condition ($\alpha = 1$).

In the second test, we monitor the phase of entry of $FV_L(t^*)$, $FV_N(t^*)$, $FV_L^{\text{asym}}(t^*)$ and $FV_N^{\text{asym}}(t^*)$ with maximum modulus. We restrict to $t^* = 2\pi + 2\pi Mm$ for $m = 0, 1, \ldots$. For this choice the only non-zero entry of $FV_L^{\text{asym}}(t^*)$ will have constant phase. See Figure 2.7.3 for a demonstration of a fundamental difference between the linear and nonlinear problem. Due to the logarithmic term in (2.6.1) the phase will always differ as Figure 2.7.3 displays.

2.7.3 Small amplitude limit

In this section we analyze the effect of nonlinearity through the limit $\alpha \to 0$. Specifically, define

$$q_{L,\alpha}(x,t) = q_L(x,t)/\alpha, \quad \text{and} \quad q_{N,\alpha}(x,t) = q_N(x,t)/\alpha.$$

Therefore, $q_{L,\alpha}(x,t)$ is the solution of (2.1.1) with $q_0(x,t) = (x+1)e^{-x^2}$, by linearity. For (2.5.1) we are in essence computing the Fréchet derivative of the solution operator evaluated near zero, acting on $q_0(x) = (x+1)e^{-x^2}$. This should, for small time, be close to the solution of the linear problem. This approximation breaks down for large time. We demonstrate both of these facts numerically. In Figure 2.7.4 we demonstrate the decay rate of $\sup_{x\in[-40,40]} |q_{L,\alpha}(x) - q_{N,\alpha}(x)|$ as $\alpha \to 0$. Much of the detail of the solution is destroyed by the absolute value. In Figure 2.7.5 we show the convergence of both the real and imaginary parts of $q_{N,\alpha}$ to $q_{L,\alpha}$. It is apparent that the amplitude of the linear solutions plays a role in the convergence rate.

We have demonstrated the convergence of $q_{N,\alpha}$ to $q_{L,\alpha}$ as $\alpha \to 0$ for a fixed time. We now demonstrate that we may take a sequence of times $\{t_j\}$, a sequence $\{\alpha_j\}$ with $\alpha_j \to 0$ along with appropriate sets S_j so that

$$D_j = \sup_{x\in S_j} |q_{N,\alpha_j}(x,t_j) - q_{L,\alpha_j}(x,t_j)|\sqrt{t_j} \not\to 0 \ \text{ as } \ \alpha_j \to 0. \tag{2.7.1}$$

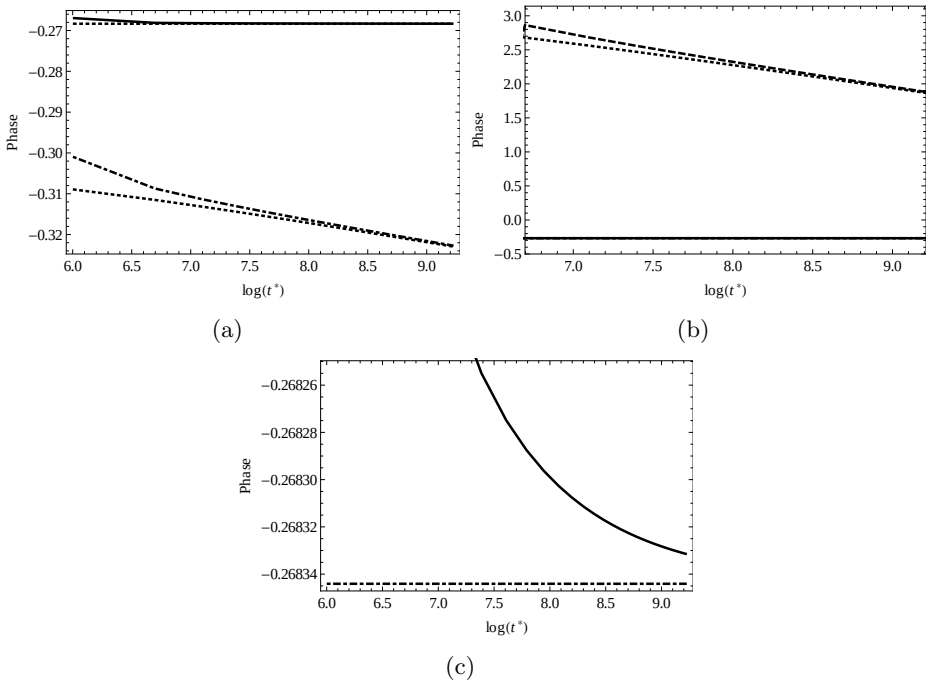

Figure 2.7.3: This figure shows the phase of the entry of $FV_L(t^*)$ (solid), $FV_L^{\text{asym}}(t^*)$ (dot-dashed), $FV_N(t^*)$ (dashed) and $FV_N^{\text{asym}}(t^*)$ (dotted) with maximum modulus. (a) A small amplitude initial condition ($\alpha = 1$), and (b) A larger amplitude initial condition ($\alpha = 1$). (c) A zoomed comparison of the dominant mode of $FV_L(t^*)$ and $F_L^{\text{asym}}(t^*)$ when $\alpha = 1$.

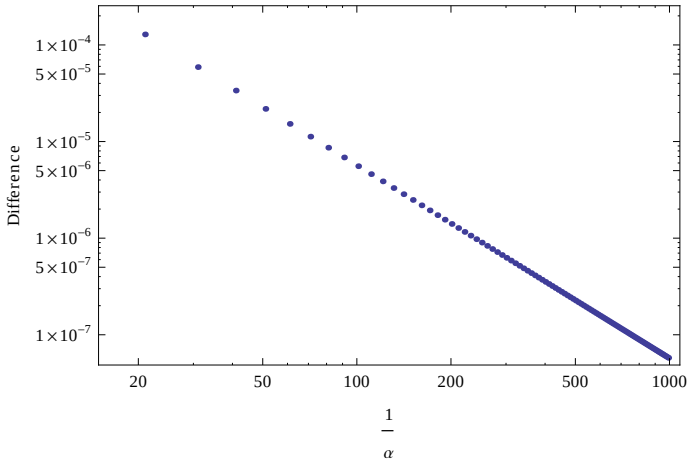

Figure 2.7.4: The difference $\sup_{x\in[-40,40]} |q_{L,\alpha}(x,10) - q_{N,\alpha}(x,10)|$ as $\alpha \to 0$ plotted versus $1/\alpha$ as $\alpha \to 0$. This demonstrates that the difference is $\mathcal{O}(\alpha)$.

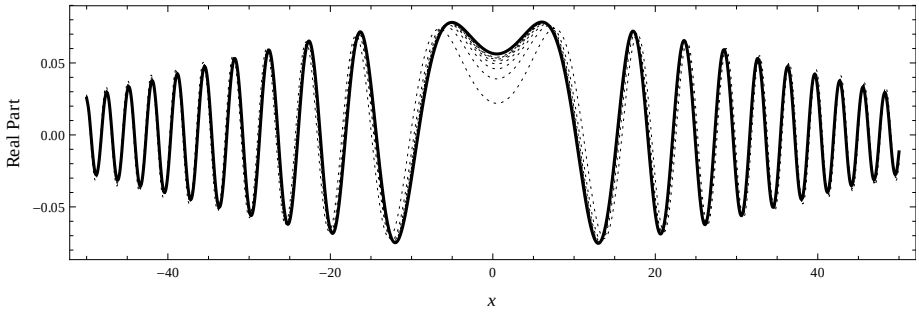

(a)

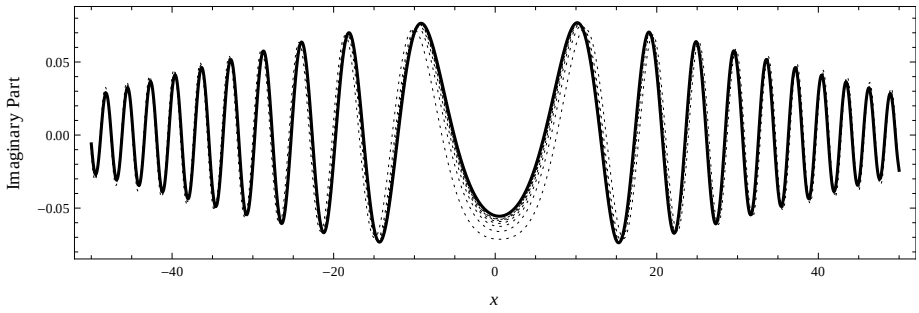

(b)

Figure 2.7.5: This figure shows the convergence of $q_{N,\alpha}$ to $q_{L,\alpha}$ in the $\alpha \to 0$ limit when $t = 10$. The dashed line represents $q_{N,\alpha}$ for α varying from 1 to 1/4. (a) Convergence of the real part. (b) Convergence of the imaginary part.

The factor $\sqrt{t_j}$ is used since the asymptotics (see (2.2.3) and (2.6.1)) indicate that $q_{L,N,\alpha}(x,t) = \mathcal{O}(1/\sqrt{t})$ and D_j is an estimate of relative error. We let $t_j = j$, $S_j = [-10+j, 10+j]$ and $\alpha_j = 1/j$ for $j = 1, 2, \ldots$. In Figure 2.7.6 we see that the solution of the nonlinear problem does not converge to the solution of the linear problem in this particular limit.

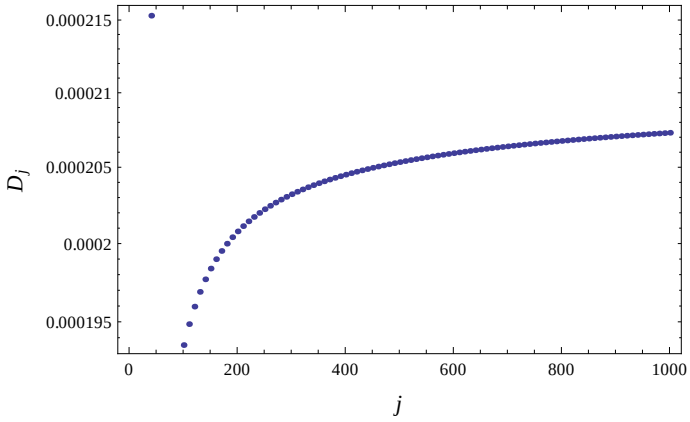

Figure 2.7.6: The difference D_j in (2.7.1) plotted versus j. This demonstrates the lack of convergence of the solution $q_{N,\alpha}$ to $q_{L,\alpha}$ in the $\alpha \to 0$ limit for long time.

Chapter 3

Riemann–Hilbert Problems

We present a thorough discussion of RHPs. The goal of this chapter is to introduce the subject in a comprehensive yet accessible way. Many proofs of well-known results are included below. The proofs are often omitted in the literature and we believe they are instructive. Standard references on the subject are [24, 4, 116, 18]. On first reading, many proofs may be skipped. It should be noted that much of the development below concerning the *Sobolev zero-sum spaces* is new.

The development here proceeds in the following way. We first introduce the fundamental ideas of RHPs using Hölder continuity. In particular, we develop the theory of Cauchy integrals over closed contours. We discuss the solution of scalar RHPs and extend the theory to non-closed contours. This leads to the study of matrix RHPs. In some cases, a matrix RHP can be reduced to a series of scalar RHPs. When this is not the case the approach is to provide conditions for the unique solvability of the RHP. This requires the study of appropriate Hardy and Sobolev spaces along with the development of the theory of Cauchy integrals on Lipschitz curves and associated singular integral equations.

The essential idea behind a RHP is that of finding a piecewise analytic function, which we often refer to as *sectionally analytic*, that is discontinuous across a contour $\Gamma \subset \mathbb{C}$. We specify how the function behaves at this discontinuity through a *jump condition*. To be more precise we divide $\mathbb{C} \setminus \Gamma = \Omega_+ \cup \Omega_-$ into disjoint components Ω_+ lying to the left of Γ and Ω_- lying to the right. Of course, for a general contour Γ this division is not possible. It turns out that Γ can be augmented so this is true, see Section 3.10.

Definition 3.0.1. *Γ is said to be a complete contour if Γ can be oriented in such a way that $\mathbb{C} \setminus \Gamma = \Omega_+ \cup \Omega_-$, $\Omega_+ \cap \Omega_- = \varnothing$ and $\Omega_+ (\Omega_-)$ lies to the left (right) of Γ. The set of self-intersections of Γ is denoted by γ_0.*

Often, it is beneficial to decompose $\Gamma = \Gamma_1 \cup \cdots \cup \Gamma_l$ so that each Γ_i is non-self-intersecting.

A RHP is the task of finding a (hopefully unique) function $\phi(z)$ that satisfies the following jump condition

$$\lim_{z \to s,\ z \in \Omega_+} \phi(z) = \left(\lim_{z \to s,\ z \in \Omega_-} \phi(z) \right) g(s) + f(s), \quad s \in \Gamma,$$

for some definite functions f, g defined on Γ. We always assume the limit is taken in a

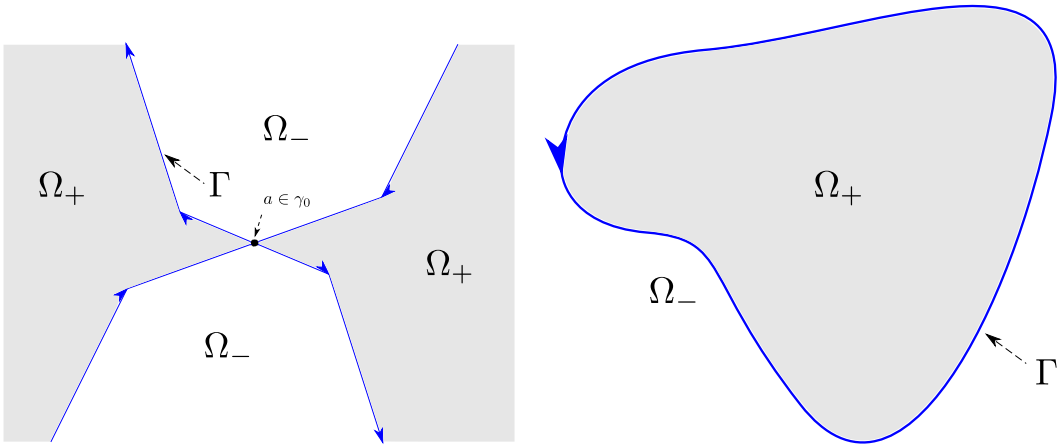

(a) (b)

Figure 3.0.1: (a) An admissible self-intersecting contour Γ with $\Omega_\pm$ labeled. (b) An admissible non-self-intersecting contour.

non-tangential manner. In what follows we use the notation

$$\phi_+(z) = \phi^+(z) = \lim_{z \to s,\ z \in \Omega_+} \phi(z),$$
$$\phi_-(z) = \phi^-(z) = \lim_{z \to s,\ z \in \Omega_+} \phi(z).$$

The $+$ or $-$ may be placed in the subscript or superscript for notational convenience.

Many remarks are in order. The jump condition

$$\phi^+(s) = \phi^-(s)g(s) + f(s),$$

will be used in the case that ϕ is matrix or vector valued. In this case g is a matrix and f is a matrix or vector. Throughout what follows we make many analogies between RHPs and differential equations. For our first analogy, one must specify what is meant by $\phi^\pm$. In relation to differential equations this is analogous to when one must specify classical versus weak derivatives. There are many natural meanings of $\phi^\pm$, two common interpretations are:

1. $\phi^\pm(s)$ should exist at every interior point of the contour and be continuous functions except at endpoints of Γ where they should be locally integrable, or

2. $\phi^\pm(s)$ should exist almost everywhere (with respect to Lebesgue measure) and be in an appropriate L^p space.

The first case is that of a *continuous RHP* and the second is that of an *L^p RHP*.

The definition used might affect the possibility of solving a specific RHP. In practice, many difficult problems are reduced to RHPs and conditions on $\phi^\pm$ fall out of the reduction process.

In addition to boundary behavior we often specify the behavior of ϕ at some point in

the complex plane, usually at ∞. A function ϕ is of finite degree at infinity if

$$\limsup_{|z|\to\infty} |z|^{-n}|\phi(z)| < \infty, \quad \text{for some } n.$$

We require that for a function to solve a RHP it must be of finite degree at infinity. We also consider matrix-valued functions and in this case we replace $|\cdot|$ with some matrix norm, see Section 1.5.4.

In practice we usually specify some terms in the asymptotic series of ϕ at ∞, say $\phi(z) = 1+\mathcal{O}(z^{-1})$, or $\phi(z) = 1+1/z+\mathcal{O}(z^{-2})$. In the former case we write $\phi(\infty) = 1$. These conditions share an analogy with boundary/initial condition in the context of differential equations. Unless otherwise stated we use uniform convergence, *i.e.*

$$\phi(z) = p(z) + \mathcal{O}(z^{-n}) \text{ as } z \to \infty \Leftrightarrow \limsup_{R\to\infty} \sup_{|z|=R} |\phi(z) - p(z)||z|^n < \infty.$$

3.1 Hölder theory of Cauchy integrals

The fundamental object of study in the theory of RHPs is the Cauchy integral. Given an oriented contour Γ and a function $f : \Gamma \to \mathbb{C}$, the Cauchy integral is defined by

$$\mathcal{C}_\Gamma f(z) = \int_\Gamma \frac{f(s)}{s-z} \bar{d}s, \quad \bar{d}s = \frac{ds}{2\pi i}. \tag{3.1.1}$$

The Cauchy integral maps functions on a contour to analytic functions off the contour. We shall see later that under specific regularity conditions these functions can be put into a one-to-one correspondence. In this sense, Cauchy integrals are critical in the solution of RHPs both from a numerical and an analytical perspective.

RHPs are the construction of sectionally analytic functions with specified boundary behavior on some contour Γ. We must understand the limiting values of (3.1.1), specifically issues related to existence and regularity.

We describe a class of functions on which the Cauchy integral has nice properties.

Definition 3.1.1. *Given a domain $\Omega \subset \mathbb{C}$, a function $f : \Omega \to \mathbb{C}$ is α-Hölder continuous on Ω if for each $s \in \Omega$, there exists $\Lambda(s)$, $\delta(s) > 0$ such that*

$$|f(s) - f(x)| \le \Lambda(s)|s - x|^\alpha, \text{ for } |s - x| < \delta(s).$$

Note that this definition is useful when $\alpha \in (0, 1]$. If $\alpha = 1$, f is Lipschitz continuous and if $\alpha > 1$, f must be constant.

Definition 3.1.2. *A function $f : \Gamma \to \mathbb{C}$ is uniformly α-Hölder continuous on a bounded contour Γ if Λ and δ can be chosen independently of s.*

Lemma 3.1.3. *Each uniformly α-Hölder continuous function with corresponding constants δ and Λ satisfies*

$$\sup_{s_1\neq s_2,\ s_1,s_2\in\Gamma} \left\{ \frac{|f(s_1) - f(s_2)|}{|s_1 - s_2|^\alpha} \right\} < C\Lambda < \infty,$$

where C depends only on δ and Γ.

Proof. It suffices to show that $|f(s_1) - f(s_2)| \leq C\Lambda|s_1 - s_2|^\alpha$ for any choice of s_1, s_2. We select a uniform grid on Γ: $\{p_1, p_2, \ldots, p_N\}$ such that $|p_i - p_j| \geq \delta/2$ for $i \neq j$ and $|p_i - p_{i+1}| = \delta/2$. We assume Γ is oriented from s_1 to s_2. Let p_i be the first element of the partition after s_1 and p_j, the first before s_2. We assume $|s_1 - s_2| \geq \delta$, then

$$\begin{aligned}\frac{|f(s_1) - f(s_2)|}{|s_1 - s_2|} &\leq \frac{|f(s_1) - f(p_i)|}{|s_1 - s_2|} + \frac{|f(p_i) - f(p_{i+1})|}{|s_1 - s_2|} + \cdots + \frac{|f(p_j) - f(s_2)|}{|s_1 - s_2|} \\ &\leq \frac{|f(s_1) - f(p_i)|}{|s_1 - p_i|} + \frac{|f(p_i) - f(p_{i+1})|}{|p_i - p_{i+1}|} + \cdots + \frac{|f(p_j) - f(s_2)|}{|p_j - s_2|} \leq N\Lambda.\end{aligned}$$

□

Remark 3.1.4. *We use a definition of uniformly Hölder functions that differs slightly from the classical definition. The results stated below will be necessarily local, which makes this definition more convenient.*

We end this section with a number of technical lemmas.

Lemma 3.1.5. *If Γ is a bounded, smooth contour then there exists $\delta > 0$, such that for every $s^* \in \Gamma$, $|\bar{d}s| \leq C|dr|$ where $r = |s - s^*|$ and $s \in B(s^*, \delta)$.*

Proof. Introduce a parametrization of Γ, $s(t) = \alpha(t) + i\beta(t)$. Let t^* be so that $s(t^*) = s^* = a + ib$. Then

$$r = [(\alpha(t) - a)^2 + (\beta(t) - b)^2]^{1/2}, \quad dr = r^{-1}(t)[(\alpha(t) - a)\alpha'(t) + (\beta(t) - b)\beta'(t)]dt.$$

Near $t = t^*$, we use Taylor's theorem to write

$$\begin{aligned}(\alpha(t) - a)\alpha'(t) + (\beta(t) - b)\beta'(t) &= (t - t^*)\left[\alpha'(t^*)(\alpha'(t^*) + \mathcal{O}(t - t^*)) + \beta'(t^*)(\beta'(t^*) + \mathcal{O}(t - t^*))\right] \\ &= (t - t^*)[(\alpha'(t^*))^2 + (\beta'(t^*))^2] + \mathcal{O}(t - t^*)^2.\end{aligned}$$

Additionally,

$$r(t) = |t - t^*|[(\alpha'(t^*))^2 + (\beta'(t^*))^2]^{1/2}(1 + \mathcal{O}(|t - t^*|^2)).$$

From boundedness and smoothness we know that there exists a constant $C > 1$ such that

$$\frac{1}{C} \leq [(\alpha'(t))^2 + (\beta'(t))^2]^{1/2} \leq C.$$

It follows that

$$\left|\frac{(\alpha(t) - a)\alpha'(t) + (\beta(t) - b)\beta'(t)}{r(t)}\right| \leq C + \mathcal{O}(|t - t^*|).$$

Therefore for $t \in (t^* - \gamma, t^* + \gamma)$, $\gamma > 0$,

$$|dt| \leq (1 + C)|dr|,$$

where γ depends on the magnitude of the second derivatives and can be made small enough so that it does not depend on t^* (or s^*). The smoothness of $s(t)$ and the non-vanishing of $s'(t)$ gives $|\bar{d}s| \leq C|dr|$ for a new constant. This is valid in $B(s^*, \delta)$ where $\delta = \sup_{t\in(t^*-\gamma,t^*+\gamma)} |s(t) - s^*|$. □

3.1.1 Boundary values

We use the notation $B_\theta(x, \delta) = \{y \in B(x, \delta) : |\mathrm{Im}(x - y)|/|x - y| > \sin\theta\}$. This is a ball with two cones subtracted, see Figure 3.1.1. To allow for rotations define $B_{\theta,\phi}(x, \delta) = (B_\theta(x, \delta) - x)e^{i\phi} + x$. The following lemma begins to illustrate the importance of the class of Hölder continuous functions.

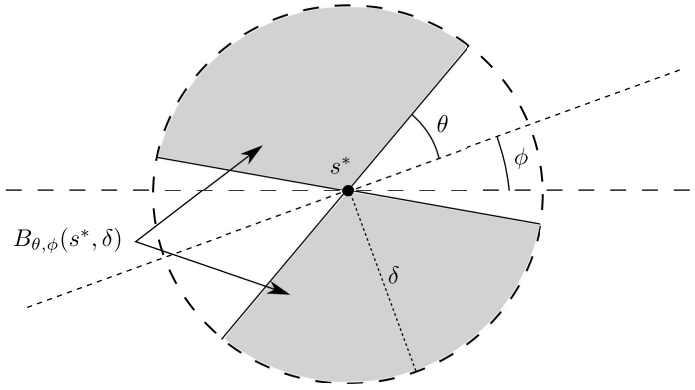

Figure 3.1.1: A representation of $B_{\theta,\phi}(s^*, \delta)$.

Lemma 3.1.6. *Let Γ be a bounded, smooth contour. Let $f : \Gamma \to \mathbb{C}$ be α-Hölder continuous and $f(s^*) = 0$ for a center s^* in Γ. Then*

1. *$\mathcal{C}_\Gamma f(s^*)$ exists, and*
2. *there exists $\delta > 0$ such that $\mathcal{C}_\Gamma f(z)$ is continuous in $B_{\theta,\phi}(s^*, \delta)$ for all $\theta > 0$ where ϕ is the angle the tangent at s^* makes with the horizontal.*

Proof. We prove each part separately.

1. This follows from the Hölder condition on f. The only unboundedness of the integrand behaves like $|s - s^*|^{\alpha-1}$, which is integrable.

2. Examine

$$I(z) = \int_\Gamma \frac{f(s)}{s - z}\bar{d}s - \int_\Gamma \frac{f(s)}{s - s^*}\bar{d}s = \int_\Gamma f(s)\left(\frac{1}{s - z} - \frac{1}{s - s^*}\right)\bar{d}s$$
$$= \int_\Gamma \frac{(f(s) - f(s^*))(z - s^*)}{(s - z)(s - s^*)}\bar{d}s.$$

We decompose $\Gamma = \Gamma_\delta \cup \Gamma_\delta^c$ where $\Gamma_\delta = \Gamma \cap B(s^*, \delta)$ and Γ_δ^c is the complement relative to Γ. We assume $z \in B(s^*, \delta)$ and set up some elementary inequalities. For $s \in \Gamma_\delta^c$:

- $|z - s^*| < \delta$,
- $|z - s| > \delta$, and
- $|s - s^*| \geq \delta$.

For $s \in \Gamma_\delta$ we use the Law of Sines (see Figure 3.1.2) to obtain $|z-s^*|/|z-s| \leq 1/\sin\theta$ where θ is then angle between the line from z to s^* and that from s^* to s. Note that θ is bounded away from zero (and $\pm\pi$) provided δ is sufficiently small.

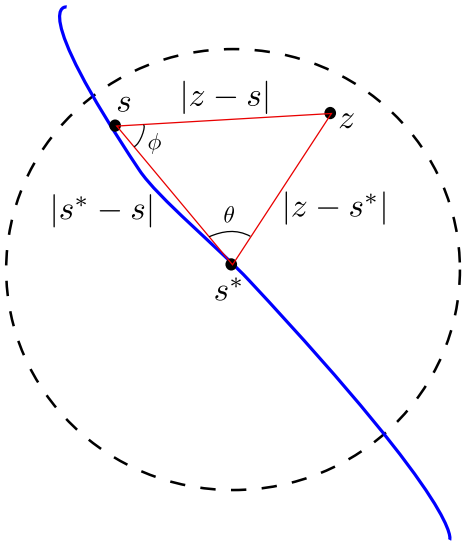

Figure 3.1.2: A pictorial representation of $|z - s^*|$ and $|z - s|$.

For $\delta > 0$,

$$\left| \int_{\Gamma_\delta^c} \frac{(f(s) - f(s^*))(z - s^*)}{(s - z)(s - s^*)} \bar{d}s \right| \leq |z - s^*|\delta^{-2} \int_{\Gamma_\delta^c} |f(s) - f(s^*)||\bar{d}s| \leq C|z - s^*|\delta^{-2}$$

The right-hand side tends to zero as $z \to s^*$. We estimate the remaining terms.

$$\left| \int_{\Gamma_\delta} \frac{(f(s) - f(s^*))(z - s^*)}{(s - z)(s - s^*)} \bar{d}s \right| \leq \frac{\Lambda(s^*)}{\sin\theta} \int_{\Gamma_\delta} |s - s^*|^{\alpha-1}|\bar{d}s|.$$

Set $r = |s - s^*|$. The final estimate we need is that for δ sufficiently small, $|\bar{d}s| \leq C|dr|$ (see Lemma 3.1.5). Thus

$$|I(z)| \leq C \left(2\frac{\Lambda(s^*)}{\alpha \sin\theta} \delta^\alpha + |z - s^*|\delta^{-2} \right). \tag{3.1.2}$$

For any $\epsilon > 0$, we choose δ so that the first term is less than ϵ and let $z \to s^*$. This proves that $I(z) \to 0$ as $z \to s^*$.

□

Remark 3.1.7. *If f is uniformly α-Hölder continuous then the right-hand side of* (3.1.2) *can be modified to depend on s^* just though $|z - s^*|$.*

Now we discuss the limiting values of $\mathcal{C}_\Gamma f$ when f is α-Hölder continuous. We assume that Γ is a bounded, closed curve. We denote the region lying to the left of Γ by Ω_+ and that to the right by Ω_-. For any point $s^* \in \Gamma$ consider

$$\mathcal{C}_\Gamma f(z) = \int_\Gamma \frac{f(s) - f(s^*)}{s - z} \bar{d}s + f(s^*) \int_\Gamma \frac{\bar{d}s}{s - z}$$

Then, using Lemma 3.1.6

$$\lim_{z \to s^*,\ z \in \Omega_+} \mathcal{C}_\Gamma f(s) = \mathcal{C}_\Gamma^+ f(s^*) = f(s^*) + \int_\Gamma \frac{f(s) - f(s^*)}{s - s^*} \bar{d}s, \tag{3.1.3}$$

$$\lim_{z \to s^*,\ z \in \Omega_-} \mathcal{C}_\Gamma f(s) = \mathcal{C}_\Gamma^- f(s^*) = \int_\Gamma \frac{f(s) - f(s^*)}{s - s^*} \bar{d}s. \tag{3.1.4}$$

We assume all limits are taken non-tangentially. We rewrite the integral appearing in this formula. For $s^* \in \Gamma$ we define the Cauchy principal value integral

$$⨍_\Gamma \frac{f(s)}{s - s^*} \bar{d}s = \lim_{\delta \to 0^+} \int_{\Gamma \setminus B(s^*, \delta)} \frac{f(s)}{s - s^*} \bar{d}s.$$

Again, let $\Gamma_\delta = \Gamma \cap B(s^*, \delta)$:

$$\begin{aligned} \int_\Gamma \frac{f(s) - f(s^*)}{s - s^*} \bar{d}s &= \lim_{\delta \to 0^+} \int_{\Gamma \setminus \Gamma_\delta} \frac{f(s) - f(s^*)}{s - s^*} \bar{d}s \\ &= \lim_{\delta \to 0^+} \int_{\Gamma \setminus \Gamma_\delta} \frac{f(s)}{s - s^*} \bar{d}s - \lim_{\delta \to 0^+} \int_{\Gamma \setminus \Gamma_\delta} \frac{\bar{d}s}{s - s^*}. \end{aligned}$$

The existence of the second limit shows the existence of the first:

$$\lim_{\delta \to 0^+} \int_{\Gamma_\delta} \frac{\bar{d}s}{s - s^*} = \frac{1}{2\pi i} \lim_{\delta \to 0^+} \log\left(\frac{s^* - s_+}{s^* - s_-}\right) = -\frac{1}{2},$$

where $s_\pm$ are the end points of the arc Γ_δ.

Remark 3.1.8. *The contour Γ need not be closed. We can close Γ and define $f = 0$ on the added portion. These results still follow provided we stay away from the end points of Γ.*

We arrive at the following:

Lemma 3.1.9 (Plemelj)**.** *Let Γ be a smooth arc from a to b and f be α-Hölder continuous on Γ. Then for $x \in \Gamma \setminus \{a, b\}$*

$$\mathcal{C}_\Gamma^+ f(x) = \frac{1}{2} f(x) + ⨍ \frac{f(s)}{s - x} \bar{d}s, \tag{3.1.5}$$

$$\mathcal{C}_\Gamma^- f(x) = -\frac{1}{2} f(x) + ⨍ \frac{f(s)}{s - x} \bar{d}s, \tag{3.1.6}$$

and

$$\mathcal{C}_\Gamma^+ f(x) - \mathcal{C}_\Gamma^- f(x) = f(x),$$
$$\mathcal{C}_\Gamma^+ f(x) + \mathcal{C}_\Gamma^- f(x) = 2\fint \frac{f(s)}{s-x}\bar{d}s.$$

3.1.2 Regularity and singularity behavior of boundary values

We take up the issue of understanding the continuity properties of the functions $\mathcal{C}_\Gamma^\pm f$ when f is α-Hölder.

Lemma 3.1.10. *Let Γ be a bounded, smooth arc and let f be uniformly α-Hölder continuous on Γ. Let $\Gamma' \subset \Gamma$ be an arc with endpoints lying a finite distance from the endpoints a and b of Γ. Then $\mathcal{C}_\Gamma^\pm f$ is uniformly α-Hölder continuous on Γ'.*

Proof. Let $s_1, s_2 \in \Gamma'$, then

$$\mathcal{C}_\Gamma^\pm f(s_1) - \mathcal{C}_\Gamma^\pm f(s_2) = \pm\frac{1}{2}(f(s_1) - f(s_2)) + \int_\Gamma f(s)\left(\frac{1}{s-s_1} - \frac{1}{s-s_2}\right)\bar{d}s.$$

This can be rewritten using Lemma 3.1.9:

$$\mathcal{C}_\Gamma^\pm f(s_1) - \mathcal{C}_\Gamma^\pm f(s_2) = \left(\frac{1}{2} \pm \frac{1}{2}\right)(f(s_1) - f(s_2)) + I(s_1, s_2),$$
$$I(s_1, s_2) = \int_\Gamma \left(\frac{f(s) - f(s_1)}{s - s_1} - \frac{f(s) - f(s_2)}{s - s_2}\right)\bar{d}s.$$

Thus the study of Hölder continuity for both $\mathcal{C}_\Gamma^\pm f$ is reduced to the study of $I(s_1, s_2)$. Define $\Gamma'_\delta = \Gamma' \cap B(s_1, \delta)$ for $\delta > 0$ such that $s_2 \in \partial B(s_1, \delta/2)$, see Figure 3.1.3. Separate

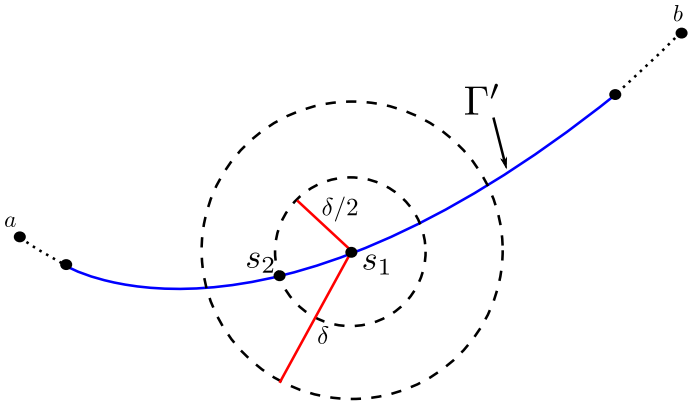

Figure 3.1.3: The positioning of s_1 and s_2 on Γ.

$I(s_1, s_2) = I_0(s_1, s_2) + I_1(s_1, s_2)$ where I_0 contains an integral over Γ'_δ and I_1, over the

compliment, relative to Γ, of Γ'_δ. For I_0, using the Hölder condition, we obtain

$$|I_0(s_1,s_2)| \leq \Lambda \int_{\Gamma'_\delta} |s-s_1|^{\alpha-1}|\bar{d}s| + \Lambda \int_{\Gamma'_\delta} |s-s_2|^{\alpha-1}|\bar{d}s|.$$

Define $r_1 = |s-s_1|$ and $r_2 = |s-s_2|$. For sufficiently small δ, depending only on Γ, (see Lemma 3.1.5) there exists a constant C that depends only on Γ such that $|\bar{d}s| \leq C|dr_1|$ and $|\bar{d}s| \leq C|dr_2|$. Thus

$$\begin{aligned} |I_0(s_1,s_2)| &\leq C\Lambda 2 \int_0^\delta r^{\alpha-1}dr + C\Lambda \int_0^{\delta/2} r^{\alpha-1}dr + C\Lambda \int_0^{3\delta/2} r^{\alpha-1}dr \\ &\leq 5C\Lambda\alpha^{-1}\delta^\alpha. \end{aligned}$$

For I_1, we write

$$I_1(s_1,s_2) = (f(s_2)-f(s_1)) \int_{(\Gamma'_\delta)^c} \frac{\bar{d}s}{s-s_1} + \int_{(\Gamma'_\delta)^c} (f(s)-f(s_2)) \left(\frac{1}{s-s_1} - \frac{1}{s-s_2} \right) \bar{d}s. \tag{3.1.7}$$

The first integral is bounded, showing that the first term satisfies a uniform α-Hölder condition. We simplify the second integral

$$\begin{aligned} I_2(s_1,s_2) &= \int_{(\Gamma'_\delta)^c} (f(s)-f(s_2)) \left(\frac{1}{s-s_1} - \frac{1}{s-s_2} \right) \bar{d}s \\ &= \int_{(\Gamma'_\delta)^c} (f(s)-f(s_2)) \frac{s_1-s_2}{(s-s_1)(s-s_2)} \bar{d}s. \end{aligned}$$

We find that for $s \in (\Gamma'_\delta)^C$

$$\frac{|s-s_2|}{|s-s_1|} \geq \frac{|s-s_2|}{|s-s_2|+|s_2-s_1|} \geq \frac{2}{2+\delta/|s-s_2|} \geq \frac{1}{2}.$$

We estimate

$$|I_2(s_1,s_2)| \leq \Lambda|s_1-s_2| \int_{(\Gamma'_\delta)^c} \frac{|s-s_2|^{\alpha-1}}{|s-s_1|}|\bar{d}s| \leq 2^{1-\alpha}\Lambda|s_1-s_2| \int_{(\Gamma'_\delta)^c} |s-s_1|^{\alpha-2}|\bar{d}s|.$$

This integral is easily bounded:

$$|I_2(s_1,s_2)| \leq 2^{1-\alpha}\Lambda\delta^{\alpha-2}|(\Gamma'_\delta)^c||s_1-s_2|.$$

This proves the lemma. □

Define the space $C^{0,\alpha}(\Gamma)$, for Γ smooth, bounded and closed, consisting of uniformly α-Hölder continuous functions. We introduce the semi-norm

$$|f|_{0,\alpha} = \sup_{s_1 \neq s_2,\ s_1,s_2 \in \Gamma} \frac{|f(s_1)-f(s_2)|}{|s_1-s_2|^\alpha},$$

which is finite for every function in $C^{0,\alpha}(\Gamma)$ by Lemma 3.1.3. $C^{0,\alpha}(\Gamma)$ is a Banach space when equipped with the norm [48]

$$\|f\|_{0,\alpha} = \sup_{s\in\Gamma} |f(s)| + |f|_{0,\alpha}.$$

Corollary 3.1.11. *$\mathcal{C}_\Gamma^\pm$ are bounded linear operators on $C^{0,\alpha}(\Gamma)$.*

Proof. The bounds in the previous lemma and Lemma 3.1.3 depend only on δ, Λ and C. This shows

$$|\mathcal{C}_\Gamma^\pm f|_{0,\alpha} \le C\|f\|_{0,\alpha}.$$

It remains to show $\sup_{s\in\Gamma} |\mathcal{C}_\Gamma^\pm f(s)| \le C\|f\|_{0,\alpha}$. For $s^* \in \Gamma$, consider Γ_δ and Γ_δ^c as above. We write

$$\mathcal{C}_\Gamma^+ f(s^*) = \int_{\Gamma_\delta^c} \frac{f(s)}{s-s^*} d\bar{s} + f(s^*) + \int_{\Gamma_\delta} \frac{f(s)-f(s^*)}{s-s^*} d\bar{s}.$$

Thus

$$|\mathcal{C}_\Gamma^+ f(s^*)| \le |f(s^*)| + \sup_{s\in\Gamma} |f(s)|\delta^{-1} \int_{\Gamma_\delta^c} |d\bar{s}| + |f|_{0,\alpha} \int_{\Gamma_\delta} |s-s^*|^{\alpha-1} |d\bar{s}| \le C\|f\|_{0,\alpha},$$

by previous arguments. Taking a supremum proves the corollary for $\mathcal{C}_\Gamma^+$. The result for $\mathcal{C}_\Gamma^-$ can be inferred from Lemma 3.1.9. □

Definition 3.1.12. *A function f satisfies an (α,γ)-Hölder condition on a contour Γ if f is α-Hölder away from the endpoints of Γ and if at each endpoint c, f satisfies*

$$f(s) = \frac{\tilde{f}(s)}{(s-c)^\gamma}, \quad \gamma = a+ib, 0 \le a < 1,$$

$\tilde{f}$ is α-Hölder.

Now, we discuss the important features of Cauchy integrals near endpoints of the contours through the following lemma.

Lemma 3.1.13. *Let Γ be a smooth arc from a to b with $\Omega_+(\Omega_-)$ defined as regions lying directly to the left(right) of Γ, see Figure 3.1.4. Assume f satisfies an (α,γ)-Hölder condition. The following holds for any endpoint $c = a$ or b.*

1. *If $\gamma = 0$, then:*

   (a) *As $z \to c$, $z \in \Omega_\pm$*

$$\mathcal{C}_\Gamma f(z) = \mp \frac{f(c)}{2\pi i} \log \frac{1}{z-c} + F_0(z).$$

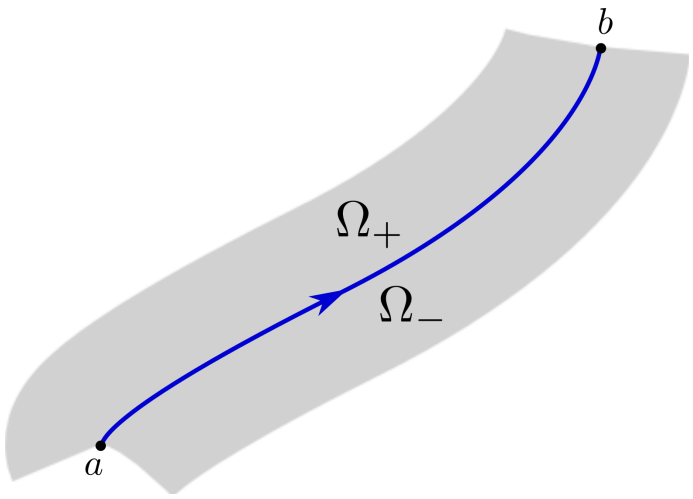

Figure 3.1.4: An open contour with $\Omega_\pm$ labelled.

(b) As $s \to c$, $s \in \Gamma$

$$\mathcal{C}_\Gamma f(s) = \mp \frac{f(c)}{2\pi i} \log \frac{1}{s-c} + H_0(s).$$

Here H_0 and F_0 both tend to definite limits at c. The upper sign is taken for $c = b$, the lower for $c = a$. The branch cut for the logarithm is taken along Γ.

2. $\gamma \neq 0$

(a) As $z \to c$, $z \in \Omega_\pm$

$$\mathcal{C}_\Gamma f(z) = \mp \frac{e^{\pm i\gamma\pi}}{2i \sin(\gamma\pi)} \frac{\tilde{f}(c)}{(z-c)^\gamma} + F_0(z).$$

(b) As $s \to c$, $s \in \Gamma$

$$\mathcal{C}_\Gamma f(s) = \mp \frac{\cot(\gamma\pi)}{2i} \frac{\tilde{f}(c)}{(s-c)^\gamma} + H_0(s).$$

In this case, if $\alpha = 0$ then F_0 and H_0 behave as above. The upper sign is taken for $c = b$, the lower for $c = a$. If $\operatorname{Re}\gamma > 0$ then for some $0 < \alpha^* < \operatorname{Re}\gamma$,

$$|F_0(z)| < \frac{A_0}{|z-c|^{\alpha^*}}, \quad |H_0(s)| < \frac{B_0}{|s-c|^{\alpha^*}}.$$

Proof. We prove Part 1 here. For the proof of Part 2 see [81]. Write

$$\int_a^b \frac{f(s)}{s-z} \bar{d}s = f(c) \int_a^b \frac{\bar{d}s}{s-z} + \int_a^b \frac{f(s)-f(c)}{s-z} \bar{d}s.$$

Thus

$$f(c)\int_a^b \frac{\bar{d}s}{s-z} = \mp\frac{f(c)}{2\pi i}\log\frac{1}{z-c} + V_0(z),$$

where V_0 is analytic near $z = c$. Thus

$$F_0(z) = V_0(z) + \int_a^b \frac{f(s)-f(c)}{s-z}\bar{d}s,$$

which tends to a definite limit as $z \to c$ by Lemma 3.1.6. The limit $z \to \Gamma$, $z \in \Omega_\pm \setminus B(c,\delta)$, $\delta > 0$ of $F_0(z)$ is $H_0(s)$ which also tends to a definite limit as $s \to c$.

□

Remark 3.1.14. *An important consequence of this result is that for functions bounded at the end of a contour, a singularity is introduced. For functions singular at the end of a contour, the singularity structure is preserved. More precisely, if f is (α,γ)-Hölder with $\gamma \neq 0$ then $\mathcal{C}_\Gamma^\pm f$ is (α',γ')-Hölder with $\operatorname{Re}\gamma = \operatorname{Re}\gamma'$.*

3.2 The solution of scalar Riemann–Hilbert problems

We have presented a fairly wide class of functions, the α-Hölder continuous functions, for which the limits of Cauchy integrals are well defined and regular. We continue with the solution of the simplest RHP on smooth, closed and bounded contours.

3.2.1 Smooth, closed and bounded contours

Problem 3.2.1. *Consider the continuous RHP*

$$\phi^+(s) - \phi^-(s) = f(s), \quad s \in \Gamma, \quad \phi(\infty) = 0, \quad f \in C^{0,\alpha}(\Gamma), \tag{3.2.1}$$

where Γ is a smooth, bounded and closed contour.

This problem is solved directly by the Cauchy integral $\phi(z) = \mathcal{C}_\Gamma f(z)$. Indeed, Lemma 3.1.9 gives

$$\phi^+(s) - \phi^-(s) = \mathcal{C}_\Gamma^+ f(s) - \mathcal{C}_\Gamma^- f(s) = f(s), \quad s \in \Gamma. \tag{3.2.2}$$

To show $\phi(\infty) = 0$ we use the following lemma which provides more precise details.

Lemma 3.2.2. *Let f be a bounded, measurable function and Γ a bounded contour, then*

$$\mathcal{C}_\Gamma f(z) = \sum_{n=1}^{N} \alpha_n z^{-n} + \mathcal{O}(z^{N+1}),$$
$$\alpha_n = -\int_\Gamma s^n f(s)\bar{d}s$$

Proof. We use the geometric series. For $|z|$ sufficiently large, $|s/z| \leq 1/2$ for all $s \in \Gamma$. Therefore

$$\frac{1}{s-z} = \left(-\frac{1}{z}\right)\frac{1}{1-(s/z)} = -\frac{1}{z}\left(\sum_{n=0}^{N}(s/z)^n + \frac{(s/z)^{N+1}}{1-(s/z)}\right).$$

We obtain the estimate

$$\left|\frac{1}{s-z} - \left(-\frac{1}{z}\right)\sum_{n=0}^{N}(s/z)^n\right| \leq 2\left(\sup_{s\in\Gamma}|s|\right)^{N+1} z^{-(N+2)}.$$

Using the Cauchy integral again for $\sup_{s\in\Gamma}|s/z| \leq 1/2$

$$\left|\int_\Gamma \frac{f(s)}{s-z}\bar{d}s + \sum_{n=1}^{N}\left(\int_\Gamma s^{n-1}f(s)\bar{d}s\right)z^{-n}\right| \leq \left(2\sup_{s\in\Gamma}|f(s)|\cdot|\Gamma|\left(\sup_{s\in\Gamma}|s|\right)^{N+2}\right)z^{-(N+1)},$$

where $|\Gamma|$ is the arclength of Γ. □

We have addressed existence in a constructive way. Now we address uniqueness. Let $\psi(z)$ be another solution of Problem 3.2.1. The function $D(z) = \psi(z) - \phi(z)$ satisfies

$$D^+(s) - D^-(s) = 0, \quad s \in \Gamma, D(\infty) = 0.$$

Since D is continuous up to Γ, D must be entire. By Liouville's theorem, it must be identically zero. This shows the uniqueness of our solution of Problem 3.2.1.

We wish to extend these results to the case of unbounded contours such as $\mathbb{R}$. This case is dealt with in a more straightforward way using L^p and Sobolev spaces. All solution formulas hold with slight changes in interpretation. We defer this to Section 3.6. We move to the next simplest case for scalar RHPs.

Problem 3.2.3. *Consider the homogeneous, continuous RHP*

$$\phi^+(s) = \phi^-(s)g(s), \quad s \in \Gamma, \quad \phi(\infty) = 1, \quad g \in C^{0,\alpha}(\Gamma), \tag{3.2.3}$$

where Γ *is a smooth, bounded and closed contour, and* $g \neq 0$.

Formally, this problem can be solved via the logarithm. Consider the RHP solved by $X(z) = \log\phi(z)$:

$$X^+(s) = X^-(s) + G(s) \Leftrightarrow X^+(s) - X^-(s) = G(s), \quad G(s) = \log g(s).$$

If $\log g(s)$ is well-defined and Hölder continuous the solution is given by

$$\phi(z) = \exp(\mathcal{C}_\Gamma G(z)). \tag{3.2.4}$$

For a general Hölder continuous function g, $\log g$ may not be well-defined. Indeed, even if one fixes the branch of the logarithm, $\log g$ will generically suffer from discontinuities. To rectify this issue we define the index of a function g with respect to traversing Γ in the

positive direction to be the normalized increment of its argument:

$$\operatorname{ind}_\Gamma g(s) = \frac{1}{2\pi}[\arg g(s)]_\Gamma = \frac{1}{2\pi i}[\log g(s)]_\Gamma = \int_\Gamma \bar{d} \log g(s). \tag{3.2.5}$$

First, if g is α-Hölder continuous and $\operatorname{ind}_\Gamma g(s) = 0$ then $\log g(s)$ is also α-Hölder continuous. Indeed, in this case the branch cut of $\log s$ can be taken so that it is Lipschitz continuous in an open set containing $\{g(s) : s \in \Gamma\}$. If $\operatorname{ind}_\Gamma g(s) = \kappa \neq 0$ and (without loss of generality) $z = 0$ is in Ω_+, the region to the left of Γ, then $\operatorname{ind} s^{-\kappa} g(s) = 0$. Thus we can uniquely solve the problem

$$\psi^+(z) = \psi^-(s) s^{-\kappa} g(s), \quad s \in \Gamma, \quad \psi(\infty) = 1,$$

with the expression (3.2.4) for the index zero case. There are two cases:

- If $\kappa > 0$, then

$$\phi(z) = P(z) \begin{cases} \psi(z), & z \in \Omega_+, \\ \psi(z) z^{-\kappa}, & z \in \Omega_-, \end{cases}$$

  where P is a polynomial of degree κ with leading coefficient 1, solves Problem 3.2.3.

- If $\kappa < 0$, then

$$\phi(z) = P(z) \begin{cases} \psi(z), & z \in \Omega_+, \\ \psi(z) z^{-\kappa}, & z \in \Omega_-, \end{cases}$$

  cannot satisfy $\phi(\infty) = 1$ for any polynomial $P \neq 0$. Thus the only solution bounded at ∞ is the zero solution.

In both cases, when $P = 1$ we call the function ϕ the *fundamental solution.*

We move to consider inhomogeneous scalar RHPs. We will see a direct parallel between the methods presented here and the method of variation of parameters for ordinary differential equations.

Problem 3.2.4. *Consider the inhomogeneous, continuous RHP*

$$\phi^+(s) = \phi^-(s) g(s) + f(s), \quad s \in \Gamma, \quad \phi(\infty) = 0, \quad g, f \in C^{0,\alpha}(\Gamma), \tag{3.2.6}$$

where Γ *is a smooth, bounded and closed contour, and* $g \neq 0$.

To solve this problem we first find the fundamental solution of the homogeneous problem. Just as in the case of variation of parameters for differential equations the solution of the homogeneous problem allows us to solve the inhomogeneous problem. We use $\nu(z)$ to denote the fundamental solution. Assume $\operatorname{ind}_\Gamma g(s) = \kappa$. The Hölder continuity of $s^{-\kappa} g(s)$ shows us that ν does not vanish in the finite plane. Dividing (3.2.6) by ν and using that $\nu^+(s) = \nu^-(s) g(s)$,

$$\frac{\phi^+(s)}{\nu^+(s)} = \frac{\phi^-(s)}{\nu^-(s)} + \frac{f(s)}{\nu^+(s)}, \quad \frac{\phi(z)}{\nu(z)} = \mathcal{O}(z^{\kappa-1}) \text{ as } z \to \infty.$$

Again, there are two cases:

- If $\kappa \geq 0$, then we obtain an expression for $\phi(z)/\nu(z)$ using the Plemelj formula (Lemma 3.1.9)

$$\frac{\phi(z)}{\nu(z)} = \int_\Gamma \frac{f(s)}{\nu^+(s)(s-z)} \bar{d}s = \mathcal{O}(z^{\kappa-1}) \text{ as } z \to \infty. \tag{3.2.7}$$

- If $\kappa < 0$, then the asymptotic condition here requires higher-order decay of a Cauchy integral. The solution formula is still (3.2.7) but we use Lemma 3.2.2 to find the conditions

$$\int_\Gamma s^n \frac{f(s)}{\nu^+(s)} \bar{d}s = 0, \quad n = 0, \ldots, \kappa - 1. \tag{3.2.8}$$

  If any of these conditions are satisfied then no solution of Problem 3.2.4 that vanishes at infinity exists.

Once a valid expression for $\phi(z)/\nu(z)$ is obtained, the general solution is given by

$$\phi(z) = \nu(z) \left(\int_\Gamma \frac{f(s)}{\nu^+(s)(s-z)} \bar{d}s + P(z) \right),$$

where $P(z)$ is a polynomial of degree $< \kappa$ if $\kappa > 0$. otherwise P is zero.

Remark 3.2.5. *This method is in direct analogy with Lagrange's method of variation of parameters for differential equations. The solution to the homogeneous problem is used to express the general solution of the inhomogeneous problem in term of an integral involving the homogeneous solution and the inhomogeneous term.*

Remark 3.2.6. *The definition of index in* (3.2.5) *is in correspondence with that of the Fredholm index. As we will see, a solution vanishing at infinity of the homogeneous problem corresponds to an element of the kernel of an integral operator. Furthermore,* (3.2.8) *are the conditions for f to lie in the range of the same integral operator.*

3.3 Smooth, bounded and open contours

The solution procedure for scalar RHPs is not much more difficult in practice when the contour Γ is not closed. When a non-self-intersecting contour is not closed, we say it is open.

Definition 3.3.1. *A contour Γ is said to be open (not closed) if a parameterization $\gamma : [0,1] \to \Gamma$ of Γ satisfies $\gamma(0) \neq \gamma(1)$.*

A complication comes from the fact that in the case of open contours, additional solutions are introduced. To highlight this, consider the continuous RHP

$$\phi^+(s) = \phi^-(s) g(s), \quad s \in \Gamma, \quad \phi(\infty) = 1, \quad g \in C^{0,\alpha}(\Gamma), \tag{3.3.1}$$

where Γ is a smooth, bounded and open contour extending from $z = a$ to $z = b$. If $\phi(z)$ satisfies the jump condition then so does $\frac{1}{2}(1 + \frac{z-a}{z-b})^k \phi(z)$, away from a, b for any integer

k. We impose local integrability in our definition of the solution of a continuous RHP, otherwise we would have an infinite number of solutions.

We discuss the solution of Problem 3.2.1 in the case that Γ has open endpoints and f is (α,γ)-Hölder. One solution is certainly $\mathcal{C}_\Gamma f(z)$ (see Lemma 3.1.13). To see uniqueness, let ψ be another solution then $\mathcal{C}_\Gamma f(z)-\psi(z)$ is an analytic function away from the endpoints of Γ that decays at infinity. The local integrability condition precludes the existence of poles at the these endpoints. Again, Liouville's theorem shows $\mathcal{C}_\Gamma f(z)=\psi(z)$.

We move to the solution of Problem 3.2.3 when Γ is an open contour from $z=a$ to $z=b$ and g is α-Hölder. A simplifying assumption is that g does not vanish on Γ. We proceed as if Γ is closed. Define $G(s)=\log g(s)$ taking the principal branch of the logarithm. Taking any other branch would modify $G(s)$ by $2\pi i n$ for some integer n. It can be shown that the choices of n_a and n_b below remove the dependence on n.

Define

$$\psi(z)=\exp\left(\mathcal{C}_\Gamma G(z)\right).$$

A straightforward calculation shows that ψ satisfies the appropriate jump condition. We must determine if ψ is locally integrable and if not, modify. Using Lemma 3.1.13 we see that for a contour from a to b

$$\begin{aligned}\psi(s)&=(s-b)^{\zeta(b)}H_b(s),\quad \zeta(c)=\mp\frac{\log g(c)}{2\pi i},\\ \psi(s)&=(s-a)^{\zeta(a)}H_a(s)\end{aligned}$$

where the $-(+)$ sign is taken if $c=b$ ($c=a$). Here $H_a(s)$, $H_b(s)$ tend to definite limits as $s\to a$ and b, respectively. Let $\zeta_c=\lambda_c+i\mu_c$ and let n_c be an integer such that $-1<n_c+\lambda_c<1$ for $c=a,b$. It follows that

$$\nu(z)=(z-a)^{n_a}(z-b)^{n_b}X(z),$$

is a solution of (3.3.1) since it is locally integrable. Note that if $\lambda_c\in\mathbb{Z}$ then n_c is uniquely specified. Specifically, if g takes only positive values then the solution is unique. In the case of open contours, any locally integrable $\nu(z)$ is called a *fundamental solution*.

We follow the same procedure as above to solve Problem 3.2.4 in the case of Γ being an open contour. Divide (3.2.6) by ν and write

$$\frac{\phi^+(s)}{\nu^+(s)}=\frac{\phi^-(s)}{\nu^-(s)}+\frac{f(s)}{\nu^+(s)},\quad \frac{\phi(z)}{\nu(z)}=\mathcal{O}(z^{n_a+n_b-1})\text{ as }z\to\infty. \tag{3.3.2}$$

We assume f satisfies an α-Hölder condition. Thus $f(s)/\nu^+(s)$ satisfies an $(\alpha,-\zeta(a))$-Hölder condition near $z=a$ and a similar condition near $z=b$. A solution of (3.3.2), assuming possible moment conditions (3.2.8) are satisfied, is given by

$$\phi(z)=\nu(z)\int_\Gamma\frac{f(s)}{\nu^+(s)(s-z)}\bar{d}s.$$

From Remark 3.1.14 we see that $\phi(z)$ has bounded singularities at the endpoints of Γ

whenever $\zeta(c) \neq 0$, otherwise there is a logarithmic singularity present. As before,

$$\phi(z) = \nu(z)\left(\int_\Gamma \frac{f(s)}{\nu^+(s)(s-z)}\bar{d}s + P(z)\right),$$

is the solution, where $P(z)$ is a polynomial of degree less than $-(n_a+n_b)$ if $n_a+n_b<0$, otherwise $P=0$ and we have n_a+n_b orthogonality conditions for a solution to exist, see (3.2.8) with $\kappa = n_a+n_b$.

Example 3.3.2. *Consider the RHP*

$$\phi^+(s)+\phi^-(s) = s^2-1, \quad s\in[-\ell,\ell], \quad \ell>0, \quad \phi(\infty)=0.$$

Assume we want ϕ to be uniformly bounded in the plane. We first find the fundamental solution, ν, taking any branch of the logarithm:

$$\begin{aligned} \log g(s) &= -i\pi, \\ \exp\left(\int_{-\ell}^{\ell}\frac{\log g(s)}{s-z}\bar{d}s\right) &= \sqrt{\frac{z+\ell}{z-\ell}}, \\ -\zeta(-\ell) = \zeta(\ell) &= -\frac{1}{2}. \end{aligned}$$

For ν to be bounded $n_\ell = 1$ and $n_{-\ell}=0$ so that $\mathrm{Re}(\zeta(\pm\ell))+n_{\pm\ell}>0$. Thus

$$\nu(z) = \sqrt{(z-\ell)(z+\ell)}.$$

The solution ϕ is given by ($P=0$)

$$\phi(z) = \nu(z)\left(\int_{-\ell}^{\ell}\frac{(1-s)}{(s-z)}\frac{\bar{d}s}{\sqrt{(s-\ell)(s+\ell)}^+}\right),$$

provided that

$$\int_{-\ell}^{\ell}(1-s)\frac{\bar{d}s}{\sqrt{(s-\ell)(s+\ell)}^+} = -\frac{i}{2}\left(\ell^2-2\right) = 0.$$

The solution exists if $\ell=\sqrt{2}$. This example is directly related to that of equilibrium measures, see Chapter 10.

We conclude this section with another fairly simple example that is of use later.

Example 3.3.3. *Consider the RHP*

$$\phi^+(s) = \alpha\phi^-(s), \quad s\in[a,b], \quad \phi \text{ of finite degree at } \infty.$$

Set $\alpha = |\alpha|e^{i\theta}$ so that $\log\alpha = \log|\alpha| + i\theta$. We find a solution

$$\psi(z) = \exp\left(\frac{\log|\alpha|+i\theta}{2\pi i}\log\left(\frac{z-b}{z-a}\right)\right) = \left(\frac{z-b}{z-a}\right)^{-i\log|\alpha|/(2\pi)+\theta/(2\pi)}.$$

The general form of a solution is

$$\phi(z) = (z-a)^{n_a}(z-b)^{n_b}\psi(z),$$

with integers n_a, n_b chosen so that $-1 < n_a - \theta/(2\pi) < 1$ and $-1 < n_b + \theta/(2\pi) < 1$.

3.4 The solution of some matrix Riemann–Hilbert problems

The general form for the jump condition of a matrix RHP defined for a contour Γ is

$$\Phi^+(s) = \Phi^-(s)G(s) + F(s), \quad s \in \Gamma,$$

where $\Phi : \mathbb{C} \setminus \Gamma \to \mathbb{C}^{m\times n}$, $G : \Gamma \to \mathbb{C}^{n\times n}$ and $F : \Gamma \to \mathbb{C}^{m\times n}$. Most often in our applications, $m = n = 2$. We assume $m = n$ in what follows. Unlike scalar RHPs, matrix RHPs cannot, in general, be solved in closed form. Issues related to existence and uniqueness are also more delicate. The general theory involves the analysis of singular integral operators. Specifically, it involves questions related to their invertibility. We address this in Section 3.8. Here we take a constructive approach and describe a procedure for solving three types of RHPs: diagonal problems, constant jump matrix problems, and triangular problems.

All solution techniques in this section rely on the reduction of the matrix problem to a sequence of scalar problems. When these techniques fail we must develop a completely new theory that is in some sense independent of dimensionality. This will be developed in the remaining sections of this chapter.

3.4.1 Diagonal Riemann–Hilbert problems

Problem 3.4.1. *Consider RHPs of the form*

$$\Phi^+(s) = \Phi^-(s)D(s), \quad s \in \Gamma, \quad \Phi(\infty) = I, \quad \Phi : \mathbb{C} \setminus \Gamma \to \mathbb{C}^{n\times n}, \tag{3.4.1}$$

and $D(s) = \operatorname{diag}(d_1(s), \ldots, d_{nn}(s))$ with $\det D(s) \neq 0$. We assume that $\log d_i(s) \in C^{0,\alpha}(\Gamma)$ for each i and some $\alpha > 0$.

This problem decouples into n scalar RHPs:

$$\phi_i^+(k) = \phi_i^-(k)d_i(k), \quad k \in \Gamma, \quad \phi_i(\infty) = 1, \quad i = 1, \ldots, n. \tag{3.4.2}$$

Each of these has a solution

$$\phi_i(z) = \exp\left(\int_\Gamma \frac{\log d_i(s)}{s-z}\bar{d}s\right),$$

provided that $\operatorname{ind} \log d_i(s) = 0$. We assume this in what follows. A solution of (3.4.1) is given by $\Phi(z) = \operatorname{diag}(\phi_1(z), \ldots, \phi_n(z))$. If we restrict to smooth, closed and bounded contours the solution is unique. To see this let Ψ be another solution. It is clear $\Phi^{-1}(z)$ exists for all $z \in \mathbb{C} \setminus \Gamma$. Thus

$$\Psi^+(s)\Phi_-^{-1}(s) = \Psi^-(s)D(s)D^{-1}(s)\Phi_-^{-1}(s) = \Psi^-(s)\Phi_-^{-1}(s).$$

Liouville's theorem applied to each element shows that $\Psi(s)\Phi^{-1}(s)$ is constant. The condition at infinity implies Ψ and Φ are the same function. As one would imagine, the theory for diagonal matrix RHPs on open contours mimics that of scalar problems on open contours. This will be explored to some extent in the following section.

3.4.2 Constant jump matrix problems

Problem 3.4.2. *Consider the RHP*

$$\Phi^+(s) = \Phi^-(s)A, \quad s \in (a,b), \quad \Phi \text{ of finite degree at } \infty,$$

where A is an invertible, diagonalizable matrix $A = U\Lambda U^{-1}$, $\Lambda = \operatorname{diag}(\lambda_1, \ldots, \lambda_n)$.

The condition that the matrix is diagonalizable reduces this to a diagonal RHP for $H(s) = \Phi(s)U$:

$$H^+(s) = H^-(s) \begin{bmatrix} \lambda_1 & & & \\ & \lambda_2 & & \\ & & \ddots & \\ & & & \lambda_n \end{bmatrix}.$$

We decouple this as we did for (3.4.1):

$$H_i^+(s) = H_i^-(s)\lambda_i.$$

Example 3.3.3 gives us the form of all the possible solutions of this problem. Thus $\phi(z) = \operatorname{diag}(H_1(z), \ldots, H_n(z))U^{-1}$ is a solution. Note that if $\lambda_i = 0$ for some i the solution procedure fails.

Example 3.4.3. *Consider the RHP*

$$\Phi^+(s) = \Phi^-(s) \begin{bmatrix} 0 & c \\ 1/c & 0 \end{bmatrix}, \quad s \in (a,b), \quad c \neq 0, \quad \Phi \text{ of finite degree at } \infty.$$

First, diagonalize

$$\begin{bmatrix} 0 & 1/c \\ c & 0 \end{bmatrix} = U \begin{bmatrix} -1 & 0 \\ 0 & 1 \end{bmatrix} U^{-1}, \quad U^{-1} = \begin{bmatrix} -1/c & 1 \\ 1/c & 1 \end{bmatrix}.$$

We solve the two auxiliary problems

$$\begin{aligned} H_1^+(z) &= -H_1^-(z), \\ H_2^+(z) &= H_2^-(z). \end{aligned}$$

It is clear that $H_2(z) = 1$ and

$$H_1(z) = (z-a)^{n_a}(z-b)^{n_b}\sqrt{\frac{z-b}{z-a}}, \quad n_a = 0,1, \quad n_b = -1,0,$$

are the corresponding fundamental solutions. The solution is

$$\Phi(z) = \begin{bmatrix} -H_1(z)/c & H_1(z) \\ H_2(z)/c & H_2(z) \end{bmatrix}.$$

We can multiply Φ on the left by any matrix of polynomials to obtain another solution of finite degree.

We include one more example that is used later.

Example 3.4.4. *Consider the RHP*

$$\Phi^+(s) = \Phi^-(s) \begin{bmatrix} 0 & 1 \\ -1 & 0 \end{bmatrix}, \quad s \in (a,b), \quad \Phi \text{ of finite degree at } \infty.$$

First, diagonalize

$$\begin{bmatrix} 0 & 1 \\ -1 & 0 \end{bmatrix} = U \begin{bmatrix} i & 0 \\ 0 & -i \end{bmatrix} U^{-1}, \quad U^{-1} = \begin{bmatrix} -i & 1 \\ i & 1 \end{bmatrix}.$$

We solve the two auxiliary problems

$$\begin{aligned} H_1^+(z) &= iH_1^-(z), \\ H_2^+(z) &= -iH_2^-(z). \end{aligned}$$

We find that

$$\begin{aligned} H_1(z) &= \exp\left(\int_a^b \frac{\log i}{s-z} \bar{d}s\right) = \left(\frac{z-b}{z-a}\right)^{1/4}, \\ H_2(z) &= \exp\left(\int_a^b \frac{\log -i}{s-z} \bar{d}s\right) = \left(\frac{z-b}{z-a}\right)^{-1/4}, \end{aligned}$$

are the corresponding fundamental solutions. The solution is

$$\Phi(z) = \begin{bmatrix} -iH_1(z) & H_1(z) \\ iH_2(z) & H_2(z) \end{bmatrix}.$$

Again, we can multiply Φ on the left by any matrix of polynomials to obtain another solution of finite degree.

3.4.3 Triangular Riemann–Hilbert problems

We restrict attention to smooth, closed and bounded contours. Consider the RHP of the form

$$\Phi^+(s) = \Phi^-(s)U(s), \quad s \in \Gamma, \quad \Phi(\infty) = I,$$

where $U(s)$ is upper triangular. To ensure unique solvability, assume $\operatorname{ind}_\Gamma U_{i,i}(s) = 0$ for $i = 1, \ldots, n$. This can be generalized. In essence, this problem is solved solving successive

scalar RHPs. It is important to note that each row can be solved independent of other rows. The first row of the solution is determined by the following scalar problems

$$\begin{aligned}
&\Phi^+_{1,1}(s) = \Phi^-_{1,1}(s)U_{1,1}(s), && \Phi_{1,1}(\infty) = 1,\\
&\Phi^+_{1,2}(s) = \Phi^-_{1,2}(s)U_{2,2}(s) + \Phi^-_{1,1}(s)U_{1,2}(s), && \Phi_{1,2}(\infty) = 0,\\
&\Phi^+_{1,3}(s) = \Phi^-_{1,3}(s)U_{3,3}(s) + \Phi^-_{1,1}(s)U_{1,3}(s) + \Phi^-_{1,2}(s)U_{2,3}(s), && \Phi_{1,3}(\infty) = 0,\\
&\quad\vdots
\end{aligned}$$

Note that $\Phi^-_{1,1}(s)U_{1,2}(s)$ in the second equation above can be considered an inhomogeneous term since $\Phi_{1,1}$ is known for the first equation. For the second row,

$$\begin{aligned}
&\Phi^+_{2,1}(s) = \Phi^-_{2,1}(s)U_{1,1}(s), && \Phi_{2,1}(\infty) = 0,\\
&\Phi^+_{2,2}(s) = \Phi^-_{2,2}(s)U_{2,2}(s) + \Phi^-_{2,1}(s)U_{1,2}(s), && \Phi_{2,2}(\infty) = 1,\\
&\Phi^+_{2,3}(s) = \Phi^-_{2,3}(s)U_{3,3}(s) + \Phi^-_{2,1}(s)U_{1,3}(s) + \Phi^-_{2,2}(s)U_{2,3}(s), && \Phi_{2,3}(\infty) = 0,\\
&\quad\vdots
\end{aligned}$$

From the condition $\operatorname{ind} U_{1,1}(s) = 0$ we know $\Phi_{2,1}(z) = 0$ which means that the RHP for $\Phi_{2,2}$ is homogeneous and the condition at infinity can be satisfied. In general, for row j, the first $j-1$ entries vanish identically. We present the general procedure.

1. Solve

$$\Phi^+_{j,j}(s) = \Phi^-_{j,j}(s)U_{j,j}(s), \quad \Phi_{j,j}(\infty) = 1, \quad j = 1, \dots, n.$$

   All of these solutions exist and are unique by the imposed index conditions.

2. For each $j = 1, \dots, n$, solve for $i = 1, \dots, n-j$

$$\begin{aligned}
\Phi^+_{j,j+i}(s) &= \Phi^-_{j,j+i}(s)U_{j+1,j+1}(s) + F_{i,j}(s),\\
F_{i,j}(s) &= \sum_{k=1}^{i-1} \Phi_{i,i-k}(s)U_{i-k,j}(s).
\end{aligned}$$

The resulting solution is unique. This can be shown by the same argument used at the end of Section 3.4.1.

Remark 3.4.5. *We can solve a general problem of the form*

$$\Phi^+(s) = \Phi^-(s)A,$$

where A is a constant, possibly non-normal, matrix. We find its Jordan normal form and apply the method for upper triangular RHPs.

We end this section with an important example that connects matrix RHPs with scalar RHPs.

Example 3.4.6. *Consider the RHP*

$$\Phi^+(s) = \Phi^-(s) \begin{bmatrix} 1 & f(s) \\ 0 & 1 \end{bmatrix}, \quad f \in C^{0,\alpha}(\Gamma), \quad \Phi(\infty) = I.$$

We follow the general procedure. First solve

$$\Phi^+_{1,1}(s) = \Phi^-_{1,1}(s), \quad \Phi_{1,1}(\infty) = 1,$$
$$\Phi^+_{2,2}(s) = \Phi^-_{2,2}(s), \quad \Phi_{2,2}(\infty) = 1.$$

It is clear that $\Phi_{1,1} = \Phi_{2,2} = 1$. *It remains to find* $\Phi_{1,2}$*:*

$$\Phi^+_{1,2}(s) = \Phi^-_{1,2}(s) + f(s), \quad \Phi_{1,2}(\infty) = 0.$$

Therefore $\Phi_{1,2}(z) = \mathcal{C}_\Gamma f(z)$ *and*

$$\Phi(z) = \begin{bmatrix} 1 & \mathcal{C}_\Gamma f(z) \\ 0 & 1 \end{bmatrix}.$$

3.5 Hardy spaces

In this section we discuss functions analytic off a contour which have boundary values (in some sense) on that contour. This is a natural setting in which to study RHPs. This allows the extension of the Cauchy integral formula to a larger class of functions and it allows precise properties of the Cauchy integral to be established. The following results are closely related to L^p spaces. All results are proved for $p = 2$. When the generality does not distract from the end goal, we state results for general p.

3.5.1 Hardy spaces on the unit disk

Let $f(z)$ be analytic for $z \in \mathbb{U} = \{|z| < 1\}$. For $r < 1$ and $0 < p \leq \infty$ we define the quantity

$$M_p(f, r) = \int_{|z|=r} |f(z)|^p |dz|.$$

Definition 3.5.1. *We say that a function is of class* $\mathcal{H}^p$ *if*

$$\sup_{r<1} M_p(f, r) < \infty.$$

We state an essential result, see [47].

Theorem 3.5.2. *If* $f \in \mathcal{H}^p$ *for* $0 < p < \infty$*, define* $f(z) = \lim_{r\to 1^-} f(rz)$ *for* $z \in \mathbb{U}$ *whenever the limit exists. Then* f *is defined a.e. (*i.e*, the limit exists a.e.),*

$$\lim_{r\to 1^-} M_p(f, r) = M_p(f, 1),$$

and

$$\lim_{r\to 1^-}\int_{\partial\mathbb{U}}|f(rz)-f(z)|^p|dz|=0.$$

Another result that is of fundamental importance for what follows is also found in [47]:

Theorem 3.5.3. *Every function $f\in\mathcal{H}^1$ can be expressed as the Cauchy integral of its boundary function. In fact,*

$$f^{(k)}(z)=k!\int_{\partial\mathbb{U}}\frac{f(\zeta)}{(\zeta-z)^{k+1}}d\bar{\zeta},\quad |z|<1,\quad k\in\mathbb{N},$$

and this integral vanishes identically for $|z|>1$.

Since $\partial\mathbb{U}$ is of finite measure, $\mathcal{H}^p\subset\mathcal{H}^1$ for all $p>1$.

3.5.2 Hardy spaces on general domains

The theory for the unit circle does not suffice for the RHPs we consider. We could deal with general domains by conformal mapping. In going from the unit circle to the real line we can use the fractional transformation

$$k=i\frac{z+1}{z-1},$$

to map the unit circle in the z-plane to the real line in the k-plane. If this is used as a change of variables in an integral then

$$dz\mapsto\frac{2}{i(k-i)^2}dk.$$

Proceeding this way, the Hardy space on the line will not share a nice relationship with $L^p(\mathbb{R})$. It is clear below why such a straightforward relationship is beneficial. To develop a different definition we follow [47], Chapter 10 for bounded domains. Then we make the extension to unbounded domains. Assume $D\subset\mathbb{C}$ is simply connected and ∂D is a rectifiable Jordan curve (*i.e.* a non-self-intersecting, continuous closed curve).

Definition 3.5.4. *A function $f(z)$ analytic in D is of class $\mathcal{E}^p(D)$ if there exists a sequence C_i, $i=1,2,\ldots$, of rectifiable curves tending to ∂D in the sense that C_i eventually encloses every compact subset of D on the Riemann sphere, such that*

$$\limsup_{i\to\infty}\int_{C_i}|f(z)|^p|dz|<\infty.$$

We summarize some results from [47] in the following theorem:

Theorem 3.5.5. *Let $\phi(w)$ map $\{|w|<1\}$ conformally onto D, and let Γ_r be the image of $|w|=r$ under ϕ. Then the following are equivalent:*

- $\sup_{r<1}\int_{\Gamma_r}|f(z)|^p|dz|<\infty$,

- $f(z) \in \mathcal{E}^p(D)$,
- $F(w) = f(\varphi(w))[\varphi'(w)]^{1/p} \in \mathcal{H}^p$ *for some conformal mapping* $\varphi(w)$ *of* $|w| < 1$ *onto* D,
- $F(w) \in \mathcal{H}^p$ *for all such mappings* φ.

Furthermore, Theorem 3.5.3 holds with $\partial\mathbb{U}$ replaced by ∂D. This shows that Definition 3.5.4 is a consistent extension of Definition 3.5.1.

Remark 3.5.6. *If there exists* $C > 1$ *such that*

$$\frac{1}{C} < |\varphi'(w)| < C,$$

then $\mathcal{E}^p(D)$ *and* $\mathcal{H}^p$ *are isomorphic.*

Define the space $\mathcal{E}^p(D_-)$ which is the class of functions analytic on $\mathbb{C} \setminus \overline{D}$ with finite L^p norms as curves approach ∂D in analogy with Definition 3.5.4. For the Cauchy integral formula to hold we need to impose the restriction that $f(\infty) = 0$.

Denote the class of Jordan curves which tend to straight lines at infinity by Σ_∞. We now use all of these ideas to deal with a simply connected, unbounded domain. We still need to ensure that ∂D is regular enough at ∞ so we ask that $\partial D \in \Sigma_\infty$. This will always be assumed unless specified otherwise.

Definition 3.5.7. *When* D *is unbounded, a function* $f(z)$ *analytic in* D *is of class* $\mathcal{E}^p(D)$ *if there exists a sequence* $C_n \in \Sigma_\infty$, $n = 1, 2, \ldots$, *of curves tending to* ∂D, *in the sense that* C_n *eventually surrounds every compact subset of* D, *such that*

$$\int_{C_n} |f(z)|^p |dz| \leq M < \infty.$$

Theorem 3.5.8 ([117])**.** *The Cauchy integral formula holds for every* $f \in \mathcal{E}^p(D)$, $1 \leq p < \infty$, *even when* $\infty \in \partial D$.

Proof. Assume that $0 \in \mathbb{C} \setminus \overline{D}$. Consider the conformal map $z \mapsto 1/z$. It is clear that the Cauchy integral formula holds if and only if

$$\frac{1}{z} f\left(\frac{1}{z}\right) = \int_{\partial D^{-1}} \frac{\frac{1}{\zeta} f\left(\frac{1}{\zeta}\right)}{\zeta - z} d\bar{\zeta}, \quad z \in \partial D,$$

where $D^{-1} = \{z : 1/z \in D\}$. Let $\Gamma \in \Sigma_\infty$ be a curve in D. Then Γ^{-1} is a rectifiable curve in $\overline{D^{-1}}$ and

$$\int_{\Gamma^{-1}} |1/zf(1/z)||dz| = \int_\Gamma |1/zf(z)||dz| \leq \|1/z\|_{L^q(\Gamma)} \|f\|_{L^p(\Gamma)}, \quad (1/p + 1/q = 1).$$

So $\|1/z\|_{L^q(\partial D)} < \infty$ since $q > 1$. This shows that $1/zf(1/z) \in \mathcal{E}^p(D^{-1})$ since $\|1/z\|_{L^q(\Gamma)} < C$ where C only depends on D and q. Therefore the Cauchy integral formula holds and the conclusion follows. ∎

We look to provide an additional characterization of $\mathcal{E}^p(D)$. To do this we need to restrict the class of curves. First, we assume ∂D is Lipschitz and in Σ_∞. After possible rotation, we assume the form

$$\partial D = \{x + i\nu(x) : x \in \mathbb{R}\},$$

where ν is real-valued and $\|\nu'\|_\infty < \infty$. Such a curve will be referred to as a *Lipschitz graph*. We restrict the approximating curves C_n. Assume the sequence C_n is given by a shift of ∂D:

$$C_n = \{z + i\nu(x) + i/n : z \in \partial D\}.$$

Other choices of C_n yield the same result. In particular this says that the curves C_n are Lipschitz with uniformly bounded Lipschitz constant. As before, let $C_n^+ = \{z : \operatorname{Im} z > |\nu(x) + 1/n|\}$. Define the distance to the curve

$$d_\Gamma(z) = \inf_{a\in\Gamma} |a - z|.$$

It is clear that

$$|d_\Gamma(z) - d_{C_n}(z)| < 1/n, \quad \forall z \in C_n^+.$$

Lemma 3.5.9. *The map $f \mapsto \|f\|_{\mathcal{E}^p(D)} = \limsup_{n\to\infty} \|f\|_{C_n}$ satisfies*

$$\|f\|_{L^p(\partial D)} \le \|f\|_{\mathcal{E}^p(D)}. \tag{3.5.1}$$

Additionally, $\|f\|_{\mathcal{E}^p(D)}$ defines a norm on $\mathcal{E}^p(D)$.

Proof. It is clear that $\|\cdot\|_{\mathcal{E}^p(D)}$ defines a semi-norm. Since the Cauchy integral formula holds for each $f \in \mathcal{E}^p(D)$, (3.5.1) shows it is a norm. Now we prove (3.5.1). It follows from previous results that $z^{-1}f(z^{-1}) \in \mathcal{E}^p(D^{-1})$ and has limits a.e. on ∂D^{-1}. This implies

$$f(z + i/n) \to f(z) \text{ a.e. }.$$

We have for $n > 1$

$$\int_{C_n} |f(z)|^p |dz| = \int_\Gamma |f(z + i/n)|^p |dz|.$$

Fatou's Lemma gives

$$\begin{aligned}\int_\Gamma |f(z)|^p |dz| \le \liminf_{n\to\infty} \int_\Gamma |f(z + i/n)|^p |dz| &\le \limsup_{n\to\infty} \int_{C_n} |f(z)|^p |dz| \\ &= \limsup_{n\to\infty} \int_{C_n} |f(z)|^p |dz|,\end{aligned}$$

and the lemma is proved. ∎

Given a Lipschitz graph Γ, define the weighted Bergman space by

$$\mathcal{B}^+(\Gamma) = \{f \text{ holomorphic in } \Gamma^+ : \|f\|_{\mathcal{B}^+(\Gamma)} < \infty\},$$

with norm defined by

$$\|f\|_{\mathcal{B}^+(\Gamma)} = \left(\iint_{\Gamma^+} |f(z)|^2 d_\Gamma(z) dxdy \right)^{1/2}.$$

$\mathcal{B}^+(\Gamma)$ is a Hilbert space [19].

We pause for some technical lemmas that are required in what follows. Note that the following results make explicit use of the Hilbert space structure. Therefore we restrict to $p = 2$. The main results here, Lemma 3.5.12 and Theorem 3.5.13, hold for $1 < p < \infty$ [76].

Lemma 3.5.10 ([19])**.** *Suppose $f \in L^2(\Gamma)$ and define $F = \mathcal{C}_\Gamma f$. Then*

$$\|F\|_{L^2(\Gamma)} \leq C(1 + \|\nu'\|_\infty)\|F'\|_{\mathcal{B}^+(\Gamma)}.$$

Lemma 3.5.11 ([19])**.** *Let $f \in \mathcal{H}^+(\Gamma)$ and define*

$$Tf(\zeta) = \int \int_{\Gamma^+} \frac{f(z) d_\Gamma(z)}{(z-\zeta)^2} dxdy, \quad \zeta \in \Gamma.$$

Then $\|Tf\|_{L^2(\Gamma)} \leq C(1 + \|\nu'\|_\infty)\|f\|_{\mathcal{B}^+(\Gamma)}$.

Lemma 3.5.12. *Let $\Gamma_1 = \{x + i\nu_1(x) : x \in \mathbb{R}\}$ be a Lipschitz graph in $\overline{\Gamma^+}$. Then for $f \in L^2(\Gamma)$,*

$$\|\mathcal{C}_\Gamma^+ f\|_{L^2(\Gamma_1)} \leq C(1 + \|\nu_1'\|_\infty)(1 + \|\nu'\|_\infty)\|f\|_{L^2(\Gamma)}.$$

Proof. To prove this we follow [19]. Let

$$B = \{h \in \mathcal{H}^+(\Gamma) : \|h\|_{\mathcal{H}^+(\Gamma)} \leq 1, \ h \text{ compactly supported in } \Gamma^+\}.$$

Then we know that for any $f \in \mathcal{H}^+(\Gamma)$, $\|f\|_{\mathcal{H}^+(\Gamma)} = \sup_{h \in B} |\langle f, h \rangle_{\mathcal{H}^+(\Gamma)}|$. Also define $\mathcal{C}_\Gamma^{+\prime} f(z) = d/dz \mathcal{C}_\Gamma^+ f(z)$. Lemma 3.5.10 applied to Γ_1 and Γ_1^+ along with Fubini's Theorem gives

$$\begin{aligned} \|\mathcal{C}_\Gamma^+ f\|_{L^2(\Gamma_1)} &\leq C(1 + \|\nu_1'\|_\infty)\|\mathcal{C}_\Gamma^{+\prime} f\|_{\mathcal{H}^+(\Gamma_1^+)} \\ &= C(1 + \|\nu_1'\|_\infty) \left(\iint_{\Gamma_1^+} |\mathcal{C}_\Gamma^{+\prime} f(z)|^2 d_{\Gamma_1}(z) dxdy \right)^{1/2}. \end{aligned}$$

From the choice of Γ_1 we have that $d_{\Gamma_1}(z) \leq d_\Gamma(z)$, so

$$\begin{aligned}
\iint_{\Gamma_1^+} |\mathcal{C}_\Gamma^{+\prime} f(z)|^2 d_{\Gamma_1}(z)dxdy &\leq \int\int_{\Gamma^+} |\mathcal{C}_\Gamma^{+\prime} f(z)|^2 d_\Gamma(z)dxdy \\
&= \sup_{h\in B} |\langle \mathcal{C}_\Gamma^{+\prime} f, h\rangle_{\mathcal{H}^+(\Gamma)}|^2 \\
&= \sup_{h\in B} \left| \int\int_{\Gamma^+} \left(-\int_\Gamma \frac{f(\zeta)d\zeta}{(z-\zeta)^2} \right) \overline{h(z)} d_\Gamma(z)dxdy \right|^2 \\
&= C \sup_{h\in B} \left| \int_\Gamma f(\zeta) T(\overline{h})(\zeta) d\zeta \right|^2 \\
&\leq \sup_{h\in B} \|f\|_{L^2(\Gamma)} \|T(\overline{h})\|_{L^2(\Gamma)}^2 \\
&\leq C(1+\|\nu'\|_\infty)^2 \|f\|_{L^2(\Gamma)}^2.
\end{aligned}$$

This proves the lemma. □

Theorem 3.5.13. *$\mathcal{C}_\Gamma^+ g \in \mathcal{E}^2(\Gamma^+)$ whenever $g \in L^2(\Gamma)$.*

Proof. It suffices to show that $\mathcal{C}_\Gamma^+$ is a bounded operator from $L^2(\Gamma)$ to $L^2(C_n)$ and the bound can be taken to be uniform in n. Applying Lemma 3.5.12 to the sequence $\{C_n\}$ proves the result. □

Corollary 3.5.14. *The following are direct consequences of Theorem 3.5.13. Assume that $\Gamma \in \Sigma_\infty$, then*

- *$\mathcal{E}^2(\Gamma^+) = \{\mathcal{C}_\Gamma^+ f : f \in L^2(\Gamma)\}$,*
- *$\|\cdot\|_{L^2(\Gamma)}$ and $\|\cdot\|_{\mathcal{E}^2(\Gamma^+)}$ define equivalent norms,*
- *$\mathcal{E}^2(\Gamma^+)$ is a Hilbert Space, and*
- *$\mathcal{C}_\Gamma^\pm$ is well-defined and bounded from $L^2(\Gamma)$ to itself.*

Since the Cauchy integral formula holds when applied to $\mathcal{E}^2(\Gamma^+)$ functions we have that $\mathcal{C}_\Gamma^+ f - f = 0$ a.e on Γ for $f \in \mathcal{E}^2(\Gamma^+)$. It follows from Theorem 3.5.13 that

$$\left\| \frac{d}{dz} \mathcal{C}_\Gamma (\mathcal{C}^+{}_\Gamma f - f) \right\|_{\mathcal{B}^+(\Gamma)} \leq \|\mathcal{C}_\Gamma^+ f - f\|_{L^2(\infty)} = 0.$$

Therefore $\mathcal{C}_\Gamma^+(\mathcal{C}_\Gamma^+ f - f)$ is constant. That constant must be zero from the $z \to \infty$ limit. We obtain

$$\mathcal{C}_\Gamma^+ \mathcal{C}_\Gamma^+ f = \mathcal{C}_\Gamma^+ f, \tag{3.5.2}$$

and C_Γ^+ is a projector on $L^2(\Gamma)$. Also, it is well-known that the Plemelj formula holds:

$$\mathcal{C}_\Gamma^+ f - \mathcal{C}_\Gamma^- f = f, \tag{3.5.3}$$

for $f \in L^2(\Gamma)$. This can be seen by the fact that for $f \in L^2(\Gamma)$, $F(x) = f(\ell(x)) \in L^2(\mathbb{R})$, $\ell(x) = x + i\nu(x)$. Approximate F by step functions F_n in $L^2(\mathbb{R})$. Then $f_n = F_n \circ \ell^{-1}$ converges to f in $L^2(\Gamma)$. It is straightforward to check that $\mathcal{C}_\Gamma^+ f_n(s) - \mathcal{C}_\Gamma^- f_n(s) = f_n(s)$ a.e.. This implies the Plemelj formula for all $L^2(\Gamma)$ functions. Alternatively, the result follows from Theorem A.0.13.

We know that if $f \in \mathcal{E}^2(\Gamma^+)$ then $C_\Gamma^+ f = f$. This implies that

$$\mathcal{C}_\Gamma^- f = 0, \quad f \in \mathcal{E}^2(\Gamma^+). \tag{3.5.4}$$

If we consider $\mathcal{E}^2(\Gamma^-)$ then we replace + with − in (3.5.4) and (3.5.2) becomes

$$\mathcal{C}_\Gamma^- \mathcal{C}_\Gamma^- f = -\mathcal{C}_\Gamma^- f, \tag{3.5.5}$$

when we take orientation into account.

Example 3.5.15. *Consider the derivation of* (2.1.4) *and more specifically,* (2.1.6)*. We relax the assumption $q_0 \in \mathcal{S}_\delta(\mathbb{R})$ to $q_0 \in H^1(\mathbb{R})$. What follows is performed assuming global existence of a solution in $H^1(\mathbb{R})$. We have two claims to show:*

- *$\mu^\pm(x,t;\cdot) \in \mathcal{E}^2(\Gamma^\pm)$, and*
- *$q(x,t) = i \lim_{|k|\to\infty} k\mu(x,t;k)$.*

Then (2.1.6) *follows since $\hat{q}_0 \in L^1(\mathbb{R})$ (see Lemma 3.6.9). We show the claims only for μ^+ since they follow for μ^- follows in precisely the same way. Let $k = k_r + ik_i$ and it is clear that*

$$\left\| \int_{-\infty}^{x} e^{i(\cdot + ik_i)(x-s)} q(s,t) ds \right\|_{L^2(\mathbb{R})} \leq \|q(\cdot,t)\|_{L^2((-\infty,x))} \leq \|q(\cdot,t)\|_{L^2(\mathbb{R})} \tag{3.5.6}$$

since the Fourier transform is unitary on $L^2(\mathbb{R})$. This shows $\mu^+(x,t;\cdot) \in \mathcal{E}^2(\mathbb{R}^+)$. To show the second claim it suffices to show that $\mu_x(x,t;k) = o(1)$ as $|k| \to \infty$ for k bounded away from the real line. We integrate the expression for μ_x^+ by parts:

$$\mu_x(x,t;k) = q(x,t) + ik \int_{-\infty}^{x} e^{ik(x-s)} q(s,t) ds = \int_{-\infty}^{x} e^{ik(x-s)} q_x(s,t) ds.$$

Replacing q with q_x in (3.5.6) *shows that $\mu_x(x,t;\cdot) \in \mathcal{E}^2(\mathbb{R}^-)$. To prove the last claim we appeal to Lemma 3.6.11.*

It may seem unsatisfactory that we have used properties of the Fourier transform in this derivation. One often thinks of the Lax pair as a replacement for guessing the necessary transform. Invoking properties of the Fourier transform becomes necessary as one reduces regularity. Note that the derivation of (2.1.6) *under more restrictive conditions required no knowledge of the Fourier transform.*

3.6 Cauchy integrals on intersecting contours

As seen above, the theory of Cauchy integrals is more naturally developed in L^p spaces. This development extends in a straightforward way to contours with self intersections,

provided that the contour can be separated into Lipschitz components. We concentrate on $p = 2$ but the results extend to $1 < p < \infty$. We have shown that if Γ is a Lipschitz graph then

$$\|\mathcal{C}_\Gamma f\|_{L^2(\Gamma)} \leq C(K)\|f\|_{L^2(\Gamma)},$$

where $C(K)$ depends continuously on the Lipschitz constant of Γ.

Corollary 3.6.1. *Assume Γ is a Lipschitz graph defined by $x+i\varphi(x)$, $x \in \mathbb{R}$, after possible rotation. Let $\Gamma_{a,b} = \{x + i\varphi(x) : x \in (a, b)\}$ for $a < b$ in the extended real numbers. Then for $f \in L^2(\Gamma_{a,b})$, and $c < d$*

1. *$\|\mathcal{C}_{\Gamma_{a,b}} f\|_{L^2(\Gamma_{c,d})} \leq C(K)\|f\|_{L^2(\Gamma_{a,b})}$, and specifically,*
2. *$\|\mathcal{C}_{\Gamma_{a,b}} f\|_{L^2(\Gamma_{a,b})} \leq C(K)\|f\|_{L^2(\Gamma_{a,b})}$,*

with the same constant $C(K)$ as in Lemma 3.5.12 with $\nu_1 = \nu$.

Proof. Let f be defined on $\Gamma_{a,b}$. Extend it to Γ by $f = 0$ on $\Gamma \setminus \Gamma_{a,b}$. Then

$$\|\mathcal{C}_{\Gamma_{a,b}} f\|_{L^2(\Gamma_{c,d})} = \|\mathcal{C}_\Gamma f\|_{L^2(\Gamma_{c,d})} \leq \|\mathcal{C}_\Gamma f\|_{L^2(\Gamma)} \leq C(K)\|f\|_{L^2(\Gamma)} = C(K)\|f\|_{L^2(\Gamma_{a,b})}.$$

Set $c = a,\ d = b$ to obtain the second claim. □

Remark 3.6.2. *This corollary states that if one can extend a finite or semi-infinite contour Γ to be a Lipschitz graph by adding contours then $\mathcal{C}_\Gamma^\pm$ is a bounded operator on $L^2(\Gamma)$. This can be done by adding contours with constant slope that do not increase the Lipschitz constant.*

Lemma 3.6.3. *Let $\Gamma = \Gamma_1 \cup \cdots \cup \Gamma_l$ where each Γ_i is a smooth non-self-intersecting contour. Assume there exist constants C_{ij} such that for $f \in L^2(\Gamma_j)$, $\|\mathcal{C}_{\Gamma_j} f\|_{L^2(\Gamma_i)} \leq C_{ji}\|f\|_{L^2(\Gamma_j)}$ Then*

$$\|\mathcal{C}_\Gamma f\|_{L^2(\Gamma)} \leq C\|f\|_{L^2(\Gamma)}, \quad C = \max_{1\leq j\leq n} \left(\sum_{i=1}^n C_{ji}^2\right)^{1/2}.$$

Proof. Define χ_i to be the characteristic function of Γ_i. We write

$$\begin{aligned}
\|\mathcal{C}_\Gamma f\|_{L^2(\Gamma)} &= \left\| \sum_{i=1}^n \chi_i \mathcal{C}_\Gamma \left(\sum_{j=1}^n \chi_j f \right) \right\|_{L^2(\Gamma)} = \left\| \sum_{i=1}^n \chi_i \sum_{j=1}^n \mathcal{C}_{\Gamma_j} f \right\|_{L^2(\Gamma)} \\
&\leq \sum_{i=1}^n \sum_{j=1}^n \left\| \chi_i \mathcal{C}_{\Gamma_j} f \right\|_{L^2(\Gamma)} = \sum_{i=1}^n \sum_{j=1}^n \left\| \mathcal{C}_{\Gamma_j} f \right\|_{L^2(\Gamma_i)} \\
&\leq \sum_{j=1}^n \sum_{i=1}^n C_{ji} \|f\|_{L^2(\Gamma_j)} \leq \max_j \left(\sum_{i=1}^n C_{ji}^2 \right)^{1/2} \left(\sum_{j=1}^n \|f\|_{L^2(\Gamma_j)}^2 \right)^{1/2}.
\end{aligned}$$

The final inequality follows from the Cauchy-Schwarz inequality. □

The lemma can be used to extend the boundedness of $\mathcal{C}_\Gamma^\pm$ to curves that can be decomposed into a finite number of Lipschitz components with transverse intersections. It is worth nothing that this process does not result in the optimal bound on the Cauchy integral operator. The following lemma demonstrates how the decomposition leads us to an extension, in a simple case.

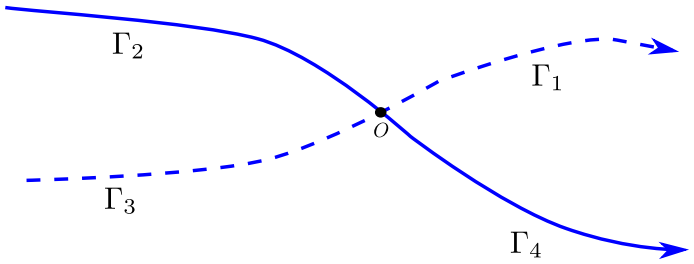

Figure 3.6.1: The intersection of two Lipschitz graphs Γ (dashed) and Γ' (solid).

Lemma 3.6.4. *Let Γ and Γ' be two Lipschitz graphs that intersect at a single point in the finite plane, see Figure 3.6.1. Without loss of generality we assume the intersection point is the origin. Let Γ_i, $i = 1, \dots, 4$ be the components of $\Gamma \cup \Gamma' \setminus \{0\}$. Assume that every combination $\Gamma_{ij} = \Gamma_i \cup \Gamma_j$ for $i \neq j$ is a Lipschitz graph. Then $\mathcal{C}_{\Gamma\cup\Gamma'}$ is bounded on $L^2(\Gamma \cup \Gamma')$ with a constant that depends only on the Lipschitz constants of Γ_{ij}.*

Proof. By Lemma 3.6.3 it suffices to show the existence of $C_{ji} > 0$, depending on just Lipschitz constants, such that $\|\mathcal{C}_{\Gamma_i} f\|_{L^2(\Gamma_j)} \leq C_{ji} \|f\|_{L^2(\Gamma_i)}$. Corollary 3.6.1 shows their existence. □

More generally, if Γ can be broken up into contours $\{\Gamma_i\}_{i=1}^n$ such that for $i \neq j$, there exists a Lipschitz graph Γ_{ij} such that $\Gamma_i \cup \Gamma_j \subset \Gamma_{ij}$ then $\mathcal{C}_\Gamma^\pm$ is bounded on $L^2(\Gamma)$. Using these ideas, we aim to define Hardy spaces of functions when Γ has intersections. The following three definitions accomplish this.

Definition 3.6.5. *Γ is said to be an admissible contour if*

- *Γ is complete with only transverse self-intersections and*
- *for each $D \Subset \Omega_\pm$, ∂D is piecewise smooth and if ∂D is unbounded, it is a Lipschitz graph.*

Remark 3.6.6. *From Lemma 3.5.12, Corollary 3.6.1 and Lemma 3.6.3 it follows that $\mathcal{C}_\Gamma^\pm$ are bounded as operators on $L^2(\Gamma)$ whenever Γ is admissible.*

Definition 3.6.7. *If Γ is an admissible contour then $\mathcal{E}^\pm(\Gamma)$ consists of functions F holomorphic in $\Omega_\pm$, such that $F \in \mathcal{E}^2(D_i)$ for each $D_i \Subset \Omega_\pm$. It is clear that $\mathcal{E}^\pm(\Gamma)$ may be identified with*

$$\bigoplus_i \mathcal{E}^2(D_i).$$

Definition 3.6.8. *A function Φ is a $\mathcal{E}^{\pm}(\Gamma)$ solution of a RHP if it satisfies the jump condition and $(\Phi - I)|_{\Omega_\pm} \in \mathcal{E}^{\pm}(\Gamma)$ or $\Phi - I \in \mathcal{E}^{+}(\Gamma) \oplus \mathcal{E}^{-}(\Gamma)$.*

Note that this definition, in some sense, captures the $\Phi(\infty) = I$ condition and that the Cauchy integral formula holds for these functions, for each $D \Subset \Omega_\pm$ we have $\Phi = I + \mathcal{C}_{\partial D} u$ for $u \in \mathcal{E}^2(D)$, implying $u \in L^2(\partial D)$. From above, (3.5.4) implies that $\mathcal{C}_{\partial D} u$ vanishes identically outside D. By patching together these representations we find that $\Phi = I + \mathcal{C}_\Gamma \hat{u}$ for some $\hat{u} \in L^2(\Gamma)$.

We end this section with estimates that are useful in what follows.

Lemma 3.6.9. *If $f(s),\ sf(s) \in L^2(\Gamma)$ then the following estimate holds:*

$$\int_\Gamma \frac{f(s)}{s-z} \bar{d}s = -\frac{1}{z} \int_\Gamma f(s) \bar{d}s + \mathcal{O}(z^{-2}),$$

if z, sufficiently large, satisfies $\inf_{s\in\Gamma} |\arg z - \arg s| > c > 0$.

Proof. Consider

$$\left| \int_\Gamma \frac{f(s)}{s-z} \bar{d}s + \frac{1}{z} \int_\Gamma f(s) \bar{d}s \right| \le |z|^{-1} \left(\int_\Gamma |(1+|s|) f(s)|^2 \bar{d}s \right)^{1/2} \left(\int_\Gamma \frac{1}{(1+|s|)^2} |H(s,z)|\, \bar{d}s \right)^{1/2},$$

$$H(s,z) = \frac{1}{(s/z) - 1} + 1.$$

Since $(1+|s|)^{-2}$ is integrable, by the Dominated Convergence Theorem it suffices to show that $H(s,z)$ is bounded, uniformly in s and z and tends to zero as $z \to \infty$ for each fixed s. The latter statement is clear. We prove the former. Assume $z \ge 1$ and let $s/z = |r| e^{i\theta}$, $|\theta| > c$. Therefore

$$|(s/z) - 1|^2 = (r\cos\theta - 1)^2 + r^2 \sin^2\theta > \begin{cases} (r\cos\theta - 1)^2, & \text{if } r < 1/(2\cos\theta), \\ r^2 \sin^2\theta, & \text{if } r \ge 1/(2\cos\theta). \end{cases}$$

Thus

$$|(s/z) - 1|^2 \ge \begin{cases} 4, & \text{if } r < 1/(2\cos\theta), \\ \frac{1}{2}\tan^2\theta, & \text{if } r \ge 1/(2\cos\theta). \end{cases}$$

Thus $H(s,z)$ is bounded uniformly in z and s. □

The assumptions in this lemma can be relaxed at the expense of weaker asymptotics.

Lemma 3.6.10. *For $f \in L^1(\Gamma)$,*

$$\lim_{z\to\infty} z \int_\Gamma \frac{f(s)}{s-z} \bar{d}s = -\int_\Gamma f(s) \bar{d}s,$$

where the limit is taken in a direction that is not tangential to Γ.

Different results hold for $f \in L^2(\Gamma)$:

Lemma 3.6.11. *If $f \in L^2(\Gamma)$ then the following estimate holds:*

$$\int_\Gamma \frac{f(s)}{s-z}\bar{d}s = o(1),$$

if z, sufficiently large, satisfies $\inf_{s\in\Gamma} |\arg z - \arg s| > c > 0$.

Proof. Consider

$$\left|\int_\Gamma \frac{f(s)}{s-z}\bar{d}s\right| \leq \|f\|_{L^2(\Gamma)} \left(\int_\Gamma \frac{|\bar{d}s|}{|s-z|^2}\right)^{1/2}. \tag{3.6.1}$$

The calculations in the proof of Lemma 3.6.9 show that under the hypothesis $\inf_{s\in\Gamma} |\arg z - \arg s| > c > 0$ $|s-z|^{-2} \leq C(1+|s|)^2$ for some constant $C > 0$. The Dominated Convergence Theorem applied to the last integral in (3.6.1) proves the result. □

3.7 Sobolev spaces

In applications stemming from RHPs and in the numerical solution of RHPs, the smoothness of the solutions on the boundary is a necessary object of study. We begin with a discussion of differentiability on oriented contours.

Let Γ be a smooth contour and $f : \Gamma \to \mathbb{C}$. We say f is Γ-differentiable if for each $s^* \in \Gamma$ there exists a value $f'(s^*)$ such that for $s \in \Gamma$

$$f(s) = f(s^*) + f'(s^*)(s-s^*) + (s-s^*)E_{s^*}(s-s^*),$$

where $|E_{s^*}(s-s^*)| \to 0$ as $|s-s^*| \to 0$. Note that this is weaker than complex differentiability since we restrict to $s \in \Gamma$.

Example 3.7.1. *The function $f(z) = |z|^2$ is Γ-differentiable for any smooth contour Γ but it is nowhere analytic.*

Assume $\Gamma = \Gamma_1 \cup \cdots \cup \Gamma_l$ where each Γ_i is non-self-intersecting and C^∞ smooth. It will be clear that a finite degree of smoothness is sufficient. We define, D, the distributional differentiation operator for functions defined on $\Gamma \setminus \gamma_0$ where γ_0 is, as before, the set of self-intersections of Γ. For a function $\varphi \in C_c^\infty(\Gamma_i)$ we represent a linear functional g via the dual pairing

$$g(\varphi) = \langle g, \varphi\rangle_{\Gamma_i}.$$

To $D_i g$ we associate the functional

$$-\langle g, \varphi_i'\rangle_{\Gamma_i}.$$

For $f \in L^2(\Gamma)$ consider $f_i = f|_{\Gamma_i}$, the restriction of f to Γ_i. In the case that the distribution $D_i f_i$ corresponds to a locally integrable function

$$\langle D_i f_i, \varphi\rangle_{\Gamma_i} = \int_{\Gamma_i} D_i f_i(z)\varphi(z)dz = -\int_{\Gamma_i} f_i(z)\varphi'(z)dz,$$

for each i, we define

$$Df(z) = D_i f_i(z) \text{ if } z \in \Gamma_i \setminus \gamma_0.$$

This allows us to define

$$H^k(\Gamma) = \left\{ f \in L^2(\Gamma) : D^j f \in L^2(\Gamma), \quad j = 0, \ldots, k \right\},$$

with norm

$$\|f\|^2_{H^k(\Gamma)} = \sum_{j=0}^{k} \|D^{(j)} f\|^2_{L^2(\Gamma)}.$$

We write $W^{k,\infty}(\Gamma)$ for the Sobolev space with the L^2 norm replaced with the L^∞ norm. An important note is that we will be dealing with matrix-valued functions, and hence the definitions of all these spaces must be suitably extended. Since all finite-dimensional norms are equivalent, we can use the above definitions in conjunction with any matrix norm to define a norm for matrix-valued functions provided the norm is sub-additive. If the Hilbert space structure of $H^k(\Gamma)$ is needed then a specific choice of the matrix norm is necessary so that it originates from an inner product.

Remark 3.7.2. *It is clear that this construction works in any L^p space allowing for the definition of the space $W^{k,p}(\Gamma)$.*

We state a well-known result concerning Sobolev spaces on the line. This may be deduced from the results in [48].

Theorem 3.7.3. *If $f \in H^k((a,b))$ then*

- *f is differentiable a.e. in (a,b) and $f^{(j)}(z) = D^j f(z)$ a.e., $j \leq k$ and*

$$f^{(j)}(x) - f^{(j)}(a) = \int_a^x f^{(j+1)}(s)ds, \quad 0 \leq j < k, \tag{3.7.1}$$

- $\sum_{i=0}^{k-1} \|f^{(i)}\|_u \leq C\|f\|_{H^k(\Gamma)}$,
- $\lim_{x\to a} f^{(j)}(x)$ *and* $\lim_{x\to b} f^{(j)}(x)$ *exist for* $0 \leq j < k$,
- *f has a unique $C^{k-1}([a,b])$ representation,*
- *multiplication is continuous: $\|fg\|_{H^k((a,b))} \leq C\|f\|_{H^k((a,b))}\|g\|_{H^k((a,b))}$, and*
- *$f^{(j)}$ is uniformly 1/2-Hölder continuous on $[a,b]$ for $0 \leq j < k$.*

If a or b is infinite the same conclusions follow but with C^{k-1} replaced with C_0^{k-1}, the space of C^{k-1} functions, decaying at infinity. If Γ is bounded and $\alpha : [-1,1] \to \Gamma$ is a C^∞ parametrization of Γ then it is clear that $H^k((-1,1))$ and $H^k(\Gamma)$ are isomorphic for every k.

Remark 3.7.4. *Since $f \in H^k(\Gamma)$ may be arbitrary on a set of measure zero, we always assume we are working with the C^{k-1} extension.*

Given a contour Γ, let γ_0 be the set of self-intersections. The behavior of functions at these intersection points is important for what follows. In particular, $\mathcal{C}_\Gamma^\pm f$ will not be smooth if is not sufficiently well-behaved at intersection points, even if f is smooth.

Definition 3.7.5. *Assume that $a \in \gamma_0$ and let $\Gamma_1, \ldots, \Gamma_m$ be a counter-clockwise ordering of sub-components of Γ which contain $z = a$ as an endpoint. For $f \in H^k(\Gamma)$, define*

$$f_i^{(j)} = \begin{cases} -\lim_{z\to a} \left(\frac{d}{dz}\right)^j f|_{\Gamma_i}(z) & \text{if } \Gamma_i \text{ is oriented away from } a, \\ \lim_{z\to a} \left(\frac{d}{dz}\right)^j f|_{\Gamma_i}(z) & \text{if } \Gamma_i \text{ is oriented toward } a. \end{cases} \tag{3.7.2}$$

We say that f satisfies the $(k-1)$th-order zero-sum condition if for all $a \in \gamma_0$

$$\sum_{i=1}^m f_i^{(j)} = 0, \text{ for } j = 0, \ldots, k-1. \tag{3.7.3}$$

Remark 3.7.6. *These definitions imply $f^{(j)} = 0$, $j = 0, \ldots, k-1$ when f satisfies the zero-sum condition and Γ has an isolated endpoint (in which case Γ is not complete and hence, not admissible). This is discussed further in Section 3.10.*

Definition 3.7.7. *Define*

$$H_z^k(\Gamma) = \{f \in H^k(\Gamma) : f \text{ satisfies the } (k-1)\text{th-order zero-sum condition}\}.$$

By Theorem 3.7.3, point evaluation of any of the $k-1$ derivatives of an H^k function is a bounded linear functional. Thus $H_z^k(\Gamma)$ is a closed subspace of $H^k(\Gamma)$. We see below that $H_z^k(\Gamma)$ is the appropriate Sobolev space on which to consider the operators $\mathcal{C}_\Gamma^\pm$. With this motivation, we begin with a lemma.

Lemma 3.7.8. *Let Γ be a smooth, non-closed curve from $z = a$ to $z = b$, oriented from a to b. If $f \in H^1(\Gamma)$, then*

$$D\int_\Gamma \frac{f(\zeta)}{\zeta - z} d\zeta = \frac{f(a)}{a - z} - \frac{f(b)}{b - z} + \int_\Gamma \frac{Df(\zeta)}{\zeta - z} d\zeta.$$

The important consequence of this lemma is that D^j, $0 \le j \le k$, commutes with the Cauchy operators $\mathcal{C}_\Gamma^\pm$ for functions in $H_z^k(\Gamma)$. Thus $\mathcal{C}_\Gamma^\pm$ are bounded from $H_z^k(\Gamma)$ to $H^k(\Gamma)$ with the operator norm being the same as the $L^2(\Gamma)$ norm. Indeed, a stronger statement is true.

Theorem 3.7.9. *Let Γ be an admissible contour with $\|\mathcal{C}_\Gamma f\|_{L^2(\Gamma)} \le C\|f\|_{L^2(\Gamma)}$. If $f \in H_z^k(\Gamma)$ then $\mathcal{C}_\Gamma^\pm f \in H_z^k(\Gamma)$ and hence $\|\mathcal{C}_\Gamma f\|_{H_z^k(\Gamma)} \le C\|f\|_{H_z^k(\Gamma)}$.*

Lemma 3.7.10 (Uniform Hölder continuity near intersection points)**.** *Let Γ be an admissible contour, $f \in H_z^1(\Gamma)$ and $a \in \gamma_0$. There exists $\delta > 0$ such that $\mathcal{C}_\Gamma^\pm f$ is uniformly 1/2-Hölder continuous in each $D \Subset B(a, \delta) \setminus \Gamma$ and hence in $\overline{D}$.*

Proof. Let the components of $\Gamma' = (\Gamma \cap B(a, \delta)) \setminus \{0\}$ be denoted by $\Gamma_1, \ldots, \Gamma_n$, with counter-clockwise ordering, see Figure 3.7.1. Choose $\delta > 0$ sufficiently small so that $\Gamma_i \cup \Gamma_j$,

$i \neq j$, is a Lipschitz graph. Let $x_1 \in \Gamma_1$, $x_2 \in \Gamma_2$ and let Λ be the line segment from x_1 to x_2. For $i = 1, 2$, define $r_i = |x_i - a|$. Assume $r_i < \delta/2$.

For $f \in H^1_z(\Gamma)$, extend f trivially to vanish on Λ. Set $F = \mathcal{C}_{\Gamma'} f$. Then f still satisfies the zero-sum condition on $\Gamma' \cup \Lambda$ and F is H^1 on Λ:

$$|F(x) - F(x')| \leq \|\mathcal{C}_{\Gamma'} f'\|_{L^2(\Lambda)} \sqrt{|x - x'|}.$$

But we know that $\|\mathcal{C}_{\Gamma'} f'\|_{L^2(\Lambda)} = \|\mathcal{C}_{\Gamma' \cup \Lambda} f'\|_{L^2(\Lambda)} \leq C(\Lambda) \|f\|_{L^2(\Gamma' \cup \Lambda)} = C(\Lambda) \|f\|_{H^1(\Gamma')}$. We estimate how $C(\Lambda)$ varies with respect to Λ.

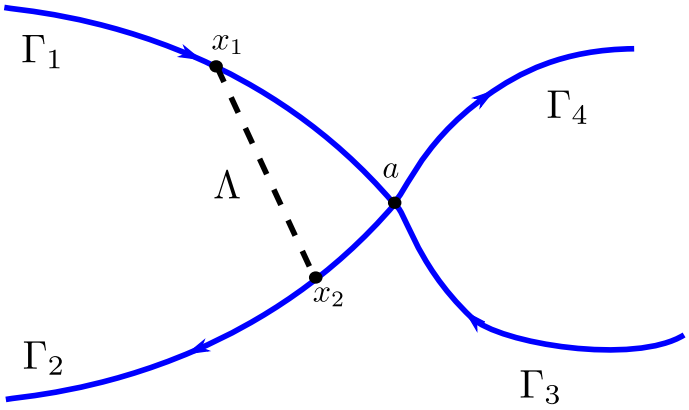

Figure 3.7.1: Zooming in on the intersection point a with a counter-clockwise ordering of the components Γ'.

We extend each Γ_i to $\tilde{\Gamma}_i$ by adding semi-infinite rays at each end point of Γ_i, while minimizing the Lipschitz constant for $\tilde{\Gamma}_i$. The same is done for Λ, giving $\tilde{\Lambda}$. If the smallest of the angles made by the intersection of $\tilde{\Gamma}_i$ with $\tilde{\Lambda}$ is greater than $\pi/4$ then we connect Γ_i to Λ with a Lipschitz contour (passing through the intersection of $\tilde{\Gamma}_i$ and $\tilde{\Lambda}$ to obtain a Lipschitz contour with bounded Lipschitz constant, independent of Λ. This is a 'nearly' perpendicular intersection. If this is not true we apply Lemma 3.5.12, after possible extensions. These extensions will have bounded Lipschitz constants, independent of Λ, since the contours are 'nearly' parallel. This process is described in Figure 3.7.2. Thus, there exists constants C_i, C_i', independent of x_1, x_2 and hence independent of Λ such that

$$\|\mathcal{C}^{\pm}_{\Gamma_i} f\|_{L^2(\Lambda)} \leq C_i \|f\|_{L^2(\Gamma_i)}, \quad f \in L^2(\Gamma_i),$$
$$\|\mathcal{C}^{\pm}_{\Lambda} f\|_{L^2(\Gamma_i)} \leq C_i' \|f\|_{L^2(\Lambda)}, \quad f \in L^2(\Lambda).$$

By Lemma 3.6.3 we know that $\mathcal{C}^{\pm}_{\Gamma' \cup \Lambda}$ has norm independent of x_1, x_2. It is clear that the effect of $\mathcal{C}_{\Gamma \setminus \Gamma'} f$ is analytic in a neighborhood of Λ. This proves the lemma. □

Proof. We return to the proof of Theorem 3.7.9. For $f \in H^k_z(\Gamma)$ we extend f to a function $\tilde{f}$ by defining it to be zero on Λ. Then $\tilde{f} \in H^k_z(\Gamma \cup \Lambda)$ so that $D^j(\mathcal{C}_\Gamma \tilde{f}) = \mathcal{C}_\Gamma D^j \tilde{f}$. Since $D^j \tilde{f} \in H^{k-j}(\Gamma \cup \Lambda)$ for $0 \leq j \leq k$, we apply Lemma 3.7.10. Then $D^j(\mathcal{C}_\Gamma \tilde{f})$ is uniformly Hölder in the sense of Lemma 3.7.10. Choose $a \in \gamma_0$. By the orientation of an admissible Γ, for every contour Γ_1 oriented towards a there exists a contour Γ_2 oriented away such

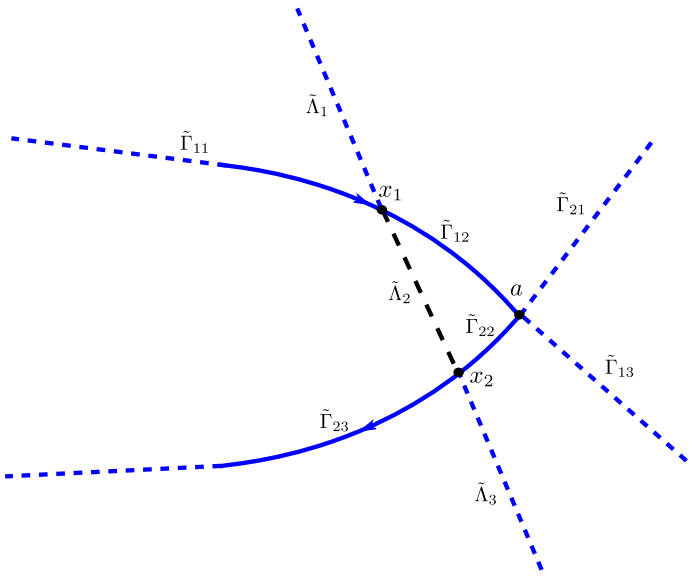

Figure 3.7.2: The extensions $\tilde{\Gamma}_1$, $\tilde{\Gamma}_2$ and $\tilde{\Lambda}$ of Γ_1, Γ_2 and Λ. The combination $\tilde{\Gamma}_1$ and $\tilde{\Lambda}$ display the nearly parallel case whereas the combination of $\tilde{\Gamma}_2$ and $\tilde{\Lambda}$ display the nearly perpendicular case. We see that $\tilde{\Gamma}_{11} \cup \tilde{\Lambda}_2 \cup \tilde{\Lambda}_3$ is a Lipschitz graph lying above (after rotation) $\tilde{\Lambda}_1 \cup \tilde{\Gamma}_{12} \cup \tilde{\Gamma}_{13}$. Thus Lemma 3.5.12 is applicable in this case to find a bound for the Cauchy integral along Γ_1, evaluated on Λ and vice versa. Also $\tilde{\Gamma}_{23} \cup \tilde{\Lambda}_2 \cup \tilde{\Lambda}_1$ and $\tilde{\Lambda}_1 \cup \tilde{\Lambda}_2 \cup \tilde{\Gamma}_{22} \cup \tilde{\Gamma}_{21}$ are Lipschitz graphs and this fact provides a bound for the Cauchy integral along Γ_2 evaluate on Λ (and vice versa).

that both contours are part of the boundary of the same component of $\Omega_\pm$. By the uniform Hölder continuity of $\mathcal{C}_\Gamma^\pm f$

$$\lim_{z\to a}\left(\frac{d}{dz}\right)^j \mathcal{C}_\Gamma^\pm f|_{\Gamma_1}(z) = \lim_{z\to a}\left(\frac{d}{dz}\right)^j \mathcal{C}_\Gamma^\pm f|_{\Gamma_2}(z).$$

This implies the zero-sum condition. □

3.7.1 The Sobolev spaces of Zhou

The spaces $H_z^k(\Gamma)$ have not appeared in the classical theory of RHPs. In the influential paper of Zhou [116], he considered the two Sobolev spaces (for an admissible Γ)

$$H_\pm^k(\Gamma) = \{f \in L^2(\Gamma) : f \in H_z^k(\partial D) \text{ for every } D \Subset \Omega_\pm\},$$

Both are equipped with the standard H^k norm. These spaces fit nicely within the framework of the Gohberg–Krein matrix factorization theory [18] that is discussed in Section 3.8. It is easy to see that $H_\pm^k(\Gamma) \subset H_z^k(\Gamma)$. Furthermore, Lemma 3.7.10 shows that if $f \in H_z^k(\Gamma)$ then $\mathcal{C}_\Gamma^\pm f \in H_\pm^k(\Gamma)$. Since $f = \mathcal{C}_\Gamma^+ f - \mathcal{C}_\Gamma^- f$ we can express

$$H_z^k(\Gamma) = H_+^k(\Gamma) + H_-^k(\Gamma),$$

where a decomposition is given by $\mathcal{C}_\Gamma^+ f$ and $-\mathcal{C}_\Gamma^- f$. The following additional properties follow [117, 116]:

- $\mathcal{C}_\Gamma^\pm : H_\pm^k(\Gamma) \to H_\pm^k(\Gamma)$, and
- $\mathcal{C}_\Gamma^\pm : H_\mp^k(\Gamma) \to H_+^k(\Gamma) \cap H_-^k(\Gamma)$.

3.8 Singular integral equations

We discuss the theory of singular integral equations (SIEs), focusing on the solution of RHPs through SIEs. Consider the solution of an L^p RHP of the form

$$\Phi^+(s) = \Phi^-(s)G(s) + F(s), \quad s \in \Gamma, \quad \Gamma \text{ admissible}, \quad \Phi(\infty) = I. \tag{3.8.1}$$

Assume for simplicity that all functions above are $n \times n$ matrices.

3.8.1 Singular integral equations on $L^2(\Gamma)$

We look for solutions where $\Phi^\pm(s)$ exist almost everywhere and $\Phi^\pm - I \in L^2(\Gamma)$. It is clear that if Φ is an $\mathcal{E}^\pm(\Gamma)$ solution then it is a solution in the above sense. It turns out that considering the seemingly more restrictive class of $\mathcal{E}^\pm(\Gamma)$ solutions is sufficient.

Remark 3.8.1. *It can be inferred from the results in [76, p. 163] that an L^2 solution is an $\mathcal{E}^\pm(\Gamma)$ solution.*

If we can find an $\mathcal{E}^\pm(\Gamma)$ solution then $\Phi(z) = I + \mathcal{C}_\Gamma u(z)$ for some $u \in L^2(\Gamma)$. We make this substitution in (3.8.1) and use Lemma 3.1.9 (more precisely, (3.5.3)) to find

$$u(s) - \mathcal{C}_\Gamma^- u(s)(G(s) - I) = G(s) - I + F(s), \quad s \in \Gamma. \tag{3.8.2}$$

This is a singular integral equation for u. We use this equation extensively. We write

$$\Phi^+(s) - I = \Phi^-(s)(G(s) - I) + F(s) + \Phi^-(s) - I, \quad s \in \Gamma.$$

After making mild assumptions on G and F (made clear below), we apply $\mathcal{C}_\Gamma^-$ noting that $\mathcal{C}_\Gamma^-(\Phi^+(s) - I) = 0$ and $\mathcal{C}_\Gamma^-(\Phi^-(s) - I) = -(\Phi^-(s) - I)$ from (3.5.2) and (3.5.4). Rearranging, we obtain

$$\Phi^- - \mathcal{C}_\Gamma^-[\Phi^-(\cdot)(G(\cdot) - I)] = I + F, \quad s \in \Gamma. \tag{3.8.3}$$

This is the equation introduced by Beals and Coifman [8] and studied by Zhou [116]. It is a fundamental aspect of the method of nonlinear steepest descent [33].

The discussion turns to function spaces and the mapping properties of these operators. To ease notation, define

$$\mathcal{C}[G;\Gamma]u = u - \mathcal{C}_\Gamma^- u(G - I),$$
$$\mathcal{C}'[G;\Gamma]\Phi^- = \Phi^- - \mathcal{C}_\Gamma^-[\Phi^-(\cdot)(G(\cdot) - I)].$$

It is clear that if $G(s) \in L^\infty(\Gamma)$ then $\mathcal{C}[G;\Gamma]$ is bounded on $L^2(\Gamma)$. We impose that the right-hand side of (3.8.2) is an $L^2(\Gamma)$ function. Thus, we require that $G - I, F \in L^2(\Gamma)$. In the second case, since $\Phi^- = f + I$, $f \in L^2(\Gamma)$. Thus

$$\Phi^-(G - I) = f(G - I) + G - I,$$

which is also in $L^2(\Gamma)$ provided the same conditions on G hold.

3.8.2 Singular integral equations on Sobolev spaces

It is easy to see that for $u \in H^k_z(\Gamma)$ with Γ having self-intersections that $\mathcal{C}^-_\Gamma u(s)(G(s) - I)$ does not generically satisfy the zero-sum condition. This is the case no matter how smooth G is. If one wishes to find smooth solutions of (3.8.2), a regularity condition for G must be satisfied at each intersection point, in addition to G being smooth away from intersection points.

Definition 3.8.2. *A jump matrix G defined on Γ is k-regular if Γ is admissible and G has a factorization*

$$G(s) = X_-^{-1}(s)X_+(s),$$

where $X_\pm - I, X_\pm^{-1} - I \in H^k_\pm(\Gamma)$.

It is clear that this requires $G - I, G^{-1} - I \in H^k(\Gamma)$.

Definition 3.8.3. *Assume $a \in \gamma_0$, the set of self-intersections of Γ. Let $\Gamma_1, \ldots, \Gamma_m$ be a counter-clockwise ordering of sub-components of Γ which contain $z = a$ as an endpoint. For $G \in H^k(\Gamma)$ we define $\hat{G}_i$ by $G|_{\Gamma_i}$ if Γ_i is oriented outwards and by $(G|_{\Gamma_i})^{-1}$ otherwise. We say that G satisfies the $(k-1)$th-order product condition if, using the $(k-1)$th-order Taylor expansion of each $\hat{G}_i$, we have*

$$\prod_{i=1}^{m} \hat{G}_i = I + \mathcal{O}\left(|z - a|^k\right), \quad \forall a \in \gamma_0. \tag{3.8.4}$$

The product condition is precisely the condition that produces smooth solutions. The classical theory on elliptic PDEs would indicate that singularities should be present at every corner of the domain. A kth-order product condition indicates that the singularity still posses some differentiability. In the case that each $\hat{G}_i$ is analytic in a neighborhood of an intersection point, we see there is no singularity and solutions will be infinitely smooth (actually, analytic).

Remark 3.8.4. *In analogy with the product condition, if Γ is not complete this implies that $\partial_z^{(j)}(G - I) = 0$, $j = 0, \ldots, k-1$ at each isolated endpoint. See Section 3.10 for a deeper discussion of this.*

Theorem 3.8.5 ([117])**.** *$G - I, G^{-1} - I \in H^k(\Gamma)$ and G satisfies the $(k-1)$th-order product condition if and only if G is k-regular.*

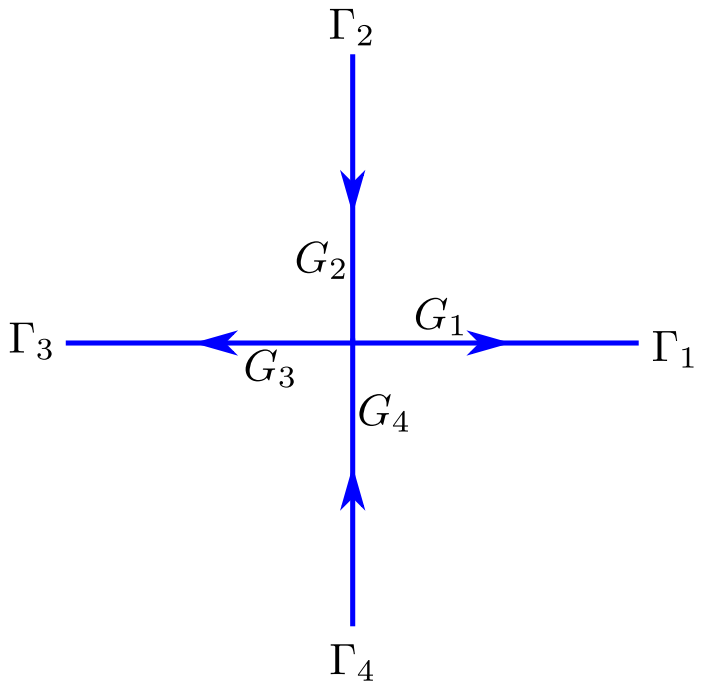

Figure 3.8.1: A sample self-intersection with consistent orientation and G_i labelled.

The proof of this theorem is straightforward when viewed from the correct angle although it is lengthy. We prove it for the simple case of $\Gamma = \mathbb{R} \cup i\mathbb{R}$, see Figure 3.8.1. To ensure we have the orientation correct we define

$$\begin{aligned}\Gamma_1 &= (0, \infty),\\ \Gamma_2 &= i(\infty, 0),\\ \Gamma_3 &= (0, -\infty),\\ \Gamma_4 &= i(-\infty, 0).\end{aligned}$$

Also, define

$$G_i(s) = \tilde{G}_i(s) + \mathcal{O}(s^k), \quad \tilde{G}_i(s) = \sum_{j=0}^{k-1} A_j s^j, \quad s \in \Gamma_i, \quad i = 1, 2, 3, 4.$$

First, assume that $G_i = \tilde{G}_i$ and we do not care about large s behavior. We must find the proper $X_\pm$ factorization of the full jump G. We start with Γ_1. Define $X_-|_{\Gamma_1} = I$ so that $X_+|_{\Gamma_1} = \tilde{G}_1$. We move counter-clockwise around Figure 3.8.1. Set $X_+|_{\Gamma_2} = \tilde{G}_1$ which requires $X_-|_{\Gamma_2} = \tilde{G}_1\tilde{G}_2^{-1}$. Set $X_-|_{\Gamma_3} = \tilde{G}_1\tilde{G}_2^{-1}$ which requires $X_+|_{\Gamma_3} = \tilde{G}_1\tilde{G}_2^{-1}\tilde{G}_3$. Finally, $X_+|_{\Gamma_4} = \tilde{G}_1\tilde{G}_2^{-1}\tilde{G}_3$ and $X_-|_{\Gamma_4} = \tilde{G}_1\tilde{G}_2^{-1}\tilde{G}_3\tilde{G}_4^{-1}$. Under the assumptions that the jump satisfies the $(k-1)$th-order product condition we see that $X_-|_{\Gamma_4} = I + \mathcal{O}(|s|^k)$.

We move to the general case where $G_i = \tilde{G}_i + \mathcal{O}(s^k)$. Let $\phi \in C^\infty(\Gamma)$ satisfy

$$\phi(s) = \begin{cases} I, & \text{if } |s| < r, \\ 0, & \text{if } |s| > 2r. \end{cases}$$

We note that if we can find a local factorization in a small neighborhood of $s = 0$, $G = \tilde{X}_-^{-1} X_+$ such that $\tilde{X}_-$ is invertible in this neighborhood then $\tilde{X}_-\phi + (I - \phi)$ is a good candidate for X_- provided that its determinant does not vanish. We must show that ϕ can be chosen so that $(\tilde{X}_- - I)\phi + I$ is non-singular. This only needs to be discussed for $r \le |s| \le 2r$. For simplicity, we choose ϕ to be a scalar-valued function $t(s)$ multiplied by the identity matrix. A little thought shows that the problem on Γ_1 reduces to choosing $t(s) : [r, 2r] \to \mathbb{C}$ so that $t(r) = 1$, $t(2r) = 0$ and the eigenvalues of $(\tilde{X}_- - I)\phi$ are never -1. The eigenvalues of $\tilde{X}_- - I$ for $s \in [r, 2r]$ will be located in a collection of balls in the complex plane with radii that tend to zero as $s \to 2r$. We see that ϕ will rotate and shrink these towards the origin as s increases from r to $2r$. It follows that $t(s)$ can always be chosen provided that r is sufficiently small. With this choice $X_- = (\tilde{X}_- - I)\phi + I$ and $X_+ = X_- G$. The definition of t differs on each contour Γ_i. We now construct $\tilde{X}_\pm$. Define

$$\begin{aligned}
\tilde{X}_-|_{\Gamma_1} &= I \\
\tilde{X}_+|_{\Gamma_1} &= \tilde{G}_1 + G_1 - \tilde{G}_1 \\
\tilde{X}_+|_{\Gamma_2} &= \tilde{G}_1 \\
\tilde{X}_-|_{\Gamma_2} &= \tilde{G}_1 \tilde{G}_2^{-1} + \tilde{G}_1(\tilde{G}_2^{-1} - \tilde{G}_2^{-1}) \\
\tilde{X}_-|_{\Gamma_3} &= \tilde{G}_1 \tilde{G}_2^{-1} \\
\tilde{X}_+|_{\Gamma_3} &= \tilde{G}_1 \tilde{G}_2^{-1} \tilde{G}_3 + \tilde{G}_1 \tilde{G}_2^{-1}(G_3 - \tilde{G}_3) \\
\tilde{X}_+|_{\Gamma_4} &= \tilde{G}_1 \tilde{G}_2^{-1} \tilde{G}_3 \\
\tilde{X}_-|_{\Gamma_4} &= \tilde{G}_1 \tilde{G}_2^{-1} \tilde{G}_3 \tilde{G}_4^{-1} + \tilde{G}_1 \tilde{G}_2^{-1} \tilde{G}_3 (G_4^{-1} - \tilde{G}_4^{-1}).
\end{aligned}$$

It is easy to see that, $\tilde{X}_-^{-1} \tilde{X}_+ = G$ and $\tilde{X}_\pm$ agrees with $\tilde{X}_\pm$ on the next contour up to $\mathcal{O}(|s|^k)$.

The factorization $G = X_-^{-1} X_+$ is now applied to (3.8.2).

$$\begin{aligned}
u - \mathcal{C}_\Gamma^- u(X_-^{-1} X_+ - I) &= X_-^{-1} X_+ - I + F, \\
u X_+^{-1} - \mathcal{C}_\Gamma^- u(X_-^{-1} - X_+^{-1}) &= X_-^{-1} - X_+^{-1} + F X_+^{-1}, \\
\mathcal{C}_\Gamma^+ u X_+^{-1} - \mathcal{C}_\Gamma^- u X_+^{-1} - \mathcal{C}_\Gamma^- u(X_-^{-1} - X_+^{-1}) &= X_-^{-1} - X_+^{-1} + F X_+^{-1}, \\
\mathcal{C}_\Gamma^+ u X_+^{-1} - \mathcal{C}_\Gamma^- u X_-^{-1} &= X_-^{-1} - X_+^{-1} + F X_+^{-1}.
\end{aligned} \tag{3.8.5}$$

Note that if $f \in H_\pm^k(\Gamma)$ and $g \in H_z^k(\Gamma)$ then $f\mathcal{C}_\Gamma^\pm g \in H_\pm^k(\Gamma) \subset H_z^k(\Gamma)$. This operation is continuous since multiplication is continuous in H^k. Thus

$$\mathcal{C}[X_+, X_-; \Gamma]u = \mathcal{C}_\Gamma^+ u X_+^{-1} - \mathcal{C}_\Gamma^- u X_-^{-1}$$

is an operator on $H_z^k(\Gamma)$. This is especially convenient since this transformation does not change u. For the right-hand side to be an $H_z^k(\Gamma)$ function, we require that $F \in H_+^k(\Gamma)$.

We turn our attention to (3.8.3).

$$\Phi^- - \mathcal{C}_\Gamma^-[\Phi^-(\cdot)(X_-^{-1}(\cdot)X_+(\cdot) - I)] = I + F.$$

Define $\Psi = \Phi^- X_-^{-1}$. Then

$$\begin{aligned} \Psi X_- - \mathcal{C}_\Gamma^-[\Psi(\cdot)(X_+(\cdot) - X_-(\cdot))] &= I + F, \\ \mathcal{C}_\Gamma^+[\Psi(\cdot)X_-(\cdot)] - \mathcal{C}_\Gamma^-[\Psi(\cdot)X_-(\cdot)] - \mathcal{C}_\Gamma^-[\Psi(\cdot)(X_+(\cdot) - X_-(\cdot))] &= I + F, \\ \mathcal{C}_\Gamma^+[\Psi(\cdot)X_-(\cdot)] - \mathcal{C}_\Gamma^-[\Psi(\cdot)X_+(\cdot)] &= I + F. \end{aligned} \tag{3.8.6}$$

To property interpret this equation we define $\tilde{H}^k_\pm(\Gamma) = H^k_\pm(\Gamma) \oplus \mathbb{C}^{n\times n}$. For $A \in \mathbb{C}^{n\times n}$ we define $\mathcal{C}_\Gamma^+ A = A$ and $\mathcal{C}_\Gamma^- A = 0$ so that Lemma 3.1.9 holds. For $\Psi \in \tilde{H}^k_-(\Gamma) \cap \tilde{H}^k_+(\Gamma)$, $\Psi X_\pm \in \tilde{H}^k_\pm(\Gamma)$. Thus using $\mathcal{C}_\Gamma^\pm : H^k_\pm(\Gamma) \to H^k_\pm(\Gamma)$ we find that $\mathcal{C}_\Gamma^\pm[\Psi X_\mp] \in \tilde{H}^k_-(\Gamma) \cap \tilde{H}^k_+(\Gamma)$. The operator

$$\mathcal{C}'[X_+, X_-; \Gamma]\Psi = \mathcal{C}_\Gamma^+[\Psi(\cdot)X_-(\cdot)] - \mathcal{C}_\Gamma^-[\Psi(\cdot)X_+(\cdot)],$$

is bounded on $\tilde{H}^k_-(\Gamma) \cap \tilde{H}^k_+(\Gamma)$ and we require in $F \in \tilde{H}^k_-(\Gamma) \cap \tilde{H}^k_+(\Gamma)$.

Fredholm properties

We first state our main rational approximation theorem that is proved in Appendix A.

Definition 3.8.6. *When Γ is admissible, let $R_\pm(\Gamma)$ be functions r such that $r|_{\partial D}$ is equal a.e. to a rational function for every $D \Subset \Omega_\pm$.*

Remark 3.8.7. *When $\Omega_\pm$ has more than one component (on the Riemann sphere) a function $f \in R_\pm(\Gamma)$ does not have to agree a.e. on Γ with a rational function. For example, let Γ be the contour in Figure 3.8.1. The function*

$$f(z) = \begin{cases} (z - e^{i5\pi/4})^{-n}, & \text{if } z \in \Gamma_1 \cup \Gamma_2, \\ (z - e^{i\pi/4})^{-n}, & \text{if } z \in \Gamma_3 \cup \Gamma_4, \end{cases}$$

is an $R_\pm(\Gamma)$ function but it is clearly not a true rational function.

Theorem 3.8.8. *If Γ is admissible then $R_\pm(\Gamma) \cap L^2(\Gamma)$ is dense in $H^k_\pm(\Gamma)$ and $L^2(\Gamma) \cap R_\pm(\Gamma) \oplus C^{n\times n}$ is dense in $\tilde{H}^k_\pm(\Gamma)$.*

Remark 3.8.9. *In light of these results there is a simple way to define the above spaces. $H^k_\pm(\Gamma)$ is the closure of functions f such that $f|_{\partial D}$, $D \subset \Omega_\pm$, is rational in the $H^k(\Gamma)$ norm. Furthermore, $H^k_z(\Gamma) = H^k_+(\Gamma) + H^k_-(\Gamma)$ with $\pm\mathcal{C}_\Gamma^\pm$ providing a decomposition. Note that these definitions coincide only when Γ is sufficiently regular (piecewise C^k is sufficient).*

Throughout this section we assume that Γ is admissible and that the jump matrix $G = X_-^{-1}X_+$ is k-regular.

Theorem 3.8.10. *The following operators are Fredholm*

- $\mathcal{C}[\Gamma; X_+, X_-]$ *on* $H^k_z(\Gamma)$ *and*

- $\mathcal{C}[\Gamma; G]$ *on* $L^2(\Gamma)$.

Proof. We begin the proof with a lemma.

Lemma 3.8.11. *If* $g \in \tilde{H}^k_{\mp}(\Gamma)$*, the operator* $L^{\pm}_g$ *defined by*

$$L^{\pm}_g u = \mathcal{C}^{\pm}_\Gamma[[\mathcal{C}^{\mp}_\Gamma u]g],$$

is compact on $H^k_z(\Gamma)$*,* $H^k_+(\Gamma) \cap H^k_-(\Gamma)$ *and* $L^2(\Gamma)$*.*

Proof. We prove this for the upper sign. The result follows analogously for the lower sign. Assume $g \in \tilde{H}^k_-(\Gamma)$ and let g_n be a sequence of $R_-(\Gamma)$ functions that converge to g in $H^k_-(\Gamma)$. Let $D \Subset \Omega_-$, $F^{\pm} = \mathcal{C}^{\pm}_\Gamma u$ and let $\tilde{g}_n$ be the rational function that agrees with $g_n|_{\partial D}$ a.e. We note that

$$\operatorname{Res}\left\{\frac{F(s)\tilde{g}_n(s)}{s-z}; s = k\right\}, \tag{3.8.7}$$

when k is a pole of g_n is a bounded, rank-one operator on all Sobolev spaces we consider here. We show that $\mathcal{C}_\Gamma[[\mathcal{C}^-_\Gamma u]g_n]$ is a finite sum of such residues for $z \in \Omega_+$. For $z \in \Omega_+$ we express

$$\mathcal{C}_\Gamma[[\mathcal{C}^-_\Gamma u]g_n] = -\sum_{D \Subset \Omega_-} \mathcal{C}_{\partial D}[[\mathcal{C}^-_\Gamma u]g_n],$$

where the minus sign comes from orientation. On ∂D for all $D \Subset \Omega_-$, $[\mathcal{C}^-_\Gamma u]g_n$ has a meromorphic extension in D and therefore $\mathcal{C}_{\partial D}[[\mathcal{C}^-_\Gamma u]g_n]$ must be a finite sum of residues of the form (3.8.7). Note that $z \notin D$. Summing over every component of Ω_- we see that the operator is finite rank. Since $\|L^{\pm}_{g_n} - L^{\pm}_g\|_{\mathcal{L}(H^k_z(\Gamma))} \to 0$ as $n \to \infty$, we conclude that $L^{\pm}_g$ is compact because the limit of compact operators is itself compact.

Note that the operators are compact on $L^2(\Gamma)$ provided $g \in H^1_{\pm}(\Gamma)$ to allow (uniform) rational approximation.

□

We return to the proof the theorem. We show that $\mathcal{C}[X_+^{-1}, X_-^{-1}; \Gamma]$ is a regulator for $\mathcal{C}[X_+, X_-; \Gamma]$.

$$\begin{aligned} Hu = \mathcal{C}[X_+, X_-; \Gamma][\mathcal{C}[X_+^{-1}, X_-^{-1}; \Gamma]u] =& \mathcal{C}^+_\Gamma(u + \mathcal{C}^+_\Gamma u(X_+^{-1} - I) - \mathcal{C}^-_\Gamma u(X_-^{-1} - I))X_+ \\ &- \mathcal{C}^-_\Gamma(u + \mathcal{C}^+_\Gamma u(X_+^{-1} - I) - \mathcal{C}^-_\Gamma u(X_-^{-1} - I))X_- \\ =& \mathcal{C}^+_\Gamma(u + \mathcal{C}^+_\Gamma u(X_+^{-1} - I))X_+ - \mathcal{C}^-_\Gamma(u - \mathcal{C}^-_\Gamma u(X_-^{-1} - I))X_- \\ &- \mathcal{C}^+_\Gamma(\mathcal{C}^-_\Gamma u(X_-^{-1} - I))X_+ - \mathcal{C}^-_\Gamma(\mathcal{C}^+_\Gamma u(X_+^{-1} - I))X_-. \end{aligned}$$

We concentrate on the first two terms since the last two are compact by Lemma 3.8.11.

$$\begin{aligned} \mathcal{C}^+_\Gamma(u + \mathcal{C}^+_\Gamma u(X_+^{-1} - I))X_+ &= \mathcal{C}^+_\Gamma(u + \mathcal{C}^+_\Gamma u X_+^{-1} - \mathcal{C}^+_\Gamma u)X_+ \\ &= \mathcal{C}^+_\Gamma(\mathcal{C}^+_\Gamma u X_+^{-1} - \mathcal{C}^-_\Gamma)X_+ = \mathcal{C}^+_\Gamma(\mathcal{C}^+_\Gamma u X_+^{-1})X_+, \\ \mathcal{C}^-_\Gamma(u - \mathcal{C}^-_\Gamma u(X_-^{-1} - I))X_- &= -\mathcal{C}^-_\Gamma(\mathcal{C}^-_\Gamma u X_-^{-1})X_-. \end{aligned}$$

Then,

$$\begin{aligned}\mathcal{C}_\Gamma^+(u+\mathcal{C}_\Gamma^+u(X_+^{-1}-I))X_+ - \mathcal{C}_\Gamma^-(u-\mathcal{C}_\Gamma^-u(X_-^{-1}-I))X_- \\ &= \mathcal{C}_\Gamma^+(\mathcal{C}_\Gamma^+uX_+^{-1})X_+ + \mathcal{C}_\Gamma^-(\mathcal{C}_\Gamma^-uX_-^{-1})X_- \\ &= \mathcal{C}_\Gamma^+u + \mathcal{C}_\Gamma^-(\mathcal{C}_\Gamma^+uX_+^{-1})X_+ - \mathcal{C}_\Gamma^-u + \mathcal{C}_\Gamma^+(\mathcal{C}_\Gamma^-uX_-^{-1})X_- \\ &= u + \mathcal{C}_\Gamma^-(\mathcal{C}_\Gamma^+uX_+^{-1})X_+ + \mathcal{C}_\Gamma^+(\mathcal{C}_\Gamma^-uX_-^{-1})X_-.\end{aligned}$$

Adding this all together we obtain

$$\begin{aligned}Hu &= u + \mathcal{C}_\Gamma^-(\mathcal{C}_\Gamma^+uX_+^{-1})X_+ + \mathcal{C}_\Gamma^+(\mathcal{C}_\Gamma^-uX_-^{-1})X_- - \\ &\quad \mathcal{C}_\Gamma^+(\mathcal{C}_\Gamma^-u(X_-^{-1}-I))X_+ - \mathcal{C}_\Gamma^-(\mathcal{C}_\Gamma^+u(X_+^{-1}-I))X_- \\ &= u + Tu,\end{aligned}$$

where T is compact and therefore the operator is right Fredholm. Changing the roles of $X_\pm$ and $X_\pm^{-1}$ we obtain that the operator is indeed Fredholm.

To see that $\mathcal{C}[G;\Gamma]$ is Fredholm on $L^2(\Gamma)$ note that $\mathcal{C}[X_+,X_-;\Gamma]u\cdot X_+ = \mathcal{C}[G;\Gamma]u$. Thus the operator defined by $u\mapsto \mathcal{C}[X_+^{-1},X_-^{-1};\Gamma](uX_+^{-1})$ is a regulator for $\mathcal{C}[G;\Gamma]$. □

Similar calculations show that $\mathcal{C}'[X_+,X_-;\Gamma]$ and $\mathcal{C}'[G;\Gamma]$ are Fredholm:

Theorem 3.8.12 ([116]). *The following operators are Fredholm*

- $\mathcal{C}'[\Gamma,X_+,X_-]$ *on* $\tilde{H}_+^k(\Gamma)\cap\tilde{H}_-^k(\Gamma)$, *and*
- $\mathcal{C}'[G;\Gamma]$ *on* $L^2(\Gamma)$.

3.8.3 Determining the index and kernel

We have shown that singular integral operators associated with RHPs are Fredholm under some precise conditions on the jump matrix. We aim to determine conditions under which the associated integral operators are invertible. To do this we must briefly discuss Gohberg–Krein (GK) matrix factorization theory in a simplified form. This theory may be discussed in great depth and detail. It is an elegant theory with profound results. In view of the density of rational functions, we use GK theory to only discuss the RHPs with jump matrices that are the product of an $R_-(\Gamma)$ and an $R_+(\Gamma)$ function.

GK factorization of rational matrix functions

Let Γ be a rectifiable Jordan curve. A matrix $A:\Gamma\to\mathbb{C}^{n\times n}$ with each entry being a rational function (*i.e.* a rational matrix function) is said to admit a right-standard factorization relative to Γ if

$$A = A_-\theta A_+,$$

Where $A_\pm$ are bounded rational functions with all poles in $\Omega_\mp$ such that $\det A_\pm \neq 0$ in $\overline{\Omega}_\pm$. Furthermore,

$$\theta(z) = \operatorname{diag}\left(\left(\frac{z-z_+}{z-z_-}\right)^{\kappa_1}, \ldots, \left(\frac{z-z_+}{z-z_-}\right)^{\kappa_n}\right),$$

for $z_\pm \in \Omega_\pm$. These conditions imply that $A_\pm^{-1}$ has no poles in $\overline{\Omega}_\pm$. The integers $\kappa_1 \geq \ldots \geq \kappa_n$ are the right-partial indices, or just partial indices, and $\kappa = \sum_{i=1}^n \kappa_i$ is the total index . We will see that κ has a direct relationship to the Fredholm index of the associated singular integral operators. The following theorem is a fundamental result from the first chapter of [18].

Theorem 3.8.13. *Let A be a rational matrix function with non-vanishing determinant on Γ. Then A admits a right-standard factorization relative to Γ for any $z_\pm \in \Omega_\pm$ and the partial indices are determined uniquely.*

We extend this result to intersecting contours. We abuse notation and call the matrix $A = X_-^{-1}X^+$ where $X_\pm \in R_\pm(\Gamma)$ a rational matrix function. It is important to note that A may not itself be a true rational function.

Theorem 3.8.14. *Assume that Γ is admissible and that A is a rational matrix function. Then A admits a right-standard factorization relative to Γ.*

Proof. We follow [116] and perform induction on the number of components of $\Omega_\pm$ as subsets of the Riemann sphere. First, we assume $X_+ = I$ so that $A = X_-^{-1} \in R_-(\Gamma)$. The general case is reduced to this case below.

If Ω_- has one component, Theorem 3.8.13 implies the result. Now assume $A = X_-^{-1}$ admits a right-standard factorization if Ω_- has $m < n$ components. We show it admits a factorization when Ω_- has n components.

Assume Ω_- has n components. Let $D \subset \Omega_-$ be a component. Then $\hat{A} = A|_{\overline{\Gamma \setminus \partial D}} \in R_-(\overline{\Gamma \setminus \partial D})$ admits a GK factorization since $\overline{\Gamma \setminus \partial D}$ is admissible and $\mathbb{C} \setminus (\overline{\Gamma \setminus \partial D}) = \Omega'_+ \cup \Omega'_-$, a disjoint union, similar to $\Omega_\pm$. Thus

$$\hat{A} = m_{1-}\theta_1 m_{1+}, \quad \theta_1(z) = \operatorname{diag}\left(\left(\frac{z-z_+}{z-z_-}\right)^{\kappa_1}, \ldots, \left(\frac{z-z_+}{z-z_-}\right)^{\kappa_n}\right),$$

$z_+ \in \Omega_+$ and $z_- \in \Omega_-$. We use m_1 to denote either function $m_{1\pm}$ away from $(\overline{\Gamma \setminus \partial D})$.

This factorization is used to, in effect, reduce the factorization problem to one on ∂D. Fix $z'_- \in \Omega'_+$ and define

$$\hat{\theta}_1(z) = \operatorname{diag}\left(\left(\frac{z-z_-}{z-z'_-}\right)^{\kappa_1}, \ldots, \left(\frac{z-z_-}{z-z'_-}\right)^{\kappa_n}\right).$$

Next, define $\tilde{A} = m_{1-}\hat{v}m_{1+}^{-1}\hat{\theta}_1$ for $\hat{v} = v|_{\partial D}$. Since $\tilde{A}$ is a rational function on a rectifiable Jordan curve Theorem 3.8.13 gives that $\tilde{A}$ admits a right-standard factorization relative to ∂D according to Theorem 3.8.14:

$$\tilde{A} = m_{2-}\theta_2 m_{2+}, \quad \theta_2(z) = \operatorname{diag}\left(\left(\frac{z-z_+}{z-z'_-}\right)^{\nu_1}, \ldots, \left(\frac{z-z_+}{z-z'_-}\right)^{\nu_n}\right).$$

To be consistent we must also decompose $\mathbb{C} \setminus \partial D = \Omega''_+ \cup \Omega''_-$. Define

$$\theta(z) = \operatorname{diag}\left(\left(\frac{z-z_-}{z-z'_-}\right)^{\nu_1}, \ldots, \left(\frac{z-z_-}{z-z'_-}\right)^{\nu_n}\right),$$

and $\hat{\theta}_2 = \theta_2\theta^{-1}$. We construct a sectionally analytic function

$$m = \begin{cases} \hat{\theta}_2 m_2 \hat{\theta}_1^{-1} m_1, & \text{if } z \in \Omega_+, \\ m_1\theta_1\hat{\theta}_1 m_2^{-1}\theta_2^{-1}, & \text{if } z \in \Omega'_- \cap \Omega_-, \\ m_1^{-1} m_2, & \text{if } z \in \Omega''_- \cap \Omega_-. \end{cases}$$

For $z \in \Gamma \setminus \partial D$

$$m_-\theta m_+ = m_{1-}\theta_1\hat{\theta}_1 m_{2-}^{-1}\theta_2^{-1}\theta\hat{\theta}_2 m_{2+}\hat{\theta}_1^{-1} m_{1+} = m_{1-}\theta_1 m_{1+} = \hat{A},$$

since $m_{2-} = m_{2+}$ on $\Gamma \setminus \partial D$. For $z \in \Gamma \setminus \partial D$ we have

$$m_-\theta m_+ = m_{1-}^{-1}\tilde{v}\theta_1^{-1} m_{1+} = A|_{\partial D}.$$

Thus $m_-\theta m_+$ is the desired factorization. Switching $-$ with $+$ we see that we may find a right-standard factorization if $A \in R_+(\Gamma)$.

For the general case $A = X_-^{-1}X_+$ we find $X_+ = m_{1-}\theta_1 m_{1+}$. We factor $X_-^{-1}m_{1-}\theta_1 = m_{2-}\theta_2 m_{2+}$. Thus $A = m_{2-}\theta_2(m_{2+}m_{1+})$. This is the desired factorization. □

Theorem 3.8.15 ([116])**.** *The partial indices $\kappa_1 \geq \cdots \geq \kappa_n$ are unique.*

Proof. Assume two factorizations of $A = m_{1-}\theta_1 m_{1+} = m_{2-}\theta_2 m_{2+}$ with

$$\begin{aligned} \theta_1(z) &= \operatorname{diag}\left(z^{\kappa_1}, \ldots, z^{\kappa_n}\right), \\ \theta_2(z) &= \operatorname{diag}\left(z^{\nu_1}, \ldots, z^{\nu_n}\right), \\ \kappa_i \leq \kappa_{i+1}, &\quad \nu_i \leq \nu_{i+1}. \end{aligned}$$

We may assume θ_1, θ_2 are of this simple form by using a Möbius transformation that takes rational functions to rational functions. After this transformation assume $0 \in \Omega_-$, $\infty \in \Omega_+$. We obtain

$$n_+\theta_1 = \theta_2 n_-, \quad n_- = m_{2-}^{-1}m_{1-}, \quad n_+ = m_{2+}m_{1+}^{-1}. \tag{3.8.8}$$

Set $n_- = (n_{ij}^-)_{1\leq i,j\leq n}$ and $n_+ = (n_{ij}^+)_{1\leq i,j\leq n}$. Assume that $\kappa_l < \nu_l$ for some l. Then

$$\nu_1 \leq \ldots \leq \nu_l < \kappa_l \Rightarrow \nu_i - \kappa_j < 0, \quad j \geq l, \quad i \leq l.$$

From (3.8.8)

$$n_{ij}^+(z) z^{\kappa_j - \nu_i} = n_{ij}^-(z).$$

If $\kappa_j - \nu_i < 0$, then $n_{ij}^-(z)z^{\kappa_j-\nu_i}$ is an entire function that decays at infinity: it must be identically zero.

Thus $n^-_{ij}(z) = 0$ for $j \geq l$, $i \leq l$, *i.e.* n_- has an $l \times (n-l)+1$ block of zeros. The span of the last $(n-l)+1$ columns of n_- is at most $n-l$ (the dimension of the non-zero block below the zero-block). Thus the rank of n_- is at most $l-1+n-l = n-1$ contradicting the fact that n_- is invertible. The case $\kappa_l < \nu_l$ can be treated with a slightly modified version of this argument. □

Now that we have established that the partial indices are unique we relate them to the Fredholm index of an operator. We begin with a lemma.

Lemma 3.8.16. *Assume G is k-regular. If $X_\pm$ and $X'_\pm$ represent two (algebraic) factorizations of G then*

$$u \mapsto uX_\pm(X'_\pm)^{-1}$$

is an invertible operator on $H^k_z(\Gamma)$.

Proof. It is clear that $X_\pm(X'_\pm)^{-1}$ is bounded and invertible on $H^k(\Gamma)$. We need to show it preserves the zero-sum conditions. With

$$X_-^{-1}X_+ = (X'_-)^{-1}X'_+,$$

we find

$$X_+(X'_+)^{-1} = X_-(X'_-)^{-1} \in H^k_-(\Gamma) \cap H^k_+(\Gamma).$$

Since a function in $H^k_-(\Gamma) \cap H^k_+(\Gamma)$ has limits agreeing from every direction at an intersection point it is clear that the zero-sum condition is preserved under multiplication by such functions. □

Theorem 3.8.17. *Let Γ be an admissible contour and $G : \Gamma \to \mathbb{C}^{n\times n}$ be a rational matrix function. Assume G has partial indices $\kappa_1 \geq \cdots \geq \kappa_n$. Then for any (algebraic) factorization of $G = X_-^{-1}X_+$ we have*

- $\dim\ker \mathcal{C}[X_+, X_-; \Gamma] = n\sum_{\kappa_i>0} |\kappa_i|$,
- $\operatorname{codim}\operatorname{ran} \mathcal{C}[X_+, X_-; \Gamma] = n\sum_{\kappa_i<0} |\kappa_i|$, *and*
- $\operatorname{ind} \mathcal{C}[X_+, X_-; \Gamma] = -n\sum_{i=1}^n \kappa_i$.

Proof. Let $G = R_-^{-1}\theta R_+$ be a right-standard factorization of G. We claim that

$$[\mathcal{C}[\Gamma; I, \theta]\mathcal{C}[R_+, R_-; \Gamma]u]R_+X_+^{-1} = \mathcal{C}[X_+, X_-; \Gamma].$$

This can be verified using the projection properties of the Cauchy operator. We digress for an important lemma.

Lemma 3.8.18. *If a k-regular RHP with jump matrix G has a solution $\Phi \in \mathcal{E}^\pm(\Gamma)$ with $\Phi_\pm - I, \Phi_\pm^{-1} - I \in H^k_\pm(\Gamma)$ then*

$$\mathcal{C}[X_+, X_-; \Gamma]^{-1}u = \mathcal{C}^+_\Gamma[uX_+\Phi_+^{-1}]\Phi_+ - \mathcal{C}^-_\Gamma[uX_+\Phi_+^{-1}]\Phi_-.$$

Proof. Let $Tu = \mathcal{C}_\Gamma^+[uX_+\Phi_+^{-1}]\Phi_+ - \mathcal{C}_\Gamma^-[uX_+\Phi_+^{-1}]\Phi_-$ First we find that

$$(\mathcal{C}[X_+, X_-; \Gamma]u)X_+\Phi_+^{-1} = \mathcal{C}_\Gamma^+ u\Phi_+^{-1} - \mathcal{C}_\Gamma^- u\Phi_-^{-1}.$$

The projection properties of $\mathcal{C}_\Gamma^\pm$ show that $\mathcal{C}_\Gamma^+ u\Phi_+^{-1} - \mathcal{C}_\Gamma^- u\Phi_-^{-1}$ and $\mathcal{C}_\Gamma^+ u\Phi_+ - \mathcal{C}_\Gamma^- u\Phi_-$ are inverses. Thus $T \circ \mathcal{C}[X_+, X_-; \Gamma] = I$. We show the other composition. We find

$$\begin{aligned}\mathcal{C}[X_+, X_-; \Gamma] \circ Tu &= \mathcal{C}_\Gamma^+[uX_+\Phi_+^{-1}]\Phi_+X_+^{-1} - \mathcal{C}_\Gamma^-[uX_+\Phi_+^{-1}]\Phi_-X_-^{-1}, \\ &= u + \mathcal{C}_\Gamma^-[uX_+\Phi_+^{-1}]\Phi_+X_+^{-1} - \mathcal{C}_\Gamma^-[uX_+\Phi_+^{-1}]\Phi_-X_-^{-1}.\end{aligned}$$

It is clear from previous calculations that $\Phi_+X_+^{-1} = \Phi_-X_-^{-1}$, proving the identity. □

We return to the theorem. It is clear that $u \mapsto uR_+X_+^{-1}$ defines an invertible operator. The lemma shows that $\mathcal{C}[\Gamma; R_+, R_-]$ is also invertible. Thus any deficiency of $\mathcal{C}[\Gamma, X_+, X_-]$ must come from

$$\mathcal{C}[I, \theta; \Gamma] = \mathcal{C}_\Gamma^+ \cdot - \mathcal{C}_\Gamma^- \cdot \theta.$$

Recall that

$$\theta(z) = \operatorname{diag}\left(\left(\frac{z - z_+}{z - z_-}\right)^{\kappa_1}, \ldots, \left(\frac{z - z_+}{z - z_-}\right)^{\kappa_n}\right).$$

We convert this to an equivalent RHP. We look for solutions of

$$\Phi^+(s) = \Phi^-(s)\theta(s), \quad s \in \Gamma, \Phi(\infty) = 0.$$

This is a diagonal RHP. We use the methods of Section 3.4.1, determining n scalar problems

$$\phi_i^+(s) = \phi_i^-(s)M^{\kappa_i}(s), \quad M(s) = \frac{s - z_+}{s - z_-}, \quad s \in \Gamma, \quad \phi_i(\infty) = 0, \quad i = 1, \ldots, n. \tag{3.8.9}$$

It is easy to check that if $\kappa_i > 0$ then

$$\phi_i^+(z) = \sum_{l=0}^{\kappa_i - 1} \alpha_l M^l(z), \quad \phi_i^-(z) = \sum_{l=0}^{\kappa_i - 1} \alpha_l M^{-\kappa_i + l}(z),$$

is a solution of (3.8.9) for any choice of $\{\alpha_l\}$ and therefore $\Phi^\pm(z) = \operatorname{diag}(\phi_1^\pm(z), \ldots, \phi_n^\pm)$ and $u(s) = \Phi^+(s) - \Phi^-(s)$ is an element of the kernel of $\mathcal{C}[I, \theta; \Gamma]$. For $\kappa_i \leq 0$, solutions must be of this same form but we may change what l ranges over. Since all exponents on ϕ_i^- must be negative, we find $\kappa_i > l$. Considering ϕ_i^+ we see that for it to be analytic, $\alpha_l = 0$ for all l. We have characterized the kernel by $\sum_{\kappa_i > 0} \kappa_i$ elements.

To analyze the range we set $u = u_+ + u_-$ where $u_\pm \in \mathcal{C}_\Gamma^\pm H_z^k(\Gamma)$. If we choose $u_- = 0$ we find $\mathcal{C}[I, \theta; \Gamma]u_+ = u_+$. Therefore $C_\Gamma^+ H_z^k(\Gamma)$ is in the range. Now choose $u_+ = 0$. We find $\mathcal{C}[I, \theta; \Gamma]u = \mathcal{C}_\Gamma^- u_-\theta$. We break this into components and consider

$$\mathcal{C}_\Gamma^- u_i^- M^{\kappa_i}.$$

If $\kappa_i \geq 0$ and $u \in \mathcal{E}^-(\Gamma)$ then $M^{-\kappa_i} u \in \mathcal{E}^-(\Gamma)$ implying that

$$\mathcal{C}_\Gamma^-(M^{-\kappa_i} u) M^{\kappa_i} = u.$$

Thus this component maps onto $\mathcal{C}_\Gamma^- H_z^k(\Gamma)$. Now if $\kappa_i < 0$ then $\mathcal{C}_\Gamma^- u_i^- M^{\kappa_i}$ will always have a $(-\kappa_i)$-th order zero at $z = z_-$. Implying that if $g \in \operatorname{ran} \mathcal{C}_\Gamma^- \cdot M^{\kappa_i}$ then $\frac{d}{dz}\mathcal{C}_\Gamma^- g(z_-) = 0$ for $j = 0, \ldots, -\kappa_i - 1$. This amounts to $\sum_{\kappa_i<0} |\kappa_i|$ orthogonality conditions. Thus we have characterized the deficiency of the range by $\sum_{\kappa_i<0} |\kappa_i|$ bounded linear functionals. We have constructed the kernel and identified deficiency of the range when $\mathcal{C}[I, \theta; \Gamma]$ acts on vectors. Since each row is acted on independently, the dimension of the kernel and codimension of the range is multiplied by the number of rows. □

Remark 3.8.19. *If we apply $\mathcal{C}[X_+, X_-; \Gamma]$ on $m \times n$ matrices then*

- $\dim \ker \mathcal{C}[X_+, X_-; \Gamma] = m \sum_{\kappa_i>0} |\kappa_i|$,
- $\operatorname{codim} \operatorname{ran} \mathcal{C}[X_+, X_-; \Gamma] = m \sum_{\kappa_i<0} |\kappa_i|$, *and*
- $\operatorname{ind} \mathcal{C}[X_+, X_-; \Gamma] = -m \sum_{i=1}^n \kappa_i$.

We connect the total index κ to something easily computable. If A is a rational matrix function with a right-standard factorization then

$$A = A_- \theta A_+ \Rightarrow \det A = \det A_- \left(\frac{z - z_+}{z - z_-}\right)^\kappa \det A_+.$$

It follows that

$$\begin{gathered} \operatorname{ind}_{\partial D} \det A_\pm = 0, \quad D \Subset \Omega_\pm, \\ \operatorname{ind}_{\partial D} \left[\left(\frac{z - z_+}{z - z_-}\right)^\kappa\right] = \begin{cases} \kappa, & \text{if } z_+ \in D, \\ 0, & \text{otherwise,} \end{cases} \end{gathered} \tag{3.8.10}$$

using the argument principle. Orientation is taken into account in the second expression (3.8.10). Summing over components,

$$\sum_{D \subset \Omega_+} \int_{\partial D} \bar{d} \log \left(\det A_+ \left(\frac{z - z_+}{z - z_-}\right)^\kappa\right) = \kappa, \qquad \sum_{D \subset \Omega_-} \int_{\partial D} \bar{d} \log \det A_- = 0.$$

We decompose $\Gamma = \Gamma_1 \cup \cdots \cup \Gamma_l$, with Γ_l smooth and non-self-intersecting. Then

$$\kappa = \sum_{D \subset \Omega_+} \int_{\partial D} \bar{d} \log \left(\det A_+ \left(\frac{z - z_+}{z - z_-}\right)^\kappa\right) - \sum_{D \subset \Omega_-} \int_{\partial D} \bar{d} \log \det A_- = \sum_{j=1}^{l} \int_{\Gamma_j} \bar{d} \log \det A.$$

We obtain the following theorem.

Theorem 3.8.20. *Let Γ be admissible and G be a rational matrix function with an algebraic factorization $X_\pm \in H^k_\pm(\Gamma)$ then*

$$\operatorname{ind} \mathcal{C}[X_+, X_-; \Gamma] = n \sum_{j=1}^{l} \int_{\Gamma_l} \bar{d} \log \det G,$$

as an operator on $H^k_z(\Gamma)$.

Theorem 3.8.21. *Theorem 3.8.20 holds when G is k-regular.*

Proof. Let $G = X_-^{-1} X_+$ and approximate $X_\pm$ with a convergent sequence of rational matrix functions $\{X^n_\pm\}$. It follows that

$$\|\mathcal{C}[X_+, X_-; \Gamma] - \mathcal{C}[X^n_+, X^n_-; \Gamma]\|_{\mathcal{L}(H^k_z(\Gamma))} \to 0 \text{ as } n \to \infty.$$

Thus for n sufficiently large $\mathcal{C}[\Gamma; X^n_+, X^n_-]$ has the same index as $\mathcal{C}[X_+, X_-; \Gamma]$. We express

$$\begin{aligned} \operatorname{ind} \mathcal{C}[X^n_+, X^n_-; \Gamma] &= n \sum_{j=1}^{l} \int_{\Gamma_l} \bar{d} \log \det X^n_+ - \bar{d} \log \det X^n_+ \\ &= n \sum_{D \subset \Omega_+} \operatorname{ind}_{\partial D} \det X^n_+ - \sum_{D \subset \Omega_-} \operatorname{ind}_{\partial D} \det X^n_-. \end{aligned}$$

Since $X^n_\pm \to X_\pm$ in $L^\infty(\Gamma)$, we have that for sufficiently large n

$$\begin{aligned} \operatorname{ind} \mathcal{C}[X^n_+, X^n_-; \Gamma] &= n \sum_{D \subset \Omega_+} \operatorname{ind}_{\partial D} \det X_+ - n \sum_{D \subset \Omega_-} \operatorname{ind}_{\partial D} \det X_- \\ &= n \sum_{j=1}^{l} \int_{\Gamma_l} \bar{d} \log \det G = \operatorname{ind} \mathcal{C}[X_+, X_-; \Gamma]. \end{aligned}$$

□

Remark 3.8.22. *Note that the index is independent of k and if G is k-regular then the invertibility of $\mathcal{C}[X_+, X_-; \Gamma]$ on $H^j_k(\Gamma)$ for one $j \in [0, k]$ implies invertibility for any j. Similar statements follow for $\mathcal{C}[G; \Gamma]$.*

Remark 3.8.23. *Let Φ be a bounded L^2 solution of the RHP with jump G, $\operatorname{ind}_\Gamma \det G = 0$. Then*

$$\det \Phi^+ = \det \Phi^- \det G, \quad \det \Phi(\infty) = 1. \tag{3.8.11}$$

Assume that $\operatorname{ind}_\Gamma \det G = 0$ and that $\det G$ be 1-regular. The theory presented thus far shows that $\det \Phi$ is the only solution to this problem (the only partial index is zero). Indeed, in many cases, $G = X_-^{-1} X_+$, so that $\det G$ must satisfy the (scalar) product condition. We find a possibly new algebraic factorization $\det G = Y_+ / Y_-$ for scalar-valued functions $Y_\pm$. Enumerate $\{D^+_i\}$ and $\{D^-_i\}$ where $D^\pm_i \Subset \Omega_\pm$. Select points $z^\pm_i \in D^\pm_i$ and define the

integers

$$\kappa_i^{\pm} = \operatorname{ind}_{D_i^{\pm}} Y_{\pm}.$$

Let

$$P(z) = \prod_{D_i^+ \Subset \Omega_+} (z - z_i^+)^{-\kappa_i^+},$$
$$M(z) = \prod_{D_i^- \Subset \Omega_-} (z - z_i^-)^{-\kappa_i^-}.$$

It follows from $\operatorname{ind}_\Gamma G = 0$ *that* $\lim_{|z|\to\infty} P(z)/M(z) = 1$ *and*

$$\kappa_i^+ = \operatorname{ind}_{D_i^+} Y_+ P/M = 0, \quad \kappa_i^- = \operatorname{ind}_{D_i^-} Y_- M/P = 0.$$

Define $Z_+ = Y_+ P/M$ *and* $Z_- = Y_- M/P$ *so that* $G = 1/Z_- Z_+$. *Again* $Z_\pm$ *are scalar-valued. We find a representation for* $\det \Phi$*:*

$$\log \det \Phi(z) = \int_\Gamma \frac{\log Z_+(s) - \log Z_-(s)}{s - z} ds = \sum_{D_i^+ \Subset \Omega_+} \int_{D_i^+} \frac{\log Z_+(s)}{s - z} ds - \sum_{D_i^- \Subset \Omega_-} \int_{D_i^-} \frac{\log Z_-(s)}{s - z} ds.$$

From this it is clear that $\det \Phi$ *cannot vanish; both Cauchy integrals are bounded. It is worth noting that if* $\det G = 1$ *then* $\det \Phi = 1$.

Some remarks are in order.

Remark 3.8.24. *Theorems 3.8.17 and 3.8.20 hold for* $\mathcal{C}[G;\Gamma]$ *and* $\mathcal{C}'[G;\Gamma]$ *in* $L^2(\Gamma)$ *provided* $k \geq 1$ *and* $\mathcal{C}'[X_+, X_-;\Gamma]$ *on* $\tilde{H}_+^k(\Gamma) \cap \tilde{H}_-^k(\Gamma)$.

Remark 3.8.25. *In applications it is often the case that* $\det G = 1$. *This immediately shows that the index is zero.*

We have shown there is a one-to-one correspondence between $\mathcal{E}^{\pm}(\Gamma)$ solutions of a RHP with jump matrix G and solutions of $\mathcal{C}[\Gamma; X_+, X_-]u = X_+^{-1} - X_-^{-1}$. The question of solvability of a RHP is reduced to the question of invertibility of a Fredholm singular integral operator. To show this, one usually determines that the singular integral operator has index zero. Additional results show that the kernel must be trivial. An appeal to the open mapping theorem and one of its well-known corollaries proves the invertibility of the operator:

Theorem 3.8.26 (Open Mapping)**.** *Let* X *and* Y *be Banach spaces. If* $T \in \mathcal{L}(X, Y)$ *is surjective, then* T *is open.*

Corollary 3.8.27. *If* X *and* Y *are Banach spaces and* $T \in \mathcal{L}(X, Y)$ *is bijective, then* T *is an isomorphism:* $T^{-1} \in \mathcal{L}(Y, X)$.

To get a handle on the kernel we present an incarnation of the so-called *vanishing lemma*.

Definition 3.8.28. *A contour is said to be Schwarz invariant if* $\bar{\Gamma} = \Gamma$*, respecting orientation. The Schwartz conjugate of a function* f *is defined by* $f^\dagger(z) = \overline{f(\bar{z})}^T$.

Theorem 3.8.29 (Vanishing Lemma [116])**.** *Let* G *be defined on a Schwarz invariant, admissible contour* Γ*. If* G *is* k*-regular,* $\operatorname{Re} G$ *is positive semi-definite on* $\mathbb{R}$*, positive definite on a set of positive measure, and* $G = G^\dagger$ *on* $\Gamma \setminus \mathbb{R}$ *then* $\dim \ker \mathcal{C}[X_+, X_-; \Gamma] = 0$.

Proof. Let Φ be a vanishing solution of the associated RHP:

$$\Phi^+(s) = \Phi^-(s)G(s), \quad \Phi(\infty) = 0.$$

Thus $u = \Phi^+ - \Phi^- \in \ker \mathcal{C}[X_+, X_-; \Gamma]$. Let $D \Subset \mathbb{C} \setminus \Gamma$, then $D^\dagger \Subset \mathbb{C} \setminus \Gamma$. Further, $\partial D^\dagger = (\partial D)^\dagger$, respecting orientation. Set $u_1 = \Phi|_{\partial D}$ and $u_2 = \Phi|_{\partial D^\dagger}$. Since $u_1 \in \mathcal{E}^2(D)$ we know that $\int_{\partial D} u_1(z) r(z) dz = 0$ for any rational function r with poles outside D. Since $u_2^\dagger$ may be approximated with rational functions in $L^2(\partial D)$ satisfying this condition, we find

$$\int_{\partial D} u_1(z) u_2^\dagger(z) dz = 0.$$

Summing over all components in the upper-half plane we find

$$\sum_{D \subset \mathbb{C}^+ \setminus \Gamma} \int_{\pm \partial D} u_1(z) u_2^\dagger(z) dz = 0. \tag{3.8.12}$$

We choose $\pm$ to make ∂D is positively oriented. Let Γ_i be smooth components of Γ in the open upper-half plane. Then Γ_i is part of the boundary of two components $D_\pm \subset \Omega_\pm$, and Φ has boundary values $u_1^\pm$ from $\Omega_\pm$ on Γ_i. Boundary values for u_2, $u_2^\pm$ exist analogously on $\Gamma_i^\dagger$. Integrals along Γ_i appear twice in (3.8.12):

$$\begin{aligned}
\int_{\Gamma_i} u_1^+(z)(u_2^-)^\dagger(z) dz &= \int_{\Gamma_i} u_1^-(z) G(z) (u_2^-)^\dagger(z) dz, \\
\int_{-\Gamma_i} u_1^-(z)(u_2^+)^\dagger(z) dz &= \int_{-\Gamma_i} u_1^-(z) G^\dagger(z) (u_2^-)^\dagger(z) dz.
\end{aligned}$$

Using $G = G^\dagger$ off the real line, we see that these integrals cancel. Only integrals on the real line survive, producing

$$\sum_{D \subset \mathbb{C}^+ \setminus \Gamma} \int_{\pm \partial D} u_1(z) u_2^\dagger(z) dz = \int_{\mathbb{R}} u_1^+(x) u_2^-(x) dx = \int_{\mathbb{R}} u_1^-(x) \tilde{G}(x) u_1^-(x) dx.$$

Where $\tilde{G} = G$ or $G^\dagger$ depending on how each subset of the real line is oriented. This equation is added to (subtracted from) its Schwarz reflection providing us with

$$0 = \int_{\mathbb{R}} u_1^-(x)(G(x) + G^\dagger(x)) u_1^-(x) dx.$$

Thus $u_1^- = 0$ and hence Φ^- is zero a.e. on $\mathbb{R}$ by positive definiteness. It is known that any

function in $\mathcal{E}^2(D)$ which vanishes on a set of positive measure on the boundary must be identically zero. If Φ is zero in any component of $\mathbb{C}\setminus\Gamma$ then the jump condition forces Φ to be zero in all neighboring components. We conclude that $\Phi = 0$ and $\dim\ker \mathcal{C}[X_+, X_-; \Gamma] = 0$. □

Remark 3.8.30. *The notion of partial indices can be generalized to so-called decomposing algebras. If these are used Theorem 3.8.29 can be strengthened to show invertibility of the operator without appealing to a zero index statement. We do not elaborate on this here but note that for our purposes* $\det G$ *is constant. Establishing zero index is then trivial.*

3.9 Additional smoothness aspects of Riemann–Hilbert problems

We expand on the theory above by providing estimates for the derivatives of solutions of singular integral equations. This provides criteria in terms of the jump matrix to test when the solution of one problem is "close" to the solution of another problem. To simplify notation we associate $[G;\Gamma]$ with the L^2 RHP

$$\Phi^+(s) = \Phi^-(s)G(s), \quad s\in\Gamma, \quad \Phi(\infty) = I.$$

If G is k-regular we also say $[G;\Gamma]$ is k-regular.

Theorem 3.9.1. *Given a RHP* $[G;\Gamma]$ *which is* k*-regular, assume* $\mathcal{C}[G;\Gamma]$ *is invertible on* $L^2(\Gamma)$*. Then the solution of* (3.8.2)*,* $u\in H^k_z(\Gamma)$*, satisfies*

$$D^k u = \mathcal{C}[G;\Gamma]^{-1}\Big(D^k(G-I) + D^k(\mathcal{C}^-_\Gamma u\cdot(G-I)) - \mathcal{C}^-_\Gamma D^k u\cdot(G-I)\Big), \tag{3.9.1}$$

where the right-hand side of (3.9.1) *does not depend on* $D^k u$*.*

Corollary 3.9.2. *Under the hypotheses of Theorem 3.9.1,* u *satisfies an inequality of the form*

$$\|u\|_{H^k(\Gamma)} \le p_k\left(\|G-I\|_{W^{k,\infty}(\Gamma)}\|\mathcal{C}[G;\Gamma]^{-1}\|_{\mathcal{L}(L^2(\Gamma))}\right)\|\mathcal{C}[G;\Gamma]^{-1}\|_{\mathcal{L}(L^2(\Gamma))}\|G-I\|_{H^k(\Gamma)}, \tag{3.9.2}$$

where p_k *is a polynomial of degree* k *whose coefficients depend on* $\|\mathcal{C}^-_\Gamma\|_{\mathcal{L}(L^2(\Gamma))}$*.*

Proof. Taking the norm of (3.9.1) gives a bound on the semi-norm $\|D^k u\|_{L^2(\Gamma)}$ in terms of $\|u\|_{H^{k-1}(\Gamma)}$. Using (3.9.1) for $k-1$ gives a bound in terms of $\|u\|_{H^{k-2}(\Gamma)}$. This process produces a bound of the form (3.9.2). □

Remark 3.9.3. *The expression for the derivative in Theorem 3.9.1 can be used to bound Sobolev norms of the solution in terms of Sobolev norms of the jump matrix if a bound on the norm of the inverse operator is known. In some cases, when the jump matrix depends on a parameter, and the Sobolev norms of the jump matrix are bounded or decaying, the resulting bounds are useful.*

We often use the following theorem which is derived from the results in [51].

Lemma 3.9.4. *Consider a sequence of k-regular RHPs $\{[G_\xi;\Gamma]\}_{\xi\geq 0}$ on the fixed contour Γ. Assume $G_\xi \to G$ in $W^{k,\infty}(\Gamma)\cap H^k(\Gamma)$ as $\xi\to\infty$, then*

- *If $\mathcal{C}[G;\Gamma]$ is invertible on $L^2(\Gamma)$ then there exists a $T>0$ such that $\mathcal{C}[G_\xi;\Gamma]$ is also invertible for $\xi > T$.*
- *If Φ_ξ is the solution of $[G_\xi,\Gamma]$, and Φ is the solution of $[G;\Gamma]$, then $\Phi_\xi^\pm - \Phi^\pm \to 0$ in $H^k(\Gamma)$.*
- *$\|\Phi_\xi - \Phi\|_{W^{j,\infty}(S)} \to 0$, for all $j\geq 1$, whenever S is bounded away from Γ.*

Proof. The first statement follows from the fact that $\mathcal{C}[G_\xi;\Gamma]$ converges to $\mathcal{C}[G;\Gamma]$ in the operator norm. The second property follows from Corollary 3.9.2. The final property is a consequence of the Cauchy-Schwartz inequality and the fact that $\|u_\xi - u\|_{L^2(\Gamma)}\to 0$. □

3.10 Truncation, augmentation and practical aspects of Riemann–Hilbert problems

When RHPs are used in practice the contour involved is often not complete. Furthermore, we aim to solve RHPs numerically (in Chapter 5) and contours of infinite length may cause problems. In this section we discuss what can be done when a contour is not complete and how for most RHPs on infinite contours there exists a 'nearby' problem on a bounded contour.

3.10.1 Augmentation

Throughout much of the above discussion we assumed Γ is complete. Here we demonstrate that this can be assumed for all L^2 RHPs without loss of generality. Let Γ be an incomplete but piecewise smooth contour with only transverse intersections. We describe a procedure that converts Γ to complete contour. We start with a definition.

Definition 3.10.1. *Let γ_0 be the set of self-intersections of the contour Γ. We say a point $a\in\Gamma$ is an open endpoint if a is a limit point of only one of the connected components of $\Gamma\setminus(\gamma_0\cup\{a\})$.*

For example, the interval $[-1,1]$ has ± 1 as open endpoints. We join all open endpoints back to Γ or to ∞ with smooth contours. Define the resulting contour to be Γ'. Now $\Omega = \mathbb{C}\setminus\Gamma'$ consists of disjoint open sets D such that ∂D is piecewise smooth with only transverse intersections. Note this is not necessarily true of $\mathbb{C}\setminus\Gamma$. Choose $D_1 \Subset \Omega$ and re-orient (if necessary) Γ' so that $\Gamma'\cap\bar{D}_1 = \partial D_1$ (positively oriented) where orientation is accounted for in the equality. Look at all neighboring components $D_2,\ldots,D_m$ of D_1. Either Γ' can be reoriented so that $\Gamma'\cap\bar{D}_2 = -\partial D_2$ (negatively oriented), or not. If not, additional contours are added resulting in Γ'' so that this can be accomplished. We repeat this process until the contour is complete. We demonstrate this procedure in Figure 3.10.1. This procedure works for any such contour Γ

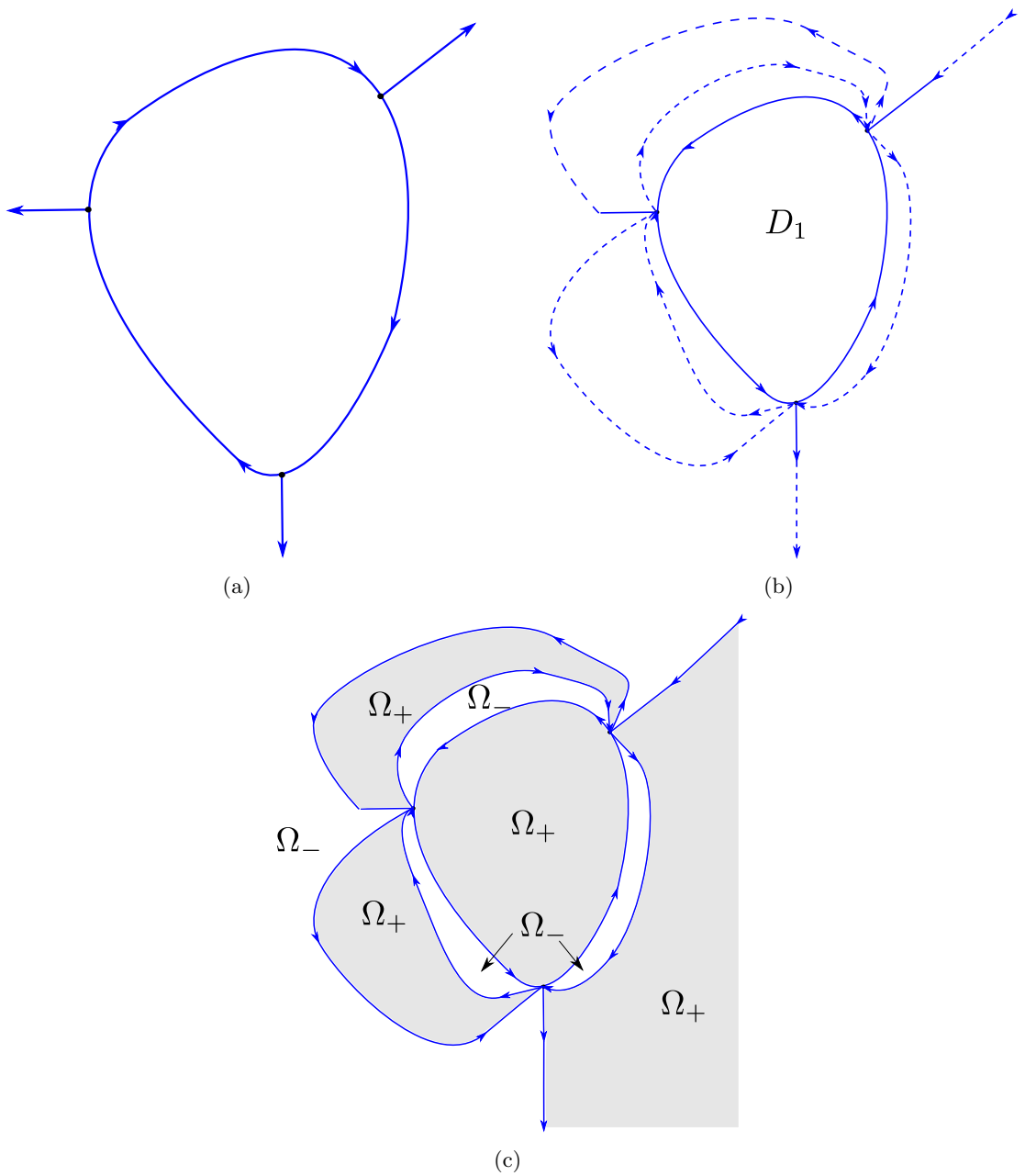

Figure 3.10.1: The augmentation of an incomplete contour with open endpoints to a complete contour. For this sketch we assume all contours are finite. (a) The initial contour. (b) Fixing D_1 and adding contours, as needed to obtain Γ'. (c) The resulting contour Γ'' is now complete with $\Omega_\pm$ clearly defined.

For a RHP $[G;\Gamma]$ we discuss the extension to a new RHP, $[\tilde{G},\Gamma'']$, and the conditions needed so that $[\tilde{G},\Gamma'']$ will be k-regular. First, define $\tilde{G}=I$ on $\Gamma''\setminus\Gamma$. Next if a given component Γ_i of Γ had its orientation reversed as a component of Γ'', define $\tilde{G}=G^{-1}$ on Γ_i. It is easily seen that if G satisfies the $(k-1)$th-order product condition on Γ then $[\tilde{G},\Gamma'']$ is k-regular. Also, it is clear that the solutions of $[G;\Gamma]$ and $[\tilde{G};\Gamma'']$ are in a one-to-one correspondence.

Next, we compare the singular integral equations

$$\mathcal{C}[G,\Gamma]u = G-I, \quad \text{on } \Gamma, \tag{3.10.1}$$

$$\mathcal{C}[\tilde{G},\Gamma'']\tilde{u} = \tilde{G}-I, \quad \text{on } \Gamma''. \tag{3.10.2}$$

It follows that (3.10.2) is equivalent to (3.10.1). Indeed, on $\Gamma''\setminus\Gamma$

$$\mathcal{C}[\tilde{G},\Gamma'']\tilde{u} = \tilde{u} - \mathcal{C}^-_{\Gamma''}u\cdot(\tilde{G}-I) = \tilde{u} = 0. \tag{3.10.3}$$

Furthermore, let $\Gamma_i\subset\Gamma$ have reversed orientation $-\Gamma_i\subset\Gamma''$. Let Γ_i^c be the complement of Γ_i with respect to Γ''. On Γ_i

$$\begin{aligned}
\tilde{u} - \mathcal{C}^-_{\Gamma''}\tilde{u}\cdot(\tilde{G}-I) &= \tilde{G}-I,\\
(\mathcal{C}^+_{-\Gamma_i}+\mathcal{C}^+_{\Gamma_i^c})\tilde{u} - (\mathcal{C}^-_{-\Gamma_i}+\mathcal{C}^-_{\Gamma_i^c})\tilde{u}\cdot\tilde{G} &= \tilde{G}-I,\\
(\mathcal{C}^+_{-\Gamma_i}+\mathcal{C}^+_{\Gamma_i^c})\tilde{u} - (\mathcal{C}^-_{-\Gamma_i}+\mathcal{C}^-_{\Gamma_i^c})\tilde{u}\cdot G^{-1} &= G^{-1}-I,\\
(\mathcal{C}^+_{-\Gamma_i}+\mathcal{C}^+_{\Gamma_i^c})\tilde{u}\cdot G - (\mathcal{C}^-_{-\Gamma_i}+\mathcal{C}^-_{\Gamma_i^c})\tilde{u} &= I-G.
\end{aligned}$$

On Γ_i we have $\mathcal{C}^+_{\Gamma_i^c}\tilde{u} = \mathcal{C}^-_{\Gamma_i^c}\tilde{u}$ and using the orientation $\mathcal{C}^\pm_{-\Gamma_i} = \mathcal{C}^\mp_{\Gamma_i}$. We obtain

$$(\mathcal{C}^+_{\Gamma_i}+\mathcal{C}^+_{\Gamma_i^c})\tilde{u} - (\mathcal{C}^-_{\Gamma_i}+\mathcal{C}^-_{\Gamma_i^c})\tilde{u}\cdot G = G-I.$$

This argument applied to each re-oriented contour combined with (3.10.3) shows

$$\tilde{u} - \mathcal{C}^-_{\Gamma}\tilde{u}\cdot(G-I) = G-I.$$

Thus proving equivalence. We arrive at the following theorem.

Theorem 3.10.2. *Let Γ be a possibly incomplete contour and let G satisfy the $(k-1)$th-order product condition on Γ. If for any augmentation Γ'' of Γ and extension $\tilde{G}$ of G, $\mathcal{C}[\tilde{G};\Gamma'']$ is invertible on $L^2(\Gamma)$, so is $\mathcal{C}[G;\Gamma]$, and $u=\mathcal{C}[G;\Gamma]^{-1}(G-I)\in H^k_z(\Gamma)$.*

Remark 3.10.3. *A theoretical contribution of this work is that the Sobolev spaces of Zhou do not make sense on incomplete contours. As we have seen, the spaces $H^k_z(\Gamma)$ are ideal when Γ is incomplete. This is one reason for considering $\mathcal{C}[G;\Gamma]$ instead of $\mathcal{C}'[G;\Gamma]$.*

3.10.2 Truncation

Thus far we have justified augmenting incomplete contours to obtain an equivalent RHP on complete contours. Often, in practice, we start with a RHP posed on an unbounded contour and we wish to truncate it to a problem on a finite contour. The following result justifies this process.

Proposition 3.10.4. *Assume $[G;\Gamma]$ is k-regular. For every $\epsilon > 0$ there exists a function G_ϵ defined on Γ and a bounded contour $\Gamma_\epsilon \subset \Gamma$ such that:*

- $G_\epsilon = I$ *on* $\Gamma \setminus \Gamma_\epsilon$,
- $\|G_\epsilon - G\|_{W^{k,\infty}(\Gamma)\cap H^k(\Gamma)} < \epsilon$
- $[G_\epsilon, \Gamma_\epsilon]$ *is k-regular and*

$$\|\mathcal{C}[G;\Gamma] - \mathcal{C}[G_\epsilon,\Gamma]\|_{\mathcal{L}(L^2(\Gamma))} < \epsilon \|\mathcal{C}_\Gamma^-\|_{\mathcal{L}(L^2(\Gamma))}.$$

Proof. A matrix-valued function f is chosen such that

- $f|_{\Gamma_i} \in C^\infty(\Gamma_i)$,
- $f = I$ in a neighborhood of all intersection points,
- f has compact support, and
- $\|(G-I)f + I - G\|_{W^{k,\infty}(\Gamma)\cap H^k(\Gamma)} < \epsilon$.

Equate $G_\epsilon = (G-I)f + I$. The last property follows immediately. □

This justifies the truncation of infinite contours to bounded contours and it shows this process preserves smoothness. For numerical computations in the next chapter, we truncate contours when the jump matrix is, to machine precision, the identity matrix.

3.10.3 Lensing

Here we go over, in detail, the process of lensing a RHP. This is one of the many deformation techniques that are useful both in the numerical method presented in the following chapter and for the method of nonlinear steepest descent. We start with a RHP (Figure 3.2(b))

$$\begin{aligned} &\Phi_1^+(k) = \Phi_1^-(k)G(k), \quad k \in \Gamma \subset \mathbb{R}, \\ &\Phi_1(\infty) = I. \end{aligned}$$

We choose $\Gamma \subset \mathbb{R}$ for simplicity and assume $0 \in \Gamma$. Assume that G has a factorization

$$G(k) = M_3(k)M_2(k)M_1(k).$$

Assume for simplicity that all matrices are nonsingular. Fix an $r > 0$ and define the regions Ω_i, $i = 1,2,3,4$, see Figure 3.2(a), by

$$\begin{aligned} \Omega_1 &= \{k \in \mathbb{C} : \operatorname{Im} k > 0 \text{ and } |k| > r\}, \\ \Omega_2 &= \{k \in \mathbb{C} : \operatorname{Im} k < 0 \text{ and } |k| > r\}, \\ \Omega_3 &= \{k \in \mathbb{C} : \operatorname{Im} k > 0 \text{ and } |k| < r\}, \\ \Omega_4 &= \{k \in \mathbb{C} : \operatorname{Im} k > 0 \text{ and } |k| < r\}. \end{aligned}$$

Further assume that M_3 has an analytic extension in a neighborhood of Ω_4 and M_1 has an analytic extension in a neighborhood of Ω_3. We wish to change the RHP on $(-r, r)$ by a lensing process. Define a new function Φ_2 by (Figure 3.2(c))

$$\Phi_2(k) = \begin{cases} \Phi_1(k)M_1^{-1}(k), & \text{if } k \in \Omega_3, \\ \Phi_1(k)M_3(k), & \text{if } k \in \Omega_4, \\ \Phi_1(k), & \text{otherwise.} \end{cases}$$

Define new contours Γ_i, $i = 1, 2, 3, 4, 5$, all oriented in the direction of increasing real part, by

$$\begin{aligned} \Gamma_1 &= \Gamma \cap (-\infty, r), \\ \Gamma_2 &= \{k \in \mathbb{C} : \operatorname{Im} k > 0 \text{ and } |k| = r\}, \\ \Gamma_3 &= (-r, r), \\ \Gamma_4 &= \{k \in \mathbb{C} : \operatorname{Im} k < 0 \text{ and } |k| - r\}, \\ \Gamma_5 &= \Gamma \cap (r, \infty). \end{aligned}$$

We compute the jumps of Φ_2 on these contours. As an example consider Γ_2. Set

$$\Phi_2^+(k) = \Phi_2^-(k)U(k), \quad k \in \Gamma_2,$$

for some matrix $U(k)$ to be determined. In this case $\Phi_2^+(k) = \Phi_1^+(k) = \Phi_1^-(k) = \Phi_2^-(k)M_1(k)$. We find that $U(k) = M_1(k)$. Repeating this process on all contours shows that Φ_2 satisfies the following RHP (Figure 3.2(d))

$$\Phi_2^+(k) = \begin{cases} \Phi_2^-(k)G(k), & \text{if } k \in \Gamma_1, \\ \Phi_2^-(k)M_1(k), & \text{if } k \in \Gamma_2, \\ \Phi_2^-(k)M_2(k), & \text{if } k \in \Gamma_3, \\ \Phi_2^-(k)M_3(k), & \text{if } k \in \Gamma_4, \\ \Phi_2^-(k)G(k), & \text{if } k \in \Gamma_5, \end{cases}$$
$$\Phi_2(\infty) = I.$$

It is clear that this generalizes to contours off the line and is only limited by the analyticity properties of the factorization. Furthermore, if $M_1, M_3 \to I$ as $k \to \infty$ in the proper regions the lensing can be employed in infinite regions. Note that one of the matrices M_i could be the identity in which case that contour is dropped from the RHP.

3.10.4 Conjugation

Conjugation is a simple concept but it allows additional deformations of a RHP. Consider a RHP $[G; \Gamma]$ with solution Φ. Let $\Psi_\pm, \Psi_\pm^{-1} \in L^\infty(\Gamma)$ be a solution of another problem $[H; \Gamma]$. Then

$$\Phi_+\Psi_+^{-1} = \Phi_-\Psi_-^{-1}\Psi_- G H^{-1}\Psi_-^{-1}.$$

Concisely, $\Phi\Psi^{-1}$ is a solution of $[\Psi_- G H^{-1}\Psi_-^{-1}; \Gamma]$. If $H = G$ then the jump becomes the identity. This method is especially useful in conjunction with lensing.

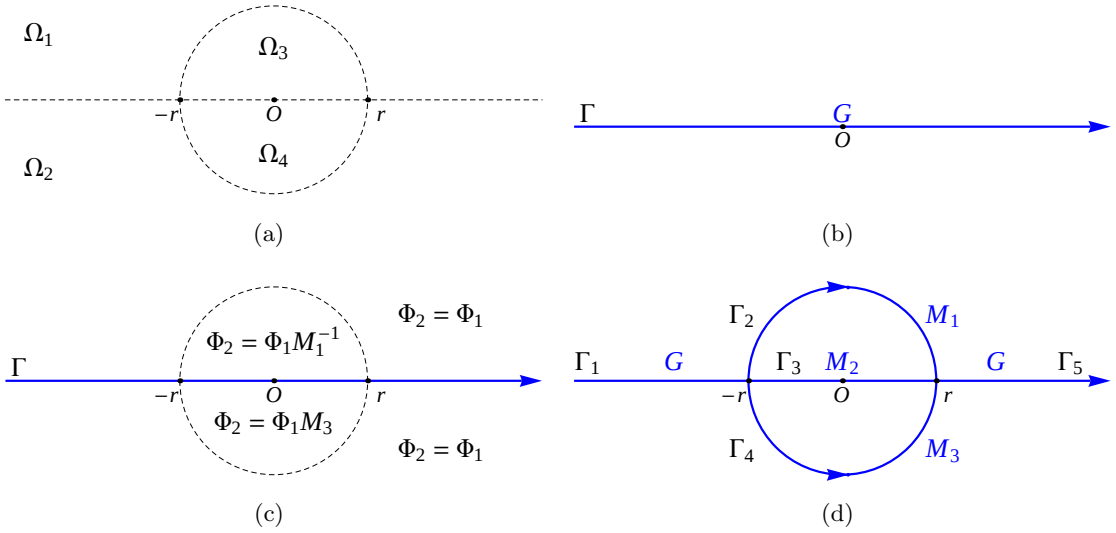

Figure 3.10.2: The lensing process. (a) Regions in the complex k-plane, (b) Contours and jump matrices for the RHP for Φ_1, (c) Definition of Φ_2, (d) Contours and jump matrices for the RHP for Φ_2.

Example 3.10.5. *Assume M_2 (Figure 3.10.2) is diagonal. The problem $[M_2;\Gamma_3]$ (see Figure 3.10.2 for Γ_3) can be solved with the techniques in Section 3.4.1. Let Ψ be this solution. By Lemma 3.1.13 we know that Ψ will have singularities at $\pm r$. The function $\Sigma = \Phi_2\Psi^{-1}$ satisfies*

$$\begin{aligned}
\Sigma^+ &= \Sigma_-\Psi_- G\Psi_+^{-1}, && \text{on } \Gamma_1, \Gamma_5,\\
\Sigma^+ &= \Sigma_-\Psi_- M_1\Psi_+^{-1}, && \text{on } \Gamma_2,\\
\Sigma^+ &= \Sigma_-\Psi_- M_3\Psi_+^{-1}, && \text{on } \Gamma_4,\\
\Sigma^+ &= \Sigma_-, && \text{on } \Gamma_3.
\end{aligned}$$

This process has removed the jump on Γ_3 from the RHP at the expense of singularities at $\pm r$. This will be used in the numerical solution of many RHPs. If the entries of M_2 are real-valued $\pm$ it can be shown using Lemma 3.1.13 that the solution of $[M_1;\Gamma_3]$ is bounded in the whole plane.

3.10.5 Contour scaling and decoupling

For simplicity, assume the RHP $[G^\xi, \Gamma^\xi]$ depends on a single parameter $\xi \geq 0$. Further, assume $\Gamma^\xi = \alpha(\xi)\Lambda + \beta(\xi)$ where Λ is a fixed contour. It follows that the matrix-valued function

$$H^\xi(k) = G^\xi(\alpha(\xi)k + \beta(\xi))$$

is defined on Λ.

We introduce a parameter into the problem to demonstrate a situation in which the

RHPs on each disjoint contour decouple from each other in the limit.

Example 3.10.6. *Assume* $\Gamma^\xi = \Gamma_1^\xi \cup \Gamma_2^\xi$ *and*

$$\begin{aligned}\Gamma_1^\xi &= \alpha_1(\xi)\Lambda_1 + \beta_1,\\ \Gamma_2^\xi &= \alpha_2(\xi)\Lambda_2 + \beta_2, \quad |\beta_1 - \beta_2| > 0.\end{aligned}$$

Assume that both Λ_1 *and* Λ_2 *are bounded. We consider the* L^2 *norm of the Cauchy operator applied to a function defined on* Γ_1^ξ *and evaluated on* Γ_2^ξ*:* $\mathcal{C}_{\Gamma_1^\xi} u(z)|_{\Gamma_2^\xi}$*. Explicitly,*

$$\mathcal{C}_{\Gamma_1^\xi} u(z) = \int_{\Gamma_1^\xi} \frac{u(s)}{s-z} \bar{d}x.$$

This is a Hilbert–Schmidt operator, and

$$\|\mathcal{C}_{\Gamma_1^\xi}\|^2_{\mathcal{L}(L^2(\Gamma_1^\xi), L^2(\Gamma_2^\xi))} \leq \int_{\Gamma_1^\xi}\int_{\Gamma_2^\xi} \frac{|dxdk|}{|x-k|^2}. \tag{3.10.4}$$

A simple change of variables shows that

$$\|\mathcal{C}_{\Gamma_1^\xi}\|^2_{\mathcal{L}(L^2(\Gamma_1^\xi), L^2(\Gamma_2^\xi))} \leq |\alpha_1(\xi)\alpha_2(\xi)| \int_{\Lambda_1}\int_{\Lambda_2} \frac{|dsdy|}{|\alpha_1(\xi)s - \alpha_2(\xi)y + \beta_1 - \beta_2|^2}. \tag{3.10.5}$$

Since the denominator in the integral in (3.10.5) *is bounded away from zero and both* Λ_i *are bounded, the right-hand side tends to zero if either* α_1 *or* α_2 *tend to zero.*

This argument, with more contours, is used in Chapter 5 to justify Algorithm 5.1.11 in this limit by noting that this type of Cauchy operator (evaluation off the contour of integration) constitutes the operator $\mathcal{T}$ *in Section 5.1. We have the representation*

$$\mathcal{C}[G^\xi; \Gamma^\xi] = \begin{bmatrix} \mathcal{C}[G_1^\xi; \Gamma_1^\xi] & 0 \\ 0 & \mathcal{C}[G_2^\xi; \Gamma_2^\xi] \end{bmatrix} + \mathcal{T}^\xi,$$

where $\|\mathcal{T}^\xi\|_{\mathcal{L}(L^2(\Gamma))} \to 0$ *as* $\xi \to \infty$*.*

Similarly, this analysis follows in some cases when β_i *depends on* ξ*. For example, when*

$$\inf_{t\in S} |\beta_1(\xi) - \beta_2(\xi)| = \delta > 0. \tag{3.10.6}$$

One can extend this to the case where (3.10.6) *is not bounded away from zero but approaches zero slower than* $a_1(\xi)a_2(\xi)$*.*

Chapter 4

Inverse Scattering and Nonlinear Steepest Descent

We present a unified discussion of the solution of IVP for the defocusing NLS equation

$$\begin{aligned} iq_t + q_{xx} - 2\lambda|q|^2 q = 0, \quad \lambda = 1 \\ q(x,0) = q_0(x) \in \mathcal{S}_\delta(\mathbb{R}). \end{aligned} \tag{4.0.1}$$

The full development presented in this chapter requires $q_0 \in \mathcal{S}_\delta(\mathbb{R})$ but the assumptions on q_0 for each individual result is made explicit. The use of spaces of non-smooth functions illustrates the parallels between the inverse scattering transform and the Fourier transform. First, we present the solution of this problem using the inverse scattering transform with the formalism of Fokas [49]. As presented in (2.5.7) and (2.5.8), the solution of the NLS equation can be recovered from the solution of a matrix RHP. The development up to this point makes no use of $\lambda = 1$ ($\lambda = -1$ for the focusing NLS equation). We apply the Deift and Zhou method of nonlinear steepest descent to this RHP to extract the long-time asymptotics with $\lambda = 1$. This whole process invokes much of the theory of Chapter 3.

4.1 The inverse scattering transform

Our starting point is the expressions for μ_1 and μ_2 in (2.5.6):

$$\begin{aligned} \mu_1(x,t,k) &= I + \int_{(-\infty,t)}^{(x,t)} e^{-ik(x-\xi)\hat{\sigma}_3}[Q(\xi,\tau)\mu(\xi,\tau,k)]d\xi, \\ \mu_2(x,t,k) &= I + \int_{(\infty,t)}^{(x,t)} e^{-ik(x-\xi)\hat{\sigma}_3}[Q(\xi,\tau)\mu(\xi,\tau,k)]d\xi, \end{aligned} \tag{4.1.1}$$

and the relationship

$$\mu_1(x,t,k) = \mu_2(x,t,k)e^{-i(kx+2k^2t)\hat{\sigma}_3}S(k). \tag{4.1.2}$$

Define the operator $T_{\pm,k}$ by

$$T_{\pm,k}u(x) = \int_{(\pm\infty,0)}^{(x,0)} e^{-i(k(x-\xi))\hat{\sigma}_3}[Q(\xi,0)u(\xi)]d\xi.$$

Since each component of $Q(x,0)$ is an $L^1(\mathbb{R})$ function, it is easily seen that $T^k_{\pm,k}$ is bounded on $L^\infty(\mathbb{R})$.

Lemma 4.1.1. *For $q_0 \in L^1(\mathbb{R})$ and $k \in \mathbb{R}$, $\|T^n_{\pm,k}\|_{\mathcal{L}(L^\infty(\mathbb{R}))} \leq C\|q_0\|^n_{L^1(\mathbb{R})}/n!$.*

Proof. Since $k \in \mathbb{R}$ we consider

$$e^{ikx\hat{\sigma}_3}[T_{\pm,k}u(x)] = \int_{(\pm\infty,0)}^{(x,0)} e^{ik\xi\hat{\sigma}_3}Q(\xi,0)e^{ik\xi\hat{\sigma}_3}u(\xi)d\xi.$$

So as to consider a kernel that is applied by left multiplication only, define $\hat{u}(x) = e^{ikx\hat{\sigma}_3}u(x)$ and $\hat{Q}(\xi,0) = e^{ikx\hat{\sigma}_3}Q(x,0)$. It is clear that the claim follows if we show that

$$\hat{T}_{\pm,k}\hat{u}(x) = \int_{(\pm\infty,0)}^{(x,0)} \hat{Q}(\xi,0)\hat{u}(\xi)d\xi. \tag{4.1.3}$$

It is also clear that, after switching the order of integration using Fubini's theorem, the operator $\hat{T}^n_{\pm,k}$ has the iterated kernel defined by

$$\begin{aligned}\hat{Q}_0(x,\xi) &= \hat{Q}(\xi,0),\\ \hat{Q}_n(x,\xi) &= \hat{Q}(\xi,0)\int_\xi^x \hat{Q}_{n-1}(x,s)ds.\end{aligned}$$

Therefore

$$\|\hat{T}^n_{\pm,k}\|_{\mathcal{L}(L^\infty(\mathbb{R}))} \leq \int_{-\infty}^{\infty} |\hat{Q}(\xi,0)| \left(\int_\xi^\infty |\hat{Q}(\xi,0)|\right)^{n-1} d\xi,$$

where $|\hat{Q}(\xi,0)|$ denotes any consistent sub-multiplicative matrix norm. This right-hand side simplifies:

$$\|\hat{T}^n_{\pm,k}\|_{\mathcal{L}(L^\infty(\mathbb{R}))} \leq \left(\int_{-\infty}^{\infty} |\hat{Q}(\xi,0)|d\xi\right)^n /n!.$$

This proves the result. □

This lemma combined with Theorem 1.5.8 shows the existence of $\mu_1(x,0,k)$ and $\mu_2(x,0,k)$ for x and k on the real line. In what follows we wish to have the same existence statement in a neighborhood of the real line. There is necessarily some exponential growth/decay involved.

Lemma 4.1.2. *Assume $q_0 \in \mathcal{S}_\delta(\mathbb{R})$. Then $\mu_1(x,0,k)$ and $\mu_2(x,0,k)$ are uniquely defined by* (4.1.1) *for $|\operatorname{Im} k| < \delta/2$.*

Proof. We consider μ_1. The argument for μ_2 follows in precisely the same way. Define $\hat{\mu}_1(x,k) = e^{ikx\sigma_3}\mu_1(x,0,k)$. From (4.1.1) we have

$$(I - \hat{T}_{-,k})\hat{\mu}_1 = I.$$

This equation is uniquely solvable via iteration for $\hat{\mu}_1 \in L^\infty(\mathbb{R})$ since $\hat{Q}(\xi,0) \in L^1(\mathbb{R})$. Therefore μ_1 is uniquely defined by (4.1.1) despite the fact that it contains exponentially growing components for $k \notin \mathbb{R}$. □

Next, we discuss the analyticity properties of μ_1 and μ_2 with respect to k. For now, we consider $q_0 \in \mathcal{S}_\delta(\mathbb{R})$ and generalize after. The analyticity of μ_1 follows from the analyticity of $\hat{\mu}_1$. Choose k and h so that $|\operatorname{Im} k| < \delta/2$ and $|\operatorname{Im}(k+h)| < \delta/2$ and consider

$$\begin{aligned}
&\frac{\hat{\mu}_1(x,k+h) - \hat{\mu}_1(x,k)}{h} \\
&= \frac{1}{h}\int_{-\infty}^{x} \left(e^{i(k+h)(x-\xi)\hat{\sigma}_3} Q(\xi,0)\hat{\mu}_1(\xi,k+h) - e^{ik(x-\xi)\hat{\sigma}_3} Q(\xi,0)\hat{\mu}_1(\xi,k) \right) d\xi \\
&= \int_{-\infty}^{x} e^{ik(x-\xi)\hat{\sigma}_3} Q(\xi,0) \left(\frac{\hat{\mu}_1(\xi,k+h) - \hat{\mu}_1(\xi,k)}{h} \right) d\xi \\
&+ \int_{-\infty}^{x} \left(\frac{e^{i(k+h)(x-\xi)\hat{\sigma}_3} Q(\xi,0) - e^{ik(x-\xi)\hat{\sigma}_3} Q(\xi,0)}{h} \right) \hat{\mu}_1(\xi,k+h) d\xi.
\end{aligned}$$

The complex differentiability of $\hat{\mu}_1$ follows once we show that the last term tends to a definite limit in the $L^\infty(\mathbb{R})$ norm. A straightforward calculation shows that

$$\int_{-\infty}^{\infty} \left| \left(e^{i(k+h)\xi\sigma_3} - e^{ik\xi\sigma_3} \right) Q(\xi,0) \right| d\xi \leq \int_{-\infty}^{\infty} 2e^{\gamma\xi} |Q(\xi,0)| d\xi,$$
$$\gamma = \max\{|\operatorname{Im}(k+h)|, |\operatorname{Im} k|\}.$$

Therefore the Dominated Convergence Theorem demonstrates that this integral tends to zero as $h \to 0$. This proves the continuity of $\hat{T}_{\pm,k}$, $(I - \hat{T}_{\pm,k})^{-1}$ and hence $\hat{\mu}_1(x,k)$ with respect to k for $|\operatorname{Im} k| < \delta/2$. A similar calculation, along with the continuity of $\hat{\mu}_1(x,k)$ shows that

$$\begin{aligned}
\lim_{h\to 0} \int_{-\infty}^{x} \left(\frac{e^{i(k+h)\xi\hat{\sigma}_3} Q(\xi,0) - e^{ik\xi\hat{\sigma}_3} Q(\xi,0)}{h} \right) \hat{\mu}_1(\xi,k+h) d\xi \\
= \int_{-\infty}^{x} i\xi [e^{ik\xi\sigma_3}, Q(\xi,0)] \hat{\mu}_1(\xi,k) d\xi,
\end{aligned}$$

in $L^\infty(\mathbb{R})$, see [53, Theorem 2.17]. Furthermore, similar methods and integration by parts indicates that $\mu_1(x,0,k) - I = \mathcal{O}(1/k)$ and $\mu_2(x,0,k) - I = \mathcal{O}(1/k)$ as $k \to \infty$. For fixed x, the same is true of all k derivatives of μ_1 and μ_2. We obtain the following result:

Lemma 4.1.3. *If $q_0 \in \mathcal{S}_\delta(\mathbb{R})$ then $\mu_1(x,0,k)$ and $\mu_2(x,0,k)$ are analytic functions of k in*

the open strip $|\operatorname{Im} k| < \delta/2$. *For fixed* x *and* $|\operatorname{Im} k| \le C < \delta/2$

$$\partial_k^n(\mu_1(x,0,k) - I) = \mathcal{O}(1/k) \quad as \quad k \to \infty,$$
$$\partial_k^n(\mu_2(x,0,k) - I) = \mathcal{O}(1/k) \quad as \quad k \to \infty.$$

We turn to results for q_0 in more general spaces. It follows that each column of μ_1 and μ_2 is determined independently of the other. Furthermore, the only exponential present in the first column of the equation for μ_1 is $e^{2ik(x-\xi)}$ implying that the first column μ_1^+ of μ_1 is analytic in the open upper-half plane. Indeed, μ_1^+ satisfies

$$\mu_1^+(x,0,k) = \begin{bmatrix} 1 \\ 0 \end{bmatrix} + \int_{-\infty}^{x} Q(\xi,0) \begin{bmatrix} e^{2ik(x-\xi)} & 0 \\ 0 & 1 \end{bmatrix} \mu_1^+(\xi,0,k)d\xi. \tag{4.1.4}$$

The methods of Lemma 4.1.3 applied to this equation prove the desired analyticity properties. Note that this follows assuming only that $q_0 \in L^1(\mathbb{R})$. Similarly, the second column μ_1^- is analytic in the open lower-half plane. For μ_2 the reverse is true. The first (second) column μ_2^- (μ_2^+) of μ_2 is analytic in the open lower- (upper-) half plane. We consider (4.1.4) in more detail.

Lemma 4.1.4. *If* $q_0 \in L^1 \cap L^2(\mathbb{R})$, $v_1^+ = \mu_1^+ - [1,0]^T$ *is an element of the Hardy space* $\mathcal{E}(\mathbb{R}^+)$.

Proof. Consider the equation satisfied by v_1^+:

$$v_1^+(x,0,k) - \int_{-\infty}^{x} Q(\xi,0) \begin{bmatrix} e^{2ik(x-\xi)} & 0 \\ 0 & 1 \end{bmatrix} v_1^+(\xi,0,k)d\xi = \int_{-\infty}^{x} Q(\xi,0) \begin{bmatrix} e^{2ik(x-\xi)} \\ 0 \end{bmatrix} d\xi.$$

We have already demonstrated that for $k \in \mathbb{R}$ this equation can be solved by iteration. The iterated kernel is given by

$$\mathcal{K}_0(x,\xi) = Q(\xi,0) \begin{bmatrix} e^{2ik(x-\xi)} & 0 \\ 0 & 1 \end{bmatrix},$$
$$\mathcal{K}_n(x,\xi) = \mathcal{K}_0(x,\xi) \int_s^x \mathcal{K}_{n-1}(x,s)ds.$$

Then

$$v_1^+(x,0,k) = f(x,k) + \sum_{n=0}^{\infty} \int_{-\infty}^{x} \mathcal{K}_n(x,\xi) f(\xi,k)d\xi, \tag{4.1.5}$$
$$f(x,k) = \int_{-\infty}^{x} Q(\xi,0) \begin{bmatrix} e^{2ik(x-\xi)} \\ 0 \end{bmatrix} d\xi.$$

We estimate the $L^2(\mathbb{R})$ norm

$$\left(\int_{-\infty}^{\infty}\left|\int_{-\infty}^{x}\mathcal{K}_n(x,\xi)f(\xi,k)d\xi\right|^2 dk\right)^{1/2} \leq \int_{-\infty}^{x}\left(\int_{-\infty}^{\infty}|\mathcal{K}_n(x,\xi)f(\xi,k)|^2 dk\right)^{1/2}$$
$$\leq \int_{-\infty}^{x}\sup_{k\in\mathbb{R}}|\mathcal{K}_n(x,\xi)|d\xi \times \sup_{\xi\in\mathbb{R}}\|f(\xi,\cdot)\|_{L^2(\mathbb{R})},$$

where the first inequality follows from Minkowski's inequality for integrals [53, Theorem 6.19]. We estimate the two factors separately. First,

$$\int_{-\infty}^{x}\sup_{k\in\mathbb{R}}|\mathcal{K}_n(x,\xi)|d\xi \leq \int_{-\infty}^{\infty}|Q(\xi,0)|\left(\int_{\xi}^{\infty}|Q(\xi,0)|d\xi\right)^{n-1} \leq C\|q_0\|^n_{L^1(\mathbb{R})}/n!. \tag{4.1.6}$$

A simple change of variables relates f to the Fourier transform

$$f(\xi,k) = \frac{1}{2}\int_{-\infty}^{0} e^{iks}Q(\xi+s/2)\begin{bmatrix} e^{-iks} \\ 0 \end{bmatrix} ds,$$

and therefore $\|f(\xi,\cdot)\|_{L^2(\mathbb{R})} \leq C\|Q\|_{L^2(\mathbb{R}}$. Since $\sum_n C^n/n!$ converges for any $C>0$, we have shown the L^2 norm of $v_1^+(x,0,\cdot)$ is bounded on the real axis. For $\mathrm{Im}(k)>0$ we note that all bounds hold, showing that $v_1^+ \in \mathcal{E}(\mathbb{R}^+)$. □

Similar arguments apply to μ_1^- and $\mu_2^\pm$ to show that once $[1,0]^T$ or $[0,1]^T$ is subtracted they are elements of an appropriate Hardy space. We also look at decay properties of the columns of $\mu_1 - I$ and $\mu_2 - I$.

Lemma 4.1.5. *For $q_0 \in L^1(\mathbb{R})$, $|f(x,k)| = o(1)$ as $|k|\to\infty$ for $\mathrm{Im}(k)\geq 0$.*

Proof. Fix $\epsilon>0$. We approximate $\lambda\bar{q}$ with a simple function $\sum_j \alpha_j\chi_{A_j}$ so that $\|\bar{q} - \sum_j \alpha_j\chi_{A_j}\|_{L^1(\mathbb{R})} < \epsilon/2$. Let $|k| > 4\sum_j|\alpha_j|/\epsilon$. Then for $|k|>1$

$$|f(x,k)| \leq \left|\int_{-\infty}^{x} e^{ik(x-\xi)}\left((\lambda\bar{q}(\xi) - \sum_j \alpha_j\chi_{A_j}(\xi)\right)d\xi\right| + \left|\int_{-\infty}^{x} e^{ik(x-\xi)}\sum_j \alpha_j\chi_{A_j}(\xi)d\xi\right| \leq \epsilon.$$

□

Lemma 4.1.6. *For $q_0 \in L^1\cap L^2(\mathbb{R})$, $\mu_1^+(x,0,k) = [1,0]^T + o(1)$ as $|k|\to\infty$ for $\mathrm{Im}(k)\geq 0$.*

Proof. Taking a supremum over $k\in\mathbb{R}$ in (4.1.5), while noting that $f(x,k)$ has the desired decay and the estimate (4.1.6) can still be applied, produces the result. □

Remark 4.1.7. *Similar statements to Lemma 4.1.6 follow for μ_1^- in $\mathbb{C}^-$ and $\mu_2^\pm$ in $\mathbb{C}^\pm$.*

We move to a discussion of the matrix $S(k)$ that is defined by (4.1.2). Abel's identity shows that $\mu_1(x,0,k)$ and $\mu_2(x,0,k)$ have determinant independent of x. Indeed, both satisfy

$$\left(e^{ikx\hat{\sigma}_3}\mu\right)_x = e^{ikx\hat{\sigma}_3}Q(e^{ikx\hat{\sigma}_3}\mu).$$

Since $e^{ikx\hat{\sigma}_3}Q$ is traceless, $\det\mu_1$ and $\det\mu_2$ are independent of x. Then for each k we let $x \to -\infty$ for μ_1 and $x \to \infty$ for μ_2 to see that $\det\mu_1(x,0,k) = \det\mu_2(x,0,k) = 1$. Therefore $\det S(k) = 1$. For $j = 1, 2$, the first column v_1 of μ_j satisfies

$$v_{1x} + ik \begin{bmatrix} 0 & 0 \\ 0 & -2 \end{bmatrix} v_1 = Qv_1, \quad v_1((-1)^j\infty) = \begin{bmatrix} 1 \\ 0 \end{bmatrix},$$

while the second column v_2 satisfies

$$v_{2x} + ik \begin{bmatrix} 2 & 0 \\ 0 & 0 \end{bmatrix} v_2 = Qv_2, \quad v_2((-1)^j\infty) = \begin{bmatrix} 0 \\ 1 \end{bmatrix}.$$

Let $v_2(x,0,k) = [v_{21}(x,0,k), v_{22}(x,0,k)]^T$ and define

$$v_2^*(x,0,k) = \begin{bmatrix} \overline{v_{22}(x,0,\bar{k})} \\ \overline{\lambda v_{21}(x,0,\bar{k})]} \end{bmatrix}.$$

It follows that $v_1(x,0,k) = v_2^*(x,0,k)$. This means that swapping rows and columns, followed by Schwarz conjugation and multiplication on the off-diagonal by λ leaves any solution μ invariant. Let

$$S(k) = \begin{bmatrix} a(k) & \mathcal{B}(k) \\ b(k) & \mathcal{A}(k) \end{bmatrix}.$$

A tedious, but simple calculation shows that $\mathcal{A}(k) = \overline{a(\bar{k})}$ and $\mathcal{B}(k) = \lambda\overline{b(\bar{k})}$ where $\lambda^2 = 1$ is used explicitly. Furthermore $\det S(k) = 1$ implies

$$|a(k)|^2 - \lambda|b(k)|^2 = 1 \quad \text{for} \quad k \in \mathbb{R}. \tag{4.1.7}$$

Using $\det\mu_1 = \det\mu_2 = 1$ and the fact that each entry of μ_1 and μ_2 is in $L^\infty \cap L^2(\mathbb{R})$ we find that $a - 1, b \in L^\infty \cap L^2(\mathbb{R})$. If $q_0 \in \mathcal{S}_\delta(\mathbb{R})$ it follows that $S(k)$ is analytic in the strip $|\operatorname{Im} k| < \delta/2$. If we only require $q_0 \in L^1 \cap L^2(\mathbb{R})$, b cannot, in general, be analytically extended off $\mathbb{R}$ but $a - 1 \in \mathcal{E}(\mathbb{R}^+)$.

Following Lemma 4.1.6, for sufficiently large $k \in \overline{\mathbb{C}^+}$, $a(k)$ must be bounded away from zero. We assume here that $a(k)$ does not vanish in the finite plane, implying that $1/a(k)$ is bounded in $\mathbb{C}^+$. This assumption is known to be true when $\lambda = 1$ [8]. Define

$$\Phi = \begin{cases} \Phi^+, & \text{in } \mathbb{C}^+, \\ \Phi^-, & \text{in } \mathbb{C}^-, \end{cases}$$

$$\Phi^+ = \begin{bmatrix} \dfrac{\mu_1^+}{a(k)}, \mu_2^+ \end{bmatrix}, \quad \Phi^- = \begin{bmatrix} \mu_2^-, \dfrac{\mu_1^-}{\overline{a(\bar{k})}} \end{bmatrix}.$$

It follows that $\Phi(x,t,k)$ solves the following RHP when $t=0$:

$$\Phi^+(x,t,s) = \Phi^-(x,t,s)G(x,t,s), \quad s\in\mathbb{R}, \quad \Phi(x,0,\infty) = I, \tag{4.1.8}$$
$$G(x,t,k) = \begin{bmatrix} 1-\lambda\overline{\rho(\bar{k})}\rho(k) & -\lambda\overline{\rho(\bar{k})}e^{-2ikx-4ik^2t} \\ \rho(k)e^{2ikx+4ik^2t} & 1 \end{bmatrix}$$

and

$$Q(x,0) = -i\lim_{|k|\to\infty}[\sigma_3, k\Phi(x,0,k)].$$

This is seen by noting that Φ solves (2.5.2) and $\Phi_x = \mathcal{O}(1/k)$ if $q_0\in\mathcal{S}_\delta(\mathbb{R})$. Indeed, the arguments in Remark 4.1.7 show the decay of Φ_x.

We derive another representation for $a(k)$. Note that

$$M(x,k) = \begin{bmatrix} \mu_1^+(x,0,k) & \mu_2^+(x,0,k) \end{bmatrix}$$

is a solution of (2.5.2). Furthermore, it follows that $a(k) = \det M(x,k)$. Since $\mu_2^+\to[0,1]^T$ as $x\to\infty$ we find that $a(k) = \lim_{x\to\infty}\mu_{11}^+(x,0,k)$ where μ_{11}^+ denotes the first component of μ_1^+. We look at the large x behavior of $f(x,k)$. We find

$$\begin{aligned}\|f(x,k)\| &\le \left|\int_{-\infty}^{\infty} e^{-2ik\xi}q_0(\xi)d\xi\right| + \left|\int_x^{\infty} e^{-2ik\xi}q_0(\xi)d\xi\right| \\ &\le |\hat{q}_0(2k)| + I(x),\end{aligned}$$

where $I(x)\to 0$ as $x\to\infty$. For the remainder of this section we assume $q_0\in\mathcal{S}_\delta(\mathbb{R})$, so that the Fourier transform satisfies $\hat{q}_0(k)\in\mathcal{S}(\mathbb{R})$. This implies that $a(k) = 1+\mathcal{O}(1/k^n)$ as $k\to\infty$ for every $n>0$. Combining this with (4.1.7) we see $b(k) = \mathcal{O}(1/k^n)$ for every $n>0$. Also, following Lemma 4.1.3 we see that $a-1, b\in H^k(\mathbb{R})$ for every $k>0$ whenever $q_0\in\mathcal{S}_\delta(\mathbb{R})$. These facts suffice for the theory we present here, yet more regularity can be shown: for $q_0\in\mathcal{S}(\mathbb{R})$ it is known that $b/a\in\mathcal{S}(\mathbb{R})$ [8].

Remark 4.1.8. *The RHP for Φ has a unique solution. The jump matrix G has unit determinant so the Fredholm index of the associated singular integral operator $\mathcal{C}[J;\mathbb{R}]$ is zero (Theorem 3.8.20). Furthermore, the symmetry of $G(x,t,k)$ is such that the vanishing lemma applies (Theorem 3.8.29).*

We prove a result that concerns the differentiability of Φ with respect to x or t.

Lemma 4.1.9. *Consider a RHP of the form*

$$\Psi^+(x,s) = \Psi^-(x,s)K(x,s), \quad s\in\Gamma, \quad \Phi(x,\infty) = I,$$
$$K(x,s) = H_d(s) + e^{i\gamma(s)x\hat{\sigma}_3}H_o(s), \quad x\in\mathbb{R}, \quad \gamma:\Gamma\to\mathbb{R},$$

where H_d contains the diagonal elements of K and $e^{\gamma(s)x\hat{\sigma}_3}H_o$, the off-diagonal elements. With Γ being admissible, assume $K(x,\cdot)-I\in L^2\cap L^\infty(\mathbb{R})$ and $\mathcal{C}[K,\Gamma]$ is invertible on $L^2(\Gamma)$ with bounded inverse. If $\gamma(s)H_0(s)\in L^2\cap L^\infty(\Gamma)$ then $\partial_x\Psi(x,k)$ exists for every x and $k\in\mathbb{C}\setminus\Gamma$.

Proof. Let $u^{(x)}$ be the solution of $u^{(x)} - \mathcal{C}_\Gamma^- u^{(x)}(K(x,\cdot) - I) = K(x,\cdot) - I$. Consider the difference

$$\frac{u^{(x+h)} - u^{(x)}}{h} - \frac{1}{h}\left(\mathcal{C}_\Gamma^- u^{(x)}(K(x,\cdot) - I) - \mathcal{C}_\Gamma^- u^{(x+h)}(K(x+h,\cdot) - I)\right) = \frac{K(x,\cdot) - K(x+h,\cdot)}{h},$$

Define $v^{(x,h)} = (u^{(x+h)} - u^{(x)})/h$. We find

$$\mathcal{C}[K(x,\cdot),\Gamma]v^{(x,h)} = (I + C_\Gamma^- u^{(x+h)})\frac{K(x,\cdot) - K(x+h,\cdot)}{h}.$$

The right-hand side tends to $(I + C_\Gamma^- u^{(x)})\partial_x K(x,\cdot)$ in $L^2(\Gamma)$. Using the boundedness of the inverse operator we find that $v^{(x)} = \lim_{h\to 0} v^{(x,h)}$ exists in $L^2(\Gamma)$. Therefore $\partial_x \Psi(x,k) = \mathcal{C}_\Gamma v^{(x)}$. □

We state a result from [49] that allows us to complete the solution of the initial value problem for the NLS equations.

Proposition 4.1.10 (The dressing method [49])**.** *Assume Γ is an admissible contour. Let $M(x,t,k)$ satisfy the 2×2 RHP*

$$M^+(x,t,s) = M(x,t,s)e^{-i(sx+2s^2t)\hat{\sigma}_3}S(s), \quad s\in\Gamma, \quad M(x,t,\infty) = I,$$

where $\det S(k) = 1$. Here the subscripts denote the $(1,1)$ component. Assume this RHP has a unique solution that is differentiable in x and t for every $k\notin\Gamma$. Then M satisfies (2.5.2) *and* (2.5.3) *with*

$$Q(x,t) = \begin{bmatrix} 0 & q_1(x,t) \\ q_2(x,t) & 0 \end{bmatrix}.$$

defined by

$$Q(x,t) = i\lim_{k\to\infty}[\sigma_3, kM(x,t,k)].$$

Furthermore, Q satisfies $iQ_t - Q_{xx}\sigma_3 + 2Q^3\sigma_3 = 0$.

Choosing jumps so that $q_2 = \lambda\bar{q}_1$ produces solutions of NLS equations. We combine Proposition 4.1.10 with Lemma 4.1.9 to obtain the final result of this section.

Theorem 4.1.11. *Assume $q_0\in\mathcal{S}_\delta(\mathbb{R})$. Then $S(k)$ is analytic for $|\operatorname{Im} k| < \delta/2$ and $e^{i(kx-2k^2t)\hat{\sigma}_3}S(k) - I \in H^1(\mathbb{R})$ for all $k>0$ and $\rho\in\mathcal{S}(\mathbb{R})$. Furthermore, the RHP in* (4.1.8) *has a unique solution for every x and t. The solution of NLS with $q(x,0) = q_0(x)$ is given by*

$$-i\lim_{|k|\to\infty}[\sigma_3, k\Phi(x,t,k)]_{12} = -2i\lim_{|k|\to\infty} k\Phi_{12}(x,t,k),$$

where the limit is taken in a direction that is not tangential to $\mathbb{R}$.

4.2 Nonlinear steepest descent

We discuss the Deift and Zhou method of nonlinear steepest descent as applied to (4.1.8). Nonlinear steepest descent has been used to analyze the asymptotic behavior of many RHPs [24, 34, 35, 37, 38]. The full theory for the NLS equation applies to initial conditions lying in appropriate weighted Sobolev spaces [38]. For simplicity and ease of exposition we restrict to $q_0 \in \mathcal{S}_\delta(\mathbb{R})$.

We begin by introducing factorizations of $G(x,t,k)$. It turns out that $\sup_{k\in\mathbb{R}} |\rho(k)| < 1$ [8] and this implies that G admits both an UL and an LDU factorization for all $x,t,k \in \mathbb{R}$:

$$
\begin{aligned}
G(x,t,k) &= M(k)P(k) = L(k)D(k)U(k),\\
P(k) &= \begin{bmatrix} 1 & 0 \\ \rho(k)e^{2i(kx+2k^2t)} & 1 \end{bmatrix}, \qquad M(k) = \begin{bmatrix} 1 & \lambda\overline{\rho(\bar{k})}e^{-2i(kx+2k^2t)} \\ 0 & 1 \end{bmatrix},\\
L(k) &= \begin{bmatrix} 1 & 0 \\ \frac{\rho(k)}{\tau(k)}e^{2i(kx+2k^2t)} & 1 \end{bmatrix}, \qquad D(k) = \begin{bmatrix} \tau(k) & 0 \\ 0 & 1/\tau(k) \end{bmatrix},\\
U(k) &= \begin{bmatrix} 1 & \frac{\lambda\overline{\rho(\bar{k})}}{\tau(k)}e^{-2i(kx+2k^2t)} \\ 0 & 1 \end{bmatrix}, \qquad \tau(k) = 1-\lambda\rho(k)\overline{\rho(\bar{k})}.
\end{aligned}
$$

From the results of the previous section, each of these factors is analytic and limits rapidly to the identity in the strip $|\operatorname{Im} k| < \delta/2$. The deformations of the RHP that follow are centered around the stationary phase point for $e^{-2i(kx+2k^2t)}$: $k_0 = -x/(4t)$, see Section 2.2. We break the asymptotic calculations up into two cases: $t = 0$ and $t \gg 0$.

4.2.1 Asymptotics for $t = 0$ as $|x| \to \infty$.

These asymptotics are already known since we have specified the initial condition. It is instructive to see how this behavior can be extracted from the RHP. For $x < 0$, we use only the LDU factorization and the lensing process, see Section 3.10.3. Define for $0 < \delta' < \delta/2$

$$
\Phi_1(k) = \begin{cases} \Phi(k)U^{-1}(k), & \text{if } 0 < \operatorname{Im} k < \delta',\\ \Phi(k)L(k), & \text{if } -\delta' < \operatorname{Im} k < 0,\\ \Phi(k), & \text{if } |\operatorname{Im} k| > \delta', \end{cases}
$$

where we have suppressed the x and t dependence for convenience. The function Φ_1 solves the RHP

$$
\Phi_1^+(k) = \Phi_1^+(k)G_1(k), \quad G_1(k) = \begin{cases} U(k), & \text{if } \operatorname{Im} k = \delta',\\ L(k), & \text{if } \operatorname{Im} k = -\delta',\\ D(k), & \text{if } \operatorname{Im} k = 0. \end{cases}
$$

The exponential in $U(k)$, the only jump in the upper-half plane, is of the form $\exp(2x\delta' + 2ixs)$ for $s \in \mathbb{R}$. It is clear that

$$
\|U-I\|_{L^1\cap L^\infty(\mathbb{R}+i\delta')} < Ce^{2x\delta'} \quad \text{and} \quad \|L-I\|_{L^1\cap L^\infty(\mathbb{R}-i\delta')} < Ce^{2x\delta'}.
$$

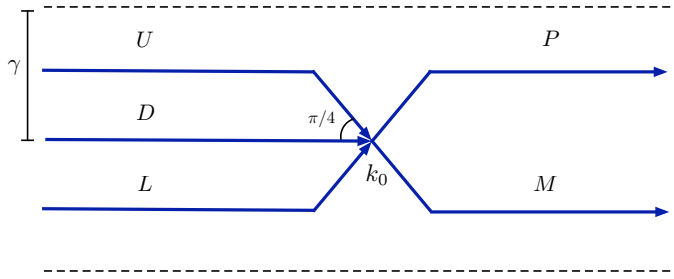

Figure 4.3.1: Jump contours after lensing for the RHP for Φ_2. The distance between the horizontal contours in the upper/lower-half planes is δ'.

Hence the same bounds hold for $L^2(\mathbb{R} \pm i\delta)$. Lemma 3.9.4 implies that u, the solution of $\mathcal{C}[G_1; \Gamma_1]u = G - I$ with $\Gamma_1 = \mathbb{R} \cup (\mathbb{R} + i\delta') \cup (\mathbb{R} - i\delta)$ tends exponentially to the solution of $\mathcal{C}[D; \mathbb{R}]v = D - I$ in the L^2 norm. The solution of this diagonal problem can be found explicitly (see Section 3.4.1):

$$\Delta(k; k_0) = \begin{bmatrix} \delta(k; k_0) & 0 \\ 0 & \delta^{-1}(k; k_0) \end{bmatrix}, \qquad \delta(k; k_0) = \exp\left(\mathcal{C}_{(-\infty, k_0)}\tau(k)\right),$$

with $k_0 = \infty$. It is important that the $(1, 2)$ component of $\Delta(k; k_0)$ is identically zero. From the expression

$$u = \mathcal{C}^-_{\Gamma_1} u(G_1 - I) + G_1 - I,$$

we use that u has bounded L^2 norm as $x \to -\infty$ and see that the $(1, 2)$ component of u satisfies

$$\|u_{12}\|_{L^1(\Gamma_1)} \leq C\|u\|_{L^2(\Gamma_1)}\|G_1 - I\|_{L^2(\Gamma_1)} + \|G_1 - I\|_{L^1(\Gamma_1)} \leq C' e^{2x\gamma'},$$

for a new constant C'. From Lemma 3.6.9, $q(x, 0)$ does indeed exponentially decay as $x \to -\infty$. Similar arguments show the same exponential behavior as $x \to +\infty$ when the UL factorization is used.

4.3 Asymptotics as $t \to \infty$

We concern ourselves with the asymptotics of the solution in the more physically relevant region $|k_0| = |-x/(4t)| < M$ for some $M > 0$ as $t \to \infty$. The derivation of these asymptotics requires significantly more machinery. We follow [36]. We lens the RHP for Φ on $(-\infty, k_0)$ using the LDU factorization and lens it on (k_0, ∞) using the UL factorization. Let Φ_2 denote the new function we seek after lensing. The jump contours and jump matrices for Φ_2 are shown in Figure 4.3.1.

With the exception of the jump matrix on $(-\infty, k_0)$, all jump matrices associated with Φ_2 tend to the identity matrix exponentially away from the stationary phase point k_0. We remove the jump on $(-\infty, k_0)$. Define $\Phi_3(k) = \Phi_2(k)\Delta^{-1}(k; k_0)$. A simple exercise shows that Φ_3 satisfies the jumps in Figure 4.3.2.

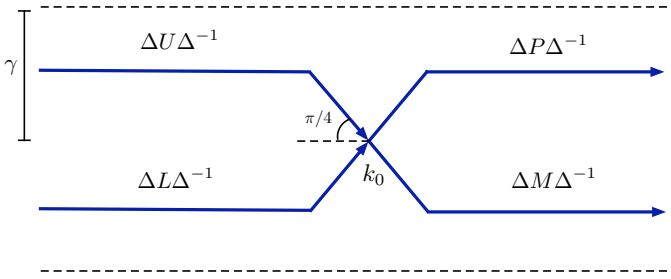

Figure 4.3.2: The jump matrices and jump contours for Φ_3. This incorporates the removal of the jump on $(-\infty, k_0)$.

The exponent present in the jump matrices can be written in the form $\exp(\pm\, t(-4k_0^2 + 4i(k-k_0)^2))$. This indicates increased localization as $t \to \infty$. Define $h(k) = -4k_0^2 + 4i(k-k_0)^2$. Near the stationary point we should be able to approximate the jump matrices by

$$
\begin{aligned}
[M](k) &= \begin{bmatrix} 1 & \lambda\overline{\rho(\bar{k}_0)}e^{-th(k)} \\ 0 & 1 \end{bmatrix}, \qquad [P](k) = \begin{bmatrix} 1 & 0 \\ \rho(k_0)e^{th(k)} & 1 \end{bmatrix}, \\
[L](k) &= \begin{bmatrix} 1 & 0 \\ \frac{\rho(k_0)}{\tau(k_0)}e^{th(k)} & 1 \end{bmatrix}, \qquad [D](k) = \begin{bmatrix} \tau(k_0) & 0 \\ 0 & 1/\tau(k_0) \end{bmatrix}, \\
[U](k) &= \begin{bmatrix} 1 & \frac{\lambda\overline{\rho(\bar{k}_0)}}{\tau(k_0)}e^{-th(k)} \\ 0 & 1 \end{bmatrix}, \qquad [\Delta](k;k_0) = \Delta_s(k;k_0)\Delta_r(k_0;k_0),
\end{aligned}
\tag{4.3.1}
$$

with

$$
\begin{aligned}
\Delta_s(k;k_0) &= \operatorname{diag}((k_0-k)^{f(k_0)/(2\pi i)}, (k_0-k)^{-f(k_0)/(2\pi i)}), \\
f(z) &= \log(\tau(z/\sqrt{8t} + k_0)), \\
\Delta_r(k;k_0) &\text{ is Hölder continuous at } k = k_0.
\end{aligned}
$$

In the next section we solve a problem with the localized jumps explicitly in terms of parabolic cylinder functions.

4.3.1 Construction of the global parametrix

We define global parametrix to be the solution of

$$
\Psi(z)^+ = \Psi^-(z) \begin{cases} [P]_\Delta(z), & \text{if } z \in e^{i\pi/4}(0,\infty), \\ [U]_\Delta(z), & \text{if } z \in e^{i3\pi/4}(0,\infty), \\ [L]_\Delta(z), & \text{if } z \in e^{i5\pi/4}(0,\infty), \\ [M]_\Delta(z), & \text{if } z \in e^{i7\pi/4}(0,\infty), \end{cases} \qquad \Psi(\infty) = I,
$$

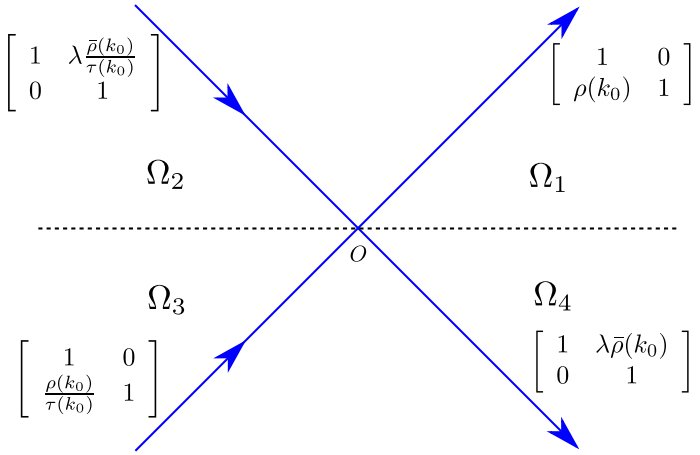

Figure 4.3.3: The jump contours for Φ with piecewise definition V_{k_0} and the regions Ω_i, $i = 1, \ldots, 4$.

where $[P]_\Delta(z) = [\Delta](z/\sqrt{8t} + k_0; k_0)[P](z/\sqrt{8t} + k_0)[\Delta]^{-1}(z/\sqrt{8t} + k_0; k_0)$ and similarly for L, U, and M. Note that the $(1,1)$ component of $\Delta_s(k_0; k_0)$ can be written as

$$(\Delta_s)_{11}(z/\sqrt{8t} + k_0; k_0) = (8t)^{f(k_0)/(4\pi i)} z^{f(k_0)/(2\pi i)}.$$

The RHP can be simplified. It is clear that $(8t)^{f(k_0)/(4\pi i)}$ and $\Delta_r(k_0; k_0)$ have no dependence on z (or on k), we define

$$\Psi_1(k) = \Delta_r^{-1}(k_0; k_0)(8t)^{-f(k_0)/(4\pi i)\sigma_3} \Psi(k)(8t)^{f(k_0)/(4\pi i)\sigma_3} \Delta_r(k_0; k_0). \tag{4.3.2}$$

It follows that Ψ_1 solves

$$\Psi_1^+(z) = \Psi_1^-(z)\ z^{f(k_0)/(4\pi i)\hat\sigma_3}[e^{(-2ik_0^2 t - iz^2/4)\hat\sigma_3} V_{k_0}], \quad z \in e^{i\pi/4} \times (\mathbb{R} \cup i\mathbb{R}), \quad \Psi_1(\infty) = I,$$

where V_{k_0} and the orientation of $e^{i\pi/4} \times (\mathbb{R} \cup i\mathbb{R})$ is shown in 4.3.3. This RHP is now deformed to one on the real line using a reverse lensing process. The resulting problem is not a classical L^2 RHP but it is exactly solvable. For $z \notin e^{i\pi/4} \times (\mathbb{R} \cup i\mathbb{R})$, define

$$\Psi_2(z) = \Psi_1(z) \begin{cases} z^{f(k_0)/(4\pi i)\hat\sigma_3} \left(e^{(-2ik_0^2 t - iz^2/4)\hat\sigma_3} \begin{bmatrix} 1 & 0 \\ \rho(k_0) & 1 \end{bmatrix} \right), & \text{if } z \in \Omega_1, \\ z^{f(k_0)/(4\pi i)\hat\sigma_3} \left(e^{(-2ik_0^2 t - iz^2/4)\hat\sigma_3} \begin{bmatrix} 1 & \frac{\lambda\bar\rho(k_0)}{\tau(k_0)} \\ 0 & 1 \end{bmatrix} \right), & \text{if } z \in \Omega_2, \\ z^{-f(k_0)/(4\pi i)\hat\sigma_3} \left(e^{(-2ik_0^2 t - iz^2/4)\hat\sigma_3} \begin{bmatrix} 1 & 0 \\ -\frac{\rho(k_0)}{\tau(k_0)} & 1 \end{bmatrix} \right), & \text{if } z \in \Omega_3, \\ z^{-f(k_0)/(4\pi i)\hat\sigma_3} \left(e^{(-2ik_0^2 t - iz^2/4)\hat\sigma_3} \begin{bmatrix} 1 & -\lambda\bar\rho(k_0) \\ 0 & 1 \end{bmatrix} \right), & \text{if } z \in \Omega_4. \end{cases}$$

It follows that Ψ_2 satisfies for $z \in \mathbb{R}$

$$\Psi_2^+(z) = \Psi_2^-(z) e^{(-2ik_0^2 t - iz^2/4)\hat{\sigma}_3} \left(z_-^{f(k_0)/(4\pi i)\sigma_3} G(0,0,k_0) z_+^{-f(k_0)/(4\pi i)\sigma_3} \right), \quad \Psi_2(\infty) = I.$$

We introduce a final transformation. Define $\Psi_3(z) = \Psi_2(z) z^{f(k_0)/(4\pi i)\sigma_3} e^{(2ik_0^2 t + iz^2/4)\hat{\sigma}_3}$, which satisfies

$$\Psi_3^+(z) = \Psi_3^-(z) G(0,0,k_0), \quad z \in \mathbb{R}, \tag{4.3.3}$$

$$\Psi_3(z) = (I + \Psi_{2,1}/z + \cdots) z^{f(k_0)/(4\pi i)\sigma_3} e^{2ik_0^2 t + iz^2/4\hat{\sigma}_3}, \quad \text{as } z \to \infty. \tag{4.3.4}$$

Since the jump matrix has no z dependence it can be seen that $\partial_z \Psi_3(z) \cdot \Psi_3^{-1}(z) = \mathcal{O}(z)$ has no jump on the real axis. Liouville's theorem shows that $\partial_z \Psi_3(z) \cdot \Psi^{-1}(z)$ must be a first-degree polynomial. A straightforward calculation shows

$$\begin{aligned} \partial_z \Psi_3 \Psi_3^{-1} = &\left(-\frac{iz}{2}\sigma_3 - \frac{i}{2}\Psi_{31}\sigma_3 + \mathcal{O}(1/z) \right) \\ &\times \left(I - \frac{1}{2}\Psi_{2,1} + \mathcal{O}(1/z^2) \right) = -\frac{iz}{2}\sigma_3 + \frac{i}{2}[\sigma_3, \Psi_{21}]. \end{aligned}$$

We obtain a differential equation for Ψ_3:

$$\partial_z \Psi_3(z) = \begin{bmatrix} -iz/2 & \kappa \\ \bar{\kappa} & iz/2 \end{bmatrix} \Psi_3(z), \quad \kappa = (\Psi_{2,1})_{12},$$

where the subscripts denote the $(1,2)$ component of Ψ_{31}. Note that at this point κ is not known and once we obtain it, we have determined the leading asymptotic behavior of the $(1,2)$-component of Ψ_2. Examining the first column and differentiating, we see

$$\begin{aligned} \partial_z (\Psi_3)_{11}(z) &= -z\frac{i}{2}(\Psi_3)_{11}(z) + \kappa(\Psi_3)_{21}(z), \\ \partial_z (\Psi_3)_{21}(z) &= \bar{\kappa}(\Psi_3)_{11}(z) + z\frac{i}{2}(\Psi_3)_{21}(z), \\ \partial_z^2 (\Psi_3)_{11}(z) &= -z\frac{i}{2}\partial_z(\Psi_3)_{11}(z) - \frac{i}{2}(\Psi_3)_{11}(z) + \kappa\partial_z(\Psi_3)_{21}(z). \end{aligned}$$

Therefore

$$\partial_z^2 (\Psi_3)_{11}(z) = \left(-\frac{z^2}{4} - \frac{i}{2} + |\kappa|^2 \right) (\Psi_3)_{11}(z), \tag{4.3.5}$$

$$\partial_z^2 (\Psi_3)_{21}(z) = \left(-\frac{z^2}{4} + \frac{i}{2} + |\kappa|^2 \right) (\Psi_3)_{21}(z). \tag{4.3.6}$$

The parabolic cylinder function $D_\nu(z)$ solves [84]:

$$\frac{d^2 D_\nu(z)}{dz^2} + \left(-\frac{1}{4}z^2 + \frac{1}{2} + \nu \right) = 0. \tag{4.3.7}$$

It follows that $(\Psi_3(z))_{11} = \alpha_{11} D_{i|\kappa|^2}(e^{i\pi/4}z)$ and similarly $(\Psi_3(z))_{21} = \alpha_{21} D_{-1+i|\kappa|^2}(e^{i\pi/4}z)$. Applying this reasoning to the second column of Ψ_3 we find the expression

$$\Psi_3(z) = \begin{bmatrix} \alpha_{11} D_{i|\kappa|^2}(e^{i\pi/4}z) & \alpha_{12} D_{-1-i|\kappa|^2}(e^{-i\pi/4}z) \\ \alpha_{21} D_{-1+i|\kappa|^2}(e^{i\pi/4}z) & \alpha_{22} D_{i|\kappa|^2}(e^{-i\pi/4}z) \end{bmatrix} X(z),$$

for some undetermined matrix $S(z)$. We choose $X(z)$ to be piecewise constant so that condition (4.3.4) is satisfied. It is shown in [40] that necessarily

$$\alpha_{11} = e^{\pi|\beta|^2/4}, \quad \alpha_{12} = e^{\pi|\beta|^2/4 - 3i\pi/4}\kappa, \quad \alpha_{21} = \bar{\alpha}_{12}, \quad \alpha_{22} = \alpha_{11},$$

and

$$X(z) = \begin{cases} \begin{bmatrix} 1 & 0 \\ \frac{2\pi}{\kappa\ \Gamma(-i|\kappa|^2)} e^{-\pi|\kappa|^2/2 + i\pi/4} & 1 \end{bmatrix}, & \text{if } \operatorname{Im} z > 0, \\ \begin{bmatrix} 1 & \frac{2\pi}{\bar{\kappa}\ \Gamma(i|\kappa|^2)} e^{-\pi|\kappa|^2/2 - i\pi/4} \\ 0 & 1 \end{bmatrix}, & \text{if } \operatorname{Im} z < 0, \end{cases}$$

here $\Gamma(z)$ is the Gamma function [84]. The condition $X^+(z) = X^-(z)G(0,0,k_0)$ from (4.3.3) dictates the choice of κ:

$$\begin{bmatrix} \tau(k_0) & -\lambda\bar{\rho}(k_0) \\ \rho(k_0) & 1 \end{bmatrix} = \begin{bmatrix} e^{-2\pi|\kappa|^2} & -\frac{\sqrt{2\pi}}{\kappa\ \Gamma(i|\kappa|^2)} e^{-\pi|\kappa|^2/2 - i\pi/4} \\ \frac{\sqrt{2\pi}}{\bar{\kappa}\ \Gamma(-i|\kappa|^2)} e^{-\pi|\kappa|^2/2 + i\pi/4} & 1 \end{bmatrix},$$

where we used that $\Gamma(z)\Gamma(-z) = -\pi/(z\sin(\pi z))$. Thus

$$|\kappa|^2 = -\frac{1}{2\pi}\log\tau(k_0),$$
$$\arg\kappa = \frac{\pi}{4} + \arg\Gamma(i|\kappa|^2) - \arg\rho(k_0).$$

This determines κ and hence $\lim_{z\to\infty}(\Psi_2)_{12}$. Since $\Psi_1(z) = \Psi_2(z)$ on the positive imaginary axis, we take the large z limit along it. We find $\kappa = \lim_{z\to\infty}(\Psi_1)_{12}$. From (4.3.2)

$$\lim_{z\to\infty} z\Psi_{12}(z) = (8t)^{-f(k_0)/(2\pi i)} e^{-2r(k_0) + 4itk_0^2}\kappa,$$

where

$$e^{-r(k_0)} = \Delta_r(k_0; k_0),$$
$$r(k_0) = \frac{1}{2\pi i}\int_{-\infty}^{k_0} \log(s - k_0) d(\log(1 - \lambda|\rho(s)|^2) ds.$$

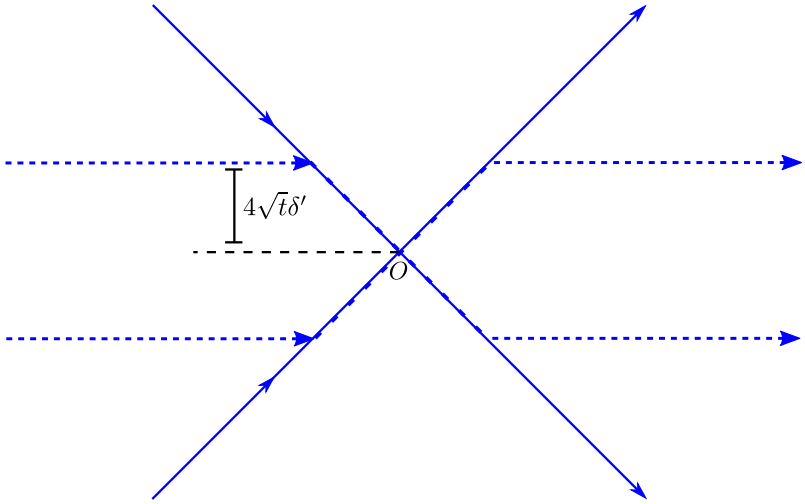

Figure 4.3.4: The contours Γ (solid) and $\hat{\Gamma}$ (dashed) and their overlap region C_0.

This is derived by integrating $\mathcal{C}_{(-\infty,k_0)} \log \tau(k)$ by parts. If we can show that after scaling Ψ approximates Φ_2 in an appropriate way, we have shown (2.6.1) without the error bound:

$$q(x,t) \sim i\frac{1}{\sqrt{2t}}(8t)^{-f(k_0)/(2\pi i)}e^{-2r(k_0)+4itk_0^2}\kappa.$$

The factor of $1/\sqrt{t}$ appears from the transformation back to the k-plane:

$$\lim_{k\to\infty} k(\Psi_2(k))_{12} = \frac{1}{\sqrt{8t}} \lim_{z\to\infty} z(\Psi_2(z/\sqrt{8t}+k_0))_{12}. \tag{4.3.8}$$

4.3.2 Error analysis

The error analysis is best performed in the z plane. That is, we must scale and shift the jump contour and jump matrices for Φ_2: define $\hat{\Phi}_2(z) = \Phi_2(z/\sqrt{8t}+k_0)$. The jump contour Γ for Ψ and $\hat{\Gamma}$ for $\hat{\Phi}_2$ are shown in Figure 4.3.4. Let V be the jump matrix for Ψ and $\hat{V}$ be the jump matrix for $\hat{\Psi}_2$. We extend both jump matrices to $\Gamma \cup \hat{\Gamma}$ by defining them to be the identity matrix outside of their initial domain of definition. We show that

$$\|u - \hat{u}\|_{L^1(\Gamma\cup\hat{\Gamma})} = \mathcal{O}(t^{-1/2}\log t).$$

We claim that it suffices to show that

$$\|V - \hat{V}\|_{L^1\cap L^\infty(\Gamma\cup\hat{\Gamma})} = \mathcal{O}(t^{-1/2}\log t). \tag{4.3.9}$$

Indeed, in this case Lemma 3.9.4 shows that

$$\|u - \hat{u}\|_{L^2(\Gamma\cup\hat{\Gamma})} = \mathcal{O}(t^{-1/2}\log t). \tag{4.3.10}$$

From the integral equations satisfied by u and $\hat{u}$:

$$u - \hat{u} = \mathcal{C}_{\Gamma\cup\hat{\Gamma}}(u-\hat{u})(V-I) - \mathcal{C}_{\Gamma\cup\hat{\Gamma}}u(V-\hat{V}) + V - \hat{V}.$$

The Cauchy-Schwarz inequality along with the triangle inequality proves the result. Indeed, $\|V-I\|_{L^2(\Gamma\cup\hat{\Gamma})}$ and $\|u\|_{L^2(\Gamma\cup\hat{\Gamma})}$ are uniformly bounded and (4.3.10) along (4.3.9) shows the sufficiency.

It follows that the contour of intersection $C_0 = \Gamma \cap \hat{\Gamma}$ is defined by

$$C_0 = 4t\delta' e^{i\pi/4}\left([-1,1]\cup[-i,i]\right),$$

with appropriate orientation. The contribution to the solution from $\hat{\Gamma}\setminus C_0$ is exponentially small with respect to t. This follows directly from the arguments given in Section 4.2.1. Next, we consider the difference $\|V-\hat{V}\|_{L^1\cap L^\infty(\Gamma\setminus C_0)}$. Since $\sup_{z\in\mathbb{C}}|z^{ic}| < \infty$, $c\in\mathbb{R}$, it is clear that the contribution on each connected component of $\Gamma\setminus C_0$ is bounded by a constant multiplied by

$$I(t) = \int_{4\sqrt{t}\delta'}^{\infty} e^{-x^2/4}dx.$$

The asymptotics of the error function shows $I(t)$ decays beyond all orders as $t\to\infty$.

We consider $\|V-\hat{V}\|_{L^1\cap L^\infty(C_0)}$. We must analyze the difference for $k(z) = z/\sqrt{8t}+k_0$,

$$\Delta(k(z))P(k(z))\Delta^{-1}(k(z);k_0) - [P](z).$$

We return to the k-plane. Since ρ can be recovered from a Cauchy integral of its boundary values on the boundary of any strip about the real axis with width less than δ, we know that it must be uniformly Lipschitz in the strip $|\operatorname{Im} k| < \delta'$ for $\delta' < \delta/2$. Therefore, with $4t\delta' > 1$ and for some $C > 0$,

$$\begin{aligned}
|U(k_0)-U(k)| &< C|k-k_0|,\\
|L(k_0)-L(k)| &< C|k-k_0|,\\
|P(k_0)-P(k)| &< C|k-k_0|,\\
|M(k_0)-M(k)| &< C|k-k_0|.
\end{aligned}$$

When setting $k(z) = z/\sqrt{8t}+k_0$ we obtain bounds on the L^∞ norms of these differences that are $\mathcal{O}(t^{-1/2})$. In addition, we consider

$$\Delta(k;k_0) - \Delta_r(k_0;k_0)\Delta_s(k;k_0) = (\Delta_r(k;k_0)-\Delta_r(k_0;k_0))\Delta_s(k;k_0). \tag{4.3.11}$$

This can be simplified further. Since $0<\tau(k)<1$, for $y>0$

$$1 \geq |\delta(x+iy;k_0)| \geq \exp\left(\frac{1}{2\pi}\int_{-\infty}^{k_0}\frac{\log\tau(s)}{(s-x)^2+y^2}yds\right) \geq (1-\|\rho\|_{L^\infty(\mathbb{R})})^{1/2},$$

where we used that the Poisson kernel integrates to unity. Similar arguments show for $y<0$ that $1 \leq |\delta(x+iy,k_0)| \leq (1-\|\rho\|_{L^\infty(\mathbb{R})})^{-1/2}$. Thus δ is uniformly bounded in both

k and k_0. To analyze the difference (4.3.11) it suffices to consider

$$I - \Delta_r^{-1}(k;k_0)\Delta_r(k_0;k_0).$$

This is further reduced to the study of

$$I_1(k;k_0) = \int_{-\infty}^{k_0} \log\left(\frac{s-k}{s-k_0}\right) d\log\tau(s) = (k_0-k)\log(k_0-k)\frac{\tau'(k_0)}{\tau(k_0)}$$
$$-(k_0-k)\int_{-\infty}^{k_0}\log(s-k_0)d\left(\frac{\tau'(s)}{\tau(s)}\right) + \int_{-\infty}^{k_0}\log(s-k)\log\left(\frac{s-k}{s-k_0}\right)d\left(\frac{\tau'(s)}{\tau(s)}\right).$$

For k in a neighborhood of $k = k_0$, we have $|I_1(k;k_0)| \le |k_0-k|\log|k_0-k|$. Therefore $\|V-\hat{V}\|_{L^\infty(C_0)} = \mathcal{O}(t^{-1/2}\log t)$. To bound the L^1 norm we notice that it involves integrals of the form

$$\int_0^{4\delta'\sqrt{t}} e^{-x^2/4}\delta^{-2}(\varphi(x);k_0)\left[\rho(\varphi(x)) - \rho(\varphi(0))e^{I_1(\varphi(x);k_0)/(\pi i)}\right]dx,$$
$$\varphi(x) = x\frac{e^{i\theta}}{\sqrt{8t}} + k_0 \quad \text{for} \quad \theta = (2n-1)\pi/4.$$

Since the L^∞ norm of the term in the brackets is $\mathcal{O}(t^{-1/2}\log t)$ we find $\|V-\hat{V}\|_{L^1(C_0)} = \mathcal{O}(t^{-1/2}\log t)$. This shows that $\|u-\hat{u}\|_{L^1(\Gamma\cup\hat{\Gamma})} = \mathcal{O}(t^{-1/2}\log t)$. Upon considering (4.3.8) we obtain the error bound in (2.6.1).

Chapter 5

The Numerical Solution of Riemann–Hilbert Problems

In this chapter we build up to the efficient and effective numerical solution of Riemann–Hilbert problems. Two main topics must be discussed. The first and obvious topic is the construction of a numerical method. A method is derived in [89] and we review the details in Section 5.3. The method is based around solving

$$\mathcal{C}[G;\Gamma]u = G - I. \tag{5.0.1}$$

The second topic is the preconditioning of (5.0.1). To understand the need for preconditioning, consider the jump matrix in (2.5.7). We consider the solution of

$$u - \mathcal{C}_\Gamma^- u \cdot (G - I) = G - I, \quad G(x,t,k) = \begin{bmatrix} 1 & -\lambda\overline{\rho(\bar{k})}e^{-2ikx-4ik^2t} \\ \rho(k)e^{2ikx+4ik^2t} & 1 - \lambda\overline{\rho(\bar{k})}\rho(k) \end{bmatrix}. \tag{5.0.2}$$

Rearranging, we find $u = (I + \mathcal{C}_\Gamma^- u)(G - I)$. The matrix $G(x,t,k)$ has rapid oscillations for x and t non-zero and unless there is some highly unlikely cancellation, u will also contain rapid oscillations. The conditioning and convergence of a numerical method is highly correlated to the magnitude of the derivatives of the solution. We expect to lose accuracy for large x and t and in practice, due to finite-precision arithmetic, one can solve (5.0.2) accurately only in a small neighborhood of the origin in the (x,t)-plane. This is in direct analogy to the complication one encounters if (2.1.6) is integrated numerically without contour deformation. The deformations of Section 2.3 turn the oscillations into exponential decay and quadrature remains accurate.

As is demonstrated in Chapter 4, the method of nonlinear steepest descent allows the transformation of an oscillatory Riemann–Hilbert problem to a Riemann–Hilbert problem isolated near the associated stationary points of an oscillatory term in the jump matrix. From a numerical point of view, the contours for the isolated Riemann–Hilbert problem must be scaled in much the same way as for the linear problem in Section 2.3. The analysis of this technique is more difficult and the focus of this chapter is to first derive sufficient conditions for which we can prove that the approach of solving RHPs numerically

on scaled contours is guaranteed to be accurate in asymptotic regimes, *i.e.*, for arbitrarily large values of parameters. We refer to this type of behavior as *asymptotic stability* or *uniform approximation*.

The choice of these scaling factors for contours is not a trivial task. We use the following rule of thumb:

Assumption 5.0.1. *If the jump matrix G has a factor $e^{\xi\theta}$ and β_j corresponds to a qth order stationary point (*i.e., *$\theta(z) \backsim C_1 + C_2(z-\beta_j)^q$), then the scaling which achieves asymptotic stability is $\alpha_j(\xi) = |\xi|^{-1/q}$.*

The heuristic reason for this choice is as follows. If $z = |\xi|^{-1/q}k + \beta_j$, then for k in a bounded set we have

$$\xi\theta(z) = C_1\xi + C_2 e^{i\arg\xi}k^q + o(1) \text{ as } |\xi| \to \infty.$$

It turns out in many cases that $C_1\xi$ is purely imaginary. This has ideal boundedness properties. We prove the validity of this assumption for the deformations below on a case-by-case basis. Note that this is in direct correspondance with the technique described in Chapter 2 for (2.1.1).

In addition, we show the deep connection between the success of the numerical method and the success of the method of nonlinear steepest descent [33]. A notable conclusion is that one can expect that whenever the method of nonlinear steepest descent produces an asymptotic formula, the numerical method can be made asymptotically stable. Achieving this requires varying amounts of preconditioning of the RHP. This can vary from not deforming the RHP at all, all the way to using the full deformation needed by the analytical method. An important question is: "when can we stop deforming to a have a reliable numerical method?" Our main results are in Section 5.2 and these results provide an answer to this question. In short, although we do not require the knowledge of local parametrices to construct the numerical method, their existence ensures that the numerical method remains accurate, and their explicit knowledge allows us to analyze the error of the approximation directly.

It is often the case that RHPs as originally stated in the method of nonlinear steepest descent are not tractable with known numerical methods. For example, in Chapter 6 the jump matrix of the RHP at an intermediate stage of deformation has two singularities in the finite complex plane. We demonstrate additional deformation techniques in Chapter 6 (and every chapter that follows) that allow one to move contours away from the singularity. Other singular cases may arise. In some RHPs the jump matrix may not tend to the identity at an endpoint of the contour. A RHP of this form does not satisfy the *product condition* (see Definition 3.8.3) and does not initially fit into the framework we lay out. An approach for rectifying this issue — based on removing the singularities using local parametrices — is worked out in Chapter 9. Finally, in the theory of orthogonal polynomials there exists RHPs that have no known closed-form parametrix for the asymptotic analysis, such as the higher-order Tracy–Widom distributions [16]. Despite no explicit parametrix being known, the method described here can effectively compute solutions, see Chapter 10.

This chapter is structured as follows. We use an abstract framework for the numerical solution of RHPs which allows us to address asymptotic accuracy in a more concise way (Section 5.1). Additionally, other numerical methods (besides the one used for the appli-

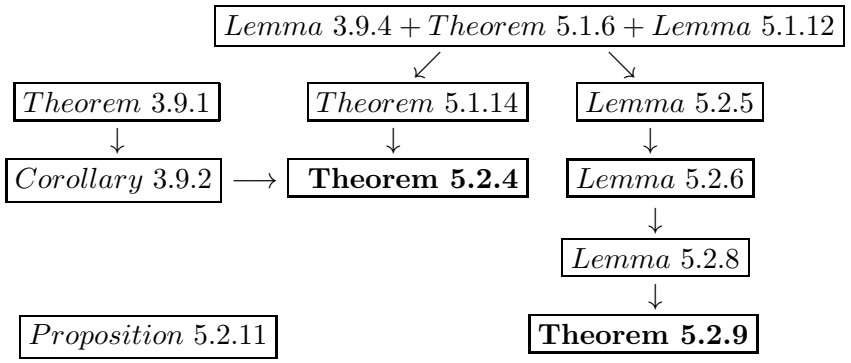

Figure 5.0.1: The interdependency of results related to the development of the framework. The fundamental results of this chapter are listed in bold.

cations) may fit within the framework. Then, we prove our main results which provide sufficient conditions for uniform approximation (Section 5.2). The numerical approach of [89] is placed within the general framework, along with necessary assumptions which allows a realization of uniform approximation (Section 5.3).

The fundamental results of this chapter are necessarily encoded in the notation, definitions and intermediate results that follow. Here we provide a road map to guide the reader through this chapter, see Figure 5.0.1. Theorems 5.2.4 and 5.2.9 represent the fundamental results of this chapter. Both present a detailed asymptotic analysis of Algorithm 5.1.11. To enhance readability we present a summary of each theorem and proposition:

- **Theorem 5.1.6:** Sufficient conditions for the convergence of projection-based numerical methods for operator equations are derived.

- **Algorithm 5.1.11:** The approach of scaling contours and solving a sequence of RHPs is encoded.

- **Theorem 5.1.14:** General conditions for the convergence of Algorithm 5.1.11 are proved.

- **Theorem 5.2.4:** One set of sufficient conditions for the uniform accuracy of Algorithm 5.1.11 is provided.

- **Theorem 5.2.9:** A set of relaxed conditions, with weakened results, for the uniform accuracy of numerical methods is provided. This result is derived using a *numerical parametrix*, see Definition 5.2.7.

- **Proposition 5.2.11:** Checking the conditions of Theorem 5.2.4 or the requirements of Definition 5.2.7 can be difficult. This proposition assists in that process.

5.1 The numerical solution of Riemann–Hilbert problems

The goal of this section is to introduce the necessary tools to approximate the solution of the operator equation

$$\mathcal{C}[G;\Gamma]u = G - I. \tag{5.1.1}$$

We start with two projections $\mathcal{I}_n$ and $\mathcal{P}_n$, both of finite rank. Assume $\mathcal{P}_n$ is defined on $H^1_z(\Gamma)$ and $\mathcal{I}_n$ is defined on $H^1(\Gamma)$. Define $X_n = \operatorname{ran}\mathcal{P}_n$ and $Y_n = \operatorname{ran}\mathcal{I}_n$ equipping both spaces with the inherited $L^2(\Gamma)$ norm. We obtain a finite-dimensional approximation of $\mathcal{C}[G;\Gamma]$ by defining

$$\mathcal{C}_n[G;\Gamma]u = \mathcal{I}_n\mathcal{C}[G;\Gamma]u.$$

It follows that $\mathcal{C}_n[G;\Gamma] : X_n \to Y_n$. This is useful under the assumption that we can compute $\mathcal{C}[G;\Gamma]$ exactly for all $u \in X_n$. An approximate solution of (5.1.1) is obtained by

$$u_n = \mathcal{C}_n[G;\Gamma]^{-1}\mathcal{I}_n(G - I),$$

whenever the operator is invertible. We use the pair $(\mathcal{I}_n, \mathcal{P}_n)$ to refer to this numerical method.

Remark 5.1.1. *In the numerical framework of [89], solving the associated linear system results in a solution that must satisfy the first-order zero-sum condition, justifying the theoretical construction above, see Theorem 5.3.8.*

To simplify notation, we define $\mathcal{T}[G;\Gamma]u = \mathcal{C}^-_\Gamma u(G - I)$ (so that $\mathcal{C}[G;\Gamma] = I - \mathcal{T}[G;\Gamma]$) and $\mathcal{T}_n[G;\Gamma] = \mathcal{I}_n\mathcal{T}[G;\Gamma]$. We use a few definitions to describe the required properties of the projections.

Definition 5.1.2. *The approximation $\mathcal{C}_n[G;\Gamma]$ to $\mathcal{C}[G;\Gamma]$ is said to be of type (α,β,γ) if, whenever $\mathcal{C}[G;\Gamma]$ is invertible for $n > N$, $\mathcal{C}_n[G;\Gamma]$ is invertible and*

- $\|\mathcal{C}_n[G;\Gamma]\|_{\mathcal{L}(H^1_z(\Gamma),Y_n)} \le C_1 n^\alpha(1 + \|G - I\|_{L^\infty(\Gamma)}\|\mathcal{C}^-_\Gamma\|_{\mathcal{L}(L^2(\Gamma))})$,
- $\|\mathcal{C}_n[G;\Gamma]^{-1}\|_{\mathcal{L}(Y_n,X_n)} \le C_2 n^\beta\|\mathcal{C}[G;\Gamma]^{-1}\|_{\mathcal{L}(L^2(\Gamma))}$ *and*
- $\|\mathcal{T}_n[G;\Gamma]\|_{\mathcal{L}(X_n,Y_n)} \le C_3 n^\gamma\|G - I\|_{L^\infty(\Gamma)}\|\mathcal{C}^-_\Gamma\|_{\mathcal{L}(L^2(\Gamma))}$.

The constants C_1, C_2 and C_3 are allowed to depend on Γ.

The first and second conditions in Definition 5.1.2 are necessary for the convergence of the numerical method. This will be made more precise below. The first and third conditions are needed to control operator norms as G varies. It is not surprising that the first and the third conditions are intimately related. In Section 5.3 we demonstrate the connection.

Remark 5.1.3. *Some projections, mainly those used in Galerkin methods, can be defined directly on $L^2(\Gamma)$. In this case we replace the first condition in Definition 5.1.2 with*

$$\|\mathcal{C}_n[G;\Gamma]\|_{\mathcal{L}(L^2(\Gamma),Y_n)} \le C_1 n^\alpha(1 + \|G - I\|_{L^\infty(\Gamma)}\|\mathcal{C}^-_\Gamma\|_{\mathcal{L}(L^2(\Gamma))}).$$

This condition and the second condition with $\alpha = \gamma$ are implied by requiring

$$\|\mathcal{I}_n\|_{\mathcal{L}(L^2(\Gamma),Y_n)} \leq C_1 n^{\alpha}.$$

In this sense Galerkin methods are more natural for RHPs, although we use the collocation method of [89] below because a Galerkin method has yet to be developed.

Definition 5.1.4. *The pair $(\mathcal{I}_n, \mathcal{P}_n)$ is said to produce an admissible numerical method if*

- *The method is of type (α, β, γ).*
- *For all $m > 0$ there exists $s > 0$ such that $\|\mathcal{I}_n u - u\|_{H^1(\Gamma)}$ and $\|\mathcal{P}_n u - u\|_{H^1(\Gamma)}$ tend to zero faster than n^{-m} as $n \to \infty$ for all $u \in H^s(\Gamma)$.*
- *$\mathcal{I}_n$ is bounded from $C(\Gamma)$ to $L^2(\Gamma)$, uniformly in n.*

Remark 5.1.5. *We assume spectral convergence of the projections. This assumption can be relaxed but one has to spend considerable effort to ensure α, β and γ are sufficiently small. The absence of an infinite number of bounded derivatives does not mean the method will not converge, but that a proof of convergence is more difficult.*

Next, we prove the generalized convergence theorem.

Theorem 5.1.6. *Assume that $(\mathcal{I}_n, \mathcal{P}_n)$ produces an admissible numerical method. If $[G;\Gamma]$ is 1-regular and $\mathcal{C}[G;\Gamma]$ is invertible on $L^2(\Gamma)$, we have*

$$\|u - u_n\|_{L^2(\Gamma)} \leq (1 + cn^{\alpha+\beta})\|\mathcal{P}_n u - u\|_{H^1(\Gamma)} \quad \textit{with} \tag{5.1.2}$$

$$c = C\|\mathcal{C}[G;\Gamma]^{-1}\|_{\mathcal{L}(L^2(\Gamma))}(1 + \|G - I\|_{L^\infty(\Gamma)}\|\mathcal{C}_\Gamma^-\|_{\mathcal{L}(L^2(\Gamma))}). \tag{5.1.3}$$

Proof. First, for notational simplicity, define $\mathcal{K}_n = \mathcal{C}_n[G;\Gamma]$, $\mathcal{K} = \mathcal{C}[G;\Gamma]$ and $f = G - I$. Then $u_n = \mathcal{K}_n^{-1}\mathcal{I}_n f = \mathcal{K}_n^{-1}\mathcal{I}_n\mathcal{K}u$. Further, since $u \in H^1_z(\Gamma)$,

$$\begin{aligned}
u - u_n =& u - \mathcal{P}_n u + \mathcal{P}_n u - u_n \\
=& u - \mathcal{P}_n u + \mathcal{P}_n u - \mathcal{K}_n^{-1}\mathcal{I}_n\mathcal{K}u \\
=& u - \mathcal{P}_n u + \mathcal{K}_n^{-1}\mathcal{K}_n\mathcal{P}_n u - \mathcal{K}_n^{-1}\mathcal{I}_n\mathcal{K}u \\
=& u - \mathcal{P}_n u + \mathcal{K}_n^{-1}(\mathcal{K}_n\mathcal{P}_n u - \mathcal{I}_n\mathcal{K}u) \\
=& u - \mathcal{P}_n u + \mathcal{K}_n^{-1}\mathcal{I}_n\mathcal{K}(\mathcal{P}_n u - u).
\end{aligned}$$

We used $\mathcal{K}_n\mathcal{P}_n u = \mathcal{I}_n\mathcal{K}\mathcal{P}_n u$ for $u \in H^1_z(\Gamma)$ in the last line. Taking an $L^2(\Gamma)$ norm, we have

$$\|u - u_n\|_{L^2(\Gamma)} \leq \|(I + \mathcal{K}_n^{-1}\mathcal{I}_n\mathcal{K})(u - \mathcal{P}_n u)\|_{L^2(\Gamma)} \leq (1 + cn^{\alpha+\beta})\|u - \mathcal{P}_n u\|_{H^1(\Gamma)}.$$

□

Remark 5.1.7. *In the case mentioned above where $\mathcal{I}_n$ and $\mathcal{P}_n$ can be defined directly on $L^2(\Gamma)$ we obtain a purely $L^2(\Gamma)$-based bound*

$$\|u - u_n\|_{L^2(\Gamma)} \leq (1 + cn^{\alpha+\beta})\|u - \mathcal{P}_n u\|_{L^2(\Gamma)}.$$

Corollary 5.1.8. *Under the assumptions of Theorem 5.1.6 and assuming that $[G;\Gamma]$ is k-regular for large k (large is determined by Definition 5.1.4) we have that $\Phi_n = I + \mathcal{C}_\Gamma u_n$ is an approximation of Φ, the solution of $[G;\Gamma]$, in the following sense.*

- $\Phi_n^\pm - \Phi^\pm \to 0$ *in* $L^2(\Gamma)$ *and*
- $\|\Phi_n - \Phi\|_{W^{j,\infty}(S)} \to 0$ *for all* $j \geq 0$, *whenever* S *is bounded away from* Γ.

Proof. The first claim follows from the boundedness of the Cauchy operator on $L^2(\Gamma)$ and, as before, the Cauchy–Schwarz inequality gives the second. □

Below we always assume the numerical method considered is admissible. The ideas presented thus far are general. In specific cases the contour Γ consists of disjoint components. We take a different approach to solving the RHP in this case.

Example 5.1.9. *Consider the RHP $[G;\Gamma]$ with $\Gamma = \Gamma_1 \cup \Gamma_2$ where Γ_1 and Γ_2 are disjoint. To solve the full RHP, we first solve for Φ_1 — the solution of $[G|_{\Gamma_1};\Gamma_1]$ — assuming that this sub-problem has a unique solution. The jump on Γ_2 is modified through conjugation by Φ_1. Define*

$$\tilde{G}_2 = \Phi_1 G|_{\Gamma_2} \Phi_1^{-1}.$$

Next, the solution Φ_2 of $[\tilde{G}_2;\Gamma_2]$ is found. A simple calculation shows that $\Phi = \Phi_2\Phi_1$ solves the original RHP $[G;\Gamma]$. This process parallels the method used in Theorem 3.8.14.

This idea allows us to treat each disjoint contour separately, solving in an iterative way. When using this algorithm numerically, the dimension of the linear system solved at each step is a fraction of that of the full discretized problem. This produces significant computational savings. We now generalize these ideas.

Consider a RHP $[G;\Gamma]$ where $\Gamma = \Gamma_1 \cup \cdots \cup \Gamma_\ell$. Here each Γ_i is disjoint and $\Gamma_i = \alpha_i\Lambda_i + \beta_i$ for some contour Λ_i. We define $G_i(z) = G(z)|_{\Gamma_i}$ and $H_i(k) = G_i(\alpha_i k + \beta_i)$. As a notational remark, in this chapter we always associate H_i and G in this way.

Remark 5.1.10. *The motivation for introducing the representation of the contours in this fashion is made clear below. Mainly, this formulation is important when α_i and/or β_i depend on a parameter but Λ_i does not.*

We now describe the general iterative solver.

Algorithm 5.1.11. *(Scaled and Shifted RH Solver)*

1. *Solve the RHP $[H_1;\Lambda_1]$ to obtain $\tilde{\Phi}_1$. We denote the solution of the associated SIE as U_1 with domain Λ_1. Define $\Phi_1(z) = \tilde{\Phi}_1\left(\frac{z-\beta_1}{\alpha_1}\right)$.*
2. *For each $j = 2,\ldots,\ell$ define $\Phi_{i,j}(z) = \Phi_i(\alpha_j z + \beta_j)$ and solve the RHP $[\tilde{H}_j;\Lambda_j]$ with*

$$\tilde{H}_j = \Phi_{j-1,j} \cdots \Phi_{1,j} H_j \Phi_{1,j}^{-1} \cdots \Phi_{j-1,j}^{-1},$$

to obtain $\tilde{\Phi}_j$. Again, the solution of the integral equation is denoted by U_j with domain Λ_j. Define $\Phi_j(z) = \tilde{\Phi}_j\left(\frac{z-\beta_j}{\alpha_j}\right)$.

3. Construct $\Phi = \Phi_\ell \cdots \Phi_1$*, which satisfies the original problem.*

When this algorithm is implemented numerically, the jump matrix corresponding to $\tilde{H}_j$ is not exact. It depends on the approximations of each of the Φ_i for $i < j$ and more specifically, it depends on the order of approximation of the RHP on Λ_i for $i < j$. We use the notation $\boldsymbol{n}_i = (n_1, \ldots, n_i)$ where each n_i is the order of approximation on Λ_i. Further, we use $\boldsymbol{n} > \boldsymbol{m}$ whenever the vectors are of the same length and $n_j > m_j$ for all j. The statement $\boldsymbol{n} \to \infty$ means that each component of $\boldsymbol{n}$ tends to ∞. Let $\Phi_{i,j,\boldsymbol{n}_i}$ be the approximation of $\Phi_{i,j}$ and define

$$\tilde{H}_{j,\boldsymbol{n}_j} = \Phi_{j-1,j,\boldsymbol{n}_{j-1}} \cdots \Phi_{1,j,\boldsymbol{n}_1} H_j \Phi^{-1}_{1,j,\boldsymbol{n}_1} \cdots \Phi^{-1}_{j-1,j,\boldsymbol{n}_{j-1}}.$$

If the method converges then $\tilde{H}_{j,\boldsymbol{n}_j} \to \tilde{H}_j$ uniformly as $\boldsymbol{n}_j \to \infty$.

A significant question remains: "how do we know solutions exist at each stage of this algorithm?" In general, solutions may not exist. $\mathcal{C}[G;\Gamma]$ can be expressed in the form $\mathcal{K} - \mathcal{T}$ where $\mathcal{K}$ is the block-diagonal operator with blocks $\mathcal{C}[G_i;\Gamma_i]$ and $\mathcal{T}$ is a compact operator. Here $\mathcal{T}$ represents the effect of one contour on another and if the operator norm of $\mathcal{T}$ is sufficiently small, solutions exist at each iteration of Algorithm 5.1.11. This is true if the arclength of each Γ_i is sufficiently small. A thorough discussion of this was presented in Example 3.10.6. An implicit assumption in our numerical framework is that such equations are uniquely solvable.

Additionally, it is worth nothing that if each of the scale factors $\alpha_i = \alpha_i(\xi)$ are parameter dependent such that $\alpha_i(\xi) \to 0$ as $\xi \to 0$ then the norms of the inverse operators are related. When each of the $\alpha_i(\xi)$ are sufficiently small, there exists $C > 1$ such that

$$\frac{1}{C}\|\mathcal{C}[G;\Gamma]^{-1}\|_{\mathcal{L}(L^2(\Gamma))} \leq \max_i \|\mathcal{C}[G_i;\Gamma_i]^{-1}\|_{\mathcal{L}(L^2(\Gamma_i))} \leq C\|\mathcal{C}[G;\Gamma]^{-1}\|_{\mathcal{L}(L^2(\Gamma))}. \tag{5.1.4}$$

Due to the simplicity of the scalings we allow the norms of the operators $\mathcal{C}[G_i;\Gamma_i]$ and $\mathcal{C}[G_i;\Gamma_i]^{-1}$ are equal to that of their scaled counterparts $\mathcal{C}[H_i;\Lambda_i]$ and $\mathcal{C}[H_i;\Lambda_i]^{-1}$.

The final question is one of convergence. For a single fixed contour we know that if $(\mathcal{I}_n, \mathcal{P}_n)$ produces an admissible numerical method and the RHP is sufficiently regular, the numerical method converges. This means that the solution of this RHP converges uniformly, away from the contour it is defined on. This is the basis for proving that Algorithm 5.1.11 converges. Theorem 3.9.4 aids us when considering the infinite-dimensional operator for which the jump matrix is uniformly close, but we need an additional result for the finite-dimensional case.

Lemma 5.1.12. *Consider a family of RHPs* $\{[G_\xi;\Gamma]\}_{\xi\geq 0}$ *on the fixed contour* Γ *which are* k*-regular. Assume* $G_\xi \to G$ *in* $L^\infty(\Gamma) \cap L^2(\Gamma)$ *as* $\xi \to \infty$ *and* $[G;\Gamma]$ *is* k*-regular, then*

- *If* $\mathcal{C}_n[G;\Gamma]$ *is invertible, then there exists* $T(n) > 0$ *such that* $\mathcal{C}_n[G_\xi;\Gamma]$ *is also invertible for* $\xi > T(n)$*.*
- *If* $\Phi_{n,\xi}$ *is the approximate solution of* $[G_\xi;\Gamma]$ *and* Φ_n *is the approximate solution of* $[G;\Gamma]$*, then* $\Phi_{n,\xi} - \Phi_n \to 0$ *in* $L^2(\Gamma)$ *as* $\xi \to \infty$ *for fixed* n*.*
- $\|\Phi_{n,\xi} - \Phi_n\|_{W^{j,\infty}(S)} \to 0$*, as* $\xi \to \infty$*, for all* $j \geq 1$*, whenever* S *is bounded away from* Γ *for fixed* n*.*

Proof. We consider the two equations

$$\mathcal{C}_n[G_\xi;\Gamma]u_{n,\xi} = \mathcal{I}_n(G_\xi - I),$$
$$\mathcal{C}_n[G;\Gamma]u_n = \mathcal{I}_n(G - I).$$

Since the method is of type (α,β,γ), we have (see Definition 5.1.2),

$$\|\mathcal{C}_n[G_\xi;\Gamma] - \mathcal{C}_n[G;\Gamma]\|_{\mathcal{L}(X_n,Y_n)} \leq C_3 n^\gamma \|\mathcal{C}_\Gamma^-\|_{\mathcal{L}(L^2(\Gamma))}\|G_\xi - G\|_{L^\infty(\Gamma)} = E(\xi)n^\gamma.$$

For fixed n, by increasing ξ, we can make $E(\xi)$ small, so that

$$\|\mathcal{C}_n[G_\xi;\Gamma] - \mathcal{C}_n[G;\Gamma]\|_{\mathcal{L}(X_n,Y_n)} \leq \frac{1}{C_2}\frac{1}{\|\mathcal{C}[G;\Gamma]^{-1}\|_{\mathcal{L}(L^2(\Gamma))}}n^{-\beta} \leq \frac{1}{\|\mathcal{C}_n[G;\Gamma]^{-1}\|_{\mathcal{L}(Y_n,X_n)}}.$$

Specifically, we choose ξ small enough so that

$$E(\xi) \leq \frac{1}{2}\frac{1}{C_2C_3}\frac{1}{\|\mathcal{C}[G;\Gamma]^{-1}\|_{\mathcal{L}(L^2(\Gamma))}}n^{-\gamma-\beta}.$$

Using Theorem 1.5.7 $\mathcal{C}_n[G_\xi;\Gamma]$ is invertible, and we bound

$$\|\mathcal{C}_n[G_\xi;\Gamma]^{-1} - \mathcal{C}_n[G;\Gamma]^{-1}\|_{\mathcal{L}(Y_n,X_n)} \leq 2C_2 n^{2\beta+\gamma}\|\mathcal{C}[G;\Gamma]^{-1}\|^2_{\mathcal{L}(L^2(\Gamma))}E(\xi). \tag{5.1.5}$$

Importantly, the quantity on the left tends to zero as $\xi \to \infty$. We use a triangle inequality:

$$\begin{aligned}\|u_n - u_{n,\xi}\|_{L^2(\Gamma)} \leq{}& \|(\mathcal{C}_n[G_\xi;\Gamma]^{-1} - \mathcal{C}_n[G;\Gamma]^{-1})\mathcal{I}_n(G-I)\|_{L^2(\Gamma)}\\ &+ \|\mathcal{C}_n[G;\Gamma]^{-1}\mathcal{I}_n(G-G_\xi)\|_{L^2(\Gamma)}.\end{aligned}$$

Since we have assumed that Γ is bounded and that the norm of $\mathcal{I}_n : C(\Gamma) \to L^2(\Gamma)$ is uniformly bounded in n, we obtain L^2 convergence of u_n to $u_{n,\xi}$ as $\xi \to \infty$:

$$\|u_n - u_{n,\xi}\|_{L^2(\Gamma)} \leq C_3 n^{2\beta+\gamma}E(\xi)\|G-I\|_{L^\infty(\Gamma)} + C_4 n^\beta \|G - G_\xi\|_{L^\infty(\Gamma)} \leq C_5 n^{2\beta+\gamma}E(\xi). \tag{5.1.6}$$

This proves the three required properties. □

Remark 5.1.13. *A good way to interpret this result is to see $E(\xi)$ as the difference in norm between the associated infinite-dimensional operator which is proportional to the uniform difference in the jump matrices. Then* (5.1.5) *gives the resulting error between the finite-dimensional operators. It is worthwhile to note that if $\alpha = \beta = \gamma = 0$ then T can be chosen independent of n.*

Now we have the tools needed to address the convergence of the solver. We introduce some notation to simplify matters. At stage j in the solver we solve a SIE on Λ_j. On this domain we need to compare two RHPs:

$$[\tilde{H}_j;\Lambda_j] \quad \text{and} \quad [\tilde{H}_{j,\boldsymbol{n}_j};\Lambda_j].$$

Let U_j be the exact solution of this SIE which is obtained from $[\tilde{H}_j;\Lambda_j]$. As an intermediate

step we need to consider the numerical solution of $[\tilde{H}_j;\Lambda_j]$. We use U_{j,n_j} to denote the numerical approximation of U_j of order n_j. Also, $U_{j,\boldsymbol{n}_j}$ is used to denote the numerical approximation of the solution of the SIE associated with $[\tilde{H}_{j,\boldsymbol{n}_j};\Lambda_j]$.

Theorem 5.1.14. *Assume that each problem in Algorithm 5.1.11 is solvable and k-regular for sufficiently large k. Then the algorithm converges to the true solution of the RHP. More precisely, there exists $\boldsymbol{N}_i$ such that for $\boldsymbol{n}_i > \boldsymbol{N}_i$ we have*

$$\|U_{i,\boldsymbol{n}_i} - U_i\|_{L^2(\Lambda_i)} \leq C_k \left[(\max \boldsymbol{n}_i)^{\alpha+\beta} + (\max \boldsymbol{n}_i)^{2\alpha+\gamma}\right]^i \max_{j\leq i} \|\mathcal{I}_n U_j - U_j\|_{H^1(\Lambda_j)},$$

where $\mathcal{I}_n$ is the appropriate projection for Λ_j.

Proof. We prove this by induction. Since $U_{1,\boldsymbol{n}_1} = U_{1,n_1}$ the claim follows from Theorem 5.1.6 for $i = 1$. Now assume the claim is true for all $j < i$. We use Lemma 5.1.12 to show it is true for i. Using the triangle inequality we have

$$\|U_{i,\boldsymbol{n}_i} - U_i\|_{L^2(\Lambda_i)} \leq \|U_{i,\boldsymbol{n}_i} - U_{i,n_i}\|_{L^2(\Lambda_i)} + \|U_i - U_{i,n_i}\|_{L^2(\Lambda_i)}.$$

Using Theorem 5.1.6, we bound the second term:

$$\|U_i - U_{i,n_i}\|_{L^2(\Lambda_i)} \leq C n_i^{\alpha+\beta} \|\mathcal{I}_n U_i - U_i\|_{H^1(\Lambda_i)}.$$

To bound the first term we use (5.1.6),

$$\|U_{i,\boldsymbol{n}_i} - U_{i,n_i}\|_{L^2(\Lambda_i)} \leq C n_i^{2\beta+\gamma} E(\boldsymbol{n}_{i-1}). \tag{5.1.7}$$

$E(\boldsymbol{n}_{i-1})$ is proportional to the uniform difference of $\tilde{H}_i$ and its approximation obtained through the numerical method, $\tilde{H}_{i,\boldsymbol{n}_{i-1}}$. By the induction hypothesis, if k is sufficiently large, Lemma 5.1.12, tells us that this difference tends to zero as $\boldsymbol{n}_{i-1} \to \infty$, and the use of (5.1.6) is justified. More precisely, the Cauchy–Schwarz Inequality for each Λ_j, $j < i$ and repeated triangle inequalities results in

$$\|\tilde{H}_i - \tilde{H}_{i,\boldsymbol{n}_{i-1}}\|_{L^\infty(\Lambda_i)} \leq C \sum_{j=1}^{i-1} \|U_j - U_{j,n_j}\|_{L^2(\Lambda_j)}. \tag{5.1.8}$$

Combining (5.1.7) and (5.1.8) we complete the proof. □

Remark 5.1.15. *The requirement that k is large can be made more precise using Definition 5.1.4 with $m = \max\{l(2\alpha+\gamma), l(\alpha+\beta)\}$ where l is the number of disjoint contours Γ_i that make up the full contour Γ. There is little restriction if $(\alpha,\beta,\gamma) = (0,0,0)$.*

5.2 Uniform approximation

We describe briefly how to obtain an explicit asymptotic approximation. Second, we use the ideas presented above to explain how numerics can be used to provide asymptotic approximations. The idea we continue to exploit is that the set of invertible operators

between Banach spaces is open. Before we proceed, we define two types of uniform approximation. Let $\{U_n^\xi\}_{\xi\geq 0}$ be a sequence, depending on the parameter ξ, in a Banach space such that for each ξ, $\|U_n^\xi - U^\xi\| \to 0$ as $n \to \infty$ for some U^ξ.

Definition 5.2.1. *We say the sequence* $\{U_n^\xi\}_{\xi\geq 0}$ *is* weakly uniform *if for every* $\epsilon > 0$ *there exists a function* $N(\xi) : \mathbb{R}^+ \to \mathbb{N}$ *taking finitely many values such that*

$$\|U_{N(\xi)}^\xi - U^\xi\| < \epsilon.$$

Definition 5.2.2. *We say the sequence* $\{U_n^\xi\}_{\xi\geq 0}$ *is* strongly uniform *(or just* uniform*) if for every* $\epsilon > 0$ *there exists* $N \in \mathbb{N}$ *such that for* $n \geq N$

$$\|U_n^\xi - U^\xi\| < \epsilon.$$

The necessity for the definition of a weakly uniform sequence is mostly a technical detail, as we do not see it arise in practice. To illustrate how it can arise we give an example.

Example 5.2.3. *Consider the sequence*

$$\{U_n^\xi\}_{n,\xi\geq 0} = \left\{\sin\xi + e^{-n^2} + e^{-(\xi-n)^2}\right\}_{n,\xi\geq 0}.$$

For fixed ξ, $U_n^\xi \to \sin\xi$. *We want, for* $\epsilon > 0$, *while keeping* n *bounded,*

$$|U_n^\xi - \sin\xi| = |e^{-n^2} + e^{-(\xi-n)^2}| < \epsilon.$$

We choose $n > \xi$ *or if* ξ *is large enough we choose* $0 < n < \xi$. *To maintain error that is uniformly less then* ϵ *we cannot choose a fixed* n*; it must vary with respect to* ξ. *When relating to RHPs the switch from* $n > \xi$ *to* $0 < n < \xi$ *is related to transitioning into the asymptotic regime.*

5.2.1 Direct estimates

As before, we are assuming we have a RHP $[G^\xi; \Gamma^\xi]$ that depends on a parameter ξ and Γ^ξ is bounded. Here we use *a priori* bounds on the solution of the associated SIE which are uniform in ξ to prove the uniform approximation. In general, when this is possible, it is the simplest way to proceed.

Our main tool is Corollary 3.9.2. We can easily estimate the regularity of the solution of each problem $[H_i; \Lambda_i]$ provided we have some information about $\|\mathcal{C}[G_i^\xi; \Gamma_i^\xi]^{-1}\|_{\mathcal{L}(L^2(\Gamma_i))}$ or equivalently $\|\mathcal{C}[H_i^\xi; \Lambda_i]^{-1}\|_{\mathcal{L}(L^2(\Lambda_i))}$. We address how to estimate this later in this section. First, we need a statement about how regularity is preserved throughout Algorithm 5.1.11. Specifically, we use information from the scaled jumps H_i and the local inverses $\mathcal{C}[H_i; \Lambda_i]^{-1}$ to estimate global regularity. The following theorem uses this to prove strong uniformity of the numerical method.

Theorem 5.2.4. *Assume*

- $\{[G^\xi, \Gamma^\xi]\}_{\xi\geq 0}$ *is a sequence of* k*-regular RHPs,*

- *the norm of* $\mathcal{C}[H_i^\xi, \Lambda_i]^{-1}$ *is uniformly bounded in* ξ,
- $\|H_i^\xi\|_{W^{k,\infty}(\Lambda_i)} \leq C$, *and*
- $\alpha_i(\xi) \to 0$ *as* $\xi \to \infty$.

Then if k *and* ξ *are sufficiently large*

- *Algorithm 5.1.11 applied to* $\{[G^\xi, \Gamma^\xi]\}_{\xi \geq 0}$ *has solutions at each stage,*
- $\|U_j^\xi\|_{H^k(\Lambda_i)} \leq P_k$ *where* P_k *depends on* $\|H_i^\xi\|_{H^k(\Lambda_i)\cap W^{k,\infty}(\Lambda_i)}$, $\|\mathcal{C}[H_i^\xi; \Lambda_i]^{-1}\|_{\mathcal{L}(L^2(\Lambda_i))}$ *and* $\|U_j^\xi\|_{L^2(\Lambda_j)}$ *for* $j < i$ *and*
- *the approximation* $U_{i,\boldsymbol{n_i}}^\xi$ *of* U_i^ξ *(the solution of the SIE) at each step in Algorithm 5.1.11 converges uniformly in* ξ *as* $\boldsymbol{n}_i \to \infty$. *In other words, the convergence is strongly uniform.*

Proof. First, we note that since $\alpha_i(\xi) \to 0$, (3.10.5) shows that jump matrix $\tilde{H}_i^\xi$ for the RHP solved at stage i in Algorithm 5.1.11 tends uniformly to H_i^ξ. This implies the solvability of the RHPs at each stage in Algorithm 5.1.11, as well as the bound

$$\|\mathcal{C}[\tilde{H}_i^\xi; \Lambda_i]^{-1}\|_{\mathcal{L}(L^2(\Gamma))} \leq C\|\mathcal{C}[H_i^\xi; \Lambda_i]^{-1}\|_{\mathcal{L}(L^2(\Gamma))},$$

for sufficiently large ξ. As before, C can be taken to be independent of ξ. We claim that $\|U_i^\xi\|_{H^k(\Lambda_i)}$ is uniformly bounded. We prove this by induction. When $i = 1$, $U_1^\xi = \mathcal{C}[H_i^\xi, \Lambda_i]^{-1}(H_i^\xi - I)$ and the claim follows from Corollary 3.9.2. Now assume the claim is true for $j < i$. All derivatives of the jump matrix $\tilde{H}_i^\xi$ depend on the Cauchy integral of U_j^ξ evaluated away from Λ_j and H_i^ξ. The former is bounded by the induction hypothesis and the later is bounded by assumption. Again, using Corollary 3.9.2 we obtain the uniform boundedness of $\|U_i^\xi\|_{H^k(\Lambda_i)}$. Theorem 5.1.14 implies that convergence is uniform in ξ. □

The most difficult part about verifying the hypotheses of this theorem is establishing an estimate of $\|\mathcal{C}[H_i^\xi; \Lambda_i^\xi]^{-1}\|_{\mathcal{L}(L^2(\Lambda_i))}$ as a function of ξ. A very useful fact is that once the solution Ψ^ξ of the RHP $[G^\xi; \Gamma^\xi]$ is known then the inverse of the operator is also known (see Lemma 3.8.18):

$$\mathcal{C}[G^\xi; \Gamma^\xi]^{-1}u = \mathcal{C}^+_{\Gamma^\xi}[u[(\Psi^\xi)^{-1}]^+](\Psi^\xi)^+ - \mathcal{C}^-_{\Gamma^\xi}[u[(\Psi^\xi)^{-1}]^+](\Psi^\xi)^-. \tag{5.2.1}$$

When Ψ^ξ is known approximately, *i.e.*, when a parametrix is known, then estimates on the boundedness of the inverse can be reduced to studying the L^∞ norm of the parametrix. Then (5.1.4) can be used to relate this to each $\mathcal{C}[G_i^\xi; \Gamma_i^\xi]^{-1}$ which gives an estimate on the norm of $\mathcal{C}[H_i^\xi; \Lambda_i]^{-1}$. We study this further in the chapters that follow (see Sections 7.6 and 8.3.2).

5.2.2 Failure of direct estimates

We study a toy RHP to motivate where the direct estimates can fail. Let $\phi(x)$ be a smooth function with compact support in $(-1, 1)$ satisfying $\max_{[-1,1]} |\phi(x)| = 1/2$. Consider the

following scalar RHP for a function μ:

$$\mu^+(x) = \mu^-(x)(1 + \phi(x)(1 + \xi^{-1/2}e^{i\xi x})), \tag{5.2.2}$$

$$\mu(\infty) = 1, \quad x \in [-1, 1], \quad \xi > 0. \tag{5.2.3}$$

This problem can be solved explicitly but we study it from the linear operator perspective instead. From the boundedness assumption on ϕ, a Neumann series argument gives the invertibility of the singular integral operator and uniform boundedness of the L^2 inverse in ξ. Using the estimates in Corollary 3.9.2 we obtain useless bounds, that all grow with ξ. Intuitively, the solution to (5.2.2) is close, in L^2 to the solution to

$$\nu^+(x) = \nu^-(x)(1 + \phi(x)), \tag{5.2.4}$$

$$\nu(\infty) = 1, \quad x \in [-1, 1], \quad \xi > 0, \tag{5.2.5}$$

which trivially has uniform bounds on its Sobolev norms. In the next section we introduce the idea of a numerical parametrix which resolves this complication.

5.2.3 Extension to indirect estimates

In this section we assume minimal hypotheses for dependence of the sequence $\{[G^\xi; \Gamma^\xi]\}_{\xi \geq 0}$ on ξ. Specifically we require only that the map $\xi \mapsto H_i^\xi$ is continuous from $\mathbb{R}^+$ to $L^\infty(\Lambda_i)$ for each i. We do not want to hypothesize more as that would alter the connection to the method of nonlinear steepest descent which only requires uniform convergence of the jump matrix. In specific cases, stronger results can be obtained by requiring the map $\xi \mapsto H_i^\xi$ to be continuous from $\mathbb{R}^+$ to $W^{k,\infty}(\Lambda_i)$.

The fundamental result we need to prove a uniform approximation theorem is the continuity of Algorithm 5.1.11 with respect to uniform perturbations in the jump matrix. With the jump matrix G we associated H_j, the scaled restriction of G to Γ_j. With G we also associated U_j, the solution of the SIE obtained from $[\tilde{H}_j; \Lambda_j]$. In what follows we have another jump matrix J and analogously we use K_j to denote the scaled restriction of J and P_j to denote the solution of the SIE obtained from $[\tilde{K}_j, \Lambda_j]$.

Lemma 5.2.5. *Assume $\{[G^\xi, \Gamma^\xi]\}_{\xi \geq 0}$ is a sequence of 1-regular RHPs such that $\xi \mapsto H_i^\xi$ is continuous from $\mathbb{R}^+$ to $L^\infty(\Lambda_i)$ for each i. Then for sufficiently large but fixed $\boldsymbol{n}_i$, the map $\xi \mapsto U^\xi_{i,\boldsymbol{n}_i}$ is continuous from $\mathbb{R}^+$ to $L^2(\Lambda_i)$ for each i.*

Proof. We prove this by induction on i. For $i = 1$ the claim follows from Lemma 5.1.12. Now assume the claim is true for $j < i$. We prove it holds for i. We show the map is continuous at η for $\eta \geq 0$. First, from Lemma 5.1.12

$$\|U^\eta_{i,\boldsymbol{n}_i} - U^\xi_{i,\boldsymbol{n}_i}\|_{L^2(\Lambda)} \leq C n_i^{2\alpha+\gamma} E(\xi, \eta),$$

where $E(\xi, \eta)$ is proportional to $\|\tilde{H}^\eta_{i,\boldsymbol{n}_{i-1}} - \tilde{H}^\xi_{i,\boldsymbol{n}_{i-1}}\|_{L^\infty(\Lambda_i)}$. A similar argument as in Theorem 5.1.14 gives

$$\|\tilde{H}^\eta_{i,\boldsymbol{n}_{i-1}} - \tilde{H}^\xi_{i,\boldsymbol{n}_{i-1}}\|_{L^\infty(\Lambda_i)} \leq C(\eta, \boldsymbol{n}_i) \sum_{j=1}^{i-1} \|U^\eta_{j,\boldsymbol{n}_j} - U^\xi_{j,\boldsymbol{n}_j}\|_{L^2(\Lambda_j)},$$

for $|\xi - \eta|$ sufficiently small. By assumption, the right-hand side tends to zero as $\xi \to \eta$, which proves the lemma. □

It is worthwhile noting that the arguments in Lemma 5.2.5 show the same continuity for the infinite-dimensional, non-discretized problem. Now we show weak uniform convergence of the numerical scheme on compact sets. It is clear that the arguments can be generalized to ξ being an element of a general metric space.

Lemma 5.2.6. *Assume $\{[G^\xi, \Gamma^\xi]\}_{\xi \geq 0}$ is a sequence of k-regular RHPs such that all the operators in Algorithm 5.1.11 are invertible for every ξ. Assume that k is sufficiently large so that the approximations from Algorithm 5.1.11 converge for every $\xi \geq 0$. Then there exists a vector-valued function $\boldsymbol{N}(i, \xi)$ that takes finitely many values such that*

$$\|U^\xi_{i,\boldsymbol{N}(i,\xi)} - U^\xi_i\|_{L^2(\Lambda_i)} < \epsilon.$$

Moreover if the numerical method is of type $(0, 0, 0)$ then convergence is strongly uniform.

Proof. Let $S \subset \mathbb{R}^+$ be compact. It follows from Lemma 5.2.5 that the function $E(\xi, \boldsymbol{n}, i) = \|U^\xi_{i,\boldsymbol{n}} - U^\xi_i\|_{L^2(\Gamma_i)}$ is a continuous function of ξ for fixed $\boldsymbol{n}$. For $\epsilon > 0$ find $\boldsymbol{n}_\xi$ such that $E(\xi, \boldsymbol{n}_\xi, i) < \epsilon/2$. By continuity, define $\delta_\xi(\boldsymbol{n}_\xi) > 0$ so that $E(s, \boldsymbol{n}_\xi, i) < \epsilon$ for $|s - \xi| < \delta_\xi$. The open sets $\{B(\xi, \delta_\xi)\}_{\xi \in S}$ cover S and we can select a finite subcover $\{B(\xi_j, \delta_{\xi_j})\}_{j=1}^N$. We have $E(s, \boldsymbol{n}_{\xi_j}, i) < \epsilon$ whenever $s \in B(\xi_j, \delta_{\xi_j})$. To prove the claim for a method of type $(0, 0, 0)$, we use the fact that δ_ξ can be taken independent of $\boldsymbol{n}_\xi$ and that $E(s, \boldsymbol{n}, i) < \epsilon$ for every $\boldsymbol{n} > \boldsymbol{n}_\xi$. □

Definition 5.2.7. *Given a sequence of k-regular RHPs $\{[G^\xi, \Gamma^\xi]\}_{\xi \geq 0}$ such that*

- $\Gamma^\xi = \Gamma^\xi_1 \cup \cdots \cup \Gamma^\xi_\ell$, *and*
- $\Gamma^\xi_i = \alpha_i(\xi)\Lambda_i + \beta_i$,

another sequence of k-regular RHPs $\{[J^\xi, \Sigma^\xi]\}_{\xi \geq 0}$ is said to be a numerical parametrix if

- $\Sigma^\xi = \Sigma^\xi_1 \cup \cdots \cup \Sigma^\xi_\ell$,
- $\Sigma^\xi_i = \gamma_i(\xi)\Lambda_i + \sigma_i$,
- *For all i*

$$J^\xi(\gamma_i(\xi)k + \sigma_i) - G^\xi(\alpha_i(\xi)k + \beta_i) \to 0, \tag{5.2.6}$$

  uniformly on Λ_i as $\xi \to \infty$,

- *the norms of the operators and inverse operators at each step in Algorithm 5.1.11 are uniformly bounded in ξ, implying uniform boundedness of J^ξ in ξ, and*
- *the approximation $P^\xi_{i,\boldsymbol{n_i}}$ of P^ξ_i (the solution of the SIE) at each step in Algorithm 5.1.11 converges uniformly as $\min \boldsymbol{n}_i \to \infty$.*

This definition hypothesizes desirable conditions on a nearby limit problem for the sequence $\{[G^\xi, \Gamma^\xi]\}_{\xi \geq 0}$. Under the assumption of this nearby limit problem we are able to obtain a uniform approximation for the solution of the original RHP.

Lemma 5.2.8. *Assume there exists a numerical parametrix $\{J_\xi, \Sigma_\xi\}_{\xi>0}$ for a sequence of RHPs $\{[G_\xi, \Gamma_\xi]\}_{\xi \geq 0}$. Then for every $\epsilon > 0$ there exists $\boldsymbol{N}_i$ and $T > 0$ such that, at each stage in Algorithm 5.1.11,*

$$\|U^\xi_{i,\boldsymbol{N}_i} - U^\xi_i\|_{L^2(\Lambda_i)} < \epsilon \text{ for } \xi > T. \tag{5.2.7}$$

Furthermore, if the numerical method is of type $(0,0,0)$, then (5.2.7) is true with $\boldsymbol{N}_i$ replaced by any $\boldsymbol{M}_i > \boldsymbol{N}_i$.

Proof. At each stage in Algorithm 5.1.11 we have

$$\|U^\xi_{i,\boldsymbol{n}_i} - U^\xi_i\|_{L^2(\Lambda_i)} \leq \|U^\xi_{i,\boldsymbol{n}_i} - P^\xi_{i,\boldsymbol{n}_i}\|_{L^2(\Lambda_i)} + \|P^\xi_{i,\boldsymbol{n}_i} - P^\xi_i\|_{L^2(\Lambda_i)} + \|P^\xi_i - U^\xi_i\|_{L^2(\Lambda)}. \tag{5.2.8}$$

Since $P^\xi_{i,\boldsymbol{n}_i}$ originates from a numerical parametrix we know that $\|P^\xi_{i,\boldsymbol{n}_i} - P^\xi_i\|_{L^2(\Lambda_i)} \to 0$ uniformly in ξ as $\boldsymbol{n}_i$ is increased. Furthermore, $\|P^\xi_i - U^\xi_i\|_{L^2(\Lambda)}$ depends only on ξ and tends to zero as $\xi \to \infty$. The main complication comes from the fact that a bound on $\|U^\xi_{i,\boldsymbol{n}_i} - P^\xi_{i,\boldsymbol{n}_i}\|_{L^2(\Lambda_i)}$ from (5.1.5) depends on both $\boldsymbol{n}_{i-1}$ and ξ if the method is not of type $(0,0,0)$. The same arguments as in Lemma 5.2.5 show this tends to zero. Therefore we choose $\boldsymbol{n}_i$ large enough so that the second term in (5.2.8) is less than $\epsilon/3$. Next, we choose ξ large enough so that the sum of the remaining terms is less than $2/3\epsilon$. If the method is of type $(0,0,0)$ this sum remains less than ϵ if $\boldsymbol{n}_i$ is replaced with $\boldsymbol{n}$ for $\boldsymbol{n} > \boldsymbol{n}_i$. This proves the claims. □

Now we prove the uniform approximation theorem.

Theorem 5.2.9. *Assume $\{[G^\xi, \Gamma^\xi]\}_{\xi \geq 0}$ is a sequence of k-regular RHPs for k sufficiently large so that Algorithm 5.1.11 converges for each ξ. Assume there exists a numerical parametrix as $\xi \to \infty$. Then Algorithm 5.1.11 produces a weakly uniform approximation to the solution of $\{[G^\xi, \Gamma^\xi]\}_{\xi \geq 0}$. Moreover, convergence is strongly uniform if the method is of type $(0,0,0)$.*

Proof. Lemma 5.2.8 provides an $M > 0$ and $\boldsymbol{N}_1(i)$ such that if $\xi > M$ then

$$\|U^\xi_{i,\boldsymbol{N}_1(i)} - U^\xi_i\|_{L^2(\Lambda_i)} < \epsilon, \text{ for every } i.$$

According to Theorem 5.2.6 there is $\boldsymbol{N}_2(\xi, i)$ such that

$$\|U^\xi_{i,\boldsymbol{N}_2(\xi,i)} - U^\xi_i\|_{L^2(\Lambda_i)} < \epsilon, \text{ for every } i.$$

The function

$$\boldsymbol{N}(\xi, i) = \begin{cases} \boldsymbol{N}_1(i), & \text{if } \xi > M, \\ N_2(\xi, i), & \text{if } \xi \leq \boldsymbol{M}, \end{cases}$$

satisfies the required properties for weak uniformity. Strong uniformity follows in a similar way from Lemma 5.2.8 and Theorem 5.2.6. □

Remark 5.2.10. *This proves weak uniform convergence of the numerical method for the toy problem introduced in Section 5.2.2: we can take the RHP for ν as a numerical parametrix.*

The seemingly odd restrictions for the general theorem are a consequence of poorer operator convergence rates when n is large. A well-conditioned numerical method does not suffer from this issue. It is worth noting that using direct estimates is equivalent to requiring that the RHP itself satisfies the properties of a numerical parametrix.

In what follows, we want to show a given sequence of RHPs is a numerical parametrix. The reasoning for the following result is two-fold. First, we hypothesize only conditions which are easily checked in practice. Second, we want to connect the stability of numerical approximation with the use of local, model problems in nonlinear steepest descent.

Proposition 5.2.11. *Assume*

- $\{[J^\xi, \Sigma^\xi]\}_{\xi\geq 0}$ *is a sequence of k-regular RHPs,*
- *the norm of* $\mathcal{C}[K_i^\xi, \Lambda_i]^{-1}$ *is uniformly bounded in* ξ*,*
- $\|K_i^\xi\|_{W^{k,\infty}(\Lambda_i)} \leq C$*, and*
- $\gamma_i(\xi) \to 0$ *as* $\xi \to \infty$*.*

Then, if k and ξ are sufficiently large,

- *Algorithm 5.1.11 applied to* $\{[J^\xi, \Sigma^\xi]\}_{\xi\geq 0}$ *has solutions at each stage and*
- $\{[J^\xi, \Sigma^\xi]\}_{\xi\geq 0}$ *satisfies the last two properties of a numerical parametrix (Definition 5.2.7).*

Proof. The proof is essentially the same as Theorem 5.2.4 □

Remark 5.2.12. *Due to the decay of γ_i, the invertibility of each of* $\mathcal{C}[K_i^\xi; \Lambda_i]$ *is equivalent to that of* $\mathcal{C}[G^\xi; \Gamma^\xi]$*.*

This proposition states that a numerical parametrix only needs to be locally reliable; we can consider each shrinking contour as a separate RHP as far as the analysis is concerned.

Remark 5.2.13. *The basic philosophy of this work is that to apply the numerical method described in Section 5.3, we must transform the RH problem for Φ into a form suitable for numerical solution. To accomplish this, we transform Φ by representing it explicitly in terms of new functions which satisfy the following properties:*

- $\Phi \mapsto \Psi$ *so that $\Psi \sim I$ at infinity: This is a prerequisite to apply the numerical method of Section 5.3. Most RHPs satisfy this condition but the RHPin Problem 10.3.1 does not satisfy this condition.*

- $\Psi \mapsto \Delta$ *so that the oscillatory jumps of* Ψ *become exponential decaying jumps of* Δ*: This is the first step in the process to guarantee that the solution of the corresponding SIE has bounded Sobolev norms.*

- $\Delta \mapsto \Sigma$ *so that the jumps of* Σ *are localized and scaled: This is the step that produces a method that is asymptotically stable.*

5.3 A numerical realization

In [89], S. Olver constructed a numerical framework for computing solutions to RHPs, based on a method used in [87] for computing solutions to the undeformed Painlevé II RHP. This framework is based on Chebyshev interpolants. Consider the RHP $[G;\Gamma]$, $\Gamma = \Gamma_1 \cup \cdots \cup \Gamma_\ell$, where each Γ_i is bounded and is a Möbius transformation of the unit interval:

$$M_i([-1,1]) = \Gamma_i.$$

Definition 5.3.1. *The Chebyshev points of the second kind are*

$$\boldsymbol{x}^{[-1,1],n} = \begin{bmatrix} x_1^{[-1,1],n} \\ \vdots \\ x_n^{[-1,1],n} \end{bmatrix} = \begin{bmatrix} -1 \\ \cos\pi\left(1 - \frac{1}{n-1}\right) \\ \vdots \\ \cos\frac{\pi}{n-1} \\ 1 \end{bmatrix}.$$

The mapped Chebyshev points are denoted

$$\boldsymbol{x}^{i,n} = M_i(\boldsymbol{x}^{[-1,1],n}).$$

Given a continuous function f_i defined on Γ_i we find a unique interpolant at $\boldsymbol{x}^{i,n}$ using mapped Chebyshev polynomials of the first kind. Given a function, f defined on the whole of Γ, we define $\mathcal{I}_n$ to be this interpolation projection applied to the restriction of f on each Γ_i. Clearly,

$$\mathcal{I}_n : H^1(\Gamma) \to H^1(\Gamma)$$

and because $\boldsymbol{x}^{j,n}$ contains all junction points,

$$\mathcal{I}_n : H^1_z(\Gamma) \to H^1_z(\Gamma).$$

5.3.1 Computing Cauchy integrals

The framework in [89] is given by the pair $(\mathcal{I}_n, \mathcal{I}_n)$ and the matrix $\mathcal{C}_n[G;\Gamma]$ is equal to $\mathcal{I}_n\mathcal{C}[G;\Gamma]\mathcal{I}_n$ with some unbounded components subtracted; obeying the requirement that the two operators agree on $H^1_z(\Gamma)$. The construction of $\mathcal{C}_n[G;\Gamma]$ is now discussed.

Define $\mathbb{T}$ to be the unit circle with typical counter-clockwise orientation and $\mathbb{I} = [-1,1]$ with left-to-right orientation. The numerical method relies on a matrix representation of

the action of these operators on the Laurent monomials, $L_k(z) = z^k$, in the case of $\mathbb{T}$ and the Chebyshev polynomials of the first kind, $T_k(z)$, in the case of $\mathbb{I}$. The following representations are derived in [89, 87]. For $\Gamma = \mathbb{T}$ the action is given by

$$\mathcal{C}^+_{\mathbb{U}} L_k(s) = \begin{cases} L^k(s), & \text{if } k \geq 0, \\ 0, & \text{otherwise,} \end{cases}$$
$$\mathcal{C}^-_{\mathbb{U}} L_k(s) = \begin{cases} -L^k(s), & \text{if } k < 0, \\ 0, & \text{otherwise.} \end{cases}$$

If $\Gamma = \mathbb{I}$, the expressions are much more complicated. The idea used is similar to computing the discrete cosine transform. First $\mathbb{T}$ is mapped to $\mathbb{I}$ using the map $z \mapsto T(z) = \frac{1}{2}\left(z + z^{-1}\right)$. This allows us to map functions on $\mathbb{I}$ to functions on $\mathbb{T}$. Furthermore, if we map a polynomial on $\mathbb{I}$ we obtain a Laurent polynomial on $\mathbb{T}$ and we know how the Cauchy operator acts there. Using the correct inverses of the map T we obtain $\mathcal{C}^{\pm}_{\mathbb{I}}$. The inverses needed are

$$T_+^{-1}(x) = x - \sqrt{x-1}\sqrt{1+x},$$
$$T_-^{-1}(x) = x + \sqrt{x-1}\sqrt{1+x},$$
$$T_\downarrow^{-1}(x) = x - i\sqrt{1-x}\sqrt{1+x},$$
$$T_\uparrow^{-1}(x) = x + i\sqrt{1-x}\sqrt{1+x}.$$

Denoting the floor function by $\lfloor \cdot \rfloor$, we define the auxiliary functions

$$\mu_m(z) = \sum_{j=1}^{\lfloor \frac{m+1}{2} \rfloor} \frac{z^{2j-1}}{2j-1}, \quad \psi_0(z) = \frac{2}{i\pi} \operatorname{arctanh} z,$$
$$\psi_m(z) = z^m \left(\psi_0(z) - \frac{2}{i\pi} \begin{cases} \mu_{-m-1}(z) & \text{if } m < 0 \\ \mu_m(1/z) & \text{if } m > 0 \end{cases} \right).$$

Then

$$\mathcal{C}_{\mathbb{I}} T_k(x) = -\frac{1}{2}\left(\psi_k(T_+^{-1})) + \psi_{-k}(T_+^{-1}(x)) \right), \tag{5.3.1}$$

and taking limits,

$$\begin{aligned} \mathcal{C}^+_{\mathbb{I}} T_k(x) &= -\frac{1}{2}\left(\psi_k(T_\downarrow^{-1}(x)) + \psi_{-k}(T_\downarrow^{-1}(x)) \right) \\ &= -\frac{2}{i\pi} T_k(x) \operatorname{arctanh} T_\downarrow^{-1}(x) + \frac{1}{i\pi} \sum_{j=1}^{\lfloor \frac{k+1}{2} \rfloor} \frac{T_{k-2j+1}(x)}{2j-1} \begin{cases} 1, & \text{if } k-2j+1 = 0, \\ 2, & \text{otherwise,} \end{cases} \\ \mathcal{C}^-_{\mathbb{I}} T_k(x) &= -\frac{1}{2}\left(\psi_k(T_\uparrow^{-1}(x)) + \psi_{-k}(T_\uparrow^{-1}(x)) \right) \\ &= -\frac{2}{i\pi} T_k(x) \operatorname{arctanh} T_\uparrow^{-1}(x) + \frac{1}{i\pi} \sum_{j=1}^{\lfloor \frac{k+1}{2} \rfloor} \frac{T_{k-2j+1}(x)}{2j-1} \begin{cases} 1, & \text{if } k-2j+1 = 0, \\ 2, & \text{otherwise.} \end{cases} \end{aligned} \tag{5.3.2}$$

Remark 5.3.2. *In practice ψ_m is computed stably using the ${}_2F_1$ hypergeometric function. See [89] for details.*

Remark 5.3.3. *Notice that if $f(\pm 1) \neq 0$ then we expect a logarithmic singularity of $\mathcal{C}_{\mathbb{I}} f$ at the end points.*

We need to deal with more complicated contours. Assume Γ is a contour for which there exists a conformal mapping $M : \mathbb{I} \to \Gamma$ which maps infinity to infinity. Assume f vanishes at the endpoints of Γ and is smooth. $\mathcal{C}^{\pm}_{\Gamma} f$ is the unique function, analytic off Γ, which satisfies $F^+(k) - F^-(k) = f(k)$ for $k \in \Gamma$ with $F(\infty) = 0$. Then we have $F^+(M(z)) - F^-(M(z)) = f(M(z))$ for $z \in \mathbb{I}$ and $F(M(\infty)) = 0$. From the Plemelj formulae

$$\begin{aligned} F(M(z)) &= \mathcal{C}_{\mathbb{I}}(f \circ M)(z), \\ \Rightarrow F(k) &= \mathcal{C}_{\mathbb{I}}(f \circ M)(M^{-1}(k)). \end{aligned}$$

Remark 5.3.4. *If M does not map infinity to infinity we modify the result by subtracting the behavior at infinity*

$$F(k) = \mathcal{C}_{\mathbb{I}}(f \circ M)(M^{-1}(k)) - \mathcal{C}_{\mathbb{I}}(f \circ M)(M^{-1}(\infty)).$$

The last task is to deal with contours that have corners and self-intersections. We need the behavior of $\mathcal{C}_{\mathbb{I}} f$ at ± 1 in the case that f does not vanish at the end points. In terms of the auxiliary functions above we have [89] (see also Lemma 3.1.13),

$$\begin{aligned} \mathcal{C}_{\mathbb{I}} T_k(x) &\backsim -\frac{1}{2i\pi}(-1)^k[\log(-x-1) - \log 2] + \frac{1}{\pi i}(-1)^k[\mu_{k-1}(-1) + \mu_k(-1)], \quad \text{as } x \to -1, \\ \mathcal{C}_{\mathbb{I}} T_k(x) &\backsim \frac{1}{2i\pi}[\log(x-1) - \log 2] + \frac{1}{\pi i}[\mu_{k-1}(1) + \mu_k(1)], \quad \text{as } x \to 1. \end{aligned}$$

Assume Γ_1 and Γ_2 are as in Figure 5.3.1. Let $f \in H^1_z(\Gamma_1 \cup \Gamma_2)$ and let $f_i = f|_{\Gamma_i}$ be its restriction. For each Γ_i we have a conformal map $M_i : \mathbb{I} \to \Gamma_i$ with a fixed point at ∞. We expand in a Chebyshev series

$$\begin{aligned} f_1(M_1(x)) &= \sum_{n=0}^{\infty} \hat{f}^1_n T_n(x), \\ f_2(M_2(x)) &= \sum_{n=0}^{\infty} \hat{f}^2_n T_n(x). \end{aligned}$$

Then, taking orientation into account,

$$\mathcal{C}_{\Gamma_1 \cup \Gamma_2} f(z) = \sum_{k=0}^{\infty} \hat{f}^1_k \mathcal{C}_{\mathbb{I}} T_k(M_1^{-1}(z)) - \sum_{k=0}^{\infty} \hat{f}^2_k \mathcal{C}_{\mathbb{I}} T_k(M_2^{-1}(z)).$$

It is not clear, due to the singularities, how to define $\mathcal{C}^{\pm}_{\Gamma_1 \cup \Gamma_2}$. We assume that $a = M_i(-1)$ corresponds to the intersection point and we examine the behavior of this formula at this

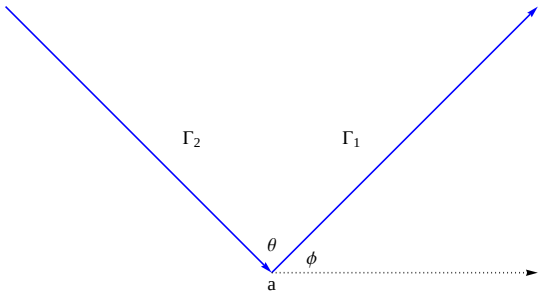

Figure 5.3.1: Intersecting contours

intersection point. As $z \to a$,

$$\begin{aligned}
\mathcal{C}_{\Gamma_1\cup\Gamma_2} f(z) \backsim & \sum_{k=0}^{\infty} \hat{f}_k^1 \left(-\frac{1}{2i\pi}(-1)^k[\log(-M_1^{-1}(z)-1) - \log 2] + \frac{1}{\pi i}(-1)^k[\mu_{k-1}(-1) + \mu_k(-1)] \right) \\
& - \sum_{k=0}^{\infty} \hat{f}_k^2 \left(-\frac{1}{2i\pi}(-1)^k[\log(-M_2^{-1}(z)-1) - \log 2] + \frac{1}{\pi i}(-1)^k[\mu_{k-1}(-1) + \mu_k(-1)] \right), \\
= & \sum_{k=0}^{\infty} (\hat{f}_k^1 - \hat{f}_k^2) \frac{(-1)^k}{2ik} \log 2 + \sum_{k=0}^{\infty} (\hat{f}_k^1 - \hat{f}_k^2) \frac{1}{\pi i}[\mu_{k-1}(-1) + \mu_k(-1)] \\
& - \sum_{k=0}^{\infty} \frac{(-1)^k}{2\pi i} \left(\hat{f}_k^1 \log(-M_1^{-1}(z)-1) - \hat{f}_k^2 \log(-M_2^{-1}(z)-1) \right).
\end{aligned} \tag{5.3.3}$$

Expanding we see

$$\begin{aligned}
-M_1^{-1}(z) - 1 &= -\partial_z M_1^{-1}(a)(z-a) + \dots, \\
-M_2^{-1}(z) - 1 &= -\partial_z M_2^{-1}(a)(z-a) + \dots.
\end{aligned}$$

Equating $z = a + \epsilon e^{i\gamma}$ we obtain

$$\begin{aligned}
\arg(-M_1^{-1}(z)-1) \backsim & \arg(-|\partial_z M_1^{-1}(a)| e^{i\gamma}), \quad \text{as } \epsilon \to 0, \\
\arg(-M_2^{-1}(z)-1) \backsim & \arg(-|\partial_z M_2^{-1}(a)| e^{i\gamma}), \quad \text{as } \epsilon \to 0.
\end{aligned}$$

We choose $\arg z \in (-\pi, \pi]$. Defining θ and ϕ by the angles in Figure 5.3.1,

$$\begin{aligned}
\arg(-M_1^{-1}(z)-1) &\backsim \begin{cases} \gamma - \phi + \pi, & \text{if } \phi - 2\pi < \gamma \le \phi, \\ \gamma - \phi - \pi, & \text{if } \phi < \gamma \le \pi, \end{cases} \\
\arg(-M_2^{-1}(z)-1) &\backsim \begin{cases} \gamma - \phi - \theta + \pi, & \text{if } \phi + \theta - 2\pi < \gamma \le \phi + \theta, \\ \gamma - \phi - \theta - \pi, & \text{if } \phi + \theta < \gamma \le \pi. \end{cases}
\end{aligned}$$

Combining all of this,

$$-\arg(-M_1^{-1}(z)-1)+\arg(-M_2^{-1}(z)-1)\backsim\begin{cases}2\pi-\theta, & \text{if } \phi<\gamma<\phi+\theta,\\ -\theta, & \text{otherwise.}\end{cases}$$

We use that $\sum_{n=0}^{\infty}\hat{f}_k^i(-1)^k=f|_{\Gamma_i}(a)=f(a)$ and examine the last term in (5.3.3) more closely:

$$\begin{aligned}&-\frac{1}{2\pi i}\sum_{k=0}^{\infty}(-1)^k(\hat{f}_k^1\log(-M_1^{-1}(z)-1)-\hat{f}_k^2\log(-M_2^{-1}(z)-1))\\&=-\frac{f(a)}{2\pi i}(\log(-M_1^{-1}(z)-1)-\log(-M_2^{-1}(z)-1))\\&\backsim i\frac{f(a)}{2\pi i}(-\arg(-M_1^{-1}(z)-1)+\arg(-M_2^{-1}(z)-1))\\&=\frac{1}{2\pi i}\begin{cases}f(a)(2\pi i-\theta) & \text{if } \phi<\arg(z)<\phi+\theta,\\ -f(a)\theta & \text{otherwise,}\end{cases}.\end{aligned}$$

This is consistent with Lemma 3.1.9. We alter M_2 so that $M_2(1)=a$ and derive the following result.

Lemma 5.3.5. *Let Γ_1,Γ_2 be smooth contours. Let Γ_1 be oriented from $z=a$ to $z=b$ with $M_1:\mathbb{I}\to\Gamma_1$, $M_1(-1)=a$ and $M_1(1)=b$. Furthermore, let Γ_2 be oriented from $z=c$ to $z=a$ with $M_2:\mathbb{I}\to\Gamma_2$, $M_2(-1)=c$ and $M_2(1)=a$. Define $\theta_i\in(-\pi,\pi]$ to be the angle of the tangent line to Γ_i at $z=a$ makes with the line $\{a+s:s\in\mathbb{R}^+\}$.*

- *For smooth function $f_1:\Gamma_1\to\mathbb{C}$,*

$$\begin{aligned}\mathcal{C}_{\Gamma_1}f_1(z)&=\frac{f_1(a)}{2\pi i}\log(z-c)+H_L(f_1),\ \text{as } z\to a, z\notin\Gamma_1,\\&=\frac{f_1(a)}{2\pi i}\log|z-c|+\frac{\theta_2}{2\pi}f_1(a)+H_L(f_1),\ \text{as } z\to a, z\in\Gamma_2,\end{aligned}$$

  and

$$H_L(f_1)=\sum_{k=0}^{\infty}\hat{f}_k^1\left(\frac{1}{2i\pi}(-1)^k\log 2+\frac{1}{\pi i}(-1)^k[\mu_{k-1}(-1)+\mu_k(-1)]\right),$$

  where $\hat{f}_k^1$ are the Chebyshev coefficients of $f_1\circ M_1$.

- *For smooth function $f_2:\Gamma_2\to\mathbb{C}$,*

$$\begin{aligned}\mathcal{C}_{\Gamma_2}f_2(z)&=-\frac{f_2(a)}{2\pi i}\log(z-c)+H_R(f_2),\ \text{as } z\to a, z\notin\Gamma_2,\\&=-\frac{f_2(a)}{2\pi i}\log|z-c|-\frac{\theta_1}{2\pi}f(a)+H_R(f_2),\ \text{as } z\to a, z\in\Gamma_1,\end{aligned}$$

and

$$H_R(f_2) = \sum_{k=0}^{\infty} \hat{f}_k^2 \left(\frac{-1}{2i\pi} \log 2 + \frac{1}{\pi i}[\mu_{k-1}(1) + \mu_k(1)] \right),$$

where $\hat{f}_k^2$ *are the Chebyshev coefficients of* $f_2 \circ M_2$.

Remark 5.3.6. *If we choose the conformal maps* M_i *so that they preserve orientation from* $\mathbb{I}$ *to* Γ_i *then Lemma 5.3.5 describes the limiting values at either endpoint.*

Define the finite Cauchy operator for Γ_i oriented from a to b:

$$\hat{\mathcal{C}}^{\pm}_{\Gamma_i}[\theta_1, \theta_2] f(z) = \begin{cases} \mathcal{C}^{\pm}_{\Gamma_i} f(z), & \text{if } z \in \Gamma_i \setminus \{a, b\}, \\ \lim_{r \to 0^+} \left(\mathcal{C}^{\pm}_{\Gamma_i} f(a + re^{i\theta_1}) - \frac{f(a)}{2\pi i} \log |r| \right), & \text{if } z = a, \\ \lim_{r \to 0^+} \left(\mathcal{C}^{\pm}_{\Gamma_i} f(b + re^{i\theta_2}) + \frac{f(b)}{2\pi i} \log |r| \right), & \text{if } z = b, \\ \mathcal{C}_{\Gamma} f(z), z \notin \Gamma_i, \end{cases}$$

where the values are dependent on the direction of approach for $z = a, b$. This function is clearly computable for any z in the complex plane.

We generalize the method so that we may deal with an arbitrary number of intersecting contours. With $a \in \gamma_0$, the set of self-intersections of Γ, let $\Gamma_1, \ldots, \Gamma_p$ be a counter-clockwise ordering of the components of Γ that have $z = a$ as an endpoint. For $f \in H^1_z(\Gamma)$ it is clear how to define $\mathcal{C}^{\pm}_{\Gamma} f(z^*)$ if $z^* \in \boldsymbol{x}^{i,n}$ when z^* is not an endpoint. Note that for each $i = 1, \ldots, p$, $M_i(1) = a$ or $M_i(-1) = a$. Thus, $z = a$ appears in $\boldsymbol{x}^{i,n}$ for $i = 1, \ldots, p$. An important complication is that in general

$$\lim_{z \to a, z \in \Gamma_i} \mathcal{C}^{\pm}_{\Gamma} f(z) \neq \lim_{z \to a, z \in \Gamma_j} \mathcal{C}^{\pm}_{\Gamma} f(z), \quad i \neq j,$$

and $\mathcal{C}^{\pm}_{\Gamma}(a)$ for $z \in \boldsymbol{x}^{i,n}$ is different from $\mathcal{C}^{\pm}_{\Gamma}(a)$ for $z \in \boldsymbol{x}^{j,n}$ if $i \neq j$. Lemma 5.3.5 informs us as to what these values are and we construct a well-defined method for computing limits of boundary values. Recall that $\Gamma = \Gamma_1 \cup \cdots \cup \Gamma_l$.

Theorem 5.3.7. *Let the tangent to* Γ_i *at* $z = a_i$ *make an angle* $\theta_{a_i} \in (-\pi, \pi]$ *with the horizontal and let the tangent at* $z = b$ *make an angle* $\theta_{b_i} \in (-\pi, \pi]$ *with the horizontal. Then if* $f \in H^1_z(\Gamma)$,

$$\sum_{i=1}^{l} \hat{\mathcal{C}}^{\pm}_{\Gamma_i}[\theta_{a_i}, \theta_{a_i}] f(z) = \sum_{i=1}^{l} \hat{\mathcal{C}}^{\pm}_{\Gamma_i}[\theta_{b_i}, \theta_{b_i}] f(z) = \mathcal{C}^{\pm}_{\Gamma} f(z), \quad z \notin \gamma_0,$$

$$\sum_{i=1}^{l} \hat{\mathcal{C}}^{\pm}_{\Gamma_i}[\theta_{a_i}, \theta_{a_i}] f(z) = \lim_{z \to a,\ z \in \Gamma_1} \mathcal{C}^{\pm}_{\Gamma} f(z),$$

$$\sum_{i=1}^{l} \hat{\mathcal{C}}^{\pm}_{\Gamma_i}[\theta_{b_i}, \theta_{b_i}] f(z) = \lim_{z \to b,\ z \in \Gamma_1} \mathcal{C}^{\pm}_{\Gamma} f(z).$$

Proof. Note that the same angle is used twice since it is not specified if $M_j(\pm) = a_i$ when a_i is an endpoint. The zero-sum condition ensures that the $\log |r|$ term in the definition of

the finite Cauchy operator drops out. □

Using this definition we effectively compute $\mathcal{C}_\Gamma^\pm u$, $u \in H_z^1(\Gamma)$ at every point $\boldsymbol{x}^{i,n}$, computing the limiting values at the endpoints of Γ_i. Therefore we compute the operator

$$\mathcal{C}[G;\Gamma]\mathcal{I}_n u,$$

exactly for every interpolation point in $\boldsymbol{x}^{i,n}$, $i = 1,\ldots,l$ implying that $\mathcal{I}_n\mathcal{C}[G;\Gamma]\mathcal{I}_n u$ is computable. This defines an operator that acts on sums of mapped Chebyshev polynomials u_n and returns $\mathcal{C}[G;\Gamma]u_n$ at each point of $\boldsymbol{x}^{i,n}$, $i = 1,\ldots,l$ that is not an endpoint of Γ_i. Furthermore, this operator returns

$$u_n(z) - \sum_{i=1}^{n} \hat{\mathcal{C}}_{\Gamma_i}^\pm[\theta,\theta]u_n(z)\cdot(G(z)-I),$$

at each endpoint of Γ_i with θ appropriately chosen as in Theorem 5.3.7. This is guaranteed to return finite values $\boldsymbol{u}_n^i$ at every point in $\boldsymbol{x}^{i,n}$, $i = 1,\ldots,l$. We output the interpolant of the values $\boldsymbol{u}_n^i$ using mapped Chebyshev polynomials. This is the definition of operator $\mathcal{C}_n[G;\Gamma]$ and as promised it agrees with $\mathcal{C}[G;\Gamma]$ if $u_n \in H_z^1(\Gamma)$. From a computational standpoint, a linear system is set up to solve for $\boldsymbol{f}^i$ by enforcing that

$$\mathcal{C}_n[G;\Gamma]u_n(x) = G(x) - I, \quad \text{for all } x \in \boldsymbol{x}^{i,n}, \quad i = 1,\ldots,l. \tag{5.3.4}$$

The following theorem is found in [89], and finalizes the theoretical development of the numerical method.

Theorem 5.3.8 ([89])**.** *If the linear system* (5.3.4) *is nonsingular, then the calculated* $u_n(x)$ *satisfies the zero-sum condition.*

In conclusion, the fact that the linear system is nonsingular implies that the numerically constructed solution of the Riemann–Hilbert problem $\Phi_n = I + \mathcal{C}_\Gamma u_n$ satisfies the correct jumps at the collocation points.

Remark 5.3.9. *A* `Mathematica` *implementation of the framework in [89] is available online [85]. This method is discussed deeper in [89] with all implementational details .*

5.3.2 Properties of $\mathcal{C}_n[G;\Gamma]$

We address the properties required in Definition 5.1.4.

Lemma 5.3.10. *When* $G \in W^{1,\infty}(\Gamma)$*, the numerical method in [89] satisfies:*

- $\mathcal{I}_n$ *is uniformly bounded in* n *from* $C(\Gamma)$ *to* $L^2(\Gamma)$ *when* Γ *is bounded.*
- $\|\mathcal{C}_n[G;\Gamma]\|_{\mathcal{L}(H_z^1(\Gamma),Y_n)} \le C(1 + \|G-I\|_{L^\infty(\Gamma)}\|\mathcal{C}_\Gamma^-\|_{\mathcal{L}(L^2(\Gamma))})$.
- $\|\mathcal{T}_n[G;\Gamma]\|_{\mathcal{L}(X_n,Y_n)} \le Cn^2\|G-I\|_{L^\infty(\Gamma)}\|\mathcal{C}_\Gamma^-\|_{\mathcal{L}(L^2(\Gamma))}$.
- $\|\mathcal{I}_n u - u\|_{H^1(\Gamma)} \le C_s n^{2-s}\|u\|_{H^s(\Gamma)}$.

Proof. First, note that these constants depend on Γ. Using the Dirichlet kernel one proves that $\mathcal{I}_n$ is uniformly bounded from $C(\Gamma)$ to an L^2 space with the Chebyshev weight [7]. The norm on this weighted space dominates the usual $L^2(\Gamma)$ norm, proving the first result. For the second statement we take $u \in H^1_z(\Gamma)$ and consider

$$\begin{aligned} &\|\mathcal{I}_n - \mathcal{I}_n(G-I)\mathcal{C}_\Gamma^- u\|_{L^2(\Gamma)} \\ &\leq \|\mathcal{I}_n\|_{\mathcal{L}(C(\Gamma),L^2(\Gamma))}(1 + \|G-I\|_{L^\infty(\Gamma)}\|\mathcal{C}_\Gamma^-\|_{\mathcal{L}(H^1_z(\Gamma),H^1(\Gamma))}\|u\|_{H^1(\Gamma)}). \end{aligned}$$

Since Y_n is equipped with the $L^2(\Gamma)$ norm and $\|\mathcal{C}_\Gamma^-\|_{\mathcal{L}(H^1_z(\Gamma),H^1(\Gamma))} = \|\mathcal{C}_\Gamma^-\|_{\mathcal{L}(L^2(\Gamma))}$ we obtain the second property. We then use for $u \in X_n$ (see Section 5.1) that $\|u\|_{H^1(\Gamma)} \leq Cn^2\|u\|_{L^2(\Gamma)}$ to obtain

$$\|\mathcal{T}_n[G;\Gamma]\|_{\mathcal{L}(X_n,Y_n)} \leq Cn^2\|G-I\|_{L^\infty(\Gamma)}\|\mathcal{C}_\Gamma^-\|_{\mathcal{L}(L^2(\Gamma))}.$$

The last statement follows from estimates in [98] for the pseudo-spectral derivative. □

The final property we need to obtain an admissible numerical method, the boundedness of the inverse, is a very difficult problem. We can verify, *a posteriori*, that the norm of the inverse does not grow too much. In general, for this method, we see at most logarithmic growth. We make the following assumption.

Assumption 5.3.11. *For the framework in [89] we assume that whenever* $[G;\Gamma]$ *is* 1*-regular and* $\mathcal{C}[G;\Gamma]^{-1}$ *exists on* $L^2(\Gamma)$ *as a bounded operator, we have for* $n > N$

$$\|\mathcal{C}_n[G;\Gamma]^{-1}\|_{\mathcal{L}(Y_n,X_n)} \leq Cn^\beta\|\mathcal{C}[G;\Gamma]^{-1}\|_{\mathcal{L}(L^2(\Gamma))}, \quad \beta > 0. \tag{5.3.5}$$

Remark 5.3.12. *This assumption is known to hold for a similar collocation method on the unit circle using Laurent monomials [97].*

With this assumption the numerical method associated with $(\mathcal{I}_n, \mathcal{I}_n)$ is of type $(0, \beta, 2)$. In light of Theorem 5.1.6, we expect spectral convergence and the bound in Assumption 5.3.11 does not prevent convergence. We combine Assumption 5.3.11, Theorem 5.1.6 and Theorem 3.9.1 to obtain

$$\|u - u_n\|_{L^2(\Gamma)} \leq C(\|\mathcal{C}[G;\Gamma]^{-1}\|_{\mathcal{L}(L^2(\Gamma))}(1 + \|G-I\|_{L^\infty(\Gamma)}\|\mathcal{C}_\Gamma^-\|_{\mathcal{L}(L^2(\Gamma))})n^{2+\beta-k}\|u\|_{H^k(\Gamma)}. \tag{5.3.6}$$

Therefore, we realize L^2 convergence of our approximations to the function u. Since $\Phi = I + \mathcal{C}_\Gamma u$, we find (see Lemma 3.6.9)

$$\Phi \sim I + \frac{\Phi_1}{z} + \mathcal{O}(z^{-2}), \quad \Phi_1 = -\int_\Gamma u\bar{d}z \sim -\int_\Gamma u_n\bar{d}z. \tag{5.3.7}$$

Here L^2 convergence implies L^1 convergence since Γ is bounded. An approximation of Φ_1 is critical in inverse scattering, see (2.5.8). To efficiently and accurately compute $\int_\Gamma u_n dz$ we note that the values u_n takes at mapped Chebyshev nodes is known and therefore Clenshaw-Curtis quadrature computes this integral effectively .

Note that if Algorithm 5.1.11 is used then an approximation of u such that $\Phi = I + \mathcal{C}_\Gamma u$ is not directly returned from the algorithm since SIEs are solved on each disjoint contour at

each stage, not on all of Γ. But since an approximation $\Phi_{\boldsymbol{n}} = \phi_\ell \cdots \phi_1$ (with $\phi_j = I + \mathcal{C}_\Gamma u_j$) to the solution Φ is known we find, in the notation of Algorithm 5.1.11:

$$\Phi_1 \sim -\sum_{j=1}^{\ell} \int_{\Gamma_J} u_j \bar{d}z. \tag{5.3.8}$$

Chapter 6

The Korteweg-de Vries and Modified Korteweg-de Vries Equations

We consider the initial-value problem on the whole line for the Korteweg–de Vries equation (KdV)

$$\begin{aligned} q_t + 6qq_x + q_{xxx} &= 0, \\ q(x,0) &= q_0(x) \in \mathcal{S}_\delta(\mathbb{R}). \end{aligned} \tag{6.0.1}$$

We also consider the defocusing modified KdV equation, given by

$$\begin{aligned} q_t - 6q^2q_x + q_{xxx} &= 0, \\ q(x,0) &= q_0(x) \in \mathcal{S}_\delta(\mathbb{R}). \end{aligned} \tag{6.0.2}$$

The KdV equation describes the propagation of long waves in dispersive media, e.g. long surface water waves [69]. Historically, the KdV equation is the first known case of a PDE that is solvable by the inverse scattering transform [56]. The KdV equation and the modified KdV equation can also be thought of as dispersive regularizations of the Burgers and modified Burgers equations, respectively.

The presence of dispersion makes the quantitative approximation of solutions of the KdV equation and the modified KdV equation through numerical methods especially difficult, see Section 6.5 for a detailed discussion. Section 6.5 demonstrates that while the oscillatory nature of the solution is reproduced in many numerical methods a high degree of accuracy for moderate times is elusive. To see this heuristically, in Figure 6.0.1 we approximate the solution of the KdV equation with $q(x,0) = A\,\mathrm{sech}^2(x)$ where $A = 3.2$ using the numerical scheme presented in this chapter. With $A = 3$ the solution would be a two-soliton solution without any dispersive tail [42]. Notice that a significant dispersive tail forms even though the solution is close to a soliton solution. The issue becomes worse when we consider solutions that are farther from a soliton solution, see Figure 6.0.2.

To combat this dispersive complication, we exploit the integrability of the KdV equation and the modified KdV equation and evaluate the inverse scattering transform numerically.

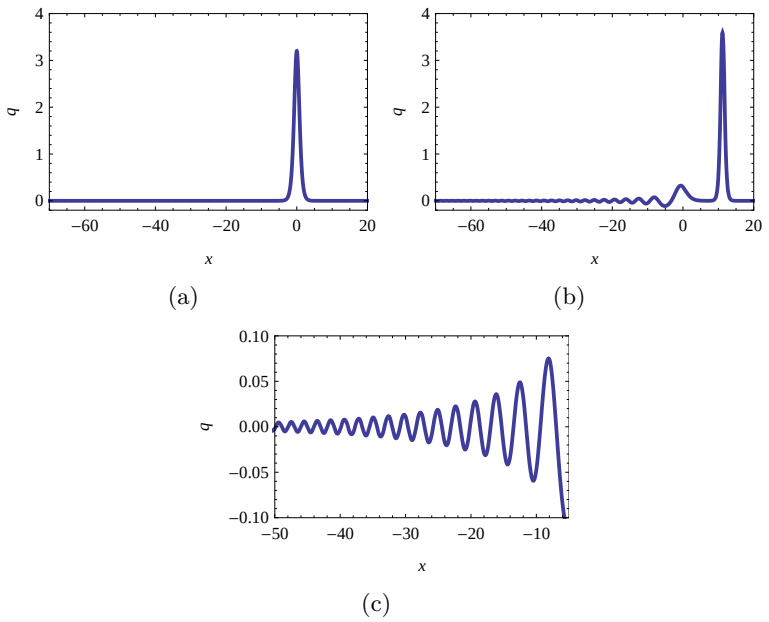

Figure 6.0.1: Numerical solution of the KdV equation with initial data that is close to a two-soliton solution. (a) Initial condition, (b) Solution at $t = 1.5$. The two largest peaks each correspond to a soliton. (c) Dispersive tail at $t = 1.5$.

Computing the inverse scattering transform involves developing techniques to compute the forward transform (direct scattering) and the inverse transform (inverse scattering). Our approach to direct scattering employs collocation methods for ODEs (see Appendix B and existing spectrum approximation techniques. For inverse scattering we use the numerical method for RHPs presented in [89]. After deforming the RHP in the spirit of Deift and Zhou [34, 39, 60], the numerical method becomes *asymptotically stable*: the work required to compute the solution at a point to a desired accuracy is bounded for all x and t. In this method the roles of x and t are reduced to that of parameters. No time-stepping or spatial discretization is needed and the code can trivially be run in parallel.

The numerical direct and inverse scattering for the defocusing modified KdV equation is presented along with numerical results. The RHP for the modified KdV equation has a simple form and the deformations are straightforward. All RHPs we solve are well-posed:

Definition 6.0.13. *A RHP is well-posed if it has a unique solution of the form*

$$\Phi(k) = I + \mathcal{C}_\Gamma u \tag{6.0.3}$$

for some function $u \in L^2(\Gamma)$.

This is demonstrated using Theorem 3.8.21 and Theorem 3.8.29

Next, the KdV equation is considered. Now one has to deal with the addition of solitons to the problem. After deformation, the RHP for the KdV equation has a singularity and this requires two additional deformations. We introduce a new deformation that is not present, to our knowledge, in the existing literature. This new transition region allows for

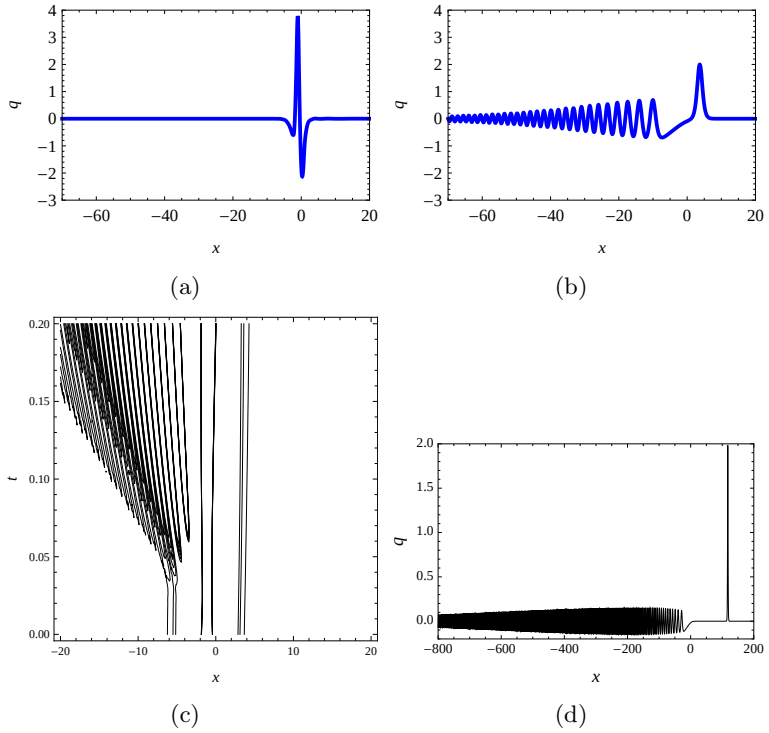

Figure 6.0.2: Numerical solution of the KdV equation for an initial condition which is far from a pure soliton initial condition. (a) Initial condition obtained by adding a soliton to the RHP associated with $q(x,0) = -2.3\,\mathrm{sech}^2(x)$, (b) Solution at $t = 1.5$, (c) A contour plot showing the birth of the dispersive tail, (d) Solution at $t = 30$. It is not practical to use conventional methods to capture this solution quantitatively for longer times.

stable asymptotic computation of the solution in a region where the classical deformations break down numerically. Numerical results for the KdV equation are presented. Finally, the numerical solutions of the modified KdV equation and the KdV equation are compared using the Miura transformation.

We solve the modified KdV equation because the complexity associated with its solution is what should be expected when solving other integrable equations with this method. We solve the KdV equation because it is a more difficult problem, and demonstrates that the method is general enough to handle the added difficulties, though it requires the introduction of significantly more machinery.

Through the comparison of our results with existing asymptotic expressions we can guarantee the accuracy of the method. It is accurate for small-time and for long-time. Traditionally, numerical analysts favor integrable equations because of the large class of explicit solutions available for comparison. All of these explicit cases do not exhibit a dispersive tail. This method expands the class of solutions which we can compute accurately and, importantly, it provides a benchmark test to guide the development of new numerical methods designed to capture dispersion.

6.0.3 Integrability and Lax pairs

The mKdV and the KdV equation and are both completely integrable [1]. We take this to mean that for each equation there exist two linear systems of ordinary differential equations depending on a parameter k

$$\begin{aligned}\mu_x &= L(k,q)\mu,\\ \mu_t &= M(k,q)\mu,\end{aligned}$$

such that $\mu_{xt} = \mu_{tx}$ if and only if q satisfies the PDE in question. Systems of this form are called Lax pairs. Note that we use a slightly different form than that in Chapter 2. The Lax pair is also known as the *scattering problem* for the PDE. We introduce the modified Zakharov–Shabat scattering problem given by

$$\begin{aligned}\mu_x &= \begin{bmatrix} -ik & q \\ r & ik \end{bmatrix}\mu,\\ \mu_t &= \begin{bmatrix} A & B \\ C & D \end{bmatrix}\mu,\end{aligned}$$

where r, A, B, C and D are scalar functions to be determined [1]. If we make the choice

$$\begin{aligned}A &= -4ik^3 + 2ikqr - (r_x q - q_x r),\\ B &= 4qk^2 + 2ikq_x - 2q^2 r - q_{xx},\\ C &= 4rk^2 - 2ikr_x + 2qr^2 - r_{xx},\\ D &= -A,\end{aligned} \tag{6.0.4}$$

we can obtain Lax pairs for both the modified KdV equation and the KdV equation.

The modified Korteweg–de Vries equation

To obtain a Lax pair for the (defocusing) modified KdV equation (6.0.2), let $r = q$, so that the x equation of the Lax pair takes the form

$$\mu_x = \begin{bmatrix} -ik & q \\ q & ik \end{bmatrix}\mu. \tag{6.0.5}$$

In what follows we do not need the explicit form of the equation for μ_t.

Remark 6.0.14. *As above, we perform scattering in a more restricted space of functions. We assume $q(x,0) \in \mathcal{S}_\delta(\mathbb{R})$. This simplifies some technical details as is noted below. This assumption is relaxed on a case-by-case basis. The decay rate is needed for analyticity properties and the smoothness is needed to numerically compute the scattering data, defined below.*

1. *Definition of the Scattering Data.* Consider the problem (6.0.5). Assume $q \in \mathcal{S}_\delta(\mathbb{R})$,

it follows that there are two matrix-valued eigenfunctions

$$\phi(x;k) \backsim \begin{bmatrix} e^{-ikx} & 0 \\ 0 & -e^{ikx} \end{bmatrix} \text{ as } x \to -\infty, \quad \psi(x;k) \backsim \begin{bmatrix} e^{-ikx} & 0 \\ 0 & e^{ikx} \end{bmatrix} \text{ as } x \to \infty. \tag{6.0.6}$$

From Abel's formula, the determinants of these solutions are constant in x; evaluating at $\pm\infty$ we see that the columns do indeed form a linearly independent solution set and hence span the solution space. There exists a transition matrix

$$T(k) = \begin{bmatrix} a(k) & \mathcal{B}(k) \\ b(k) & \mathcal{A}(k) \end{bmatrix},$$

such that

$$\phi(x;k) = \psi(x;k)T(k).$$

Define $\rho(k) = b(k)/a(k)$ to be the reflection coefficient. For the defocusing modified KdV equation we define the scattering data to be only the reflection coefficient [1]. The conventions for the reflection coefficient in [1] and [34] differ. The reflection coefficient used by Ablowitz and Segur [1] is i times that used by Deift and Zhou [34].

2. *The Inverse Problem.*We phrase the inverse problem in terms of a RHP. We seek a 2×2 matrix-valued function Φ that satisfies

$$\begin{aligned} \Phi^+(k) &= \Phi^-(k)G(k), \quad k \in \mathbb{R}, \\ \Phi(\infty) &= I, \\ G(k) &= \begin{bmatrix} 1 - \rho(k)\rho(-k) & -\rho(-k)e^{-\theta(k)} \\ \rho(k)e^{\theta(k)} & 1 \end{bmatrix}, \\ \theta(k) &= 2ikx + 8ik^3t. \end{aligned}$$

The solution to the modified KdV equation is given by

$$q(x,t) = -2i \lim_{k\to\infty} k\Phi(k)_{21}, \tag{6.0.7}$$

where the subscript denotes the 2-1 component [34]. We suppress the x and t dependence for notational simplicity.

Remark 6.0.15. *The well-posedness of this RHP can be established by considering a specific singular integral equation and showing it is of the form $(I-K)u = f$ where $\|K\| < 1$. This fact relies on $\sup_{k\in\mathbb{R}} |\rho(k)| < 1$, see [34] for details. Additionally, the well-posedness follows from Theorems 3.8.21 and 3.8.29 because $\det G = 1$ and $G + G^\dagger$ is positive definite.*

The Korteweg–de Vries equation

To obtain the KdV equation (6.0.1) from (6.0.4) we set $r = -1$ and the x portion of the Lax pair takes the form

$$\mu_x = \begin{bmatrix} -ik & q \\ -1 & ik \end{bmatrix} \mu.$$

This can be simplified to the time-independent Schrödinger equation

$$\mu_{xx} + (k^2 - q)\mu = 0. \tag{6.0.8}$$

As before, we do not need the explicit form of the equation for μ_t.

1. *Definition of the Scattering Data.* We consider the problem (6.0.8) and assume $q \in \mathcal{S}_\delta(\mathbb{R})$. There are two vector-valued eigenfunctions

$$\phi \backsim \begin{bmatrix} e^{-ikx} & e^{ikx} \end{bmatrix} \text{ as } x \to -\infty, \quad \psi \backsim \begin{bmatrix} e^{-ikx} & e^{ikx} \end{bmatrix} \text{ as } x \to \infty.$$

   It follows from Abel's formula that the Wronskian of these solutions is constant in x and evaluating at $\pm\infty$ we see the two entries form a linearly independent solution set which spans the solution space. There is a transition matrix

$$T(k) = \begin{bmatrix} a(k) & b(k) \\ \mathcal{B}(k) & \mathcal{A}(k) \end{bmatrix},$$

   such that $\phi(x,t;k) = \psi(x,t;k)T(k)$. Define $\rho(k) = b(k)/a(k)$ to be the reflection coefficient. It is known that $a(k)$ has simple zeros in the upper-half plane, on the imaginary axis. We denote the set of these n zeros by $\{\kappa_j\}_{j=1}^n$ and we assume that $\rho(k)$ can be analytically extended above these poles. In this case let $C_j = \text{Res}\{\rho(k), k = \kappa_j\}$ and form the set $\{C_j\}_{j=1}^n$. Define the set

$$\{\rho(k), \{\kappa_j\}_{j=1}^n, \{C_j\}_{j=1}^n\}, \tag{6.0.9}$$

   to be the scattering data for the KdV equation.

2. *The Inverse Problem.*We can pose the meromorphic RHP for the solution of the KdV equation. We seek a function $\Phi : \mathbb{R} \to \mathbb{C}^{1\times 2}$ that is meromorphic off $\mathbb{R}$ with simple poles at $\pm\kappa_j$ such that

$$\begin{aligned} \Phi^+(k) &= \Phi^-(k)G(k), \quad k \in \mathbb{R}, \\ \text{Res}\{\Phi(k), k = \kappa_j\} &= \lim_{k\to\kappa_j} \begin{bmatrix} 0 & 0 \\ C_j e^{\theta(\kappa_j)} & 0 \end{bmatrix} \Phi(k), \\ \text{Res}\{\Phi(k), k = -\kappa_j\} &= \lim_{k\to-\kappa_j} \begin{bmatrix} 0 & -C_j e^{\theta(\kappa_j)} \\ 0 & 0 \end{bmatrix} \Phi(k), \\ \Phi(\infty) &= \begin{bmatrix} 1 & 1 \end{bmatrix}. \end{aligned}$$

The solution to the KdV equation is given by the reconstruction formula [3],

$$q(x,t) = 2i \lim_{k\to\infty} k\Phi_x(k)_1.$$

Remark 6.0.16. *This meromorphic problem can be turned into an analytic problem by introducing small circles around each pole and using the appropriate jump on this new contour [60]. Fix* $0 < \epsilon < \min_{k\neq j} |\kappa_j - \kappa_k|/2$, *with* $\epsilon < \min_j |\kappa_j|$. *This* ϵ *is chosen so that the circles* $A_j^{\pm} = \{k \in \mathbb{C} : |k - \pm\kappa_j| < \epsilon\}$ *do not intersect each other or the real axis. We define* $\hat{\Phi}$ *by*

$$\hat{\Phi}(k) = \begin{cases} \Phi(k) \begin{bmatrix} 1 & 0 \\ -C_j e^{\theta(\kappa_j)}/(k-\kappa_j) & 1 \end{bmatrix}, & \text{if } |k-\kappa_j| < \epsilon,\ j = 1,\dots,n, \\ \Phi(k) \begin{bmatrix} 1 & 0 \\ C_j e^{\theta(\kappa_j)}/(k+\kappa_j) & 1 \end{bmatrix}, & \text{if } |k+\kappa_j| < \epsilon,\ j = 1,\dots,n, \\ \Phi(k), & \text{otherwise.} \end{cases}$$

It is straightforward to show that $\hat{\Phi}$ *solves the RHP*

$$\hat{\Phi}^+(k) = \begin{cases} \hat{\Phi}^-(k)G(k), & \text{if } k \in \mathbb{R}, \\ \hat{\Phi}^-(k) \begin{bmatrix} 1 & 0 \\ -C_j e^{\theta(\kappa_j)}/(k-\kappa_j) & 1 \end{bmatrix}, & \text{if } k \in A_j^+, \\ \hat{\Phi}^-(k) \begin{bmatrix} 1 & -C_j e^{\theta(\kappa_j)}/(k+\kappa_j) \\ 0 & 1 \end{bmatrix}, & \text{if } k \in A_j^-, \end{cases}$$

$$\hat{\Phi}(\infty) = \begin{bmatrix} 1 & 1 \end{bmatrix},$$

where A_j^- *(*A_j^+*) has (counter-)clockwise orientation.*

Remark 6.0.17. *Due to the fact that generically* $\rho(0) = -1$ *for the KdV equation, the well-posedness of this RHP is in principle more difficult to establish. One must appeal to Theorems 3.8.21 and 3.8.29. In the language of the vanishing lemma, Theorem 3.8.29,* $(A_j^+)^\dagger = A_j^-$. *Furthermore, the jump matrices share the correct Schwartz invariance. Furthermore,* $\det G = 1$ *and* $G + G^\dagger$ *is positive definite on* $\mathbb{R} \setminus 0$. *This proves the unique solvability of the RHP.*

6.0.4 Asymptotic regions

In this section we present the classical results on the long-time asymptotics of the solution of the modified KdV equation and the KdV equation. We introduce constants, c_i, to divide regions. While any valid choice of these will work, the numerical method can be improved by adjusting them on a case-by-case basis.

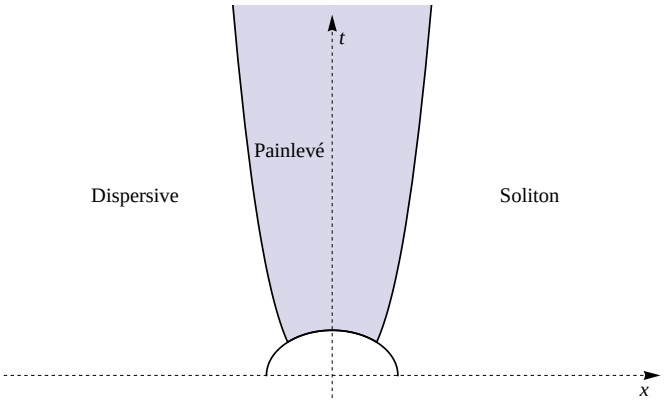

(a)

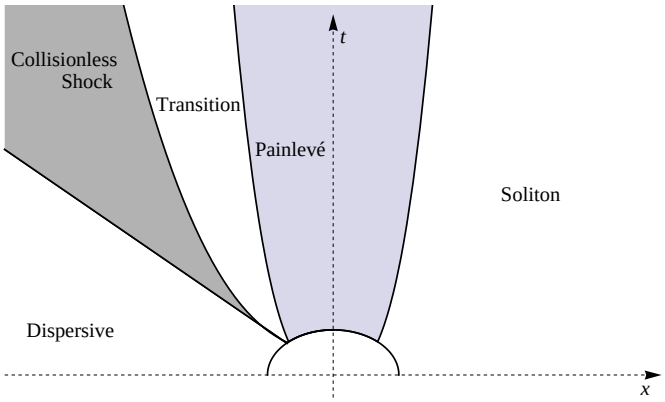

(b)

Figure 6.0.3: (a) Regions for the asymptotic analysis for the modified KdV equation, (b) Regions for the asymptotic analysis for the KdV equation.

The modified Korteweg–de Vries equation

The results presented here are found in [34]. In the (x,t)-plane, the long-time evolution of the modified KdV equation is described in three fundamentally different ways. For a diagram of these regions see Figure 6.3(a).

1. *The Soliton Region.* This region is defined for $x \geq c_1 t^{1/3},\ c_1 > 0$. The name "soliton region" is a misnomer because there are no solitons present in the defocusing modified KdV equation [1] but for the sake of uniformity with the KdV equation we retain the name. Here the solution $q(x,t)$ decays beyond all orders, *i.e.*,

$$q(x,t) = \mathcal{O}((x+t)^{-j}), \quad \text{for all } j > 0. \tag{6.0.10}$$

2. *The Painlevé Region.* This region is defined for $|x| \leq c_1 t^{1/3}$. More general results can be found in [34]. Along a trajectory $x = -Ct^{1/3}$, $C > 0$, the solution satisfies

$$q(x,t) - U(x,t) = \mathcal{O}(t^{-2/3}), \tag{6.0.11}$$

where

$$U(x,t) = (3t)^{-1/3} v(x/(3t)^{1/3}), \tag{6.0.12}$$

and v is the Ablowitz–Segur solution to Painlevé II with Stokes' constants $\{s_1, s_2, s_3\} = \{-i\rho(0), 0, i\rho(0)\}$. See Chapter 8 for a numerical method to compute this solution.

3. *The Dispersive Region.* Historically, this region is defined for $-x > c_2 t > 0$, $c_2 > 0$. For our purposes, we use $-x > c_1 t^{1/3}$ for the definition of this region. The reasoning for this will become clear below. Along a trajectory $-x = Ct$, $C > 0$, the solution satisfies

$$q(x,t) - R(x,t) = \mathcal{O}(log(t)t^{-1}), \tag{6.0.13}$$

where

$$R(x,t) = \sqrt{\frac{\nu(k_0)}{3tk_0}} \cos\left(16tk_0^3 - \nu(k_0)\log(192tk_0^3) + \delta(k_0)\right),$$

and

$$\begin{aligned} k_0 &= \sqrt{-x/(12t)}, \\ \nu(k_0) &= -\frac{1}{2\pi}\log(1-\rho(k_0)\overline{\rho}(k_0)), \\ \delta(k_0) &= \frac{\pi}{4} - \arg(\rho(k_0)) + \arg(\Gamma(i\nu(k_0))) \\ &\quad - \frac{1}{\pi}\int_{-k_0}^{k_0} \log\left(\frac{1-\rho(\eta)\overline{\rho}(\eta)}{1-\rho(k_0)\overline{\rho}(k_0)}\right)\frac{1}{\eta - k_0}d\eta. \end{aligned}$$

The Korteweg–de Vries equation

The results presented here are found in [39, 60]. See Figure 6.3(b) for a diagram of these regions.

1. *The Soliton Region.* This region is defined for $x \geq c_1 t^{1/3}$, $c_1 > 0$. For $x > Ct$, $C > 0$, the solution of the KdV equation in this region satisfies

$$q(x,t) - S(x,t) = \mathcal{O}((x+t)^{-j}),$$

where

$$S(x,t) = \sum_{j=1}^{n} 2\kappa_j^2 \operatorname{sech}^2(\kappa_j x - 4\kappa_j^3 t - p_j),$$
$$p_j = \frac{1}{2}\log\left(\frac{C_j^2}{2\kappa_j}\prod_{l=j+1}^{n}\left(\frac{\kappa_l - \kappa_j}{\kappa_l + \kappa_j}\right)^2\right).$$

The constants κ_j and C_j are defined in (6.0.9).

2. *The Painlevé Region.* This region is defined for $|x| < c_2 t^{1/3}$, $c_2 > 0$. Along a trajectory $x = \pm Ct^{1/3}$, $C > 0$, the solution to the KdV equation satisfies

$$q(x,t) - U(x,t) = \mathcal{O}(t^{-1}), \tag{6.0.14}$$

where

$$U(x,t) = \frac{1}{(3t)^{2/3}}\left(v^2\left(\frac{x}{(3t)^{1/3}}\right) + v'\left(\frac{x}{(3t)^{1/3}}\right)\right),$$

and v is the Hastings–McLeod solution to Painlevé II with Stokes' constants $\{s_1, s_2, s_3\} = \{i, 0, -i\}$ [63] (see also Chapter 8). The error bound is not present in [39] but we infer it from (6.0.11) through the Miura transformation, Section 6.2.4.

3. *Transition Region.* This region is, to our knowledge, not present in the literature. It is defined by the relation $c_3 t^{1/3}(\log t)^{2/3} \leq -x \leq c_4 t^{1/3}$, $c_3, c_4 > 0$. Asymptotics are not known in this region.

4. *The Collisionless Shock Region.* This region is defined by $c_5 t \leq -x \leq c_6 t^{1/3}(\log t)^{2/3}$, $0 < c_5 \leq 12$ and $c_6 > 0$. This is the region in the (x,t)-plane where our deformations are valid. The asymptotic formula in [39] is given with the constraint $1/C \leq -x/(t^{1/3}(\log t)^{2/3}) \leq C$ for $C > 1$. With this constraint the RHP limits to a

RHP on $(-b(s), b(s))$ of the form [39]

$$\zeta^+(k) = \begin{cases} \zeta^-(k) \begin{bmatrix} 0 & e^{-24i\tau \int_0^{a(s)} f(p)dp} \\ -e^{24i\tau \int_0^{a(s)} f(p)dp} & 0 \end{bmatrix}, & \text{if } a(s) < k < b(s), \\ \zeta^-(k) \begin{bmatrix} 2\nu k^2 & 0 \\ 0 & (2\nu k^2)^{-1} \end{bmatrix}, & \text{if } -a(s) < k < a(s), \\ \zeta^-(k) \begin{bmatrix} 0 & e^{-24i\tau \int_0^{-a(s)} f(p)dp} \\ -e^{24i\tau \int_0^{-a(s)} f(p)dp} & 0 \end{bmatrix}, & \text{if } -b(s) < k < -a(s), \end{cases}$$
$$\zeta(\infty) = \begin{bmatrix} 1 & 1 \end{bmatrix},$$
$$f(p) = \sqrt{(a^2 - p^2)(b^2 - p^2)}. \tag{6.0.15}$$

The definitions of a, b, s and τ can be found in Section 6.4. See Section 6.2.2 for the definition of ν. Note that the only x and t dependence enters through a, b and τ. The approximation W of the solution of the KdV equation is obtained by

$$W(x,t) = 2i\sqrt{-x/(12t)} \lim_{k\to\infty} \partial_x \zeta(k).$$

We remark that no bound is present in [39]. See (6.2.6) for a numerical conjecture of this error bound.

Remark 6.0.18. *By adjusting c_2 and c_6, the collisionless shock region can be made to overlap with the Painlevé region up to a finite time. In the absence of the transition region, this will always leave a gap in the (x,t)-plane that is not contained in any region. From a numerical point of view, we introduce the transition region precisely to compute the solution of the KdV equation in this gap. This region seems to be not needed in the asymptotic analysis because the solution in the collisionless shock region can be asymptotically matched with the solution in the Painlevé region [5].*

5. *The Dispersive Region.* This region is defined by $-x > c_7 t > 0$, $c_7 > 0$. Along a trajectory $x = -Ct$, $C > 0$, the solution to the KdV equation satisfies

$$q(x,t) - R(x,t) = \mathcal{O}(t^{-1}), \tag{6.0.16}$$

where

$$R(x,t) = -\sqrt{\frac{4\nu(k_0)k_0}{3t}} \sin\left(16tk_0^3 - \nu(k_0)\log(192tk_0^3) + \delta(k_0)\right),$$

and

$$\begin{aligned} k_0 &= \sqrt{-x/(12t)}, \\ \nu(k_0) &= -\frac{1}{2\pi}\log(1-\rho(k_0)\overline{\rho}(k_0)), \\ \delta(k_0) &= \frac{\pi}{4} - \arg(\rho(k_0)) + \arg(\Gamma(i\nu(k_0))) + \sum_{j=1}^{n} \arctan\left(\frac{\kappa_j}{k_0}\right) \\ &\quad - \frac{1}{\pi}\int_{-k_0}^{k_0} \log\left(\frac{1-\rho(\eta)\overline{\rho}(\eta)}{1-\rho(k_0)\overline{\rho}(k_0)}\right)\frac{1}{\eta-k_0}d\eta. \end{aligned}$$

6.1 The modified Korteweg–de Vries equation

6.1.1 Numerical computation of the scattering data

We look for solutions of the form (6.0.6) to (6.0.5). Define

$$\sigma_3 = \begin{bmatrix} 1 & 0 \\ 0 & -1 \end{bmatrix}, \quad \sigma_1 = \begin{bmatrix} 0 & 1 \\ 1 & 0 \end{bmatrix},$$

and two new functions

$$\begin{aligned} J(k) &= \phi(k)\sigma_3 e^{ikx\sigma_3} - I, \\ K(k) &= \psi(k)e^{ikx\sigma_3} - I. \end{aligned} \tag{6.1.1}$$

Therefore $J \to 0$ as $x \to -\infty$ and $K \to 0$ as $x \to \infty$. Rewriting (6.0.6),

$$\mu_x = q\sigma_1\mu - ik\sigma_3\mu,$$

and we find that K and J both solve

$$M_x - ik[M, \sigma_3] - q\sigma_1 M = q\sigma_1.$$

For each k, this can be solved with a Chebyshev collocation method on $(-L, 0]$ for J and on $[0, L)$ for K using the appropriate boundary condition at $\pm L$. See Appendix B for a discussion of the method. If we use n collocation points, this gives two approximate solutions J_n and K_n for J and K, respectively. From J_n and K_n we obtain ϕ_n and ψ_n, approximations of ϕ and ψ, respectively, by inverting (6.1.1). Furthermore, ϕ_n and ψ_n share the point $x = 0$ in their domain of definition. Define

$$T_n(k) = \psi_n^{-1}(0; k)\phi_n(0; k).$$

This is an approximation of the transition matrix, from which we extract an approximation of the reflection coefficient.

6.1.2 Numerical solution of the inverse problem

The RHPs considered here have the key feature that the jump matrices are highly oscillatory. Deift and Zhou adapted ideas from the asymptotic evaluation of integrals to this

problem to obtain asymptotic formulae with rigorous error bounds [34, 33, 39]. The main idea of this method is to deform the contours of the RHP so that it limits (in some sense) to a simple problem that can be solved explicitly. In general, these same ideas translate to the numerics. The exponential decay that is sought in the analytic method also enables the fast convergence of the numerical approximation, as the smoothness of the resulting asymptotic expansions ensure that the solution to the RHP can be well represented by mapped Chebyshev polynomials. In what follows we deform the RHP for the modified KdV equation. The deformations are guided by the desire to remove oscillations from the jump contours. This is generally accomplished by factoring the jump matrix and deforming the contours so that each factor is isolated near saddle points, away from which they approach the identity exponentially fast.

To remove oscillations from the jump matrix, we need to examine the exponential that appears in these expressions, which we represent as $\exp\theta(k)$, where $\theta(k) = 2ikx + 8ik^3t$. For $x < 0$, in analogy with the method of steepest descent for integrals, we deform the RHP through the saddle points of θ. We find that $\theta'(k) = 2ix + 24ik^2t$, and solving for $\theta'(k) = 0$ gives the saddle points $k = \pm k_0$, with $k_0 = \sqrt{-x/(12t)}$. The directions of steepest descent, at $\pm k_0$ — along which the oscillations of the jump matrix become exponential decay — are given by

$$\begin{aligned}\theta_s^+ &= 3\pi/4 \pm \pi/2,\\ \theta_s^- &= \pi/4 \pm \pi/2.\end{aligned}$$

The dispersive region

We present the full deformation from the initial RHP on the real line. We introduce two factorizations of the original jump matrix $G(k)$:

$$\begin{aligned}
&G(k) = M(k)P(k),\\
&M(k) = \begin{bmatrix} 1 & -\rho(-k)e^{-\theta(k)} \\ 0 & 1 \end{bmatrix}, \quad P(k) = \begin{bmatrix} 1 & 0 \\ \rho(k)e^{\theta(k)} & 1 \end{bmatrix},\\
&G(k) = L(k)D(k)U(k), \quad L(k) = \begin{bmatrix} 1 & 0 \\ \rho(k)e^{\theta(k)}/(1-\rho(k)\rho(-k)) & 1 \end{bmatrix},\\
&D(k) = \begin{bmatrix} 1-\rho(k)\rho(-k) & 0 \\ 0 & 1/(1-\rho(k)\rho(-k)) \end{bmatrix},\\
&U(k) = \begin{bmatrix} 1 & -\rho(-k)e^{-\theta(k)}/(1-\rho(k)\rho(-k)) \\ 0 & 1 \end{bmatrix}.
\end{aligned}$$

In what follows, we often suppress x and t dependence for notational simplicity. The factorizations are suggestively defined. M (for 'minus') will be deformed into the lower-half plane and P (for 'plus') will be deformed into the upper-half plane. L is lower triangular and will be deformed into the lower-half plane, D is diagonal and will not be deformed. Finally, U is upper triangular and will be deformed into the upper-half plane. Throughout our deformations we use the notation $\Phi_{n,\alpha}$ for the solution of the deformed problem. The number n indicates how many deformations have been performed, with $n = 1$ being the original RHP. The characters α are used to denote the region (*e.g.* $\alpha = cs$ for the

collisionless shock region).

Since $q \in \mathcal{S}_\delta(\mathbb{R})$ for some $\delta > 0$, ρ has an analytic continuation off the real line so that all the deformations are justified [1, 3]. These factorizations are used so that only one of $\exp\theta(k)$ or $\exp(-\theta(k))$ is present in each matrix. This makes it possible to deform the contours to new contours which have angles $\theta_s^{\pm}$ with the real axis, along which the jump matrices approach the identity exponentially fast. The 'ghost' contours introduced in Figure 6.1(a) all satisfy this desired property, and hence we define a new matrix function $\Phi_{2,d}$ based on these regions. Notice that the new definitions still satisfy the condition at infinity. We compute the jumps that $\Phi_{2,d}$ satisfies to phrase a RHP for $\Phi_{2,d}$, see Figure 6.1(b). This process is referred to as lensing and is presented in more detail in Section 3.10.3.

In order to achieve asymptotic stability (see Section 2) in the sense of Section 5.2 we need the jump matrix to approach the identity away from $\pm k_0$, *i.e.*, we need to remove the contour on $(-k_0, k_0)$. Indeed, numerical results show that the solution on this contour is increasingly oscillatory as $|x| + |t|$ becomes large. We introduce the unique 2×2 matrix-valued function Δ that satisfies the diagonal RHP

$$\Delta^+(k; k_0) = \Delta^-(k; k_0)D(k), \quad k \in (-k_0, k_0), \quad \Delta(\infty; k_0) = I. \tag{6.1.2}$$

See Section 3.4.1 for the exact form of Δ. Notice that in general Δ has singularities at $\pm k_0$. To combat this issue we introduce circles around both $\pm k_0$, see Figure 6.1(c). We define $\Phi_{3,d}$ by the definitions in Figure 6.2(a) where $\Phi_{3,d} = \Phi_{2,d}$ when no definition is specified. Computing the jumps we see that $\Phi_{3,d}$ satisfies the RHP in Figure 6.2(b). We apply the same procedure at $-k_0$ and obtain the problem shown graphically in Figure 6.3(a). Finally, we define $\Phi_{4,d} = \Phi_{3,d}\Delta^{-1}$ and $\Phi_{4,d}$ satisfies the RHP shown in Figure 6.3(b). We solve this resulting RHP numerically.

Remark 6.1.1. *To obtain a RHP valid for $t = 0$ and $x < 0$ one can take the limit of the above RHP as $t \to 0^+$. In this limit $k_0 \to \infty$ and Δ has a jump on all of $\mathbb{R}$.*

The Painlevé region

For $x > 0$ this region intersects with the soliton region defined below, and we use that deformation. For $x < 0$, the saddle points are coalescing and this allows for a new deformation. In this region we reduce the number of contours present, in order to reduce the overall computational cost. Indeed, consider the interval between the two saddle points $[-k_0, k_0]$, where

$$|k| \leq \sqrt{\frac{C}{12}}t^{-1/3} \Rightarrow |2kx + 8k^3t| \leq 2Ct^{1/3}k + 8k^3t \leq \frac{2}{\sqrt{12}}C + \frac{8}{12\sqrt{12}}C^{3/2}.$$

This implies that the oscillations are controlled between the two saddle points and the LDU factorization is not needed. See Figure 6.4(a) for the RHP in this region.

Remark 6.1.2. *The deformations for the dispersive region and the Painlevé regions are valid in overlapping regions of the (x,t)-plane. As $x \to 0, x < 0$, the deformation for the dispersive region can be used until the Painlevé region is reached. Using these deformations*

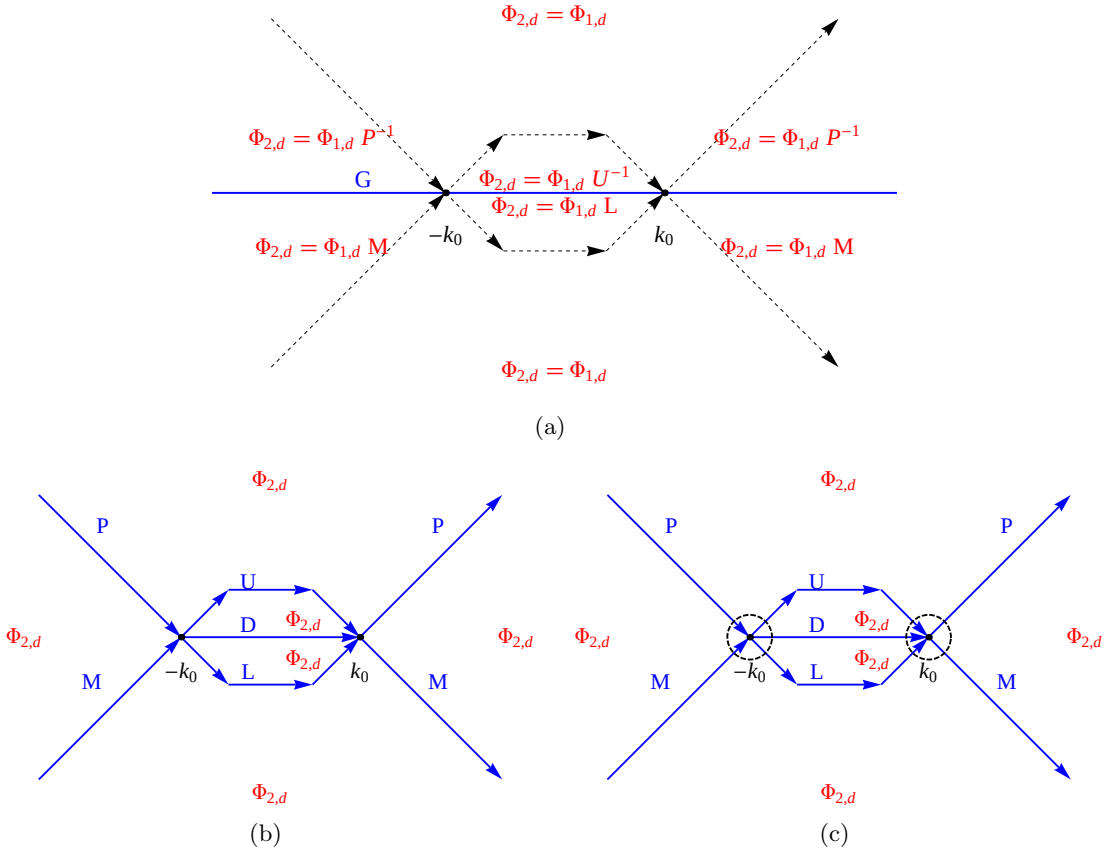

Figure 6.1.1: (a) The jump contours and matrices of the initial RHP with 'ghost' contours, (b) Graphical representation of the jump contours and matrices of the RHP satisfied by $\Phi_{2,d}$, (c) Ghost circles in preparation for the singularities of Δ.

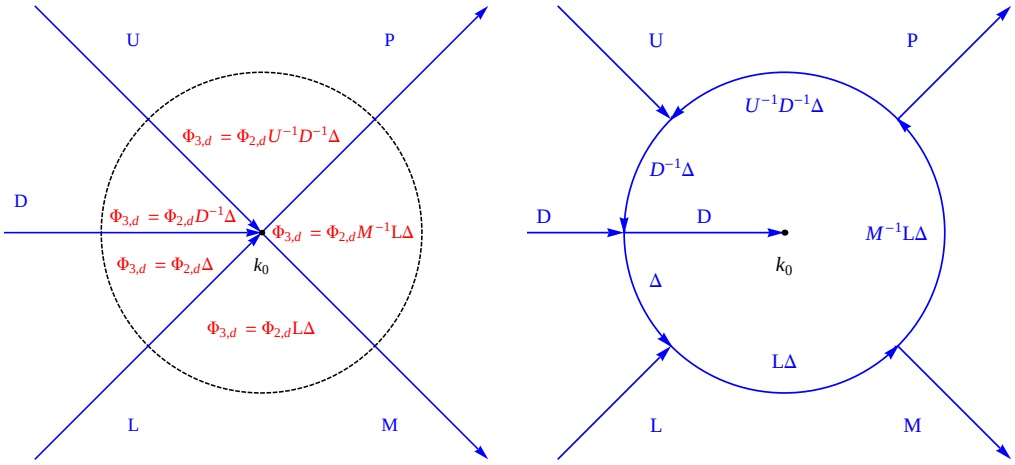

Figure 6.1.2: (a) Definition of $\Phi_{3,d}$ near k_0, (b) The jump contours and matrices of the RHP satisfied by $\Phi_{3,d}$ near k_0.

in tandem allows the method to retain accuracy in the region $x < 0$, $t \geq 0$ for $|x|$ and t large. Note that for the deformation for the dispersive region to be valid as $k_0 \to 0$ it is necessary that $\|\rho\|_\infty < 1$ because of the form of D.

The Soliton region

Choose a function $\alpha(x,t)$ so that $0 \leq \alpha(x,t) < \sqrt{3}|k_0|$, then the deformation used in this region is given in Figure 6.4(b). Note that the angle of the contours is chosen so that $\operatorname{Re}\theta(k) \leq 0$ on all contours with $\operatorname{Im} k > 0$, whereas $\operatorname{Re}\theta(k) > 0$ on all contours with $\operatorname{Im} k \leq 0$.

Remark 6.1.3. *There is a lot of freedom in choosing α. For simplicity, we assume the reflection coefficient is analytic and decays in the strip $\{s + ti : s \in \mathbb{R},\ t \in (-T,T),\ T > 0.5\}$, and therefore we use $\alpha(x,t) = \min\{.5, \sqrt{3}k_0\}$.*

6.1.3 Numerical results

There are additional issues that have to be addressed before these RHPs can be efficiently solved numerically. First, in Section 6.1.2 we opened up circles around two singularities at $\pm k_0$. This deformation is valid provided the radius of the circles is sufficiently small. In addition, we need to shrink the radius of these circles if $|x|$ or t is large. We use the following rule of thumb. Assume the saddle point is at zero and a parametrix has introduced a singularity at zero. Further assume the oscillator is $\exp(wk^r)$, $r > 1$, where w is a parameter. We scale the radius of the circle following Assumption 5.0.1. Second, we truncate contours when the jump matrices are to machine precision, the identity matrix. This allows us to have only finite contours present in the problem. Furthermore, it allows the contours to shrink as x and t increase since the exponential decay is more drastic. The

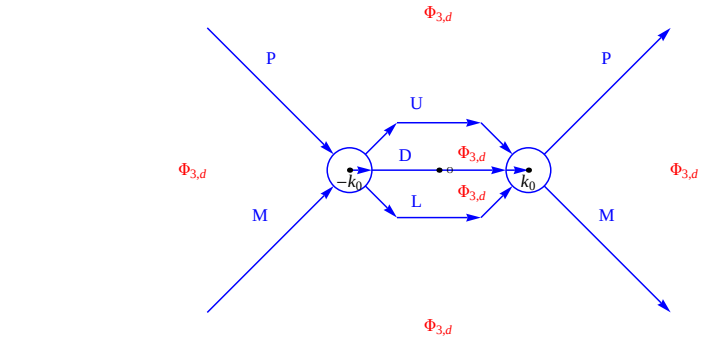

(a)

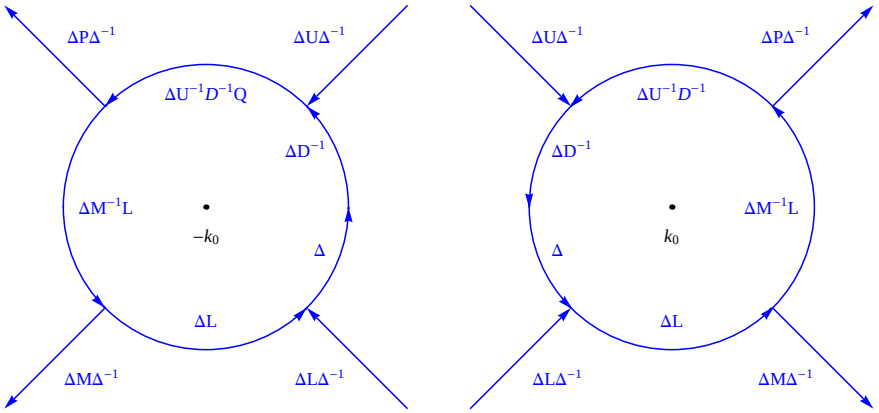

(b)

Figure 6.1.3: (a) The jump contours and matrices of the RHP satisfied by $\Phi_{3,d}$, (b) The jump contours and matrices of the RHP satisfied by $\Phi_{4,d}$. Note that the contours with jumps $\Delta U\Delta^{-1}$ and $\Delta L\Delta^{-1}$ connect.

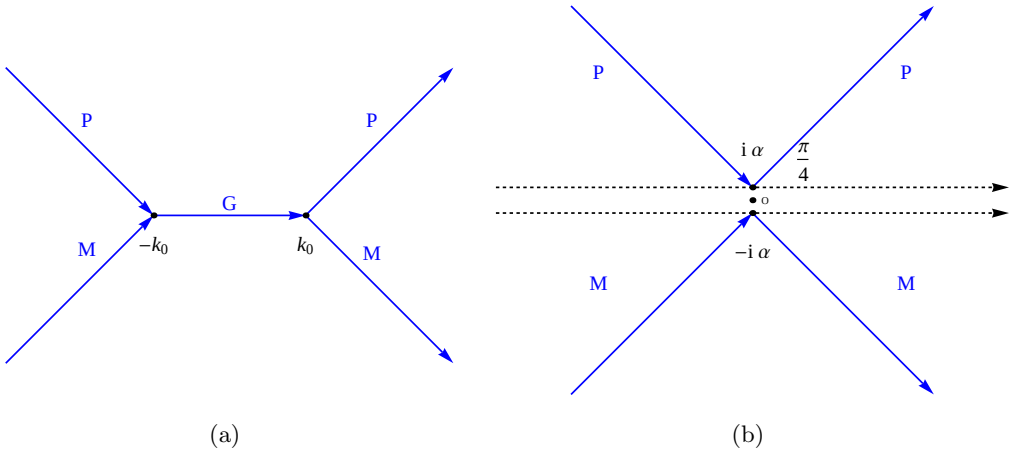

(a) (b)

Figure 6.1.4: (a) The jump contours and matrices of the RHP for the modified KdV equation in the Painlevé region with $x < 0$. (b) The jump contours and matrices of the RHP for the modified KdV equation in the soliton region.

scaling on these contours is the same as for the circles around the saddle points. Note that if all jump contours are decaying to the identity as x and t becomes large, it is possible that we truncate all contours and approximate the solution by zero.

Finally, we define $q(n, x, t)$ as the approximation to the solution of the modified KdV equation with n collocation points on each contour where the initial condition is implied from context.

Direct scattering

For an initial condition where the reflection coefficient is not known explicitly we can verify our direct, and in the process, inverse scattering computations by evaluating the solution to the inverse problem at $t = 0$. As an example we start with the initial condition $q(x, 0) = -1.3\,\mathrm{sech}^2(x)$. In Figure 6.5(a) we plot the error, $|q(x, 0) - q(80, x, 0)|$, while varying the number of collocation points. Define $\rho(m, k)$ to be the approximation of the reflection coefficient obtained using m collocation points. In Figure 6.5(b) we show spectral convergence of the computation of the reflection coefficient when $k = 1$.

Inverse scattering

Throughout this section we proceed as if the reflection coefficient is obtained to machine precision. This is often not the case since we do not have an explicit formula for the reflection coefficient. This does limit the accuracy obtained in the plots below.

1. *Convergence.* To analyze the error, we introduce some notation. Define

$$Q_n^m(x, t) = |q(n, x, t) - q(m, x, t)|.$$

Using this notation, Figure 6.2.12 demonstrates the spectral (Cauchy) convergence with each of the deformations.

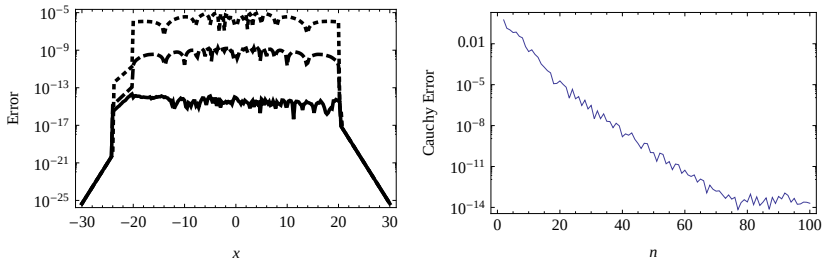

(a) (b)

Figure 6.1.5: (a) Error in performing the full inverse scattering transformation at $t = 0$ while varying the number of collocation points m for the direct scattering. ($m = 20$: dotted line, $m = 40$: dashed line, $m = 80$: solid line.) Note that for moderate $|x|$ we approximate $q(x, 0)$ by zero after the truncating contours and obtain very small absolute error. (b) The Cauchy error, $|\rho(200, 1) - \rho(n, 1)|$, plotted for $n = 2$ to $n = 100$ on a log scale to show the spectral convergence of the reflection coefficient.

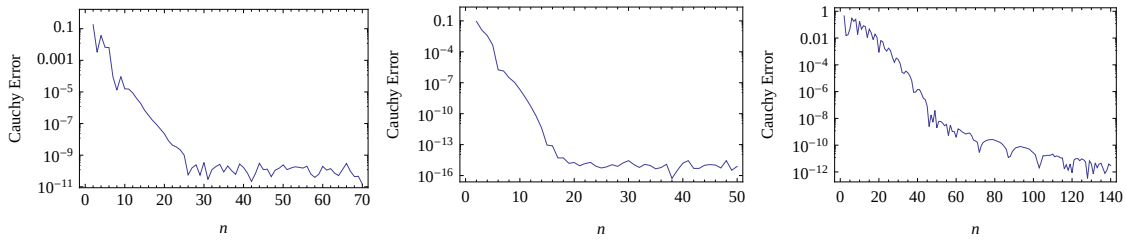

(a) (b) (c)

Figure 6.1.6: Demonstration of spectral convergence for the modified KdV equation with $q(x, 0) = -1.3\,\mathrm{sech}^2(x)$. All plots have $Q^n_{2m}(x, t)$ plotted as a function of n as n ranges from 2 to m. (a) Dispersive Region: $m = 70$ at the point $(x, t) = (-8.8, 0.6)$, (b) Painlevé Region: $m = 50$ at the point $(x, t) = (-0.8, 0.6)$, (c) Soliton/Painlevé Region: $m = 140$ at the point $(x, t) = (0.2, 2.6)$. This deformation requires more collocation points because it only has four contours, so that each contour contains more information about the solution. Machine precision is not achieved since some errors are present in the computation of the reflection coefficient.

2. *Asymptotic Stability.* For the method to be asymptotically stable we require that, for a given n and m, $Q_n^m(x,t)$ remains bounded (and small) as $|x| + |t|$ becomes large. In fact, what we numerically demonstrate is that $Q_n^m(x,t)$ tends to zero in all regions. See Figure 6.1.7 for the demonstration of this. Note that we expect $Q_n^m(x,t)$ to approach zero only when the solution approaches zero as well.

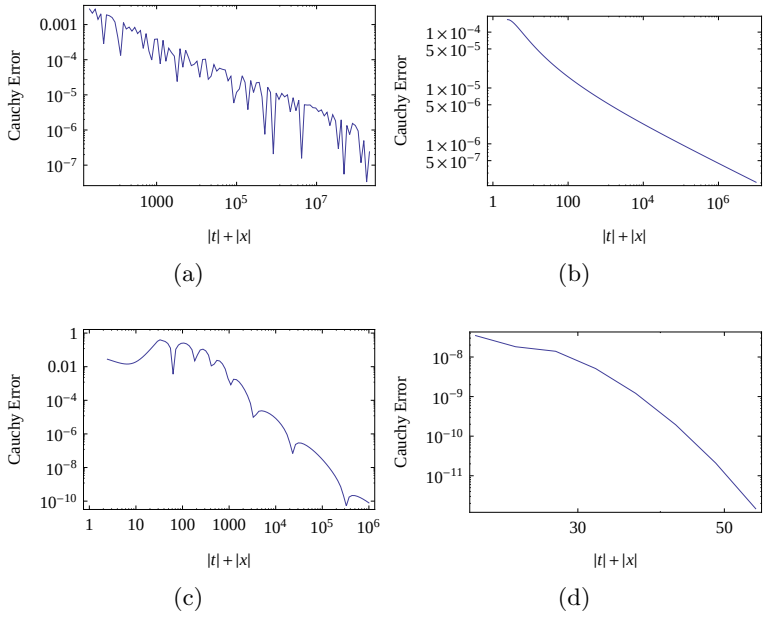

Figure 6.1.7: Demonstration of asymptotic stability for the modified KdV equation with $q(x,0) = -1.3\,\mathrm{sech}^2(x)$. All plots have $Q_m^n(x,t)$ plotted as a function of $|t| + |x|$. (a) *The Dispersive Region*: $m = 10$, $n = 5$ along the trajectory $x = -20t$, (b) *The Painlevé Region*: $m = 10$, $n = 5$ along the trajectory $x = -(3t)^{1/3}$, (c) *The Painlevé Region*: $m = 20$, $n = 10$ along the trajectory $x = (3t)^{1/3}$, (d) *The Soliton Region*: $m = 10$, $n = 5$ along the trajectory $x = 20t$.

Comparison with asymptotic formulae

In Section 6.0.4 asymptotic formulae in various regions for the modified KdV equation were presented. In this section we compare numerical results with these formulae. We skip the soliton region because the asymptotic formula approximates the solution by zero, which is uninteresting. Taking into account the verifiable convergence and the fact that convergence of the numerical method has no long-time requirements, it seems reasonable to assume that the computed solutions in the plots below approximate the true solution better than the asymptotic formulae.

1. *The Dispersive Region.* In Figure 6.1.8 we present a numerical verification of the error bound (6.0.13) along with a plot of both approximations in the dispersive region.

2. *The Painlevé Region.* In Figure 6.1.8 we present a numerical verification of the error bound (6.0.11) along with a plot of both approximations in the Painlevé region.

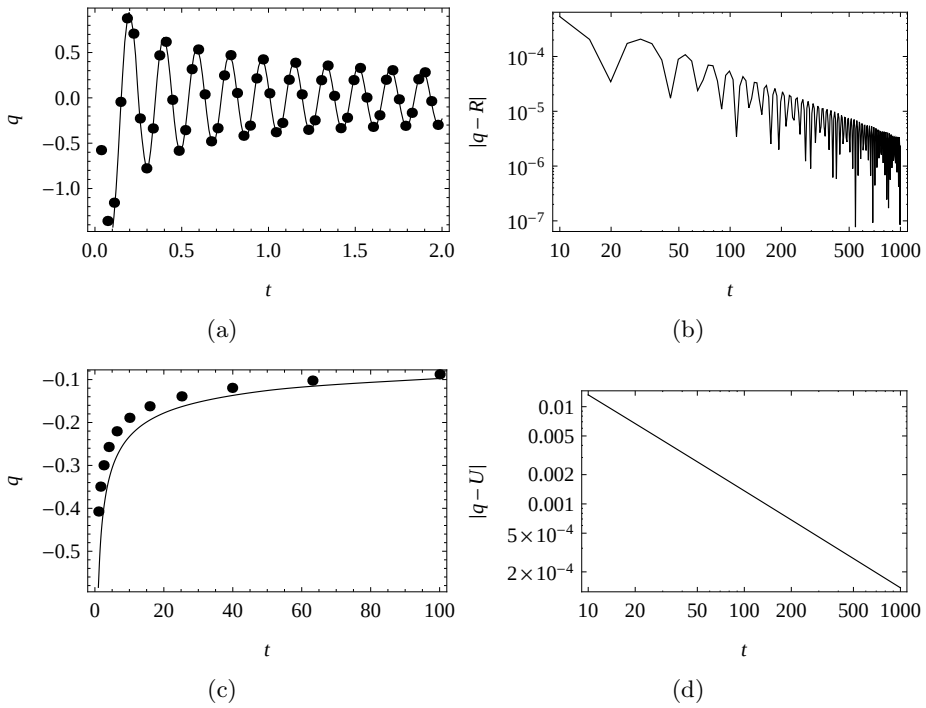

Figure 6.1.8: Comparison of numerical results with the asymptotic formulae in the dispersive and Painlevé regions for the modified KdV equation. (a) *The Dispersive Region:* $q(10, x, t)$ and $R(x, t)$ plotted as a function of t with $x = -20t$. The computed solution is shown by the solid line and the asymptotic formula by the dots, (b) *The Dispersive Region:* $|q(10, x, t) - R(x, t)|$ plotted as a function of t with $x = -20t$. A least-squares fit gives $|q(10, x, t) - R(x, t)| = \mathcal{O}(t^{-1.2})$, in agreement with the error formula, (c) *The Painlevé Region:* $q(10, x, t)$ and $U(x, t)$ plotted as a function of t with $x = -t^{1/3}$. The computed solution is shown by the solid line and the asymptotic formula by dots, (d) *The Painlevé Region:* $|q(10, x, t) - U(x, t)|$ plotted as a function of t with $x = -t^{1/3}$. A least-squares fit gives $|q(10, x, t) - U(x, t)| = \mathcal{O}(t^{-0.65})$, in agreement with the error formula.

With minimal deformations we obtain a numerical method for the defocusing modified KdV equation that is not only asymptotically accurate but also converges spectrally fast. The roles of x and t are reduced to that of parameters and we have no need for spatial grids or time-stepping. The dispersive nature of the modified KdV equation is captured exactly. The amount of effort required to solve the modified KdV equation should be typical when considering other integrable equations with Riemann–Hilbert formulations. Below we solve the KdV equation and in the process expand the scope of the numerical method to deal with RHPs that have singularities. This complication is not typical but we proceed to show that it can be dealt with.

6.2 The Korteweg–de Vries equation

We discuss numerical inverse scattering for the KdV equation. We can adjust the constants c_2 and c_7 in Section 6.0.4 to make the dispersive region overlap with the Painlevé region up to some finite t. This essentially allows one to use only the deformations needed for the modified KdV equation for small time, eliminating the collisionless shock and transition regions. For practical purposes this is sufficient. However, the regions never overlap for sufficiently large time and since we are interested in the development of an asymptotically stable method, we need to construct the deformations in the collisionless shock and transition regions. These deformations are more complicated.

The RHP for the KdV equation is generally a meromorphic problem which alters the deformations for $x > 0$. Additionally, $\rho(0) = -1$, generically, which complicates the deformations for $x < 0$. The deformation for the dispersive region is only stable in its original region of definition, $-x > \alpha t$, $\alpha > 0$; it cannot be extended into the Painlevé region for large t. For concreteness we use $-x > 12t > 0$. As a consequence, the three regions defined in the case of the modified KdV equation do not overlap for the KdV equation. To overcome this issue Deift, Zhou and Venakides used a new deformation of the RHP for the collisionless shock region [39] (see [5] for the first appearance of this region). This deformation is valid into the dispersive region but does not extend to the Painlevé region. Below we present the deformations for the RHP associated with the KdV equation in these four classical regions. To fill the final gap we introduce a new deformation to transition from the collisionless shock region into the Painlevé region.

6.2.1 Numerical computation of the scattering data for the KdV equation

Calculating the scattering data numerically relies on two spectral methods: a Chebyshev collocation method for ODEs and Hill's method [22] for computing the spectrum of a linear operator.

- Computing ρ.

  For $k \in \mathbb{R}$ we are looking for solutions of $\mu_{xx} + q_0(x)\mu = -k^2\mu$ which behave like $\exp(\pm ikx)$ as $x \to \pm\infty$. If $q_0(x) \in \mathcal{S}_\gamma(\mathbb{R})$ the eigenfunctions limit to this asymptotic behavior exponentially fast. For illustration purposes we concentrate on the eigenfunctions at $-\infty$. We set $u(x) = \mu(x)e^{\pm ikx} - 1$ where the $\pm$ is chosen when $\mu \backsim e^{\mp ikx}$.

Then $u(x)$ satisfies the ODE

$$u_{xx} \mp 2iku_x + q_0(u+1) = 0, \quad u(\pm\infty) = u'(\pm\infty) = 0.$$

The Chebyshev collocation method in Appendix B is used to solve this equation on $(-L, 0]$ for each choice of $\pm$. The same ideas apply to the eigenfunctions whose behavior is specified at $+\infty$. We solve for these on $[0, L)$. We enforce the boundary condition at $\pm L$. As in the case of the modified KdV equation, matching the solutions at the origin produces an approximation of the reflection coefficient.

- Computing $\{\kappa_1, \ldots, \kappa_n\}$.

  Calculating these values is equivalent to calculating the $L^2(\mathbb{R})$ eigenvalues of the operator $\partial_x^2 + q_0(x)$ [3]. Through the transformation $x = 2\tan(y/2)$ we map the original ODE to the interval $[-\pi, \pi]$. This is well defined because of the decay of q_0. If $m(y) = \mu(2\tan(y/2))$ and $Q(y) = q_0(2\tan(y/2))$, then m satisfies the problem

$$\cos^2(y/2)\left(\cos^2(y/2)m_y\right)_y + Q(y)m = \lambda m, \quad \lambda = -k^2, \quad m(x) = m(x+\pi). \tag{6.2.1}$$

  Define $C_p^k([a,b]) = \{f \in C^k([a,b]) : f^{(j)}(a) = f^{(j)}(b), \quad 0 \le j \le k\}$. To show the equivalence of this problem with solving the original scattering problem we have the following lemma.

  Lemma 6.2.1. *Assume $q_0(x) \in \mathcal{S}(\mathbb{R})$ and $m \in C_p^2([-\pi,\pi])$ solves (6.2.1) with $\lambda > 0$ then $\mu(x) = m(2\arctan(x/2))$ is an L^2 eigenfunction of $\partial_x^2 + q_0(x)$. Furthermore, all L^2 eigenfunctions for $\partial_x^2 + q_0(x)$ can be found this way.*

  Proof. The behavior of the coefficients of (6.2.1) at $\pm\pi$ forces $m(\pm\pi) = 0$. Also, m is Lipschitz with constant $C = \sup_{y\in[-\pi,\pi]} |m'(y)|$. Therefore

$$|m(y) - m(\pm\pi)| \le C|y \mp \pi| \Rightarrow |m(y)| \le C|y \mp \pi|.$$

  Using the asymptotic expansion of $2\arctan(x/2)$ we see that

$$|\mu(x)| \le \min\{C|2\arctan(x/2) - \pi|, C|2\arctan(x/2) + \pi|\} \le C'/(1+|x|),$$

  for a new constant C'. This shows μ is an L^2 eigenfunction. Now assume that μ is an L^2 eigenfunction of the operator $\partial_x^2 + q_0(x)$. We know that $\lambda > 0$ and $\mu \backsim \exp(-\sqrt{\lambda}|x|)$ as $|x| \to \infty$ [3]. Since q is smooth μ must be smooth and $\mu(2\tan(y/2))$ is a $C_p^2([-\pi,\pi])$ solution of (6.2.1). Therefore these eigenvalues and eigenfunctions are in direct correspondence. □

  Applying the spectrum approximation techniques in [22] to (6.2.1) allows us to obtain $\{\kappa_1, \ldots, \kappa_n\}$ with spectral accuracy.

- Computing $\{C_1, \ldots, C_n\}$.

  As mentioned above, all poles of $\rho(k) = b(k)/a(k)$ are simple. Since the above method for calculating $\rho(k)$ gives a method for computing $b(k)$ we reduce the problem to

computing $a'(\kappa_j)$. We use the relationship [3]

$$a'(\kappa_j) = \frac{1}{ib(\kappa_j)} \int_{\mathbb{R}} \mu(x;\kappa_j)^2 dx,$$

where μ is the eigenfunction of the operator $\partial_x + q_0(x)$ with eigenvalue $\lambda = \kappa_j^2$ such that $\mu \backsim \exp(-|\lambda x|)$ as $|x| \to \infty$. This is evaluated using Clenshaw–Curtis quadrature.

6.2.2 Numerical solution of the inverse problem

The dispersive region

We proceed as in the case of the modified KdV equation. Assume we performed the deformation in Remark 6.0.16 to introduce small circles around each pole. Examining the exponent, $\exp(2i\kappa_j x + 8i\kappa_j^3 t)$, and further recalling that $\kappa_j \in i\mathbb{R}^+$, we see that the exponent is unbounded in this region. Following the approach in [60] we define

$$\Phi_{1,d}(k) = \begin{cases} \Phi(k) \begin{bmatrix} 1 & -(k-\kappa_j)/(C_j e^{\theta(k_0)}) \\ C_j e^{\theta(k_0)}/(k-\kappa_j) & 0 \end{bmatrix} Q(k), & \text{if } |k-\kappa_j| < \epsilon, \\ \Phi(k) \begin{bmatrix} 0 & -C_j e^{\theta(k_0)}/(k+\kappa_j) \\ (k+\kappa_j)/(C_j e^{\theta(k_0)}) & 1 \end{bmatrix} Q(k), & \text{if } |k+\kappa_j| < \epsilon, \\ \Phi(k)Q(k), & \text{otherwise,} \end{cases}$$

for

$$Q(k) = \begin{bmatrix} \prod_{j=0}^n (k-\kappa_j)/(k+\kappa_j) & 0 \\ 0 & \prod_{j=0}^n (k+\kappa_j)/(k-\kappa_j) \end{bmatrix}.$$

Note that the matrix

$$\begin{bmatrix} 1 & -(k-\kappa_j)/(C_j e^{\theta(k_0)}) \\ C_j e^{\theta(k_0)}/(k-\kappa_j) & 0 \end{bmatrix} Q(k)$$

has a removable pole at κ_j and $\Phi_{1,d}$ still tends to the identity at infinity. Recall $A_j^{\pm} = \{k \in \mathbb{C} : |k \mp \kappa_j| = \epsilon\}$ where Aj^+ has counter-clockwise orientation, and A_j^- clockwise. Further ϵ is chosen small enough so that the $A_j^{\pm}$ do not intersect any other contour. We compute

the jumps of $\Phi_{1,d}$:

$$\Phi^+_{1,d}(k) = \begin{cases} \Phi^-_{1,d}(k)Q^{-1}(k)G(k)Q(k), & \text{if } k \in \mathbb{R}, \\ \Phi^-_{1,d}(k)Q^{-1}(k) \begin{bmatrix} 1 & -(k-\kappa_j)/(C_j e^{\theta(k_0)}) \\ 0 & 1 \end{bmatrix} Q(k), & \text{if } k \in A_j^+, \\ \Phi^-_{1,d}(k)Q^{-1}(k) \begin{bmatrix} 1 & 0 \\ -(k+\kappa_j)/(C_j e^{\theta(k_0)}) & 1 \end{bmatrix} Q(k), & \text{if } k \in A_j^-, \end{cases}$$
$$\Phi_{1,d}(\infty) = \begin{bmatrix} 1 & 1 \end{bmatrix}.$$

This effectively inverts the exponent and turns exponential blowup into decay to the identity. This demonstrates that the solitons exhibit exponential decay. To simplify the notation, define

$$T_+(k,j;x,t) = \begin{bmatrix} 1 & 0 \\ -C_j e^{\theta(\kappa_j)}/(k-\kappa_j) & 1 \end{bmatrix}, \quad T_-(k,j;x,t) = \begin{bmatrix} 1 & -C_j e^{\theta(\kappa_j)}/(k+\kappa_j) \\ 0 & 1 \end{bmatrix},$$
$$S_+(k,j;x,t) = \begin{bmatrix} 1 & -(k-\kappa_j)/(C_j e^{\theta(\kappa_j)}) \\ 0 & 1 \end{bmatrix}, \quad S_-(k,j;x,t) = \begin{bmatrix} 1 & 0 \\ -(k+\kappa_j)/(C_j e^{\theta(\kappa_j)}) & 1 \end{bmatrix}.$$

As before, the 'ghost' contours introduced in Figure 6.1(a) pass along the directions of steepest descent. We define a new matrix function $\Phi_{2,d}$ based on these regions. Notice that the new definitions still satisfy the normalization condition at infinity. We compute the jumps that $\Phi_{2,d}$ satisfies to phrase a RHP for $\Phi_{2,d}$, see Figure 6.1(b). Throughout the figures in this section, the dot inside the circles with jumps $T_\pm$ or $S_\pm$ represent $\pm\kappa_j$.

We decompose G into its LDU and MP factorizations and deform the jump contour off $\mathbb{R}$ as we did in Section 6.1.2. However, there is a significant difference: if we examine the matrix D, we see that there is a singularity at the origin, since generically $\rho(0) = -1$ [3]. We need to remove this singularity in order to represent the solution by Chebyshev polynomials. Additionally, we need to remove the contour on $(-k_0, k_0)$ to attain asymptotic stability as mentioned in Section 6.1.2 using Δ in Section 3.4.1. We proceed in the same way and arrive at the RHP in Figure 6.2.2, noting that the circles (corresponding to solitons) and presence of the matrix Q are the only aspects that are different.

Remark 6.2.2. *We assumed that $\rho(0) = -1$. If it happens that $|\rho(0)| < 1$ then the deformations reduce to those done for the modified KdV equation but now in the (possible) presence of solitons. Numerical results show that this can happen when an initial condition for the KdV equation is obtained through the Miura transformation, see Section 6.2.4. In this case, the deformations for the dispersive, Painlevé and soliton regions cover the (x,t)-plane.*

The Painlevé region

As in the case of the modified KdV equation, for $x > 0$ we have an intersection with the soliton region defined below. We use that deformation. The final deformation for the KdV

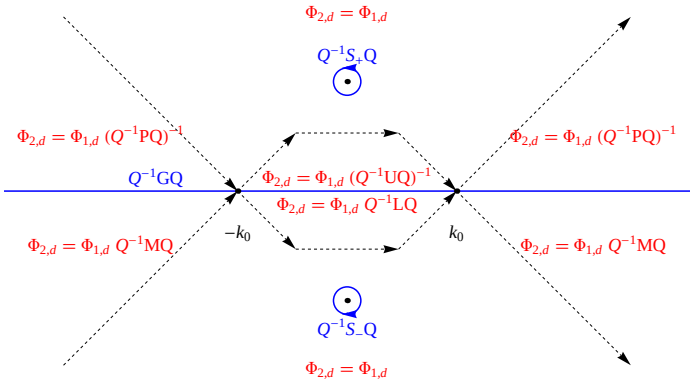

(a)

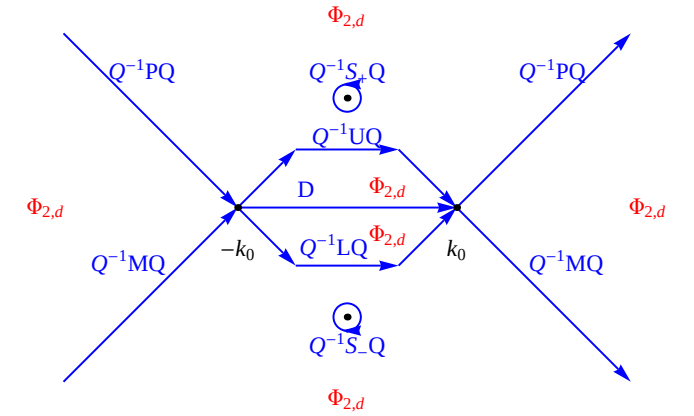

(b)

Figure 6.2.1: (a) Jump contours and matrices for the initial RHP with 'ghost' contours, (b) Jump contours and matrices for the RHP satisfied by $\Phi_{2,d}$.

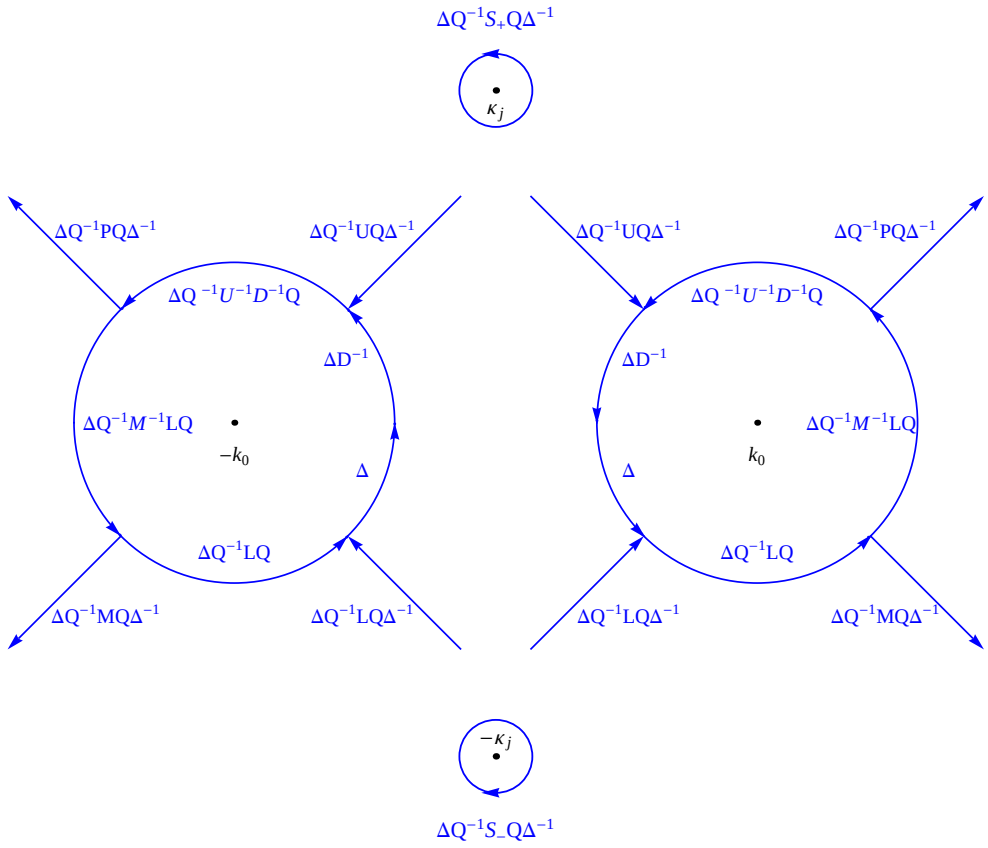

Figure 6.2.2: A zoomed view of the jump contours and matrices for the RHP in the dispersive region of the KdV equation. Note that the contours with jumps $\Delta Q^{-1}UQ\Delta^1$ and $\Delta Q^{-1}LQ\Delta^1$ connect.

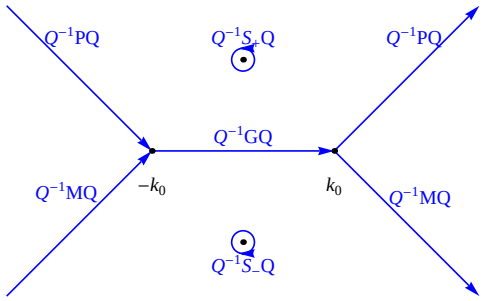

Figure 6.2.3: The jump contours and matrices for the RHP in the Painlevé Region with $x < 0$.

equation when $x < 0$ is nearly the same as in the case of the modified KdV equation, see Figure 6.2.3.

The collisionless shock region

The singularity at $k = 0$ in the matrix $D(k)$ destroys the boundedness of $\Delta(k; k_0)$ which poses problems that do not occur for the modified KdV equation. As $k \to 0$ the matrices $\Delta Q^{-1}PQ\Delta^{-1}$ and $\Delta Q^{-1}MQ\Delta^{-1}$ are unbounded and we cannot link up the dispersive region with the Painlevé region, as we did for the modified KdV equation. By choosing C large we can make the dispersive and Painlevé regions overlap up to some finite t. We wish to obtain a method which is stable for large t. We need to introduce additional deformations to bridge the dispersive and Painlevé regions. The first region we address is the collisionless shock region. Ablowitz and Segur [5] introduced this region, and Deift, Zhou and Venakides derived the needed deformations [39].

The results presented below for this region are from [39]. As x increases in the dispersive region, the saddle points of $\exp\theta$, $\pm k_0$, approach the singularity ($k = 0$) of the parametrix Δ. To prevent this, we replace θ by a so-called g-function [32], whose saddle points, after scaling, do not approach a singularity. For $b > a > 0$, we determine constants D_1, D_2 so that there exists a function $g(k)$ which is bounded in the finite plane and satisfies the following properties:

$$
\begin{aligned}
&g^-(k) + g^-(k) = \begin{cases} D_1 & \text{if } k \in (-b, -a), \\ -D_1 & \text{if } k \in (a, b), \end{cases} \\
&g^+(k) - g^-(k) = D_2, \quad k \in (-a, a), \\
&\quad g(k) \text{ analytic in } k \text{ off } [-b, b], \\
&\quad g(k) \text{ has saddle points at } \pm(a, b), \\
&\quad g(k) \backsim 4k^3 - 12k \text{ as } k \to \infty.
\end{aligned}
$$

The constants D_1 and D_2 depend on a and b and have desired properties to scale away singularities. These will be determined below. Also, once all these constants are fixed, g is uniquely determined.

Remark 6.2.3. *For the KdV equation, g can be determined explicitly (Section 6.4) but it is more instructive to introduce it as above. It is more convenient to compute it numerically from this formulation since the method in [88] is easily adapted to ensure spectral accuracy.*

Define the function $\gamma(k) = -i\tau[4k^3 - 12k - g(k)]$, $\tau = tk_0^3$ and construct

$$\phi(k) = \begin{bmatrix} e^{\gamma(k)} & 0 \\ 0 & e^{-\gamma(k)} \end{bmatrix} \to I \text{ as } k \to \infty.$$

It is advantageous to introduce a scaling operator, $\tilde{\ }$, defined by $\tilde{f}(\cdot; x, t) = f(k_0\cdot; x, t)$ and solve for $\tilde{\Phi}(k)$. For $k \in \mathbb{R}$ the jump satisfied by $\tilde{\Phi}(k)\phi(k)$ is $\phi_-^{-1}(k)\tilde{G}(k)\phi^+(k)$. This assumes the absence of solitons, otherwise we replace G by $Q^{-1}GQ$. Explicitly

$$\phi_-^{-1}(k)\tilde{G}(k)\phi^+(k) = \begin{bmatrix} [1-\rho(k_0k)\rho(-k_0k)]e^{\gamma^+(k)-\gamma^-(k)} & -\rho(-k_0k)e^{-\theta(k_0k)-\gamma^+(k)-\gamma^-(k)} \\ \rho(k_0k)e^{\theta(k_0k)+\gamma^+(k)+\gamma^-(k)} & e^{-\gamma^+(k)+\gamma^-(k)} \end{bmatrix}.$$

Note that $\theta(k_0k) = 2ik_0kx + 8ik_0^3k^3t = 2i\tau(-12k + 4k^3)$, and γ satisfies

$$\begin{aligned} \gamma^+(k) - \gamma^-(k) &= i\tau(g^+(k) - g^-(k)) = 0 \text{ for } k \notin [-b, b], \\ \gamma^+(k) + \gamma^-(k) &= i\tau(g^+(k) + g^-(k)) - \theta(k_0k) \to 0 \text{ as } k \to \infty. \end{aligned}$$

We write

$$\phi_-^{-1}(k)\tilde{G}(k)\phi(k)_+ = \begin{cases} \begin{bmatrix} 1-\rho(k_0k)\rho(-k_0k) & -\rho(-k_0k)e^{2i\tau g(k)} \\ \rho(k_0k)e^{2i\tau g(k)} & 1 \end{bmatrix}, \\ \qquad\qquad \text{if } k \in (-\infty, -b), \\ \begin{bmatrix} [1-\rho(k_0k)\rho(-k_0k)]e^{i\tau(g^+(k)-g^-(k))} & -\rho(-k_0k)e^{-C_1} \\ \rho(k_0k)e^{C_1} & e^{i\tau(-g^+(k)+g^-(k))} \end{bmatrix}, \\ \qquad\qquad \text{if } k \in (-b, -a), \\ \begin{bmatrix} [1-\rho(k_0k)\rho(-k_0k)]e^{C_2} & -\rho(-k_0k)e^{i\tau(-g^+(k)-g^-(k))} \\ \rho(k_0k)e^{i\tau(g^+(k)+g^-(k))} & e^{-C_2} \end{bmatrix}, \\ \qquad\qquad \text{if } k \in [-a, a], \\ \begin{bmatrix} [1-\rho(k_0k)\rho(-k_0k)]e^{i\tau(g^+(k)-g^-(k))} & -\rho(-k_0k)e^{C_1} \\ \rho(k_0k)e^{C_1} & e^{i\tau(-g^+(k)+g^-(k))} \end{bmatrix}, \\ \qquad\qquad \text{if } k \in (a, b), \\ \begin{bmatrix} 1-\rho(k_0k)\rho(-k_0k) & -\rho(-k_0k)e^{-2i\tau g(k)} \\ \rho(k_0k)e^{2i\tau g(k)} & 1 \end{bmatrix}, \\ \qquad\qquad \text{if } k \in [b, \infty), \end{cases} \tag{6.2.2}$$

where $C_1/i\tau = g^+(k) + g^-(k)$ for $k \in [a, b]$ and $C_2/i\tau = g^+(k) - g^-(k)$ for $k \in [-a, a]$. This successfully removes θ from the problem. As in the dispersive region, we proceed to

factor $\tilde{G} = \tilde{L}\tilde{D}\tilde{U}$ on $[-a, a]$. Again, $\tilde{D}$ has a singularity at the origin that we must remove. Before we remove this singularity let us analyze the system in the limit as $k_0 \to 0$ as this will guide the choice of the parametrix and the constants C_1 and C_2. On the interval $[-a, a]$ we have

$$\phi_-^{-1}(k)\tilde{D}(k)\phi_+(k) = \begin{bmatrix} [1-\rho(k_0k)\rho(-k_0k)]e^{C_2} & 0 \\ 0 & \left([1-\rho(k_0k)\rho(-k_0k)]e^{C_2}\right)^{-1} \end{bmatrix}.$$

Using $\rho(0) = -1$ and the analyticity of $\rho(k)$ neighborhood of the origin, we obtain that $1 - \rho(k_0k)\rho(-k_0k) = 2\nu k^2 k_0^2 + \mathcal{O}((kk_0)^4)$ near $k = 0$ for some constant ν. We left $b > a > 0$ mostly arbitrary above. It follows (Section 6.4) that the boundedness condition along with the prescribed asymptotic behavior requires $a^2 + b^2 = 2$, leaving a single degree of freedom. We use this degree of freedom to enforce $k_0^2 \exp(C_2) = 1$, so that $(1 - \rho(k_0k)\rho(-k_0k)) \exp(C_2) \backsim 2\nu k^2 + \mathcal{O}(k_0^2 k^4)$. Removing, to second order, the dependence on k_0. To see that there does exist an a that satisfies this condition, we refer to the explicit construction of g in Section 6.4. As $k, k_0 \to 0$ there is a constant $C > 1$ so that

$$\frac{1}{C} \leq \frac{1-\rho(k_0k)\rho(-k_0k)}{k^2} e^{C_2} \leq C, \quad \text{for } k \in [-a, a].$$

Thus, to obtain a local parametrix, we should solve the RHP

$$\psi_+(k) = \psi_-(k)\phi_-^{-1}(k)\tilde{D}(k)\phi^+(k), \quad k \in (-a, a), \quad \psi(\infty) = I.$$

This diagonal RHP can be solved explicitly using the method in Section 3.4.1. We conjugate the problem by ψ in the same way as was done with Δ in Section 6.2.2.

The full deformation for this region now follows. We lens the scaled problem into the form shown in Figure 6.4(a). Near a, b the jumps on the contours are also given there. Define $\Phi_{2,cs} = \Phi_{1,cs}\phi$. Near a, b, $\Phi_{2,cs}$ satisfies the problem shown in Figure 6.2.5. We conjugate by the local parametrix , defining $\Phi_{3,cs} = \Phi_{2,cs}\psi^{-1}$. See Figure 6.2.5 for the RHP near a, b for $\Phi_{3,cs}$. By symmetry, what happens at $-a, -b$ is clear. More work is necessary. Define the two functions β_m and β_p via diagonal RHPs

$$\begin{aligned} \beta_m^+(k) &= \beta_m^-(k)(\phi_-^{-1}\tilde{D}\phi_+)^{-1}, \quad k \in (-b, -a), \quad \beta_m(\infty) = I, \\ \beta_p^+(k) &= \beta_p^-(k)(\phi_-^{-1}\tilde{D}\phi_+)^{-1}, \quad k \in (a, b), \quad \beta_m(\infty) = I. \end{aligned}$$

For the final deformation define

$$\Phi_{4,cs} = \begin{cases} \Phi_{3,cs}\phi^{-1} & \text{inside the circle centered at } -b, \\ \Phi_{3,cs}\beta_m & \text{inside the circle centered at } -a, \\ \Phi_{3,cs}\beta_p & \text{inside the circle centered at } a, \\ \Phi_{3,cs}\phi^{-1} & \text{inside the circle centered at } b, \\ \Phi_{3,cs} & \text{otherwise.} \end{cases}$$

It follows that $\Phi_{4,cs}$ solves the RHP shown in Figure 6.2.6.

Remark 6.2.4. *Note that $s = 0$ when $k_0 = 1$ or $x = -12t$ and we switch to the dispersive*

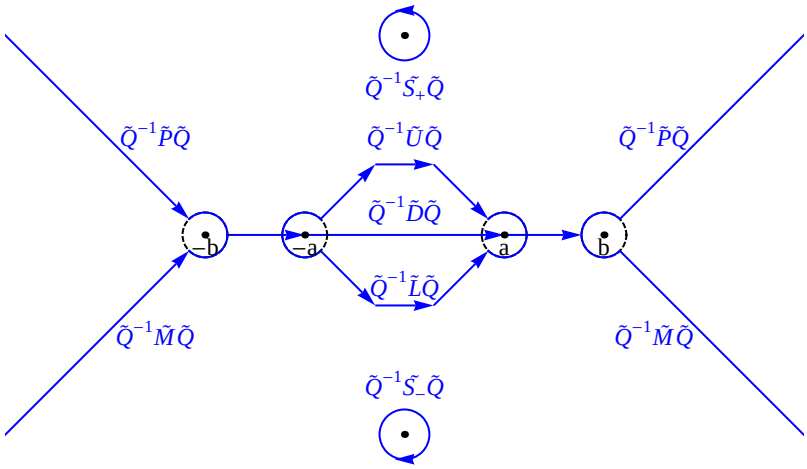

(a)

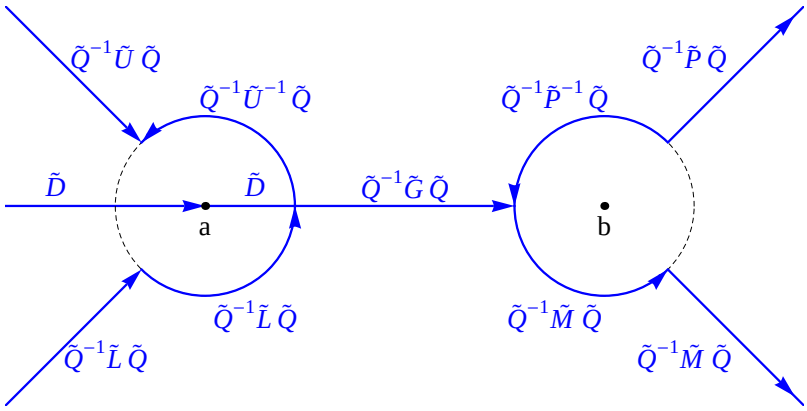

(b)

Figure 6.2.4: (a) The initial deformation of the RHP in the collisionless shock region for a function $\Phi_{1,cs}$. (b) The initial jump contours and matrices near a, b.

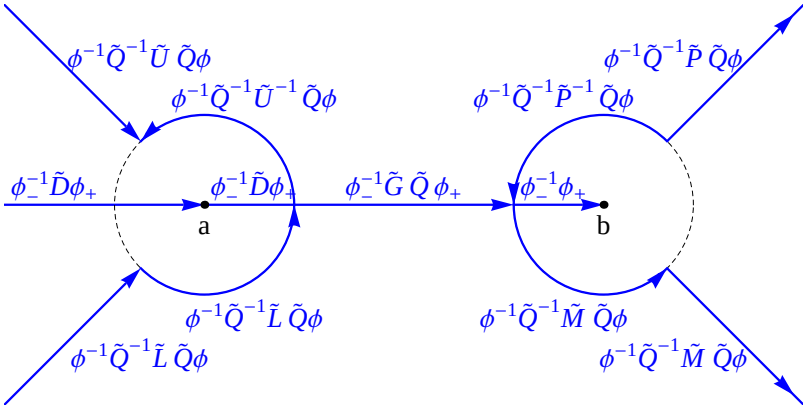

(a)

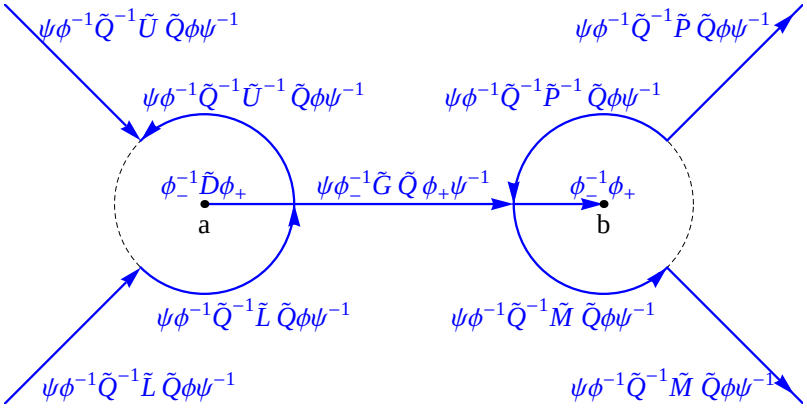

(b)

Figure 6.2.5: (a) The jump contours and matrices for the RHP for $\Phi_{2,cs}$ near a, b, (b) The jump contours and matrices for the RHP for $\Phi_{3,cs}$ near a, b.

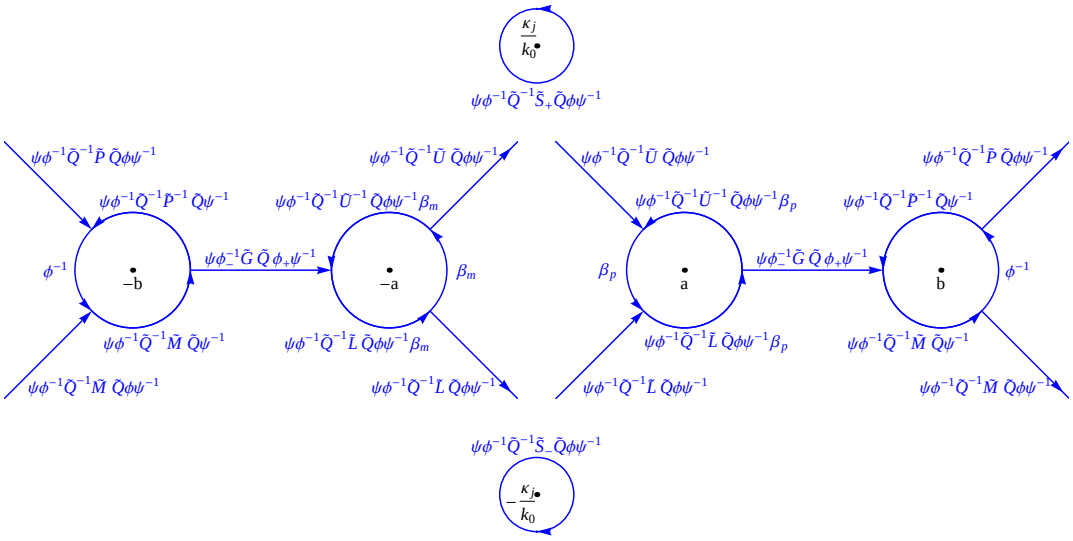

Figure 6.2.6: A zoomed view of the jump contours and matrices of the final deformation of the RHP in the collisionless shock region.

region. This switch is continuous in the sense that $s = 0 \Rightarrow a = b = 1$ *and* ϕ *is the identity. The deformation automatically reduces to the deformation in the dispersive region. On the other side of the region, the curve defined by* $8^{2/3} = -\log k_0^2/\tau$ *lies to the right of the curve defined by* $x = -(3t)^{1/3}\log(t)^{2/3}$*. In the next section we address what happens as the curve defined by* $8^{2/3} = -\log k_0^2/\tau$ *is approached.*

The transition region

While the collisionless shock region has extended the values of (x,t) for which there exists a well-behaved RHP past that of the dispersive region, it is not asymptotically reliable as we approach the Painlevé region: as $|x|$ decreases, a approaches the singularity of the local parametrix at zero. To avoid this issue, we collapse the lensing. To maintain numerical accuracy, we choose a to ensure that the oscillations are controlled on $[-b,b]$. For simplicity let $x = -t^{1/3}R(t)$, where

$$\lim_{t\to\infty}\frac{R(t)}{\log(t)^{2/3}} = 0, \text{ and } \lim_{t\to\infty} R(t) = \infty.$$

Given a positive bounded function $f(x,t)$, we choose a so that

$$i\tau(g^+(k) + g^-(k)) = if(x,t), \quad k \in [a,b], \tag{6.2.3}$$

which implies

$$i\tau(g^+(k) + g^-(k)) = -if(x,t), \quad k \in [-b,-a].$$

In light of (6.4.3) this is equivalent to solving

$$f(x,t)/\tau = 24\int_0^a \sqrt{(a^2-p^2)(b^2-p^2)}dp, \tag{6.2.4}$$

for a and b. By adjusting f this can be solved since the right-hand side is a monotone function of a, under the constraint $a^2+b^2=2$, which increases from 0 to 16 as a increases from 0 to 1. Furthermore, $\tau\to\infty$ in this region.

The RHP, after conjugation by ϕ, is of the form (6.2.2) and we claim that all entries of the matrices in (6.2.2) are bounded and the oscillations are controlled. In choosing (6.2.3) we have that $|i\tau(g^+(k)+g^-(k))|\le f(x,t)$ on $[-b,b]$ which implies that the $(1,2)$ and $(2,1)$ components of the matrix have controlled oscillations and are bounded. Next, consider $i\tau(g^+(k)-g^-(k))$. The choice (6.2.3) implies

$$h(x,t)/\tau = 24\int_a^b \sqrt{(p^2-a^2)(b^2-p^2)}dp, \tag{6.2.5}$$

for a positive function h such that $1/C < h(x,t)/\tau + f(x,t)/\tau < C$, $C>1$. This comes from the fact that both (6.2.5) and (6.2.4) cannot vanish simultaneously. Since f is chosen to be bounded, $h=\mathcal{O}(\tau)$ and $\tau=\mathcal{O}(R^{3/2}(t))$. Using these facts along with $k_0^2=\mathcal{O}(R(t)/t^{2/3})$ we obtain

$$\lim_{t\to\infty} e^{-h(x,t)}=0,\quad \lim_{t\to\infty} k_0^2 e^{h(x,t)}\to 0.$$

This shows that the $(1,1)$ and $(2,2)$ components of the matrices in (6.2.2) are bounded. These matrices are stable asymptotically for numerics without any lensing on $[-b,b]$. After lensing on $(-\infty,-b)\cup(b,\infty)$ we obtain a RHP for $\Phi_{1,t}$, see Figure 6.7(a). Define $\Phi_{2,t}=\Phi_{1,t}\phi$ and refer to Figure 6.2.8 for the jump contours and jump matrices of the RHP for $\Phi_{2,t}$ near a,b. Finally, define

$$\Phi_{3,t}=\begin{cases}\Phi_{2,t}\phi^{-1} & \text{inside the circles centered at } \pm b,\pm a,\\ \Phi_{2,t} & \text{otherwise.}\end{cases}$$

Refer to Figure 6.2.9 for the jump contours and jump matrices of the final RHP in the transition region.

The soliton region

This is the region where $x>0, x=\mathcal{O}(t)$. We present a deformation that is very similar to that used for the modified KdV equation. We use the $G=MP$ factorization, and the only complication arises from dealing with the jumps on $A_j^{\pm}$. As $|k_0|$ increases, the line $\operatorname{Im} k=\sqrt{3}|k_0|$ eventually overtakes the circles, corresponding to solitons, or to the poles in the RHP. This means that we need to invert the exponentials on some of these circles but not on others. We illustrate this process. Define

$$Q_{k_0}=\begin{bmatrix}\prod_{|\kappa_j|<\sqrt{3}|k_0|}(k+\kappa_j)/(k-\kappa_j) & 0\\ 0 & \prod_{|\kappa_j|<\sqrt{3}|k_0|}(k-\kappa_j)/(k+\kappa_j)\end{bmatrix}.$$

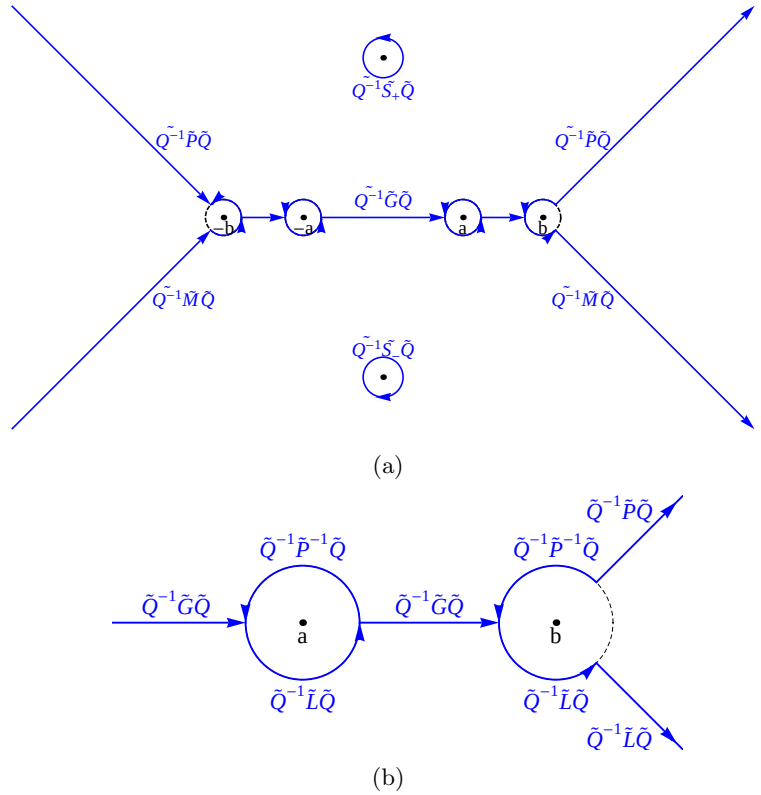

Figure 6.2.7: (a) The jump contours and matrices of the RHP for $\Phi_{1,t}$. (b) The jump contours and matrices of the RHP for $\Phi_{1,t}$ near a, b.

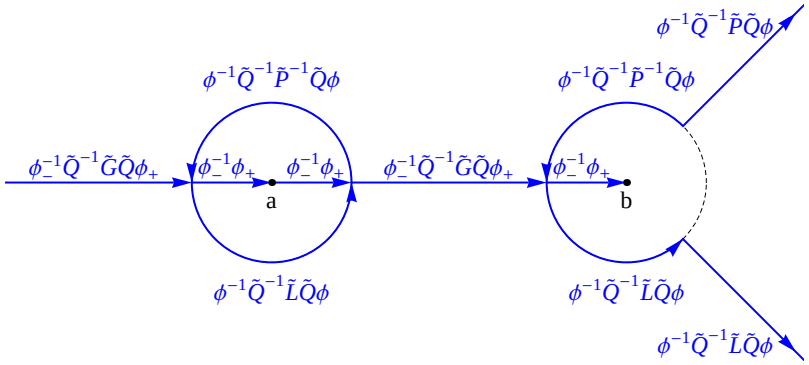

Figure 6.2.8: The jump contours and matrices of the RHP for $\Phi_{2,t}$ near a, b.

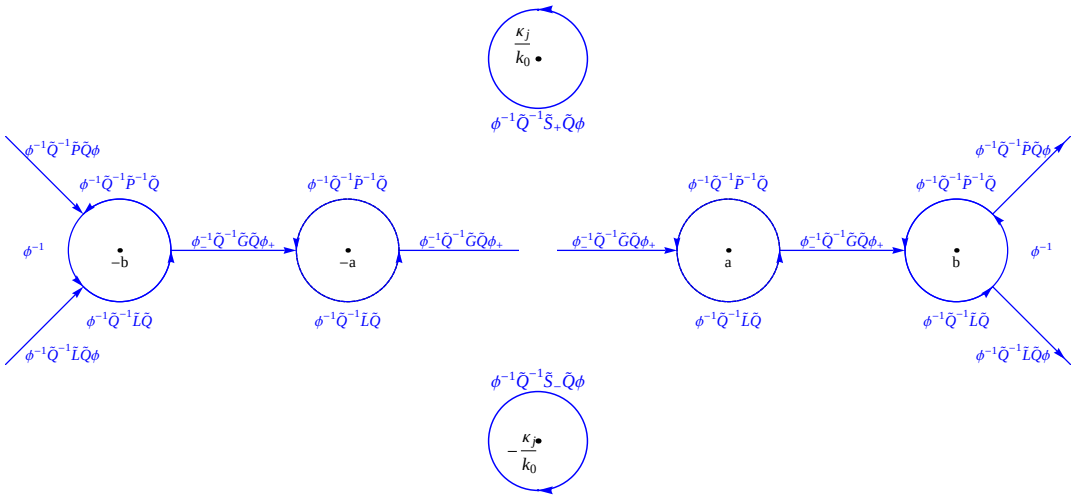

Figure 6.2.9: A zoomed view of the jump contours and matrices of the final deformation of the RHP in the transition region.

This matrix allows us to change the matrix $T_\pm$ to $S_\pm$ as we did in Section 6.2.2 for just those of the $A_j^\pm$ such that $|\kappa_j| < \sqrt{3}|k_0|$. Again we use a function $0 \le \alpha(x,t) < \sqrt{3}|k_0|$. The reader is referred to Figure 6.2.10 for the final deformation.

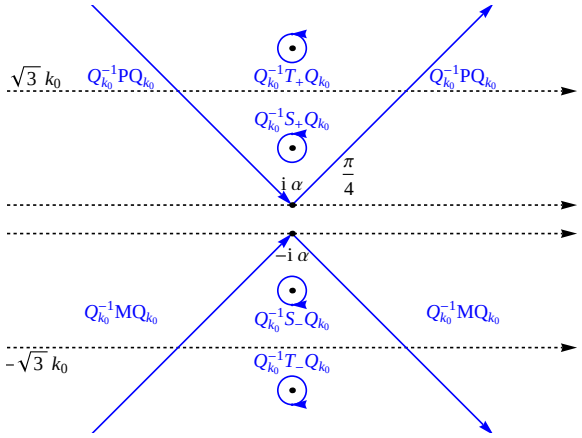

Figure 6.2.10: The final deformation of the RHP in the soliton region for the KdV equation. The solution to this problem contains two solitons to illustrate when $T_\pm$ needs to be replaced with $S_\pm$.

6.2.3 Numerical results

As in Section 6.1.3 we scale and truncate the contours appropriately and $q(n,x,t)$ is defined to be the solution obtained with n collocation points on each contour.

Direct scattering

As a test case to verify the computed reflection coefficient we use an exact form given in [42]. If $q(x,0) = A\ \mathrm{sech}^2(x)$ then

$$\rho(k) = \frac{a(k)\Gamma(\tilde{c}(k))\Gamma(\tilde{c}(k)-\tilde{a}(k)-\tilde{b}(k))}{\Gamma(\tilde{c}(k)-\tilde{a}(k))\Gamma(\tilde{c}(k)-\tilde{b}(k))}, \quad a(k) = \frac{\Gamma(\tilde{a}(k))\Gamma(\tilde{b}(k))}{\Gamma(\tilde{c}(k))\Gamma(\tilde{a}(k)+\tilde{b}(k)-\tilde{c}(k))},$$
$$\tilde{a}(k) = 1/2 - ik + (A+1/4)^{1/2}, \quad \tilde{b}(k) = 1/2 - ik - (A+1/4)^{1/2}, \quad \tilde{c}(k) = 1 - ik,$$

where Γ is the Gamma function [84]. If $A > 0$ the set of poles is not empty. The poles are located at

$$\kappa_j = i((A+1/4)^{1/2} - (j+1/4)), \quad j = 1, \ldots \quad \text{while} \quad ((A+1/4)^{1/2} - (j+1/4)) > 0,$$

and the corresponding residues C_j are computed from the expression for ρ. Figure 6.11(a) shows the error between this relation and the computed reflection coefficient when $A = 2.4$ for a varying number of collocation points.

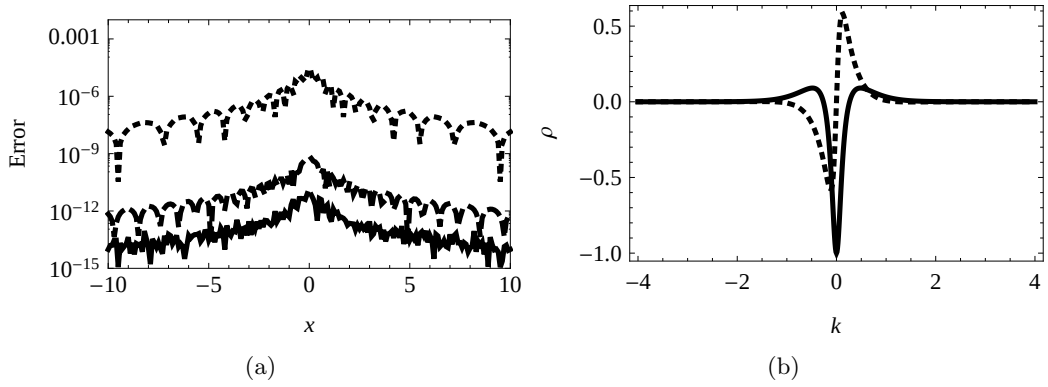

Figure 6.2.11: Numerical computation of the reflection coefficient $\rho(k)$ with $q(x,0) = 2.4\ \mathrm{sech}^2(x)$. (a) Absolute error between computed and actual reflection coefficient plotted vs. k when the number of collocation points is 25 (dotted), 50 (dashed) and 100 (solid), (b) Plot of the computed reflection coefficient with 100 collocation points. The real part is shown as a curve and the imaginary part as a dashed graph.

Inverse scattering

As before, throughout this section we assume the reflection coefficient is obtained to machine precision.

1. *Convergence.* To analyze error we again use

$$Q_n^m(x,t) = |q(n,x,t) - q(m,x,t)|.$$

See Figure 6.2.12 for a demonstration of spectral convergence with all deformations.

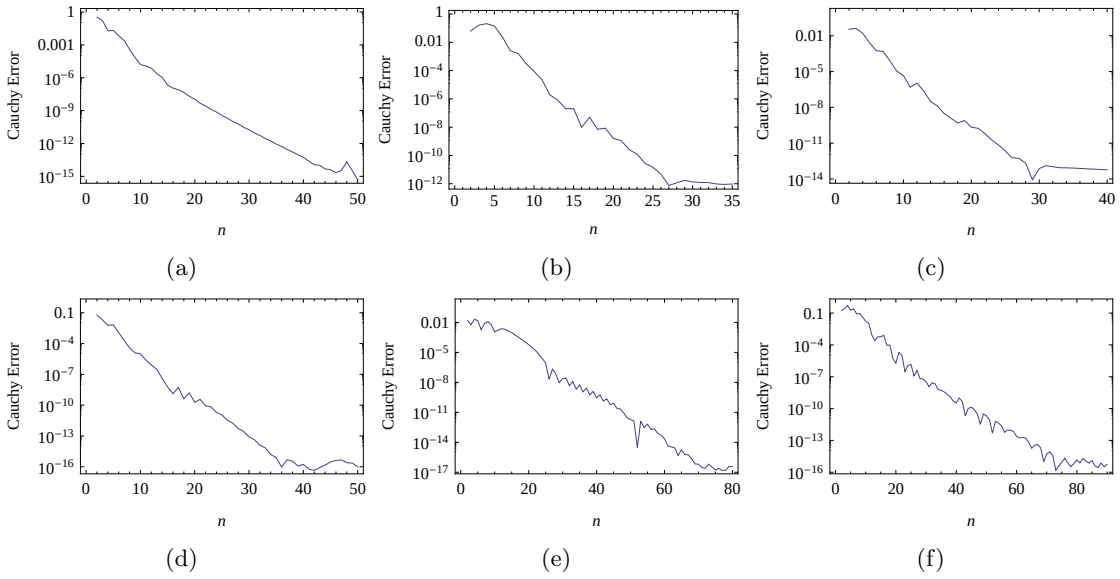

Figure 6.2.12: Demonstration of spectral convergence for the KdV equation with $q(x,0)$ shown in Figure 6.2(a). All plots have $Q^n_{2m}(x,t)$ plotted as a function of n as n ranges from 2 to m. (a) *The Dispersive Region*: $m = 50$ at the point $(x,t) = (-10, 1/2)$, (b) *The Collisionless Shock Region*: $m = 30$ at the point $(-9.86, 2.8)$, (c) *The Transition Region*: $m = 40$ at the point $(-3.12, 7.)$, (d) *The Painlevé Region*: $m = 50$ at the point $(-2.76, 7)$, (e) *The Painlevé Region*: $m = 80$ at the point $(2.76, 7)$, (f) *The Soliton Region*: $m = 90$ at the point $(1.2, .1)$. The smallest errors achieved in (b) and (c) are greater than in the other plots due to errors accumulating from the larger number of functions computed to setup the corresponding RHP.

2. *Asymptotic Stability.* As mentioned before, for the method to be stable we need that for a given n and m, $Q_n^m(x,t)$ should remain bounded (and small) as $|x|+|t|$ becomes large. Again, what we numerically demonstrate is that $Q_n^m(x,t)$ tends to zero in all regions. See Figure 6.2.13 for the demonstration of this. As mentioned before, we expect $Q_n^m(x,t)$ to approach zero only when the solution approaches zero.

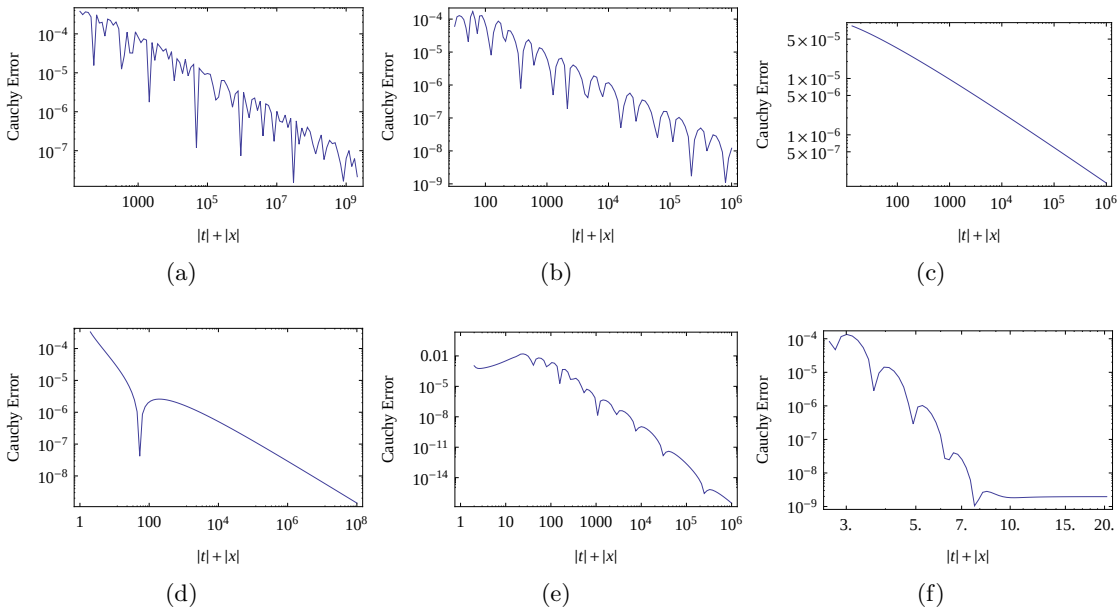

Figure 6.2.13: Demonstration of asymptotic stability for the KdV equation with $q(x,0)$ shown in Figure 6.2(a). All plots have $Q_m^n(x,t)$ plotted as a function of $|x|+|t|$. (a) *The Dispersive Region*: $m=16$, $n=8$ along the trajectory $x=-20t$, (b) *The Collisionless Shock Region*: $m=20$, $n=20$ along the trajectory $x=-4(3t)^{1/3}\log(t)^{2/3}$. (c) *The Transition Region*: $m=16$, $n=8$ along the trajectory $x=-(3t)^{1/3}\log(t)^{1/6}$, (d) *The Painlevé Region*: $m=16$, $n=8$ along the trajectory $x=-t^{1/3}$, (e) *The Painlevé Region*: $m=32$, $n=16$ along the trajectory $x=t^{1/3}$, (f) *The Soliton Region*: $m=32$, $n=16$ along the trajectory $x=4t-2.3$, in order to track the soliton. We do not expect the error to decay to zero when the solution does not.

Comparison with asymptotic formulae

In this section we compare our numerics with the asymptotic formulae for the KdV equation. We skip the soliton region because the numerics limit to the linear system related to the soliton solutions exponentially fast. We also skip the transition region because, as mentioned before, no asymptotic results are known. As before, we emphasize that in view of the verified convergence, the numerical results are believed to be more accurate than the asymptotic results.

1. *The Dispersive Region.* Numerical results are compared with the asymptotic formula (6.0.16) in Figure 6.2.14. The difference between the numerical approximation and

the asymptotic approximation is of the correct order.

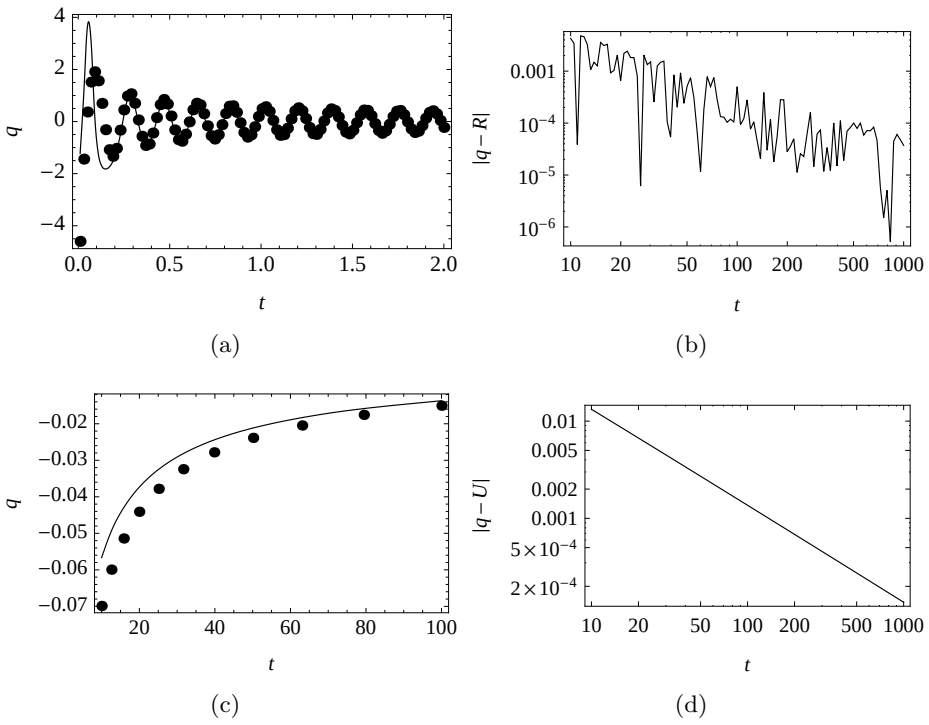

Figure 6.2.14: Numerical asymptotics in the dispersive and Painlevé regions for the KdV equation. (a) *The Dispersive Region:* $q(10, x, t)$ and $R(x, t)$ plotted as a function of t with $x = -20t$. $R(x, t)$ is defined in (6.0.16). Solid: Computed solution, Dots: Asymptotic formula, (b) *The Dispersive Region:* $|q(10, x, t) - R(x, t)|$ plotted as function of t with $x = -20t$. A least-squares fit gives $|q(10, x, t) - R(x, t)| = \mathcal{O}(t^{-1.1})$, (c) *The Painlevé Region:* $q(10, x, t)$ and $U(x, t)$ plotted as a function of t with $x = -t^{1/3}$. $U(x, t)$ is defined in (6.0.14). Solid: Computed solution, Dots: Asymptotic formula, (d) *The Painlevé Region:* $|q(10, x, t) - U(x, t)|$ plotted as a function of t with $x = -t^{1/3}$. A least-squares fit gives $|q(10, x, t) - U(x, t)| = \mathcal{O}(t^{-0.99})$ which is in agreement with the error bound.

2. *The Painlevé Region.* Numerical results are compared with the asymptotic formula in (6.0.14) in Figure 6.2.14. As before, we use the Riemann–Hilbert based techniques in Chapter 8 to compute v.

3. *The Collisionless Shock Region.* Numerical results are compared with the W from (6.0.15) in Figure 6.2.15. From Figure 6.15(b) we estimate the amplitude of the solution to be on the order of $|x|/t$. This allows us to estimate relative error, Figure 6.15(c). We see the relative error is on the order of $(\log t)^{-2/3}$ along the trajectory $x = 4(3t)^{1/3}(\log t)^{2/3}$. Numerically, in absolute error

$$q(x, t) - W(x, t) = \mathcal{O}\left(\frac{|x|}{t}(\log t)^{-2/3}\right).$$

Since there is not an error bound present in [39] we conjecture

$$q(x,t) - W(x,t) = \mathcal{O}(t^{-2/3}) \text{ as } t \to \infty, \quad x = C(3t)^{1/3}(\log t)^{2/3}, \quad C > 0. \tag{6.2.6}$$

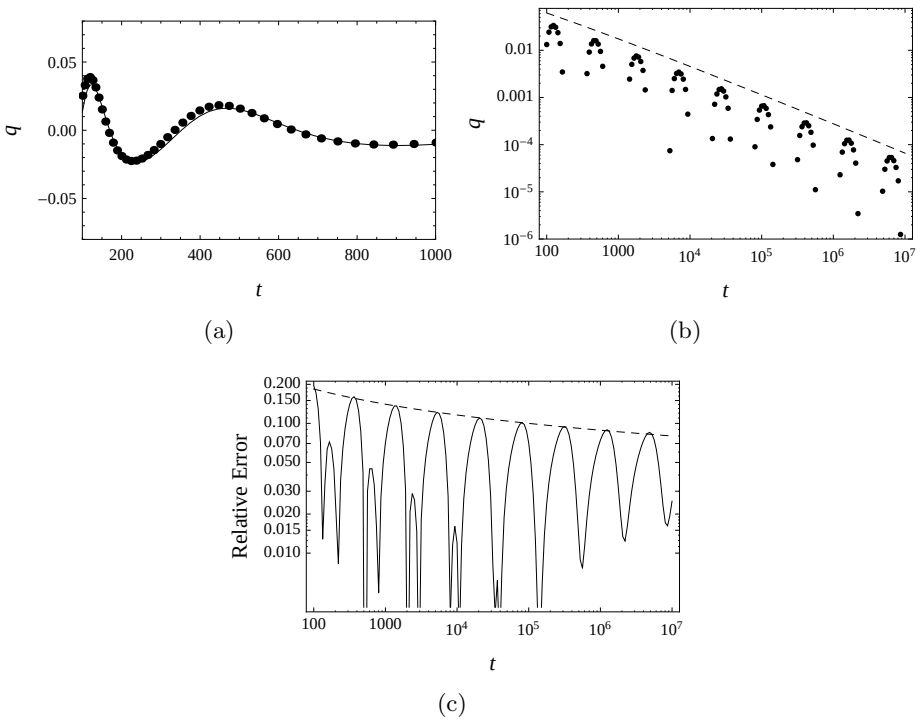

Figure 6.2.15: Numerical asymptotics in the collisionless shock region for the KdV equation. (a) $q(10,x,t)$ and $W(x,t)$ plotted as a function or t with $x = 4(3t)^{1/3}(\log t)^{2/3}$. Solid: Computed solution, Dots: Computed solution to (6.0.15), (b) Confirmation that the amplitude is on the order of $|x|/t$ along the same trajectory. Dots: Computed solution, Dashed: $t \mapsto -x/(12t)$, (c) Confirmation that the relative error is on the order of $(\log t)^{-2/3}$. Solid: $t \mapsto |q(10,x,t) - W(x,t)|/(|x|/t)$, Dashed: $t \mapsto (\log t)^{-2/3}$, along the same trajectory.

Remark 6.2.5. *In the collisionless shock region we compute the asymptotic expression by directly solving the limiting RHP numerically, instead of using the formula given in [39]. In our numerical experiments, this formula did not agree with Figure 6.15(a). This discrepancy will be explored further in a future paper.*

6.2.4 Miura transformation

Assume q satisfies the defocusing version of the modified KdV equation (6.0.2) then $u = -q^2 - q_x$ satisfies the KdV equation (6.0.1). This is the well-known Miura transformation [80]. The numerical approach used here allows for q_x to be computed in a straightforward way, by essentially differentiating the linear system resulting from the collocation method for RHPs [87]. In Figure 6.2.16 we use the Miura transformation to check the consistency of

our numerics for $q(x,0) = -1.3\,\mathrm{sech}^2(x)$. As expected, the evolution of the KdV equation and the Miura transformation of the modified KdV equation coincide. The error in Figure 6.16(f) could be made much smaller, as the above convergence results indicate. The figure is not meant to estimate the rate of convergence but to just demonstrate that the absolute difference between two solutions does decrease as we increase the number of collocation points.

6.3 Uniform approximation of solutions of the modified KdV equation

In this section we prove asymptotic stability for the numerical solution of the modified KdV equation (6.0.2) for $x < 0$. The analysis presented below demonstrates the ease at which the ideas in Chapter 5 can be applied in certain situations.

Recall, the RHP for the modified KdV equation is

$$\begin{aligned}
&\Phi^+(s) = \Phi^-(s)G(s), \quad s \in \mathbb{R}, \quad \Phi(\infty) = I,\\
&G(k) = \begin{bmatrix} 1-\rho(k)\rho(-k) & -\rho(-k)e^{-\theta(k)} \\ \rho(k)e^{\theta(k)} & 1 \end{bmatrix},\\
&\theta(k) = 2ikx + 8ik^3t.
\end{aligned}$$

In the cases we consider ρ is analytic in a strip that contains $\mathbb{R}$. If $x \ll -ct^{1/3}$ the deformation is similar to the case considered in the following chapter for Painlevé II and asymptotic stability follows by the same arguments. We assume $x = -12c^2t^{1/3}$ for some positive constant c. This deformation is found in [110]. We rewrite θ:

$$\theta(k) = -24ic^2(kt^{1/3}) + 8i(kt^{1/3})^3.$$

We note that $\theta'(k_0) = 0$ for $k_0 = \pm\sqrt{-x/(12t)} = \pm ct^{-1/3}$. We introduce a new variable $z = kt^{1/3}/c$ so that

$$\theta(zct^{-1/3}) = -24ic^3z + 8ic^3z^3 = 8ic^3(z^3 - 3z).$$

For a function of $f(k)$ we use the scaling $\tilde{f}(z) = f(zct^{-1/3})$. The functions $\tilde{\theta}$, $\tilde{G}$ and $\tilde{\rho}$ are identified similarly. After deformation and scaling, we obtain the following RHP for $\tilde{\Phi}(z)$:

$$\begin{aligned}
&\tilde{\Phi}^+(s) = \tilde{\Phi}^-(s)J(s), s \in \Sigma = [-1,1] \cup \Gamma_1 \cup \Gamma_2 \cup \Gamma_3 \cup \Gamma_4,\\
&J(z) = \begin{cases}
\tilde{G}(z), & \text{if } z \in [-1,1],\\
\begin{bmatrix} 1 & 0 \\ \tilde{\rho}(z)e^{\tilde{\theta}(z)} & 1 \end{bmatrix}, & \text{if } z \in \Gamma_1 \cup \Gamma_2,\\
\begin{bmatrix} 1 & -\tilde{\rho}(-z)e^{-\tilde{\theta}(z)} \\ 0 & 1 \end{bmatrix}, & \text{if } z \in \Gamma_3 \cup \Gamma_4,
\end{cases}
\end{aligned}$$

where Γ_i, $i = 1,2,3,4$, shown in Figure 6.3.1, are locally deformed along the path of steepest descent. To reconstruct the solution to the modified KdV equation we use the

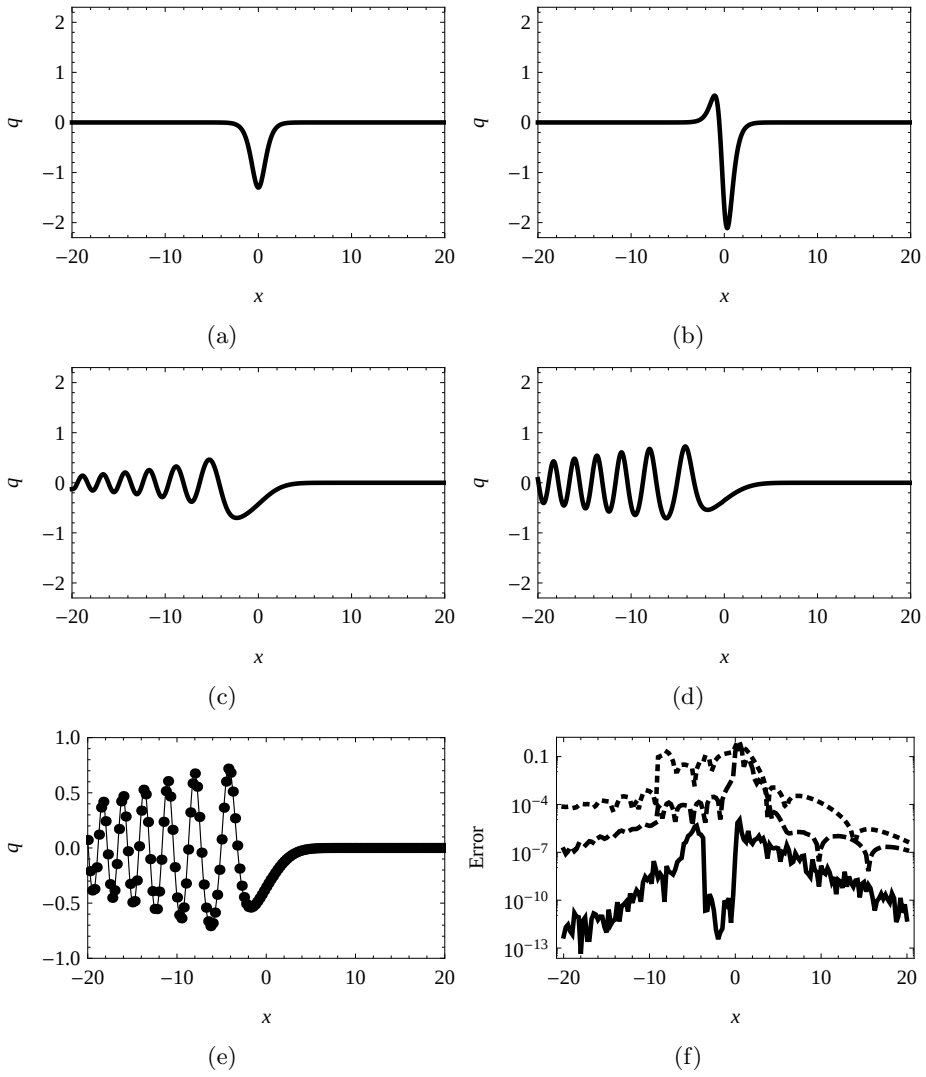

Figure 6.2.16: Numerical demonstration of the consistency of the numerical methods for the KdV equation and the modified KdV equation through the Miura transformation. (a) Initial condition for the modified KdV equation, $q(x,0) = q_0(x) = -1.3\ \mathrm{sech}^2(x)$, (b) Initial condition for the KdV equation, $q(x,0) = -q_0^2(x) - \frac{d}{dx}q_0(x)$, (c) Evolution using the modified KdV equation at $t = .75$, (d) Evolution using the KdV equation at $t = .75$, (e) Solid: Evolution using the KdV equation at $t = .75$, Dots: Miura transformation of the evolution using the modified KdV equation at $t = .75$. (f) Absolute difference between the Miura transformed the modified KdV equation and the KdV equation. We vary the number of collocation points per contour, m. Dotted: $m = 5$, Dashed: $m = 10$, Solid: $m = 40$. The jumps in the error are caused by switching deformations.

formula

$$u(x,t) = 2ik_0 \lim_{z\to\infty} z\tilde{\Phi}_{12}(z). \tag{6.3.1}$$

Remark 6.3.1. *We assume ρ decays rapidly at ∞ and is analytic in a strip that contains the real line. This allows us to perform the initial deformation which requires modification of the contours at ∞. As t increases, the analyticity requirements on ρ are reduced; the width of the strip can be taken to be smaller if needed. We only require that each Γ_i lies in the domain of analyticity for $\tilde{\rho}$. More specifically, we assume t is large enough so that when we truncate the contours for numerical purposes using Proposition 3.10.4, they lie within the strip of analyticity for $\tilde{\rho}$.*

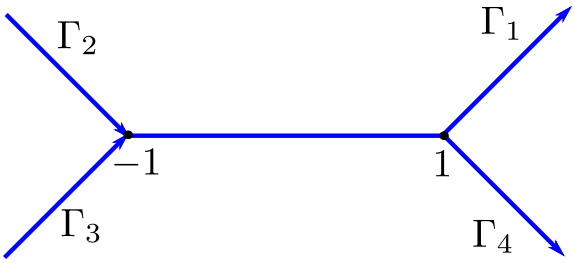

Figure 6.3.1: Jump contours for the RHP for the modified KdV equation.

The parametrix derived in [34] is used to show that $\mathcal{C}[J,\Sigma]$ has an inverse that is uniformly bounded by using (5.2.1) as was done in the previous section. We use the analyticity and decay of ρ at ∞ along with the fact that the contours pass along the paths of steepest descent.

The contour is fixed (*i.e.*, independent of x, t and c), and this situation is more straightforward to analyze than the previous example. Repeated differentiation of $J(k)$ proves that this deformation yields a uniform numerical approximation. Furthermore, replacing c by any smaller value yields the same conclusion. This proves the uniform approximation of the modified KdV equation in the Painlevé region

$$\{(x,t) : t \geq \epsilon, \quad x \leq -\epsilon, x \geq -12c^2t^{1/3}\}, \quad \epsilon > 0.$$

where ϵ is determined by the analyticity of ρ.

6.3.1 Numerical results

In Figure 6.3.2 we show the solution with initial data $u(x,0) = -2e^{-x^2}$ with $c = \sqrt{9/4}$. The reflection coefficient is obtained using the method described in [110]. We use the notation $u(n,x,t)$ to denote the approximate solution obtained with n collocation points per contour. We see that the absolute error tends to zero rapidly. More importantly, the relative error remains small. We approximate the solution uniformly on the fixed, scaled contour. When we compute the solution using (6.3.1) we multiply by z_0 which is decaying to zero along this trajectory. This is how the method maintains accuracy even when comparing relative error.

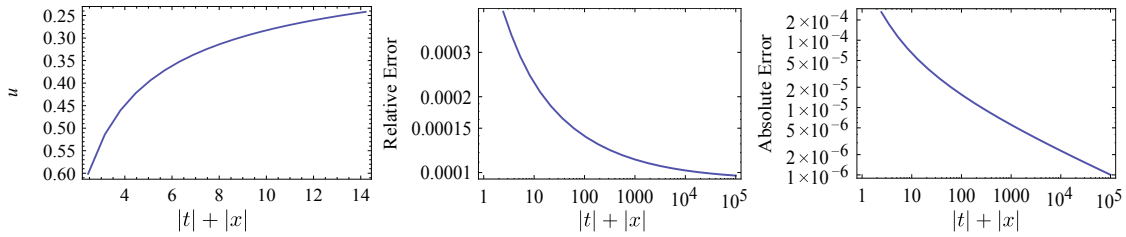

(a) (b) (c)

Figure 6.3.2: (a) Plot of the solution along $x = -(3t)^{1/3}$ for small time. (b) Absolute error, $|u(5,x,t) - u(10,x,t)|$, for long time (c) Relative error $|u(5,x,t) - u(10,x,t)|/|u(10,x,t)|$ for long time.

6.4 The collisionless shock g-function

We give the explicit form of g from Section 6.2.2. Restricting to $a^2 + b^2 = 2$, the expression

$$s = 24 \int_a^b \sqrt{(p^2 - a^2)(b^2 - p^2)}dp, \quad \tau = tk_0^3, \quad s = -\log k_0^2/\tau \in [0, 8^{2/3}],$$

defines both $a(s)$ and $b(s)$ since it is a monotone function of a. Define the g-function to be

$$g(k) = 12 \int_{b(s)}^{k} \sqrt{(p^2 - a^2(s))(p^2 - b^2(s))}dp + 12 \int_0^{a(s)} \sqrt{(p^2 - a^2(s))(p^2 - b^2(s))}dp, \tag{6.4.1}$$

we choose the branch cuts for $\sqrt{(p^2 - a^2(s))(p^2 - b^2(s))}$ to be the straight line segments along $[-b(s), -a(s)]$ and $[a(s), b(s)]$. In order for g to be single-valued it is necessary to add a branch cut on $[-a(s), a(s)]$.

Lemma 6.4.1. *The g-function given by* (6.4.1) *satisfies:*

1. *g is bounded in the finite plane,*

2.

$$g^+(k) - g^-(k) = \begin{cases} 24 \int_{b(s)}^{k} \sqrt{(p^2 - a^2(s))(p^2 - b^2(s))}dp, & \text{if } k \in [a(s), b(s)], \\ 24 \int_{b(s)}^{a(s)} \sqrt{(p^2 - a^2(s))(p^2 - b^2(s))}dp, & \text{if } k \in (-a(s), a(s)), \\ 24 \int_{-b(s)}^{k} \sqrt{(p^2 - a^2(s))(p^2 - b^2(s))}dp, & \text{if } k \in [-b(s), -a(s)], \\ 0, & \text{otherwise}, \end{cases} \tag{6.4.2}$$

3.

$$g^+(k)+g^-(k)=\begin{cases} 24\int_0^{a(s)}\sqrt{(p^2-a^2(s))(p^2-b^2(s))}dp, & \text{if } k\in[a(s),b(s)],\\ 24\int_0^{k}\sqrt{(p^2-a^2(s))(p^2-b^2(s))}dp, & \text{if } k\in(-a(s),a(s)),\\ 24\int_0^{-a(s)}\sqrt{(p^2-a^2(s))(p^2-b^2(s))}dp, & \text{if } k\in[-b(s),-a(s)],\\ 2g(k), & \text{otherwise,}\end{cases} \tag{6.4.3}$$

4.

$$g(k)=4k^3-12k+\mathcal{O}(k^{-1}) \text{ as } k\to\infty,$$

5.

$$k_0^2e^{i\tau(g^+(k)+g^-(k))}=1, \text{ for } k\in(-a(s),a(s)).$$

Proof. *(1) is clear from* (6.4.1). *(2) and (3) follow from contour integration and the fact that the integrand is invariant under $p\mapsto -p$. To prove (4) we look at the expansion of the integrand*

$$12\sqrt{(p^2-a^2(s))(p^2-b^2(s))}=12p^2\sqrt{(1-(a(s)/p)^2-(b(s)/p)^2-(a(s)/p)^2(b(s)/p)^2)}.$$

We use

$$\sqrt{1-y}=1-\frac{1}{2}y-\frac{1}{8}y^2+\dots,$$

to obtain (for large p)

$$12\sqrt{(p^2-a^2(s))(p^2-b^2(s))}=12p^2(1-(a(s)/p)^2-(b(s)/p)^2)+\mathcal{O}(p^{-2}).$$

After integrating this we find

$$f(k)=\int_{a(s)}^{k}\sqrt{(p^2-a^2(s))(p^2-b^2(s))}dp=4k^3-6(a^2(s)+b^2(s))k+C+\mathcal{O}(k^{-1}),$$

for some complex constant C. To find C notice that $f(k)$ is the sum of a constant and odd

powers of k,

$$\begin{aligned} f(k)+f(-k) &= 2C, \\ &= \int_{a(s)}^{k} \sqrt{(p^2-a^2(s))(p^2-b^2(s))}dp + \int_{a(s)}^{-k} \sqrt{(p^2-a^2(s))(p^2-b^2(s))}dp \\ &= \int_{a(s)}^{k} \sqrt{(p^2-a^2(s))(p^2-b^2(s))}dp + \int_{k}^{-a(s)} \sqrt{(p^2-a^2(s))(p^2-b^2(s))}dp \\ &= -\int_{-a(s)}^{a(s)} \sqrt{(p^2-a^2(s))(p^2-b^2(s))}dp \\ &= -2\int_{0}^{a(s)} \sqrt{(p^2-a^2(s))(p^2-b^2(s))}dp. \end{aligned}$$

Therefore $g(k) \backsim 4k^3 - 12k + \mathcal{O}(k^{-1})$, *where we used* $a^2(s)+b^2(s)=2$. *Finally, for (5) assume* $k \in (-a(s), a(s))$,

$$\begin{aligned} -\log k_0^2/\tau &= 24\int_{a(s)}^{b(s)} \sqrt{(p^2-a^2(s))(b^2(s)-p^2)}dp, \\ \log k_0^2/\tau &= 24i\int_{a(s)}^{b(s)} \sqrt{(p^2-a^2(s))(p^2-b^2(s))}dp = i(g^+(k)-g^-(k)), \\ k_0^2 e^{i\tau(g^+(k)-g^-(k))} &= 1. \end{aligned}$$

These are all the properties mentioned in Section 6.2.2.

6.5 Comparison with existing numerical methods

We close this chapter with a comparison between the method described above and methods that exist in the literature. The numerical aspects of dispersion are studied in great detail in [55, 58]. In these studies the authors invoke fourth-order time-stepping and the Fast Fourier Transform (FFT) in space. This type of method is very efficient for approximating the solution of the Cauchy problem for small time and, when only a small time solution is needed, the method in [58] is surely the method of choice. Approximation for larger time is complicated by the large velocity and increasingly oscillatory nature of the dispersive tail. If the dispersive tail reaches the boundary, errors are immediately introduced into the approximation of the Cauchy problem.

For a quantitative analysis we consider the asymptotic formula for the dispersive tail of KdV ([39], see also (6.0.16)), which we write as

$$q(x,t) = t^{-1/2}\sqrt{\frac{\nu(k_0)}{3k_0}}\cos(-4/3k_0x + \cdots) + \mathcal{O}(t^{-1}),$$

where ν is a function depending on q_0 which decays to zero, at a rate depending on the regularity of q_0. To find the leading edge of the propagating tail, we choose the largest k' such that $\sqrt{\nu(k')/(3k')} > 10^{-10}$. Since k_0 depends only on the ratio x/t, we know

the solution will be greater than machine precision for $t < 10^8$ in the neighborhood of the values of (x,t) such that $k' = k_0$. We estimate the number of operations required to compute the solution accurately. Assume the spatial computational domain is $[-L,L]$ with N equally spaced grid points. We solve from $t=0$ to $t=T$ with a time step Δt. Since the solution behaves roughly like $\cos(-4/3k'x)$ with non-zero amplitude, we need to use a sufficient number of grid points to at least resolve this frequency, i.e., $\pi N/L \geq 4/3k'$ must be satisfied. Furthermore, using $k' = k_0 = \sqrt{-x/(12t)}$ we obtain that the point $(-12tk'^2, t)$ should be in our computational domain if $t \leq T$, requiring that $L > 12Tk'^2$. From these inequalities we obtain

$$N > \frac{16}{\pi} k'^3 T. \tag{6.5.1}$$

To ensure CFL stability of the method we require $\Delta t = c/N,\ \ c \leq 1$ [58]. Since the FFT costs, on the order of, $N \log N$ operations, the number of operations required to evaluate the spatial derivatives via an FFT is larger than $4N \log N$. The number of operations required for the fourth order time–stepper to evolve a point up to time T is greater than $4NTc^{-1}$. This combines to give a total number of operations larger than $16c^{-1}N^2 T \log N$ which is $\mathcal{O}(T^3 \log T)$. For the initial condition used in Figure 6.0.2 we estimate $k' = 8$, which means that to evolve the solution to $T = 30$ requires more than 10^{13} flops, even with $c = 1$. This is manageable. However, it become prohibitively expensive very quickly with increasing T, or for less regular initial conditions so that ν decays slower. The above calculation is optimistic, since convergence considerations and the presence of the nonlinearity can further increase the numerical effort required.

Next, we briefly discuss other computational approaches which, just like our own, rely on the integrability of the equation being solved. Osborne and Boffetta [93, 12] compute the scattering data using an algorithm in the spirit of the FFT for which they expect second-order convergence. Our use of spectral methods achieves higher rates of convergence. Additionally, Hald [61] used a trapezoidal method to solve the Gel'fand–Levitan–Marchenko formulation of the inverse problem. This method lacked spectral accuracy and the flexibility to deform contours. Bornemann has also computed the solution of the inverse problem through the use of Fredholm determinants [14] for $t = 0$ but this method suffers from ill-conditioning for $t > 0$.

Chapter 7

The Focusing and Defocusing Nonlinear Schrödinger Equations

We consider the initial-value problem on the whole line for the Nonlinear Schrödinger (NLS) equations

$$\begin{aligned} iq_t + q_{xx} + 2\lambda|q|^2 q = 0, \quad \lambda = \pm 1, \\ q(x,0) = q_0(x) \in \mathcal{S}_\delta(\mathbb{R}). \end{aligned} \tag{7.0.1}$$

When $\lambda = 1$ we obtain the focusing NLS equation and for $\lambda = -1$, the defocusing NLS equation. The NLS equations describe physical phenomena in optics [71], Bose–Einstein condensates [59, 94], as well as water waves [114]. Together with the KdV equation, these equations are the canonical examples of $(1+1)$-dimensional integrable partial differential equations. In this chapter we solve the NLS equation, both focusing and defocusing, numerically via the inverse scattering transform. These results initially appeared in [109].

The presence of an oscillatory dispersive tail is seen for both the focusing and defocusing NLS equations. Examination of the linear dispersion relationship for the PDEs indicates that small amplitude waves will travel at a speed proportional to their wave number. Unlike the KdV equation, solitons do no separate from dispersion asymptotically. These factors make traditional numerics inefficient to capture the solution for large time. The computational cost to compute the solution using time-stepping methods grows rapidly in time. The methods in [55, 58] are well suited for solving dispersive problems for small time. When a periodic approximation to the whole-line problem is used, one has to resolve the dispersive oscillations and increase the domain size as time increases. A thorough discussion of this can be found in Section 6.5 for the case of the KdV equation. In particular, it is shown that the computational costs grows at least like $t^3 \log t$.

The main benefit of the method presented here is that the computational cost to compute the solution at a given x and t value is seen to be independent of x and t. In Chapter 6 this claim is verified with numerical tests for the KdV and modified KdV equations. In this chapter we prove this fact using results from Section 5.1.

In addition to solving the problem on the whole line, we use symmetries to solve specific boundary-value problems on $\mathbb{R}^+$. To our knowledge this is the first time the solution of

a boundary-value problem has been computed effectively through the inverse scattering transform . We compute unbounded solutions to the defocusing NLS equation which have poles. Lastly, we prove that our approximation, under a specific assumption on the underlying numerical scheme, approximates solutions of (7.0.1) uniformly away from possible poles in the entire (x,t) plane. It should also be noted that the scattering problem (see Section 7.1) for the focusing NLS equation is a non-self adjoint spectral problem and this complicates the asymptotic analysis of the problem [25]. The numerical method outlined in Chapter 5 is not adversely affected by this additional complication.

7.1 Integrability and Riemann–Hilbert problems

The focusing and defocusing NLS equations are both completely integrable [3, p. 110]. We look for Lax pairs of the form

$$\begin{aligned}\mu_x &= L(k,q)\mu,\\ \mu_t &= M(k,q)\mu,\end{aligned}$$

through the modified Zakharov–Shabat scattering problem (see Section 6.0.3) given by

$$\mu_x = \begin{bmatrix} -ik & q \\ r & ik \end{bmatrix}\mu, \tag{7.1.1}$$

$$\mu_t = \begin{bmatrix} A & B \\ C & D \end{bmatrix}\mu. \tag{7.1.2}$$

In this case, choosing

$$A = -4ik^2 + iqr, \qquad B = 2qk + iq_x, \qquad C = -2rk + ir_x, \qquad D = -A, \tag{7.1.3}$$

and $r = -\lambda\overline{q}$, we obtain Lax pairs for both the focusing and defocusing NLS equations.

We briefly describe the inverse scattering transform. Some conventions used here differ from that in Chapter 2 but the unification is easily seen. We retain these conventions for historical comparisons. The analyticity properties in k of the solutions of (7.1.1) are studied. For simplicity, we assume $q \in \mathcal{S}_\delta(\mathbb{R})$. Piecewise-smooth initial data with exponential decay can also be treated but this is beyond the scope of this paper. We define two matrix solutions of (7.1.1) by their corresponding asymptotic behaviour:

$$\mu^-(x;k) \backsim \begin{bmatrix} e^{-ikx} & 0 \\ 0 & -e^{ikx} \end{bmatrix} \text{ as } x \to -\infty, \quad \mu^+(x;k) \backsim \begin{bmatrix} e^{-ikx} & 0 \\ 0 & e^{ikx} \end{bmatrix} \text{ as } x \to \infty. \tag{7.1.4}$$

Liouville's Formula implies that the determinants of these solutions are constant in x. Since the determinants are non-zero at $\pm\infty$ these matrix solutions define a linearly independent set which spans the solution space. There must exist a transition matrix

$$T(k) = \begin{bmatrix} a(k) & \mathcal{B}(k) \\ b(k) & \mathcal{A}(k) \end{bmatrix},$$

such that $\mu^+(x;k) = \mu^-(x;k)T(k)$. Define $\rho(k) = b(k)/a(k)$ to be the reflection coefficient. Some symmetry properties of T follow [3]:

$$a(k) = -\overline{\mathcal{A}(\bar{k})}, \qquad b(k) = -\lambda\overline{\mathcal{B}(\bar{k})}. \tag{7.1.5}$$

For the focusing NLS equation ($\lambda = 1$) there may exist values $\kappa_j \notin \mathbb{R}$ and $\operatorname{Im}\kappa_j > 0$ such that

$$\mu_1^-(x;\kappa_j) = T(\kappa_j)\mu_2^+(x;\kappa_j), \quad a(\kappa_j) = 0,$$

where the subscripts refer to columns. This implies that $\mu_1^-(x;\kappa_j)$ decays at both $\pm\infty$, exponentially. Thus, $\mu_1^-(x;\kappa_j)$ is an $L^2(\mathbb{R})$ eigenfunction of (7.1.1). From the symmetries (7.1.5) $\bar{\kappa}_j$ is also an $L^2(\mathbb{R})$ eigenvalue. For these values of k we define the norming constants

$$C_j = \frac{b(\kappa_j)}{a'(\kappa_j)}.$$

For the defocusing NLS equation ($\lambda = -1$) it is known there are no such eigenfunctions [3]. This implies there are no smooth soliton solutions with spatial decay for the defocusing NLS equation. We define the set

$$\left\{\rho(k), \{\kappa_j\}_{j=1}^n, \{C_j\}_{j=1}^n\right\}, \tag{7.1.6}$$

to be the scattering data, noting that the sets of eigenvalues and norming constants could be empty. As in Chapter 6, the process of finding the scattering data is called *direct scattering*.

Remark 7.1.1. *We assume $q_0 \in \mathcal{S}_\delta(\mathbb{R})$ for $\delta > 0$. This allows $T(k)$ to be analytically extended to a neighbourhood of the real line. But it may happen that $T(k)$ (in particular $b(k)$) cannot be extended above κ_j. Thus $b(\kappa_j)$ is really an abuse of notation and should be replaced with a constant, b_j.*

The solutions $\mu^\pm$ can be grouped and transformed in such a way that they satisfy a RHP[3].

The RHP associated with the NLS equations is

$$\begin{aligned} &\Phi^+(k) = \Phi^-(k)\begin{bmatrix} 1+\lambda\rho(k)\overline{\rho(\bar{k})} & \lambda\overline{\rho(\bar{k})}e^{-\theta(k)} \\ \rho(k)e^{\theta(k)} & 1 \end{bmatrix}, \quad k \in \mathbb{R} \\ &\Phi(\infty) = I, \qquad \theta(k) = 2i(xk + 2tk^2), \end{aligned} \tag{7.1.7}$$

with the residue conditions (when $\lambda = 1$),

$$\begin{aligned} \operatorname{Res}\{\Phi(k), k = \kappa_j\} &= \lim_{k\to\kappa_j}\Phi(k)\begin{bmatrix} 0 & 0 \\ C_j e^{\theta(\kappa_j)} & 0 \end{bmatrix}, \\ \operatorname{Res}\{\Phi(k), k = \kappa_j\} &= \lim_{k\to\kappa_j}\Phi(k)\begin{bmatrix} 0 & -\bar{C}_j e^{-\theta(\bar{\kappa}_j)} \\ 0 & 0 \end{bmatrix}. \end{aligned}$$

Once the solution of the RHP is known the solution to the corresponding NLS equations

is given by the expression

$$q(x,t) = 2i \lim_{|k|\to\infty} k\Phi(k)_{12},$$

where the subscript denotes the $(1,2)$ component of the matrix. The process of solving the RHP and reconstructing the solution is called *inverse scattering*.

We follow the standard procedure (see *e.g.*. Chapter 6) to turn the residue conditions into jump conditions. Fix $0 < \epsilon$ so that the circles $A_j^+ = \{k \in \mathbb{C} : |k - \kappa_j| = \epsilon\}$ and $A_j^- = \{k \in \mathbb{C} : |k - \bar{\kappa}_j| = \epsilon\}$ do not intersect each other or the real axis. We define $\hat{\Phi}$ by

$$\hat{\Phi}(k;x,t) = \begin{cases} \Phi(k;x,t) \begin{bmatrix} 1 & 0 \\ -C_j e^{\theta(\kappa_j)}/(k-\kappa_j) & 1 \end{bmatrix}, & \text{if } |k-\kappa_j| < \epsilon,\ j = 1,\dots,n, \\ \Phi(k;x,t) \begin{bmatrix} 1 & 0 \\ \bar{C}_j e^{-\theta(\bar{\kappa}_j)}/(k-\bar{\kappa}_j) & 1 \end{bmatrix}, & \text{if } |k-\bar{\kappa}_j| < \epsilon,\ j = 1,\dots,n, \\ \Phi(k;x,t), & \text{otherwise.} \end{cases} \tag{7.1.8}$$

It is straightforward to show that $\hat{\Phi}$ solves the RHP:

$$\hat{\Phi}^+(k) = \begin{cases} \hat{\Phi}^-(k)G(k), & \text{if } k \in \mathbb{R}, \\ \hat{\Phi}^-(k) \begin{bmatrix} 1 & 0 \\ -C_j e^{\theta(\kappa_j)}/(k-\kappa_j) & 1 \end{bmatrix}, & \text{if } k \in A_j^+, \\ \hat{\Phi}^-(k) \begin{bmatrix} 1 & -\bar{C}_j e^{-\theta(\bar{\kappa}_j)}/(k-\bar{\kappa}_j) \\ 0 & 1 \end{bmatrix}, & \text{if } k \in A_j^-, \end{cases} \quad , \qquad \hat{\Phi}(\infty) = I,$$

where $A_j^-(A_j^+)$ has clockwise(counter-clockwise) orientation.

In addition to $q_0 \in \mathcal{S}_\delta(\mathbb{R})$, we assume that the set $\{\kappa_j\}$ is bounded away from the real line. This is sufficient to ensure that all RHPs we address are well posed.

7.2 Numerical direct scattering

We describe a procedure to compute the scattering data (7.1.6). This follows Chapter 6. We look for solutions of the form (7.1.4) of (7.1.1). Define

$$\sigma_3 = \begin{bmatrix} 1 & 0 \\ 0 & -1 \end{bmatrix}, \quad Q = \begin{bmatrix} 0 & q \\ \lambda\bar{q} & 0 \end{bmatrix}, \quad \sigma_1 = \begin{bmatrix} 0 & 1 \\ 1 & 0 \end{bmatrix},$$

and two functions

$$J(k;x,t) = \mu^-(k;x,t)\sigma_3 e^{ikx\sigma_3} - I, \qquad K(k;x,t) = \mu^+(k;x,t)e^{ikx\sigma_3} - I. \tag{7.2.1}$$

Therefore $J \to 0$ as $x \to -\infty$ and $K \to 0$ as $x \to \infty$. Rewriting (7.1.1),

$$\mu_x = Q\mu - ik\sigma_3\mu, \tag{7.2.2}$$

we find that K and J both solve

$$N_x - ik[N, \sigma_3] - Q\sigma_1 N = Q\sigma_1.$$

For each k, this can be solved with the Chebyshev collocation method in Appendix B on $(-L, 0]$ for J and on $[0, L)$ for K using the appropriate boundary condition at $\pm L$. If we use n collocation points, this gives two approximate solutions J_n and K_n for J and K, respectively. From J_n and K_n we obtain μ_n^- and μ_n^+, approximations of μ^- and μ^+, respectively, by inverting the transformations in(7.2.1). Furthermore, μ_n^- and μ_n^+ share the point $x = 0$ in their domain of definition. Define

$$T_n(k) = (\mu_n^-)^{-1}(0; k)\mu_n^+(0; k).$$

This is an approximation of the transition matrix, from which we extract an approximation of the reflection coefficient.

This procedure works well for k in a neighbourhood of the real line. The solutions which decay at both $\pm\infty$ are all that is needed to obtain $b(k)$ when $a(k) = 0$. Furthermore, from the analyticity properties of a we have [3, p. 75]

$$a(k) - 1 = \frac{1}{2\pi i}\int_{-\infty}^{\infty} \frac{a(s) - 1}{s - k} ds, \qquad a'(k) = \frac{1}{2\pi i}\int_{-\infty}^{\infty} \frac{a'(s)}{s - k} ds.$$

Thus knowing $a(k)$ on the real line and $b(k)$ when $a(k) = 0$ allows us to compute $C_j = b(\kappa_j)/a'(\kappa_j)$. In practice we use the framework [89] discussed in Section 5.3 to compute these Cauchy integrals. Also, $a'(k)$ can be obtained accurately using spectral differentiation by mapping the real line to the unit circle.

The remaining problem is that of computing κ_j. We consider (7.2.2)

$$\mu_x - Q\mu = -ik\sigma_3\mu, \quad \Rightarrow \quad i\sigma_3\mu_x - i\sigma_3 Q\mu = k\mu. \tag{7.2.3}$$

Making the change of variables $x \mapsto \tan(s/2)$, $U(s) = \mu(\tan(s/2))$, $H(s) = Q(\tan(s/2))$ we obtain

$$2i\cos^2(s/2)\sigma_3 U_s(s) - i\sigma_3 H(s)U(s) = kU(s).$$

We use Hill's method [22] to compute the eigenvalues of the operator

$$2i\cos^2(s/2)\sigma_3\frac{d}{ds} - i\sigma_3 H(s), \tag{7.2.4}$$

in the space $L^2([-\pi, \pi])$. Following the arguments in Lemma 6.2.1 and using the convergence of Hill's method, even for non-self-adjoint operators [20, 68], the only eigenvalues we obtain off the real line are those associated with (7.2.3). This allows us to compute the discrete spectrum $\{\kappa_j\}_{j=1}^n$ with spectral accuracy. We may test to make sure all eigenvalues are captured by computing the inverse scattering transform at $t = 0$ and ensuring that

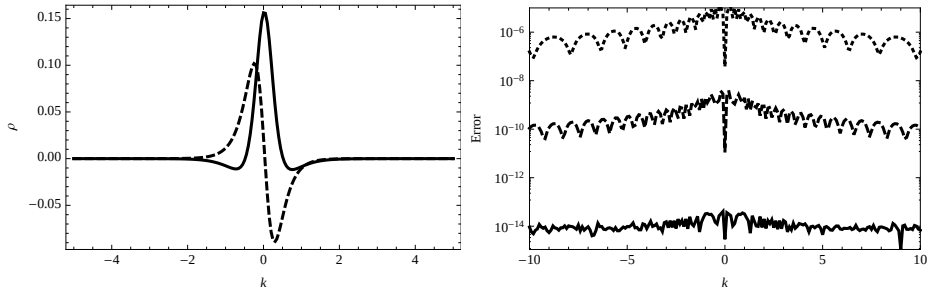

(a) (b)

Figure 7.2.1: (a) Plot of the known analytical formula for the reflection coefficient with $A = 1$ and $\mu = 0.1$ (Solid: real part, Dashed: imaginary part). (b) Demonstration of spectral convergence for the reflection coefficient (Dotted: 40 collocation points, Dashed: 80 collocation points, Solid: 120 collocation points.).

we recover the initial condition. The method has not been developed to deal with singular limits in which lots of eigenvalues are present. There is in principle no limit on card$\{\kappa_j\}$ but the computational cost grows with the size of this set.

7.2.1 Numerical results

In this section we present numerical results for direct scattering. First, we compare the result of our method with a reflection coefficient that is known analytically. Next, we present numerically computed reflection coefficients, which we use later. For the focusing NLS equation ($\lambda = 1$) the authors in [103] present an explicit reflection coefficient for initial conditions of the form

$$q_0(x) = -iA\,\mathrm{sech}(x)\exp\left(-i\mu A\log\cosh(x)\right), \quad \mu, A \geq 0. \tag{7.2.5}$$

The components of the transition matrix take the form

$$a(k) = \frac{\Gamma(w(k))\Gamma(w(k) - w_- - w_+)}{\Gamma(w - w_+)\Gamma(w - w_-)}, \qquad b(k) = iA2^{-\frac{i\mu}{2}}\frac{\Gamma(w(k))\Gamma(1 - w(k) + w_+ + w_-)}{\Gamma(w_+)\Gamma(w_-)},$$

where

$$w(k) = -ik - A\mu\frac{i}{2} + \frac{1}{2}, \quad w_+ = -iA\left(T + \frac{\mu}{2}\right), \quad w_- = iA\left(T - \frac{\mu}{2}\right), \quad \text{and} \quad T = \sqrt{\frac{\mu^2}{4} - 1}.$$

Here Γ is the Gamma function [84]. The set $\{\kappa_j\}$ is non-empty for $0 \leq \mu < 2$. Its elements are

$$\kappa_j = AT - i(j - 1/2),\ j \in \mathbb{N} \text{ and } j < 1/2 + A|T|.$$

In Figure 7.2.1 we plot the reflection coefficient for $A = 1$ and $\mu = 0.1$. These plots demonstrate spectral convergence.

In Figure 7.2.2 we show the computed reflection coefficient for $q_0(x) = 1.9\exp(-x^2 + ix)$

for both focusing and defocusing NLS. For focusing NLS we find $\kappa_1 = -0.5 + 1.11151i$, see Figure 7.2(c) for a plot of the spectrum of (7.2.4) found using Hill's method.

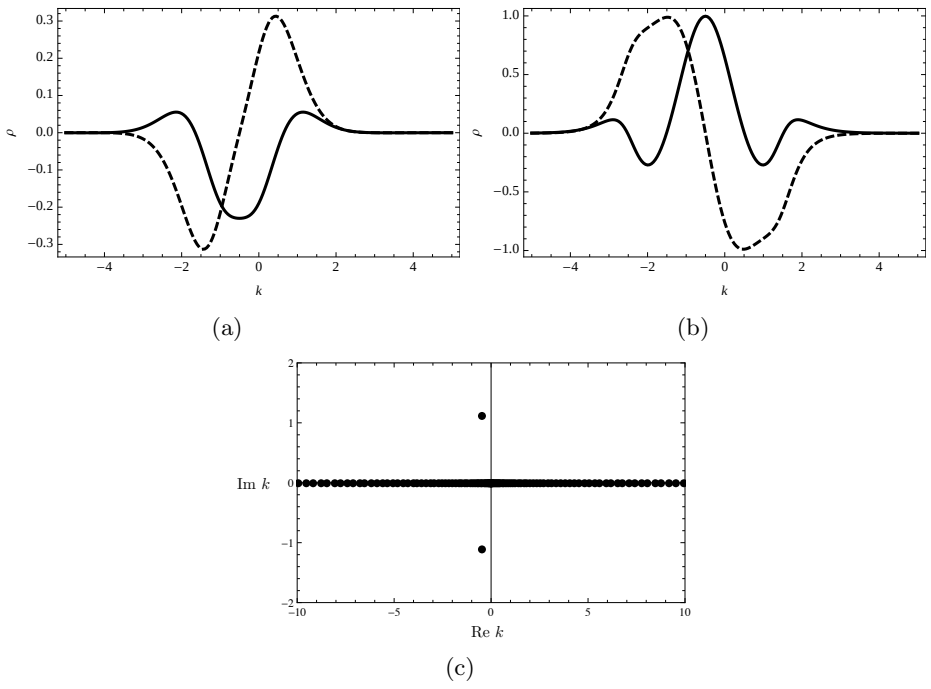

Figure 7.2.2: (a) Plot of the computed reflection coefficient for the focusing NLS equation ($\lambda = 1$) when $q_0(x) = 1.9e^{-x^2+ix}$. (Solid: real part, Dashed: imaginary part). (b) Plot of known reflection coefficient for the defocusing NLS equation ($\lambda = -1$) when $q_0(x) = 1.9e^{-x^2+ix}$. (Solid: real part, Dashed: imaginary part). (c) The spectrum of (7.2.4) found using Hill's method when $\lambda = 1$.

7.3 Numerical inverse scattering

As in the case of the KdV equation, numerical inverse scattering has two major components. The first is the use of a Chebyshev collocation method (Section 5.3) for solving RHPs and the second is the deformation of contours in the spirit of the method of nonlinear steepest descent [33]. The use of nonlinear steepest descent is essential since the jump for the RHP (7.1.7) is oscillatory for large values of x and t. An interesting and desired consequence of using nonlinear steepest descent is that the resulting numerical method is provably accurate for large values of x and t. More specifically, the computational cost to compute the solution at a given point, accurate to within a given tolerance, is shown to be independent of x and t (see Section 7.6). We use the collocation method described in Section 5.3. Additionally, we demonstrate the deformation of a the RHP. This proceeds in much the same way as in Section 4.2 and we include the full details so that this chapter may be read independently of Chapter 4.

7.3.1 Small time

When both x and t are small, the RHP needs no deformation. When t is small, but x is large, the RHP needs to be deformed. We introduce factorizations of the jump matrix. Define

$$
\begin{aligned}
G(k) &= \begin{bmatrix} 1-\lambda\overline{\rho(\bar{k})}\rho(k) & \lambda\overline{\rho(\bar{k})}e^{-\theta(k)} \\ \rho(k)e^{\theta(k)} & 1 \end{bmatrix}, M(k) = \begin{bmatrix} 1 & \lambda\overline{\rho(\bar{k})}e^{-\theta(k)} \\ 0 & 1 \end{bmatrix}, \\
P(k) &= \begin{bmatrix} 1 & 0 \\ \rho(k)e^{\theta(k)} & 1 \end{bmatrix}, \\
L(k) &= \begin{bmatrix} 1 & 0 \\ \frac{\rho(k)}{\tau(k)}e^{\theta(k)} & 1 \end{bmatrix}, \qquad D(k) = \begin{bmatrix} \tau(k) & 0 \\ 0 & 1/\tau(k) \end{bmatrix}, \\
U(k) &= \begin{bmatrix} 1 & \frac{\lambda\overline{\rho(\bar{k})}}{\tau(k)}e^{-\theta(k)} \\ 0 & 1 \end{bmatrix}, \qquad \tau(k) = 1-\lambda\rho(k)\overline{\rho(\bar{k})}.
\end{aligned}
\tag{7.3.1}
$$

Note that $G(k) = L(k)D(k)U(k) = M(k)P(k)$. We assume the sets $\{\kappa_j\}_{j=1}^n$ and $\{C_j\}_{j=1}^n$ are empty. Later, we make the proper modifications to incorporate the extra contours required.

We deform contours of (7.1.7) off the real line so that oscillations are turned to exponential decay. The matrix G contains the two factors $\exp(\pm\theta(k))$ and if one decays the other must grow. This motivates separating these factors using the process of lensing , see Section 3.10.3.

Since $q_0 \in \mathcal{S}_\delta(\mathbb{R})$ we know that (see Section 4.1) ρ is analytic in the strip $S_\gamma = \{k \in \mathbb{C} : |\operatorname{Im} k| < \gamma\}$ for $\delta/2 > \gamma > 0$. This can be seen by considering the Volterra integral equations for the eigenfunctions $\mu^\pm$. The factors in (7.3.1) allow lensing but we need to determine where to lens. We look for saddle points of the oscillator: $\theta'(k) = 0$ when $k = k_0 = -x/(4t)$. We use the LDU factorization for $k < k_0$ and MP for $k > k_0$. See Figure 7.1(b) for this deformation and note that the contours are locally deformed along the path of steepest descent, that is, the direction along with the jump matrix tends to the identity matrix most rapidly. We denote the solution of this lensed RHP by Φ_1.

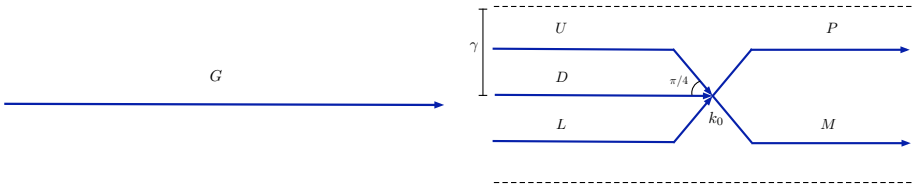

(a) (b)

Figure 7.3.1: (a) Jump contour for the initial RHP for Φ. (b) Jump contours after lensing for the RHP for Φ_1.

This RHP can be solved numerically provided t is not too large. As t increases, the solution v on the contour $(-\infty, k_0)$ is increasingly oscillatory and is not well resolved using Chebyshev polynomials.

7.3.2 Long time

Next, we provide a deformation that leads to a numerical method that is accurate for arbitrarily large x and t. In light of the results in Chapter 5, specifically Remark 5.2.13, we need to remove the contour D from the RHP so that all jumps decay to the identity matrix away from k_0 as x and t become large. The matrix-valued function

$$\Delta(k;k_0) = \begin{bmatrix} \delta(k;k_0) & 0 \\ 0 & \delta^{-1}(k;k_0) \end{bmatrix}, \qquad \delta(k;k_0) = \exp\left(\mathcal{C}_{(-\infty,k_0)}\tau(k)\right),$$

satisfies (see Section 3.4.1)

$$\Delta^+(k;k_0) = \Delta^-(k;k_0)D(k), \quad k \in (-\infty,k_0), \qquad \Delta(\infty;k_0) = I.$$

We multiply the solution of the RHP in Figure 7.1(b) by Δ^{-1} to remove the jump. To compute the solution to the new RHP we use conjugation

$$\Phi_1^+ = \Phi_1^- J \;\Leftrightarrow\; \Phi_1^+\Delta_+^{-1} = \Phi_1^- J\Delta_+^{-1} \;\Leftrightarrow\; \Phi_1^+\Delta_+^{-1} = \Phi_1^-\Delta_-^{-1}\Delta_- J\Delta_+^{-1}.$$

Indeed, we see that if $J = D$ there is no jump. Define $\Phi_2 = \Phi_1\Delta^{-1}$. See Figure 7.3.2 for a schematic overview of the new jumps. This deformation is not sufficient for a numerical solution as $\Delta(k;k_0)$ has a singularity at $k = k_0$. We must perform one last deformation in a neighbourhood of $k = k_0$ to bound contours away from this singularity. We use a piecewise definition of a function Φ_3, see Figure 7.3(a), and compute the jumps, Figure 7.3(b). This is the final RHP. It is used, after contour truncation and scaling, to compute solutions of the NLS equations for arbitrarily large time. We discuss the scaling of the RHP in more detail in Section 7.6.

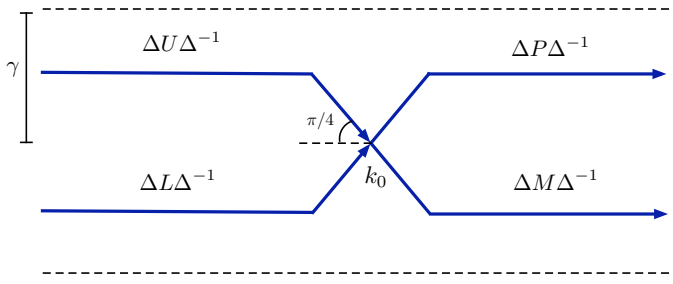

Figure 7.3.2: Removal of the jump on $(-\infty, k_0)$.

We use a combination of the deformation in Figure 7.1(b) for small time and the deformation in 7.3(b) to obtain an approximation to focusing or defocusing NLS when no solitons are present in the solution. Lastly, we deal with the addition of solitons for the

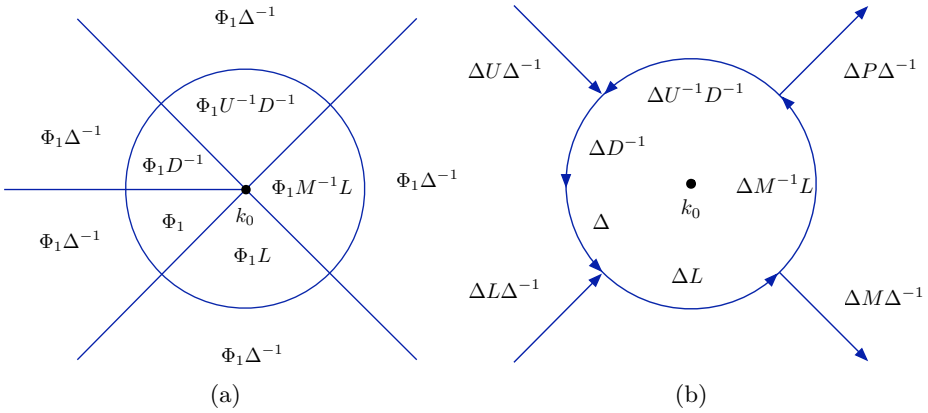

Figure 7.3.3: (a) The piecewise definition of Φ_3. (b) Jump contours and jump matrices for the RHP for Φ_3.

case of focusing NLS. There are additional jumps of the form

$$\Phi^+(k) = \begin{cases} \Phi^-(k) \begin{bmatrix} 1 & 0 \\ -C_j e^{\theta(\kappa_j)}/(k-\kappa_j) & 1 \end{bmatrix}, & \text{if } k \in A_j^+, \\ \\ \Phi^-(k) \begin{bmatrix} 1 & -\bar{C}_j e^{-\theta(\bar{\kappa}_j)}/(k-\bar{\kappa}_j) \\ 0 & 1 \end{bmatrix}, & \text{if } k \in A_j^-, \end{cases}.$$

We assume that $\mathrm{Re}(\kappa_j) > \gamma$.

For small x and t, $|e^{\theta(\kappa_j)}| = |e^{-\theta(\bar{\kappa}_j)}|$ is close to unity and the contours and jumps need to be added to one of the deformations discussed above. This will not be the case for all x and t. When $|C_j e^{\theta(\kappa_j)}| > 1$ we invert this factor through a deformation. Define the set $K_{x,t} = \{j : |C_j e^{\theta(\kappa_j)}| > 1\}$. Note that the x and t dependence enters through $\theta(\kappa_j)$. Next, define the functions

$$v(k) = \prod_{j \in K_{x,t}} \frac{k-\kappa_j}{k-\bar{\kappa}_j}, \quad \text{and} \quad V(k) = \begin{bmatrix} v(k) & 0 \\ 0 & 1/v(k) \end{bmatrix}.$$

Define the piecewise-analytic matrix-valued function $\hat{\Phi}$:

$$\hat{\Phi}(k) = \Phi(k) \begin{cases} \begin{bmatrix} 1 & -(k-\kappa_j)/(C_j e^{\theta(\kappa_j)}) \\ C_j e^{\theta(\kappa_j)}/(k-\kappa_j) & 0 \end{bmatrix} V(k), & \text{if } |k-\kappa_j| < \epsilon, \\ \\ \begin{bmatrix} 0 & -\bar{C}_j e^{-\theta(\bar{\kappa}_j)}/(k-\bar{\kappa}_j) \\ (k-\bar{\kappa}_j)/(\bar{C}_j e^{-\theta(\bar{\kappa}_j)}) & 1 \end{bmatrix} V(k), & \text{if } |k-\bar{\kappa}_j| < \epsilon, \\ \\ V(k) & \text{otherwise.} \end{cases}$$

Computing the jumps that $\hat{\Phi}$ satisfies we find, for $j \in K_{x,t}$,

$$\hat{\Phi}^+(k) = \hat{\Phi}^-(k) \begin{cases} V^{-1}(k) \begin{bmatrix} 1 & -(k-\kappa_j)/(C_j e^{\theta(\kappa_j)}) \\ 0 & 1 \end{bmatrix} V(k), & \text{if } k \in A_j^+, \\ V^{-1}(k) \begin{bmatrix} 1 & 0 \\ -(k-\bar{\kappa}_j)/(\bar{C}_j e^{-\theta(\bar{\kappa}_j)}) & 1 \end{bmatrix} V(k), & \text{if } k \in A_j^-. \end{cases}$$

This turns growth of the exponential to decay to the identity matrix. To simplify notation we define

$$T_{j,+}(k) = \begin{bmatrix} 1 & 0 \\ -C_j e^{\theta(\kappa_j)}/(k-\kappa_j) & 1 \end{bmatrix}, \qquad T_{j,-}(k) = \begin{bmatrix} 1 & -\bar{C}_j e^{-\theta(\bar{\kappa}_j)}/(k-\bar{\kappa}_j) \\ 0 & 1 \end{bmatrix}, \tag{7.3.2}$$

$$S_{j,+}(k) = \begin{bmatrix} 1 & -(k-\kappa_j)/(C_j e^{\theta(\kappa_j)}) \\ 0 & 1 \end{bmatrix}, \qquad S_{j,-}(k) = \begin{bmatrix} 1 & 0 \\ -(k-\bar{\kappa}_j)/(\bar{C}_j e^{-\theta(\bar{\kappa}_j)}) & 1 \end{bmatrix}. \tag{7.3.3}$$

In Figure 7.3.4 we present the full small-time and long-time RHPs. We use the notation $[J;\Sigma]$ to denote the RHP in Figure 7.4(b).

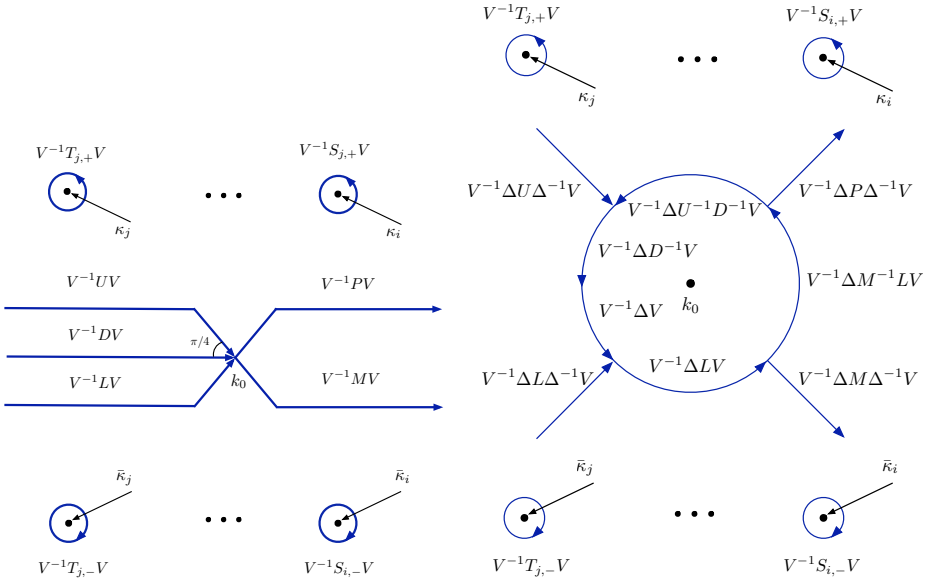

Figure 7.3.4: (a) The jump contours and jump matrices for the final deformation for small time. In this schematic $|C_j e^{\theta(\kappa_j)}| \leq 1$ and $|C_i e^{\theta(\kappa_i)}| > 1$. (b) The jump contours and jump matrices for the final deformation for large time. Again, in this schematic $|C_j e^{\theta(\kappa_j)}| \leq 1$ and $|C_i e^{\theta(\kappa_i)}| > 1$.

7.3.3 Numerical results

In Figure 7.3.5 we plot the solution of the focusing NLS equation with q_0 given by (7.2.5) with $A = 1$ and $\mu = 0.1$. The solution is nearly reflectionless but Figure 7.3.5(d) shows the important dispersive aspect of the solution. Traditional numerical methods can fail to resolve this. In Figure 7.3.7 we plot the initial condition $q_0(x) = 1.9\exp(-x^2 + ix)$. The solutions of the focusing and defocusing NLS equations with this initial condition are computed. See Figure 7.3.8 for focusing and Figure 7.3.9 for defocusing. We also note that when the initial condition is less localized the corresponding reflection coefficient is more oscillatory. This makes it more difficult to resolve the solution of the corresponding RHP. We restrict ourselves to initial data with rapid decay for this reason, *i.e.* in numerical examples we consider $q_0 \in \mathcal{S}_\delta(\mathbb{R})$ with δ large.

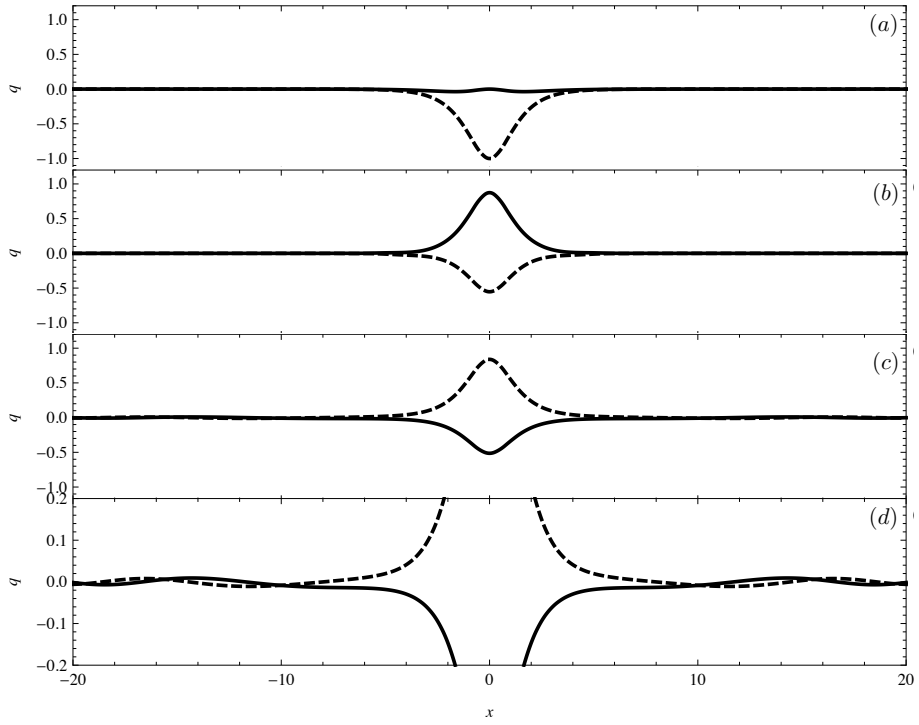

Figure 7.3.5: The solution of the focusing NLS equation with q_0 given by (7.2.5) with $A = 1$ and $\mu = .1$. (Solid: real part, Dashed: imaginary part) (a) $q(x, 0)$, (b) $q(x, 1)$, (c) $q(x, 10)$, (d) A scaled plot of $q(x, 10)$ showing the effects of dispersion. Traditional numerical methods can fail to resolve this.

We show numerical results that demonstrate spectral convergence. Let q_0 be given by (7.2.5) with $A = 1$ and $\mu = 0.1$ so that we can assume the reflection coefficient is computed to machine precision *i.e.*, $n > 80$ in Figure 7.1(b). Define $q(n, x, t)$ to be the approximate solution such that the number of collocation points per contour is proportional to n. In practice we set the number of collocation points to be n on shorter contours, like all contours in Figure 7.4(b). For larger contours, like the horizontal contours in Figure

7.4(a), we use $5n$ collocation points. To analyze the error we define

$$Q_m^n(x,t) = |q(n,x,t) - q(m,x,t)|. \tag{7.3.4}$$

Using this notation, see Figure 7.3.6 for a demonstration of spectral (Cauchy) convergence. Note that we choose x and t values to demonstrate spectral convergence in both the small time and large time regimes.

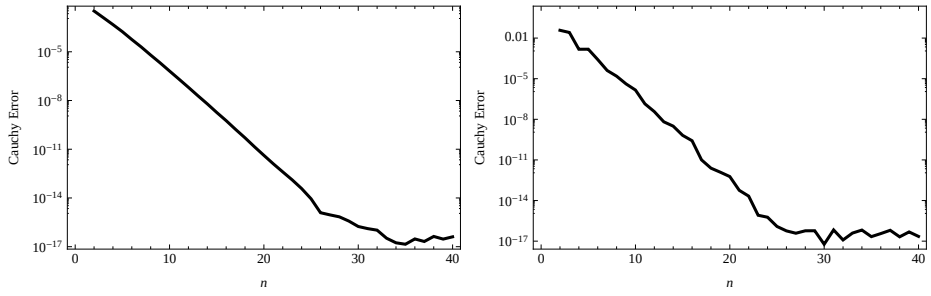

(a) (b)

Figure 7.3.6: The convergence of the numerical approximations of the solution of the focusing NLS equation with q_0 given by (7.2.5) with $A = 1$ and $\mu = .1$. (a) $Q_n^{80}(2, 0.2)$ as n ranges from 2 to 40. (b) $Q_n^{80}(110, 110)$ as n ranges from 2 to 40.

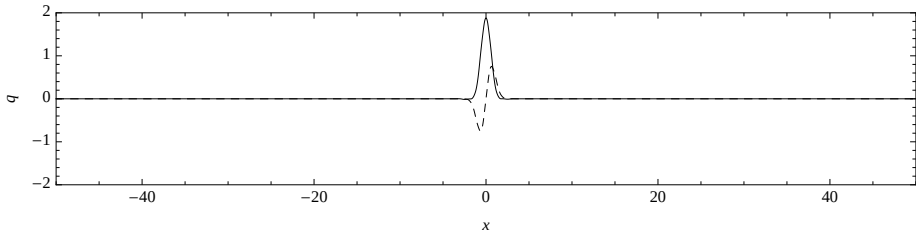

Figure 7.3.7: The initial condition $q_0(x) = 1.9e^{-x^2+ix}$. (Solid: real part, Dashed: imaginary part)

7.4 Extension to homogeneous Robin boundary conditions on the half line

Thus far, the results have been for the solution of the NLS equation posed on the whole line. We switch our attention to boundary-value problems on the half line, $x \geq 0$. Specifically, we extend the previous method to solve the following boundary-value problem:

$$\begin{aligned} iq_t + q_{xx} + 2\lambda|q|^2 q = 0, \quad \lambda = \pm 1, \\ \alpha q(0,t) + q_x(0,t) = 0, \quad \alpha \in \mathbb{R}, \\ q(x,0) = q_0(x) \in \mathcal{S}_\delta(\mathbb{R}^+), \delta > 0. \end{aligned} \tag{7.4.1}$$

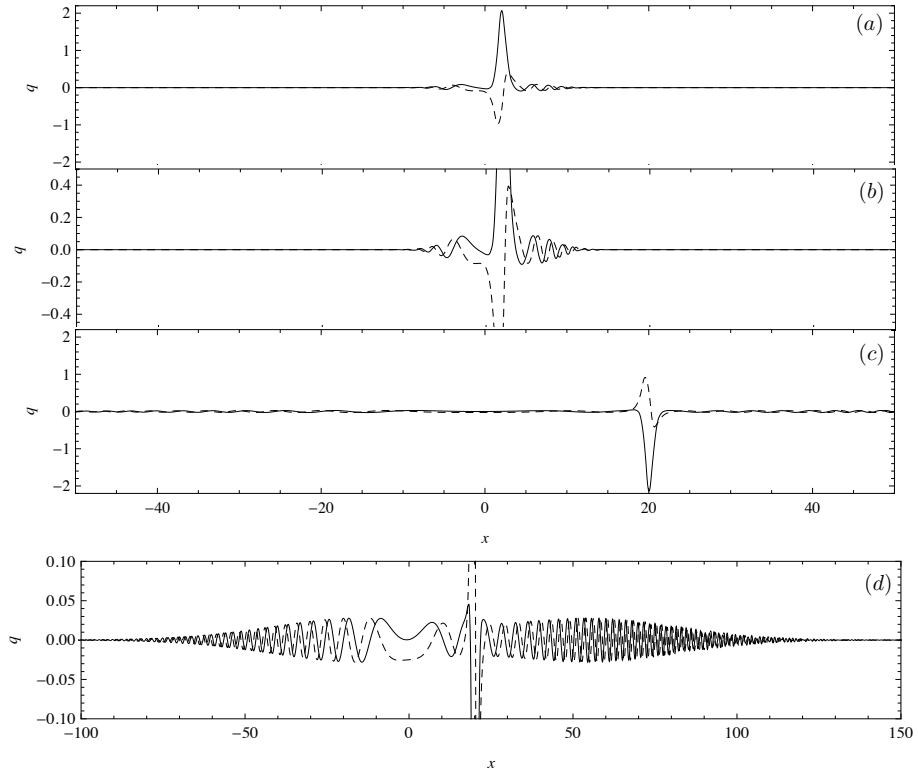

Figure 7.3.8: The solution of the focusing NLS equation with q_0 shown in Figure 7.3.7. (Solid: real part, Dashed: imaginary part) (a) $q(x,1)$ (b) A zoomed plot of $q(x,1)$ (c) $q(x,10)$ (d) A zoomed plot of $q(x,10)$, illustrating the dispersive effects in the solution.

Here $\mathcal{S}_\delta(\mathbb{R}^+)$ is the space of smooth functions f on $[0,\infty)$ such that

$$\limsup_{x\to\infty} e^{\delta x}|f(x)| < \infty.$$

If we take $\alpha = 0$ we obtain a Neumann problem. Similarly, the limit $\alpha \to \infty$ effectively produces a Dirichlet problem. A method of images approach can be used to solve this problem. The approach of Biondini and Bui [11], first introduced in [10], takes the given initial condition on $[0,\infty)$ and produces an extension to $(-\infty,0)$ using a Darboux transformation. For Neumann boundary conditions this results in an even extension and for Dirichlet boundary conditions the transformation produces an odd extension. Consider the system of ODEs

$$\begin{aligned} Y_1' &= Y_2, \\ Y_2' &= (4\lambda|q_0|^2 + \alpha^2)Y_1 - \lambda\bar{q}_0 Y_3 - q_0 Y_4, \\ Y_3' &= 2q_0' Y_1, \\ Y_4' &= 2\lambda\bar{q}_0' Y_1, \end{aligned} \tag{7.4.2}$$

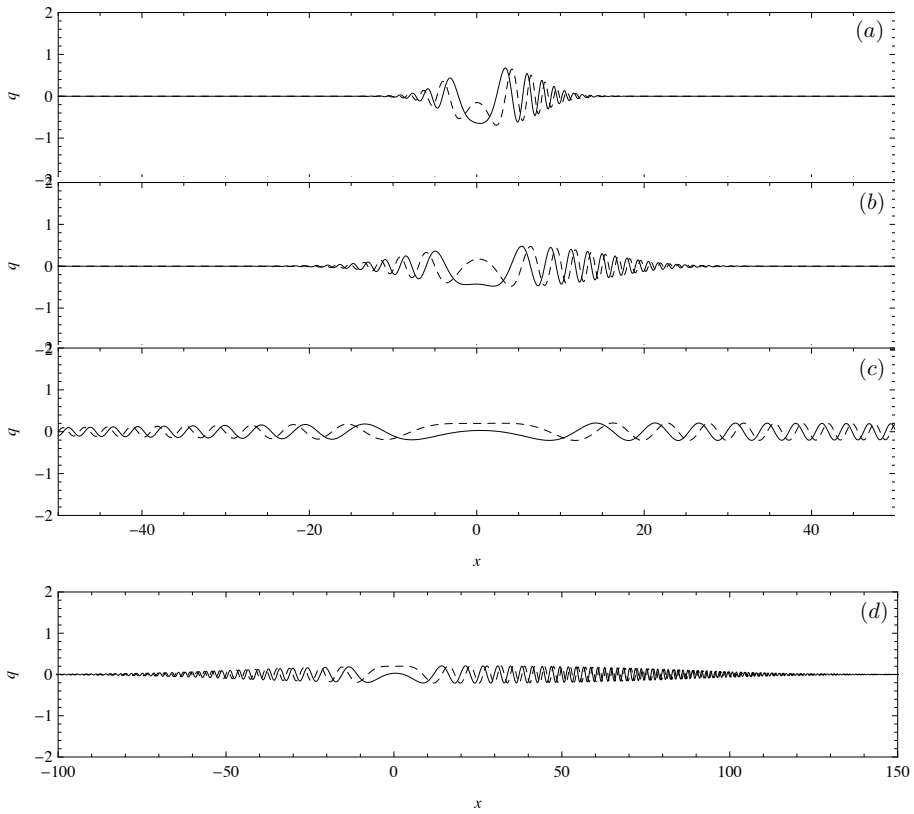

Figure 7.3.9: The solution of the defocusing NLS equation with q_0 shown in Figure 7.3.7. (Solid: real part, Dashed: imaginary part) (a) $q(x,1)$, (b) $q(x,2)$, (c) $q(x,10)$, (d) A scaled plot of $q(x,10)$ showing the dramatic effects of dispersion.

with initial conditions

$$\begin{aligned} Y_1(0) &= 1, \\ Y_2(0) &= -\alpha, \\ Y_3(0) &= 2q_0(0), \\ Y_4(0) &= 2\lambda\bar{q}_0(0), \end{aligned}$$

and the function

$$\tilde{q}(x) = \begin{cases} q_0(x), & \text{if } x \in [0,\infty), \\ -q_0(-x) + Y_3(x)/Y_1(x), & \text{if } x \in (-\infty,0). \end{cases}$$

It was shown in [11] that the solution of the Cauchy problem for NLS equation on $\mathbb{R}$ with initial data $\tilde{q}$, restricted to $[0,\infty)$, is the unique solution of (7.4.1). To compute the extended initial data $\tilde{q}$ we first solve the system (7.4.2) numerically using a combination of Runge–Kutta 4 and 5. This is implemented in `NDSolve` in `Mathematica`. The inverse scattering transform for the extended potential can be used in the previous section's framework to numerically solve (7.4.1).

Remark 7.4.1. *The method of Bikbaev and Tarasov [10] was used to derive asymptotics by Deift and Park in [31]. Another approach would be to use the method of Fokas to compute solutions [49, 65].*

7.4.1 Numerical results

In this section we show numerical results for a Robin problem and a Neumann problem. As noted above, we could treat the Dirichlet problem by using an odd extension of our initial condition.

- **Robin boundary conditions** Here we show results for the case of the focusing NLS equation ($\lambda = 1$) with $\alpha = -1$ and with initial condition $q_0(x) = 1.9\exp(-x^2 + x)$. Note that the initial condition satisfies the boundary condition at $t = 0$. In Figure 7.1(a), we give the extended initial condition $\tilde{q}$ and in Figure 7.1(b) we show the corresponding reflection coefficient. For this extended initial condition, we have four poles on the imaginary axis in the RHP which corresponds to two stationary solitons:

$$\kappa_1 = 1.84725i, \quad C_1 = -14.4092i, \quad \kappa_2 = 1.21265i, \quad C_2 = -8.17034i.$$

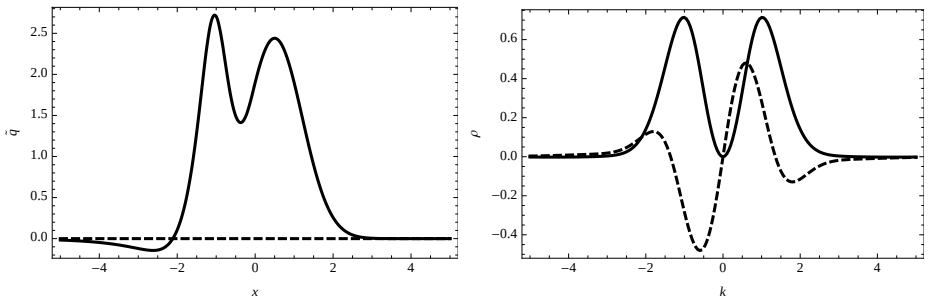

(a) (b)

Figure 7.4.1: (a) The extended initial condition $\tilde{q}$ (Solid: real part, Dotted: imaginary part). (b) The reflection coefficient for the extended initial condition $\tilde{q}$. (Solid: real part, Dotted: imaginary part)

- **Neumann boundary conditions** To show the reflection of a soliton off the boundary at $x = 0$ we solve a Neumann problem ($\alpha = 0$) with initial condition $q_0(x) = 1/2x^2\exp(-.2x^2 - ix)$. The extension $\tilde{q}$ of the initial condition can be seen in Figure 7.3(a). In this case it is just the even extension. The scattering data consists of

$$\kappa_1 = 0.497613 + 0.371208, \quad C_1 = 0.110159 + 5.35099i,$$
$$\kappa_2 = -0.497613 + 0.371208, \quad C_2 = -0.231104 - 0.0357421i.$$

  This shows that we have a pair of poles in the RHP to the right of the imaginary axis and two to left. This corresponds to one soliton moving to the left and one soliton moving to the right. The reflection coefficient is shown in Figure 7.3(b).

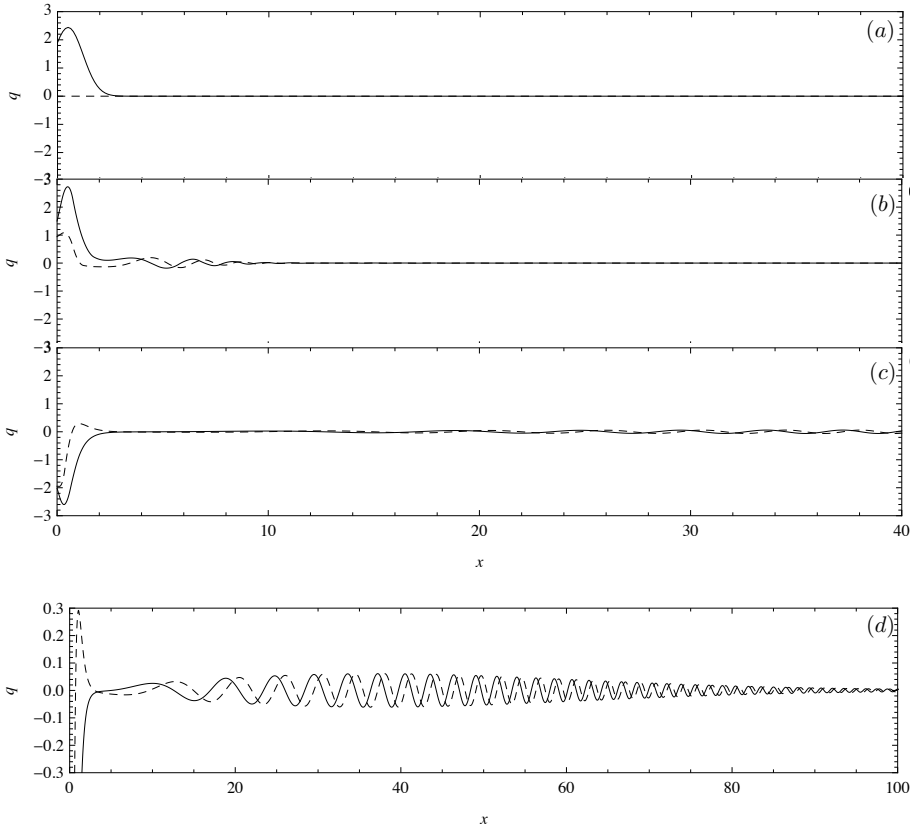

Figure 7.4.2: The solution of the focusing NLS equation with Robin boundary conditions ($\alpha = 1$) and with q_0 shown in Figure 7.1(a). (Solid: real part, Dashed: imaginary part) (a) $q(x,0)$ (b) $q(x,1)$ (c) $q(x,10)$ (d) A scaled plot of $q(x,10)$ showing the extent of the dispersive tail.

7.5 Singular solutions

As mentioned above the defocusing NLS equation does not have soliton solutions that decay at infinity. We can insert the contours $A_j^{\pm}$ (see (7.1.8)) into the RHP anyway. We introduce λ into (7.3.2) to obtain appropriate jump conditions for the defocusing NLS equations. Define

$$T_{j,+}(k) = \begin{bmatrix} 1 & 0 \\ -C_j e^{\theta(\kappa_j)}/(k-\kappa_j) & 1 \end{bmatrix}, \qquad T_{j,-}(k) = \begin{bmatrix} 1 & -\lambda \bar{C}_j e^{-\theta(\bar{\kappa}_j)}/(k-\bar{\kappa}_j) \\ 0 & 1 \end{bmatrix},$$
$$S_{j,+}(k) = \begin{bmatrix} 1 & -(k-\kappa_j)/(C_j e^{\theta(\kappa_j)}) \\ 0 & 1 \end{bmatrix}, \qquad S_{j,-}(k) = \begin{bmatrix} 1 & 0 \\ -\lambda(k-\bar{\kappa}_j)/(\bar{C}_j e^{-\theta(\bar{\kappa}_j)}) & 1 \end{bmatrix}.$$

When $\lambda = 1$ (focusing) this definition agrees with (7.3.2).

When $\lambda = -1$ (defocusing) we investigate how these additional contours will manifest themselves in the solution. Consider

$$u_1(x,t) = 2\eta e^{-4it(\xi^2-\eta^2)-2ix\xi}\,\mathrm{sech}(2\eta(4t\xi + x - x_0)),$$

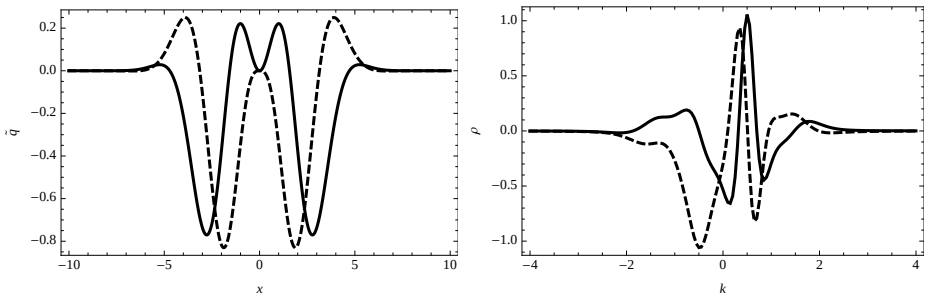

(a) (b)

Figure 7.4.3: (a) The extended initial condition $\tilde{q}$ (Solid: real part, Dotted: imaginary part). (b) The reflection coefficient for the extended initial condition $\tilde{q}$. (Solid: real part, Dotted: imaginary part)

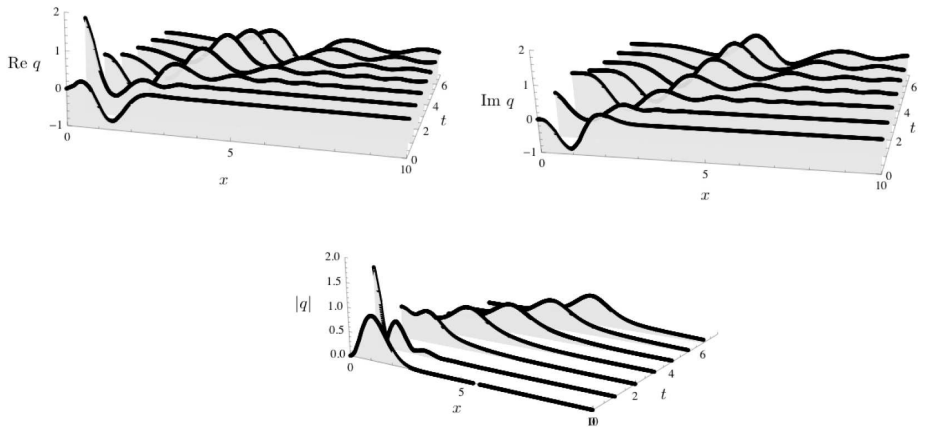

Figure 7.4.4: The solution of the focusing NLS equation with Neumann boundary ($\alpha = -1$) conditions and q_0 shown in Figure 7.3(a). The solution is shown up to $t = 7$.

which is the one soliton solution of the focusing NLS equation [2]. A simple calculation shows that

$$u_2(x,t) = 2\eta e^{-4it(\xi^2-\eta^2)-2ix\xi}\text{csch}(2\eta(4t\xi + x - x_0)),$$

is a solution of defocusing NLS. We are using the term solution loosely since this function has a pole when $4t\xi + x - x_0 = 0$. We call this a singular solution or singular soliton. These solutions are also called *positons* [43]. Reference [43] contains a deeper discussion of these solutions with applications to rogue waves.

What we obtain when adding the above contours to the RHP associated with the defocusing NLS equation is a nonlinear combination of these singular solutions in the presence of dispersion, as in the focusing case where the soliton was nonsingular. See Figure 7.5.1 for plots of a solution obtained using the reflection coefficient in Figure 7.2.2

along with

$$\kappa_1 = 2 + 2i, \quad C_1 = 1000, \quad \kappa_2 = -2 + 2i, \quad C_2 = 1/1000.$$

This corresponds to two of these singular solitons moving toward each other, until they bounce off each other (the poles never cross). They interact in the presence of dispersion. We choose large and small norming constants to have the solitons away from $x = 0$ when $t = 0$. It is not possible to obtain these types of solutions with traditional numerical methods. Not surprisingly, the relative accuracy of our numerical approximation breaks down near the poles. For points bounded away from the poles we still expect uniform convergence as discussed in the following section.

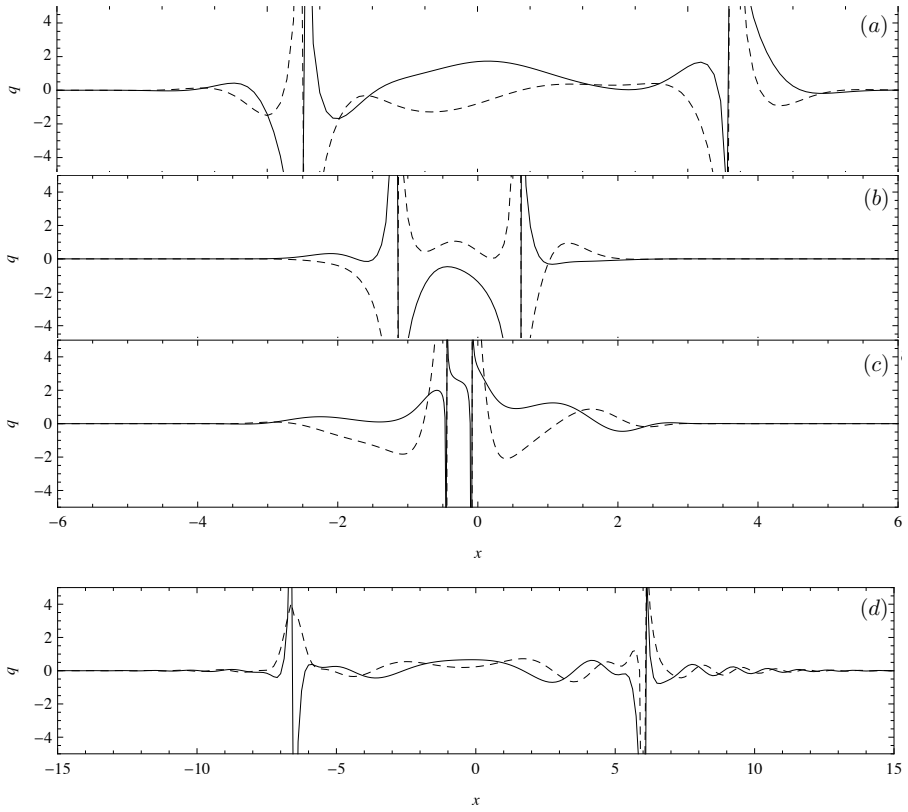

Figure 7.5.1: A singular solution of the defocusing NLS equation. Note that the vertical lines are asymptotes. (Solid: real part, Dashed: imaginary part) (a) $q(x, 0)$ (b) $q(x, 0.1)$ (c) $q(x, 0.2)$, showing the interaction of the singular solutions. (d) $q(x, 1)$, after the two poles have bounced off each other and a significant amount of dispersion is present.

7.6 Accuracy uniform in x and t

In this section we use the theory of Chapter 5 to prove the accuracy of the numerical method for arbitrarily large time when it is applied to $[J; \Sigma]$ in Figure 7(b). We assume the contours of the RHP are truncated according to Proposition 3.10.4. Define $\Sigma_1 = \bigcup_j (A_j^+ \cup A_j^-)$ and

$\Sigma_2 = \Sigma \setminus \Sigma_1$. Define the restrictions of J:

$$J_1(k) = J(k)|_{\Sigma_1},$$
$$J_2(k) = J(k)|_{\Sigma_2}.$$

We introduce some x- and t-independent domains Ω_1 and Ω_2:

$$\Sigma_1 = \frac{\Omega_1}{\sqrt{t}} - \frac{x}{4t},$$
$$\Sigma_2 = \Omega_2.$$

We use the change of variables

$$k = \frac{z}{\sqrt{t}} - \frac{x}{4t}, \tag{7.6.1}$$

and the notation $\tilde{J}_1(z) = J_1(z/\sqrt{t} - x/(4t))$. Fix the trajectory in the (x,t) plane: $x = c4t$. We wish to use Algorithm 5.1.11. First, we numerically solve $[\tilde{J}_1, \Omega_1]$ with n collocation points to obtain a solution $\tilde{\Phi}_{1,n}$. The change of variables (7.6.1) is inverted, defining

$$\Phi_{1,n}(k) = \tilde{\Phi}_{1,n}\left(\sqrt{t}(k - k_0)\right).$$

Define $\tilde{J}_{2,n}(k) = \Phi_{1,n}(k) J_2(k) \Phi_{1,n}^{-1}(k)$. Then $[\tilde{J}_{2,n}, \Omega_2]$ is solved numerically with n collocation points (for simplicity) to obtain a function $\Phi_{2,n}$. Note that there is no change of variables to invert for this RHP. The function $\Phi_n = \Phi_{1,n}\Phi_{2,n}$ is an approximation of the solution to the full RHP $[J; \Sigma]$.

Since the arc length of Σ_1 tends to zero for large t, the conditions we check are the hypotheses of Theorem 5.2.4 (or Proposition 5.2.11):

- $\mathcal{C}[\tilde{J}_1; \Omega_1]^{-1}$ exists and is uniformly bounded in t,
- $\mathcal{C}[J_2; \Omega_2]^{-1}$ exists and is uniformly bounded in t, and
- all derivatives of $\tilde{J}_1(z)$ and $J_2(z)$, in the z variable, are uniformly bounded in t and z.

It is easy to see that all derivatives of $V^{-1}T_{j,\pm}V$ and $V^{-1}S_{j,\pm}V$ will be uniformly bounded. The transformation from $T_{j,\pm}$ to $S_{j,\pm}$ guarantees this.

The only possible singular behavior of $\tilde{J}_1$ will come from either the terms $\exp(\pm\theta(k))$ or from $\Delta(k; k_0)$. We proceed to show that under the chosen scaling, all derivatives of these two functions are bounded. From the definition of θ,

$$\theta(k) = 2i(c4tk + 2tk^2) = -4ic^2t + 4iz^2.$$

We see that all derivatives $\exp(\tilde{\theta}(z))$ are bounded as long as z is bounded.

Now we consider $\Delta(k; k_0)$ in a neighborhood of k_0. We need to bound derivatives of

$\exp(Y(k))$ where

$$Y(k) = \frac{1}{2\pi i}\int_{-\infty}^{k_0} \frac{f(s)}{s-k} ds, \quad f(s) = \log(1-\lambda\rho(s)\overline{\rho(s)}),$$

because it appears in Δ. We first note that $\exp(Y(k))$ is bounded for all k since $f(s)$ is real valued. Now, since the Cauchy integral is invariant under a conformal change of variables that leaves infinity fixed, we have

$$\begin{aligned}
\tilde{Y}(z) &= \frac{1}{2\pi i}\int_{-\infty}^{0} \frac{\tilde{f}(s)}{s-z} ds, \\
\tilde{f}(s) &= f(s/\sqrt{t} - x/(4t)), \quad \tilde{Y}(z) = Y(z/\sqrt{t} - x/(4t)).
\end{aligned}$$

From [78] (see also [90]) we have

$$\begin{aligned}
\tilde{Y}^{(j)}(z) &= \frac{1}{2\pi i}\left(\int_{-\infty}^{0} \frac{\tilde{f}^{(j)}(s)}{s-z} ds - \sum_{i=1}^{j} \frac{\tilde{f}^{(j-i)}(0)}{(-z)^{i+1}}\right), \\
\tilde{f}^{(j)}(0) &= f^{(j)}\left(-\frac{x}{4t}\right) t^{-j/2}.
\end{aligned}$$

From the assumption that ρ is analytic and decays in a strip containing the real line we see that all derivatives of $\tilde{Y}$ are uniformly bounded in t.

As stated, the analysis in [90] requires that the singular integral operators on Ω_i have uniformly bounded inverses as t becomes large. We describe how this follows from the asymptotic analysis of the RHP [38, 36]. A very useful fact is that once the solution Ψ of the RHP $[G;\Gamma]$ is known then the inverse of the operator is also known [24] (see also Lemma 3.8.18):

$$\mathcal{C}[G;\Gamma]^{-1}u = \mathcal{C}_\Gamma^+[u(\Psi^+)^{-1}]\Psi^+ - \mathcal{C}_\Gamma^-[u(\Psi^+)^{-1}]\Psi^-. \tag{7.6.2}$$

If $\Psi \in L^\infty(\Gamma)$ then the inverse operator is bounded on $L^2(\Gamma)$. We show that $\mathcal{C}[\tilde{J}_1;\Omega_1]$ is close in operator norm (uniformly in t) to an operator with an explicit inverse that can be bounded uniformly in t using (7.6.2).

To construct the operator with an explicit inverse we follow the construction in Section 4.2. We factor off the singular behavior of $\Delta(k;k_0)$:

$$\begin{aligned}
\Delta(k;k_0) &= \Delta_s(k;k_0)\Delta_r(k;k_0), \\
\Delta_s(k;k_0) &= \mathrm{diag}((k_0-k)^{f(k_0)/(2\pi i)}, (k_0-k)^{-f(k_0)/(2\pi i)}), \\
\Delta_r(k;k_0) &\text{ is Hölder continuous at } k=k_0.
\end{aligned}$$

Define (compare with (7.3.1))

$$[M](k) = \begin{bmatrix} 1 & \lambda\overline{\rho(\bar{k}_0)}e^{-\theta(k)} \\ 0 & 1 \end{bmatrix}, \qquad [P](k) = \begin{bmatrix} 1 & 0 \\ \rho(k_0)e^{\theta(k)} & 1 \end{bmatrix},$$
$$[L](k) = \begin{bmatrix} 1 & 0 \\ \frac{\rho(k_0)}{\tau(k_0)}e^{\theta(k)} & 1 \end{bmatrix}, \qquad [D](k) = \begin{bmatrix} \tau(k_0) & 0 \\ 0 & 1/\tau(k_0) \end{bmatrix}, \tag{7.6.3}$$
$$[U](k) = \begin{bmatrix} 1 & \frac{\lambda\overline{\rho(\bar{k}_0)}}{\tau(k_0)}e^{-\theta(k)} \\ 0 & 1 \end{bmatrix}, \qquad [\Delta](k;k_0) = \Delta_s(k;k_0)\Delta_r(k_0;k_0).$$

We define a RHP $[[\tilde{J}_1];\Omega_1]$ by replacing each appearance of M, P, L, D and U in $\tilde{J}_1$ with $[M], [P], [L], [D]$ and $[U]$, respectively. If we assume $|k_0| \leq C$, $C > 0$, the analyticity of ρ along with the Hölder continuity of Δ_r imply that $\|\tilde{J}_1 - [\tilde{J}_1]\|_\infty \to 0$ and therefore $\mathcal{C}[\tilde{J}_1;\Omega_1] - \mathcal{C}[[\tilde{J}_1];\Omega_1] \to 0$ in operator norm. If we extend Ω_1 using augmentation (Section 3.10) so that the outward rays are infinite then $\mathcal{C}[[\tilde{J}_1];\Omega_1]^{-1}$ can be constructed explicitly out of Parabolic Cylinder functions [38] and is uniformly bounded in t. After this extension $\mathcal{C}[\tilde{J}_1;\Omega_1] - \mathcal{C}[[\tilde{J}_1];\Omega_1] \to 0$ continues to hold so we may ignore extensions/truncations and $\mathcal{C}[\tilde{J}_1;\Omega_1]^{-1}$ is uniformly bounded in t, for t sufficiently large.

The RHP $[J_2, \Omega_2]$ has rational jump matrices and can be solved explicitly [3, p. 83]. The uniform boundedness of $\mathcal{C}[J_2,\Omega_2]^{-1}$ can be established by studying the explicit solution. If the set $\{\kappa_j\}$ is large then an asymptotic approach like [60] to show the solitons separate may be more appropriate. Full details of this are beyond the scope of this chapter.

While we made the restriction $x = 4ct$ above, the bounds on derivatives and operators can be taken to be independent of c for $|c| \leq C$. Define W^i to be the exact solution of the SIE on Ω_i and W_n^i to be its approximation with n collocation points per contour. From Theorem 5.2.4 we have proved the following:

Theorem 7.6.1 (Uniform approximation)**.** *Fix $T > 0$ and $C > 0$. For every $\epsilon > 0$ there exists $N > 0$ such that for $n > N$ and $t > T$*

$$\|W_n^i - W^i\|_{L^2(\Omega_i)} < \epsilon, i = 1, 2 \text{ if } |k_0| \leq C.$$

Since the arc length of the contours is bounded we have uniform $L^1(\Gamma)$ convergence and (5.3.8) demonstrates that $q(x,t)$ is approximated uniformly.

Remark 7.6.2. *This theorem relies heavily on Assumption 5.3.11. If Assumption 5.3.11 fails to be true the numerical method may not converge.*

Remark 7.6.3. *The results of [36, 38, 40] only apply to the defocusing NLS equation. The difficulty with the focusing NLS equation is the lack of information about $\{\kappa_j\}$ and possible accumulation points on the real line [25]. We are considering cases where we assume $\{\kappa_j\}$ are known (again see [25]) and the analysis proceeds in a way similar to the defocusing NLS equation.*

Remark 7.6.4. *Despite the fact that the theorem restricts to $|k_0| < C$ we still obtain uniform convergence. If $q_0(x) \in \mathcal{S}_\delta(\mathbb{R})$, for every $\epsilon > 0$ there exists $C > 0$ such that for $|k_0| > C$, $|q(x,t)| < \epsilon$ [38]. Thus we approximate the solution with zero when $|k_0| > C$.*

7.6.1 Numerical results

To demonstrate asymptotic accuracy we use the notation in (7.3.4) and fix n and m. We let x and t become large along a specific trajectory. For our purposes we use $x = 4t$. Note that along this trajectory q is on the order of $1/\sqrt{t}$ [115] (see also [38, 36, 35]). This allows us to estimate the relative error. See Figure 7.6.1 for a demonstration of the accuracy of the method for large x and t. We see that the relative error is bounded and small using relatively few collocation points.

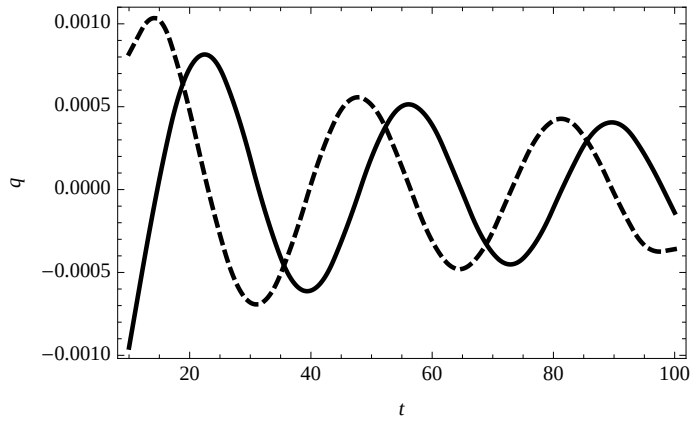

(a)

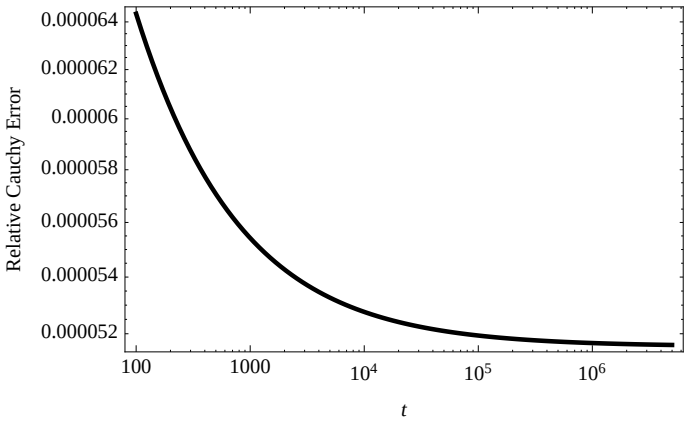

(b)

Figure 7.6.1: Asymptotic computations of solutions of the focusing NLS equation with q_0 given by (7.2.5) with $A = 1$ and $\mu = .1$. (Solid: real part, Dashed: imaginary part) (a) $q(8, 4t, t)$. (b) $Q_8^{16}(4t, t) \cdot t^{1/2}$ for large values of t.

Chapter 8

The Painlevé II Transcendents

Here we focus on the (homogeneous) Painlevé II ODE:

$$\frac{d^2u}{dx^2} = xu + 2u^3. \tag{8.0.1}$$

(For brevity we refer to the homogeneous Painlevé II equation simply as Painlevé II.) There are many important applications of this equation: the Tracy–Widom distribution (see Chapter 10) from random matrix theory is written in terms of the Hastings–McLeod solution [63] and, as we have seen, asymptotic solutions to the Korteweg–de Vries and modified Korteweg–de Vries equations can be written in terms of Ablowitz–Segur solutions [5]. The aim of this chapter is to demonstrate that the RH formulation can indeed be used effectively to compute solutions to Painlevé II.

8.1 General comments

Solutions to differential equations such as (8.0.1) are typically defined by initial conditions; at a point x we are given $u(x)$ and $u'(x)$. In the RH formulation, however, we do not specify initial conditions. Rather, the solution is specified by the *Stokes constants*; s_1, s_2, s_3 which satisfy the following condition:

Assumption 8.1.1.

$$s_1 - s_2 + s_3 + s_1 s_2 s_3 = 0. \tag{8.1.1}$$

We treat the Stokes' constants as given, as, in applications they arise naturally while initial conditions do not. Given such constants, we denote the associated solution to (8.0.1) by

$$P_{\mathrm{II}}(s_1, s_2, s_3; x). \tag{8.1.2}$$

The solution P_{II} and its derivative can be viewed as the special function which map Stokes' constants to initial conditions.

In this chapter we develop techniques to accurately and efficiently compute the Ablowitz–Segur and Hastings–McLeod solutions. For these solutions $s_2 = 0$, and $s_1 = -s_3 \in i\mathbb{R}$.

Thus we are interested in computing

$$P_{\mathrm{II}}(-i\alpha, 0, i\alpha; x), \quad \alpha \in \mathbb{R}.$$

Note that these are the solutions that appear in the asymptotic analysis of solutions of the KdV equation. We will see that for $s_2 = 0$ and $x > 0$ the method extends to general s_1, s_3 with no extra work. We break the $x < 0$ case into two subcases:

1. Case 1: $1 - s_1 s_3 > 0$ and
2. Case 2: $1 - s_1 s_3 = 0$.

For Case 1 we perform the deformation for $s_2 \in \mathbb{C}$, $1 - s_1 s_3 > 0$ and Assumption 8.1.1. Thus we obtain Case 1 with $s_2 = 0$ and $s_3 \in i\mathbb{R}$ as a special case. Case 2 is dealt with by assuming $s_2 = 0$. Either way, the deformation and computations are more complex when $x < 0$.

At first glance, computing the solutions to (8.0.1) appears trivial: given initial conditions, simply use one's favorite time-stepping algorithm, or better yet, input it into an ODE toolbox such as MATLAB's `ode45` or MATHEMATICA's `NDSolve`. Unfortunately, several difficulties immediately become apparent. In Figure 8.1.1, we plot several solutions to (8.0.1) (computed using the RH approach we are advocating): the Hastings–McLeod solution and perturbations of the Hastings–McLeod solution. Note that the computation of the solution is inherently unstable, and small perturbations cause oscillations — which make standard ODE solvers inefficient — and poles — which completely break such ODE solvers (though this issue can be resolved using the methodology of [54]).

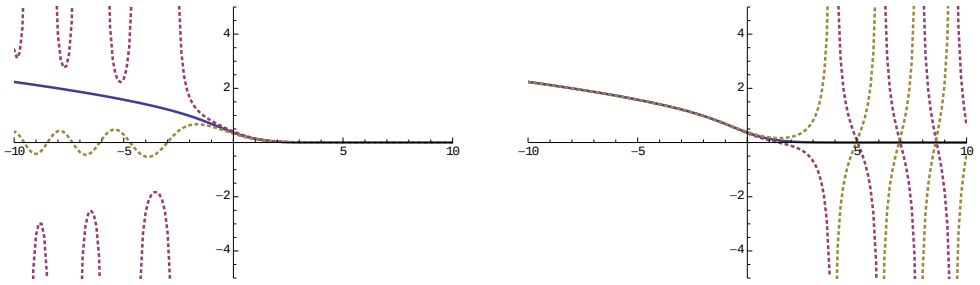

Figure 8.1.1: Solutions to Painlevé II. (a) Radically different solutions for $x < 0$. (b) Radically different solutions for $x > 0$.

Remark 8.1.2. *There are many other methods for computing the Tracy-Widom distribution itself as well as the Hastings–McLeod solution [13, 14], based on the Fredholm determinant formulation for solving a boundary value problem. Moreover, accurate data values have been tabulated using high precision arithmetic with a Taylor series method [95, 96]. However, we will see that there is a whole family of solutions to Painlevé II which exhibit similar sensitivity to initial conditions, and thus a reliable, general numerical method is needed even for this case.*

We present the RHP for the solution of Painlevé II (8.0.1). Let $\Gamma = \Gamma_1 \cup \cdots \cup \Gamma_6$ with $\Gamma_i = \{se^{i\pi(i/3-1/6)} : s \in \mathbb{R}^+\}$, *i.e.*, Γ consists of six rays emanating from the origin, see Figure 8.1.2. The jump matrix is defined by $G(\lambda) = G_i(\lambda)$ for $\lambda \in \Gamma_i$, where

$$G_i(x;\lambda) = G_i(\lambda) = \begin{cases} \begin{bmatrix} 1 & s_i e^{-i8/3\lambda^3 - 2ix\lambda} \\ 0 & 1 \end{bmatrix}, & \text{if } i \text{ is even,} \\ \begin{bmatrix} 1 & 0 \\ s_i e^{i8/3\lambda^3 + 2ix\lambda} & 1 \end{bmatrix}, & \text{if } i \text{ is odd.} \end{cases}$$

From the solution Φ of $[G;\Gamma]$, the Painlevé function is recovered by the formula

$$u(x) = \lim_{z\to\infty} z\Phi_{12}(z),$$

where the subscripts denote the $(1,2)$ entry. This RHP was solved numerically in [87] for small $|x|$.

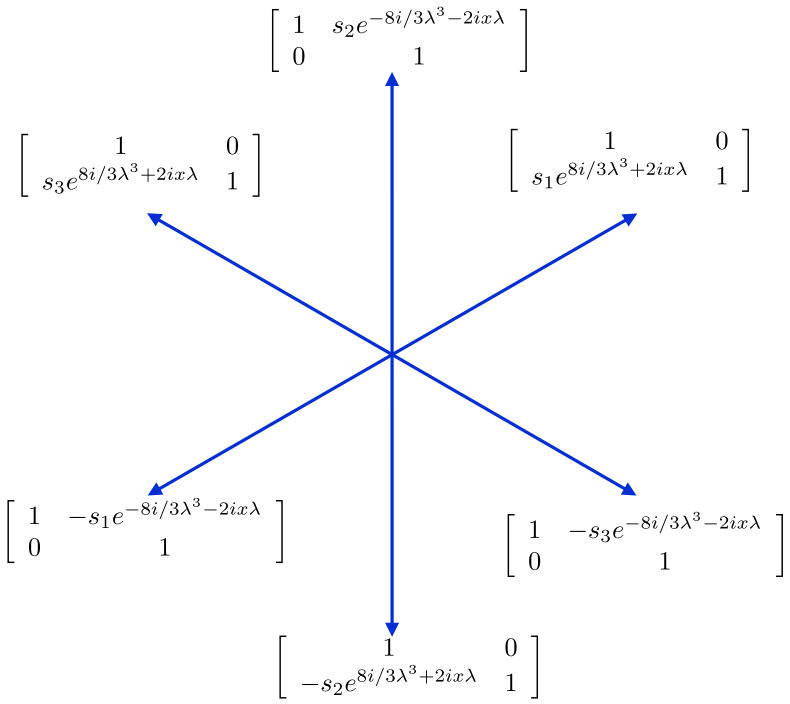

Figure 8.1.2: The contour and jump matrix for the Painlevé IIRHP.

For large $|x|$, the jump matrices G are increasingly oscillatory. We combat this issue by deforming the contour so that these oscillations turn to exponential decay. To simplify this procedure, and to start to mold the RHP into the abstract form in Section 5.2, we first rescale the RHP. If we let $z = \sqrt{|x|}\lambda$, then the jump contour Γ is unchanged, and

$$\Phi^+(z) = \Phi^+(\sqrt{|x|}\lambda) = \Phi^-(\sqrt{|x|}\lambda)G(\sqrt{|x|}\lambda) = \Phi^-(z)G(z),$$

where $G(z) = G_i(z)$ on Γ_i with

$$G_i(z) = \begin{cases} \begin{bmatrix} 1 & s_i e^{-\xi\theta(z)} \\ 0 & 1 \end{bmatrix}, & \text{if } i \text{ is even,} \\ \begin{bmatrix} 1 & 0 \\ s_i e^{\xi\theta(z)} & 1 \end{bmatrix}, & \text{if } i \text{ is odd,} \end{cases}$$

$\xi = |x|^{3/2}$ and

$$\theta(z) = \frac{2i}{3}\left(4z^3 + 2e^{i\arg x} z\right).$$

Then

$$u(x) = \lim_{\lambda\to\infty} \lambda\Phi_{12}(x;\lambda) = \sqrt{x} \lim_{\lambda\to\infty} z\Phi_{12}(x;z). \tag{8.1.3}$$

8.2 Positive x, $s_2 = 0$ and $0 \le 1 - s_1 s_3 \le 1$

We deform the RHP for Painlevé II so that numerics are asymptotically stable for positive x. We will see that the deformation is extremely simple under the following relaxed assumption:

Assumption 8.2.1. *$x > 0$ and $s_2 = 0$*

We remark that, unlike other deformations, the following deformation can be easily extended to achieve asymptotic stability for x in the complex plane such that $-\frac{\pi}{3} < \arg x < \frac{\pi}{3}$.

On the undeformed contour, $e^{\pm i|x|^{3/2}\theta(z)}$ are oscillatory as $|x|$ becomes large. However, with the right choice of curve $h(t)$, $e^{\pm i\theta(h(t))}$ has no oscillations; instead, it decays exponentially fast as $t \to \infty$. But h is precisely the path of steepest descent, which passes through the saddle points of θ, *i.e.*, the points where the derivative of θ vanishes. We readily find that

$$\theta'(z) = 2(4z^2 + 1),$$

and the saddle points are precisely $z = \pm i/2$.

We note that, since $G_2 = I$, when we deform Γ_1 and Γ_3 through $i/2$ they become completely disjoint from Γ_4 and Γ_6, which we deform through $-i/2$. We point out that $G_3^{-1} = G_1$ and $G_6^{-1} = G_4$; thus we can reverse the orientation of Γ_3 and Γ_4, resulting in the jump G_1 on the curve $\Gamma_\uparrow$ and G_4 on $\Gamma_\downarrow$, as seen in Figure 8.2.1.

Recall that

$$\theta\left(\pm\frac{i}{2}\right) = \pm\frac{i}{3}.$$

However, we now only have $\Gamma_\uparrow$ emanating from $i/2$, with jump matrix

$$G_1 = \begin{bmatrix} 1 & 0 \\ s_1 e^{i|x|^{3/2}\theta(z)} & 1 \end{bmatrix}.$$

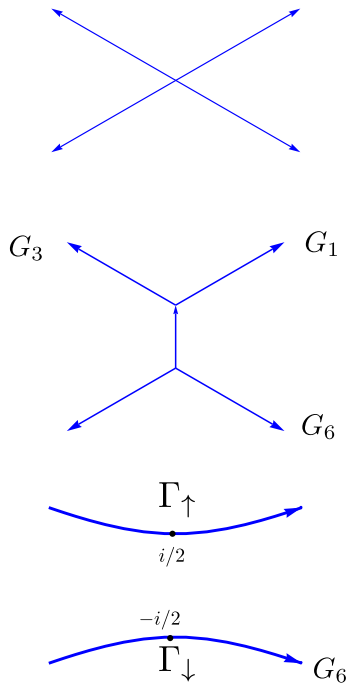

Figure 8.2.1: Deforming the RHP for positive x, with Assumption 8.2.1.

This matrix is exponentially decaying to the identity along $\Gamma_\uparrow$, as is G_4 along $\Gamma_\downarrow$. We employ the approach of Section 5.2 and Algorithm 5.1.11. We first use Lemma 3.10.4 to truncate the contours near the saddle point. What remains is to determine what "near" means. Because θ behaves like $\mathcal{O}\left(z \pm i/2\right)^2$ near the saddle points, Assumption 5.0.1 implies that we should choose the shifting of $\beta_1 = i/2$ and $\beta_2 = -i/2$, the scalings $\alpha_1 = \alpha_2 = r|x|^{-3/4}$ and the canonical domains $\Omega_1 = \Omega_2 = [-1, 1]$. Here r is chosen so that what is truncated is negligible in the sense of Lemma 3.10.4. The treatment G_6 is similar. The complete proof of asymptotic stability of the numerical method proceeds in a similar way as in Section 10.4.2.

8.3 Negative x, $s_2 = 0$ and $1 - s_1 s_3 > 0$

As mentioned above we perform this deformation under the relaxed conditions:

Assumption 8.3.1. *$x < 0$, $s_2 \in \mathbb{C}$ and $1 - s_1 s_3 > 0$*

We begin with the deformation of Γ to pass through the saddle points $\pm 1/2$, resulting in the RHP on the left of Figure 8.3.1. The function

$$G_6 G_1 G_2 = \begin{bmatrix} 1 - s_1 s_3 & s_1 e^{-\xi\theta} \\ s_2 e^{\xi\theta} & 1 + s_1 s_2 \end{bmatrix}$$

has terms with $\exp(\pm\xi\theta)$. It cannot decay to the identity when deformed in the complex plane. We can resolve this issue by using lensing, see Section 3.10.3.

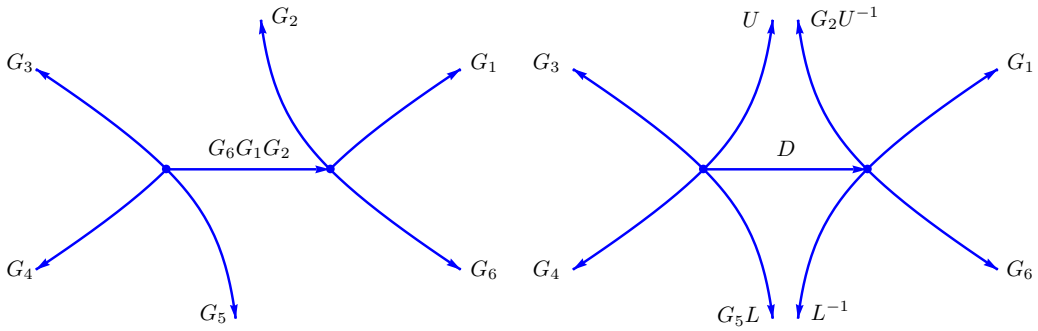

Figure 8.3.1: Left: Initial deformation along the paths of steepest descent. Right: The deformed contour after lensing.

Consider the LDU factorization:

$$G_6G_1G_2 = LDU = \begin{bmatrix} 1 & 0 \\ e^{-\zeta\theta}\frac{s_1}{1-s_1s_3} & 1 \end{bmatrix} \begin{bmatrix} 1-s_1s_3 & 0 \\ 0 & \frac{1}{1-s_1s_3} \end{bmatrix} \begin{bmatrix} 1 & e^{\zeta\theta}\frac{s_1}{1-s_1s_3} \\ 0 & 1 \end{bmatrix}.$$

The matrix U decays near $i\infty$, L decays near $-i\infty$, both approach the identity matrix at infinity and D is constant. Moreover, the oscillators in L and U are precisely those of the original G matrices. Therefore, we reuse the path of steepest descent, and obtain the deformation on the right of Figure 8.3.1. The LDU decomposition is valid under the assumption $1 - s_1s_3 \neq 0$.

8.3.1 Removing the connected contour

Although the jump matrix D is non-oscillatory (it is, in fact, constant), it is still incompatible with the theory presented in Section 5.2: we need the jump matrix to approach the identity matrix away from the saddle points. Therefore, it is necessary to remove this connecting contour. Since $D = \operatorname{diag}(d_1, d_2)$ is diagonal, we can solve $P^+ = P^-D$ with $P(\infty) = I$ on $(-1/2, 1/2)$ in closed form, see Section 3.4.1:

$$P(z) = \begin{bmatrix} \left(\frac{2x+1}{2x-1}\right)^{i\log d_1/2\pi} & 0 \\ 0 & \left(\frac{2x+1}{2x-1}\right)^{i\log d_2/2\pi} \end{bmatrix}.$$

This parametrix solves the desired RHP for any choice of branch of the logarithm. However, we must choose a branch so that the singularity is locally integrable. This is accomplished by choosing the standard choice of branch.

We write

$$\Phi = \Psi P.$$

Since P satisfies the required jump on $(-1/2, 1/2)$, Ψ has no jump there. Moreover, on each of the remaining curves we have

$$\Psi^+ = \Phi^+P^{-1} = \Phi^-GP^{-1} = \Psi^{-1}PGP^{-1},$$

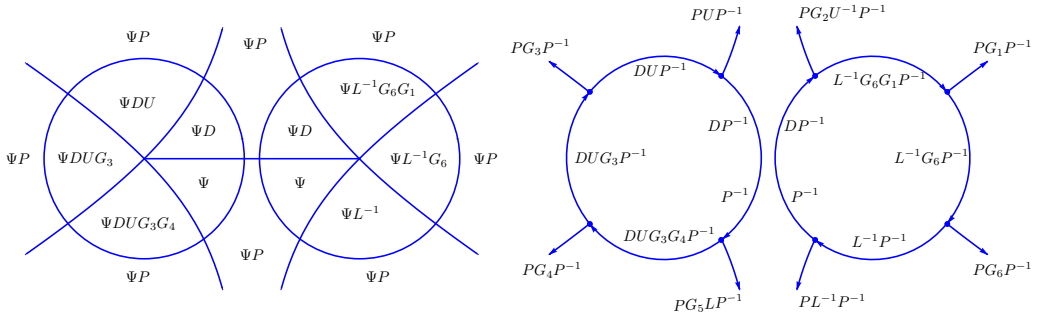

Figure 8.3.2: Left: Definition of Φ in terms of Ψ. Right: Jump contour for Ψ.

and our jump matrix becomes PGP^{-1}. Unfortunately, we have introduced singularities at $\pm 1/2$ and the theory of Section 5.2 requires smoothness of the jump matrix. This motivates alternate definitions for Ψ in circles around the saddle points similar to what was done in Chapters 6 and 7. In particular, we define Φ in terms of Ψ by the left panel of Figure 8.3.2, where Ψ has the jump matrix defined in the right panel of the figure. A quick check demonstrates that this definition of Φ satisfies the required jump relations.

We are ready to apply Algorithm 5.1.11. Define

$$\Omega = \{z : \|z\| = 1\} \cup \{re^{i\pi/4} : r \in (1,2)\} \cup \{re^{3i\pi/4} : r \in (1,2)\} \\ \cup \{re^{-3i\pi/4} : r \in (1,2)\} \cup \{re^{-i\pi/4} : r \in (1,2)\}.$$

In accordance with Assumption 5.0.1, we have

$$\Gamma_1 = \frac{1}{2} + \xi^{-1/2}\Omega \quad \text{and} \quad \Gamma_2 = -\frac{1}{2} + \xi^{-1/2}\Omega,$$

with the jump matrices defined according to Figure 8.3.2. Now, paths of steepest descent are local paths of steepest descent.

8.3.2 Uniform approximation

We have isolated the RHP near the saddle points, and constructed a numerical algorithm to solve the deformed RHP. We show that this numerical algorithm approximates the true solution to the RHP. In order to analyze the error, we introduce the local model problem for this RHP following [51]. The solution of the model problem is the the parametrix used in asymptotic analysis.

Remark 8.3.2. *It is important to note that knowledge of the parametrix is not needed to solve the RHP numerically.*

Let $\nu = i \log d_2/(2\pi)$ and define the Wronskian matrix of parabolic cylinder functions $D_\nu(\zeta)$ [84],

$$Z_0(\zeta) = 2^{-\sigma_3/2} \begin{bmatrix} D_{-\nu-1}(i\zeta) & D_\nu(\zeta) \\ \frac{d}{d\zeta} D_{-\nu-1}(i\zeta) & \frac{d}{d\zeta} D_\nu(\zeta) \end{bmatrix} \begin{bmatrix} e^{i\pi/2(\nu+1)} & 0 \\ 0 & 1 \end{bmatrix}, \tag{8.3.1}$$

along with the constant matrices

$$H_{k+2} = e^{i\pi(\nu+1/2)\sigma_3} H_k e^{i\pi(\nu+1/2)\sigma_3}, \quad H_0 = \begin{bmatrix} 1 & 0 \\ h_0 & 1 \end{bmatrix}, \quad H_1 = \begin{bmatrix} 1 & h_1 \\ 0 & 1 \end{bmatrix}, \quad \sigma_3 = \begin{bmatrix} 1 & 0 \\ 0 & -1 \end{bmatrix},$$

$$h_0 = -i\frac{\sqrt{2\pi}}{\Gamma(\nu+1)}, \quad h_1 = \frac{\sqrt{2\pi}}{\Gamma(-\nu)} e^{i\pi\nu}.$$

In addition, define

$$Z_{k+1}(\zeta) = Z_k(\zeta) H_k.$$

The sectionally holomorphic function $Z(\zeta)$ is defined as

$$Z(\zeta) = \begin{cases} Z_0(\zeta), & \text{if } \arg\zeta \in (-\pi/4, 0), \\ Z_1(\zeta), & \text{if } \arg\zeta \in (0, \pi/2), \\ Z_2(\zeta), & \text{if } \arg\zeta \in (\pi/2, \pi), \\ Z_3(\zeta), & \text{if } \arg\zeta \in (\pi, 3\pi/2), \\ Z_4(\zeta), & \text{if } \arg\zeta \in (3\pi/2, 7\pi/4). \end{cases}$$

This is used to construct the local solutions

$$\hat{\Psi}^r(z) = B(z)(-h_1/s_3)^{-\sigma_3/2} e^{it\sigma_3/2} 2^{-\sigma_3/2} \begin{bmatrix} \zeta(z) & 1 \\ 1 & 0 \end{bmatrix} Z(\zeta(z))(-h_1/s_3)^{\sigma_3/2},$$

$$\hat{\Psi}^l(z) = \sigma_2 \hat{\Psi}^r(-z)\sigma_2,$$

where

$$\sigma_2 = \begin{bmatrix} 0 & -i \\ i & 0 \end{bmatrix}, B(z) = \left(\zeta(z)\frac{z+1/2}{z-1/2}\right)^{\nu\sigma_3}, \zeta(z) = 2\sqrt{-t\theta(z) + t\theta(1/2)}.$$

Consider the sectionally holomorphic matrix-valued function $\hat{\Psi}(z)$ defined by

$$\hat{\Psi}(z) = \begin{cases} P(z), & \text{if } |z \pm 1/2| > R, \\ \hat{\Psi}^r(z), & \text{if } |z - 1/2| < R, \\ \hat{\Psi}^l(z), & \text{if } |z + 1/2| < R. \end{cases}$$

We use $[\hat{G}; \hat{\Gamma}]$ to denote the RHP solved by $\hat{\Psi}$. See the top panel of Figure 8.3.3 for $\hat{\Gamma}$. In [51], it is shown that Ψ^r satisfies the RHP for Φ exactly near $z = 1/2$ and for Ψ^l near $z = -1/2$. Notice that $\hat{\Psi}^r$ and $\hat{\Psi}^l$ are bounded near $z = \pm 1/2$. In the special case where $\log d_1 \in \mathbb{R}$, P remains bounded at $\pm 1/2$. Following the analysis in [51] we write

$$\Phi(z) = \chi(z)\hat{\Psi}(z),$$

where $\chi \to I$ as $\zeta \to \infty$.

We deform the RHP for $\hat{\Psi}$ to open up a small circle of radius r near the origin as in Figure 8.3.2. We use $[\hat{G}_1; \hat{\Gamma}_1]$ to denote this deformed RHP and solution $\hat{\Psi}_1$. See Figure 8.3.3 for $\hat{\Gamma}_1$. It follows that $\hat{\Psi}(z)P^{-1}(z)$ is uniformly bounded in z and ξ. Further, $\hat{\Psi}_1$ has the same properties. Since $\hat{\Psi}_1$ is uniformly bounded in both z and ξ we use (5.2.1)

to show that $\mathcal{C}[\hat{G}_1; \hat{\Gamma}_1]^{-1}$ has uniformly bounded norm. We wish to use this to show the uniform boundedness of the inverse $\mathcal{C}[G; \Gamma]^{-1}$. To do so we extend the jump contours and jump matrices in the following way. Set $\Gamma_e = \Gamma \cup \hat{\Gamma}_1$ and define

$$G_e(z) = \begin{cases} G(z), & \text{if } z \in \Gamma, \\ I, & \text{otherwise,} \end{cases}$$
$$\hat{G}_e(z) = \begin{cases} \hat{G}_1(z), & \text{if } z \in \hat{\Gamma}_1, \\ I, & \text{otherwise.} \end{cases}$$

The estimates in [51] show that $G_e - \hat{G}_e \to 0$ uniformly on Γ_e. It follows that $\mathcal{C}[\hat{G}_e; \Gamma_e]^{-1}$ is uniformly bounded since the extended operator is the identity operator on $\Gamma \setminus \hat{\Gamma}_1$. Theorem 3.9.4 implies that $\mathcal{C}[G_e; \Gamma_e]^{-1}$ is uniformly bounded for sufficiently large ξ, which implies that $\mathcal{C}[G; \Gamma]^{-1}$ is uniformly bounded for ξ sufficiently large, noting that the extended operator is the identity operator on the added contours. We use this construction to prove the uniform convergence of the numerical method using both direct and indirect estimates.

8.3.3 Application of direct estimates

We see that the RHP for Ψ satisfies the properties of a numerical parametrix. This requires that the jump matrices have uniformly bounded Sobolev norms. The only singularities in the jump matrices are of the form

$$s(z) = \left(\frac{z - 1/2}{z + 1/2}\right)^{iv}, v \in \mathbb{R}.$$

After transforming to a local coordinate k, $z = \xi^{-1/2}k - 1/2$, we see that

$$S(k) = s(\xi^{-1/2}k - 1/2) = \xi^{-iv/2}\left(\frac{\xi^{-1/2}k + 1}{k}\right)^{iv}.$$

The function $S(k)$ is smooth and has uniformly bounded derivatives provided k is bounded away from $k = 0$. The deformations applied thus far guarantee that k is bounded away from 0. To control the behavior of the solution for large k we look at the exponent which appears in the jump matrix

$$\theta(z) = \frac{2i}{3} - 4i\left(z + \frac{1}{2}\right)^2 + \frac{8i}{3}\left(z + \frac{1}{2}\right)^3,$$

and define

$$\tilde{\theta}(k) = \theta(\xi^{-1/2}k - 1/2) = \frac{2i}{3} - 4ik^2/\xi + \frac{8i}{3}k^3/\xi^{3/2}.$$

If we assume that the contours are deformed along the local paths of steepest descent, all derivatives of $e^{\xi\tilde{\theta}(k)}$ are exponentially decaying, uniformly in ξ. After applying the same procedure at $z = 1/2$ and after contour truncation, Theorem 3.10.4 implies the RHP for Ψ satisfies the hypotheses of Theorem 5.2.4, proving uniform convergence.

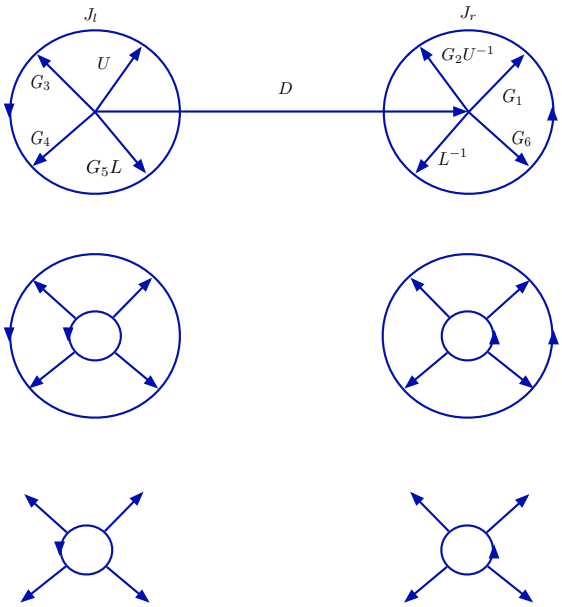

Figure 8.3.3: Top: Jump contours for the model problem with solution $\hat{\Psi}$. Note that J_r and J_l are the jumps on the outside of the circles. They tend uniformly to the identity as $\xi \to \infty$ [51]. Center: The jump contours, $\hat{\Gamma}_1$, for the function $\hat{\Psi}_1$. The inner circle has radius r and the outer circle has radius R. Bottom: Contour on which $\hat{U}$ is non-zero. This can be matched up with the right contour in Figure 8.3.2.

8.3.4 Application of indirect estimates

The second approach is to use the solution of the model problem to construct an numerical parametrix. Since we have already established strong uniform convergence we proceed to establish a theoretical link with the method of nonlinear steepest descent, demonstrating that the success of nonlinear steepest descent implies the success of the numerical method, even though the numerical method does not depend on the details of nonlinear steepest descent. We start with the RHP $[\hat{G}_1; \hat{\Gamma}_1]$ and its solution $\hat{\Psi}_1$. As before, see Figure 8.3.3 for $\hat{\Gamma}_1$. Define $\hat{u} = (\hat{\Psi}_1)^+ - (\hat{\Psi}_1)^-$ which is the solution of the associated SIE on $\hat{\Gamma}_1$. The issue here is that we cannot scale the deformed RHP in Figure 8.3.2 so that it is posed on the same contour as $[G; \Gamma]$. We need to remove the larger circle.

We define a new function $\hat{U} = \hat{u}\phi$ where ϕ is a C^∞ function with support in $(B(-1/2, R) \cup B(1/2, R)) \cap \hat{\Gamma}_1$ such that $\phi = 1$ on $(B(1/2, r) \cup B(-1/2, r)) \cap \hat{\Gamma}_1$ for $r < R$. Let $\hat{\Gamma}_2$ be the support of $\hat{U}$ (see bottom contour in Figure 8.3.3). Define $\hat{\Psi}_2 = I + \mathcal{C}_{\hat{\Gamma}_2}\hat{U}$. From the estimates in [51], it follows that

$$\hat{\Psi}_2^+ = \hat{\Psi}_2^- \hat{G}_2,$$

where $\hat{G}_2 - G$ tends uniformly to zero as $\xi \to \infty$. We have to establish the required smoothness of $\hat{U}$. We do this explicitly from the above expression for $\hat{\Psi}P^{-1}$ after using the scalings $z = \xi^{-1/2}k \pm 1/2$. The final step is to let ξ be sufficiently large so that we can truncate both $[G; \Gamma]$ and $[\hat{G}_2; \hat{\Gamma}_2]$ to the same contour. We use Proposition 5.2.11 to prove

that this produces a numerical parametrix. Additionally, this shows how the local solution of RHPs can be tied to stable numerical computations of solutions.

Remark 8.3.3. *This analysis relies heavily on the boundedness of P. These arguments fail if we let P have unbounded singularities. In this case one approach would be to solve the RHP for χ. The jump for this RHP tends to the identity. To prove weak uniformity for this problem one needs to only consider the trivial RHP with the jump being the identity matrix as a numerical parametrix. Another approach is to remove the growth in the parametrix through conjugation by constant matrices; see Chapter 10, specifically Section 10.4.2, for such an approach to rectify an unbounded global parametrix in the orthogonal polynomial RHP.*

8.3.5 Numerical results

In Figure 8.3.4 we plot the solution to Painlevé II with $(s_1, s_2, s_3) = (1, -2, 3)$ and demonstrate numerically that the computation remains accurate in the asymptotic regime. We use $u(n, x)$ to denote the approximate solution obtained with n collocation points per contour. Since we are using (8.1.3) we consider the estimated relative error by dividing the absolute error by $\sqrt{x}$. We see that we retain relative error as x becomes large.

Remark 8.3.4. *Solutions to Painlevé II often have poles on the real line, which correspond to the RHPs not having a solution. In other words, $\|\mathcal{C}[\Gamma, \Omega]^{-1}\|$ is not uniformly bounded, which means that the theory of this paper does not apply. However, the theorems can be adapted to the situation where x is restricted to a subdomain of the real line such that $\|\mathcal{C}[\Gamma, \Omega]^{-1}\|$ is uniformly bounded. This demonstrates asymptotic stability of the numerical method for solutions with poles, provided that x is bounded away from the poles, similar to the restriction of the asymptotic formulae in [51].*

8.4 Negative x, $s_2 = 0$ and $s_1s_3 = 1$

We develop deformations for the Hastings–McLeod Stokes constants. We realize numerical asymptotic stability in the aforementioned sense. The imposed conditions reduce to the following:

Assumption 8.4.1. *$x < 0$, $s_2 = 0$ and $s_1 = -s_3 = \pm i$*

We begin by deforming the RHP (Figure 8.1.2) to the one shown in Figure 8.4.1. The horizontal contour extends from $-\alpha$ to α for $\alpha > 0$. We determine α below. Define

$$G_0 = G_6G_1 = \begin{bmatrix} 0 & s_1 e^{-i|x|^{3/2}\theta(z)} \\ s_1 e^{i|x|^{3/2}\theta(z)} & 1 \end{bmatrix}.$$

Note that the assumption $s_2 = 0$ simplifies the form of the RHP substantially, see Figure 8.1(b). We use an approach similar to that of the equilibrium measure to replace θ with a function possessing more desirable properties. Define

$$\Theta(z) = e^{i|x|^{3/2}\frac{g(z)-\theta(z)}{2}\sigma_3}, \quad g(z) = (z^2 - \alpha^2)^{3/2}.$$

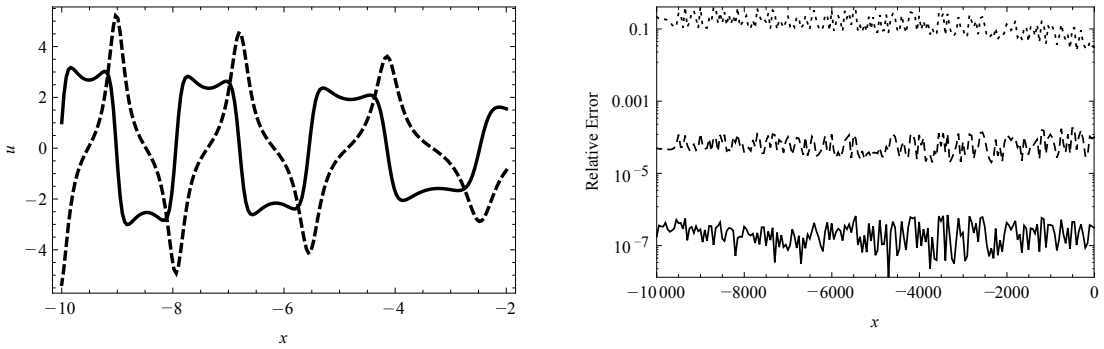

Figure 8.3.4: Left: Plot of the solution, u, for small x (Solid: real part, Dashed: imaginary part). Right: Relative error. Solid: $|x|^{-1/2}|u(12,x) - u(36,x)|$, Dashed: $|u(8,x) - u(36,x)|/\sqrt{|x|}$, Dotted: $|u(4,x) - u(36,x)|/\sqrt{|x|}$. This plot demonstrates both uniform approximation and spectral convergence.

The branch cut for $g(z)$ is chosen along $[-\alpha, \alpha]$. If we equate $\alpha = 1/\sqrt{2}$ the branch of g can be chosen so that $g(z) - \theta(z) \sim \mathcal{O}(z^{-1})$. Furthermore, $g_+(z) + g_-(z) = 0$ and $\mathrm{Im}(g_-(z) - g_+(z)) > 0$ on $(-\alpha, \alpha)$. Define $\hat{G}_i = \Theta_-^{-1} G_i \Theta_+$ and note that

$$\hat{G}_0(z) = \begin{bmatrix} 0 & s_1 e^{-i|x|^{3/2}\frac{g_+(z)+g_-(z)}{2}} \\ s_1 e^{i|x|^{3/2}\frac{g_+(z)+g_-(z)}{2}} & e^{i|x|^{3/2}\frac{g_-(z)-g_-(z)}{2}} \end{bmatrix} = \begin{bmatrix} 0 & s_1 \\ s_1 & e^{i|x|^{3/2}\frac{g_-(z)-g_-(z)}{2}} \end{bmatrix}.$$

As $x \to -\infty$, G_0 tends to the matrix

$$J = \begin{bmatrix} 0 & s_1 \\ s_1 & 0 \end{bmatrix}.$$

The solution of the RHP

$$\Psi^+(z) = \Psi^-(z)J, \quad z \in [-\alpha, \alpha], \quad \Psi(\infty) = I,$$

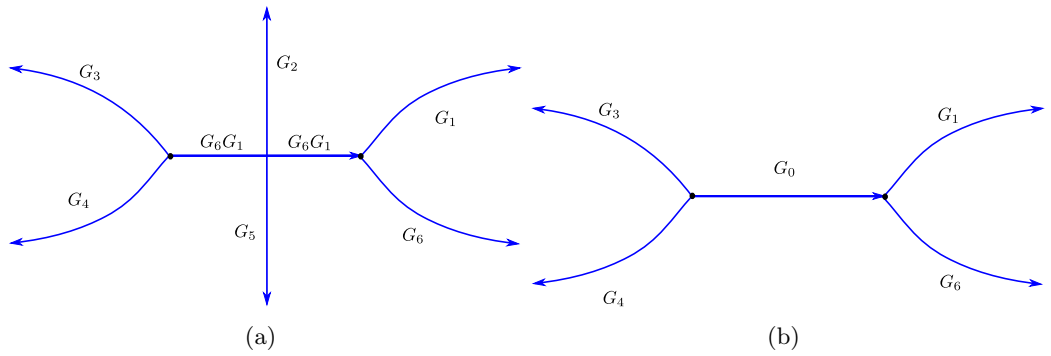

Figure 8.4.1: Deforming the RHP for negative x, with Assumption 8.4.1. The black dots represent $\pm\alpha$. (a) Initial deformation. (b) Simplification stemming from Assumption 8.4.1.

is given by

$$\Psi_{\mathrm{HM}}^{\mathrm{out}}(z) = \frac{1}{2}\begin{bmatrix} \beta(z)+\beta(z)^{-1} & -is_1(\beta(z)-\beta(z)^{-1}) \\ -is_1(\beta(z)-\beta(z)^{-1}) & \beta(z)+\beta(z)^{-1} \end{bmatrix}, \quad \beta(z) = \left(\frac{z-\alpha}{z+\alpha}\right)^{1/4}.$$

Here β has a branch cut on $[-\alpha,\alpha]$ and satisfies $\beta(z)\to 1$ as $z\to\infty$. It is clear that $(\Psi_{\mathrm{HM}}^{\mathrm{out}})_+ \hat{G}_0 (\Psi_{\mathrm{HM}}^{\mathrm{out}})_-^{-1} \to I$ uniformly on every closed subinterval of $(-\alpha,\alpha)$.

We define local parametrices near $\pm\alpha$:

$$\Psi_{\mathrm{HM}}^{\alpha} = \begin{cases} I & \text{if } -\frac{\pi}{3} < \arg(z-a) < \frac{\pi}{3} \\ \hat{G}_1^{-1} & \text{if } \frac{\pi}{3} < \arg(z-a) < \pi \\ \hat{G}_1 & \text{if } -\pi < \arg(z-a) < -\frac{\pi}{3} \end{cases},$$

$$\Psi_{\mathrm{HM}}^{-\alpha} = \begin{cases} I & \text{if } \frac{2\pi}{3} < \arg(z+a) < \pi \text{ or } -\pi < \arg(z+a) < -\frac{2\pi}{3} \\ \hat{G}_1^{-1} & \text{if } 0 < \arg(z+a) < \frac{2\pi}{3} \\ \hat{G}_1 & \text{if } -\frac{2\pi}{3} < \arg(z+a) < \frac{2\pi}{3} \end{cases}.$$

We are ready to define the global parametrix. Given $r>0$, define

$$\Psi_{\mathrm{HM}} = \begin{cases} \Psi_{\mathrm{HM}}^{\alpha} & \text{if } |z-a|<r \\ \Psi_{\mathrm{HM}}^{-\alpha} & \text{if } |z+a|<r \\ \Psi_{\mathrm{HM}}^{\mathrm{out}} & \text{if } |z+a|>r \text{ and } |z-a|>r \end{cases}.$$

It follows that Ψ_{HM} satisfies the RHP shown in Figure 8.3(b).

Let Φ be the solution of the RHP shown in Figure 8.3(a). It follows that $\Delta = \Phi\Psi_{\mathrm{HM}}^{-1}$ solves the RHP shown in Figure 8.3(b). The RHP for Δ has jump matrices that decay to the identity away from $\pm\alpha$. We use Assumption 5.0.1 to determine that we should use $r = |x|^{-1}$. We solve the RHP for Δ numerically. To compute the solution of Painlevé II used in the asymptotic analysis of the KdV equation ((6.0.14)) we use the formula

$$P_{II}(\pm i, 0, \mp i; x) = 2i\sqrt{|x|}\lim_{z\to\infty} z\Delta(z)_{12}.$$

See Figure 8.4(a) for a plot of the Hastings–McLeod solution with $s_1 = i$. To verify

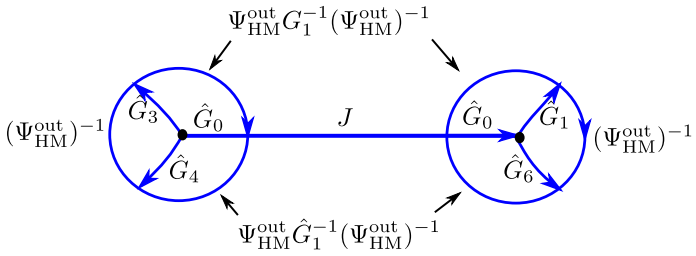

Figure 8.4.2: The jump contours and jump matrices for the RHP solved by $\Psi_{\rm HM}$. The radius for the two circles is r.

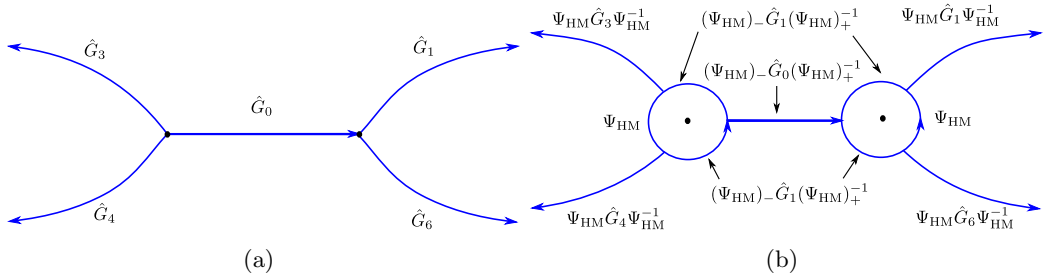

Figure 8.4.3: The final deformation of the RHP for negative x, with Assumption 8.4.1. The black dots represent $\pm\alpha$. (a) After conjugation by Θ. (b) Bounding the contours away from the singularities of g and β using $\Psi_{\rm HM}$.

our computations we may use the asymptotics [51]:

$$P_{II}(i, 0, -i; x) \sim -\sqrt{\frac{-x}{2}} + \mathcal{O}\left(x^{-5/2}\right). \tag{8.4.1}$$

We define

$$D_{\rm HM}(x) = \left| \frac{P_{II}(i, 0, -i; x)}{\sqrt{\frac{-x}{2}}} + 1 \right|,$$

to be the *relative error* which should tend to a constant for x large and negative. We demonstrate this in Figure 8.4(b).

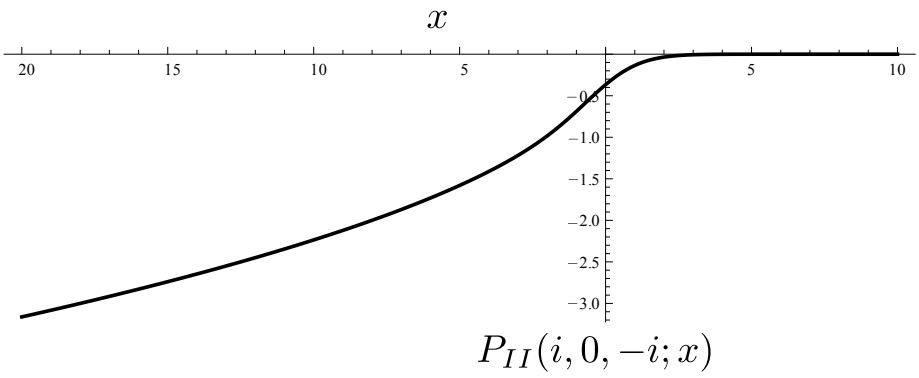

(a)

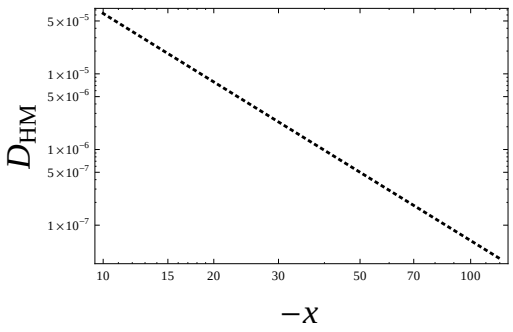

(b)

Figure 8.4.4: Plotting and analysis of the numerical approximation of $P_{II}(i, 0, -i; x)$. (a) $P_{II}(i, 0, -i; x)$ for positive and negative x. For small $|x|$ we solve the undeformed RHP. (b) A verification of the numerical approximation using the asymptotics 8.4.1 .

Chapter 9

The Finite-Genus Solutions of the Korteweg-de Vries Equation

The goal of this chapter is to present a new description for the so-called finite-genus or finite-gap solutions of the KdV equation

$$q_t + 6qq_x + q_{xxx} = 0, \quad (x,t) \in \mathbb{R} \times \mathbb{R}, \tag{9.0.1}$$

and to use this description to compute them. This material originally appeared in [108] (see [107] for a short summary). The finite-genus solutions arise in the spectral analysis of the Schrödinger operator with periodic or quasi-periodic potential, where the spectrum has only a finite number g of finite-length bands separated by g gaps. They are explicitly described in terms of Riemann theta functions, parametrized by hyperelliptic compact Riemann surface of genus g. In the context of the periodic problem for (9.0.1), these solutions play the same role that is played by trigonometric polynomials for the linear KdV equation $q_t + q_{xxx} = 0$ of (9.0.1): the general solution to the periodic problem in the space of square-integrable functions is approximated arbitrarily close by a finite-genus solution with sufficiently high g. An eloquent overview of the extensive literature on these solutions is found in McKean's review [73] of [74]. Of particular importance in the development of this literature are the pioneering works of Lax [70] and Novikov [83]. Excellent reviews are also found in Chapter 2 of [82], Dubrovin's oft-cited review article [45], and [9], parts of which focus specifically on the computation of these solutions.

The computation of the finite-genus solutions is a nontrivial matter. Although Lax's original paper [70] includes an appendix by Hyman, where solutions of genus two were obtained through a variational principle, the now-standard approach of their computation goes through their algebro-geometric description in terms of Riemann surfaces, see [21] or [55], for instance. Another approach is through the numerical solution of the so-called Dubrovin equations, a set of coupled ordinary differential equations that describe the dynamics of the zeros and poles of an auxiliary eigenfunction of the spectral problem, the Baker-Akhiezer function [9, 44]. The finite-genus solution is easily recovered from the solution of the Dubrovin equations [82, 93]. One advantage of all these approaches over the variational method employed by Lax and Hyman is that periodic and quasi-periodic solutions are constructed with equal ease. The same is true for our approach, described below.

The essence of this paper is the derivation of a Riemann–Hilbert representation of the Baker–Akhiezer function. We construct a RHP whose solution is used to find the Baker–Akhiezer function. From this, one extracts the associated solution of the KdV equation. The x- and t-dependence of the solution appear in an explicit way, so that no time or space stepping is required to obtain the value of the solution at a specific x and t. This should be contrasted with, for instance, the numerical solution of the Dubrovin equations [93]. Furthermore, just like for the method of inverse scattering (Chapters 6 and 7), the infinite-line counterpart of the problem under investigation, this dependence of the KdV solution on its independent variables appears linearly in an exponential function in the RHP.

In order to solve this RHP, we employ a regularization procedure using a g-function [32]. This simplifies the x- and t-dependence further. The resulting RHP has piecewise-constant jumps. Straightforward modifications allow the RHP to be numerically solved efficiently using the techniques in Section 5.3. This results in an approximation of the Baker–Akhiezer function that is uniformly valid on its associated Riemann surface. This, in turn, produces a uniform approximation of the associated solution of the KdV equation in the entire (x, t) plane.

In this chapter, we begin by introducing the required fundamentals from the theory of Riemann surfaces. Next we use the methods of Chapter 2 of [82] to describe how hyperelliptic Riemann surfaces are used to solve the KdV equation for a restricted class of initial conditions. The representation of the Baker–Akhiezer function in terms of a RHP is derived in the next section. The modification of this RHP is discussed in the two subsequent sections. The final form of the RHP is presented in Section 9.5. In the final section the RHP is solved numerically and the numerical convergence of the method is verified. The method is illustrated there with many numerical examples. As a notational remark, due to the wealth of defined functions in this chapter we reserve bold-face fonts for vectors and matrices.

9.1 Riemann surfaces

We use this section to introduce the fundamental ideas from the theory of Riemann surfaces that are needed below. Most of these fundamental facts can be found in [9, 44]. The unfinished lecture notes by B. A. Dubrovin [46] provide an especially readable introduction and most results stated below can also be found there. We include additional classical results on Riemann surfaces to give the reader some insight into the depth of the subject.

Definition 9.1.1. *Let*

$$F(\lambda, \mu) = \mu^2 - P_{2g+2}(\lambda), \text{ or } F(\lambda) = \mu^2 - P_{2g+1}(\lambda).$$

The algebraic curve associated with this function is the solution set in $\mathbb{C}^2$ *of the equation* $F(\lambda, w) = 0$. *The desingularization and compactification of this curve is a Riemann surface,* Γ. *Note that in this chapter* Γ *is no longer a contour. For this restricted class of polynomials the associated Riemann surface* Γ *is said to be hyperelliptic. We only consider hyperelliptic surfaces.*

Define the a cycles $\{a_j\}_{j=1}^g$ and the b cycles $\{b_j\}_{j=1}^g$ on the Riemann surface as in

Figure 9.1.1. The set $\{a_j \cup b_j\}_{j=1}^{g}$ is a basis for the homology of the Riemann surface. It is well known that the hyperelliptic surfaces in Definition 9.1.1 are of genus g; they can be identified with a sphere with g handles. It is also well known that a genus g surface has g linearly independent holomorphic differentials, denoted $\omega_1, \ldots \omega_g$. We choose the normalization

$$\oint_{a_j} \omega_k = 2\pi i \delta_{jk}, \quad j,k = 1, \ldots, g.$$

The matrix

$$\boldsymbol{B} = (B_{jk})_{1 \le j,k \le g}, \quad B_{jk} = \oint_{b_j} \omega_k,$$

is known as a Riemann matrix. Although this matrix has important properties and is necessary for computing the theta function representation of the finite-genus solutions we do not need it directly.

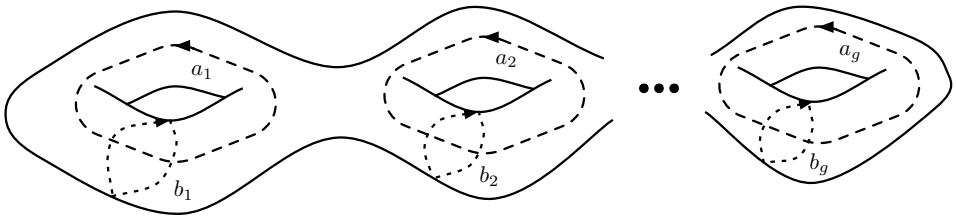

Figure 9.1.1: A cartoon of a hyperelliptic Riemann surfaces with a choice for the a and b cycles.

Lemma 9.1.2 ([45])**.** *Let ω be a holomorphic differential on a Riemann surfaces of genus g. If*

$$\oint_{a_j} \omega = 0, \ j = 1, \ldots, g,$$

then $\omega = 0$.

Lemma 9.1.3 ([45])**.** *Every holomorphic differential f on a genus g hyperelliptic Riemann surface $\mu^2 - P_{2g+1}(\lambda) = 0$ can be expressed locally as*

$$f = \frac{q(\lambda)}{\mu} d\lambda,$$

where q is a polynomial of degree at most $g-1$.

A divisor is a formal sum

$$D = \sum_{j=1}^{k} n_j Q_j, \quad n_j \in \mathbb{Z},$$

of points Q_j on the Riemann surface. Given a meromorphic function f on the Riemann surface with poles at Q_j of multiplicity n_j and zeros at R_j with multiplicity m_j we define the associated divisor

$$(f) = \sum_{j=1}^{l} m_j R_j - \sum_{j=1}^{k} n_j Q_j.$$

The degree of a divisor

$$\deg D = \sum_{j=1}^{k} n_j \text{ so that } \deg(f) = \sum_{j=1}^{k} n_j - \sum_{j=1}^{l} m_i.$$

A divisor is said to be positive if each n_j is positive and $D > D'$ holds if $D - D'$ is positive. We use $l(D)$ to denote the dimension of the space of meromorphic functions f such that $(f) \geq D$.

Lemma 9.1.4 (Riemann inequality [45]). *For a genus g surface, if $\deg D \geq g$ then*

$$l(D) \geq 1 + \deg D - g.$$

A divisor D is said to be nonspecial if the Riemann inequality is an equality. Define the Abel mapping for points on the Riemann surface by

$$A(Q) = \left[\begin{array}{ccc} \int_{Q_0}^{Q} \omega_1 & \cdots & \int_{Q_0}^{Q} \omega_g \end{array} \right], \tag{9.1.1}$$

where the path of integration is taken to be the same for all integrals. Note that this is well-defined for the appropriately normalized differentials. We extend this map to divisors $D = \sum_{j=1}^{k} n_j Q_j$ by

$$A(D) = \sum_{j=1}^{k} n_j A(Q_j).$$

Theorem 9.1.5 ([45]). *The Abel map A maps points on the symmetrized Riemann surface to the associated Jacobi variety $J(\Gamma) = \mathbb{C}^g / \{2\pi M + BN\}$ for $M, N \in \mathbb{Z}^g$. Furthermore, if the divisor $D = Q_1 + \cdots + Q_g$ is nonspecial then A has a single-valued inverse from the Jacobi variety to the symmetrized Riemann surface in a neighborhood of $A(D)$.*

We do not make use of this theorem directly but include it for completeness. Next, we describe properties of Abelian differentials of the second kind that are needed below.

Definition 9.1.6. *Given a point Q on the Riemann surface and a positive integer n, an Abelian differential of the second kind is a meromorphic differential that has a single pole of order $n+1$, so that its local representation is*

$$\nu_Q^n = \left(z^{-n-1} + \mathcal{O}(1) \right) dz,$$

with respect to a local parameter z, $z(Q) = 0$.

When Q is the point at infinity we construct these differentials explicitly. As a local parameter we take $z^2 = 1/\lambda$ since Q is a branch point. If n is even we set

$$\nu_\infty^n = -\frac{1}{2}\lambda^{n/2-1}d\lambda.$$

When n is odd, there is more to be done. First, compute

$$\frac{\lambda^j}{w}d\lambda = -2\frac{z^{-2j-3}}{\sqrt{P(z^{-2})}}dz.$$

Then

$$P(z^{-2}) = z^{-4g-2}(1-z^2\alpha_{g+1})\prod_{j=1}^{g}(1-z^2\alpha_j)(1-z^2\beta_j).$$

Thus

$$\begin{aligned}\frac{\lambda^j}{w}d\lambda &= -2z^{-2j-2+2g}\left((1-z^2\alpha_{g+1})\prod_{j=1}^{g}(1-z^2\alpha_j)(1-z^2\beta_j)\right)^{-1/2}dz\\ &= (-2z^{-2j-2+2g}+\mathcal{O}(1))dz.\end{aligned}$$

We choose $j = g + (n-1)/2$ so that

$$\nu_\infty^n = -\frac{1}{2}\frac{\lambda^{g+(n-1)/2}}{w}d\lambda.$$

Let μ_∞^n be the differential obtained from ν_∞^n by adding holomorphic differentials so that it has zero a cycles. We state a lemma concerning the b-periods of these differentials.

Lemma 9.1.7 ([46])**.** *Define $y_k(z)$ through the equality $\omega_k = y_k(z)dz$ and $z^2 = 1/\lambda$. Then*

$$\oint_{b_k}\mu_\infty^n = \frac{1}{n!}\frac{d^{n-1}}{dz^{n-1}}y_k(z)\bigg|_{z=0}, \quad k = 1,\dots,g.$$

9.2 The finite-genus solutions of the KdV equation

We begin by considering the scattering problem associated with the KdV equation. The time-independent Schrödinger equation

$$-\Psi_{xx} - q_0(x)\Psi = \lambda\Psi, \tag{9.2.1}$$

is solved for eigenfunctions $\Psi(x,\lambda)$ bounded for all x. We define the Bloch spectrum

$$\mathcal{S}(q_0) = \left\{\lambda\in\mathbb{C}:\ \text{there exists a solution such that } \sup_{x\in\mathbb{R}}|\Psi(x,\lambda)| < \infty\right\}.$$

It is well known that for $q_0(x)$ smooth and periodic the Bloch spectrum consists of a countable collection of real intervals

$$\mathcal{S}(q_0) = \bigcup_{j=1}^{\infty} [\alpha_j, \beta_j],$$
$$\alpha_j < \beta_j < \alpha_{j+1} < \beta_{j+1}.$$

If there are only $n+1$ intervals then $\beta_{n+1} = \infty$. We refer to the intervals $[\alpha_j, \beta_j]$ as bands and the intervals $[\beta_j, \alpha_{j+1}]$ as gaps.

Assumption 9.2.1. *$\mathcal{S}(q_0)$ consists of a finite number of intervals. In this case we say that q_0 is a finite-gap potential.*

Define Γ to be the hyperelliptic Riemann surface associated with the function

$$F(\lambda, \mu) = \mu^2 - P(\lambda), \quad P(\lambda) = (\lambda - \alpha_{g+1}) \prod_{j=1}^{g} (\lambda - \alpha_j)(\lambda - \beta_j).$$

See Figure 9.2.1 for a cartoon. We divide this surface into two sheets. Choose the branch cuts for the function $\sqrt{P(\lambda)}$ along $\mathcal{S}(q_0)$. We fix the branch by the requirement $\sqrt{P(\lambda)} \sim (-1)^g i|\lambda|^{g+1/2}$ as $\lambda \to -\infty$. Define $\sqrt{P(\lambda)}^+$ to be the value $\lim_{\epsilon \to 0^+} \sqrt{P(\lambda + i\epsilon)}$. This allows us to define

$$\Gamma_\pm = \{(\lambda, \pm\sqrt{P(\lambda)}^+) : \lambda \in \mathbb{C}\}.$$

When considering a function f defined on Γ we use the notation $f_\pm$ so that $f_+(f_-)$ denotes the function restricted to $\Gamma_+(\Gamma_-)$. In this way we can consider $f_\pm$ as a function of only λ. We need an explicit description of the a cycles since we take a computational approach below:

$$a_i = \{(\lambda, \sqrt{P(\lambda)}^+) : \lambda \in (\beta_i, \alpha_{i+1}]\} \cup \{(\lambda, -\sqrt{P(\lambda)}^+) : \lambda \in [\beta_i, \alpha_{i+1})\}.$$

The a_i component on $\Gamma_+(\Gamma_-)$ is oriented in the direction of decreasing (increasing) λ. This description is also useful since we will consider poles and zeros lying on the a cycles.

Remark 9.2.2. *There is some inconsistency in the notation $f_\pm$ which is also present in the literature [46]. In what follows, it will be clear from context whether we are referring to a function defined on the Riemann surface or to f_+ and f_- separately.*

We introduce further notation that will be of use later. Given a point $Q = (\lambda, w) \in \Gamma$, we follow [51] and define the involution $*$ by $Q^* = (\lambda, -w)$. This is an isomorphism from one sheet of the Riemann surface to the other. It is clear the first sheet is isomorphic to the cut plane

$$\hat{\mathbb{C}} = \mathbb{C} \setminus \left\{ [\alpha_{g+1}, \infty) \cup \bigcup_{j=1}^{g} [\alpha_j, \beta_j] \right\},$$

through the mapping $\hat{} : \Gamma_+ \to \hat{\mathbb{C}}$ defined by $\hat{Q} = \lambda$ and its inverse $\check{} : \hat{\mathbb{C}} \to \Gamma_+$ defined by $\check{\lambda} = (\lambda, \sqrt{P(\lambda)}^+)$.

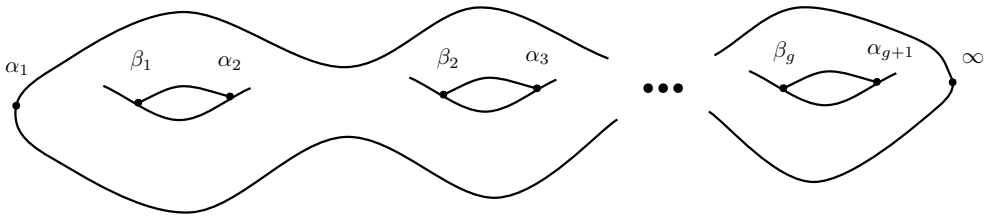

Figure 9.2.1: A cartoon of the Riemann surface associated with the finite-gap potential q_0.

Lemma 9.2.3. *[82] For every $x_0 \in \mathbb{R}$ there exist two solutions $\Psi_\pm$ of (9.2.1) such that*

- *$\Psi_\pm(x, \lambda)$ is meromorphic on $\Gamma \setminus \{\infty\}$ with g poles at*

$$D = \sum_{i=1}^{g} Q_i, \quad Q_i \in a_i,$$

and g zeros at

$$D' = \sum_{i=1}^{g} R_i, \quad R_i \in a_i.$$

- *Define $\gamma_i = \hat{R}_i$ then $\{\gamma_j\}_{j=1}^g$ satisfies*

$$\gamma_j(x_0) \in [\beta_j, \alpha_{j+1}], \tag{9.2.2}$$

$$\gamma_j' = -\frac{2i\sqrt{P(\gamma_j)}}{\prod_{k\neq j}(\gamma_j - \gamma_k)}. \tag{9.2.3}$$

- *$\Psi_\pm(x, \lambda) = e^{\pm i\sqrt{\lambda}(x-x_0)}(1 + \mathcal{O}(\lambda^{-1/2}))$ as $\lambda \to \infty$.*

For simplicity we take $x_0 = 0$ below. We will always take the branch cut for $\lambda^{1/2}$ to be along $[0, \infty)$ and fix the branch by $\lambda^{1/2} \sim i|\lambda|^{1/2}$ as $\lambda \to -\infty$. If the potential $q_0(x)$ is taken as an initial condition for the KdV equation then these zeros have both time and space dependence $\gamma_j = \gamma_j(x, t)$. This dependence is given by [44]

$$\dot{\gamma}_j = -\frac{8i(\gamma_j + q_0/2)\sqrt{P(\gamma_j)}}{\prod_{k\neq j}(\gamma_j - \gamma_k)}, \tag{9.2.4}$$

and the solution to the KdV equation can be reconstructed through

$$q(x, t) = -2\sum_{j=1}^{g} \gamma_j(x, t) + \alpha_{g+1} + \sum_{j=1}^{g}(\alpha_j + \beta_j).$$

The (now time-dependent) function $\Psi_{\pm}(x,t,\lambda)$ is known as a Baker–Akhiezer (BA) function. From the general theory of Baker–Akhiezer functions [82] it is known that it is uniquely determined by a nonspecial divisor

$$D = \sum_{i=1}^{g} Q_i,$$

for the poles and the asymptotic behavior [82]. The following lemma shows that all divisors we consider are nonspecial.

Lemma 9.2.4. *On the hyperelliptic surface $\mu^2 = P(\lambda)$ the divisor $D = \sum_{i=1}^{g} R_i$, where $R_i \in a_i$ is nonspecial.*

Proof. Assume f is meromorphic with $D \le (f)$. The differential $w = df$ has double poles with zero residues at the points R_i. We have the following representation

$$w = \sum_{i=1}^{g} y_i + \eta.$$

Here y_i are Abelian differentials of the second kind normalized so that they have zero periods along the a cycles and second-order poles at the points R_i. Since f is single valued on the Riemann surface

$$\oint_{a_k} w = 0, \quad \oint_{b_k} w = 0, \quad k = 1, \dots, g.$$

Since the a periods vanish we conclude that η must be zero. From the b period condition we obtain

$$\oint_{b_k} w = \sum_{j=1}^{g} c_j \psi_{kj}(z_j(0)) = 0, \tag{9.2.5}$$

where z_j is a local parameter near $R_j = z_j(0)$ and ψ_{kj} is determined from the equality $\omega_k = \psi_{kj}(z_j)dz_j$ near R_j. We know that ω_k can be expressed uniquely as the sum of differentials of the form

$$u_l = \frac{\lambda^{l-1}}{\mu} d\lambda, \text{ for } l = 1, \dots, g,$$

with coefficients d_{kl}. If $R_j = (z_j, \pm\sqrt{P(z_j)})$ is not a branch point we obtain

$$\psi_{k,j}(z_j) = \sum_{l=1}^{g} d_{kj} \frac{z_j^{l-1}}{\sqrt{P(z_j)}}.$$

If it is a branch point $R_j = (z_j, 0)$ we use the local parameter $s = \sqrt{\lambda - z_j}$ so that

$$\psi_{k,j}(z_j) = \sum_{l=1}^{g} d_{kl} \frac{2z_j^{l-1}}{\sqrt{P'(z_j)}}.$$

Since the matrix $\boldsymbol{d} = (d_{kl})_{1\le k,l\le g}$ is invertible the condition (9.2.5) is reduced to the study of the matrix

$$\boldsymbol{Z} = (z_j^{l-1})_{1\le j,l\le g},$$

after multiplying rows by suitable constants. This is a Vandermonde matrix, and thus invertible. This shows that $c_j = 0$ and thus $w = 0$ and $f = C \in \mathbb{C}$. This proves the result. □

Remark 9.2.5. *We have shown that the Abel map is invertible from the Jacobi variety to the symmeterized Riemann surface in a neighborhood of $A(D)$ for every divisor we consider.*

Being precise, we obtain the following unique characterization of the function $\Psi_\pm(x,t,\lambda)$ [82]:

Definition 9.2.6. *The BA function for the solution of the KdV with initial condition $q_0(x)$ is the unique function that satisfies*

- $\Psi_\pm$ *solves* (9.2.1).
- $\Psi_\pm$ *is meromorphic on* $\Gamma \setminus \{\infty\}$ *with poles at*

$$D = \sum_{i=1}^{g} Q_i, \quad Q_i \in a_i, \quad \hat{Q}_i = \gamma_i(0,0). \tag{9.2.6}$$

- $\Psi_\pm(x,t,\lambda) = e^{\pm i\lambda^{1/2}x \pm 4i\lambda^{3/2}t}(1 + \mathcal{O}(\lambda^{-1/2}))$ *as* $\lambda \to \infty$.
- $q_0(x) = -2\sum_{j=1}^{g} \gamma_j(x,0) + \alpha_{g+1} + \sum_{j=1}^{g}(\alpha_j + \beta_j)$.

Remark 9.2.7. *Instead of computing the zeros of the BA function we derive a Riemann–Hilbert formulation of the BA function to compute the function itself. The main benefit of this approach is that the roles of x and t in the problem are reduced to that of parameters. This gives an approximation to the solution of the KdV equation that is uniformly convergent in the (x,t) plane. In this sense our method is comparable to the theta function approach which can also achieve uniform convergence [55]. On the other hand, no time stepping is required, as for the direct numerical solution of the PDE or the numerical solution of 9.2.2 and 9.2.4.*

In what follows we assume without loss of generality that $\alpha_1 = 0$. If $\alpha_1 \neq 0$ we define $\tau = \lambda - \alpha_1$ and consider a modified scattering problem

$$-\Psi_{xx} - q_0(x)\Psi = (\tau + \alpha_1)\Psi, \tag{9.2.7}$$

$$-\Psi_{xx} - \tilde{q}_0(x)\Psi = \tau\Psi, \ \tilde{q}_0(x) = q_0(x) + \alpha_1. \tag{9.2.8}$$

Let $q(x,t)$ and $\tilde{q}(x,t)$ be the solutions of the KdV equation with $q_0(x)$ and $\tilde{q}_0(x)$ respectively, as initial conditions. If $\tilde{q}(x,t)$ satisfies the KdV equation then so does $\tilde{q}(x-6ct,t)+c$. Therefore, by uniqueness, $q(x,t) = \tilde{q}(x+6\alpha_1 t,t) - \alpha_1$.

9.3 From a Riemann surface of genus g to the cut plane

Consider the hyperelliptic Riemann surface Γ from Section 9.2. We represent a function $f_\pm$ defined on Γ by a vector-valued function $\boldsymbol{f}$ on $\hat{\mathbb{C}}$ by

$$\boldsymbol{f}(\lambda) = \left[\begin{array}{cc} f_+(\check{\lambda}) & f_-((\check{\lambda})^*) \end{array} \right].$$

Assume the function $f_\pm$ is continuous on all of Γ. Let $\lambda \in (\alpha_j, \beta_j)$ and define $\lambda_{\pm\epsilon} = \lambda \pm i\epsilon$. It follows that $\lim_{\epsilon\to 0^+} \check{\lambda}_{\pm\epsilon} = \lim_{\epsilon\to 0^+} (\check{\lambda}_{\mp\epsilon})^*$. From the continuity of $f_\pm$

$$\lim_{\epsilon\to 0^+} f_+(\check{\lambda}_{\pm\epsilon}) = \lim_{\epsilon\to 0^+} f_-((\check{\lambda}_{\mp\epsilon})^*).$$

Let $\boldsymbol{f}^\pm(\lambda) = \lim_{\epsilon\to 0^+} \boldsymbol{f}(\lambda \pm i\epsilon)$. Then

$$\boldsymbol{f}^+(\lambda) = \boldsymbol{f}^-(\lambda) \left[\begin{array}{cc} 0 & 1 \\ 1 & 0 \end{array} \right].$$

We form a planar representation of the BA function

$$\boldsymbol{\Psi}(\lambda) = \left[\begin{array}{cc} f_+(\check{\lambda}) & f_-((\check{\lambda})^*) \end{array} \right].$$

The function $\boldsymbol{\Psi}$ satisfies

$$\boldsymbol{\Psi}^+(x,t,\lambda) = \boldsymbol{\Psi}^-(x,t,\lambda) \left[\begin{array}{cc} 0 & 1 \\ 1 & 0 \end{array} \right], \ \lambda \in (\alpha_{n+1}, \infty) \cup \bigcup_{j=1}^{g} (\alpha_j, \beta_j),$$
$$\boldsymbol{\Psi}(x,t,\lambda) = \left[\begin{array}{cc} e^{i\lambda^{1/2}x + 4i\lambda^{3/2}} & e^{-i\lambda^{1/2}x - 4i\lambda^{3/2}} \end{array} \right] (I + \mathcal{O}(\lambda^{-1/2})).$$

The next step is to remove the oscillatory nature of $\boldsymbol{\Psi}$ for large λ. This procedure will affect the jumps, thus some care is in order. Define

$$\boldsymbol{R}(x,t,\lambda) = \left[\begin{array}{cc} e^{-\zeta(x,t,\lambda)/2} & 0 \\ 0 & e^{\zeta(x,t,\lambda)/2} \end{array} \right],$$
$$\zeta(x,t,\lambda) = 2ix\lambda^{1/2} + 8it\lambda^{3/2}.$$

The function $\mathbf{\Phi}(x,t,\lambda) = \Psi(x,t,\lambda)\boldsymbol{R}(x,t,\lambda)$ satisfies

$$\begin{aligned}
&\mathbf{\Phi}^+(x,t,\lambda) = \mathbf{\Phi}^-(x,t,\lambda)\begin{bmatrix} 0 & 1 \\ 1 & 0 \end{bmatrix},\ \lambda \in (\alpha_{n+1},\infty) \cup \bigcup_{j=1}^{g}(\alpha_j,\beta_j),\\
&\mathbf{\Phi}^+(x,t,\lambda) = \mathbf{\Phi}^-(x,t,\lambda)\begin{bmatrix} e^{-\zeta(x,t,\lambda)} & 0 \\ 0 & e^{\zeta(x,t,\lambda)} \end{bmatrix},\ \lambda \in \bigcup_{j=1}^{g}(\beta_j,\alpha_{j+1}),\\
&\mathbf{\Phi}(x,t,\lambda) = \begin{bmatrix} 1 & 1 \end{bmatrix}(I + \mathcal{O}(\lambda^{-1/2})).
\end{aligned} \tag{9.3.1}$$

This is a RHP for $\mathbf{\Phi}$ when the poles at $\gamma_j(0,0)$ coincide with α_j or β_j. The boundary values of the solution to the RHP should be at least locally integrable. A pole at a band end (α_j or β_j) corresponds to a square-root singularity. In general, we have poles in the intervals (β_j,α_{j+1}) where there are smooth jumps. In Section 9.4.1 we treat the case where $\gamma_j(0,0) = \beta_j$, $j = 1,\dots,g$ while enforcing that $\mathbf{\Phi}$ remains bounded at $\{\alpha_j\}_{j=1}^g$. No such enforcement is made at $\{\beta_j\}_{j=1}^g$. The general case of poles on the a cycles is treated in Section 9.4.2.

9.4 Regularization

We show how the jump conditions in (9.3.1) can be reduced to piecewise constant jumps. As mentioned above, we first perform the calculations in the simpler case when the poles are located at $(\beta_j,0)$ on Γ. In the general case, we use an additional BA function as a parametrix to move the poles to the band ends thus reducing the problem to the first case.

9.4.1 All poles at the band ends

We assume $\gamma_j(0,0) = \beta_j$. Define the g-function

$$\mathcal{G}(x,t,\lambda) = \frac{\sqrt{P(\lambda)}}{2\pi i}\sum_{j=1}^{g}\int_{\beta_j}^{\alpha_{j+1}} \frac{-\zeta(x,t,s) + i\Omega_j(x,t)}{\sqrt{P(s)}^+}\frac{ds}{s-\lambda}, \tag{9.4.1}$$

where $\Omega_j(x,t)$ is constant in λ. It is determined below.

Lemma 9.4.1. *The g-function satisfies*

- $\mathcal{G}^+(x,t,\lambda) + \mathcal{G}^-(x,t,\lambda) = 0$ *for* $\lambda \in (\alpha_j,\beta_j)$,
- $\mathcal{G}^+(x,t,\lambda) - \mathcal{G}^-(x,t,\lambda) = -\zeta(x,t,\lambda) + i\Omega_j(x,t)$ *for* $\lambda \in (\beta_j,\alpha_{j+1})$,
- $\mathcal{G}(x,t,\lambda)/\sqrt{P(\lambda)} = \sum_{k=1}^{g} m_k(x,t)\lambda^{-k} + \mathcal{O}(\lambda^{-g-1})$ *as* $\lambda \to \infty$ *where*

$$m_k(x,t) = -\frac{1}{2\pi i}\sum_{j=1}^{g}\int_{\beta_j}^{\alpha_{j+1}} \frac{-\zeta(x,t,s) + i\Omega_j(x,t)}{\sqrt{P(s)}^+}s^{k-1}ds.$$

Proof: *The first two properties follow from the branching properties of $\sqrt{P(\lambda)}$ and properties of Cauchy integrals. The last property follows from Lemma 3.2.2.*

Define the matrix function

$$\boldsymbol{G}(x,t,\lambda) = \begin{bmatrix} e^{-\mathcal{G}(x,t,\lambda)} & 0 \\ 0 & e^{\mathcal{G}(x,t,\lambda)} \end{bmatrix},$$

and consider the function

$$\boldsymbol{\Sigma}(x,t,\lambda) = \boldsymbol{\Phi}(x,t,\lambda)\boldsymbol{G}(x,t,\lambda).$$

Using Lemma 9.4.1 we compute the jumps of $\boldsymbol{\Sigma}$:

$$\boldsymbol{\Sigma}^+(x,t,\lambda) = \boldsymbol{\Sigma}^-(x,t,\lambda)\begin{bmatrix} 0 & 1 \\ 1 & 0 \end{bmatrix},\ \lambda \in (\alpha_{g+1},\infty) \cup \bigcup_{j=1}^{g}(\alpha_j,\beta_j), \tag{9.4.2}$$

$$\boldsymbol{\Sigma}^+(x,t,\lambda) = \boldsymbol{\Sigma}^-(x,t,\lambda)\begin{bmatrix} e^{i\Omega_j(x,t)} & 0 \\ 0 & e^{-i\Omega_j(x,t)} \end{bmatrix},\ \lambda \in \bigcup_{j=1}^{g}(\beta_j,\alpha_{j+1}). \tag{9.4.3}$$

Since $\sqrt{P(\lambda)} = \mathcal{O}(|\lambda|^{g+1/2})$, $\boldsymbol{G}$ has growth in λ at ∞ unless $m_k(x,t) = 0$ for $k = 1,\dots,g$. We wish to determine $\{\Omega_j\}_{j=1}^g$ so that $\boldsymbol{\Sigma}$ has the same asymptotic behavior as $\boldsymbol{\Phi}$ as $\lambda \to \infty$, see (9.3.1). Thus, we must solve the following problem, which we put in slightly more abstract terms since we make use of it again below.

Problem 9.4.2. *Given continuous functions*

$$f_j(\lambda) : [\beta_j,\alpha_{j+1}] \to \mathbb{C},\quad j = 1,\dots,g,$$

we seek constants Ω_j satisfying the moment conditions

$$0 = \int_{\beta_j}^{\alpha_{j+1}} \frac{-f_j(\lambda) + i\Omega_j}{\sqrt{P(\lambda)}^+}\lambda^{i-1}d\lambda,\quad j = 1,\dots,g.$$

Theorem 9.4.3. *Problem 9.4.2 has a unique solution. Further, if each f_j takes purely imaginary values then each Ω_j is real valued.*

Proof. The second claim follows from the fact that $\sqrt{P(\lambda)}^+$ takes purely imaginary values in the gaps, $[\beta_j,\alpha_{j+1}]$. To establish the first claim, notice that Problem 9.4.2 is equivalent to the linear system

$$\begin{aligned} \boldsymbol{M}\boldsymbol{\Omega} &= \boldsymbol{V}, \\ (\boldsymbol{M})_{kj} &= i\int_{\beta_j}^{\alpha_{j+1}} \frac{\lambda^{k-1}}{\sqrt{P(\lambda)}}d\lambda, \\ (\boldsymbol{\Omega})_j = \Omega_j,\quad (V)_i &= \sum_{j=1}^{g}\int_{\beta_j}^{\alpha_{j+1}} \frac{f_j(\lambda)}{\sqrt{P(\lambda)}}\lambda^{k-1}d\lambda. \end{aligned}$$

Assume the rows of M are linearly dependent. Then there exist constants d_k such that

$$\sum_{k=1}^{g} d_k \boldsymbol{M}_{kj} = 0, \text{ for } j = 1, \ldots, g.$$

Explicitly, this implies

$$\sum_{k=1}^{g} \int_{\beta_j}^{\alpha_{j+1}} \frac{d_k}{\sqrt{P(\lambda)}} \lambda^{k-1} d\lambda = \int_{\beta_j}^{\alpha_{j+1}} \left(\sum_{k=1}^{g} d_k \lambda^{k-1} \right) \frac{d\lambda}{\sqrt{P(\lambda)}}, \text{ for } j = 1, \ldots, g.$$

We show this implies that the holomorphic differential

$$f = \sum_{k=1}^{g} d_k \lambda^{k-1} \frac{d\lambda}{\sqrt{P(\lambda)}} = \sum_{k=1}^{g} d_k \lambda^{k-1} \frac{d\lambda}{w},$$

has zero a periods. Compute

$$\int_{\alpha_j}^{\beta_{j+1}} \frac{\lambda^{k-1}}{w} d\lambda = \frac{1}{2} \left(\int_{\alpha_j}^{\beta_{j+1}} \frac{\lambda^{k-1}}{w} d\lambda + \int_{\beta_{j+1}}^{\alpha_j} \frac{\lambda^{k-1}}{-w} d\lambda \right) = \frac{1}{2} \oint_{a_j} \frac{\lambda^{k-1}}{w} d\lambda.$$

Indeed, f integrates to zero around every a cycle implying that f is the zero differential, see Lemma 9.1.2. But since each of $\lambda^{k-1} w^{-1} d\lambda$ is linearly independent we conclude that $d_k = 0$, $k = 1, \ldots, g$ and the rows of $\boldsymbol{M}$ are linearly independent. □

If we select Ω_j to make all m_k vanish we use the condition

$$\lim_{\lambda \to \infty} \boldsymbol{\Sigma}(x, t, \lambda) = \begin{bmatrix} 1 & 1 \end{bmatrix},$$

in conjunction with (9.4.2) to obtain a RHP for $\boldsymbol{\Sigma}$. It is important that $\boldsymbol{\Omega}$ in Problem 9.4.2 is real valued. This implies the piecewise-constant jump matrix in (9.4.2) is bounded for all x and t.

9.4.2 Poles in the gaps

In this section we show how to use an additional BA function to, in effect, reduce the case where $\gamma_j(0,0) \in (\beta_j, \alpha_{j+1})$ to that of $\gamma_j(0,0) = \beta_j$. We assume that not all poles of $\Psi_\pm$ lie on the band ends $\{\beta_j\}_{j=1}^g$. Consider the planar representation of a BA function $(\Psi_p)_\pm$ which satisfies

$$\begin{aligned}
\boldsymbol{\Psi}_p^+(x,t,\lambda) &= \boldsymbol{\Psi}_p^-(x,t,\lambda) \begin{bmatrix} 0 & 1 \\ 1 & 0 \end{bmatrix}, \ \lambda \in (\alpha_{g+1}, \infty) \cup \bigcup_{j=1}^{g} (\alpha_j, \beta_j), \\
\boldsymbol{\Psi}_p(x,t,\lambda) &= \begin{bmatrix} e^{\kappa(\lambda)/2} & e^{-\kappa(\lambda)/2} \end{bmatrix} (I + \mathcal{O}(\lambda^{-1/2})), \\
\kappa(\lambda) &= \sum_{j=1}^{g} i t_j \lambda^{j-1/2}, \quad t_j \in \mathbb{R},
\end{aligned}$$

with poles at β_j. The goal is to choose $\{t_j\}_{j=1}^g$ so that $(\Psi_p)_\pm$ has zeros precisely at the poles of $\Psi_\pm$. Define $(\Psi_r)_\pm = \Psi_\pm(\Psi_p)_\pm$. The planar representation $\mathbf{\Psi}_r = \mathbf{\Psi}\mathbf{\Psi}_p$ with entry-wise multiplication now has poles at β_j and zeros at the zeros of $\mathbf{\Psi}$. We find $\Psi_\pm$ by first finding two functions $(\Psi_p)_\pm$ and $(\Psi_r)_\pm$ both of which have poles at $\{(0,\beta_j)\}_{j=1}^g$ and dividing. Thus, the general case of poles in gaps is reduced to poles at band ends provided we find the required $\{t_j\}_{j=1}^g$.

Remark 9.4.4. *We are using the term poles loosely. On $\hat{\mathbb{C}}$, $\mathbf{\Psi}_p$ has unbounded square-root singularities while on Γ, $(\Psi_p)_\pm$ has poles.*

We show that we can choose $\{t_j\}_{j=1}^g$ so that the zeros of $(\Psi_p)_\pm$ will be at an arbitrary divisor

$$D' = \sum_{j=1}^g R_j, \quad R_j \in a_j.$$

First, we state a lemma about the location of the zeros and poles of a BA function.

Lemma 9.4.5. *[9] Let D' be the divisor of the zeros of the BA function and D be that of the poles. Assume*

$$\Psi_\pm(\lambda) = e^{q(k)}(1 + \mathcal{O}(k^{-1})), \quad k \to \infty, \quad k^2 = \lambda. \tag{9.4.4}$$

On the Jacobi variety $J(\Gamma)$

$$A(D') = A(D) - \boldsymbol{V}, \tag{9.4.5}$$

where $\boldsymbol{V}$ is the vector of the b-periods of a normalized Abelian differential ν of the second kind that satisfies

$$\nu(Q) = dq(k) + \mathcal{O}(k^{-2})dk, \quad k = k(Q) \to \infty, \tag{9.4.6}$$

$$\oint_{a_l} \nu = 0, \quad \boldsymbol{V}_l = \oint_{b_l} \nu, \ l = 1, \ldots, g. \tag{9.4.7}$$

Conversely, if two divisors satisfy (9.4.5) *then they are the divisors of the poles and zeros of some BA function which satisfies* (9.4.4).

To determine $\mathbf{\Psi}_p$ we have D and D'. We need to show we can choose $\nu = d\kappa + \mathcal{O}(k^{-2})dk$ so that (9.4.5) holds. The following lemma provides this result.

Lemma 9.4.6. *Assume*

$$D = \sum_{j=1}^g Q_j, \quad D' = \sum_{j=1}^g R_j, \quad Q_j, R_j \in a_j.$$

Then there exists real constants $\{t_j\}_{j=1}^g$ so that the differential

$$\nu = \sum_{j=1}^g t_j \nu_j$$

satisfies the properties in (9.4.6) *with* $q(k) = \kappa(k)$, *and* ν_j *can be constructed explicitly.*

Proof: *Define* τ_j *to be the Abelian differential of the second kind with principal part (see Section 9.1)*

$$\tau_j = (2j-1)\left(k^{2j-3} + \mathcal{O}(k^{-2})\right) dk, \quad k \to \infty,$$

where $1/k$ *is a parameter in the neighborhood of* ∞. *For* $j \geq 1$, *we choose a path of integration that lies on one sheet. We have*

$$\int_{\lambda_0}^{\lambda} \tau_j = \pm\lambda^{j-1/2}(1 + \mathcal{O}(\lambda^{j-3/2})) \quad as \quad \lambda \to \infty.$$

Define

$$\nu = \sum_{j=1}^{g} it_j(\tau_j + \eta_j),$$

where η_j *is a holomorphic differential chosen so that* $\tau_j + \eta_j$ *has vanishing a periods. We define* $\nu_j = i(\tau_j + \eta_j)$. *Consider the system of equations*

$$\oint_{b_k} \nu = (V)_k, \quad k = 1, \ldots, g.$$

It follows that (see Lemma 9.1.7)

$$\oint_{b_k} \nu = \sum_{j=1}^{g} it_j \, \frac{1}{(2j-2)!} \frac{d^{2j-2}}{dz^{2j-2}} r_k(z)\Big|_{z=0}, \quad k = 1, \ldots, g.$$

Here z *is a local parameter in the neighborhood of* ∞: $z(\infty) = 0$ *and* $\omega_k = r_k(z)dz$. *To compute these derivatives we again use a convenient basis, not normalized, for the holomorphic differentials:*

$$u_j = \frac{\lambda^{j-1}}{w} d\lambda, \quad j = 1, \ldots, g.$$

Set $\lambda = 1/z^2$ *and compute*

$$\begin{aligned} u_j &= -2z^{2(g-j)} \left((1 - \alpha_{j+1}z) \prod_{i=1}^{g} (1 - \alpha_i z)(1 - \beta_i z) \right)^{-1/2} dz \\ &= s_j(z)dz. \end{aligned}$$

It is clear that the matrix

$$(A)_{kj} = \frac{d^{2k-2}}{dz^{2k-2}} s_j(z),$$

is triangular with non-vanishing diagonal entries. There exists an invertible linear trans-

formation from $\{u_j\}_{j=1}^g$ *to* $\{\omega_k\}_{k=1}^g$*, and since* $\boldsymbol{A}$ *is invertible, it follows that the system*

$$\oint_{b_k} \nu = V_k, \text{ for } k = 1, \ldots, g, \tag{9.4.8}$$

is uniquely solvable for $\{t_j\}_{j=1}^g$*. This proves the existence of a BA function with asymptotic behavior* (9.4.4) *and one arbitrary zero on each a cycle.*

In summary, the BA function $(\Psi_r)_\pm = (\Psi_p)_\pm \Psi_\pm$ has poles located at $(\beta_j, 0)$ and one zero on each a-cycle corresponding to the zeros of $\Psi_\pm$. We show below how to compute such a BA function. We use the approach of Section 9.3 to formulate a RHP for $(\Psi_p)_\pm$:

$$\boldsymbol{\Sigma}_p^+(x,t,\lambda) = \boldsymbol{\Sigma}_p^-(x,t,\lambda) \begin{bmatrix} 0 & 1 \\ 1 & 0 \end{bmatrix}, \ \lambda \in (\alpha_{n+1}, \infty) \cup \bigcup_{j=1}^g (\alpha_j, \beta_j), \tag{9.4.9}$$

$$\boldsymbol{\Sigma}_p^+(x,t,\lambda) = \boldsymbol{\Sigma}_p^-(x,t,\lambda) \begin{bmatrix} e^{iW_j} & 0 \\ 0 & e^{-iW_j} \end{bmatrix}, \ \lambda \in \bigcup_{j=1}^g (\beta_j, \alpha_{j+1}), \tag{9.4.10}$$

where each of the $W_j \in \mathbb{R}$ is chosen so that the g-function

$$\mathcal{G}_p(\lambda) = \frac{\sqrt{P(\lambda)}}{2\pi i} \sum_{j=1}^g \int_{\beta_j}^{\alpha_{j+1}} \frac{-\kappa(s) + iW_j}{\sqrt{P(\lambda)}^+} \frac{ds}{s-\lambda}, \tag{9.4.11}$$

satisfies $\mathcal{G}_p(\lambda) = \mathcal{O}(\lambda^{-1/2})$ as $\lambda \to \infty$. Theorem 9.4.3 provides a well-defined map from $\{t_j\}_{j=1}^g$ to $\{W_j\}_{j=1}^g$. Furthermore each W_j can be taken modulo 2π. The RHP for $(\Psi_r)_\pm$ is similar but $\kappa(\lambda)$ must be replaced with $\kappa(\lambda) + 2ix\lambda^{1/2} + 8it\lambda^{3/2}$ to account for the x and t dependence in $\Psi_\pm$. In this case we write $W_j(x,t)$. This is elaborated below.

9.5 A Riemann–Hilbert problem with smooth solutions

The numerical method described in [89] requires solutions of the RHP to be smooth. We need to deform the RHP to take into account the singularities explicitly if we wish to solve it numerically. In this section, we assume the divisor for the poles of the BA function is

$$D = \sum_{i=1}^g (\beta_j, 0),$$

and that the $\Omega_j(x,t)$ are chosen so that the moment conditions for $\mathcal{G}$ are satisfied. We replace $\Omega_j(x,t)$ with W_j and $W_j(x,t)$ in the case of $(\Psi_p)_\pm$ and $(\Psi_r)_\pm$, respectively. In light of the previous section, all other cases can be reduced to this. Define

$$\boldsymbol{\Delta}(x,t,\lambda) = \begin{bmatrix} \delta(x,t,\lambda) & 0 \\ 0 & 1/\delta(x,t,\lambda) \end{bmatrix}, \quad \delta(x,t,\lambda) = \prod_{j=1}^g \left(\frac{\lambda - \alpha_{j+1}}{\lambda - \beta_j} \right)^{\Omega_j(x,t)/(2\pi)}.$$

The branch cut for δ to be along the intervals $[\beta_j, \alpha_{j+1}]$ and we assume $\Omega_j(x,t) \in [0, 2\pi)$. Note that $\boldsymbol{\Delta}$ satisfies

$$\boldsymbol{\Delta}^+(x,t,\lambda) = \boldsymbol{\Delta}^-(x,t,\lambda) \begin{bmatrix} e^{i\Omega_j(x,t)} & 0 \\ 0 & e^{-i\Omega_j(x,t)} \end{bmatrix}, \quad \lambda \in (\beta_j, \alpha_{j+1}).$$

Define

$$\boldsymbol{H}(\lambda) = \frac{1}{2} \begin{bmatrix} 1 & 1+\sqrt{\lambda-\alpha_{n+1}} \\ 1 & 1-\sqrt{\lambda-\alpha_{n+1}} \end{bmatrix},$$

where the function $\sqrt{\lambda-\alpha_{n+1}}$ has its branch cut on $[\alpha_{n+1}, \infty)$, and satisfies $\sqrt{\lambda-\alpha_{n+1}} \sim i|\lambda|^{1/2}$ as $\lambda \to -\infty$ to fix the branch. The last function we need is the g-function matrix

$$\boldsymbol{G}(x,t,\lambda) = \begin{bmatrix} e^{-\mathcal{G}(x,t,\lambda)} & 0 \\ 0 & e^{\mathcal{G}(x,t,\lambda)} \end{bmatrix}.$$

Note that if we were solving for $(\Psi_p)_\pm$ or $(\Psi_r)_\pm$ we would replace $\mathcal{G}$ with (9.4.11).

We introduce a local parametrix for what follows. Consider the RHP

$$\boldsymbol{Y}^+(\lambda) = \boldsymbol{Y}^-(\lambda) \begin{bmatrix} 0 & c \\ 1/c & 0 \end{bmatrix}, \quad \lambda \in (a,b), \tag{9.5.1}$$

where we do not specify the asymptotic behavior since we wish to obtain multiple solutions. From Example 3.4.3 we find

$$\boldsymbol{Y}(\lambda; a, b, \alpha, \beta, c) = \begin{bmatrix} -i(\lambda-a)^\alpha(\lambda-b)^\beta/c & i(\lambda-a)^\alpha(\lambda-b)^\beta \\ 1/c & 1 \end{bmatrix}, \quad \alpha, \beta = \pm\frac{1}{2},$$

is a solution of (9.5.1). We choose the branch cut of $(\lambda-a)^\alpha(\lambda-b)^\beta$ to be along the interval $[a,b]$ with $(\lambda-a)^\alpha(\lambda-b)^\beta \sim \lambda^{\alpha+\beta}$ as $\lambda \to \infty$. To simplify notation we define

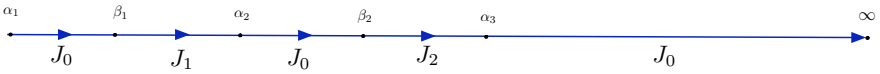

Figure 9.5.1: The contours and jump matrices of the RHP for $\boldsymbol{\Sigma}$.

$\boldsymbol{J}_j(x,t) = \operatorname{diag}(e^{-i\Omega_j(x,t)}, e^{i\Omega(x,t)})$ and

$$\boldsymbol{J}_0 = \begin{bmatrix} 0 & 1 \\ 1 & 0 \end{bmatrix}.$$

We need a local parametrix at each point α_j or β_j. This motivates the definition

$$\begin{aligned}
\boldsymbol{A}_1(x,t,\lambda) &= \boldsymbol{Y}(\lambda; \alpha_1, \beta_1, 1/2, -1/2, 1), \\
\boldsymbol{A}_j(x,t,\lambda) &= \boldsymbol{Y}(\lambda; \alpha_j, \beta_j, 1/2, -1/2, \exp(-i\Omega_{j-1}(x,t))), \quad j = 2, \dots, g+1, \\
\boldsymbol{B}_j(x,t,\lambda) &= \boldsymbol{Y}(\lambda; \alpha_j, \beta_j, 1/2, -1/2, \exp(-i\Omega_j(x,t))), \quad j = 1, \dots, g.
\end{aligned}$$

This allows us to enforce boundedness at each α_j with a possibly unbounded singularity at β_j. The matrices $\boldsymbol{A}_j$ are used locally at α_j and $\boldsymbol{B}_j$ at β_j.

Consider the following example. The general case can be inferred from this.

Example 9.5.1 (Genus two)**.** *Our initial RHP is* (9.4.2) *with the condition*

$$\lim_{\lambda\to\infty} \boldsymbol{\Sigma}(x,t,\lambda) = \begin{bmatrix} 1 & 1 \end{bmatrix},$$

see Figure 9.5.1. First, we introduce a circle around $\alpha_3 = \alpha_{g+1}$*. In addition we place a large circle around all the gaps, see Figure 9.5.2. Now, we redefine our function* $\boldsymbol{\Sigma}$ *in various regions. Define* $\boldsymbol{\Sigma}_1$ *by the piecewise definition in Figure 9.3(a). We compute the jumps satisfied by* $\boldsymbol{\Sigma}_1$*, see Figure 9.3(b). An important calculation is that if* $\boldsymbol{\Sigma}_1(x,t,\lambda) = \begin{bmatrix} 1 & 1 \end{bmatrix} + \mathcal{O}(\lambda^{-1})$ *then*

$$\begin{aligned}\boldsymbol{\Sigma}_1(x,t,\lambda)\boldsymbol{H}(\lambda) &= \frac{1}{2}\left(\begin{bmatrix} 1 & 1 \end{bmatrix} + \mathcal{O}(\lambda^{-1})\right)\begin{bmatrix} 1 & 1+\sqrt{\lambda-\alpha_{n+1}} \\ 1 & 1-\sqrt{\lambda-\alpha_{n+1}} \end{bmatrix} \\ &= \begin{bmatrix} 1 & 1 \end{bmatrix} + \mathcal{O}(\lambda^{-1/2}).\end{aligned}$$

This allows us to obtain functions with the correct asymptotic behavior.

We present the deformation in the interior of the large circle in Figure 9.3(a). See Figure 9.4(a) for the piecewise definition of $\boldsymbol{\Sigma}_2$ *and Figure 9.4(b) for the jumps and jump contours for* $\boldsymbol{\Sigma}_2$*. While this RHP can be solved numerically, we make a final deformation to reduce the number of contours present. Define* $\mathcal{D}$ *to be the region inside the large outer circle but outside each of the smaller circles around* α_j, β_j*. Define*

$$\boldsymbol{\Sigma}_3(x,t,\lambda) = \begin{cases} \boldsymbol{\Sigma}_2(x,t,\lambda), \boldsymbol{\Delta}^{-1}(x,t,\lambda) & \text{if } \lambda \in \mathcal{D}, \\ \boldsymbol{\Sigma}_2(x,t,\lambda), & \text{otherwise.} \end{cases}$$

See Figure 9.5.5 for the jumps and jump contours of the RHP for $\boldsymbol{\Sigma}_3$*. We refer to this as the deformed and regularized RHP associated with* $\Psi_\pm$*.*

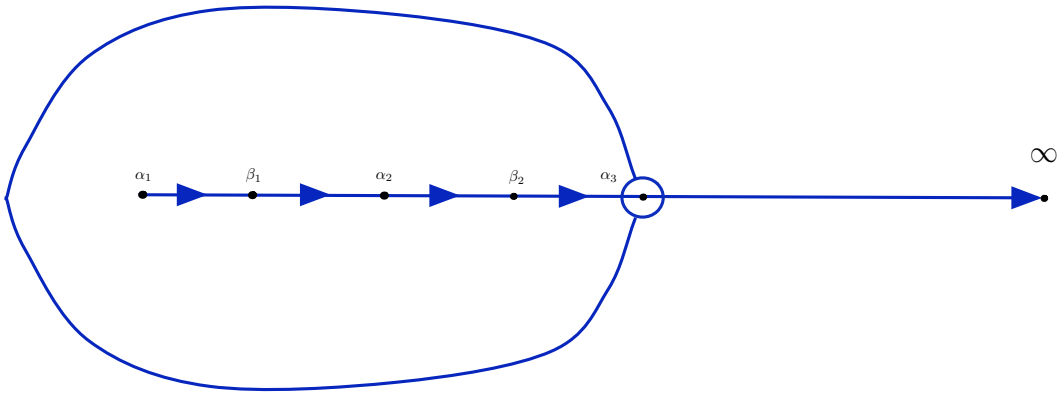

Figure 9.5.2: Introducing a large circle around α_j and β_j.

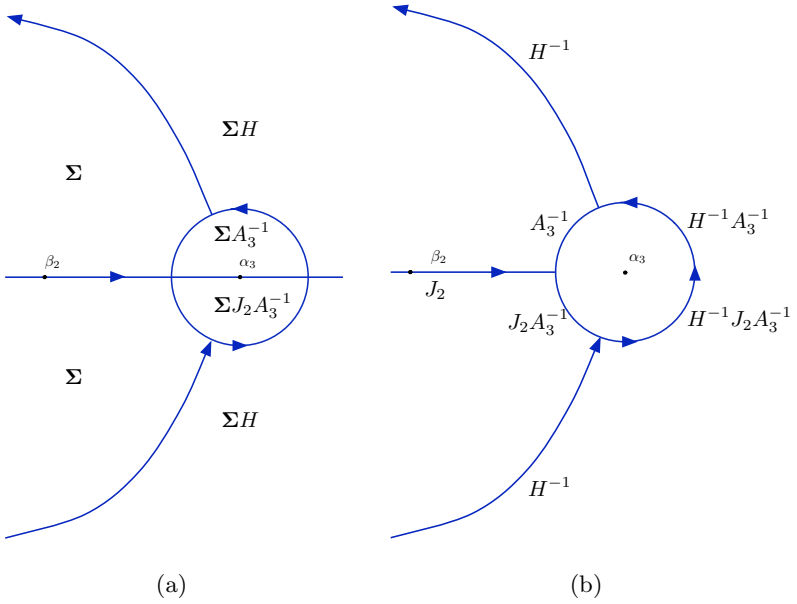

Figure 9.5.3: (a) The piecewise definition of $\mathbf{\Sigma}_1$. (b) The jump contours and jump matrices for the RHP for $\mathbf{\Sigma}_1$.

This resulting RHP has smooth solutions by the theory of Chapter 3: the RHP is k-regular for all k. Furthermore, the uniqueness of the BA function gives us existence and uniqueness of the solution of this RHP. See Appendix 9.7 for a more detailed discussion of the solvability of the RHP. This justifies solving for $\mathbf{\Sigma}_3$ numerically.

9.5.1 Reconstruction of the solution to the KdV equation

Once the function $\mathbf{\Sigma}_3$ above is known (at least numerically) we want to extract from it the solution of the KdV equation. We use that $\mathbf{\Sigma}_3$ is analytic at infinity and that each component of $\mathbf{\Psi}$ satisfies (9.2.1). For large λ we write

$$\mathbf{\Sigma}_3(x,t,\lambda) = \mathbf{\Psi}(x,t,\lambda)\boldsymbol{R}(x,t,\lambda)\boldsymbol{G}(x,t,\lambda)\boldsymbol{H}(\lambda). \tag{9.5.2}$$

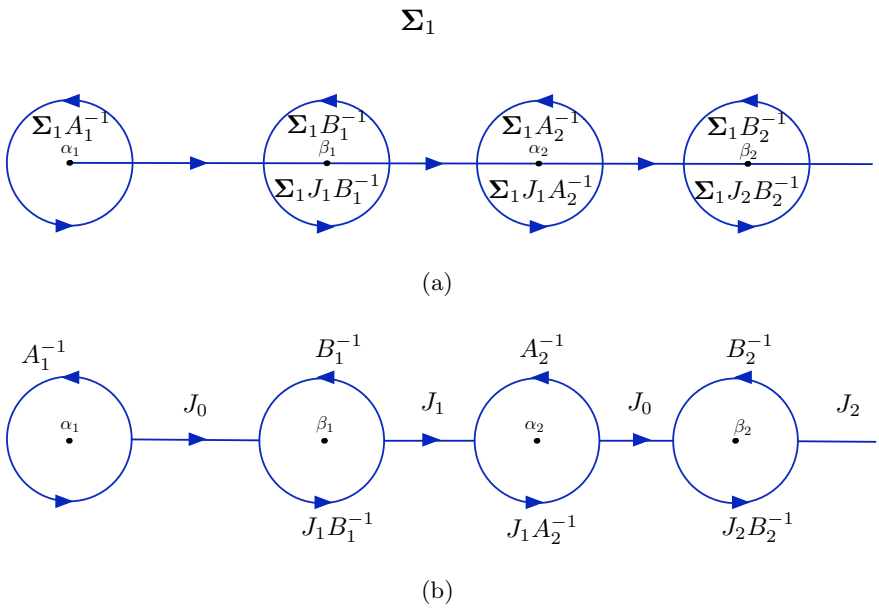

Figure 9.5.4: (a) The piecewise definition of $\mathbf{\Sigma}_2$ inside the outer circle. (b) The jump contours and jump matrices for the RHP for $\mathbf{\Sigma}_2$.

We find a differential equation for $\mathbf{\Sigma}_3$. Differentiating (9.5.2) we find

$$\begin{aligned}
\partial_x \mathbf{\Sigma}_3(x,t,\lambda) = {} & \partial_x \mathbf{\Psi}(x,t,\lambda)\boldsymbol{R}(x,t,\lambda)\boldsymbol{G}(x,t,\lambda)\boldsymbol{H}(\lambda)+ \\
& \mathbf{\Psi}(x,t,\lambda)\partial_x \boldsymbol{R}(x,t,\lambda)\boldsymbol{G}(x,t,\lambda)\boldsymbol{H}(\lambda)+ \\
& \mathbf{\Psi}(x,t,\lambda)\boldsymbol{R}(x,t,\lambda)\partial_x \boldsymbol{G}(x,t,\lambda)\boldsymbol{H}(\lambda). \\
\partial_{xx} \mathbf{\Sigma}_3(x,t,\lambda) = {} & \partial_{xx} \mathbf{\Psi}(x,t,\lambda)\boldsymbol{R}(x,t,\lambda)\boldsymbol{G}(x,t,\lambda)\boldsymbol{H}(\lambda)+ \\
& \mathbf{\Psi}(x,t,\lambda)\partial_{xx} \boldsymbol{R}(x,t,\lambda)\boldsymbol{G}(x,t,\lambda)\boldsymbol{H}(\lambda)+ \\
& \mathbf{\Psi}(x,t,\lambda)\boldsymbol{R}(x,t,\lambda)\partial_{xx} \boldsymbol{G}(x,t,\lambda)\boldsymbol{H}(\lambda)+ \\
& 2\mathbf{\Psi}(x,t,\lambda)\partial_x \boldsymbol{R}(x,t,\lambda)\partial_x \boldsymbol{G}(x,t,\lambda)\boldsymbol{H}(\lambda)+ \\
& 2\partial_x \mathbf{\Psi}(x,t,\lambda)\partial_x \boldsymbol{R}(x,t,\lambda)\boldsymbol{G}(x,t,\lambda)\boldsymbol{H}(\lambda)+ \\
& 2\partial_x \mathbf{\Psi}(x,t,\lambda)\boldsymbol{R}(x,t,\lambda)\boldsymbol{\partial}_x G(x,t,\lambda)\boldsymbol{H}(\lambda).
\end{aligned}$$

We seek to simplify this formula. Define $\boldsymbol{r}(\lambda) = \operatorname{diag}(2i\lambda^{1/2}, -2i\lambda^{1/2})$ then

$$\begin{aligned}
\partial_x \boldsymbol{R}(x,t,\lambda) &= \boldsymbol{r}(\lambda)\boldsymbol{R}(x,t,\lambda), \\
\partial_{xx} \boldsymbol{R}(x,t,\lambda) &= \boldsymbol{r}^2(\lambda)\boldsymbol{R}(x,t,\lambda).
\end{aligned}$$

It follows that each $\Omega_j(x,t)$ depends linearly on x. Define $\boldsymbol{g}(\lambda) = \operatorname{diag}(-\partial_x g(x,t,\lambda), \partial_x g(x,t,\lambda))$, therefore

$$\begin{aligned}
\partial_x \boldsymbol{G}(x,t,\lambda) &= \boldsymbol{g}(\lambda)\boldsymbol{G}(x,t,\lambda), \\
\partial_{xx} \boldsymbol{G}(x,t,\lambda) &= \boldsymbol{g}^2(\lambda)\boldsymbol{G}(x,t,\lambda).
\end{aligned}$$

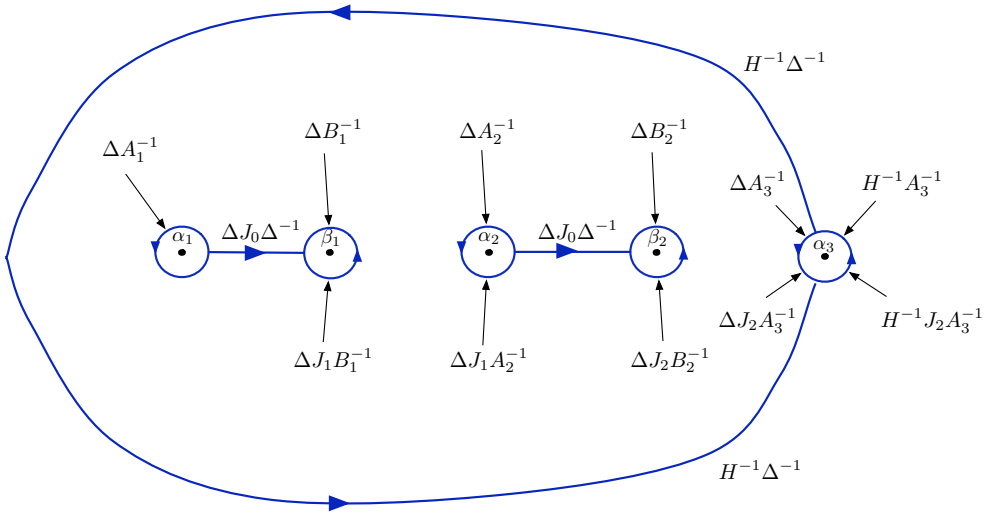

Figure 9.5.5: The final RHP for $\mathbf{\Sigma}_3$. The same deformation works for RHPs which arise from arbitrary genus BA functions by adding additional contours.

Also, $\boldsymbol{R}, \boldsymbol{G}, \boldsymbol{r}$ and $\boldsymbol{g}$ are diagonal and mutually commute. We write

$$\begin{aligned}
\partial_x \mathbf{\Sigma}_3(x,t,\lambda) &= \partial_x \mathbf{\Psi}(x,t,\lambda)\boldsymbol{R}(x,t,\lambda)\boldsymbol{G}(x,t,\lambda)\boldsymbol{H}(\lambda) \\
&\quad + \mathbf{\Psi}(x,t,\lambda)\boldsymbol{R}(x,t,\lambda)\boldsymbol{G}(x,t,\lambda)\boldsymbol{H}(\lambda)\boldsymbol{H}^{-1}(\lambda)[\boldsymbol{r}(\lambda)+\boldsymbol{g}(\lambda)]\boldsymbol{H}(\lambda), \\
\partial_{xx} \mathbf{\Sigma}_3(x,t,\lambda) &= \partial_{xx} \mathbf{\Psi}(x,t,\lambda)\boldsymbol{R}(x,t,\lambda)\boldsymbol{G}(x,t,\lambda)\boldsymbol{H}(\lambda) \\
&\quad + 2\partial_x \mathbf{\Psi}(x,t,\lambda)\boldsymbol{R}(x,t,\lambda)\boldsymbol{G}(x,t,\lambda)\boldsymbol{H}(\lambda)\boldsymbol{H}^{-1}(\lambda)[\boldsymbol{r}(\lambda)+\boldsymbol{g}(\lambda)]\boldsymbol{H}(\lambda) \\
&\quad + \mathbf{\Psi}(x,t,\lambda)\boldsymbol{R}(x,t,\lambda)\boldsymbol{G}(x,t,\lambda)\boldsymbol{H}(\lambda)\boldsymbol{H}^{-1}(\lambda)[\boldsymbol{g}^2(\lambda)+2\boldsymbol{g}(\lambda)\boldsymbol{r}(\lambda)+\boldsymbol{r}^2(\lambda)]\boldsymbol{H}(\lambda).
\end{aligned}$$

We proceed to eliminate $\mathbf{\Psi}$. Since $\partial_{xx}\mathbf{\Psi} = -\lambda\mathbf{\Psi} - q(x,t)\mathbf{\Psi}$, we obtain

$$\begin{aligned}
\partial_{xx} \mathbf{\Sigma}_3(x,t,\lambda) &= [-\lambda - q(x,t)]\mathbf{\Sigma}_3(x,t,\lambda) + 2\partial_x \mathbf{\Sigma}_3(x,t,\lambda)\boldsymbol{H}^{-1}(\lambda)[\boldsymbol{g}(\lambda)+\boldsymbol{r}(\lambda)]\boldsymbol{H}(\lambda) \\
&\quad - \mathbf{\Sigma}_3(x,t,\lambda)\boldsymbol{H}^{-1}(\lambda)[\boldsymbol{g}(\lambda)+\boldsymbol{r}(\lambda)]^2\boldsymbol{H}(\lambda).
\end{aligned} \tag{9.5.3}$$

Set $\mathbf{\Sigma}_3(x,t,\lambda) = \begin{bmatrix} 1 & 1 \end{bmatrix} + \boldsymbol{c}_1(x,t)/\lambda + \mathcal{O}(\lambda^{-2})$ and substitute, assuming each derivative of $\mathbf{\Sigma}_3$ has an induced asymptotic expansion,

$$\begin{aligned}
\partial_{xx}\boldsymbol{c}_1(x,t)/\lambda + \mathcal{O}(\lambda^{-2}) &= [-\lambda - q(x,t)](\begin{bmatrix} 1 & 1 \end{bmatrix} + \boldsymbol{c}_1(x,t)/\lambda + \mathcal{O}(\lambda^{-2})) \\
&\quad + (\begin{bmatrix} 1 & 1 \end{bmatrix} + \partial_x\boldsymbol{c}_1(x,t)/\lambda + \mathcal{O}(\lambda^{-2}))\boldsymbol{H}^{-1}(\lambda)[\boldsymbol{g}(\lambda)+\boldsymbol{r}(\lambda)]\boldsymbol{H}(\lambda) \\
&\quad + (\begin{bmatrix} 1 & 1 \end{bmatrix} + \boldsymbol{c}_1(x,t)/\lambda + \mathcal{O}(\lambda^{-2}))\boldsymbol{H}^{-1}(\lambda)[\boldsymbol{g}(\lambda)+\boldsymbol{r}(\lambda)]^2\boldsymbol{H}(\lambda).
\end{aligned}$$

It can be shown that the $\mathcal{O}(\lambda)$ terms on each side of this equation cancel. Equating the $\mathcal{O}(1)$ terms we obtain

$$\begin{aligned} q(x,t)\begin{bmatrix} 1 & 1 \end{bmatrix} = &- \lim_{\lambda\to\infty} \partial_x \boldsymbol{c}_1(x,t)/\lambda \boldsymbol{H}^{-1}(\lambda)[\boldsymbol{g}(\lambda)+\boldsymbol{r}(\lambda)]\boldsymbol{H}(\lambda) \\ &- \lim_{\lambda\to\infty} \Big(\begin{bmatrix} -\lambda & -\lambda \end{bmatrix} + \Big(\begin{bmatrix} 1 & 1 \end{bmatrix} + \boldsymbol{c}_1(x,t)/\lambda + \mathcal{O}(\lambda^{-2}) \Big) \\ &\times \boldsymbol{H}^{-1}(\lambda)[\boldsymbol{g}(\lambda)+\boldsymbol{r}(\lambda)]^2 \boldsymbol{H}(\lambda) \Big) . \end{aligned}$$

Equating $\partial_x \boldsymbol{c}_1(x,t) = \begin{bmatrix} s_1(x,t) & s_2(x,t) \end{bmatrix}$ and working this out explicitly, we find

$$\begin{aligned} q(x,t) &= 2i(s_2(x,t)-s_1(x,t)) + 2iE, \\ E &= -\frac{1}{2\pi}\sum_{n=1}^{g} \int_{\beta_n}^{\alpha_{n+1}} \frac{\partial_x \Omega_n(x,t) - 2\lambda^{1/2}}{\sqrt{P(\lambda)}^{+}} \lambda^g d\lambda. \end{aligned} \tag{9.5.4}$$

9.5.2 Regularization of the RHP with poles in the gaps

In this section we deal with the case where the divisor for the poles of the BA function is of the form

$$D = \sum_{i=1}^{g} Q_i, \quad Q_i \in a_i.$$

We have proved existence of a BA function with one arbitrary zero on each a-cycle. We consider the BA function $(\Psi_r)_\pm = (\Psi_p)_\pm \Psi_\pm$ which has poles located at $\{(0,\beta_j)\}_{j=1}^g$ and one zero on each a-cycle. In this section we assume we know $t_1, t_2, \ldots$ which are required to find $(\Psi_p)_\pm$. In the next section we discuss computing $\{t_j\}_{j=1}^g$. It follows that

$$(\Psi_r)_\pm \sim e^{\pm Z(x,t,\lambda)/2}, \tag{9.5.5}$$

where

$$Z(x,t,\lambda) = \kappa(\lambda) + 2ix\lambda^{1/2} + 8it\lambda^{3/2} = 2i(x+t_1)\lambda^{1/2} + 2i(4t+t_2)\lambda^{3/2} + 2i\sum_{j=3}^{g} t_j \lambda^{(2j-1)/2}.$$

Using the techniques in Section 9.5.1 we see this is all the information that is needed to set up a solvable RHP for $(\Psi_r)_\pm$ with smooth solutions. We have to extract the solution to the KdV equation from $(\Psi_r)_\pm$. We solve for a function $\boldsymbol{\Sigma}_3$, the deformation of $\boldsymbol{\Psi}_r$, that satisfies

$$\begin{aligned} \boldsymbol{\Sigma}_3(x,t,\lambda) &= \boldsymbol{\Psi}(x,t,\lambda)\boldsymbol{R}(x,t,\lambda)\boldsymbol{G}(x,t,\lambda)\boldsymbol{\Psi}_p'(\lambda)\boldsymbol{H}(\lambda), \\ \boldsymbol{\Psi}_p'(\lambda) &= \operatorname{diag} \boldsymbol{\Psi}_p(\lambda), \end{aligned} \tag{9.5.6}$$

for large λ. If we perform the same calculations which results in (9.5.3). We obtain

$$\begin{aligned}\partial_{xx}\boldsymbol{\Sigma}_3(x,t,\lambda) &= [-\lambda - q(x,t)]\boldsymbol{\Sigma}_3(x,t,\lambda) \\ &+ 2\partial_x\boldsymbol{\Sigma}_3(x,t,\lambda)\boldsymbol{H}^{-1}(\lambda)(\boldsymbol{\Psi}_p'(\lambda))^{-1}[\boldsymbol{g}(\lambda)+\boldsymbol{r}(\lambda)]\boldsymbol{\Psi}_p'(\lambda)\boldsymbol{H}(\lambda) \\ &- \boldsymbol{\Sigma}_3(x,t,\lambda)\boldsymbol{H}^{-1}(\lambda)(\boldsymbol{\Psi}_p'(\lambda))^{-1}[\boldsymbol{g}(\lambda)+\boldsymbol{r}(\lambda)]^2\boldsymbol{\Psi}_p'(\lambda)\boldsymbol{H}(\lambda).\end{aligned} \tag{9.5.7}$$

But $\boldsymbol{\Psi}_p'$ is diagonal and commutes with $\boldsymbol{g}$ and $\boldsymbol{h}$. Therefore, all $\boldsymbol{\Psi}_p'$ dependence cancels out. We see that (9.5.4) is invariant under multiplication by $(\Psi_p)_\pm$. Thus, the solution $q(x,t)$ to the KdV equation is extracted from $\boldsymbol{\Sigma}_3$ by (9.5.4). We summarize our results in the following theorem.

Theorem 9.5.2. *If $\boldsymbol{\Sigma}_3(x,t,\lambda)$ is the solution of the deformed and regularized RHP associated with $(\Psi_r)_\pm$ and*

$$\boldsymbol{\Sigma}_3(x,t,\lambda) = \begin{bmatrix} 1 & 1 \end{bmatrix} + \boldsymbol{c}_1(x,t)\lambda^{-1} + \mathcal{O}(\lambda^{-2}), \quad \boldsymbol{c}_1(x,t) = \begin{bmatrix} s_1(x,t) & s_2(x,t) \end{bmatrix},$$

then the corresponding solution of the KdV equation is found through

$$\begin{aligned} q(x,t) &= 2i(s_2(x,t) - s_1(x,t) + 2iE, \\ E &= -\frac{1}{2\pi}\sum_{j=1}^{g}\int_{\beta_j}^{\alpha_{j+1}} \frac{\partial_x W_j(x,t) - 2\lambda^{1/2}}{\sqrt{P(\lambda)}^+}\lambda^g d\lambda, \end{aligned}$$

where $\{W_j(x,t)\}_{j=1}^{\infty}$ are defined by the moment conditions for (9.4.11) *with $\kappa(\lambda)$ replaced with $Z(x,t,\lambda)$.*

This theorem states that despite the theoretical use of the function $(\Psi_p)_\pm$, the computation of the solution to the KdV equation does not require the computation of $(\Psi_p)_\pm$.

9.6 Numerical computation

In this section we discuss the computation of all the components of the theory. These components are:

1. Evaluating contour integrals used in the Abel map and Problem 9.4.2.
2. Computing the singular integrals used in the representation of the g-function.
3. Solving the deformed and regularized RHP for the Baker–Akhiezer function.
4. Extracting the solution to the KdV equation from the Baker–Akhiezer function.

9.6.1 Computing contour integrals

The developments above require the computation of integrals of the form

$$I_j(f) = \int_{\beta_j}^{\alpha_{j+1}} \frac{f(\lambda)}{\sqrt{P(\lambda)}^+}d\lambda, \tag{9.6.1}$$

to determine the g-function and compute Ω_j/W_j. Note that in the cases we consider f is analytic near the contour of integration. Also, we compute the Abel map of divisors whose points lie in gaps. We always choose $Q_0 = (\alpha_1, 0)$ in (9.1.1) and integrate along Γ_+ across the bands and gaps. Thus computing the Abel map of a point in a gap requires computation of integrals of the form (9.6.1) along with integrals of the form

$$\begin{aligned} K_j(f) &= \int_{\alpha_j}^{\beta_j} \frac{f(\lambda)}{\sqrt{P(\lambda)}^+} d\lambda, \\ I_j(f,\lambda) &= \int_{\beta_j}^{\lambda} \frac{f(s)}{\sqrt{P(s)}^+} ds. \end{aligned} \tag{9.6.2}$$

While numerical integration packages can handle such integrals, it is beneficial to use Chebyshev polynomials. For example, define

$$s = m(\lambda) = \frac{2}{\beta_j - \alpha_j}\lambda - \frac{\beta_j + \alpha_j}{\beta_j - \alpha_j}.$$

We change (9.6.1) to

$$I_j(f) = \int_{-1}^{1} \frac{f(m^{-1}(s))}{\sqrt{P(m^{-1}(s))}^+} dm^{-1}(s).$$

The function

$$w(s) = \frac{\sqrt{1-s^2}}{\sqrt{P(m^{-1}(s))}},$$

is analytic in a neighborhood of the interval $[-1, 1]$. We write

$$I_j(f) = \int_{-1}^{1} \left(\frac{f(m^{-1}(s))}{\sqrt{P(m^{-1}(s))}^+} w(s) \frac{d}{ds} m^{-1}(s) \right) \frac{ds}{\sqrt{1-s^2}}.$$

The Chebyshev series approximation of the function in parenthesis converges exponentially since it is analytic in a neighborhood of $[-1, 1]$. A discrete cosine transform is used to approximate the series and the first coefficient in the series gives a very good approximation to $I_j(f)$. Similar ideas work for $K_j(f)$ but we must modify our approach for $I_j(f, \lambda)$. Consider the integral

$$F_n(\lambda) = \int_{-1}^{\lambda} T_n(x) \frac{dx}{\sqrt{1-x^2}}, \quad \lambda \in (1, 1).$$

Here T_n denotes the nth-order Chebyshev polynomial of the first kind. Using the standard change of variables $x = \cos\theta$,

$$F_n(\lambda) = -\int_{\pi}^{\arccos\lambda} T_n(\cos\theta) d\theta = -\int_{\pi}^{\arccos\lambda} \cos(n\theta) d\theta.$$

Therefore

$$F_n(\lambda) = \begin{cases} -\frac{\sin(n \arccos \lambda)}{n} & \text{if } n > 0, \\ \pi - \arccos \lambda & \text{if } n = 0. \end{cases}$$

Using the change of variables $m(\lambda)$ and the discrete cosine transform we can compute each $I_j(f, \lambda)$ with this formula.

We need to compute b periods. The b cycles have a more complicated relationship. Consider the cycles $\tilde{b}_j$ in Figure 9.6.1. We compute

$$\oint_{\tilde{b}_j} w = 2 \int_{\alpha_j}^{\beta_j} f(\lambda) d\lambda.$$

From Figure 9.6.1, we see that $b_1 = \tilde{b}_1$ and $b_i = \tilde{b}_i + b_{i-1}$. This gives a recurrance relationship for b periods of a differential.

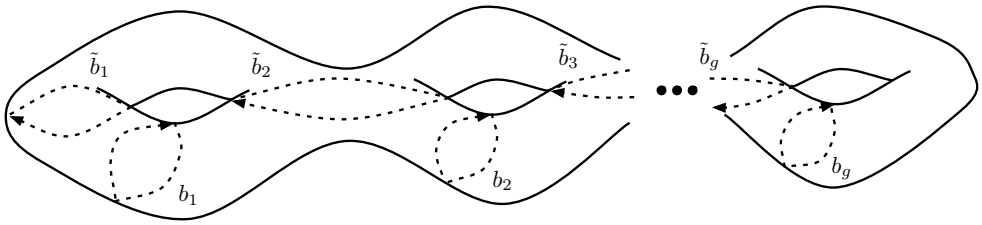

Figure 9.6.1: The cycles $\tilde{b}_j$ on a schematic of the Riemann surface.

We must know ω_k before computing the Abel map. We describe how to compute the normalized differentials. Let $\omega = f(\lambda)d\lambda$ be a holomorphic differential, we showed in the proof of Theorem 9.4.3 that

$$\oint_{a_j} w = -2 \int_{\beta_j}^{\alpha_{j+1}} f(\lambda) d\lambda.$$

Given the branch point $\alpha_j, \beta_j,\ j = 1, \ldots, g+1$ where $\beta_{g+1} = \infty$ we use the basis of unnormalized differentials

$$u_n = \frac{\lambda^{n-1}}{\mu} d\lambda, \quad n = 1, \ldots, g,$$

and compute their a and b periods. This allows us to construct the basis ω_k of normalized differentials and gives us access to the Abel map.

Assume $Q = (\lambda, \sigma\sqrt{P(\lambda)}^{+}) \in a_j$ for $\sigma = \pm 1$. Then the kth component of the Abel map is computed by

$$(A(Q))_k = \sum_{l=1}^{j-1} (I_l(f_k) + K_l(f_k)) + K_l(f_k) + \sigma I_j(f_k, \lambda),$$

where $f_k(\lambda)/w$ is the principal part of ω_k, the kth normalized holomorphic differential.

9.6.2 Computing the g-function

The g-function is defined by

$$\mathcal{G}(x,t,\lambda) = \frac{\sqrt{P(\lambda)}}{2\pi i}\sum_{j=1}^{g}\int_{\beta_j}^{\alpha_{j+1}} \frac{-\zeta(x,t,s)+i\Omega_j(x,t)}{\sqrt{P(s)}^{+}}\frac{ds}{s-\lambda}, \tag{9.6.3}$$

see (9.4.1). After mapping each interval of integration in (9.6.3) using a linear change of variables $z = m_j(s)$ ($m_j : [\beta_j, \alpha_{j+1}] \to [-1,1]$) we have the expression

$$\mathcal{G}(x,t,\lambda) = \frac{\sqrt{P(\lambda)}}{2\pi i}\sum_{j=1}^{g}\int_{-1}^{1} H_j(z)\frac{dz}{z-m_j(\lambda)},$$

where

$$H_j(z) = \frac{-\zeta(x,t,m_j^{-1}(z))+i\Omega_j(x,t)}{\sqrt{P(m_j^{-1}(z))}^{+}}.$$

Note that $F_j(z) = H_j(z)\sqrt{1-z^2}$ is analytic in a neighborhood of $[-1,1]$. We use

$$\mathcal{G}(x,t,\lambda) = \frac{\sqrt{P(\lambda)}}{2\pi i}\sum_{j=1}^{g}\int_{-1}^{1} \frac{F_j(z)}{z-m_j(\lambda)}\frac{dz}{\sqrt{1-z^2}},$$

This reduces the problem of computing the g-function to that of computing integrals of the form

$$C(\lambda) = \frac{1}{2\pi i}\int_{-1}^{1}\frac{f(s)}{(s-\lambda)}\frac{1}{\sqrt{1-s^2}}ds, \quad \lambda \notin [-1,1],$$

where f is a smooth function on $[-1,1]$. We use the known expansion of the function $1/(s-\lambda)$ in a Chebyshev series [100]

$$\frac{1}{s-\lambda} = \sum_{j=0}^{\infty} e_j(\lambda)T_j(s), \quad e_j(\lambda) = \begin{cases} -\frac{1}{\sqrt{\lambda^2-1}}, & \text{if } j=0, \\ -2\frac{(\lambda-\sqrt{\lambda^2-1})^j}{\sqrt{\lambda^2-1}}, & \text{otherwise.} \end{cases}$$

Here T_j is the jth Chebyshev polynomial of the first kind [100]. This formula is technically valid for $\lambda > 1$ but can be extended to $\mathbb{C}\setminus[-1,1]$ by analytic continuation. We use a discrete cosine transformation of order n to approximate the Chebyshev series of f:

$$f(s) \approx \sum_{j=0}^{n} c_j T_j(s).$$

Orthogonality gives

$$C(\lambda) \approx \frac{1}{2\pi i}\left(\pi c_0 e_0(\lambda) + \frac{\pi}{2}\sum_{j=0}^{n} c_j e_j(\lambda)\right).$$

Exponential convergence is guaranteed since in our case f is analytic.

Although it is not important for our purposes, one may wish to compute the limiting values $\mathcal{G}^{\pm}$ as λ approaches a gap from above or below. We use the formula [84]

$$\lim_{\epsilon\to 0^+}\frac{1}{2\pi i}\int_{-1}^{1}\frac{T_j(s)}{s-(\lambda\pm i\epsilon)}\frac{ds}{\sqrt{1-s^2}} = \pm\frac{1}{2}\frac{T_j(\lambda)}{\sqrt{1-\lambda^2}} + \frac{1}{2i}U_{j-1}(\lambda), \quad \lambda\in(-1,1),$$

where U_k is the Chebyshev polynomial of the second kind [100].

9.6.3 Computing the Baker-Akhiezer function

This section is concerned with computing $(\Psi_r)_{\pm}$. Let D' be the divisor for the desired zeros of the BA function and D be the divisor for the poles. We compute the vector (see (9.4.5))

$$\boldsymbol{V} = A(D'-D),$$

using the method for computing integrals described above. Next, consider the differentials

$$\nu_j = i\frac{\lambda^{g+j-1}}{\mu}d\lambda, \quad j=1,\ldots,g,$$

which satisfy

$$\int_{\lambda_0}^{\lambda}\nu_j = \mathcal{O}(\lambda^{-1/2+j}), \text{ as } \lambda\to\infty.$$

We accurately compute the a periods of ν_j. We construct $\{\tilde{\nu}_j\}_{j=1}^{g}$ which each have vanishing a periods by adding an appropriate linear combination holomorphic differentials. We compute the matrix

$$\boldsymbol{S} = \left(\oint_{b_k}\tilde{\nu}_j\right)_{kj}.$$

The system $\boldsymbol{SX} = \boldsymbol{V}$ is solved for the real-valued vector $\boldsymbol{X}$, giving a differential

$$l = \sum_{j=1}^{g}\boldsymbol{X}_j\tilde{x}_j,$$

that has b periods equal to the vector $\boldsymbol{V}$. The final step is to compute the coefficients $\{t_j\}_{j=1}^{g}$ in the expansion

$$\int_{\lambda_0}^{\lambda} l = \sum_{n=1}^{g} it_n \lambda^{n-1/2} + \mathcal{O}(\lambda^{-1/2}) = \kappa(\lambda)/2 + \mathcal{O}(\lambda^{-1/2}).$$

The BA function with asymptotic behavior $(\Psi_p)_\pm \sim e^{\pm\kappa(\lambda)/2}$ as $\lambda \to \infty$ has zeros at the points of D'. Theorem 9.5.2 tells us to seek $(\Psi_r)_\pm \sim e^{\pm Z(x,t,\lambda)/2}$ as $\lambda \to \infty$. We construct the deformed and regularized RHP for $(\Psi_r)_\pm$, see Section 9.5. This RHP is solved numerically.

To test the method we use $\alpha_1 = 0, \beta_1 = .25, \alpha_2 = 1, \beta_2 = 1.5$ and $\alpha_3 = 2$. Thus we have a genus two surface. We choose zeros to be at the points $(.5, \sqrt{P(.5)}^{+})$ and $(1.75, \sqrt{P(1.75)}^{+})$. To approximate the BA function we use n collocation points per contour. See Appendix 9.8 for a discussion of the numerical method for RHPs that is used and its convergence properties. The roots of the approximate BA function are found using standard Chebyshev root-finding techniques [15]. In Figure 9.6.2 we plot the absolute error of the roots as n increases. Spectral convergence of the roots is observed. See Figure 9.6.3 for a surface plot showing both the zeros and the poles of the BA function on a single sheet. See Figures 9.6.4 and 9.6.5 for contour plots of the real part, imaginary part, and modulus of the BA function on each sheet. Note that producing this plot requires the computation of the g-function. These plots are all produced in the genus two case but higher genus BA functions can also be plotted.

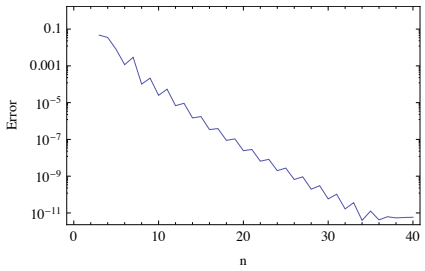

Figure 9.6.2: A demonstration of the spectral convergence of the zeros of the BA function.

9.6.4 Numerical solutions of the KdV equation

Before we move to numerical results for the KdV equation, let us review the solution process. The constants α_j $(j = 1, \ldots, g+1)$ and β_j $(j = 1, \ldots, g)$ are chosen, all positive. This determines the polynomial $P(\lambda)$ and the unnormalized differentials u_k. The a periods of these differentials are computed using Chebyshev polynomials and the normalized basis ω_k is constructed. Next, one point in each a-cycle is chosen to be a pole of the BA function. These points make up the divisor for the poles of the BA function. The Abel map of this

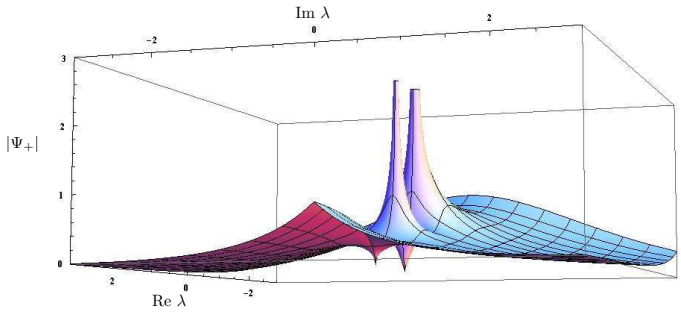

Figure 9.6.3: A three-dimensional plot of the modulus of the BA function on one sheet of the Riemann surface. We see two poles and two zeros are clearly present.

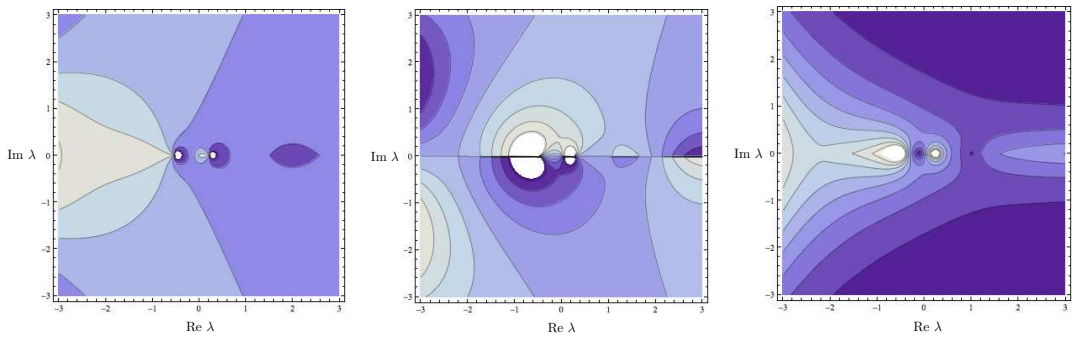

(a) (b) (c)

Figure 9.6.4: A genus two Baker–Akhiezer function. Darker shades indicate smaller values. Two poles and two zeros are clearly present. (a) The real part of Ψ_+. (b) The imaginary part of Ψ_+. (c) The modulus of Ψ_+.

divisor is computed, along with the Abel map of the divisor

$$D = \sum_{j=1}^{g} (\beta_j, 0).$$

Through the process just outlined the constants t_j, $j = 1, \ldots, g$ are computed. The Riemann–Hilbert formulation is used to compute the function $(\Psi_r)_\pm$ by noting that its asymptotic behavior is (9.5.5). The function $\mathbf{\Sigma}_3$ is found and $u(x,t)$ is computed using Theorem 9.5.2.

In this section we plot numerical solutions of the KdV equation. In the genus two case we use numerical tests to demonstrate uniform spectral convergence.

Genus one

For a genus one solution we set $\alpha_1 = 0, \beta_1 = .25$ and $\alpha_2 = 1$ with the zero of the BA function at $(.5, \sqrt{P(.5)}^{+})$ at $t = 0$. See Figure 9.6.6 for plots of the corresponding solution

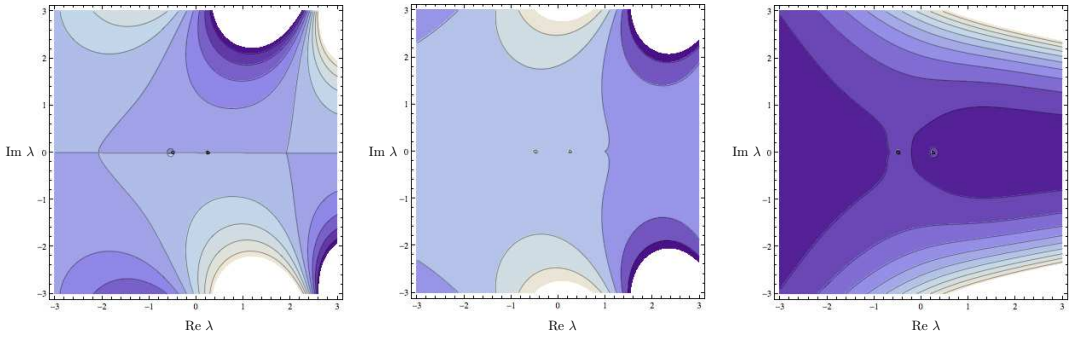

(a) (b) (c)

Figure 9.6.5: A genus two Baker–Akhiezer function. Darker shades indicate smaller values. (a) The real part of Ψ_-. (b) The imaginary part of Ψ_-. (c) The modulus of Ψ_-.

of the KdV equation. This solution is an elliptic function. Explicitly, [23],

$$q(x,t) = -\alpha_2 - \beta_1 + 2\,\mathrm{cn}^2(x - K(1-\beta_1) + 1.0768 - (8(1-\beta)^2 - 4 - \alpha_2 - \beta_1)t, 1-\beta_1),$$

where $K(k)$ is the complete elliptic integral and cn is the Jacobi cn function [84]. The shift inside the cn function is computed numerically. See Figure 9.6.6 for another solution.

Genus two

For a genus two solution we set $\alpha_1 = 0, \beta_1 = .25, \alpha_2 = 1, \beta_2 = 1.5$ and $\alpha_3 = 2$ with the zeros of the BA function at $(.5, \sqrt{P(.5)}^+)$ and $(1.75, \sqrt{P(1.75)}^+)$ at $t = 0$. See Figure 9.6.8 for plots of the corresponding solution of the KdV equation.

For this solution we numerically discuss convergence. We use $q_n(x,t)$ to denote the approximate solution of the KdV equation obtained with n collocation points per contour of the RHP. We define the Cauchy error

$$E_{n,m}(x,t) = |q_n(x,t) - q_m(x,t)|.$$

We fix $m = 80$ and let n vary: $n = 10, 20, 40$. See Figure 9.6.7 for plots of $E_{n,m}(x,t)$ for various values of x and t. This figure demonstrates uniform spectral Cauchy convergence of the function $q_n(x,t)$ to $q(x,t)$, the solution of the KdV equation.

We plot another genus two solution in Figure 9.6.8. If we shrink the widths of the bands we can obtain solutions which are closer to the soliton limit. See Figure 9.6.9 for a solution demonstrating a soliton-like interaction.

Genus three

For a genus three solution we set $\alpha_1 = 0, \beta_1 = .25, \alpha_2 = 1, \beta_2 = 2, \alpha_3 = 2.5, \beta_3 = 3$ and $\alpha_4 = 3.5$ with the zeros of the BA function at $(.5, \sqrt{P(.5)}^+)$, $(1.75, \sqrt{P(1.75)}^+)$ and $(2.75, \sqrt{P(2.75)}^+)$ at $t = 0$. In Figure 9.6.10 we show the jump contours for the RHP which are used in practice to compute the BA function. See Figure 9.6.12 for plots of the corresponding solution of the KdV equation and Figure 9.6.11 and Figure 9.6.12 for

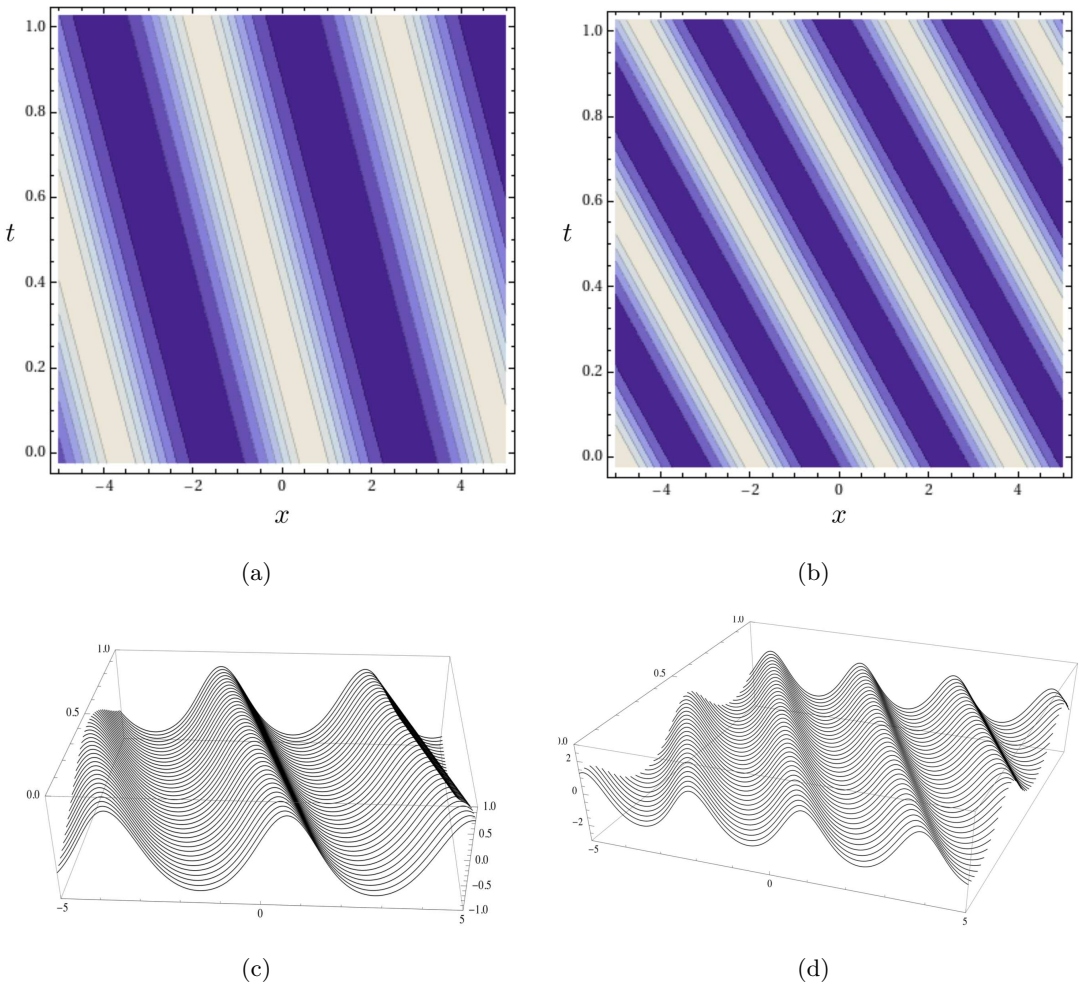

Figure 9.6.6: (a) A contour plot of the genus one solution with $\alpha_1 = 0, \beta_1 = .64$ and $\alpha_2 = 1$ with the zero of the BA function at $(.75, \sqrt{P(.75)}^{+})$ at $t = 0$. Darker shades represent troughs. (b) A contour plot of the genus one solution with $\alpha_1 = 0, \beta_1 = .64$ and $\alpha_2 = 1$ with the zero of the BA function at $(.75, \sqrt{P(.75)}^{+})$ at $t = 0$. Again, darker shades represent troughs. (c) A three-dimensional plot of the solution in (a) showing the time evolution. (d) A three-dimensional plot of the solution in (b) showing the time evolution.

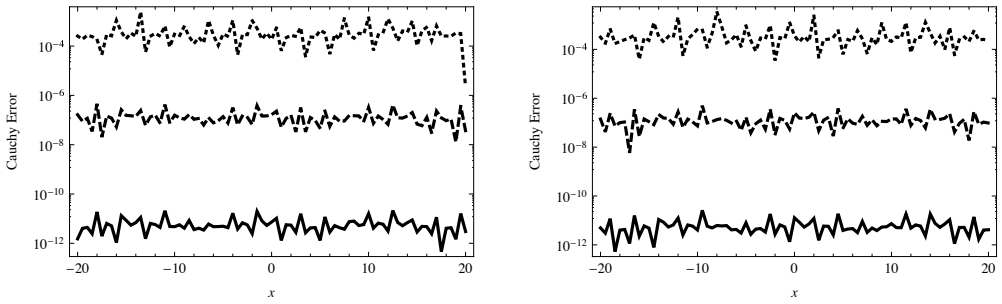

(a) (b)

Figure 9.6.7: (a) A logarithmically scaled plot of $E_{n,80}(x,0)$ for $n = 10$ (dotted), $n = 20$ (dashed) and $n = 40$ (solid). (b) A logarithmically scaled plot of $E_{n,80}(x,25)$ for $n = 10$ (dotted), $n = 20$ (dashed) and $n = 40$ (solid). This figure demonstrates uniform spectral convergence.

another genus three solution. We show the dynamics of the zeros of the BA function in Figure 9.6.11.

Genus five

Just to demonstrate the breadth of the method we compute a genus five solution. We set $\alpha_1 = 0, \beta_1 = .25, \alpha_2 = 1, \beta_2 = 2, \alpha_3 = 2.5, \beta_3 = 3, \alpha_4 = 3.3, \beta_4 = 3.5, \alpha_5 = 4, \beta_5 = 5.1$ and $\alpha_6 = 6$ with the zeros of the BA function at $(.5, \sqrt{P(.5)}^+)$, $(2.2, \sqrt{P(2,2)}^+)$, $(3.2, \sqrt{P(3.2)}^+)$, $(3.6, \sqrt{P(3.6)}^+)$ and $(5.3, \sqrt{P(5.3)}^+)$ at $t = 0$. See Figure 9.6.13 for a plot of the corresponding solution of the KdV equation. This figure shows the time evolution.

9.7 Analysis of the deformed and regularized RHP

In general we consider a RHP of the form

$$\boldsymbol{\Phi}^+(\lambda) = \boldsymbol{\Phi}^-(\lambda)\boldsymbol{G}(\lambda), \quad \lambda \in \Lambda, \quad \boldsymbol{\Phi}(\infty) = I, \tag{9.7.1}$$

where Λ is bounded and $\boldsymbol{G}$ depends on $\{\Omega_j(x,t)\}_{j=1}^g$, or alternatively $\{W_j(x,t)\}_{j=1}^g$. We use many of the results in Chapter 3. It is straightforward to check that $\boldsymbol{G}$ satisfies the first-order product condition. Analyticity may be used to see that $\boldsymbol{G}$ satisfies the $(k-1)$th-order product condition for all $k > 0$.

We apply Theorem 3.8.21 to the RHP derived in Section 9.5. We use $\boldsymbol{G}$ to denote the jump matrix. We note that when we augment the contour, $\boldsymbol{G} = I$ on all added pieces and these do not contribute to the integral. Also, $\det \boldsymbol{\Delta} = 1$ away from α_j, β_j and $\det \boldsymbol{J}_0 = -1$.

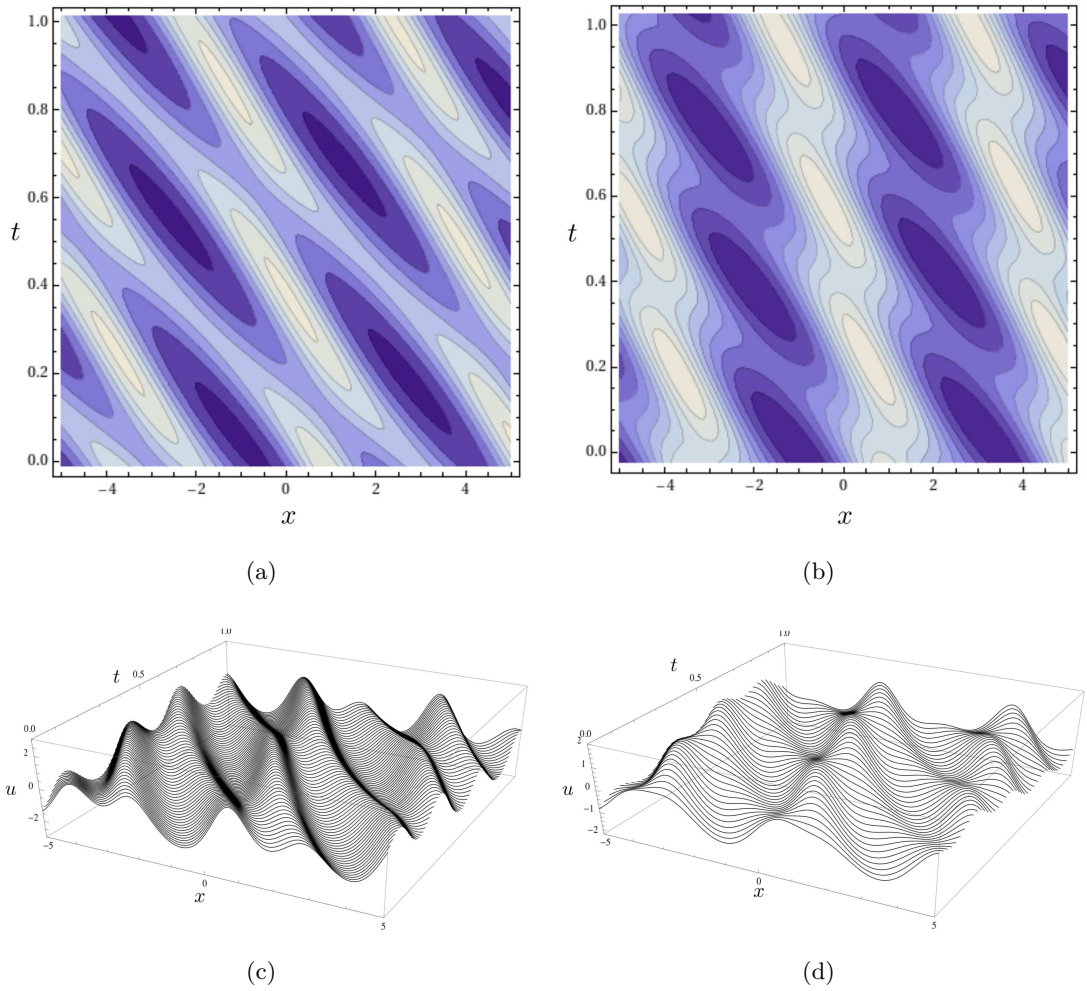

Figure 9.6.8: (a) A contour plot of the genus two solution with $\alpha_1 = 0, \beta_1 = .25, \alpha_2 = 1, \beta_2 = 1.5$ and $\alpha_3 = 2$ with the zeros of the BA function at $(.5, \sqrt{P(.5)}^{+})$ and $(1.75, \sqrt{P(1.75)}^{+})$ at $t = 0$. Darker shades represent troughs. (b) A contour plot of the genus two solution with $\alpha_1 = 0, \beta_1 = .25, \alpha_2 = 1, \beta_2 = 2$ and $\alpha_3 = 2.25$ with the zeros of the BA function at $(.5, \sqrt{P(.5)}^{+})$ and $(2.2, \sqrt{P(2.2)}^{+})$ at $t = 0$. Again, darker shades represent toughs. (c) A three-dimensional plot of the solution in (a) showing the time evolution. (d) A three-dimensional plot of the solution in (b) showing the time evolution.

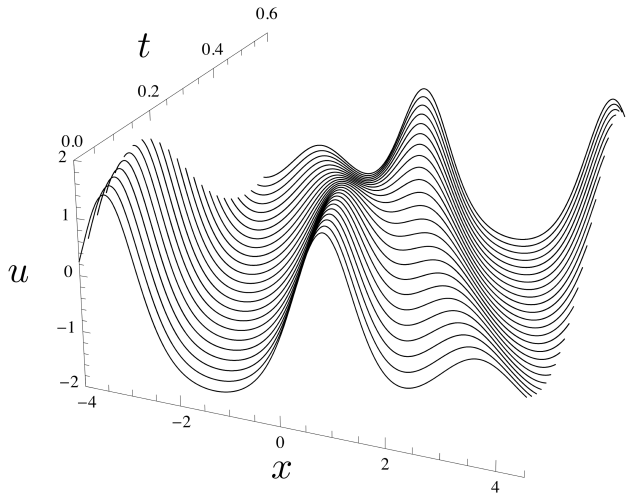

Figure 9.6.9: A genus two solution with $\alpha_1 = 0, \beta_1 = 0.1, \alpha_2 = 1, \beta_2 = 1.05$ and $\alpha_3 = 1.75$ with the zeros of the BA function at $(.5, \sqrt{P(.5)}^+)$ and $(1.2, \sqrt{P(1.2)}^+)$ at $t = 0$. This solution demonstrates a soliton-like interaction.

Both of these do not influence the index. We are left with

$$\begin{aligned}\operatorname{ind} \mathcal{C}[\boldsymbol{G}; \Lambda] = -\frac{1}{\pi i} \sum_{l=1}^{g} \left(\int_{C_{\alpha_l}} d \log \det \boldsymbol{A}_l(\lambda) + \int_{c_{\beta_l}} d \log \det \boldsymbol{B}_l(\lambda) \right) \\ -\frac{1}{\pi i} \int_{\partial \mathcal{D}} d \log \det \boldsymbol{H}(\lambda) - \frac{1}{\pi i} \int_{C_{\alpha_{g+1}}} d \log \det \boldsymbol{A}_{g+1}(\lambda).\end{aligned}$$

Here $C_{\alpha_j}, C_{\beta_j}$ are the circles around α_j, β_j, and $\mathcal{D}$ is again the region inside the large outer circle but outside each of the smaller circles, as before. Straightforward contour integration produces

$$\begin{aligned}\int_{C_{\alpha_l}} d \log \det \boldsymbol{A}_l(\lambda) = \pi i, \\ \int_{C_{\beta_l}} d \log \det \boldsymbol{B}_l(\lambda) = -\pi i, \\ \int_{\partial \mathcal{D}} d \log \det \boldsymbol{H}(\lambda) = -\pi i.\end{aligned}$$

This proves that $\operatorname{ind} \mathcal{C}[\boldsymbol{G}; \Lambda] = 0$. Every element in the kernel of $\operatorname{ind} \mathcal{C}[\boldsymbol{G}; \Lambda]$ corresponds to a solution of the RHP that vanishes at infinity [117]. Given a matrix-valued solution $\boldsymbol{\Phi}$, we sum the rows to get the vector representation of the BA function. If we have a vanishing solution we zero out the second row and assume the first is non zero. Call the new function $\boldsymbol{\Psi}$. This is still a vanishing solution. Then $\boldsymbol{\Phi} + c\boldsymbol{\Psi}$ is a solution of the RHP for any c. Summing the rows of $\boldsymbol{\Phi} + c\boldsymbol{\Psi}$ we obtain a function different from $\boldsymbol{\Phi}$ for every c. This contradicts the uniqueness of the BA function. This shows that $\operatorname{ind} \mathcal{C}[\boldsymbol{G}; \Lambda]$ must be

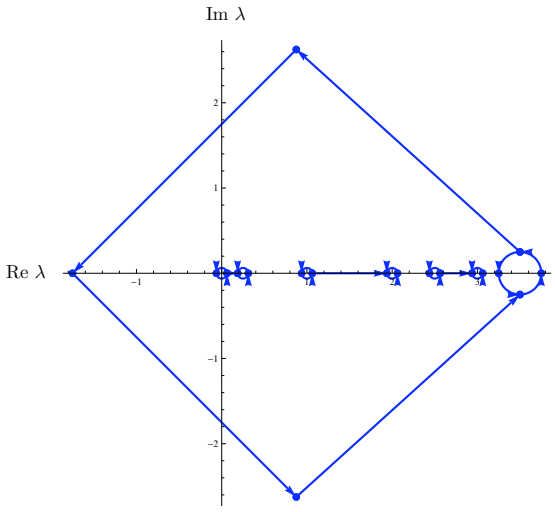

Figure 9.6.10: The jump contours for the RHP which are used in practice to compute the BA function. Here $\alpha_1 = 0, \beta_1 = .25, \alpha_2 = 1, \beta_2 = 2, \alpha_3 = 2.5, \beta_3 = 3$ and $\alpha_4 = 3.5$.

boundedly invertible by the open mapping theorem. This shows that all RHPs considered here are uniquely solvable with smooth solutions. This is the justification needed to use the numerical method for RHPs in [89].

9.8 Uniform approximation

We consider the RHP (9.7.1). We use C to denote a generic constant. In this section we explain how our approximation of the BA function changes with x and t. We use the results from Section 5.1. As before, we consider the operator $\mathcal{C}[\boldsymbol{G};\Lambda]$ defined by

$$\mathcal{C}[\boldsymbol{G};\Lambda]U = U - (\mathcal{C}_\Lambda^- U)(\boldsymbol{G} - I). \tag{9.8.1}$$

The operator equation

$$\mathcal{C}[\boldsymbol{G};\Lambda]U = \begin{bmatrix} 1 & 1 \end{bmatrix}(\boldsymbol{G} - I),$$

is discretized using the method in Section 5.3. We use $\mathcal{C}_n[\boldsymbol{G};\Lambda]$ to denote this discretization. Once an approximation U_n to U is known, an approximate solution $\boldsymbol{\Phi}_n(\lambda) = \mathcal{C}_\Lambda U_n(\lambda) + \begin{bmatrix} 1 & 1 \end{bmatrix}$ of $\boldsymbol{\Phi}$ is obtained. The method is a collocation method and $\boldsymbol{\Phi}_n$ will satisfy the RHP exactly at each collocation point. The residue of a function at ∞ is computed through

$$\lim_{\lambda\to\infty} \lambda(\boldsymbol{\Phi}(\lambda) - \begin{bmatrix} 1 & 1 \end{bmatrix}) = -\frac{1}{2\pi i}\int_\Lambda U(s)ds.$$

This is what is used to compute s_1 and s_2 in (9.5.4). We make the fundamental assumption, Assumption 5.3.11.

We establish two claims:

- $\|\mathcal{C}[\boldsymbol{G};\Lambda]^{-1}\|_{\mathcal{L}(L^2(\Lambda))} < C$ and

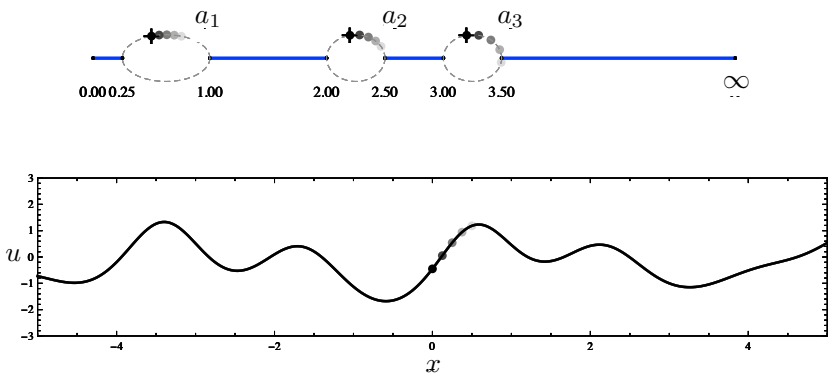

(a)

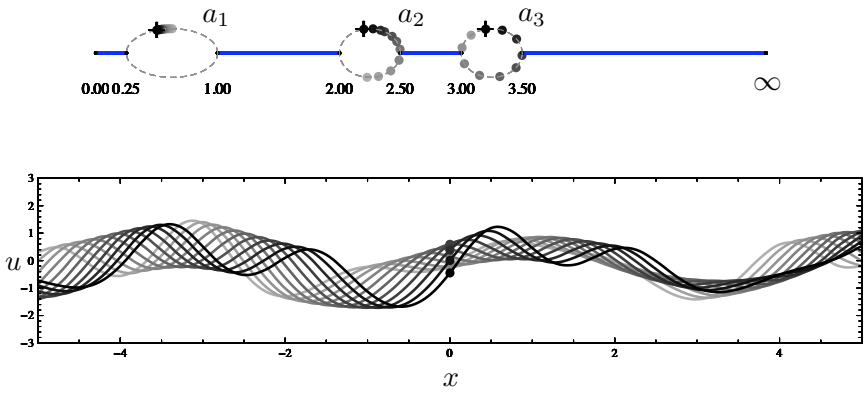

(b)

Figure 9.6.11: A genus three solution with $\alpha_1 = 0, \beta_1 = .25, \alpha_2 = 1, \beta_2 = 2, \alpha_3 = 2.5, \beta_3 = 3$ and $\alpha_4 = 3.5$ with the zeros of the BA function at $(.5, \sqrt{P(.5)}^+), (2.2, \sqrt{P(2.2)}^+)$ and $(3.2, \sqrt{P(3.2)}^+)$ at $t = 0$. These plots show the dynamics of the zeros of the BA function. The top plot in each panel gives a schematic of the Riemann surface with the a cycles labeled. Dots of the same shade across the panels are in correspondence. The + on the plots represents where the pole of the BA function is located on the Riemann surface. These points are also the locations of the zeros at $t = 0$. (a) The solution at $t = 0$. We vary x from $x = 0$ up to $x = 0.25$ and plot how the zeros $\{\gamma_1(x, 0), \gamma_2(x, 0), \gamma_3(x, 0)\}$ move on the Riemann surface. (b) The evolution of the same solution up to $t = 0.125$. We fix $x = 0$ and plot how the zeros $\{\gamma_1(0, t), \gamma_2(0, t), \gamma_3(0, t)\}$ move on the Riemann surface.

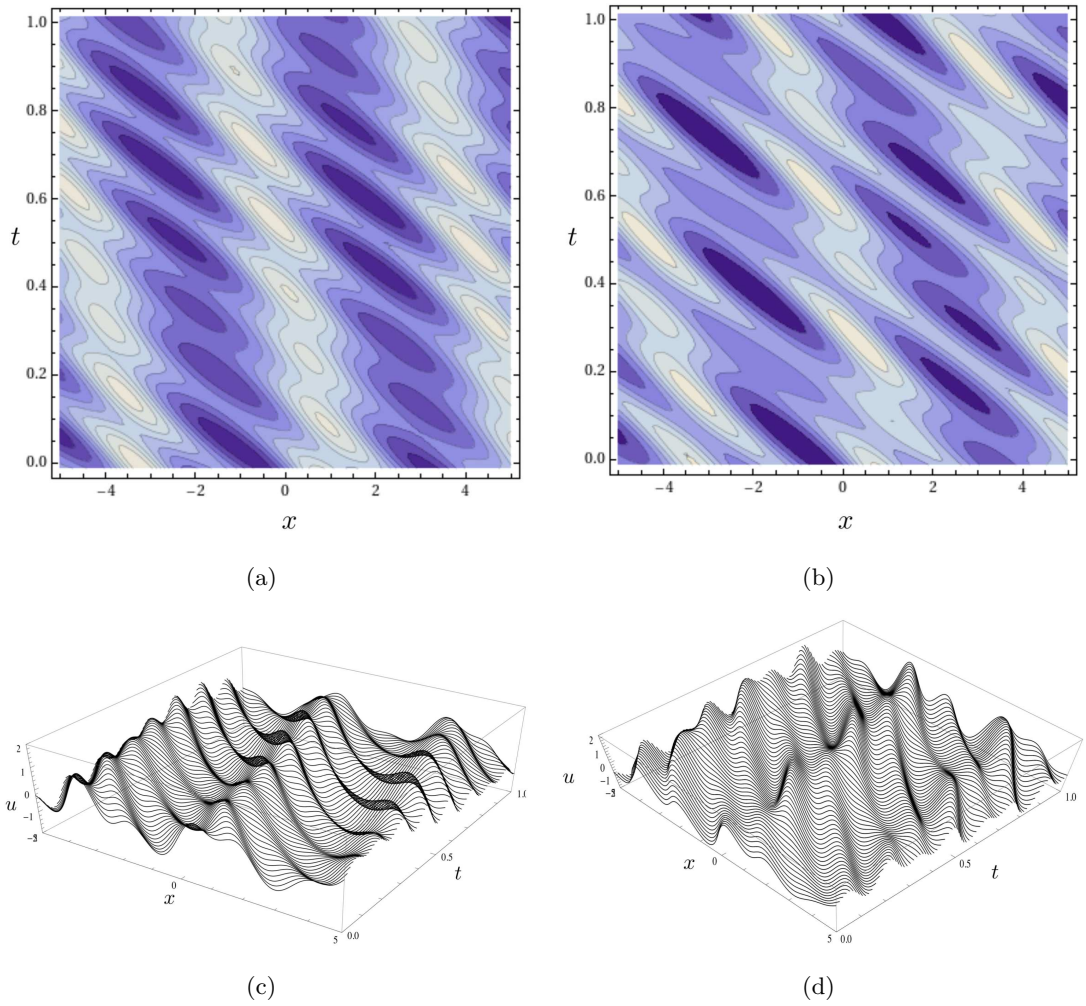

Figure 9.6.12: (a) A contour plot of the genus three solution with $\alpha_1 = 0, \beta_1 = .25, \alpha_2 = 1, \beta_2 = 2, \alpha_3 = 2.5, \beta_3 = 3$ and $\alpha_4 = 3.5$ with the zeros of the BA function at $(.5, \sqrt{P(.5)}^{+}), (2.2, \sqrt{P(2.2)}^{+})$ and $(3.2, \sqrt{P(3.2)}^{+})$ at $t = 0$. Darker shades represent troughs. (b) A contour plot of the genus three solution in Figure 9.6.11. Again, darker shades represent toughs. (c) A three-dimensional plot of the solution in (a) showing the time evolution. (d) A three-dimensional plot of the solution in Figure 9.6.11 showing the time evolution.

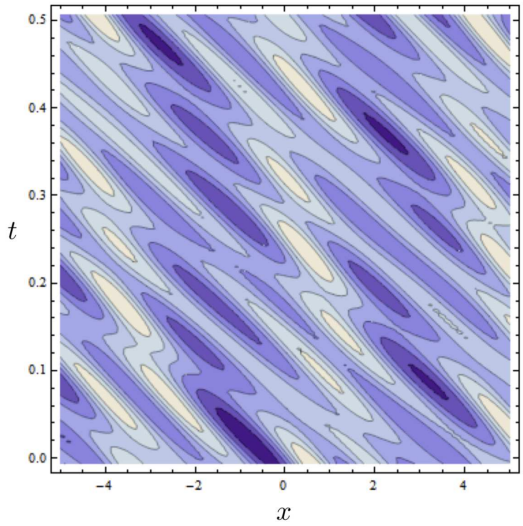

(a)

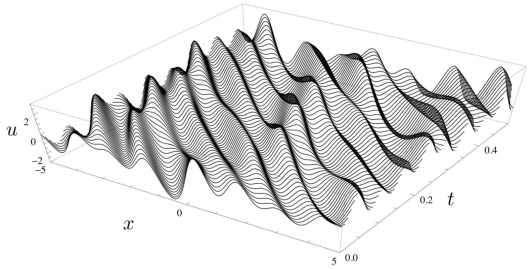

(b)

Figure 9.6.13: (a) A contour plot of the genus five solution with $\alpha_1 = 0, \beta_1 = .25, \alpha_2 = 1, \beta_2 = 2, \alpha_3 = 2.5, \beta_3 = 3, \alpha_4 = 3.3, \beta_4 = 3.5, \alpha_5 = 4, \beta_5 = 5.1$ and $\alpha_6 = 6$ with the zeros of the BA function at $(.5, \sqrt{P(.5)}^{+})$, $(2.2, \sqrt{P(2,2)}^{+})$, $(3.2, \sqrt{P(3.2)}^{+})$, $(3.6, \sqrt{P(3.6)}^{+})$ and $(5.3, \sqrt{P(5.3)}^{+})$ at $t = 0$. Darker shades represent troughs. (b) A three-dimensional plot of the solution same solution showing the time evolution.

- $\|\boldsymbol{G} - I\|_{W^{k,\infty}(\Lambda)} < D_k$ for each $k > 0$ for constants D_k.

The operator $\mathcal{C}[\boldsymbol{G}; \Lambda]^{-1}$ depends on g constants $\Omega_j \in [0, 2\pi],\ j = 1, \ldots, g$, in an analytic way. We add 2π to the interval so that we may appeal to compactness. In the notation of Section 9.7. It follows that the mapping

$$\boldsymbol{\Omega} = (\Omega_1, \ldots, \Omega_j) \mapsto \operatorname{ind} \mathcal{C}[\boldsymbol{G}; \Lambda],$$

is continuous from $[0, 2\pi)^g$ to $\mathcal{L}(L^2(\Gamma))$. Since the operator is always invertible the same statement holds for the inverse operator. This implies

$$\sup_{\boldsymbol{\Omega}} \|\mathcal{C}[\boldsymbol{G}; \Lambda]^{-1}\|_{\mathcal{L}(L^2(\Gamma))} < C.$$

The second claim can be established by differentiating the jump matrix $\boldsymbol{G}$. It is clear that all derivatives of $\boldsymbol{G}$ are bounded and this bound can be made independent of $\boldsymbol{\Omega}$. This leads to the following theorem which shows we expect uniform spectral convergence of all needed functions.

Theorem 9.8.1. *If Assumption 5.3.11 holds then $\boldsymbol{\Phi}_n = I + \mathcal{C}_\Gamma \boldsymbol{U}_n$, the numerical approximation of $\boldsymbol{\Phi} = I + \mathcal{C}_\Gamma \boldsymbol{U}$, satisfies*

$$\sup_{\boldsymbol{\Omega}} |\boldsymbol{\Phi}_n(\lambda) - \boldsymbol{\Phi}(\lambda)| < C_\alpha \epsilon^{-1} n^{-\alpha}, \quad \textit{for every } \alpha \geq 0, \ \inf_{s \in \Lambda} |\lambda - s| > \epsilon,$$
$$\sup_{\boldsymbol{\Omega}} \|\boldsymbol{U}_n - \boldsymbol{U}\|_{L^2(\Lambda)} < L_\alpha n^{-\alpha}, \quad \textit{for every } \alpha \geq 0.$$

As a consequence, (see (5.3.8)*) the approximate solution $q_n(x,t)$ of the KdV equation satisfies*

$$\sup_{\boldsymbol{\Omega}} |q_n(x,t) - q(x,t)| < S_\alpha n^{-\alpha}, \quad \textit{for every } \alpha \geq 0.$$

Chapter 10

Orthogonal Polynomials and Random Matrix Theory

Random matrix theory made a prominent appearance in nuclear physics by Wigner [112]. Random matrices were used to model the spectral lines of a heavy atom. Indeed, the eigenvalue statistics of the matrices under consideration closely predict the spectral lines as the size of the matrices become large [75]. Importantly, the statistics of the eigenvalues in the large-matrix limit are seen to be dependent only on symmetry properties of the matrices under consideration, not the exact distribution of the entries of the matrix [24, 75]. This behavior is known as *universality*.

The Riemann–Hilbert approach to random matrix theory was developed by Deift and his collaborators. See [24] for a thorough exposition of the results. In this chapter, many of the results of this manuscript are made computational. Generically, the statistics of random matrices are known explicitly only in the large-matrix limit. Here we compute random matrix statistics for a particular classes of finite-dimensional matrices. This demonstrates both the breadth and ubiquity of RHPs and the wide applicability of the methods developed in previous chapters. The results from this chapter can also be found in [91].

10.1 Introduction

We consider the problem of calculating random matrix eigenvalue statistics for unitary random matrix ensembles; *i.e.*, $n \times n$ random matrices of the form

$$M = \begin{bmatrix} M_{11} & M_{12}^{\mathrm{R}} + \mathrm{i}M_{12}^{\mathrm{I}} & \cdots & M_{1n}^{\mathrm{R}} + \mathrm{i}M_{1\mathrm{n}}^{\mathrm{I}} \\ M_{12}^{\mathrm{R}} - \mathrm{i}M_{12}^{\mathrm{I}} & M_{22} & \cdots & M_{2n}^{\mathrm{R}} + \mathrm{i}M_{2\mathrm{n}}^{\mathrm{I}} \\ \vdots & \ddots & \ddots & \vdots \\ M_{1n}^{\mathrm{R}} - \mathrm{i}M_{1\mathrm{n}}^{\mathrm{I}} & \cdots & M_{(n-1)n}^{\mathrm{R}} - \mathrm{i}M_{(\mathrm{n}-1)\mathrm{n}}^{\mathrm{I}} & M_{nn} \end{bmatrix}$$

when $M_{ij}^{\mathrm{R,I}}$ are real valued and distributed according to the probability distribution

$$\frac{1}{Z_n} e^{-n \operatorname{Tr} V(M)} dM,$$

where Z_n is the normalization constant. Furthermore,

$$dM = \prod_{i=1}^{n} dM_{ii} \prod_{i<j} (dM_{ij}^{\mathrm{R}} dM_{ij}^{\mathrm{I}}).$$

Importantly, the eigenvalue statistics of invariant ensembles are expressible in terms of the kernel

$$\mathcal{K}_n(x,y) = -\frac{\gamma_{n-1} e^{-n/2(V(x)+V(y))}}{2\pi \mathrm{i}} \frac{\pi_n(x)\pi_{n-1}(y) - \pi_{n-1}(x)\pi_n(y)}{x-y}, \qquad [24]$$

where π_k is the orthonormal polynomial with respect to the weight

$$e^{-nV(x)}dx,$$

and

$$\gamma_{n-1} = 2\pi \mathrm{i} \left[\int_{-1}^{1} \pi_{n-1}(x) w(x) dx \right]^{-1}$$

is a normalization constant. Particular statistics of interest include the *spectral density*

$$d\mu_n = \mathcal{K}_n(x,x)dx,$$

describing the global distribution of eigenvalues, and the *gap statistic*

$$\det(I - \mathcal{K}_n|_{L^2[\Omega]}),$$

where det denotes a *Fredholm determinant*, describing the local distribution of eigenvalues: the probability that no eigenvalue is inside the set Ω.

Gap statistics for unitary ensembles follow two principles of universality.

1. For x in the *bulk* — *i.e.*, inside the support of the equilibrium measure — the gap statistic of a properly scaled neighborhood of x approaches the sine kernel distribution:
$$\det(I - \mathcal{S}|_{L^2(-s,s)}) \quad \text{for} \quad \mathcal{S}(x,y) = \frac{\sin(x-y)}{x-y}.$$
This was proved rigorously in [24] by expressing the orthogonal polynomials in terms of a RHP, so that asymptotics of π_n were determinable via nonlinear steepest descent. Our approach follows this treatment.

2. Moreover, the *edge statistic* — *i.e.*, a properly scaled neighborhood of ∞ — generically approaches the Tracy–Widom distribution:
$$\det(I - \mathcal{A}|_{L^2(s,\infty)}) \quad \text{for} \quad \mathcal{A}(x,y) = \frac{Ai(x)Ai'(y) - Ai'(x)Ai(y)}{x-y},$$
where Ai is the classical Airy function [84].

Underlying these two universality laws are *Painlevé transcendents*; in the case of the Tracy–Widom distribution it is the Hastings–McLeod solution to Painlevé II [63], whereas

the sine kernel distribution is expressible in terms of a solution to Painlevé V [75]. See Chapter 8 for a discussion of a numerical Riemann–Hilbert approach for computing the Hastings–McLeod solution of Painlevé II.

The eigenvalue statistics of unitary ensembles differ from universality laws for finite n and are no longer known to be expressible in terms of Painlevé transcendents. This is in direct relation with the asymptotic formulae given in Chapters 6 and 7 for the solutions of the KdV and NLS equations. Our goal is to calculate the finite-dimensional statistics to explore the manner in which the onset of universality depends on the potential $V(x)$ present in the probability measure on matrices. To accomplish this, we calculate the associated orthogonal polynomials numerically, using their Riemann–Hilbert representation, via the framework presented in Section 5.3. By deforming the RHP, we achieve a numerical method that is uniformly accurate for large and small n, using and extending the theory in Section 5.2.

In our numerical experiments, we see that the onset of universality depends strongly on the magnitude of the equilibrium measure: where eigenvalue density is small, finite n statistics differ greatly from universality behavior.

This is related to what is observed with the KdV and NLS equation. The equilibrium measure is calculated from the probability distribution for the matrix entries. This is analogous to the reflection coefficient in Chapters 6 and 7. In those cases, the magnitude of the initial condition for the KdV and NLS equations is related to the magnitude of the reflection coefficient. A smaller amplitude reflection coefficient indicates a quicker transition into the asymptotic regime, as Section 2.7 indicates.

In this chapter, we start with a demonstration of the numerical results, plotting the finite-dimensional random matrix statistics (Section 10.2). Importantly, because we do not require the knowledge of local parametrices, our numerical approach continues to work for degenerate potentials, such as those that arise in the study of higher-order Tracy–Widom distributions [16]. We describe the manner in which orthogonal polynomials can be reduced to solutions of a Riemann–Hilbert problem that is suitable for numerics (Section 10.3). This RHP is suitable for small n. Through a regularization procedure in Section 10.4.2 we obtain a method that is provably accurate for all n.

Remark 10.1.1. *An alternative to the approach we use in this paper is to calculate the orthogonal polynomials directly for each n via Gram–Schmidt and numerical quadrature. For small n, this is likely more efficient, similar to how an FFT time-stepping method is more efficient for the KdV and NLS equations for small time, see Section 6.5. However, it is well known to be prone to instability [57]; moreover, the calculation must be restarted for each n as the weight e^{-nV} changes. On the other hand, the RH approach has computational cost independent of n, making it more practical for investigating large n behavior.*

10.2 Finite-dimensional invariant ensemble statistics

In this section, we compute the finite n statistics of unitary invariant ensembles by using the numerical method for calculating π_n and $\gamma_{n-1}\pi_{n-1}$ that we develop in later sections. It is apparent in the numerical results that the behavior of local statistics is tied strongly to the global density of eigenvalues; *i.e.*, the magnitude of the density of the equilibrium measure.

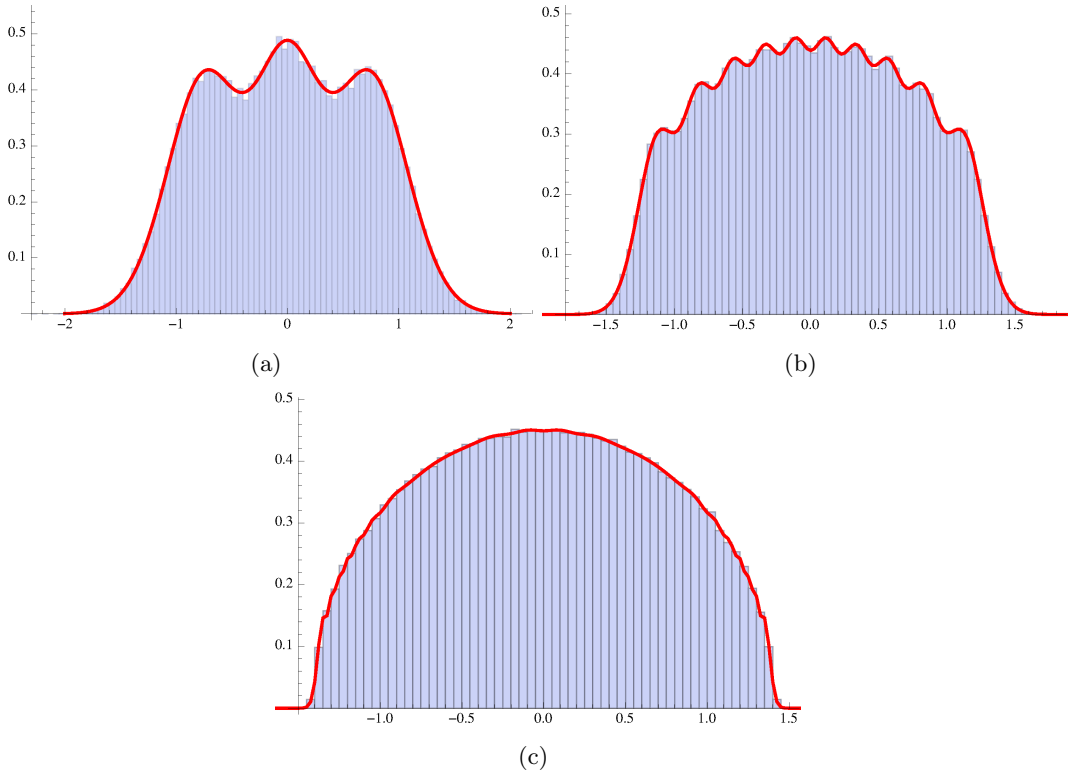

Figure 10.2.1: Calculated spectral densities for the GUE ($V(x) = x^2$) for $n = 3, 10$ and 100, compared to Monte Carlo simulation.

For unitary invariant ensembles, the spectral density is the distribution of the counting measure. In Figure 10.2.1, we compare the GUE (*i.e.*, $V(x) = x^2$) spectral density (numerically calculated using our approach) for $n = 3, 10$ and 100 to a histogram, demonstrating the accuracy of the approximation. (Because the polynomials involved are Hermite polynomials, we verify the accuracy directly as well.) This shows a phenomenon where the distribution exhibits n "bumps" of increased density, likely corresponding to the positions of the finite-charge energy minimization equilibrium; *i.e.*, the Fekete points (see [101, Chapter 3] for definition).

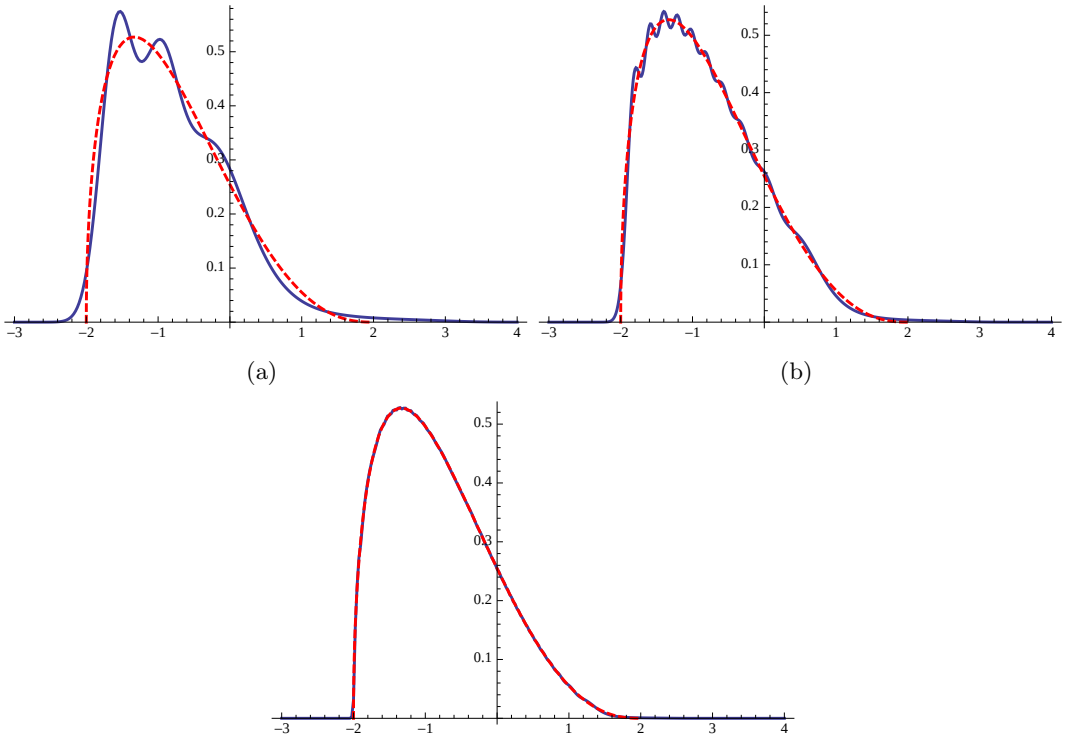

Figure 10.2.2: Calculated spectral density for $V(x) = \frac{x^2}{5} - \frac{4}{15}x^3 + \frac{x^4}{20} + \frac{8}{5}x$ for $n = 3, 10$ and 100. The dashed line denotes the density of the equilibrium measure ($n = \infty$).

In Figure 10.2.2, we plot the finite n spectral densities for the potential

$$V(x) = \frac{x^2}{5} - \frac{4x^3}{15} + \frac{x^4}{20} + \frac{8x}{5},$$

which is an example of a potential whose equilibrium measure vanishes at an endpoint, and hence the edge statistics follow a higher-order Tracy–Widom distribution [16]. Interestingly, this change in edge statistic behavior is not just present in the local statistics, but clearly visible in the decay of the tail of the global statistics.

We turn our attention to local gap statistics, which are described by the *Fredholm determinant*

$$\det(I - \mathcal{K}_n|_{L^2[\Omega]}).$$

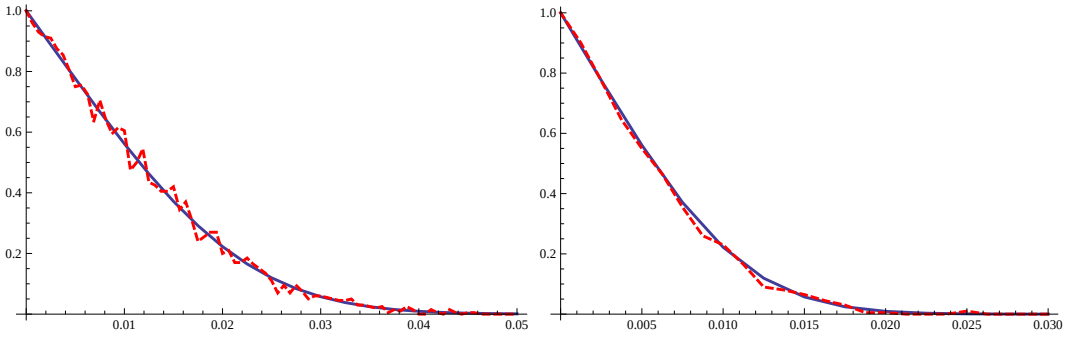

(a) (b)

Figure 10.2.3: The calculated probability that there are no eigenvalues in $(-s, s)$ for the GUE (plain) versus Monte Carlo simulation (dashed), for $n = 50$ (left) and $n = 100$ (right).

Using the method of Bornemann [14], we calculate the determinant, provided that the kernel itself can be evaluated. Thus, we successfully compute finite-gap statistics by calculating orthogonal polynomials using the RH approach. In Figure 10.2.3, we plot the gap statistics versus a histogram for the GUE[1] in the interval $(-s, s)$.

To see universality in the bulk, we scale the interval with n; in particular, we need to look at the gap probability for

$$\Omega = x + \frac{(-s, s)}{\mathcal{K}_n(x, x)}.$$

Alternatively, $\mathcal{K}_n(x, x)$ can be replaced by its asymptotic distribution to get

$$\Omega = x + \frac{(-s, s)}{n\psi(x)},$$

where $d\mu = \psi(x)dx$ is the equilibrium measure of V. For x inside the support of μ, this statistic approaches the sine kernel distribution[2]. We demonstrate this in Figure 10.2.4 for the degenerate potential, showing that the rate in which the statistics approach universality depends on the magnitude of the density of the equilibrium measure: convergence is more rapid when $\psi(x)$ has larger amplitude.

Next, we consider edge statistics. In the generic position (*i.e.*, when the equilibrium measure has precisely square root decay at its right endpoint b), the gap probability for

$$\Omega = \left(b + \frac{s}{c_V n^{2/3}}, \infty\right)$$

tends to the Tracy–Widom distribution[3]; here c_V is a constant associated with the equilibrium measure, see Section 10.3.2 for its precise definition and the numerical method for its

[1] We are not imposing the bulk scaling introduced below, to demonstrate that the numerical approach does not depend on choosing the scalings correctly.

[2] This was demonstrated in [24, Chapter 8] for an equivalent, rescaled kernel acting on $(-s, s)$. Here, we leave the kernel unmodified, and scale only Ω.

[3] We found this particular form by specializing [16, (1.15)], though it is equivalent to the rescaled kernel found in [26, (1.23)].

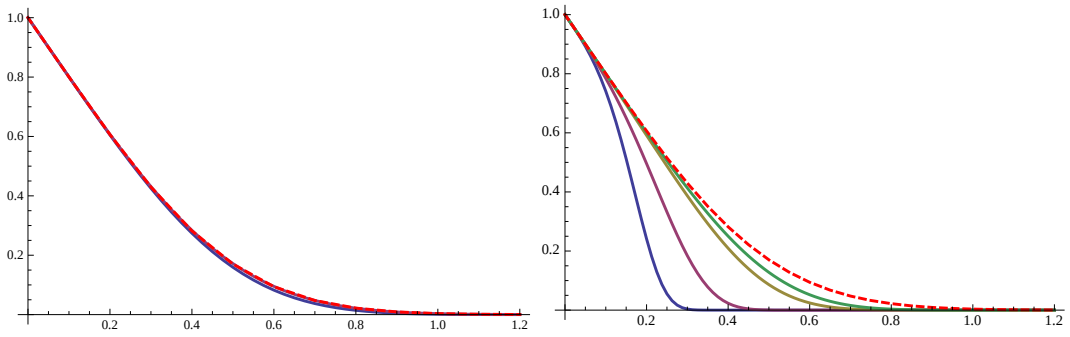

(a) (b)

Figure 10.2.4: The calculated probability that there are no eigenvalues in the scaled neighborhood $x + \frac{(-s,s)}{\mathcal{K}_n(x,x)}$ for $n = 50, 100, 200$ and 250 for $x = 1$ (left, $\psi(1) \approx .055$) and $x = 1.5$ (right, $\psi(1.5) \approx .0105$), for the potential $V(x) = x^2/5 - 4x^3/15 + x^4/20 + 8x/5$.

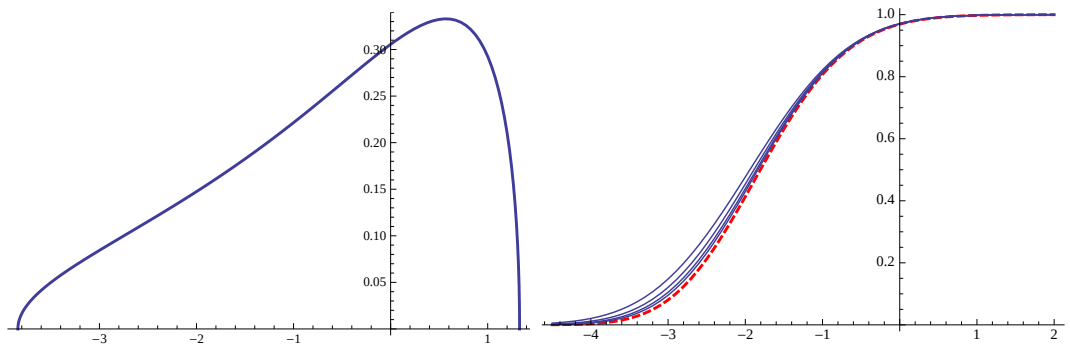

(a) (b)

Figure 10.2.5: The equilibrium measure for $V(x) = e^x - x$ (left) and the scaled gap statistic for $n = 10, 20, 40$ and 80 (right). The dashed line is the Tracy–Widom distribution ($n = \infty$).

calculation. In Figure 10.2.5, we plot the computed equilibrium measure for $V(x) = e^x - x$ (computed as described in Section 10.3.2), and its scaled edge statistic for increasing values of n. While the finite statistics are converging to the Tracy–Widom distribution, the rate of convergence is much slower than the convergence of bulk statistics where the density of the equilibrium measure is large.

Remark 10.2.1. *There are several methods for calculating universality laws* — i.e., $n = \infty$ *statistics — including using their Painlevé transcendent representations, see [13] for an overview. An additional approach based on RHPs is to represent, say,*

$$\partial_s \log\det(I - \mathcal{S}|_{L^2(-s,s)}),$$

as a RH problem. This can be solved numerically for multiple choices of s, and the results are then integrated numerically, see [17] for examples in the degenerate case. This approach is accurate in the tails, whereas the Fredholm determinant representation that we use achieves absolute accuracy only. We are not aware of similar RHPs for finite n.

10.3 Orthogonal polynomials

To calculate the kernel $\mathcal{K}_n$, we need to calculate the polynomials $\pi_n(x)$ and $\gamma_{n-1}\pi_{n-1}(x)$, where $\pi_0(x), \pi_1(x), \ldots$ are monic polynomials orthogonal to the weight $e^{-nV(x)}dx$, supported on the real line. These polynomials can be expressed in terms of the solution to a RHP:

Problem 10.3.1. *[52] The function*

$$Y(z) = \begin{bmatrix} \pi_n(z) & \mathcal{C}_{\mathbb{R}}[\pi_n e^{-nV}](z) \\ -2\pi\mathrm{i}\gamma_{n-1}\pi_{n-1}(z) & -2\pi\mathrm{i}\gamma_{n-1}\mathcal{C}_{\mathbb{R}}[\pi_{n-1}e^{-nV}](z) \end{bmatrix},$$

where

$$\gamma_{n-1} = \left[\int \pi_{n-1}^2(x)e^{-nV(x)}dx\right]^{-1},$$

solves the RHP on the real line

$$Y^+ = Y^- \begin{bmatrix} 1 & e^{-nV(x)} \\ 0 & 1 \end{bmatrix}, \qquad Y \sim \begin{bmatrix} z^n & 0 \\ 0 & z^{-n} \end{bmatrix}, \quad z \to \infty.$$

We apply the numerical method described in Section 5.3. This is discussed in detail in the following sections.

10.3.1 Equilibrium measures

Our first task is to remove the growth in Y at ∞. To accomplish this, we must compute the g-function, which has logarithmic growth at infinity so that $e^{\pm ng(z)} \sim z^{\pm n}$, but has special jump properties so that its incorporation into the RHP allows for uniform approximation.

The g function is associated with the equilibrium measure of V:

Definition 10.3.2. *The equilibrium measure μ is the minimizer of*

$$\iint \log \frac{1}{|x-y|} d\mu(x) d\mu(y) + \int V(x) d\mu(x).$$

We review the numerical approach to calculating equilibrium measures in [88], but in the context of calculating the g-function. For simplicity, we assume that the equilibrium measure of V is supported on a single interval (a, b); a sufficient condition is that V is convex [24] [4].

With the correct choice of (a, b), there exists g satisfying the following scalar RHP:

1. g is analytic off $(-\infty, b)$ and g' is bounded at a and b,
2. $g_+(x) + g_-(x) = V(x) - \ell$ for $a \le x \le b$ and some constant ℓ,
3. $g(z) \sim \log z + \mathcal{O}(\frac{1}{z})$ as $z \to \infty$, and
4. $g_+(x) - g_-(x) = 2\pi \mathrm{i}$ for $-\infty < x < a$.

To calculate g, first we calculate its derivative $\phi = g'$, which satisfies:

1. ϕ is analytic off (a, b) and is bounded at a and b,
2. $\phi_+(x) + \phi_-(x) = V'(x)$ for $a \le x \le b$,
3. $\phi(z) \sim \frac{1}{z}$ as $z \to \infty$.

Differentiating the asymptotics at infinity is justified because $g - \log z$ has an isolated singular point at infinity at which it is bounded; therefore it is analytic at infinity. In typical analysis, ϕ is defined as a Cauchy integral. For computational purposes, it is preferable to use the following representation in terms of the Chebyshev expansion of V'.

Given a candidate (a, b), we describe all functions that have the correct jump on (a, b), decay at infinity and have weaker than pole singularities at a and b.

Definition 10.3.3. *Let $\chi \in \mathbb{C}$ and*

$$f(x) = \sum_{k=0}^{\infty} f_k T_k(x),$$

where T_k is the kth-order Chebyshev polynomial of the first kind. Define

$$\mathcal{P}_\chi f(z) = \sum_{k=0}^{\infty} f_k J_+^{-1}(z)^k - \frac{f_0}{2} \frac{z}{\sqrt{z-1}\sqrt{z+1}} + \frac{\chi}{\sqrt{z-1}\sqrt{z+1}},$$

for the inverse Joukowski transform

$$J_+^{-1}(z) = z - \sqrt{z-1}\sqrt{z+1}.$$

[4] We remark that the below procedure was adapted to the multiple interval case in [88], and adapting our numerical procedure for computing orthogonal polynomials, and thence invariant ensemble statistics, to such cases is straightforward.

Denote the affine map from (a,b) *to* $(-1,1)$ *as*

$$M_{(a,b)}(z) = \frac{a+b}{2} + \frac{b-a}{2}z,$$

and define

$$\mathcal{P}_{(a,b),\chi} f(z) = \mathcal{P}_\chi[f \circ M_{(a,b)}](M^{-1}_{(a,b)}(z)).$$

Theorem 10.3.4 ([86, 88])**.** *Suppose the Chebyshev expansion of* $f(M_{(a,b)}(x))$ *converges absolutely. Then, for all* $\chi \in \mathbb{C}$, $\mathcal{P}_{(a,b),\chi} f(z)$ *is a solution to*

$$\phi_+(x) + \phi_-(x) = f(x), \quad \textit{for} \quad x \in (a,b) \quad \textit{and} \quad \phi(\infty) = 0.$$

Furthermore, every solution to this scalar RHP that has weaker singularities than poles at a *and* b *is equal to* $\mathcal{P}_{(a,b),\chi} f(z)$ *for some* χ*.*

Proof. We sketch the proof for $(a,b) = (-1,1)$. Using $x = \cos\theta$)

$$T_k(x) = \frac{J_\downarrow^{-1}(x)^k + J_\downarrow^{-1}(x)^{-k}}{2},$$

where

$$J_\downarrow^{-1}(x) = x - \mathrm{i}\sqrt{1-\mathrm{x}}\sqrt{1+\mathrm{x}} = \lim_{\epsilon \downarrow 0} \mathrm{J}_+^{-1}(\mathrm{x} + \mathrm{i}\epsilon).$$

This implies that $\mathcal{P}_\chi f$ satisfies the correct jumps, using absolute convergence of the series to interchange limits.

Suppose $\tilde{\phi}$ also satisfies

$$\tilde{\phi}_+(x) + \tilde{\phi}_-(x) = f(x) \quad \text{for} \quad x \in (-1,1) \quad \text{and} \quad \tilde{\phi}(\infty) = 0,$$

with weaker than pole singularities at ± 1. Then $\kappa = \mathcal{P} f - \tilde{\phi}$ satisfies

$$\kappa_+(x) + \kappa_-(x) = 0, \quad \text{for} \quad x \in (-1,1).$$

If we let $\delta(z) = \kappa(z)\sqrt{z-1}\sqrt{z+1}$, we have $\delta_+ = \delta_-$, *i.e.*, δ is continuous and thus analytic on $(-1,1)$. Because κ has weaker than pole singularities at ± 1, we have that δ also has weaker than pole singularities at ± 1. Since these singularities are isolated, it follows that δ is analytic at ± 1, and hence analytic everywhere: δ is constant. This shows that κ is a constant multiple of $1/(\sqrt{z-1}\sqrt{z+1})$, completing the proof. □

Based on the preceding theorem we want to choose (a,b) and χ so that $\phi = \mathcal{P}_{(a,b),\chi}[V']$. To see that ϕ has the correct properties, we need to investigate the Chebyshev coefficients of

$$V'(M_{(a,b)}(x)) = \sum_{k=0}^{\infty} V_k T_k(x).$$

To achieve the desired properties, we want ϕ to be bounded:

$$V_0 = 0 \quad \text{and} \quad \chi = 0.$$

We also want $\phi(z) \sim 1/z$:

$$\frac{b-a}{8} V_1 = 1.$$

These two conditions give a function

$$F(a,b) = \begin{bmatrix} V_0 \\ (b-a)V_1 - 8 \end{bmatrix},$$

of which we want to find a root. We calculate V_0 and V_1 to high accuracy using the composite trapezoidal rule applied to

$$\int_{-1}^{1} \frac{V'(M_{(a,b)}(x))T_k(x)}{\sqrt{1-x^2}} dx = -2\int_{-\pi}^{\pi} V'(M_{(a,b)}(\cos\theta)) \cos k\theta d\theta.$$

This calculation is trivially differentiable with respect to a and b, hence we easily apply Newton iteration to find a root of F. Convexity ensures that this root is unique [88].

Once (a,b) is computed, we calculate $\phi(z)$ by using the discrete cosine transform to calculate the Chebyshev coefficients of V'. We have the equilibrium measure [88]

$$d\mu = \frac{\mathrm{i}}{2\pi}\left[\phi^+(x) - \phi^-(x)\right] dx = \frac{\sqrt{1 - M_{(a,b)}^{-1}(x)^2}}{2\pi} \sum_{k=1}^{\infty} V_k U_{k-1}(M_{(a,b)}^{-1}(x)) dx$$

where U_k are the Chebyshev polynomials of the second kind. This expression comes from the Plemelj formulae (Lemma 3.1.9) and the fact that ϕ is the Cauchy transform of $d\mu$:

$$\phi(z) = \frac{1}{2\pi\mathrm{i}} \int \frac{d\mu(x)}{x-z}.$$

To calculate g, we compute an indefinite integral of ϕ that has the correct decay at infinity [88]:

$$g(z) = \int^z \phi(s)ds = \frac{b-a}{4}\left[V_1\left(\frac{J_+^{-1}(M_{(a,b)}^{-1}(z))^2}{2} - \log J_+^{-1}(M_{(a,b)}^{-1}(z))\right) + \sum_{k=2}^{\infty} V_k \left(\frac{J_+^{-1}(M_{(a,b)}^{-1}(z))^{k+1}}{k+1} - \frac{J_+^{-1}(M_{(a,b)}^{-1}(z))^{k-1}}{k-1}\right)\right].$$

This formula was derived by mapping $J_+^{-1}(M_{(a,b)}^{-1}(z))$ back to the unit circle, where it became a trivially integrable Laurent series. Choosing (arbitrarily) $x \in (a,b)$, we calculate

$$\ell = V(x) - g_+(x) - g_-(x).$$

The numerically calculated g consists of approximating V_k using the discrete Cosine transform and truncating the sum. Due to the analyticity of V, the errors in these computed coefficients are negligible, and the approximation of g is uniformly accurate in the

complex plane.

10.3.2 Scaling constant for edge statistics

Associated with the equilibrium measure are the *Mhaskar–Rakhmanov–Saff numbers* [77, 99] c_V — along with the analytically unneeded $d_V = b - c_V$ — which we need to know to determine the correct scaling so that the edge statistics tend to the Tracy–Widom distribution. We re-express the constant c_V as stated in [26] in terms of constants that we have already calculated: the support of the equilibrium measure and its Chebyshev coefficients. The equilibrium measure for the scaled potential $V(M_{(a,b)}(x))$ has support $(-1, 1)$. Its equilibrium measure is

$$M_{(a,b)}{}'(x)\psi(M_{(a,b)}(x))dx = \frac{b-a}{2}\psi(M_{(a,b)}(x))dx = (b-a)\frac{\sqrt{1-x^2}}{4\pi}\sum_{k=1}^{\infty} V_k U_{k-1}(x)dx$$
$$= \frac{\sqrt{1-x^2}}{2\pi}h(x)dx,$$

as in [26, (3.3)]. We define the constant

$$\alpha = \left(\frac{h(1)^2}{2}\right)^{1/3} = \frac{1}{2}\left[(b-a)\sum_{k=1}^{\infty} kV_k\right]^{2/3},$$

as in [26, (3.10)]. The scaling constant is then

$$c_V = \frac{2\alpha}{b-a} = (b-a)^{-1/3}\left[\sum_{k=1}^{\infty} kV_k\right]^{2/3}.$$

Remark 10.3.5. *For the degenerate potential of Figure 10.2.4, $c_V = 0$ and hence the scaling breaks down. This coincides with the fact that the edge statistics for the associated ensemble does not follow the standard Tracy–Widom distribution.*

10.3.3 Lensing the RHP

We rewrite Y to normalize the behavior at infinity:

$$Y = \begin{bmatrix} e^{\frac{n\ell}{2}} & 0 \\ 0 & e^{-\frac{n\ell}{2}} \end{bmatrix} T \begin{bmatrix} e^{-ng} & 0 \\ 0 & e^{ng} \end{bmatrix} \begin{bmatrix} e^{-\frac{n\ell}{2}} & 0 \\ 0 & e^{\frac{n\ell}{2}} \end{bmatrix}, \tag{10.3.1}$$

so that $T \sim I$ and T has a jump along the real line, on which it satisfies

$$T_+ = T_- \begin{bmatrix} e^{n(g_- - g_+)} & e^{n(g_+ + g_- + \ell - V)} \\ 0 & e^{n(g_+ - g_-)} \end{bmatrix}$$
$$= T_- \begin{cases} \begin{bmatrix} 1 & e^{n(g_+ + g_- + \ell - V)} \\ 0 & 1 \end{bmatrix} & \text{if } x < a, \\ \begin{bmatrix} e^{n(g_- - g_+)} & 1 \\ 0 & e^{n(g_+ - g_-)} \end{bmatrix} & \text{if } a < x < b, \\ \begin{bmatrix} 1 & e^{n(2g + \ell - V)} \\ 0 & 1 \end{bmatrix} & \text{if } b < x, \end{cases}$$

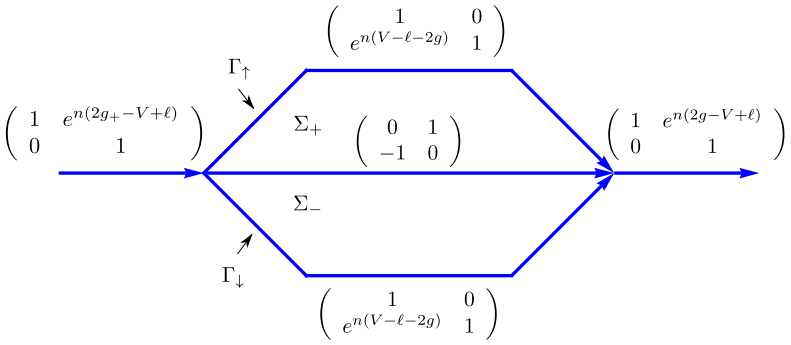

Figure 10.3.1: The jumps of S.

We appeal to properties of equilibrium measures [24, (7.57)] to assert that

$$g_+(x) + g_-(x) + \ell - V < 0,$$

for $x < a$ and $x > b$, thus those contributions of the jump matrix are isolated around a and b. On the other hand, $g_+ - g_-$ is imaginary between a and b [24, pp. 195], hence $e^{\pm n(g_+ - g_-)}$ becomes increasingly oscillatory on (a, b). We wish to deform the RH problem into the complex plane to convert oscillations into exponential decay. To accomplish this, we introduce the lensing as in Figure 10.3.1, where we rewrite T as

$$T(z) = S(z) \begin{cases} \begin{bmatrix} 1 & 0 \\ e^{n(V-\ell-2g)} & 1 \end{bmatrix}, & \text{if } z \in \Sigma_+, \\ \begin{bmatrix} 1 & 0 \\ e^{n(V-\ell-2g)} & 1 \end{bmatrix}, & \text{if } z \in \Sigma_-, \\ I, & \text{otherwise.} \end{cases} \tag{10.3.2}$$

By substituting

$$g_+ = V - g_- - \ell,$$

we see that the oscillations have been removed completely from the support of μ:

$$\begin{aligned}
S_+ &= T_+ \begin{bmatrix} 1 & 0 \\ -e^{n(V-\ell-2g_+)} & 1 \end{bmatrix} = T_+ \begin{bmatrix} 1 & 0 \\ -e^{n(g_- - g_+)} & 1 \end{bmatrix} \\
&= T_- \begin{bmatrix} e^{n(g_- - g_+)} & 1 \\ 0 & e^{n(g_+ - g_-)} \end{bmatrix} \begin{bmatrix} 1 & 0 \\ -e^{n(g_- - g_+)} & 1 \end{bmatrix} \\
&= T_- \begin{bmatrix} 0 & 1 \\ -1 & e^{n(g_+ - g_-)} \end{bmatrix} = S_- \begin{bmatrix} 1 & 0 \\ -e^{n(V-\ell-2g_-)} & 1 \end{bmatrix} \begin{bmatrix} 0 & 1 \\ -1 & e^{n(V-\ell-2g_-)} \end{bmatrix} \\
&= S_- \begin{bmatrix} 0 & 1 \\ -1 & 0 \end{bmatrix}.
\end{aligned}$$

However, we have introduced new jumps on $\Gamma_\uparrow$ and $\Gamma_\downarrow$, on which

$$S_+ = T_+ = T_- = S_- \begin{bmatrix} 1 & 0 \\ e^{n(V-\ell-2g)} & 1 \end{bmatrix}.$$

10.3.4 Removing the connecting jump

We have successfully converted oscillations to exponential decay. However, to maintain accuracy of the numerical algorithm for large n, we must isolate the jumps to neighborhoods of the endpoints a and b. To achieve this, we remove the jump along (a, b). We introduce a *parametrix* that solves the RHP exactly on this single contour. In other words, we require a function which satisfies the following RHP:

$$N_+(x) = N_-(x) \begin{bmatrix} 0 & 1 \\ -1 & 0 \end{bmatrix}, \quad \text{for} \quad a < x < b \quad \text{and} \quad N(\infty) = I.$$

The solution is [24]

$$N(z) = \frac{1}{2\nu(z)} \begin{bmatrix} 1 & \mathrm{i} \\ -\mathrm{i} & 1 \end{bmatrix} + \frac{\nu(z)}{2} \begin{bmatrix} 1 & -\mathrm{i} \\ \mathrm{i} & 1 \end{bmatrix} \quad \text{for } \nu(z) = \left(\frac{z-b}{z-a} \right)^{1/4};$$

i.e., $\nu(z)$ is a solution to

$$\nu_+(x) = \mathrm{i}\nu_-(\mathrm{x}) \quad \text{for} \quad \mathrm{a} < \mathrm{x} < \mathrm{b} \quad \text{and} \quad \nu(\infty) = 1.$$

An issue with using $N(z)$ as a parametrix is that it introduces singularities at a and b, hence we also introduce local parametrices to avoid these singularities. In the event that the equilibrium measure $\psi(x)$ has exactly *square-root decay* at the edges, asymptotically accurate local parametrices are known (see Section 10.4.1). However, if the equilibrium measure has higher-order decay (*e.g.* the higher-order Tracy–Widom distributions [16]), the asymptotically accurate local parametrices are only known in terms of a RH problem.

For numerical purposes, however, we do not need the parametrix to be asymptotically accurate: we achieve asymptotic accuracy by scaling the contours. Thus we introduce the *trivially constructed* local parametrices which satisfy the jumps of S in neighborhoods of a

and b:

$$P_a(z) = \begin{pmatrix} \begin{cases} \begin{bmatrix} 1 & 0 \\ 1 & 1 \end{bmatrix} & \text{if } \frac{\pi}{3} < \arg(z-a) < \pi \\ \begin{bmatrix} 1 & -1 \\ 1 & 0 \end{bmatrix} & \text{if } -\pi < \arg(z-a) < -\frac{\pi}{3} \\ \begin{bmatrix} 0 & -1 \\ 1 & 0 \end{bmatrix} & \text{if } -\frac{\pi}{3} < \arg(z-a) < 0 \\ I & \text{otherwise} \end{cases} \end{pmatrix} \begin{bmatrix} e^{n(V-\ell-2g)} & 0 \\ 0 & e^{-n(V-\ell-2g)} \end{bmatrix},$$

and

$$P_b(z) = \begin{pmatrix} \begin{cases} \begin{bmatrix} 1 & 0 \\ -1 & 1 \end{bmatrix} & \text{if } \frac{2\pi}{3} < \arg(z-b) < \pi \\ \begin{bmatrix} 0 & -1 \\ 1 & 1 \end{bmatrix} & \text{if } -\pi < \arg(z-b) < -\frac{2\pi}{3} \\ \begin{bmatrix} 1 & -1 \\ 0 & 1 \end{bmatrix} & \text{if } -\frac{2\pi}{3} < \arg(z-b) < 0 \\ I & \text{otherwise} \end{cases} \end{pmatrix} \begin{bmatrix} e^{n(V-\ell-2g)} & 0 \\ 0 & e^{-n(V-\ell-2g)} \end{bmatrix}.$$

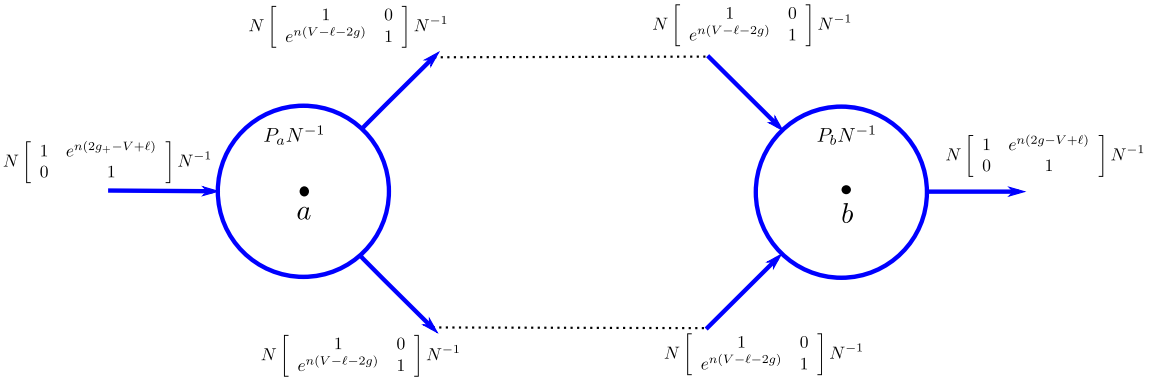

Figure 10.3.2: The jumps of Φ. We use a counter-clockwise orientation on the circles about a and b.

We write

$$S(z) = \Phi(z) \begin{cases} N(z) & \text{if } |z-a| > r \text{ and } |z-b| > r, \\ P_b(z) & \text{if } |z-b| < r, \\ P_a(z) & \text{if } |z-a| < r. \end{cases} \tag{10.3.3}$$

The final RHP for Φ satisfies the jumps depicted in Figure 10.3.2. Note that in general r depends on n. We discuss this in more detail in the next section.

In practice, we do not use infinite contours. We truncate contours when the jump matrix is to machine precision the identity matrix (see Lemma 3.10.4). In all cases we consider here, after proper deformations the jump matrices are C^∞ smooth and are exponentially decaying to the identity matrix for large z. We deform the remaining contours to be line segments connecting their endpoints. The resulting jump contour consists only of affine

transformations of the unit interval.

10.3.5 Contour scalings

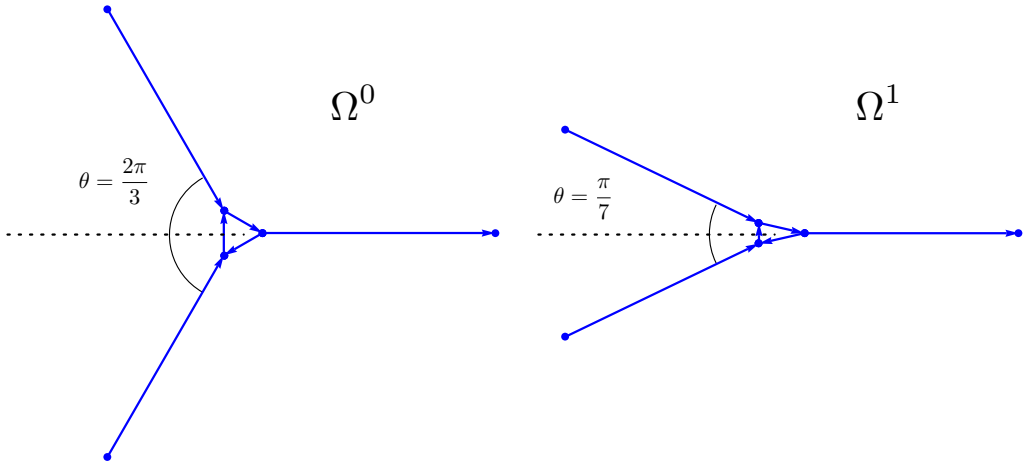

Figure 10.3.3: The pre-scaled Ω^0 used for non-degenerate endpoints and the pre-scaled Ω^1 used for first-order degenerate endpoints. These are the contours that are used in practice.

In the case of a non-degenerate equilibrium measure, $V(z) - \ell - 2g(z) \sim c_a(z-a)^{3/2}$ as $z \to a$ and $V(z) - \ell - 2g \sim c_b(z-b)^{3/2}$ as $z \to b$. In accordance with Assumption 5.0.1, we scale the contours like $n^{-2/3}$:

$$\Omega_n^1 = -n^{-2/3}\Omega^0 + a \quad \text{and} \quad d\Omega_n^2 = n^{-2/3}\Omega^0 + b,$$

where the Ω^0 that is used in practice is depicted in the left graph of Figure 10.3.3, and the angle of the contours are chosen to match the direction of steepest descent. This implies that $r \sim n^{-2/3}$. In the first-order degenerate case (e.g., $V(x) = x^2/5 - 4x^3/15 + x^4/20 + 8x/5$), $V(z) - \ell - 2g(z) \sim c_b(z-b)^{7/2}$ as $z \to b$ and we scale like $n^{-7/2}$ (implying $r \sim n^{-7/2}$) at the degenerate endpoint:

$$\Omega_n^1 = n^{-2/3}\Omega^0 + a \quad \text{and} \quad \Omega_n^2 = n^{-7/2}\Omega^1 + b,$$

where Ω^1 is depicted in the right graph of Figure 10.3.3 (the angle is sharper to attach to the new direction of steepest descent). Higher-order degenerate equilibrium measures require higher-order scalings, but this can be determined systematically by investigating the number of vanishing derivatives of the equilibrium measure. This is the final form of the RHP that is used in the numerical calculations of Section 10.2. A discussion the accuracy of the numerical solution of this scaled and shifted RHP for large n is presented below.

10.4 Achieving uniform approximation

Having described the form of the RHP which we solve numerically, we want to show that the resulting approximation remains accurate as n becomes large by satisfying the conditions of Theorem 5.2.4. While we do not use the local parametrix in the numerical algorithm, we do need it to show that the deformed contour satisfies the uniform approximation properties. Thus we introduce the local parametrix in Section 10.4.1, noting that it can also be used in the numerical scheme to achieve uniform approximation (though not for degenerate potentials). We use this parametrix to show uniform approximation properties in Section 10.4.2. To achieve this, we must adapt the jump matrix to cancel the effects of singularities resulting from the parametrix $N(z)$.

10.4.1 The classical Airy parametrix

In this section we present the deformation and asymptotic solution of the RHP, needed for the asymptotic analysis of orthogonal polynomials, as in [24, Section 7.6]. For brevity of presentation in this section we only consider potentials of the form $V(x) = x^{2m}$. For the asymptotic analysis and deformations in the more polynomial case of $V(x)$ see [27, 28, 29, 30].

The goal of the section is to construct a parametrix $\hat{\Phi}$ that is a sectionally analytic, matrix-valued function so that $S\hat{\Phi}^{-1} \to I$ as $n \to \infty$ where S is the solution of the deformed and lensed RHP in Figure 10.3.1. The RHP for the error $E = S\hat{\Phi}^{-1}$ has smooth solutions and is a near-identity RHP in the sense that the associated singular integral operator is expressed in the form $I - K_n$ with $\|K_n\|_{\mathcal{L}(L^2)} \to 0$ as $n \to \infty$. Thus E can be computed via a Neumann series for sufficiently large n.

The deformation proceeds much in the same way as in Section 10.3.4, except we have $a = -c$, $b = c$ for $c > 0$ [24]. We replace P_a and P_b with new functions ψ_{-c} and ψ_c that are constructed out of the Airy function. It is important to note that due to the near-identity nature of the problem we do not scale the jump contour (*i.e.*, $r \sim 1$). Now we construct the functions ψ_{-c} and ψ_c. As an intermediate step, define

$$\Psi(s) = \begin{cases} \begin{pmatrix} Ai(s) & Ai(\omega^2 s) \\ Ai'(s) & \omega^2 Ai(\omega^2 s) \end{pmatrix} e^{-i\frac{\pi}{6}\sigma_3} & 0 < \arg s < \frac{2\pi}{3} \\ \begin{pmatrix} Ai(s) & Ai(\omega^2 s) \\ Ai'(s) & \omega^2 Ai'(\omega^2 s) \end{pmatrix} e^{-i\frac{\pi}{6}} & \frac{2\pi}{3} < \arg s < \pi \\ \begin{pmatrix} Ai(s) & Ai(\omega^2 s) \\ Ai'(s) & \omega^2 Ai'(\omega^2 s) \end{pmatrix} e^{-i\frac{\pi}{6}\sigma_3} \begin{pmatrix} 1 & 0 \\ -1 & 1 \end{pmatrix} & \pi < \arg s < \frac{4\pi}{3} \\ \begin{pmatrix} Ai(s) & -\omega^2 Ai(\omega s) \\ Ai'(s) & -Ai'(\omega s) \end{pmatrix} e^{-i\frac{\pi}{6}\sigma_3} \begin{pmatrix} 1 & 0 \\ 1 & 1 \end{pmatrix} & \frac{4\pi}{3} < \arg s < 2\pi \end{cases},$$

with $\omega = e^{\frac{2\pi i}{3}}$.

The relations

$$Ai(s) + \omega Ai(\omega s) + \omega^2 Ai(\omega^2 s) = 0,$$
$$Ai'(s) + \omega^2 Ai'(\omega s) + \omega Ai'(\omega^2 s) = 0,$$

can be used to show that $\Psi(s)$ satisfies the following jump conditions

$$\Psi^+(s) = \Psi^-(s) \begin{cases} \begin{pmatrix} 1 & 1 \\ 0 & 1 \end{pmatrix} & s \in \gamma_1 \\ \begin{pmatrix} 1 & 0 \\ 1 & 1 \end{pmatrix} & s \in \gamma_2 \\ \begin{pmatrix} 0 & 1 \\ -1 & 0 \end{pmatrix} & s \in \gamma_3 \\ \begin{pmatrix} 1 & 0 \\ 1 & 1 \end{pmatrix} & s \in \gamma_4 \end{cases}.$$

See Figure 10.4.1 for $\gamma_i,\ i = 1, \dots 4$.

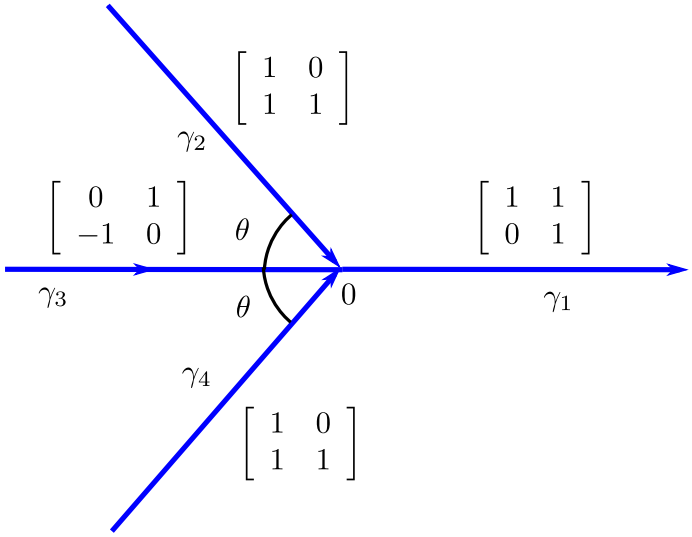

Figure 10.4.1: The jump contours for Ψ with jump matrices. We use $\theta = 2\pi/3$.

Since we only consider $V(x)$ even in this section, the equilibrium measure is supported on a symmetric interval $[-c, c]$ for $c > 0$. Define

$$\Lambda(z) = \frac{3}{2}\varphi(z)(z-c)^{-3/2}, \quad \lambda(z) = (z-c)(\Lambda(z))^{2/3},$$
$$\varphi(z) = \frac{1}{2}\left(V(z) - \ell\right) - g(z).$$

It follows from the branching properties of φ that Λ and λ are analytic in a neighborhood of c. Furthermore, since $\lambda(c) = 0$ and $\lambda'(c) = (\Lambda(c))^{2/3} \neq 0$ we use it as a conformal change of variables mapping a neighborhood of $z = c$ into a neighborhood of the origin. More precisely, fix an $\epsilon > 0$ and define $O_c = \lambda^{-1}(\{|z| < \epsilon\})$.

Define

$$\psi_c(z) = L(z)\Psi(n^{2/3}\lambda(z))e^{n\varphi(z)\sigma_3},$$
$$L(z) = \begin{pmatrix} 1 & -1 \\ -i & -i \end{pmatrix} \sqrt{\pi} e^{i\frac{\pi}{6}} n^{\sigma_3/6} ((z+c)\Lambda^{2/3}(z))^{\sigma_3/4}.$$

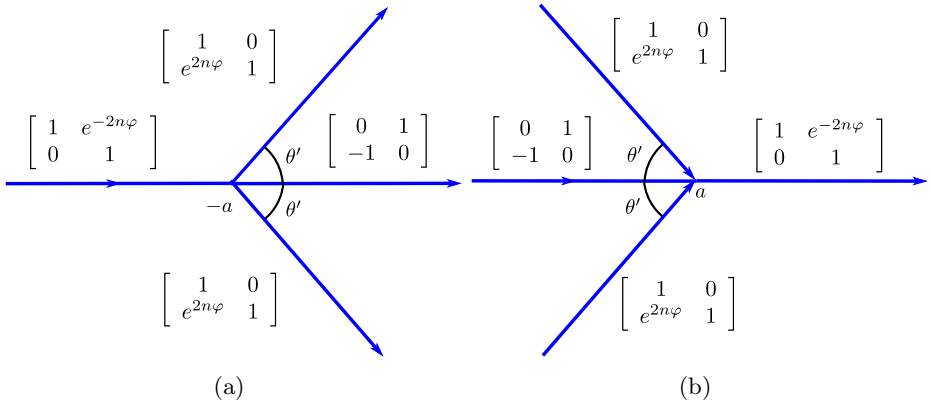

Figure 10.4.2: The local parametrices near $z = \pm c$. As above, $\theta' > 0$ is included for concreteness but its exact value is not needed. (a) The jump contours for ψ_{-c} with jump matrices. (b) The jump contours for ψ_c with jump matrices.

ψ_c solves the local RHP shown in Figure 10.2(b). The symmetry of $V(x)$ implies that $\psi_{-c}(z) = \sigma_3\psi_c(-z)\sigma_3$ satisfies the jumps shown in Figure 10.2(a). We define the full parametrix

$$\hat{\Phi}(z) = \begin{cases} \psi_c(z) & z \in O_c \\ \psi_{-c}(z) & z \in -O_c \\ N(z) & \text{otherwise} \end{cases}. \tag{10.4.1}$$

We need a result concerning the asymptotics of the Airy function:

$$Ai(s) = \frac{1}{2\sqrt{\pi}} s^{-1/4} e^{-\frac{2}{3}s^{3/2}} \left(1 + \mathcal{O}\left(\frac{1}{s^{3/2}}\right)\right),$$
$$Ai'(s) = -\frac{1}{2\sqrt{\pi}} s^{3/4} e^{-\frac{2}{3}s^{3/2}} \left(1 + \mathcal{O}\left(\frac{1}{s^{3/2}}\right)\right),$$

as $s \to \infty$ and $|\arg s| < \pi$. These asymptotics, along with the definition of $\lambda(z)$, can be used to show

$$\psi_c(z)N^{-1}(z) = I + \mathcal{O}(n^{-1}), \quad z \in \partial O_c, \tag{10.4.2}$$
$$\psi_{-c}(z)N^{-1}(z) = I + \mathcal{O}(n^{-1}), \quad z \in \partial O_{-c}, \tag{10.4.3}$$

as $n \to \infty$ uniformly in z provided $O_c \cup O_{-c}$ is contained in a sufficiently narrow strip containing the real line. See [24, Section 7.6] for the details.

We take the RHP for S in Figure 10.3.1 and label ∂O_c and ∂O_{-c}. Note that without loss of generality we take O_c and O_{-c} to be open balls around c and $-c$, respectively. (Analyticity allows us to deform any open, simply connected set containing c or $-c$ to a ball.)

Since ψ_c and ψ_{-c} solve the RHP locally in O_c and O_{-c}, respectively, the function $E = S\hat{\Psi}^{-1}$ is analytic in O_c and O_{-c}. See Figure 10.4.3 for the jump contour Ω and jump matrix J for the RHP for E. It is shown in [24, Section 7.6] using (10.4.2) that the jump

matrix for this RHP tends uniformly to the identity matrix as $n \to \infty$, again provided that all contours are in sufficiently small neighborhood of the real line. Thus

$$\| I - \mathcal{C}\left[J;\Omega\right] \|_{\mathcal{L}(L^2(\Omega))} = \mathcal{O}(n^{-1}),$$

and a Neumann series produces the unique solution u of $\mathcal{C}\left[J;\Omega\right] u = J - I$. S is found via the expression

$$S(z) = (I + \mathcal{C}_\Omega u(z))\hat{\Psi}(z).$$

10.4.2 Obtaining the bounds in Theorem 5.2.4

To prove the uniform approximation of the numerical method we apply Theorem 5.2.4. First, one has to identify the correct scalings for the contours and second, establish bounds on the relevant operator norms and function derivatives. We follow this procedure in two cases below.

The RHP for E

In this case, we consider numerically solving the RHP for E, rather than scaling and shifting the contours as we do in practice. This simplifies the proof of uniform approximation considerably though the exact form of the Airy parametrix is needed explicitly in the numerics. Unfortunately, this local parametrix does not apply to degenerate potentials. We contrast this with the analysis in the following section where the Airy parametrix is needed to prove asymptotic accuracy but is in no way needed to perform calculations.

Take $\Gamma^\xi = \Omega$ in Theorem 5.2.4 with $\xi = n$; that is, we do not scale the contour. The near-identity nature of the RHP allows us to avoid any scaling of the problem. Using the asymptotic expansions for the derivatives of Airy functions one can show that

$$\| J - I \|_{W^{k,\infty}(\Omega)\cap H^k(\Omega)} = \mathcal{O}(n^{-1}).$$

Furthermore, the fact that $\| \mathcal{C}\left[J;\Omega\right]^{-1} \|_{\mathcal{L}(L^2(\Omega))} < C$ follows easily from the Neumann series argument already given. Therefore Theorem 5.2.4 shows that the numerical method uniformly approximates solutions of this RHP for small and arbitrarily large n.

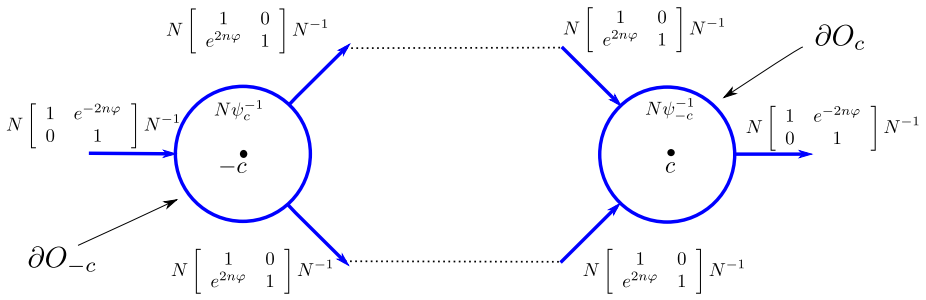

Figure 10.4.3: The jump contours Ω for the error E. The jump matrix J for E which is taken as the piecewise definition as shown. We use a counter-clockwise orientation for the circles about $\pm c$. These circles have radius $r \sim 1$.

To demonstrate the convergence properties of the solution for large n we use the following procedure. Let U_m denote the approximation of u obtained using the numerical method for RHPs discussed above with m collocation points per contour. When we break up Ω into both its non-self-intersecting components and into its components that can be represented by affine transformations of the unit interval, we end up with 14 contours. Thus, we use a total of $14m$ collocation points. We solve the RHP with $m = 10$ and then again with $m = 20$. We sample U_{10} at each collocation point for U_{20} and measure the maximum difference at these collocations points. We define this difference to be the *Cauchy error*. Figure 10.4.4 demonstrates that the error decreases as $n \to \infty$.

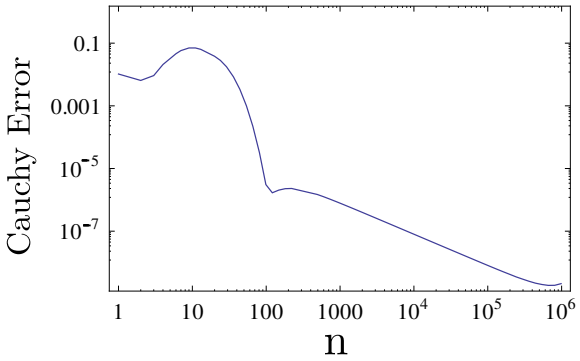

Figure 10.4.4: The *Cauchy error* between U_{10} and U_{20} as $n \to \infty$. This plot indicates that it takes fewer collocation points to approximate E as n increases.

The RHP for Φ

While for non-degenerate potentials we can solve the RHP associated with E numerically, the RHP for Φ that we use in practice is of a fundamentally simpler form. No additional special functions (*e.g* Airy functions) are needed and yet the contours are located away from the stationary points a and b (we return, for now, to allowing general potentials). All deformations are performed by a reordering and analytic continuation of previously defined functions. Thus we want to show that our strategy of scaling contours does indeed satisfy the criterion of uniform approximation of Theorem 5.2.4.

To achieve uniform approximation, we must first alter the jump matrix so that it remains bounded as $n \to \infty$. This will be achievable using only properties of $N(z)$ near a and b, and we prove that the resulting jump matrix is bounded in Lemma 10.4.3. We also need to show that the inverse of the operator is bounded. Using the local parametrix, we accomplish this in Lemmas 10.4.1 and 10.4.2.

In this section we assume the non-degenerate case. (While uniform approximation is indeed achievable for degenerate potentials, proving this is more challenging due to the lack of explicit local parametrices.) Therefore, we consider the following jump contour (see Figure 10.4.5 and compare with Algorithm 5.1.11)

$$\Gamma^\xi = \Gamma^n = \Omega_n^1 \cup \Omega_n^2,$$

for

$$\Omega_n^1 = n^{-2/3}\Omega^0 + a \quad \text{and} \quad \Omega_n^2 = n^{-2/3}\Omega^0 + b.$$

Furthermore, define G to be the jump matrix for Φ, see Figure 10.3.2.

First, we rectify the issue with the jumps on these scaled contours: as $n \to \infty$, they approach the unbounded singularities of $N(z)$, violating the condition of Theorem 5.2.4 that the jump matrix must be bounded. However, we expand

$$N(a+zn^{-2/3}) = \frac{n^{1/6}}{2}\left(\frac{b-a}{z}\right)^{\frac{1}{4}}\begin{bmatrix} 1 & -\mathrm{i} \\ \mathrm{i} & 1 \end{bmatrix} + \frac{n^{-1/6}}{2(b-a)}\left(\frac{b-a}{z}\right)^{\frac{3}{4}}\begin{bmatrix} 1 & \mathrm{i} \\ -\mathrm{i} & 1 \end{bmatrix} + \mathcal{O}(n^{-\frac{1}{2}}),$$

$$N(a+zn^{-2/3})^{-1} = \frac{n^{1/6}}{2}\left(\frac{b-a}{z}\right)^{\frac{1}{4}}\begin{bmatrix} 1 & \mathrm{i} \\ -\mathrm{i} & 1 \end{bmatrix} + \frac{n^{-1/6}}{2(b-a)}\left(\frac{b-a}{z}\right)^{\frac{3}{4}}\begin{bmatrix} 1 & -\mathrm{i} \\ \mathrm{i} & 1 \end{bmatrix} + \mathcal{O}(n^{-\frac{1}{2}}),$$

$$N(b+zn^{-2/3}) = \frac{n^{1/6}}{2}\left(\frac{b-a}{z}\right)^{\frac{1}{4}}\begin{bmatrix} 1 & \mathrm{i} \\ -\mathrm{i} & 1 \end{bmatrix} + \frac{n^{-1/6}}{2(b-a)}\left(\frac{b-a}{z}\right)^{\frac{3}{4}}\begin{bmatrix} 1 & -\mathrm{i} \\ \mathrm{i} & 1 \end{bmatrix} + \mathcal{O}(n^{-\frac{1}{2}}),$$

$$N(b+zn^{-2/3})^{-1} = \frac{n^{1/6}}{2}\left(\frac{b-a}{z}\right)^{\frac{1}{4}}\begin{bmatrix} 1 & -\mathrm{i} \\ \mathrm{i} & 1 \end{bmatrix} + \frac{n^{-1/6}}{2(b-a)}\left(\frac{b-a}{z}\right)^{\frac{3}{4}}\begin{bmatrix} 1 & \mathrm{i} \\ -\mathrm{i} & 1 \end{bmatrix} + \mathcal{O}(n^{-\frac{1}{2}}).$$

Define

$$\bar{N}_{a,n} = n^{-1/6}\begin{bmatrix} 1 & -\mathrm{i} \\ \mathrm{i} & 1 \end{bmatrix} + n^{1/6}\begin{bmatrix} 1 & \mathrm{i} \\ -\mathrm{i} & 1 \end{bmatrix},$$

and

$$\bar{N}_{b,n} = n^{-1/6}\begin{bmatrix} 1 & \mathrm{i} \\ -\mathrm{i} & 1 \end{bmatrix} + n^{1/6}\begin{bmatrix} 1 & -\mathrm{i} \\ \mathrm{i} & 1 \end{bmatrix},$$

so that

$$N(a+zn^{-2/3})\bar{N}_{a,n}, \quad \bar{N}_{a,n}^{-1}N(a+zn^{-2/3})^{-1}, \quad N(b+zn^{-2/3})\bar{N}_{b,n} \quad \text{and} \quad \bar{N}_{b,n}^{-1}N(b+zn^{-2/3})^{-1}$$

are uniformly bounded for z restricted to an annulus around zero as $n \to \infty$. These matrices are used to remove the growth of the jump matrix as $n \to \infty$. We demonstrate this procedure, which is a modification of the algorithm in Lemma 5.1.11. We truncate the contours of the RHP for Φ by removing the dashed contours in Figure 10.3.2. For $\epsilon > 0$ and small, this gives us an approximation Φ_ϵ of Φ with jump matrix G_ϵ so that $G_\epsilon - I$ is supported on $\Omega_n^1 \cup \Omega_n^2$. Additionally, G_ϵ satisfies

$$\|N^{-1}G_\epsilon N - N^{-1}GN\|_{L^2\cap L^\infty} = \mathcal{O}(\epsilon) \quad \text{and } G_\epsilon(z) = G(z) \text{ for } |z-a| = r \text{ or } |z-b| = r. \tag{10.4.4}$$

Our method of scaling contours ensures that ϵ is independent of n. We separate the RHP for Φ_ϵ into two problems $[G_1;\Omega_n^1]$ and $[G_2;\Omega_n^2]$ with solutions Φ_1 and Φ_2, respectively. See Figure 10.4.5 for the piecewise definition of G_1 and G_2. Formally, our solution procedure is as follows:

1. Scale G_1: Define $H_1(z) = G_1(b+zn^{-2/3})$.

2. Remove the growth of $H_1(z)$: If $\hat{\Phi}_1 = [H_1; \Omega_0]$ define

$$\bar{\Phi}_1(z) = \begin{cases} \bar{N}_{b,n}\hat{\Phi}_1\bar{N}_{b,n}^{-1}(z) & \text{if } z > rn^{2/3}, \\ \bar{N}_{b,n}\hat{\Phi}_1 & \text{if } z < rn^{2/3}. \end{cases} \tag{10.4.5}$$

A straightforward calculation shows that $\bar{\Phi}_1^+(z) = \bar{\Phi}^-(z)\bar{H}_1(z)$ where

$$\bar{H}_1(z) = \begin{cases} \bar{N}_{b,n}H_1(z)\bar{N}_{b,n}^{-1} & \text{if } |z| > rn^{2/3}, \\ H_1(z)\bar{N}_{b,n}^{-1}, & \text{if } |z| = rn^{2/3}. \end{cases}$$

Recall that in this case the contour is scaled according to $r \sim n^{-2/3}$.

3. Solve for $\bar{\Phi}_1 = [\bar{H}_1; \Omega_0]$. Therefore

$$\Phi_1 = [G_1; \Omega_n^1] = \bar{N}_{b,n}^{-1}\bar{\Phi}_1\left(n^{2/3}(z-b)\right)\bar{N}_{b,n}.$$

4. Modify G_2: If $\Phi_\epsilon = [G_\epsilon; \Gamma_n]$ then $\Phi_\epsilon\Phi_1^{-1}$ has the jump $\tilde{G}_2 = \Phi_1 G_2 \Phi_1^{-1}$ on Ω_n^2 and is analytic elsewhere.

5. Scale $\tilde{G}_2$: Define $\tilde{H}_2(z) = \tilde{G}_2(a + zn^{-2/3})$.

6. Remove the growth of $\tilde{H}_2(z)$: As in (10.4.5), define

$$\bar{\Phi}_2(z) = \begin{cases} \bar{N}_{a,n}\tilde{\Phi}_2\bar{N}_{a,n}^{-1}(z), & \text{if } z > rn^{2/3}, \\ \bar{N}_{a,n}\tilde{\Phi}_2, & \text{if } z < rn^{2/3}. \end{cases}$$

where $\tilde{\Phi}_2 = [\tilde{H}_2; \Omega_0]$. Then $\bar{\Phi}_2^+(z) = \bar{\Phi}_2^-(z)\bar{H}_2(z)$, where

$$\bar{H}_2(z) = \begin{cases} \bar{N}_{a,n}\tilde{H}_2(z)\bar{N}_{a,n}^{-1}, & \text{if } |z| > rn^{2/3}, \\ \tilde{H}_2(z)\bar{N}_{a,n}^{-1}, & \text{if } |z| = rn^{2/3}. \end{cases}$$

7. Solve for $\bar{\Phi}_2 = [\bar{H}_2; \Omega_0]$ and therefore

$$\Phi_2 = [\tilde{G}_2; \Omega_n^1] = \bar{N}_{a,n}^{-1}\bar{\Phi}_2\left(n^{2/3}(z-a)\right)\bar{N}_{a,n}.$$

8. $\Phi = [G; \Gamma_n] = \Phi_1\Phi_2$.

We solve two RHPs in this procedure. It is seen that the RHPs have jump matrices that are uniformly bounded in n. This is a necessary (but not sufficient!) condition for the numerical method to be asymptotically accurate. To analyse the asymptotic behavior of these RHPs we must bound the inverse of the operators by comparing the solutions with the Airy parametrix. Again, we assume that $V(x) = x^{2m}$ so that we have $a = -c$ and $b = c$, $c > 0$. We use this restriction for convenience: we have already defined the parametrix associated with this choice of $V(x)$ above.

We must alter our local parametrices to investigate their behavior both on the fixed outer contour ∂O_c and the scaled contour of the RHP on which we solve numerically.

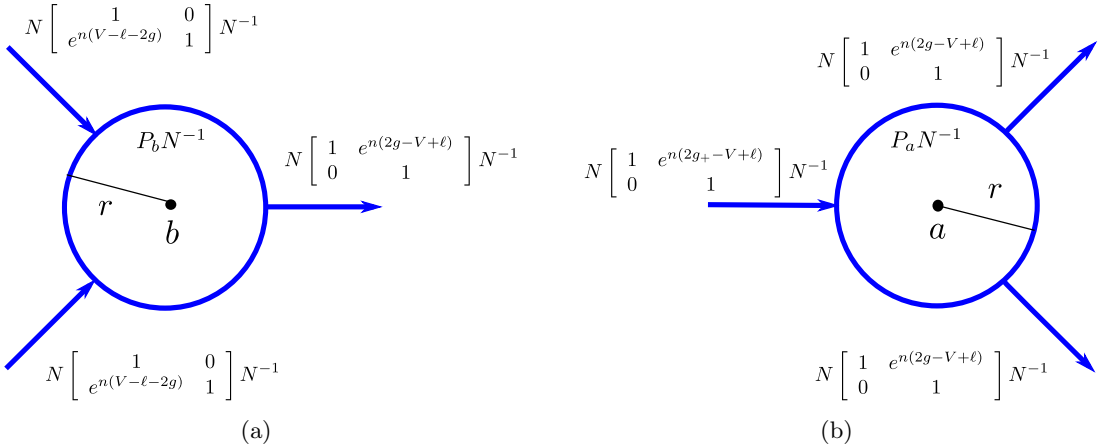

Figure 10.4.5: The separate RHPs for Φ_1 and Φ_2. All circles have counter-clockwise orientation. (a) The jump contour Ω_n^1 and jump matrices for Φ_1. (b) The jump contour Ω_n^2 and jump matrices for Φ_2.

Therefore, we alter the local parametrices by defining (compare with (10.3.3))

$$\Psi_{-c}(z) = \begin{cases} \psi_{-c}(z)P^{-1}_{a=-c}(z), & \text{if } |z+c| < r, \\ \psi_{-c}(z)N^{-1}, & \text{if } |z+c| > r \text{ and } z \in O_{-c}, \\ I, & \text{otherwise,} \end{cases}$$

$$\Psi_{c}(z) = \begin{cases} \psi_{c}(z)P^{-1}_{b=c}(z), & \text{if } |z-c| < r, \\ \psi_{c}(z)N^{-1}, & \text{if } |z-c| > r \text{ and } z \in O_{c}, \\ I, & \text{otherwise.} \end{cases}$$

The jump contours Ω_n^c and Ω_n^{-c} for the RHPs for Ψ_c and Ψ_{-c} with jump matrices J_c and J_{-c} are shown in Figure 10.4.6.

The following lemmas present a step toward our final result that proves asymptotic accuracy: they demonstrate that the local parametrices Ψ_c and Ψ_{-c} can be used to bound operator inverses. For the analysis, we extend G_1 (G_2) to Ω_n^c (Ω_n^{-c}) by defining $G_1 = I$ on $\Omega_n^c \setminus \Omega_n^1$ ($G_2 = I$ on $\Omega_n^{-c} \setminus \Omega_n^2$).

Lemma 10.4.1. *There exists a constant $C > 0$ and functions A_1, B_1 such that*

$$\begin{aligned} &G_1 J_c^{-1} = I + N[A_1(n^{-1}) + B_1(\epsilon)]N^{-1} \quad \textit{for} \quad |z-c| > r, \\ &G_1 J_c^{-1} = I, \quad \textit{for} \quad |z-c| = r \quad \textit{and}, \\ &\|\mathcal{C}[\bar{H}_1;\Omega_0]^{-1}\|_{\mathcal{L}(L^2(\Omega_0))} < C, \end{aligned} \tag{10.4.6}$$

where $\|A_1(n)\|_{L^2\cap L^\infty} = \mathcal{O}(n)$ and $\|B_1(\epsilon)\|_{L^2\cap L^\infty} = \mathcal{O}(\epsilon)$.

Proof. For (10.4.6) it follows from scaling and truncation that for sufficiently large n, $G_1 - I$ is supported inside O_c. Furthermore, on $\Omega_c^n \setminus \partial O_c$, $J_c = G$ by construction so that (10.4.4)

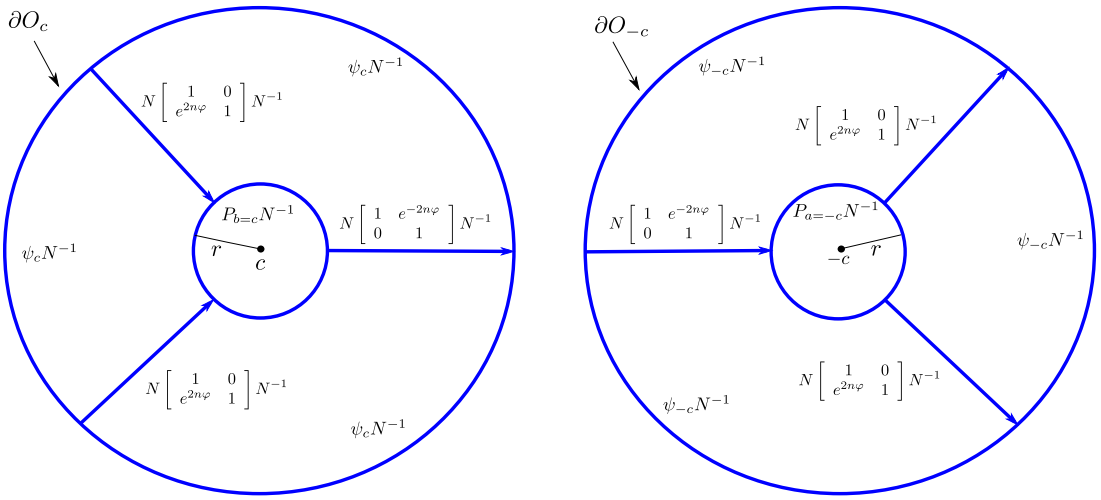

Figure 10.4.6: The separate RHPs for Ψ_c and Ψ_{-c}. The contours give a representation for Ω_n^c and Ω_n^{-c}. All circles have counter-clockwise orientation with $r \sim n^{-2/3}$. (a) The jump contours and jump matrices for Φ_c. (b) The jump contours and jump matrices for Φ_{-c}.

implies

$$N^{-1}G_\epsilon G^{-1}N = I + B_1(\epsilon),$$
$$G_\epsilon J_c^{-1} = I + NB_1(\epsilon)N^{-1}.$$

The analysis in [24, p. 227] implies on ∂O_c

$$J_c^{-1} = I + A_1(n^{-1}),$$

Since $G_1 = I$ on ∂O_c we obtain (10.4.6). To prove the remainder of the lemma, we use unscaled jumps

$$\hat{H}_1(z) = \bar{H}_1(n^{2/3}(z-c)),$$
$$\hat{J}_c(z) = \begin{cases} \bar{N}_{b=c,n}J_c(z)\bar{N}_{b=c,n}^{-1} & \text{if } |z-c| > r, \\ J_c(z)\bar{N}_{b=c,n}^{-1} & \text{if } |z-c| = r. \end{cases}$$

From (10.4.6) we have

$$\|\hat{H}_1\hat{J}_c^{-1} - I\|_{L^2\cap L^\infty(\Omega_n^c)} = \mathcal{O}(n^{-1}) + \mathcal{O}(\epsilon).$$

It follows that $\|\hat{J}_c\|_{L^\infty(\Omega_n^c)}$ is uniformly bounded in n so that

$$\|\hat{H}_1 - \hat{J}_c\|_{L^2\cap L^\infty(\Omega_n^c)} = \mathcal{O}(n^{-1}) + \mathcal{O}(\epsilon).$$

This implies that $\|\mathcal{C}[\hat{H}_1;\Omega_n^c] - \mathcal{C}[\hat{J}_c;\Omega_n^c]\|_{\mathcal{L}(L^2(\Omega_0))} = \mathcal{O}(n^{-1}) + \mathcal{O}(\epsilon)$ since $\|\mathcal{C}_{\Omega_n^c}^-\|_{\mathcal{L}(L^2(\Omega_n^c))}$ is uniformly bounded in n. Therefore it suffices to show that $\|\mathcal{C}[\hat{J}_c;\Omega_n^c]^{-1}\|_{\mathcal{L}(L^2(\Omega_n^c))}$ is

uniformly bounded in n. This is clear since the inverse operator can be written in terms of

$$\hat{\Psi}_c(z) = \begin{cases} \bar{N}_{a=c,n}\Psi_c\bar{N}^{-1}_{a=c,n}(z) & \text{if } z > r, \\ \bar{N}_{a=c,n}\Psi_c & \text{if } z < r. \end{cases} \tag{10.4.7}$$

and $\mathcal{C}^-_{\Omega_n^c}$ as was shown in Lemma 3.8.18. Both of these are uniformly bounded in n on Ω_n^c. It remains to rescale the contours. We use a simple affine scaling and this leaves the Cauchy operators invariant: it does not affect the norm. In other words:

$$\|\mathcal{C}[\bar{H}_1;\Omega_0]^{-1}\|_{\mathcal{L}(L^2(\Omega_0))} = C \Leftrightarrow \|\mathcal{C}[\hat{H}_1; c + n^{-2/3}\Omega_0]^{-1}\|_{\mathcal{L}(L^2(c+n^{-2/3}\Omega_0))} = C.$$

The final step is to notice that $\mathcal{C}[\hat{H}_1;\Omega_n^c]^{-1}$ is the identity operator on $\Omega_n^c \setminus n^{2/3}(\Omega_0 - c)$. □

We now bound the inverse operator on the second solved RHP.

Lemma 10.4.2. *There exists a constant $C > 0$ and functions A_2, B_2 such that*

$$\begin{aligned} &\tilde{G}_2 J_{-c}^{-1} = I + N[A_2(n^{-1}) + B_2(\epsilon)]N^{-1}, \quad \textit{for} \quad |z+c| > r, \\ &\tilde{G}_2 J_{-c}^{-1} = I + [A_2(n^{-1}) + B_2(\epsilon)]N^{-1}, \quad \textit{for} \quad |z+c| = r, \quad \textit{and,} \\ &\|\mathcal{C}[\bar{H}_2;\Omega_0]^{-1}\|_{\mathcal{L}(L^2(\Omega_0))} < C, \end{aligned} \tag{10.4.8}$$

where $\|A_2(n)\|_{L^2\cap L^\infty} = \mathcal{O}(n)$ and $\|B_2(\epsilon)\|_{L^2\cap L^\infty} = \mathcal{O}(\epsilon)$.

Proof. First, for Φ_1 we have the representation

$$\Phi_1(z) = I + \bar{N}^{-1}_{b=c,n}\left(\mathcal{C}_{\Omega_n^1}U(z)\right)\bar{N}_{b=c,n}, \quad U(z) = u(n^{2/3}(z-c)), \quad u = \mathcal{C}[\bar{H}_1;\Omega_0]^{-1}(\bar{H}_1 - I).$$

Lemma 10.4.1 implies that u has uniformly bounded L^2 norm on Ω_0 so that a change of variables shows $\|U\|_{L^2(\Omega_n^1)} = \mathcal{O}(n^{-1/3})$. In addition, $\|1/(\cdot - z)^k\|_{L^2(\Omega_n^1)} = \mathcal{O}(n^{-1/3})$ for z bounded away from Ω_n^1. Therefore $|\mathcal{C}_{\Omega_n^1}U(z)| = \mathcal{O}(n^{-2/3})$. This estimate can be improved. Define

$$\tilde{U} = \mathcal{C}[J_c, \Omega_n^c]^{-1}(J_c - I).$$

It can be shown that $\|U - \tilde{U}\|_{L^2(\Omega_n^c)} = \mathcal{O}(\epsilon)\cdot\mathcal{O}(n^{-1/3}) + \mathcal{O}(n^{-4/3})$ where we use the convention that $U = 0$ on $\Omega_n^c \setminus \Omega_n^1$. Furthermore, $\mathcal{C}_{\Omega_n^c}\tilde{U} = 0$ on the compliment of $\overline{O}_c$ so that

$$\mathcal{C}_{\Omega_n^1}U = \mathcal{C}_{\Omega_n^1}U - \mathcal{C}_{\Omega_n^c}\tilde{U} \quad \text{on } \Omega_n^{-c}.$$

We find that $\|\mathcal{C}_{\Omega_n^1}U\|_{L^2\cap L^\infty(\Omega_n^{-c})} = \mathcal{O}(\epsilon)\cdot\mathcal{O}(n^{-2/3}) + \mathcal{O}(n^{-5/3})$. We write

$$\Phi_1 = I + N(z)N^{-1}(z)\bar{N}^{-1}_{b=c,n}\left(\mathcal{C}_{\Omega_n^1}U(z)\right)\bar{N}_{b=c,n}N^{-1}(z),$$

and using that $N^{-1}(z)\bar{N}^{-1}_{b=c,n} = \mathcal{O}(n^{1/3})$ for $z \in \Omega_n^{-c}$ we find

$$\begin{aligned} \Phi_1 &= I + N[A_3(n^{-1}) + B_3(\epsilon)]N^{-1}, \\ \Phi_1^{-1} &= I + N[A_4(n^{-1}) + B_4(\epsilon)]N^{-1}. \end{aligned}$$

where A_3, A_4 satisfy the property stated above for A_2 and B_3, B_4 satisfy the property stated for B_2. Expand

$$\begin{aligned}\tilde{G}_2 J_{-c}^{-1} = G_2 J_{-c}^{-1} &+ G_2 N[A_3(n) + B_3(\epsilon)]N^{-1} J_{-c}^{-1} \\ &+ N[A_2(n^{-1}) + B_2(\epsilon)]N^{-1} G_2 J_{-c}^{-1} \\ &+ N[A_2(n^{-1}) + B_2(\epsilon)]N^{-1} G_2 N[A_3(n) + B_3(\epsilon)]N^{-1} J_{-c}^{-1}.\end{aligned}$$

Note that $N^{-1}G_2N$ and $N^{-1}J_{-c}^{-1}N$ are uniformly bounded on Ω_{-c}^n and $G_2J_{-c}^{-1}$ satisfies an estimate analogous to that of $G_1J_c^{-1}$ in Lemma 10.4.1. We write

$$\begin{aligned}\tilde{G}_2 J_{-c}^{-1} = I &+ N[A_1(n^{-1}) + B_1(\epsilon)]N^{-1} \\ &+ NN^{-1} G_2 N[A_3(n^{-1}) + B_3(\epsilon)]N^{-1} J_{-c}^{-1} N N^{-1} \\ &+ N[A_2(n^{-1}) + B_2(\epsilon)]N^{-1} G_2 J_{-c}^{-1} N N^{-1} \\ &+ N[A_2(n^{-1}) + B_2(\epsilon)]N^{-1} G_2 N[A_3(n^{-1}) + B_3(\epsilon)]N^{-1} J_{-c}^{-1} N N^{-1}.\end{aligned}$$

This proves (10.4.8). The proof of the second statement proceeds in precisely the same way as in Lemma 10.4.1. This proves the lemma.

□

We can now bound the jump matrices.

Lemma 10.4.3. *There exists constants $C_k > 0$, independent of n, such that for sufficiently large n we have*

$$\|\bar{H}_i\|_{W^{k,\infty} \cap H^k(\Omega_0)} < C_k, \quad i = 1, 2.$$

Proof. We consider $i = 1$ first. The only terms that may cause growth in the derivatives are

$$\kappa(z) = e^{-2n\varphi(c+n^{-2/3}z)} \quad \text{and} \quad N(c + n^{-2/3}z)\bar{N}_{b=c,n}.$$

From the analysis of [24, p. 197] it follows that $\varphi(z) = d_0(z-c)^{3/2} + d_1(z-c)^{5/2} + \mathcal{O}\left((z-c)^{7/2}\right)$. This asymptotic series can be differentiated as $\sqrt{z-c}\varphi(z)$ is analytic. Therefore,

$$\kappa(z) = \exp\left(-2d_0 z^{3/2} - 2d_0 n^{-2/3} z^{5/3} + \cdots\right).$$

and hence differentiating $\kappa(z)$ or $1/\kappa(z)$ with respect to z never causes growth in n. A similar argument applies to $N(c + n^{-2/3}z)\bar{N}_{b=c,n}$. From the expansion of $N(c + n^{-2/3}z)$ we have a series of the form

$$N(c + n^{-2/3}z)\bar{N}_{b=c,n} = f_0(z) + \sum_{j=1}^{\infty} M_{-(2j-1)/3}(n) f_j(z),$$

where $M_{-(2j+1)/3}(n) = \mathcal{O}(n^{-(2j+1)/3})$. Again, differentiation of $N(c+n^{-2/3}z)$ with respect to z never causes growth in n. This proves the claim for $i = 1$. For $i = 2$, we must bound

derivatives of $\Phi_1(-c+n^{-2/3}z)$ and $\tilde{H}_2(z)$. The boundedness of the derivatives of $\tilde{H}_2(z)$ follows from the arguments for $i=1$. Recall, for Φ_1 we have the representation

$$\Phi_1(z) = I + \bar{N}_{b=c,n}^{-1}\left(\mathcal{C}_{\Omega_n^1}U(z)\right)\bar{N}_{b=c,n},$$
$$U(z) = u(n^{2/3}(z-c)), \quad u(z) = \mathcal{C}[\bar{H}_1;\Omega_0]^{-1}(\bar{H}_1 - I).$$

Since u has uniformly bounded L^2 norm on Ω_0, $\|U\|_{L^2(\Omega_n^1)} = \mathcal{O}(n^{-1/3})$. From the fact that $\bar{N}_{b=c,n} = \mathcal{O}(n^{1/6})$ and $N_{b=c,n}^{-1} = \mathcal{O}(n^{1/6})$ we have that $\partial_z^k(\bar{N}_{b=c,n}^{-1}\left(\mathcal{C}_{\Omega_n^1}U(z)\right)\bar{N}_{b=c,n}) = \mathcal{O}(n^{-1/3})$ on Ω_n^2 where we used that $\|1/(\cdot - z)^k\|_{L^2(\Omega_n^1)} = \mathcal{O}(n^{-1/3})$ for z bounded away from Ω_n^1. This proves the lemma for $i=2$. □

In practice, we approximate Φ_1 and we never solve the exact RHP $[\bar{H}_2;\Omega_0]$. Recall that this approximation is found by first numerically approximating the solution $\bar{\Phi}_1$ of $[\bar{H}_1;\Omega_0]$ by $\bar{\Phi}_{1,m}$ (with m collocation points on each smooth component of Ω_0). Theorem 5.2.4 shows that the approximation $\bar{\Phi}_{1,m}$ converges uniformly in n with z away from Ω_0 as $m\to\infty$, subject to Assumption 5.3.11. The size of the difference $\bar{\Phi}_{1,m} - \bar{\Phi}_1$ can be traced back to an L^2 error on Ω_0. In other words,

$$\bar{\Phi}_{1,m}(z) = I + \mathcal{C}_{\Omega_0}u_m(z) \quad \text{and} \quad \bar{\Phi}_1(z) = I + \mathcal{C}_{\Omega_0}u(z),$$

where $\|u-u_m\|_{L^2(\Omega_0)} \to 0$ is satisfied as $m\to\infty$. It follows from the Cauchy–Schwarz Inequality that

$$|\bar{\Phi}_{1,m}(n^{2/3}(z-c)) - \bar{\Phi}_1(n^{2/3}(z-c))| < \|1/(\cdot - n^{2/3}(z-c))\|_{L^2(\Omega_0)}\|u-u_m\|_{L^2(\Omega_0)}n^{-2/3}.$$

Therefore from $\bar{N}_{b=c,n} = \mathcal{O}(n^{1/6})$ and $N_{b=c,n}^{-1} = \mathcal{O}(n^{1/6})$, we bound

$$\|\Phi_{1,m} - \Phi_1\|_{L^\infty(\Omega_n^2)} \le C\|u-u_m\|_{L^2(\Omega_0)}n^{-1/3}.$$

Similar arguments show that

$$\|\Phi_{1,m}^{-1} - \Phi_1^{-1}\|_{L^\infty(\Omega_n^2)} \le C\|u-u_m\|_{L^2(\Omega_0)}n^{-1/3} + \mathcal{O}(n^{-2/3}).$$

Define $\bar{H}_{2,m}$ to be $\bar{H}_2$ with Φ_1 replaced by $\Phi_{1,m}$. The final lemma we need for the fundamental result of this section follows.

Lemma 10.4.4.

$$\|\bar{H}_{2,m} - \bar{H}_2\|_{L^2\cap L^\infty(\Omega_0)} \to 0 \text{ as } m\to\infty,$$

uniformly in n.

Proof. The case $|z+c| > r$ is treated first. We use the unscaled jump matrices to show

L^∞ convergence. Consider

$$\begin{aligned}
&\bar{H}_{2,m}(n^{2/3}(z+c)) - \bar{H}_2(n^{2/3}(z+c)) \\
&= \bar{N}_{a=-c,n}\Phi_1(z)G_2(z)\Phi_1^{-1}(z)\bar{N}^{-1}_{a=-c,n} - \bar{N}_{a=-c,n}\Phi_{1,m}(z)G_2(z)\Phi^{-1}_{1,m}(z)\bar{N}^{-1}_{a=-c,n} \\
&= \bar{N}_{a=-c,n}(\Phi_1(z)-\Phi_{1,m}(z))\bar{N}^{-1}_{a=-c,n}\bar{N}_{a=-c,n}G_2(z)\bar{N}^{-1}_{a=-c,n}\bar{N}_{a=-c,n}\Phi_1^{-1}(z)\bar{N}^{-1}_{a=-c,n} \\
&+ \bar{N}_{a=-c,n}\Phi_{1,m}(z)\bar{N}^{-1}_{a=-c,n}\bar{N}_{a=-c,n}G_2(z)\bar{N}^{-1}_{a=-c,n}\bar{N}_{a=-c,n}(\Phi_1^{-1}(z)-\Phi^{-1}_{1,m})\bar{N}^{-1}_{a=-c,n}
\end{aligned}$$

We have seen that

$$\begin{aligned}
\bar{N}_{a=-c,n}\Phi_{1,m}(z)\bar{N}^{-1}_{a=-c,n} &= \mathcal{O}(1), \\
\bar{N}_{a=-c,n}\Phi_{1}(z)\bar{N}^{-1}_{a=-c,n} &= \mathcal{O}(1), \\
N_{a=-c,n}G_2(z)\bar{N}^{-1}_{a=-c,n} &= \mathcal{O}(1),
\end{aligned}$$

and finally,

$$\begin{aligned}
&\|\bar{N}_{a=-c,n}(\Phi_1-\Phi_{1,m})\bar{N}^{-1}_{a=-c,n}\|_{L^\infty(\Omega_n^2)} \le C\|u-u_m\|_{L^2(\Omega_0)}, \\
&\|\bar{N}_{a=-c,n}(\Phi_1^{-1}-\Phi^{-1}_{1,m})\bar{N}^{-1}_{a=-c,n}\|_{L^\infty(\Omega_n^2)} \le C\|u-u_m\|_{L^2(\Omega_0)} + \mathcal{O}(n^{-1/3})\cdot\mathcal{O}(\|u-u_m\|^2_{L^2(\Omega_0)}).
\end{aligned}$$

for a new constant C. This demonstrates that $\|\bar{H}_{2,m}-\bar{H}_2\|_{L^2\cap L^\infty(\Omega_0)} \to 0$ uniformly in n since Ω_0 is bounded. The case of $|z+c|<r$ follows from this analysis since fewer $\bar{N}_{a=-c,n}$ terms are present in that case. □

As before, let $u = \mathcal{C}[\bar{H}_1;\Omega_1]^{-1}(\bar{H}_1 - I)$ with u_m being its numerical approximation. Define $v = \mathcal{C}[\bar{H}_2;\Omega_2]^{-1}(\bar{H}_2 - I)$ and $v^m = \mathcal{C}[\bar{H}_{2,m};\Omega_2]^{-1}(\bar{H}_{2,m} - I)$. Let v_m denote the numerical approximation of v^m and define

$$\Phi_{2,m} = \bar{N}^{-1}_{a=-c,n}(I + \mathcal{C}_{\Omega_0}v_m(n^{2/3}(z+c))N_{a=-c,n},$$

which is an approximation of Φ_2.

We are ready to prove the main extension of the uniform approximation theory of Chapter 5.

Theorem 10.4.5. *The following limits hold, uniformly with respect to n:*

$$\begin{aligned}
\|u-u_m\|_{L^2(\Omega_0)} &\to 0 \quad as \quad m\to\infty, \\
\|v-v_m\|_{L^2(\Omega_0)} &\to 0 \quad as \quad m\to\infty.
\end{aligned}$$

Furthermore,

$$\lim_{m\to\infty}\sup_{z\in S}|\Phi(z) - \Phi_{1,m}(z)\Phi_{2,m}(z)| = \mathcal{O}(\epsilon)$$

for S bounded away from Γ_n. Here ϵ is the error associated with contour truncation, see (10.4.4).

Proof. The first limit was proved above. Lemma 10.4.4 implies $\|v^m - v\|_{L^2(\Omega_0)} \to 0$ uniformly in n. The triangle inequality produces the second limit. Finally, the Cauchy–

Schwarz Inequality applied to the Cauchy integral implies

$$\lim_{m\to\infty} \sup_{z\in S} |\Phi(z) - \Phi_{1,m}(z)\Phi_{2,m}(z)| = 0,$$

uniformly in n. Combining this with (10.4.4) proves the theorem. □

Remark 10.4.6. *We obtain convergence that is more rapid than Theorem 5.1.14 predicts. Since $\Phi_1 - I$ decays rapidly enough with respect to n we avoid the complications that arise from the use of Lemma 5.1.12 in the general case.*

Appendix A

Rational Approximation

We discuss the rational approximation of functions in appropriate L^p-based spaces. The results in this section are proved for $1 < p < \infty$ and we assume $1 < p < \infty$ throughout. It is instructive to see the generality of the methods of proof. We have defined the spaces $H^k_\pm(\Gamma)$ and $H^k_z(\Gamma)$. The spaces $W^{k,p}_\pm(\Gamma)$ and $W^{k,p}_z(\Gamma)$ are defined in an analogous way, with the L^p norm. Note that these spaces coincide when Γ is a piecewise-smooth Lipschitz graph.

Theorem A.0.7 ([47]). *If D is a bounded region such that ∂D is a piecewise differentiable, rectifiable Jordan curve then polynomials in z are dense in $\mathcal{E}^p(D)$.*

We show that for $f \in W^{k,p}_z(\partial D)$ we can approximate it with a rational functions. First, for $f \in W^{k,p}_z(\partial D) \cap \mathcal{E}^p(D)$ we approximate $D^k f$ by polynomials p_n. We have

$$\left| \int_a^s (D^k f(t) - p_n(t))|dt| \right|^p \leq \|D^k f(t) - p_n(t)\|^p_{L^p(\partial D)} \cdot |\partial D|^{p/q}, \quad 1/p + 1/q = 1,$$

where $|\partial D|$ is the arclength of ∂D. Integrating both sides over Γ with respect to $|ds|$ produces

$$\left\| \int_a^{\cdot} (D^k f(t) - p_n(t))|dt| \right\|_{L^p(\partial D)} \leq \|D^k f(t) - p_n(t)\|_{L^p(\partial D)} \cdot |\partial D|.$$

Since $\int_a^s D^k f(t)dt = D^{k-1} f + c$ for some c and $\int_a^s p_n(t)dt - c$ is a polynomial that converges to $D^{k-1} f$ in $L^2(\partial D)$. This argument can be used again to construct an polynomial that converges to $D^{k-2} f$ in $L^2(\partial D)$.

Since $f = \mathcal{C}^+_{\partial D} f - \mathcal{C}^-_{\partial D} f$ we see that we may approximate $\mathcal{C}^+_{\partial D} f$ with polynomials. We must deal with the approximation of $\mathcal{C}^-_{\partial D} f$. We bootstrap from Theorem A.0.7. Without loss of generality, assume $0 \in D$. Note that $F(z) = \mathcal{C}^-_{\partial D} f(z) \in \mathcal{E}^P(D^{-1})$ where $D^{-1} = \{z : 1/z \in D\}$. If $f \in W^{k,p}_z$ then the kth derivative $G(z) = F^{(k)}(1/z) \in \mathcal{E}^p(D^{-1})$ may be approximated in $L^p(\partial D^{-1})$ by polynomials $p_n(z)$. It follows that G must have a $(k+1)$th-order zero at $z = 0$. Thus

$$\left| \int_{\partial D^{-1}} \frac{p_n(s)}{s^j} \bar{d}s \right| \leq \left| \int_{\partial D^{-1}} \frac{p_n(s) - G(s)}{s^j} \bar{d}s \right| \leq C_j \|G - p_n\|_{L^p(\partial D^{-1})}, \quad j = 1, 2, \ldots, k+1.$$

Thus the first $(k+1)$ coefficients in p_n have magnitudes that are on the order of $\|G - p_n\|_{L^p(\partial D^{-1})}$. Define $\tilde{p}_n$ to be the polynomial obtained by dropping these terms. Since ∂D^{-1} has finite arc length we find that $\|\tilde{p}_n - p_n\|_{L^p(\partial D^{-1})} \leq C\|G - p_n\|_{L^p(\partial D^{-1})}$ for some $C > 0$, depending only on D and k. Therefore $\tilde{p}_n$ converges to G in $L^p(\partial D^{-1})$. A simple change of variables shows that $\tilde{p}_n(1/z)$ converges to F in $L^p(\partial D)$. Integrating $\tilde{p}_n(1/z)$ k-times in the same way as for $\mathcal{C}^+_{\partial D} f$ we obtain a rational approximation of $\mathcal{C}^-_{\partial D} f$ in $W^{k,p}_z$. We conclude the following:

Theorem A.0.8. *If D is a bounded region such that ∂D is a piecewise differentiable Jordan curve then, rational functions of z are dense in $W^{k,p}_z(\partial D) = W^{k,p}_+(\partial D)$.*

We turn to the density of rational functions in $W^{k,p}_z(\Gamma)$ when Γ is a piecewise smooth Lipschitz graph. It will be clear that the piecewise smooth assumption can be removed in the $k = 0$ or $L^p(\Gamma)$ case. We follow the ideas presented in [8] and complete their proof. We begin with some technical developments. Define the maximal function

$$M(f)(t) = \sup_{1 \geq \delta > 0} \frac{1}{|\Gamma \cap B(t,\delta)|} \int_{\Gamma \cap B(t,\delta)} |f(s)||ds|.$$

Lemma A.0.9 ([102])**.** *For $f \in L^p(\Gamma)$*

$$\|M(f)\|_{L^p(\Gamma)} \leq c_p \|f\|_{L^p(\Gamma)}.$$

Lemma A.0.10. *Let $P_\epsilon(s,t) = P_\epsilon(t,s) : \Gamma \times \Gamma \to \mathbb{C}$ satisfy*

1. $$1 - \int_\Gamma P_\epsilon(s,\cdot)ds \to 0 \text{ as } \epsilon \to 0^+,$$

2. $$\int_\Gamma |P_\epsilon(s,t)||ds| \leq C, \text{ uniformly in } t, \text{and}$$

3. *For $\delta > 0$,*
$$\left\| \int_\Gamma |w_\delta(s,\cdot)||P_\epsilon(s,\cdot)||ds| \right\|_\infty \to 0,$$
$$w_\delta(s,t) = \begin{cases} 0, & \text{if } |t-s| < \delta, \\ 1, & \text{otherwise.} \end{cases}$$

If Γ is a piecewise-differentiable Lipschitz graph, then for $f \in W^{1,p}_+(\Gamma)$,

$$\int_\Gamma f(t) P_\epsilon(t,s)dt \to f(s)$$

in $L^p(\Gamma)$.

Proof. Consider

$$\int_\Gamma P_\epsilon(s,t)[f(t)-f(s)]dt = \int_\Gamma P_\epsilon(s,t)w_\delta(s,t)f(t)dt - \int_\Gamma P_\epsilon(s,t)w_\delta(s,t)f(s)dt + \int_\Gamma (1-w_\delta(s,t))P_\epsilon(s,t)(f(t)-f(s))dt.$$

We show this function tends to zero in $L^p(\Gamma)$. Define $\Delta(t) = \{s \in \Gamma : |s-t| < \delta\}$ and consider

$$I_1 = \int_\Gamma \left| \int_{\Delta(t)} P_\epsilon(s,t)f(t)dt \right|^p |ds| = \int_\Gamma \left| \int_\Gamma (w_\delta(s,t))P_\epsilon(s,t)f(t)dt \right|^p |ds|.$$

It follows that [53, Theorem 6.18]

$$I_1^{1/p} \le K\|f\|_p, \quad K = \sup_{t\in\Gamma} \int_\Gamma |w_\delta(s,t)||P_\epsilon(s,t)||ds| \to 0$$

as $\epsilon \to 0$ for any $\delta > 0$ by Hypothesis 3. Now consider

$$I_2 = \int_\Gamma \left| \int_{\Delta(t)} P_\epsilon(s,t)f(s)dt \right|^p |ds| = \int_\Gamma |f(s)|^p \left| \int_\Gamma w_\delta(s,t))P_\epsilon(s,t)dt \right|^p |ds|.$$

Again, we obtain $I_2^{1/p} \le K\|f\|_{L^p(\Gamma)}$. We are left estimating the $L^p(\Gamma)$ norm of

$$I_3(s) = \int_\Gamma (1-w_\delta(s,t))P_\epsilon(s,t)(f(t)-f(s))dt.$$

A simple estimate gives

$$\begin{aligned}\left| \int_\Gamma (1-w_\delta(s,t))P_\epsilon(s,t)(f(t)-f(s))dt \right| &\le \sup_{s\in\Gamma} |(1-w_\delta(s,t))(f(t)-f(s))| \left| \int_\Gamma P_\epsilon(s,t)dt \right|, \\ &\le C \sup_{s\in\Delta(t)} |f(t)-f(s)|.\end{aligned}$$

We estimate

$$\begin{aligned}\sup_{s\in\Delta(t)} |f(t)-f(s)| &\le \frac{|\Gamma\cap B(t,\delta)|}{|\Gamma\cap B(t,\delta)|} \int_{\Gamma\cap B(t,\delta)} |Df(x)||dx| \\ &\le |\Gamma\cap B(t,\delta)| M(Df).\end{aligned}$$

From the Lipschitz nature of Γ, $|\Gamma\cap B(t,\delta)| \le C\delta$ thus

$$\|I_3\|_p \le C\delta\|M(Df)\|_p \le c_p C\delta\|Df\|_p,$$

by Lemma A.0.9. We use all these facts to find

$$I = \left\| \int_\Gamma P_\epsilon(s,t) f(t) dt - f(s) \right\|_p \leq \left\| \int_\Gamma P_\epsilon(s,t)[f(t) - f(s)] dt \right\|_p + \left\| f(s) - f(s) \int_\Gamma P_\epsilon(s,t) dt \right\|_p .$$

The second term tends to zero as $\epsilon \to 0$ by Hypothesis 1, 2, and the Dominated Convergence Theorem. Fix $\delta > 0$. We find

$$I \leq c_p C \delta \|Df\|_p + H(\epsilon, \delta), \quad H(\epsilon, \delta) \to 0 \text{ as } \epsilon \to 0.$$

Letting $\epsilon \to 0$ followed by $\delta \to 0$ proves the lemma. □

Remark A.0.11. *Similar arguments show that if $f \in W^{1,\infty}$ then convergence in Lemma A.0.10 takes place in $L^\infty(\Gamma)$.*

Lemma A.0.12. *If Γ is a piecewise smooth Lipschitz graph then $W^{1,p}_z(\Gamma)$ is dense in $L^p(\Gamma)$.*

Proof. Let $\epsilon > 0$. On each smooth component of $\Gamma_i \subset \Gamma$ we approximate f with a smooth function f^j_n so that $\int_{\Gamma_j} |f(z) - f^j_n(z)|^p |dz| \to 0$ as $n \to \infty$. We multiply f^j_n by C^∞ functions ϕ_j that take values in $[0,1]$ and vanish in a neighborhood of each non-smooth point of Γ to enforce the zero-sum condition. The functions ϕ_j are not equal to one only on a set E_j of small measure $\delta/2^j$. We find

$$\|f - \phi_j f^j_n\|_{L^p(\Gamma_j)} \leq \|f - f^j_n\|_{L^p(\Gamma_j)} + \|f^j_n - \phi_j f^j_n\|_{L^p(\Gamma_j)}.$$

We estimate the last term

$$\|f^j_n - \phi_j f^j_n\|^p_{L^p(\Gamma_j)} = \int_{E_j} |f^j_n(z) - \phi_j f^j_n(z)|^p |dz| \leq \int_{E_j} |f^j_n(z)|^p |dz|.$$

Therefore,

$$\lim_{n\to\infty} \|f - \phi_j f^j_n\|^p_{L^p(\Gamma_j)} \leq \int_{E_j} |f(z)|^p |dz|.$$

Define $f_n = \phi_j f^j_n$ on Γ_j and

$$\lim_{n\to\infty} \|f - f_n\|^p_{L^p(\Gamma)} \leq \int_{\cup_j E_j} |f(z)|^p |dz|.$$

Since $\int_{\cup_j E_j} |dz| \to 0$ as $\delta \to 0$, density is proved. □

Theorem A.0.13. *Let Γ be a piecewise differentiable Lipschitz graph. Then*

$$K_\epsilon f(s) = \int_\Gamma f(t) \frac{\epsilon}{\pi} \frac{dt}{(t-s)^2 + \epsilon^2}, \quad \epsilon > 0,$$

converges to f in $L^p(\Gamma)$ as $\epsilon \to 0$ provided $f \in L^p(\Gamma)$.

Proof. First, we show this for $f \in W^{1,p}(\Gamma)$. We must check the three hypotheses in Lemma A.0.10. First note that

$$P_\epsilon(x + i\nu(x), y + i\nu(y)) = \frac{\epsilon}{\pi} \frac{1}{(t-s)^2 + \epsilon^2} = \frac{1}{2\pi i} \left(\frac{1}{t - (s + i\epsilon)} - \frac{1}{t - (s - i\epsilon)} \right).$$

Hypothesis 1 follows by a straightforward residue calculation. As will be seen below, Hypotheses 2 and 3 follow in a straightforward way when $\Gamma = \mathbb{R}$. It suffices to show that

$$|P_\epsilon(x + i\nu(x), y + i\nu(y))||1 + i\nu'(x)| \leq C|P_\epsilon(x, y)|, \ x, y \in \mathbb{R}. \tag{A.0.1}$$

Recall $\Gamma = \{x + i\nu(x) : x \in \mathbb{R}\}$. The sufficiency is clear for Hypothesis 2 after a change of variables. For Hypothesis 3, consider

$$I = \int_\Gamma |w(s,t)||P_\epsilon(s,t)||ds| = \int_{\Gamma \setminus \Delta(t)} |P_\epsilon(s,t)||ds|.$$

The set $\Gamma \cap \Delta(t)$ contains the set $\Delta'(t) = \{x + i\nu(x) : x \in (t_1 + t, t_2 + t)\}$ where $t_1 + t + i\nu(t_1 + t), t_2 + t + i\nu(t_2 + t)$ are the two points on $\Gamma \setminus \Delta(t)$ closest to t with respect to arc length. Thus

$$\begin{aligned} I &\leq \int_{\Gamma \setminus \Delta'(t)} |P_\epsilon(s,t)||ds| = \int_{\mathbb{R} \setminus (t_1 + t, t_2 + t)} |P_\epsilon(x + i\nu(x), y + i\nu(y))||1 + i\nu'(x)|dx \\ &\leq \int_{\mathbb{R} \setminus (t - t^*, t + t^*)} |P_\epsilon(x + i\nu(x), y + i\nu(y))||1 + i\nu'(x)|dx \leq C \int_{\mathbb{R}} |P_\epsilon(x,y)|dx, \end{aligned}$$

where $t^* = \min\{-t_1, t_2\}$. Thus if Hypothesis 3 holds for $P_\epsilon(x,y)$ if $\Gamma = \mathbb{R}$ then the right-hand side tends to zero uniformly.

Now we prove Hypothesis 2 and 3 for $P_\epsilon(x,y)$ if $\Gamma = \mathbb{R}$. Since $P_\epsilon(x,y)$ is positive on for $x, y \in \mathbb{R}$, the L^1 norm can be found to be unity by contour integration. For Hypothesis 3 note that Cauchy's Theorem implies

$$\int_{\mathbb{R} \setminus (t - \delta, t + \delta)} P_\epsilon(x,y)dx + \int_{C_\delta} P_\epsilon(x,y)dx = 0,$$

where C_δ is a half-circle in the upper-half plane connecting $t - \delta$ and $t + \delta$. We find that

$$I_2 = \int_{C_\delta} P_\epsilon(x,y)dx = \frac{\epsilon}{\pi} \int_{-\pi}^{\pi} \frac{i\delta e^{i\theta} d\theta}{\delta^2 e^{2i\theta} + \epsilon^2}.$$

We estimate, for $\epsilon < \delta$, $\delta > 0$,

$$|I_2| \leq \frac{\epsilon}{\pi} \int_{-\pi}^{\pi} \frac{\delta d\theta}{\delta^2 - \epsilon^2} \to 0 \text{ as } \epsilon \to 0.$$

This establishes Hypothesis 3 in this case.

Finally, we establish (A.0.1). We consider the ratio

$$r = \frac{\epsilon^2 + (x-y)^2}{\epsilon^2 + (x-y)^2 - (\nu(x)-\nu(y))^2 + 2i(x-y)(\nu(x)-\nu(y))}.$$

We rewrite r in terms of $X = \epsilon^2/(x-y)^2$ and $Y = |(\nu(x)-\nu(y))/(x-y)|$. Note that $0 \le Y \le M$ for a constant $M > 0$ and $0 \le X \le \infty$. Thus, we are lead to

$$R(X,Y) = |r|^2 = \frac{(X+1)^2}{(X+1-Y^2)^2 + 4Y^2}, \quad (X,Y) \in [0,\infty] \times [0,M].$$

For $X + 1 > 2M^2$ we find

$$R(X,Y) \le \frac{4M^4}{M^4} \le 4.$$

Since $R(X,Y)$ is continuous in $[0, 2M^2] \times [0, M]$, and bounded on $[2M^2, \infty] \times [0, M]$ we obtain (A.0.1), establishing L^p convergence when $f \in W^{1,p}_+(\Gamma)$.

To prove the theorem we use the density of $W^{1,p}_+(\Gamma)$ in $L^p(\Gamma)$ and the fact that K_ϵ is a bounded operator on $L^p(\Gamma)$, $1 < p < \infty$, with norm that is independent of ϵ [76]. We have proved this fact in the case $p = 2$, see Lemma 3.5.12. Approximating f with a sequence $f_n \in W^{1,p}_+(\Gamma)$, we obtain

$$\begin{aligned} \|f - K_\epsilon f\|_p &\le \|f - f_n\|_p + \|f_n - K_\epsilon f_n\|_p + \|K_\epsilon(f - f_n)\|_p \\ &\le (1 + C)\|f - f_n\|_p + \|f_n - K_\epsilon f_n\|_p \end{aligned} \tag{A.0.2}$$

For $\delta > 0$ find N so that for $n > N$, $(1 + C)\|f - f_n\|_p < \delta$. For such an n let $\epsilon \to 0$ in (A.0.2)

$$\lim_{\epsilon \to 0} \|f - K_\epsilon f\|_p < \delta, \quad n > N.$$

This proves the lemma. □

Corollary A.0.14. *Define the integral operator*

$$K^j_\epsilon f(s) = \int_\Gamma f(t) \left(\frac{(-1)^j}{[t - (s + i\epsilon)]^{j+1}} - \frac{(-1)^j}{[t - (s - i\epsilon)]^{j+1}} \right) \bar{dt}$$

whose kernel is the kth derivative of the Poisson kernel. If Γ *is a piecewise smooth Lipschitz graph and* $f \in W^{k,p}_+(\Gamma)$ *then* $\|K^k_\epsilon f - D^k f\|_p \to 0$ *as* $\epsilon \to 0$.

Proof. Integration by parts and the zero-sum condition imply that $K^k_\epsilon f = K_\epsilon D^k f$. The conclusion follows from Theorem A.0.13. □

Theorem A.0.15. *If* Γ *is a piecewise smooth Lipschitz graph then* $L^p(\Gamma)$ *rational functions are dense in* $W^{k,p}_z(\Gamma)$.

Proof. Our proof is constructive. We assume $k \ge 1$. For $f \in W^{k,p}_z$ we approximate $K^k_\epsilon f$ with a Riemann sum. This is clearly a rational approximation of $D^k f$, for ϵ small. First, we

show this Riemann sum approximation converges to $K_\epsilon^k f$ in $L^p(\Gamma)$. Define $\Gamma_R = \Gamma \cap B(0,R)$ where R is undetermined for now. It suffices to show the convergence of the Riemann sums on each smooth component of Γ_R, so we assume Γ_R is smooth.

Let $\mathcal{P}_n$ be a partition of $\Gamma \cap B(0,R)$ with $\mathcal{P}_{n+1}$ being a refinement of $\mathcal{P}_n$. To simplify matters, we assume that for $x_i \in \mathcal{P}_n$, $\Delta x_i = 1/2^n$ is a constant. Define the rational function,

$$F(s;\mathcal{P}_n) = \sum_{x_i \in \mathcal{P}_n} P_\epsilon(s,x_i) f(x_i) 2^{-n},$$

which is a Riemann sum approximation of $K_\epsilon^k f$. Here P_ϵ is the kernel of K_ϵ^k. We consider the difference of Riemann sums associated with $\mathcal{P}_m$ and $\mathcal{P}_n$ with $m > n$. With $x_i \in \mathcal{P}_m$, define $x_i' \in \mathcal{P}_n$ to be the next element of $\mathcal{P}_n$ (using the orientation of Γ). Notice that

$$F(s,\mathcal{P}_n) = \sum_{x_i \in \mathcal{P}_n} 2^{m-n} P_\epsilon(s,x_i) f(x_i) 2^{-m} = \sum_{x_i \in \mathcal{P}_m} P_\epsilon(s,x_i') f(x_i') 2^{-m},$$

because 2^{m-n} elements of $\mathcal{P}_m$ map to x_i' for each i. We obtain

$$|F(s;\mathcal{P}_n) - F(s;\mathcal{P}_m)| \le 2^{-m} \sum_{x_i \in \mathcal{P}_m} |P_\epsilon(s,x_i') f(x_i') - P_\epsilon(s,x_i) f(x_i)|. \tag{A.0.3}$$

It follows that $\mathcal{P}_m$ is the union of 2^{m-n} refinements of $\mathcal{P}_n$ and we may bound (A.0.3) using the total variation. Explicitly,

$$|F(s;\mathcal{P}_n) - F(s;\mathcal{P}_m)| \le 2^{-n} TV(P(s,\cdot) f(\cdot)).$$

We use the well-known fact that for absolutely continuous functions

$$TV(F) \le \int_a^b |F'(x)| dx,$$

along with the smooth parametrization of Γ_R to find

$$\begin{aligned} |F(s;\mathcal{P}_n) - F(s;\mathcal{P}_m)| &\le C 2^{-n} \int_{\Gamma_R} |\partial_t (P_\epsilon(s,t) f(t))| |dt| \\ &\le C 2^{-n} \left(\int_{\Gamma_R} |\partial_t P_\epsilon(s,t)| |f(t))| |dt| + \int_{\Gamma_R} |\partial_t P_\epsilon(s,t)| |f'(t))| |dt| \right). \end{aligned}$$

For $k > 1$, we find that there exists positive constants $C_1(\epsilon)$ and $C_2(\epsilon)$ depending only on ϵ such that

$$\int_\Gamma |P_\epsilon(s,t)| |dt| \le C_1(\epsilon), \quad \int_\Gamma |\partial_t P_\epsilon(s,t)| |dt| \le C_2(\epsilon).$$

This implies that (see [53, Theorem 6.18])

$$\left\| \int_{\Gamma_R} |P_\epsilon(s,t)||f'(t))||dt| \right\|_p \leq C_1(\epsilon)\|f'\|_p, \quad \left\| \int_{\Gamma_R} |\partial_t P_\epsilon(s,t)||f(t))||dt| \right\|_p \leq C_2(\epsilon)\|f\|_p.$$

Thus

$$\left\| \int_{\Gamma_\delta} |\partial_t (P_\epsilon(\cdot,t)f(t))||dt| \right\|_p \leq C(\epsilon)\|f\|_{W^{1,p}(\Gamma)}.$$

This proves that our rational approximation is a Cauchy sequence. By standard Riemann integration results, our rational approximation must converge pointwise to $\tilde{K}_\epsilon^k f$ where $\tilde{K}_\epsilon^k$ has integral kernel $P_\epsilon(s,t)\chi_{\Gamma_R}(t)$. This is the required L^p convergence for $k \geq 1$.

Continuing, we find for $f \in W^{k,p}(\Gamma)$, $f \neq 0$,

$$\begin{aligned} \|F(\cdot,\mathcal{P}_n) - K_\epsilon^k f\|_p &\leq \|F(\cdot,\mathcal{P}_n) - \tilde{K}_\epsilon^k f\|_p + \|(\tilde{K}_\epsilon^k - K_\epsilon^k)f\|_p, \qquad \text{(A.0.4)} \\ \|F(\cdot,\mathcal{P}_n) - D^k f\|_p &\leq \|K_\epsilon^k f - D^k f\|_p + \|K_\epsilon^k f - F(\cdot,\mathcal{P}_n)\|_p, \\ &\leq \|K_\epsilon^k f - D^k f\|_p + \|F(\cdot,\mathcal{P}_n) - \tilde{K}_\epsilon^k f\|_p + \|(\tilde{K}_\epsilon^k - K_\epsilon^k)f\|_p. \end{aligned}$$

For $\delta > 0$, fix $\epsilon > 0$ such that $\|K_\epsilon^k f - D^k f\|_p < \delta/3$. It follows that for R sufficiently large

$$\sup_{s\in\Gamma} \int_\Gamma |P_\epsilon(s,t) - P_\epsilon(s,t)\chi_{\Gamma_R}(t)||dt| < \frac{\delta}{3\|f\|_p}.$$

This implies that $\|\tilde{K}_\epsilon^k f - K_\epsilon^k f\|_p < \delta/3$ [53, Theorem 6.18]. For such an R, we let N be large enough so that $\|F(\cdot,\mathcal{P}_n) - \tilde{K}_\epsilon^k f\|_p < \delta/3$ for $n > N$. We find

$$\|F(\cdot,\mathcal{P}_n) - D^k f\|_p \leq \delta, \quad n > N.$$

Note that $F(s,\mathcal{P}_n)$ is a finite sum of rational functions of the form $\alpha/(s-\beta)^{k+1}$. Therefore we may integrate it to obtain another rational function. Since integration is a bounded operation we find that

$$\|F(\cdot,\mathcal{P}_n) - f\|_{W_z^{k,p}(\Gamma)} \leq C\delta.$$

This proves the density of rational functions for $k \geq 1$. To obtain the claim for $L^p(\Gamma)$ we use Lemma A.0.12. □

Corollary A.0.16. *$W_+^{l,p}(\Gamma)$ is dense in $W_+^{k,p}(\Gamma)$ for $l > k$.*

We arrive at our main rational approximation theorem. See Definition 3.8.6 for the definition of $R_\pm$.

Theorem A.0.17. *If Γ is admissible then $R_\pm(\Gamma) \cap L^2(\Gamma)$ is dense in $H_\pm^k(\Gamma)$ and $L^2(\Gamma) \cap R_\pm(\Gamma) \oplus C^{n\times n}$ is dense in $\tilde{H}_\pm^k(\Gamma)$.*

Appendix B

Spectral Collocation Methods

In this appendix we discuss the numerical solution of linear differential equations using a Chebyshev collocation method. Specifically, we consider the boundary-value problems

$$\mu_x + \mathcal{L}\mu = F, \quad \mu(-\infty) = 0, \tag{B.0.1}$$

$$\mu_x + \mathcal{L}\mu = F, \quad \mu(\infty) = 0, \tag{B.0.2}$$

where $\mathcal{L}$ is a linear operator. We assume F is smooth and rapidly decaying as $|x| \to \pm\infty$. Most of the developments presented below can be found in a variety of texts. See [104] for a introduction to spectral methods including the Chebyshev method discussed below. A good reference for the rigorous treatment of such methods is [7]. The main contribution of this appendix is the analysis of the domain truncation error for problems posed on an infinite domain.

B.1 Numerical implementation

For numerical purposes, we replace (B.0.1) with differential equations posed on a finite domain

$$\tilde{\mu}_x + \mathcal{L}\tilde{\mu} = F, \quad \tilde{\mu}(-L) = 0, \tag{B.1.1}$$

$$\tilde{\mu}_x + \mathcal{L}\tilde{\mu} = F, \quad \tilde{\mu}(L) = 0. \tag{B.1.2}$$

For now, we ignore the error introduced in this truncation and we drop the tilde. This is justified later. The naive way to solve this equation is to use the Chebyshev differentiation matrix. We approximate μ with a series of mapped Chebyshev polynomials of the first kind:

$$\mu(x) \sim \sum_n \alpha_n T_n(M_{-L}(x)), \quad M_{-L}(x) = 2(x + L/2)/L. \tag{B.1.3}$$

We use the notation M_{-L} because $M_{-L}([-L,0]) = [-1,1]$. Formally differentiating we find

$$\mu_x(x) \sim \sum_n \alpha_n T_n'(M_{-L}(x)) M_{-L}'(x).$$

Let $\boldsymbol{x}^N = (x_0, x_1, \ldots, x_N)^T$, $x_j = \cos(j\pi/N)$ be the Chebyshev points. Note that in this definition the first element of $\boldsymbol{x}^N$ is 1 and the last is -1. Let $\boldsymbol{x}^{-L,N} = M_{-L}^{-1}(\boldsymbol{x}^N)$. When f is a scalar-valued function, we overload it so that $f(\boldsymbol{x}^N)$ is a vector consisting of the elements $f(x),\ x \in \boldsymbol{x}^N$. Thus

$$\mu_x(\boldsymbol{x}^{-L,N}) \sim \sum_n \alpha_n T_n'(\boldsymbol{x}^N) \cdot M_{-L}'(\boldsymbol{x}^{-L,N}).$$

We have not decided how (B.1.3) approximates μ. If we choose α_n so that

$$\mu(\boldsymbol{x}^{-L,N}) = \sum_{n=0}^{N} \alpha_n T_n(M_{-L}(\boldsymbol{x}^{-L,N})) = \sum_{n=0}^{N} \alpha_n T_n(\boldsymbol{x}^n),$$

then it follows that

$$\sum_{n=0}^{N} \alpha_n T_n'(\boldsymbol{x}^N) = D_N \mu(\boldsymbol{x}^{-L,N}),$$

where D_N is the Chebyshev differentiation matrix. As mentioned above, reference [104] provides an extremely readable introduction to D_N. In particular, it is given by

$$(D_N)_{0,0} = \frac{2N^2+1}{6}, \quad (D_N)_{N,N} = -\frac{2N^2+1}{6},$$
$$(D_N)_{jj} = \frac{-x_j}{2(1-x_j^2)}, \quad j = 1, \ldots N-1,$$
$$(D_N)_{ij} = \frac{c_i}{c_j}\frac{(-1)^{i+j}}{x_i - x_j}, \quad i \neq j, \quad i,j = 0, \ldots, N,$$

where

$$c_i = \begin{cases} 2, & \text{if } i = 0 \text{ or } N, \\ 1, & \text{otherwise.} \end{cases}$$

Thus if we can compute $\mathcal{L}\mu$, $\mu = \sum_{n=0}^{N} \alpha_n T_n(M_{-L}(x))$ exactly at $\boldsymbol{x}^{-L,N}$ we form a finite-dimensional approximation of (B.1.1). We assume this computation exists as a black box. We obtain

$$(\mathrm{diag}(M_{-L}'(\boldsymbol{x}^{-L,N})) \cdot D_n + L(\boldsymbol{x}^{-L,N})) \cdot \mu(\boldsymbol{x}^{-L,N}) = F(\boldsymbol{x}^{-L,N}). \tag{B.1.4}$$

To enforce the boundary condition $\mu(-L) = 0$ we replace the last equation in the linear system with

$$(0, \ldots, 0, 1)\mu(\boldsymbol{x}^{-L,N}) = 0.$$

Often, this system is reliably solved for an approximation of μ at the collocation points $\boldsymbol{x}^{-L,N}$: $\mu(\boldsymbol{x}^{-L,N})$. The same approach works for (B.1.2) with $M_{-L}(x)$ replaced with $M_L(x)$. Note that the boundary condition is still imposed with the last row since this transformation reverses the collocation points.

Sometimes, in practice, the matrix in (B.1.4) is ill-conditioned. This depends on $\mathcal{L}$ and F. In these cases, as a preconditioning step, we convert (B.1.1) and (B.1.2) to equivalent integral equations. Operate on (B.1.1) with $I_{-L} = \int_{-L}^{x}$ and on (B.1.2) with I_L:

$$\tilde{\mu} + I_{-L}\mathcal{L}\tilde{\mu} = I_{-L}F, \tag{B.1.5}$$

$$\tilde{\mu} + I_L\mathcal{L}\tilde{\mu} = I_L F. \tag{B.1.6}$$

Before we proceed, we must consider what the black box for $\mathcal{L}\mu$ will output. If μ is a finite mapped Chebyshev series $\mu(x) = \sum_{n=0}^{N} \alpha_n T_n(M_{-L}(x))$ we assume we obtain $\mathcal{L}(x, \mu)$ exactly at $\boldsymbol{x}^{-L,N}$. Therefore, to obtain a finite-dimensional version of (B.1.5) and (B.1.6) we must find how to apply $I_{\pm L}$ to a function when we know the values at $\boldsymbol{x}^{\pm L,N}$.

We consider the $-L$ case first. Assume f is defined on $\boldsymbol{x}^{-L,N}$. For reasons that will become clear, we interpolate $(f \cdot M'_{-L}) \circ M_{-L}^{-1}$ with Chebyshev polynomials:

$$f(x) \cdot M'_{-L}(x) \sim \sum_{n=0}^{N} \alpha_n T_n(M_{-L}(x)). \tag{B.1.7}$$

It is well known that

$$\int T_n(x)dx = \frac{1}{2}\left(\frac{T_{n+1}(x)}{n+1} - \frac{T_{n-1}(x)}{n-1}\right), \quad n \geq 2,$$

$$\int T_1(x)dx = \frac{T_2(x)}{4},$$

$$\int T_0(x)dx = T_1(x).$$

Thus using the change of variables $s = M_{-L}(t)$ in the integral $\int_{-L}^{x} f(t)dt$, we find

$$\int_{-L}^{x} f(t)dt = \int_{-1}^{M_{-L}(x)} f(M_{-L}^{-1}(s))dM_{-L}^{-1}(s).$$

It is clear that $dM_{-L}^{-1}(s) = 1/M'_{-L}(M_{-L}^{-1}(s))$ and therefore

$$\begin{aligned}\int_{-L}^{x} f(t)dt &\sim \int_{-1}^{M_{-L}(x)} \sum_{n=0}^{N} \alpha_n T_n(s)ds, \\ &= \alpha_0 T_1(M_{-L}(x)) + \alpha_1 \frac{T_2(M_{-L}(x))}{4} \\ &+ \sum_{n=1}^{N} \alpha_n \frac{1}{2} \frac{T_{n+1}(M_{-L}(x))}{n+1} - \sum_{n=1}^{N} \alpha_n \frac{1}{2} \frac{T_{n-1}(M_{-L}(x))}{n-1} + C.\end{aligned}$$

The constant C is chosen so that the integral vanishes when $x = -L$:

$$\begin{aligned}C = &- \sum_{n=1}^{N} \alpha_n \frac{1}{2} \frac{T_{n+1}(-1)}{n+1} + \sum_{n=1}^{N} \alpha_n \frac{1}{2} \frac{T_{n-1}(-1)}{n-1} \\ &- \alpha_0 T_1(-1) - \alpha_1 \frac{T_2(-1)}{4}.\end{aligned}$$

This expression simplifies using $T_n(-1) = (-1)^n$.

Next, we construct a matrix representation of I_{-L}. Let $\mathcal{F}_N$ be the matrix that maps values at $\boldsymbol{x}^N$ to the coefficients of the unique interpolating polynomial, the discrete cosine transform matrix. It can be constructed by applying the discrete cosine transform to the identity matrix, column by column. $\mathcal{F}_n^{-1}$ is found in a similarly way using the inverse discrete cosine transform. Define

$$\mathcal{I}_N = \begin{bmatrix} 0 & & & & & & \cdots & 0 \\ 1 & 0 & & & & & \cdots & 0 \\ 0 & 1/4 & 0 & -1/4 & 0 & & \cdots & 0 \\ 0 & 0 & 1/6 & 0 & -1/6 & 0 & \cdots & 0 \\ & & & \ddots & & \ddots & & \vdots \\ & & & & \ddots & & \ddots & \vdots \\ & & & & & 1/2(N-1) & 0 & -1/2(N-1) \\ & & & & & & 1/2N & 0 \end{bmatrix}.$$

Thus

$$I_{-L} f(\boldsymbol{x}^{-L,N}) \sim \mathcal{F}_N^{-1}(\mathcal{I}_N + C)\mathcal{F}_N \operatorname{diag}(M'_L(\boldsymbol{x}^{-L,N}))f(\boldsymbol{x}^{-L,N}) = \mathcal{I}_{-L,N} f(\mathbb{F}_{-L,N}).$$

Note that in this approximation we have neglected the contribution from T_{N+1} which appears after integration of the right-hand side of (B.1.7). We obtain a finite-dimensional approximation of (B.1.5):

$$(I + \mathcal{I}_{-L,N}\mathcal{L}(\boldsymbol{x}^{-L,N}))\mu(\boldsymbol{x}^{-L,N}) = \mathcal{I}_{-L,N} F(\boldsymbol{x}^{-L,N}).$$

This linear system is often better conditioned than (B.1.4). Replacing M_{-L} with M_L we obtain a method for (B.1.6).

Remark B.1.1. *We may appeal to the ideas of Theorem 5.1.6 to prove convergence as-*

suming the norm of the linear system does not grow exponentially in N. This is, of course, assuming that the solution $\tilde{\mu}$ is C^∞.

B.2 Justification of (B.1.1) and (B.1.2)

We consider (B.1.1) only. Fix $M > 0$. First, we assume that the support $\operatorname{supp} F \subset (-L, M)$ and that if $f \in L^2(-\infty, M)$, $\operatorname{supp} f \subset (-L, M)$ then $\operatorname{supp} L(x)f \subset (-L, M)$. In this case we say $\mathcal{L}$ preserves support in $(-L, M)$. We deal with the general case by approximation. We consider (B.1.5). Under our assumptions, we see that if we extend $\tilde{\mu}$ to be identically zero on $(-\infty, -L]$ we have

$$\tilde{\mu} + I_{-L}\mathcal{L}\tilde{\mu} = I_{-L}F \text{ on } (-L, M), \tag{B.2.1}$$

$$\tilde{\mu} + I_{-\infty}\mathcal{L}\tilde{\mu} = I_{-\infty}F \text{ on } (-\infty, M). \tag{B.2.2}$$

Any solution of this equation must be a solution of $\mu_x + \mathcal{L}\mu = F$. The truncation is justified in this case.

In the general case, we assume $\mathcal{L}$ can be approximated, as an operator from $C_0((-\infty, M))$ to $L^1(\mathbb{R})$, by operators $\mathcal{L}_n$ that preserve support in $(-L_n, M)$. We assume $F \in L^1((-\infty, M)$ and assume the operator $(I + I_{-\infty}\mathcal{L})$ is invertible on $C^0((-\infty, M))$. Then for sufficiently large n, $(I + I_\infty\mathcal{L}_n)$ is invertible. Note that I_∞ is bounded from $L^1((-\infty, M))$ to $C_0((-\infty, M))$ with an operator norm of unity.

We approximate F in $L^1((-\infty, M))$ with smooth functions F_m, each with compact support and consider the equation

$$(I + I_{-\infty}\mathcal{L}_n)\mu_{n,m} = F_m.$$

If $\mu_{n,m}$ solves this equation then so does $\mu_{n,m}\cdot\chi_{-\delta,M}$, $-\delta < -L_n$ such that $\operatorname{supp} F_m \subset \delta$. By uniqueness, $\mu_{n,m} = 0$ on $(-\infty, -\delta)$ for every such δ and we expect the numerical method above to converge to $\mu_{n,m}$, provided $\mu_{n,m}$ is smooth.

It remains to show that we may choose m, n so that a solution of this equation is close in $C_0((-\infty, M))$ to the solution of (B.2.2). By Theorem 1.5.7

$$\begin{aligned}\|\mu_{n,m} - \mu\|_{C_0((-\infty,M))} \leq \\ \|I + I_{-\infty}\mathcal{L}_n\|_{\mathcal{L}(C_0((-\infty,M)))}\|I_{-\infty}(\mathcal{L} - \mathcal{L}_n)\|_{\mathcal{L}(C_0((-\infty,M)))}\|\mu\|_{C_0((-\infty,M)))} \\ + \sup_{i\geq n}\|(I + I_{-\infty}\mathcal{L}_i)^{-1}\|_{\mathcal{L}(C_0((-\infty,M)))}\|I_\infty(F - F_m)\|_{C_0((-\infty,M))}.\end{aligned}$$

For sufficiently large n, $\sup_{i\geq n}\|(I + I_{-\infty}\mathcal{L}_n)^{-1}\|_{\mathcal{L}(C_0((-\infty,M)))} < \infty$ so we may choose n, m such that $\|\mu_{n,m} - \mu\|_{C_0((-\infty,M))} < \epsilon$ for any $\epsilon > 0$. The resulting equation for the chosen n, m is solved numerically. A similar calculation follows for (B.1.2).

Remark B.2.1. *As is seen above, the operator $\mathcal{L}$ is often that of multiplication by a smooth function ϕ that limits rapidly to a constant and F is smooth and rapidly decaying. In this case it is straightforward to set up such sequences $\{\mathcal{L}_n\}$ and $\{F_m\}$. In practice, we choose L so that $|F(x)|$ is less than machine precision for $x < -L$, as is $|\phi(-\infty) - \phi(x)|$.*

Bibliography

[1] M. Ablowitz and H. Segur. *Solitons and the Inverse Scattering Transform*. SIAM, Philadelpha, PA, 1981.

[2] M. J. Ablowitz. *Nonlinear dispersive waves*. Cambridge Texts in Applied Mathematics. Cambridge University Press, New York, 2011. Asymptotic analysis and solitons.

[3] M. J. Ablowitz and P. A. Clarkson. *Solitons, Nonlinear Evolution Equations and Inverse Scattering*. Cambridge University Press, 1991.

[4] M. J. Ablowitz and A. S. Fokas. *Complex Varibles: Introduction and Applications*. Cambridge University Press, second edition, 2003.

[5] M. J. Ablowitz and H. Segur. Asymptotic solutions of the Korteweg–de Vries equation. *Stud. in Appl. Math.*, 57:13–44, 1977.

[6] A. Asheim and D. Huybrechs. Asymptotic analysis of numerical steepest descent with path approximations. *Found. Comput. Math.*, 10(6):647–671, 2010.

[7] K. Atkinson and W. Han. *Theoretical Numerical Analysis*. Springer, 2009.

[8] R. Beals and R. R. Coifman. Scattering and inverse scattering for first order systems. *Comm. Pure and Appl. Math.*, 37:39–90, 1984.

[9] E. D Belokolos, A. I. Bobenko, V. Z. Enol'skii, A. R. Its, and V. B. Matveev. *Algebro-Geometric Approach to Nonlinear Integrable Equations*. Springer, 1994.

[10] R. F. Bikbaev and V. O. Tarasov. Initial-boundary value problem for the nonlinear Schrödinger equation. *J. Phys. A*, 24(11):2507–2516, 1991.

[11] G. Biondini and A. Bui. On the nonlinear Schrödinger equation on the half line with homogeneous Robin boundary conditions. *Stud. Appl. Math.*, 129(3):249–271, 2012.

[12] G. Boffetta and A. R. Osborne. Computation of the direct scattering transform for the Nonlinear Schrödinger Equation. *J. of Comp. Phys*, 102:252–264, 1995.

[13] F. Bornemann. On the numerical evaluation of distributions in random matrix theory: a review. *Markov Process. Related Fields*, 16(4):803–866, 2010.

[14] F. Bornemann. On the numerical evaluation of Fredholm determinants. *Maths. Comp.*, 79:871–915, 2010.

[15] J. P. Boyd. *Chebyshev and Fourier spectral methods*. Dover Publications Inc., Mineola, NY, second edition, 2001.

[16] T. Claeys, I. Krasovsky, and A. Its. Higher-order analogues of the Tracy-Widom distribution and the Painlevé II hierarchy. *Comm. Pure Appl. Math.*, 63, 362–412.

[17] T. Claeys and S. Olver. Numerical study of higher order analogues of the Tracy–Widom distribution. *Cont. Maths*, 2011. to appear.

[18] K. F. Clancey and I. Gohberg. *Factorization of matrix functions and singular integral operators*, volume 3 of *Operator Theory: Advances and Applications*. Birkhäuser Verlag, Basel, 1981.

[19] R. R. Coifman, P. W. Jones, and S. Semmes. Two elementary proofs of the L^2 boundedness of Cauchy integrals on Lipschitz curves. *J. Amer. Math. Soc.*, 2(3):553–564, 1989.

[20] C. W. Curtis and B. Deconinck. On the convergence of Hill's method. *Math. Comp.*, 79(269):169–187, 2010.

[21] B. Deconinck, M. Heil, A. Bobenko, M. van Hoeij, and M. Schmies. Computing Riemann theta functions. *Math. Comp.*, 73:1417–1442, 2004.

[22] B. Deconinck and J. N. Kutz. Computing spectra of linear operators using the Floquet–Fourier–Hill method. *J. of Comp. Phys.*, 291:296–321, 2007.

[23] B. Deconinck and D. O. Lovit. Data analysis and reduction using stationary solutions of the NLS equation. *Appl. Anal.*, 89:611–626, 2010.

[24] P. Deift. *Orthogonal Polynomials and Random Matrices: a Riemann-Hilbert Approach*. Amer. Math. Soc., 2000.

[25] P. Deift. *Integrable systems and random matrices: in honor of Percy Deift*, pages 419–425. Amer. Math. Soc., 2008.

[26] P. Deift and D. Gioev. Universality at the edge of the spectrum for unitary, orthogonal, and symplectic ensembles of random matrices. *Comm. Pure Appl. Math.*, 60(6):867–910, 2007.

[27] P. Deift, T. Kriecherbauer, and K. T.-R. McLaughlin. New results on the equilibrium measure for logarithmic potentials in the presence of an external field. *J. Approx. Theory*, 95(3):388–475, 1998.

[28] P. Deift, T. Kriecherbauer, K. T-R McLaughlin, S. Venakides, and X. Zhou. Asymptotics for polynomials orthogonal with respect to varying exponential weights. *Internat. Math. Res. Notices*, 16:759–782, 1997.

[29] P. Deift, T. Kriecherbauer, K. T-R McLaughlin, S. Venakides, and X. Zhou. Strong asymptotics of orthogonal polynomials with respect to exponential weights. *Comm. Pure Appl. Math.*, 52(12):1491–1552, 1999.

[30] P. Deift, T. Kriecherbauer, K. T.-R. McLaughlin, S. Venakides, and X. Zhou. Uniform asymptotics for polynomials orthogonal with respect to varying exponential weights and applications to universality questions in random matrix theory. *Comm. Pure Appl. Math.*, 52(11):1335–1425, 1999.

[31] P. Deift and J. Park. Long-time asymptotics for solutions of the NLS equation with a delta potential and even initial data. *Int. Math. Res. Not., FJOURNAL = International Mathematics Research Notices. IMRN, VOLUME = 2011, YEAR = 2011, PAGES = 5505–5624, ISSN = 1073-7928, MRCLASS = 35Q55 (35B40), MRNUMBER = 2863375, DOI = 10.1007/s11005-010-0458-5, URL = http://dx.doi.org.offcampus.lib.washington.edu/10.1007/s11005-010-0458-5,.*

[32] P. Deift, S. Venakides, and X. Zhou. An extension of the steepest descent method for Riemann-Hilbert problems: the small dispersion limit of the Korteweg-de Vries (KdV) equation. *Proc. Natl. Acad. Sci. USA*, 95:450–454, 1998.

[33] P. Deift and X. Zhou. A steepest descent method for oscillatory Riemann–Hilbert problems. *Bulletin of the Amer. Math. Soc.*, 26:119–124, 1992.

[34] P. Deift and X. Zhou. A steepest descent method for oscillatory Riemann–Hilbert problems. Asymptotics for the MKdV equation. *Annals of Mathematics*, 137:295–368, 1993.

[35] P. Deift and X. Zhou. Long-time asymptotics for integrable systems. Higher order theory. *Comm. Math. Phys.*, 165:175–191, 1994.

[36] P. Deift and X. Zhou. *Long-time behavior of the non-focusing nonlinear Schroödinger equation—a case study*, volume 5 of *Lectures in Mathematical Sciences*. University of Tokyo, 1994.

[37] P. Deift and X. Zhou. Asymptotics for the Painlevé II equation. *Comm. Pure Appl. Math.*, 48, 1995.

[38] P. Deift and X. Zhou. Long-time asymptotics for solutions of the NLS equation with initial data in a weighted Sobolev space. *Comm. Pure Appl. Math.*, 56:1029–1077, 2003.

[39] P. Deift, X. Zhou, and S. Venakides. The collisionless shock region for the long-time behavior of solutions of the KdV equation. *Comm. Pure and Appl. Math.*, 47:199–206, 1994.

[40] P. A. Deift, A. R. It·s, and X. Zhou. Long-time asymptotics for integrable nonlinear wave equations. In *Important developments in soliton theory*, Springer Ser. Nonlinear Dynam., pages 181–204. Springer, Berlin, 1993.

[41] R. G. Douglas. *Banach Algebra Techniques in Operator Theory.* Academic Press, 1972.

[42] P. G. Drazin and R. S. Johnson. *Solitons: An Introduction.* Cambridge University Press, New York, NY, 1996.

[43] P. Dubard, P. Gaillard, C. Klein, and V.B. Matveev. On multi-rogue wave solutions of the NLS equation and position solutions of the KdV equation. *The European Physical Journal - Special Topics*, 185:247–258, 2010.

[44] B. A. Dubrovin. Inverse problem for periodic finite zoned potentials in the theory of scattering. *Func. Anal. and Its Appl.*, 9:61–62, 1975.

[45] B. A. Dubrovin. Theta functions and non-linear equations. *Russian Math. Surveys*, 36:11–92, 1981.

[46] B. A. Dubrovin. Integrable Systems and Riemann Surfaces Lecture Notes. `http://people.sissa.it/~dubrovin/rsnleq_web.pdf`, 2009.

[47] P. Duren. *Theory of H^p Spaces*. Academic Press, 1970.

[48] L. C. Evans. *Partial differential equations*, volume 19 of *Graduate Studies in Mathematics*. American Mathematical Society, Providence, RI, second edition, 2010.

[49] A. S. Fokas. *A Unified Approach to Boundary Value Problems*. SIAM, Philadelphia, PA, 2008.

[50] A. S. Fokas and I. M. Gel'fand. Integrability of linear and nonlinear evolution equations and the associated nonlinear fourier transforms. *Lett. Math. Phys.*, 32:189–210, 1994.

[51] A. S. Fokas, A. R. Its, A. A. Kapaev, and V. Y. Novokshenov. *Painlevé Transcendents: the Riemann–Hilbert Approach*. Amer. Math. Soc., 2006.

[52] A. S. Fokas, A. R. Its, and A. V. Kitaev. The isomonodromy approach to matric models in 2d quantum gravity. *Comm. Math. Phys.*, 147(2):395–430, 1992.

[53] G. B. Folland. *Real analysis*. John Wiley & Sons Inc., New York, 1999.

[54] B. Fornberg and J. A. C. Weideman. A numerical methodology for the Painlevé equations. *J. Comp. Phys.*, 2011.

[55] J. Frauendiener and C. Klein. Hyperelliptic theta-functions and spectral methods: KdV and KP solutions. *Lett. Math. Phys.*, 76:249–267, 2006.

[56] C. S. Gardner, J. M. Greene, M. D Kruskal, and R. M. Miura. Method for solving the Korteweg–de Vries equation. *Phys. Rev. Lett.*, 19:1095–1097, 1967.

[57] W. Gautschi. *Orthogonal Polynomials: Applications and Computation*. Oxford University Press, 2004.

[58] T. Grava and C. Klein. Numerical solution of the small dispersion limit of Korteweg–de Vries and Whitham equations. *Comm. Pure Appl. Math.*, 60:1623–1664, 2007.

[59] E. P. Gross. Strucure of a quantized vortex in boson systems. *Il Neuvo Cimento*, 20:454–477, 1961.

[60] K. Grunert and G. Teschl. Long-time asymptotics for the Korteweg–de Vries equation via nonlinear steepest descent. *Math. Phys., Anal. and Geom.*, 12:287–324, 2008.

[61] O. H. Hald. Numerical solution of the Gel'fand–Levitan equation. *Linear Algebra Appl.*, 28:99–111, 1979.

[62] G. H. Hardy. *A course of pure mathematics*. Cambridge University Press, Cambridge, centenary edition, 2008. Reprint of the tenth (1952) edition with a foreword by T. W. Körner.

[63] Stuart P. Hastings and J. Bryce McLeod. *Classical methods in ordinary differential equations*, volume 129 of *Graduate Studies in Mathematics*. American Mathematical Society, Providence, RI, 2012. With applications to boundary value problems.

[64] A. Iserles, S. P. Nørsett, and S. Olver. Highly oscillatory quadrature: the story so far. In *Numerical mathematics and advanced applications*, pages 97–118. Springer, Berlin, 2006.

[65] A. Its and D. Shepelsky. Initial boundary value problem for the focusing nls equation with robin boundary conditions: half-line approach. *arXiv:1201.5948 [nlin.SI]*, 2012.

[66] A. R. It·s, A. V. Kitaev, and A. S. Fokas. Matrix models of two-dimensional quantum gravity, and isomonodromic solutions of Painlevé "discrete equations". *Zap. Nauchn. Sem. Leningrad. Otdel. Mat. Inst. Steklov. (LOMI)*, 187(Differentsialnaya Geom. Gruppy Li i Mekh. 12):3–30, 171, 174, 1991.

[67] M. Jimbo and T. Miwa. Studies on holonomic quantum fields. XVII. *Proc. Japan Acad. Ser. A Math. Sci.*, 56(9):405–410, 1980.

[68] M. A. Johnson and K. Zumbrun. Convergence of Hill's method for non-self adjoint operators. *SIAM J. Numer. Anal.*, 50(1):64–78, 2012.

[69] D.J. Korteweg and G. de Vries. On the change of form of long waves advancing in a rectangular canal, and on a new type of long stationary waves. *Philosophical Magazine*, 39:422–443, 1895.

[70] P. D. Lax. Periodic solutions of the KdV equation. *Comm. Pure Appl. Math.*, 28:141–188, 1975.

[71] S. V. Manakov. On the theory of two-dimensional stationary self-focusing of electromagnetic waves. *Soviet Physics JETP*, 48:248–253, 1974.

[72] B. McCoy. Ising model: exact results. *Scholarpedia*, 5(7):10313, 2010.

[73] H. P. McKean. Algebraic curves of infinite genus arising in the theory of nonlinear waves. In *Proceedings of the International Congress of Mathematicians (Helsinki, 1978)*, pages 777–783, Helsinki, 1980. Acad. Sci. Fennica.

[74] H. P. McKean and E. Trubowitz. Hill's surfaces and their theta functions. *Bull. Amer. Math. Soc.*, 84:1042–1085, 1978.

[75] M.L. Mehta. *Random Matrices*. Academic Press, 2004.

[76] Y. Meyer and R. R. Coifman. *Wavelets: Calderón-Zygmund and Multilinear Operators*. Cambridge University Press, 1997.

[77] H. N. Mhaskar and E. B. Saff. Extremal problems for polynomials with exponential weights. *Trans. Amer. Math. Soc*, 285(1):203–234, 1984.

[78] S. G. Mikhlin and S. Prössdorf. *Singular Integral Operators*. Springer, 1980.

[79] P. D. Miller. *Applied asymptotic analysis*, volume 75 of *Graduate Studies in Mathematics*. American Mathematical Society, Providence, RI, 2006.

[80] R. M. Miura. Korteweg–de Vries equation and generalizations. I. A remarkable nonlinear transformation. *J. Math. Phys.*, 9:1202–1204, 1968.

[81] N. I. Muskhelishvili. *Singular Integral Equations*. Groningen: Noordoff, (based on the second Russian edition published in 1946) edition, 1953.

[82] S. Novikov, S. V. Manakov, L. P. Pitaevskii, and V. E. Zakharov. *Theory of Solitons*. Constants Bureau, New York, 1984.

[83] S. P. Novikov. A periodic problem for the Korteweg-de Vries equation. I. *Funkcional. Anal. i Priložen.*, 8:54–66, 1974.

[84] F. W. J. Olver, D. W. Lozier, R. F. Boisvert, and C. W. Clark. *NIST Handbook of Mathematical Functions*. Cambridge University Press, 2010.

[85] S. Olver. RHPackage. `http://www.maths.usyd.edu.au/u/olver/projects/RHPackage.html`.

[86] S. Olver. Computing the Hilbert transform and its inverse. *Math. Comp.*, 2009.

[87] S. Olver. Numerical solution of Riemann–Hilbert problems: Painlevé II. *Found. Comput. Math.*, 2010.

[88] S. Olver. Computation of equilibrium measures. *J. Approx. Theory*, 163:1185–1207, 2011.

[89] S. Olver. A general framework for solving Riemann-Hilbert problems numerically. *Numer. Math.*, 122(2):305–340, 2012.

[90] S. Olver and T. Trogdon. Nonlinear steepest descent and the numerical solution of Riemann–Hilbert problems. *to appear in Comm. Pure Appl. Math.*, 2012.

[91] S. Olver and T. Trogdon. Numerical solution of Riemann–Hilbert problems: orthogonal polynomials and random matrix theory. *submitted for publication in Constr. Approx.*, 2012.

[92] L. Onsager. Crystal statistics. I. A two-dimensional model with an order-disorder transition. *Phys. Rev. (2)*, 65:117–149, 1944.

[93] Alfred R. Osborne. *Nonlinear ocean waves and the inverse scattering transform*, volume 97 of *International Geophysics Series*. Elsevier/Academic Press, Boston, MA, 2010.

[94] L. P. Pitaevskii. Vortex lines in a imperfect Bose gas. *Sov. Phys., JETP*, 13:451–454, 1961.

[95] M. Prähofer and H. Spohn. Exact scaling functions for one-dimensional stationary KPZ growth. http://www-m5.ma.tum.de/KPZ/, 2004.

[96] M. Prähofer and H. Spohn. Exact scaling functions for one-dimensional stationary KPZ growth. *J. Stat. Phys.*, 115:255–279, 2004.

[97] S. Prösdorf and B. Silbermann. *Numerical Analysis for Integral and Related Operator Equations*. Bikrhäuser, 1991.

[98] A. Quarteroni, R. Sacco, and F. Saleri. *Numerical Mathematics*. Springer, 2007.

[99] E. A. Rakhmanov. On asymptotic properties of polynomials orthogonal on the real axis. *Matematicheskii Sbornik*, 161(2):163–203, 1982.

[100] T. J. Rivlin. *Chebyshev polynomials*. Pure and Applied Mathematics (New York). John Wiley & Sons Inc., New York, second edition, 1990. From approximation theory to algebra and number theory.

[101] E. B. Saff and V. Totik. *Logarithmic Potentials with External Fields*. Springer, 1997.

[102] E. M. Stein. *Singular integrals and differentiability properties of functions*. Princeton Mathematical Series, No. 30. Princeton University Press, Princeton, N.J., 1970.

[103] A. Tovbis, S. Venakides, and X. Zhou. On semiclassical (zero dispersion limit) solution of the focusing nonlinear Schrödinger equation. *Comm. Pure and Appl. Math.*, 57:877–985, 2004.

[104] L. N. Trefethen. *Spectral methods in MATLAB*, volume 10 of *Software, Environments, and Tools*. Society for Industrial and Applied Mathematics (SIAM), Philadelphia, PA, 2000.

[105] T. Trogdon. ISTPackage. `http://students.washington.edu/trogdon/software.html`, 2013.

[106] T. Trogdon and B. Deconinck. The solution of linear constant-coefficient evolution PDEs with periodic boundary conditions. *Appl. Anal.*, 91:529–544, 2012.

[107] T. Trogdon and B. Deconinck. Numerical computation of the finite-genus solutions of the Kortewegde Vries equation via Riemann–Hilbert problems. *Appl. Math. Lett.*, 26(1):5 – 9, 2013.

[108] T. Trogdon and B. Deconinck. A Riemann–Hilbert problem for the finite-genus solutions of the KdV equation and its numerical solution. *Physica D*, 251(0):1 – 18, 2013.

[109] T. Trogdon and S. Olver. Numerical inverse scattering for the focusing and defocusing nonlinear Schrödinger equations. *Proc. R. Soc. A.*, 469, 2012.

[110] T. Trogdon, S. Olver, and B. Deconinck. Numerical inverse scattering for the Korteweg-de Vries and modified Korteweg-de Vries equations. *Physica D*, 241:1003–1025, 2012.

[111] J.-M. Vanden-Broeck. *Gravity-capillary free-surface flows.* Cambridge Monographs on Mechanics. Cambridge University Press, Cambridge, 2010.

[112] Eugene P. Wigner. Characteristic vectors of bordered matrices with infinite dimensions. *Ann. of Math. (2)*, 62:548–564, 1955.

[113] T. T. Wu, B. M. McCoy, C. A. Tracy, and E. Barouch. Spin-spin correlation functions for the two-dimensional ising model: Exact theory in the scaling region. *Phys. Rev. B*, 13:316–374, Jan 1976.

[114] V. E. Zakharov. Stability of periodic waves of finite amplitude on the surface of a deep fluid. *J of Appl. Mech. and Tech. Phys.*, 9:190–194, 1968.

[115] V. E. Zakharov and S. V Manakov. Asymptotic behavior of non-linear wave systems integrated by the inverse scattering method. *Soviet Physics JETP*, 44:106–112, 1976.

[116] X. Zhou. The Riemann–Hilbert problem and inverse scattering. *SIAM J. Math. Anal.*, 20:966–986, 1989.

[117] X. Zhou. Riemann–Hilbert problems and integrable systems. *Lectures at MSRI*, 1999.

Index